Abstract and Applied Analysis

Coupled Network Systems and Their Collective Behavior

Guest Editors: Jinde Cao, Jianquan Lu, Ahmed Elaiw, Xinsong Yang, and Qiankun Song

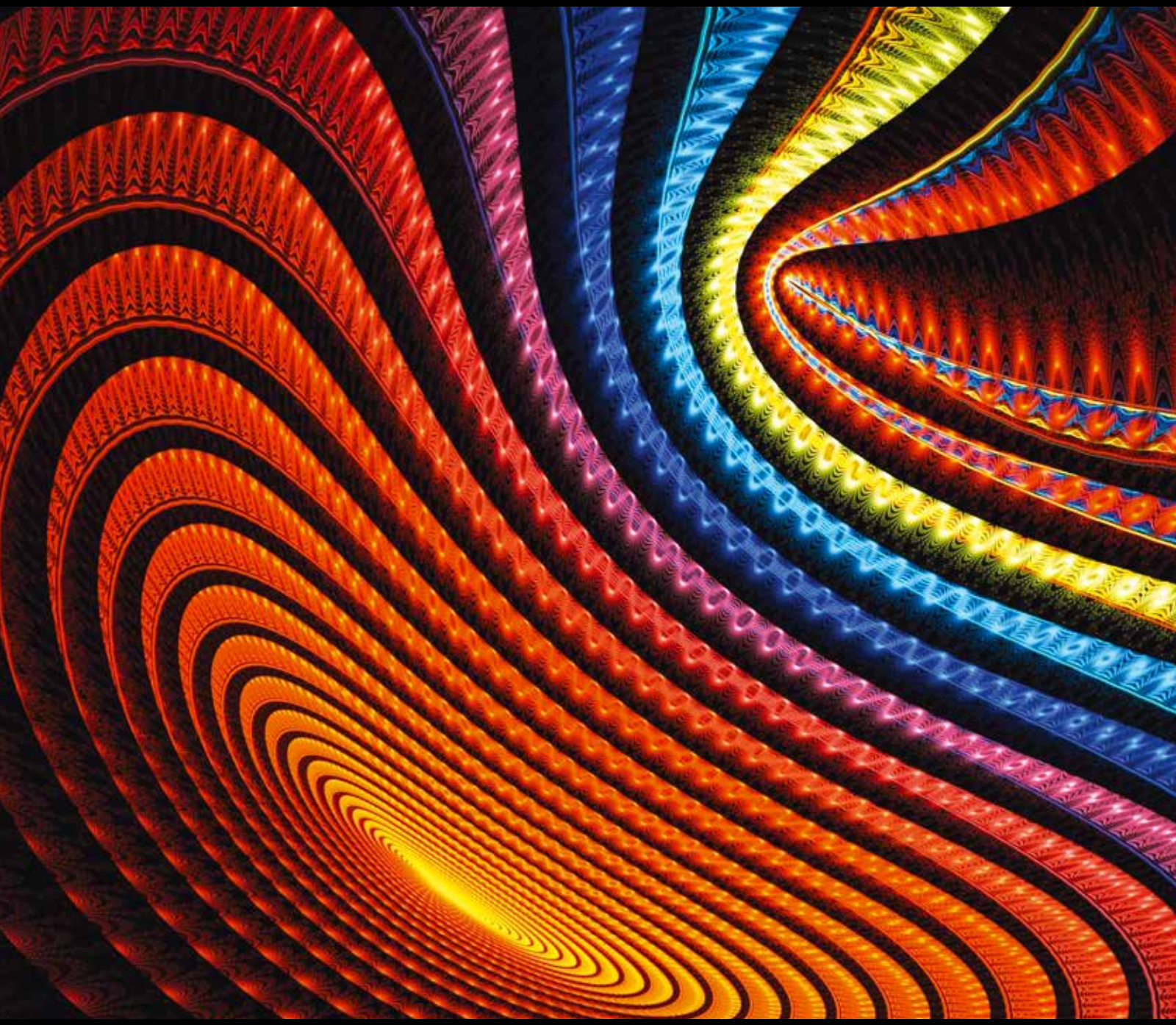

Coupled Network Systems and Their Collective Behavior

Abstract and Applied Analysis

Coupled Network Systems and Their Collective Behavior

Guest Editors: Jinde Cao, Jianquan Lu, Ahmed Elaiw, Xinsong Yang, and Qiankun Song

Editorial Board

Contents

Hindawi Publishing Corporation
Abstract and Applied Analysis
Volume 2014, Article ID 847262, 1 page
http://dx.doi.org/10.1155/2014/847262

Editorial

Coupled Network Systems and Their Collective Behavior

Jinde Cao,[1,2] Jianquan Lu,[1] Ahmed Elaiw,[2] Xinsong Yang,[3] and Qiankun Song[4]

[1] *Department of Mathematics, Southeast University, Nanjing 210096, China*
[2] *Department of Mathematics, Faculty of Science, King Abdulaziz University, Jeddah 21589, Saudi Arabia*
[3] *Department of Mathematics, Chongqing Normal University, Chongqing 401331, China*
[4] *Department of Mathematics, Chongqing Jiaotong University, Chongqing 400074, China*

Correspondence should be addressed to Jinde Cao; jdcao@seu.edu.cn

Received 12 February 2014; Accepted 12 February 2014; Published 13 May 2014

Coupled network systems (CNSs) consist of many small, inexpensive agents, in which each agent is capable of collecting signals, processing information, and communicating with neighboring agents. Due to their wide applications in many fields including mobile sensor networks and Unmanned Aerial Vehicles, CNSs have attracted many researchers from different areas of sciences and technologies, ranging from mathematics and physics to computer science. Node collaboration is the key for the success of CNSs due to the fact that each node itself is limited by communication range, power, and processing ability. In the process of the nodes' signal exchanging, an interesting aspect of the dynamics in CNSs is that certain types of globally collective behavior emerge from local interactions among the nodes. Such behavior arises ubiquitously in biological systems, ecosystems, and physical systems.

This special issue focuses on the dynamics of coupled network systems with their collective behavior and engineering applications, and it aims to bring together the most recent developments and knowledge in some related fields. Potential topics include, but are not limited to, (a) synchronization of complex dynamical networks, (b) consensus of multiagent systems, (c) stochastic resonance and some other collective behaviors, (d) network analysis and control, (e) social network analysis, and (f) network applications in different areas.

The response to this special issue on Coupled Network Systems and Their Collective Behavior was beyond our expectation. We received 38 papers in this research fields. All manuscripts submitted to this special issue went through a rigorous peer-refereeing process. Based on the reviewers' reports, twenty-four original research articles are finally accepted. The contents embrace the synchronization of complex networks under different constraints, Gossip consensus algorithm, Cucker-Smale flocking analysis, dynamic average consensus, and application of ranking algorithms on crime busting model.

It is certainly impossible to provide in this short editorial a more comprehensive description for all articles in this special issue. However, the guest editors sincerely hope that our efforts by compiling these articles can enrich our readers and inspire researchers with regard to the seemingly common but actually important issue of coupled network systems.

Acknowledgments

The guest editors would like to thank the authors who submitted papers for consideration and the reviewers whose comments are important for us to make the decisions. All the participants have made it possible to have a very stimulating interchange of ideas. Many thanks are also due to the editorial board members of this journal owing to their great support and help for this special issue.

Jinde Cao
Jianquan Lu
Ahmed Elaiw
Xinsong Yang
Qiankun Song

Hindawi Publishing Corporation
Abstract and Applied Analysis
Volume 2014, Article ID 801642, 11 pages
http://dx.doi.org/10.1155/2014/801642

Research Article

An Exploration of the Range of Noise Intensity That Affects the Membrane Potential of Neurons

Rubin Wang, Guanzheng Wang, and Jinchao Zheng

Institute for Cognitive Neurodynamics, School of Science, East China University of Science and Technology, Shanghai 200237, China

Correspondence should be addressed to Rubin Wang; rbwang@163.com

Received 20 November 2013; Accepted 4 December 2013; Published 12 February 2014

Academic Editor: Jinde Cao

Neuronal activity in the human brain occurs in a complex physiologic environment, and noise from all aspects in this physiologic environment affects all aspects of nervous-system function. An essential issue of neural information processing is whether the environmental noise in a neural system can be estimated and quantified in a proper way. In this paper, we calculated the neural energy to estimate the range of critical values of thermal noise intensity that markedly affect the membrane potential and the energy waveform, in order to define such a noisy environment which neuronal activity relies on.

1. Introduction

Thermal noise in neural system is critically vital for information processing, because it has a great influence on a variety of aspects of the central nervous system [1–6]. How to evaluate the intensity of such noise has long been a focus for scientists attempting to understand network behaviors and perception [7–11]. So far, estimations of thermal noise intensity in neurons or neural networks in published papers with regard to neural models are generally subjective, lacking a definite basis that is applicable to the range of thermal noise intensity in real systems. Sometimes, authors define thermal noise themselves in order to obtain an ideal result; however, scientific definition of thermal noise and its intensity range is extremely difficult [12–18]. From the viewpoint of quantification, there have been a lot of studies on information coding and the dynamic behaviors of networks in a noisy environment, but these studies have not attempted to answer one of the most basic questions—what principles should be used to choose the thermal noise values in models? Theoretically speaking, there will be deviations between the calculated results and experimental data, and a further discussion on the effectiveness of calculated results is also needed. Taking into account all the considerations above and based on the literature [19–21], in this paper, a range of values of the different membrane potential under the thermal noise condition studied by using the energy method and their corresponding energy waveforms.

We wanted to estimate the range of critical values of noise intensity that is capable of markedly changing the energy waveform. The principal idea of our research was inspired by the fact that since it is impossible to measure the thermal noise intensity at a neuronal level which is great enough to affect neuronal activity in an experiment, and hence, according to the rule of the only corresponding relationship between the membrane potential and its energy function, the range of thermal noise intensity obtained by our neuronal energy function can be estimated to be what it should be in a real neural system. Any kind of membrane potential can be obtained by adjusting the noise intensity, but there is no intrinsic relationship between such a membrane potential and the real neuronal energy. Therefore, we studied the membrane potential starting from the point of view of neuronal energy and observing the type of order of magnitude in noise intensity that can greatly affect the energy function of the membrane potential. As a result, we obtained a range of thermal noise intensity that neurons might have in an actual thermal noisy environment.

It follows that a further discussion of thermal noise intensity range is possible for levels of networks. This part of the research is not only significant for the application of thermal noise intensity when modeling a neuron, but is also

able to provide an adequate scientific basis for estimating the range of thermal noise intensity in networks and helping to establish neural network models.

Finally, it should be emphasized that we did not consider signal to noise ratio (SNR) that is beyond the scope of this paper.

2. Methods

Compared with the traditional simple single neuronal model, a voltage source, a current source, and an inductor are innovatively proposed in the biophysical model presented in this paper, which is shown in Figure 1. The difference in concentration between inner and external ions of neurons creates the electric voltage source that drives the ions. The current source is created by, on one hand, the chemical gradient of ions and, on the other hand, the stimuli from neighboring neurons. Moreover, in the ion channels, the flow of charged particles, such as sodium ions, potassium ions, and calcium ions, forms a loop current which is equivalent to an inductor L_m, producing self-induction. C_m is used to denote the membrane capacitance. I_m denotes the total electrical current formed by the inputs of all the neighboring neurons to the Mth neuron. U denotes the voltage source. r_m and r_{0m} denote the resistance of the current source I_m and voltage source U, respectively, showing the wastage produced by the actual sources. Due to the actions of the electric voltage source and the electric current source at different points in the neuron, the membrane resistance is divided into three parts r_{1m}, r_{2m}, and r_{3m}.

As indicated in Figure 1, the power P_m of the Mth neuron produced by the voltage source U_m and the current source I_m is obtained using the formula

$$P_m = U_m I_{0m} + U_{im} I_m, \tag{1}$$

where

$$\begin{aligned} U_m &= r_{0m} I_{0m} + r_{1m} I_{1m} + L_m \dot{I}_{1m}, \\ I_{0m} &= I_{1m} - I_m + \frac{U_{im}}{r_m} + C_m \dot{I}_{1m}, \\ U_{im} &= C_m r_{3m} \dot{U}_{0m} + U_{0m}, \end{aligned} \tag{2}$$

$$L_m \dot{I}_{1m} + r_{1m} I_m = K_{1m} \dot{U}_{0m} + K_{2m} U_{0m} - r_{2m} I_m. \tag{3}$$

The current source is calculated from the formula

$$\begin{aligned} I_m = {} & i_{1m} \\ & + \sum_{j=1}^{n} \left[i_{0m}(j-1) \sin \omega_m (j-1) \left(t_j - t_{j-1} \right) \right] \\ & + i_{0m}(n) \sin \omega_m (n) \left(t - t_n \right) \\ & t_n < t < t_{n+1}, \quad n = 1, 2, \ldots, \quad t_0 = 0, \end{aligned} \tag{4}$$

where i_{1m} is the current used to maintain resting potential, i_{0m} denotes the electric current being produced after the single neuron receives stimuli from all other neighboring neurons connected at the subthreshold level, and ω_m denotes the spiking frequency of the action potential, where

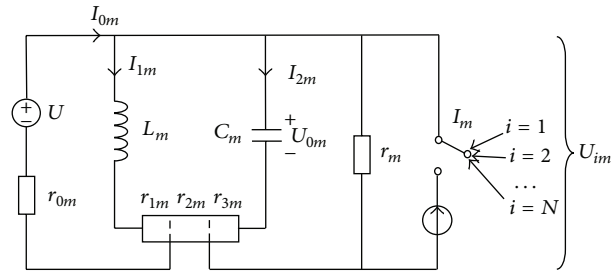

Figure 1: Physical model of the Mth neuron with coupling to other neurons.

$$K_{1m} = C_m \left(r_{2m} + r_{3m} + \frac{r_{2m} r_{3m}}{r_m} \right), \qquad K_{2m} = 1 + \frac{r_{2m}}{r_m}. \tag{5}$$

The solution of (3) is as follows:

$$\begin{aligned} I_{1m} = e^{-at} \Bigg(K + \frac{1}{L_m} \Bigg(& K_{1m} U_{0m} e^{at} + (K_{2m} - a K_{1m}) \\ & \times \int_{t_0}^{t} U_{0m} e^{at} dt - r_{2m} \int_{t_0}^{t} I_m e^{at} dt \Bigg) \Bigg), \end{aligned} \tag{6}$$

where

$$a = \frac{r_{1m}}{L_m}, \qquad K = I_{1m}(t_0) - \frac{r_m + r_{2m}}{r_m r_{1m}} U_{0m}(t_0). \tag{7}$$

When (6) satisfies the following conditions:

$$\begin{aligned} K_{2m} - a K_{1m} &= 0, \\ L_m = \frac{K_{1m}}{K_{2m}} r_{1m} &= C_m r_{1m} \left(r_{3m} + \frac{r_m r_{2m}}{r_m + r_{2m}} \right), \end{aligned} \tag{8}$$

we can obtain the following equation:

$$I_{1m} = e^{-at} \left(K + \frac{r_m r_{2m}}{r_m + r_{2m}} U_{0m} e^{at} - \frac{r_{2m}}{L_m} \int_{t_0}^{t} I_m e^{at} dt \right). \tag{9}$$

Inserting (9) and (2) into (1), the power of consumption P_m of mth neuron is obtained in the following:

$$\begin{aligned} P_m = {} & d_{1m} \dot{U}_{0m}^2 + d_{2m} \dot{U}_{0m} + d_{3m} \dot{U}_{0m} U_{0m} \\ & + d_{4m} U_{0m}^2 + d_{5m} U_{0m} + d_{6m}, \end{aligned} \tag{10}$$

where d_{1m}, d_{2m}, d_{3m}, d_{4m}, d_{5m}, and d_{6m} can be obtained from [20, 21].

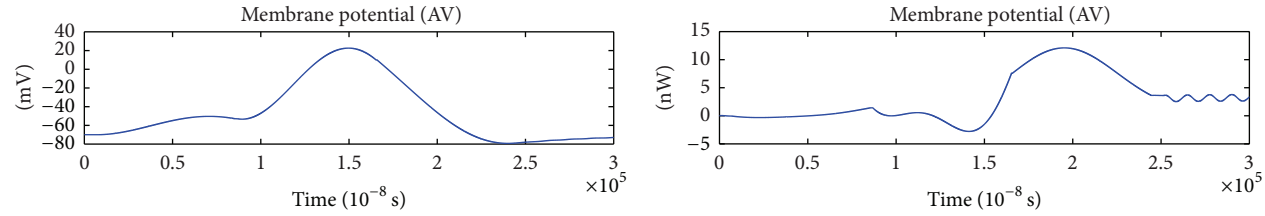

(a) (b)

Figure 2: Action potential and its corresponding energy function. $r_{0m} = 0.0001\,\Omega$, $r_{1m} = 0.1\,\Omega$, $r_{2m} = 1000\,\Omega$, $r_{3m} = 0.1\,\Omega$, $r_m = 1000\,\Omega$, $C_m = 1\,\mu$F, $L_m = 50\,\mu$H, and $i_{0m} = 70.7\,\mu$A.

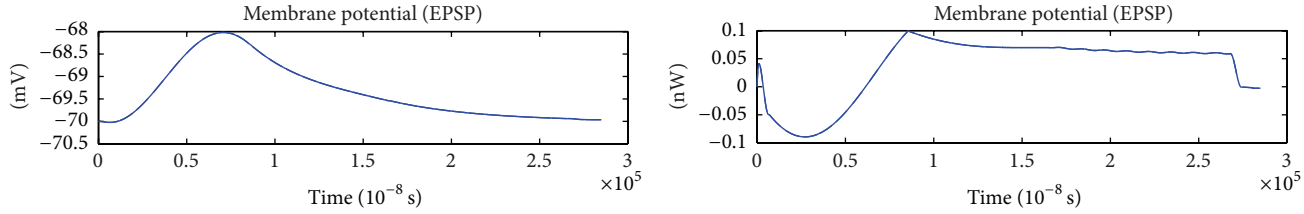

(a) (b)

Figure 3: EPSP and its corresponding energy function. $r_{0m} = 0.0001\,\Omega$, $r_{1m} = 0.1\,\Omega$, $r_{2m} = 1000\,\Omega$, $r_{3m} = 0.1\,\Omega$, $r_m = 1000\,\Omega$, $C_m = 1\,\mu$F, $L_m = 50\,\mu$H, and $i_{0m} = 7.155\,\mu$A.

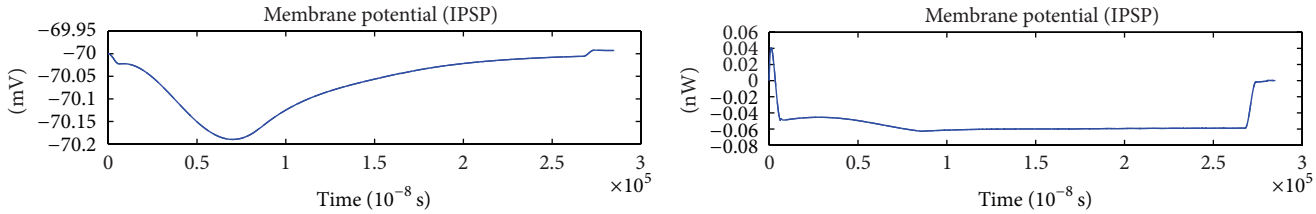

(a) (b)

Figure 4: IPSP and its corresponding energy function. $r_{0m} = 0.0001\,\Omega$, $r_{1m} = 0.1\,\Omega$, $r_{2m} = 1000\,\Omega$, $r_{3m} = 0.1\,\Omega$, $r_m = 1000\,\Omega$, $C_m = 1\,\mu$F, $L_m = 50\,\mu$H, and $i_{0m} = -0.7\,\mu$A.

According to the above equations, we can obtain the solution of the action potential U_{om}:

$$\begin{aligned} U_{0m} = &-\frac{\widehat{g}_1}{\lambda_m^2} - \frac{\widehat{g}_2 e^{-a(t-t_n)}}{\lambda_m^2 - a^2} - \frac{1}{\lambda_m^2 + \omega_m^2} \\ &\times \left(\widehat{g}_3 \sin\left(\omega_m(n)(t-t_n)\right) \right. \\ &\quad + \widehat{g}_4 \cos\left(\omega_m(n)(t-t_n)\right) \\ &\quad \times \left(U_{0m}(t_n) + \frac{\widehat{g}_1}{\lambda_m^2} + \frac{\widehat{g}_2}{\lambda_m^2 - a^2} \right. \\ &\quad \left. \left. + \frac{\widehat{g}_4}{\lambda_m^2 + \omega_m^2(n)} \right) \right) e^{-\lambda_m(t-t_n)}. \end{aligned} \tag{11}$$

To clarify our point of view, we present in a straightforward manner the action potential and its neuronal energy function represented by the corresponding power obtained by our proposed method, as shown in Figure 2.

As indicated in Figure 2, the peak voltage of the action potential is around 25 mV and the peak power of the energy function is around 12 nW. The energy waveforms of an excitatory postsynaptic potential (EPSP) and inhibitory postsynaptic potential (IPSP) are shown in Figures 3 and 4, respectively.

In the cerebral cortex, the excitatory neurons comprise 85% of the neurons, and the remaining neurons are inhibitory [22]. At the subthreshold state, the sum of the power of the EPSP and IPSP of a single neuron is negative (PP = 0.0367 + (−0.0532) = −0.0165 nW). From the overall observation, the total consumed energy is positive (PP′ = 0.0367 × 85% −0.0532 × 15% = 0.0232 nW). As seen from the results, the neural system consumes the energy supplied from blood flow, even if the neurons act at a subthreshold state; also as seen from the calculated results, neurons consume more energy at suprathreshold activities than at subthreshold activities. It is reported that a massive number of neurons in subthreshold activities consume only 20% of the total energy, whereas a small amount of neurons consume more than 80% due

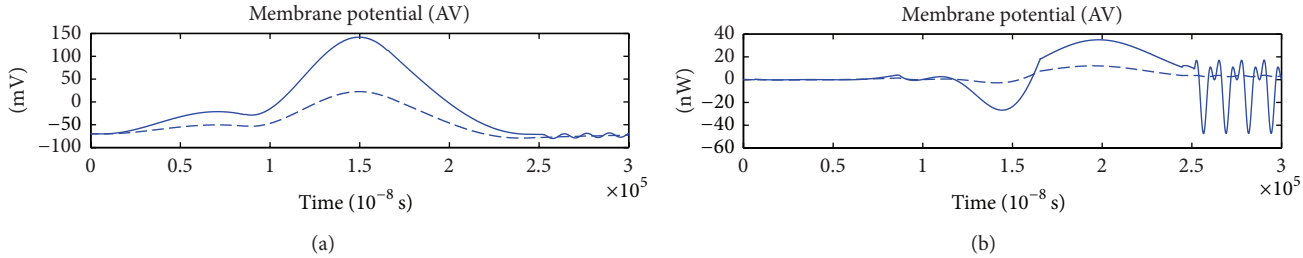

FIGURE 5: The action potential and its corresponding energy function. $r_{0m} = 0.0001\ \Omega$, $r_{1m} = 0.1\ \Omega$, $r_{2m} = 1000\ \Omega$, $r_{3m} = 0.1\ \Omega$, $r_m = 1000\ \Omega$, $C_m = 1\ \mu$F, $L_m = 50\ \mu$H, $i_{0m} = 70.7\ \mu$A, and $Q = 1 \times 10^{-4}\ \mu$A.

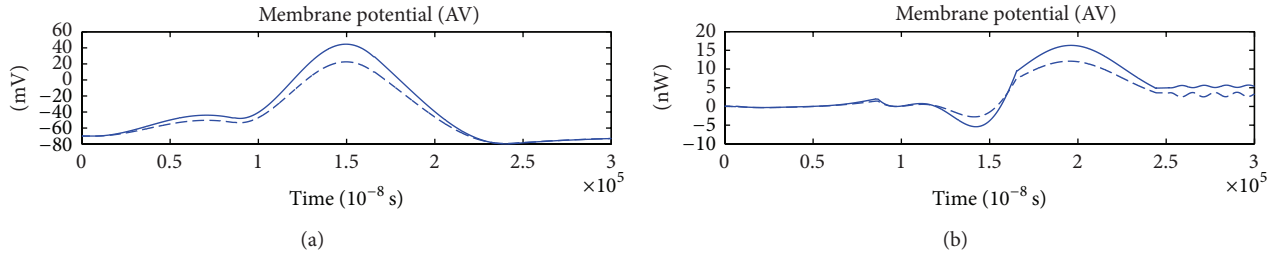

FIGURE 6: The action potential and its corresponding energy function. $r_{0m} = 0.0001\ \Omega$, $r_{1m} = 0.1\ \Omega$, $r_{2m} = 1000\ \Omega$, $r_{3m} = 0.1\ \Omega$, $r_m = 1000\ \Omega$, $C_m = 1\ \mu$F, $L_m = 50\ \mu$H, $i_{0m} = 70.7\ \mu$A, and $Q = 1 \times 10^{-5}\ \mu$A.

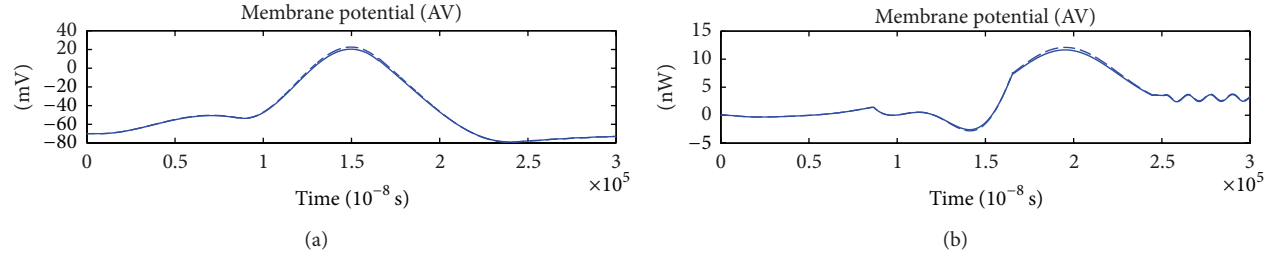

FIGURE 7: The action potential and its corresponding energy function. $r_{0m} = 0.0001\ \Omega$, $r_{1m} = 0.1\ \Omega$, $r_{2m} = 1000\ \Omega$, $r_{3m} = 0.1\ \Omega$, $r_m = 1000\ \Omega$, $C_m = 1\ \mu$F, $L_m = 50\ \mu$H, $i_{0m} = 70.7\ \mu$A, and $Q = 1 \times 10^{-6}\ \mu$A.

to action potential firing [22]. Our results conform to this conclusion.

A single neuron acts under the condition of a neural network. In other words, the interaction among the neurons makes their functional effectiveness emerge. It is in this sense that neuronal activity is performing the process of metabolism in the thermal noisy physiologic environment. To obtain the size of thermal noise intensity of the neuronal activity in the actual environment and to further obtain the noise circumstance under the condition of networks in the brain, we need to first understand the neuronal membrane potential and its corresponding energy function under the condition of no noise interference [19]. Only by obtaining the neuronal energy under an ideal condition can the physiologic influence of thermal noise on the membrane potential and its neuronal energy be better understood. Once that is obtained, it is possible to comprehend the noisy environment in a neural system and evaluate the behaviors of the network in such an environment.

3. Results

3.1. The Suprathreshold Membrane Potential and Its Neuronal Energy. Because the signal intensities of AP, EPSP, and IPSP are $7.07 \times 10^{-5}\ \mu$A, $7.155 \times 10^{-6}\ \mu$A, and $7 \times 10^{-7}\ \mu$A, so if we superpose thermal noise on the current i_{0m}, when the thermal noise intensity Q is more than $10^{-4}\ \mu$A, the influence of thermal noise on membrane potential and its energy function is far greater than that of the current i_{0m}, and when the thermal noise intensity Q is less than $10^{-7}\ \mu$A, the influence of thermal noise on membrane potential and its energy function is far weaker than that of i_{0m}. Therefore, the values of thermal noise intensity should be set as $10^{-4}\ \mu$A, $10^{-5}\ \mu$A, $10^{-6}\ \mu$A, and $10^{-7}\ \mu$A, respectively.

After adding thermal noise, the current takes the form

$$\begin{aligned} I_m = {} & i_{1m} \\ & + \sum_{j=1}^{n} \left[\left(i_{0m}(j-1) + Q \right) \sin \omega_m (j-1) \left(t_j - t_{j-1} \right) \right] \\ & + \left[i_{0m}(n) + Q \right] \sin \omega_m (n) \left(t - t_n \right), \end{aligned} \tag{12}$$

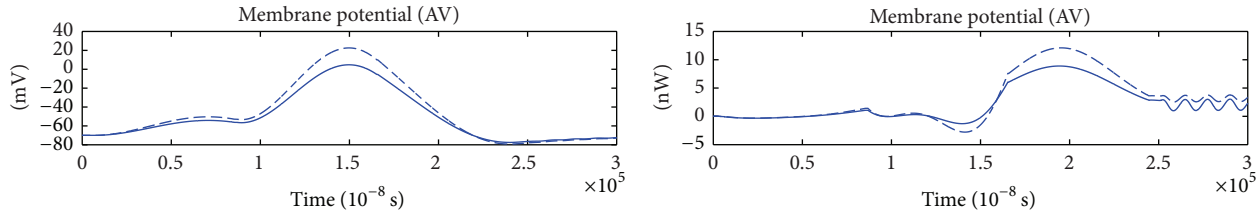

FIGURE 8: The action potential and its corresponding energy function. $r_{0m} = 0.0001\ \Omega$, $r_{1m} = 0.1\Omega$, $r_{2m} = 1000\ \Omega$, $r_{3m} = 0.1\ \Omega$, $r_m = 1000\ \Omega$, $C_m = 1\ \mu$F, $L_m = 50\ \mu$H, $i_{0m} = 70.7\ \mu$A, and $Q = 6 \times 10^{-6}\ \mu$A.

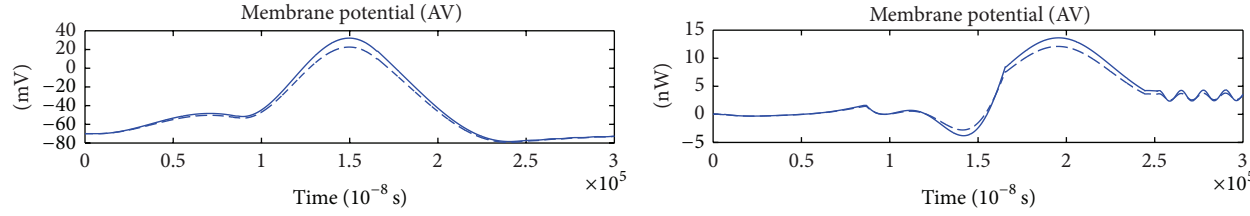

FIGURE 9: The action potential and its energy function. $r_{0m} = 0.0001\ \Omega$, $r_{1m} = 0.1\ \Omega$, $r_{2m} = 1000\ \Omega$, $r_{3m} = 0.1\ \Omega$, $r_m = 1000\ \Omega$, $C_m = 1\ \mu$F, $L_m = 50\ \mu$H, $i_{0m} = 70.7\ \mu$A, and $Q = 6 \times 10^{-6}\ \mu$A.

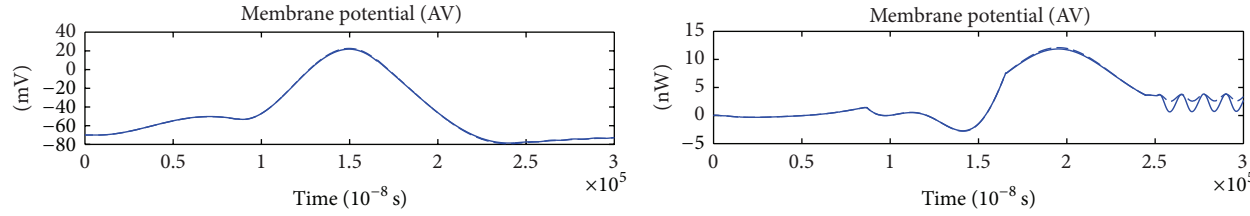

FIGURE 10: The action potential and its corresponding function. $r_{0m} = 0.0001\ \Omega$, $r_{1m} = 0.1\ \Omega$, $r_{2m} = 1000\ \Omega$, $r_{3m} = 0.1\ \Omega$, $r_m = 1000\ \Omega$, $C_m = 1\ \mu$F, $L_m = 50\ \mu$H, $i_{0m} = 70.7\ \mu$A, and $Q = 6 \times 10^{-6}\ \mu$A.

where Q denotes the synaptic noise as Gaussian white noise with the unit μA.

The action potential together with its corresponding power plotted by the energy function calculated under the condition of different noise intensity is shown as follows.

In all of Figures 5, 6, 7, 8, 9, and 10, the dotted line represents the case of no noise and the solid line represents the case of noise.

When the noise intensity Q reaches $10^{-4}\ \mu$A, the peak of the neuronal membrane potential is around 140 mV and far higher than 25 mV of the situation without noise, while the peak of the energy function is around 40 nW and far higher than the original 12 nW. Additionally, on the horizontal axis, between 2.5 ms and 3 ms, the amplitude of the energy waveform is much larger than the one in the situation without noise. Therefore, it fundamentally changes the action potential and its corresponding energy function under the ideal conditions when Q reaches $10^{-4}\ \mu$A.

When the noise intensity Q reaches $10^{-5}\ \mu$A, the influence of noise on the action potential deceases, but it is still significant. Here, the membrane potential is around 40 mV, whereas the peak of the energy function is around 15 nW. As can be seen, such noise intensity still has a great influence on the membrane potential and its corresponding energy waveform.

When the noise intensity Q reaches $10^{-6}\ \mu$A, there is hardly any influence on the action potential and its energy function. It is in such a noisy environment that the peaks of the membrane potential and energy waveform are exactly the same with those under the ideal conditions where the peaks of action potential and the energy function are 25 mV and 12 nW, respectively. In the presence of noise, the waveforms of the membrane potential and the energy function are nearly the same as without noise.

To summarize, we cannot estimate an accurate value of noise intensity for both the suprathreshold membrane potential and the corresponding neuronal energy. In estimating the range of the critical values of noise intensity, we found that when the noise intensity Q reaches about $6 \times 10^{-6}\ \mu$A (error $\pm\ 0.5 \times 10^{-6}\ \mu$A), the noise has great influence on the action potential and its corresponding energy function.

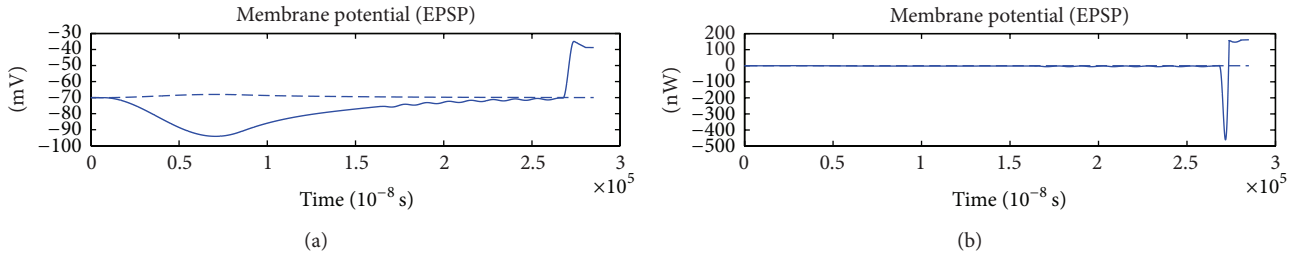

FIGURE 11: The EPSP and the corresponding energy function. $r_{0m} = 0.0001\,\Omega$, $r_{1m} = 0.1\,\Omega$, $r_{2m} = 1000\,\Omega$, $r_{3m} = 0.1\,\Omega$, $r_m = 1000\,\Omega$, $C_m = 1\,\mu$F, $L_m = 50\,\mu$H, $i_{0m} = 7.155\,\mu$A, and $Q = 1 \times 10^{-4}\,\mu$A.

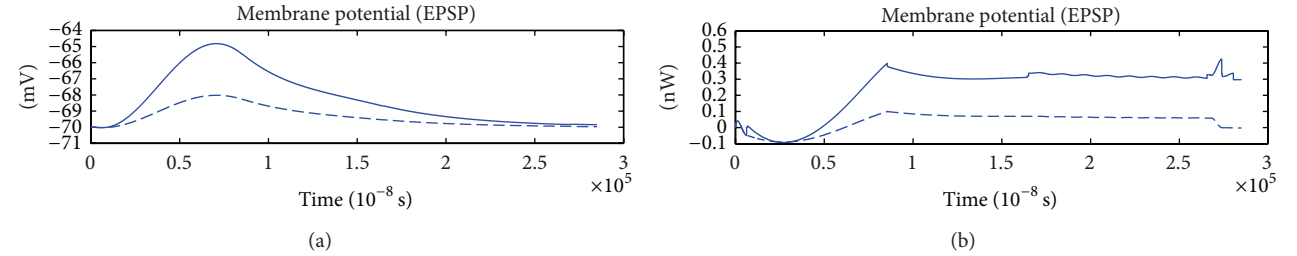

FIGURE 12: The EPSP and the corresponding energy function. $r_{0m} = 0.0001\,\Omega$, $r_{1m} = 0.1\,\Omega$, $r_{2m} = 1000\,\Omega$, $r_{3m} = 0.1\,\Omega$, $r_m = 1000\,\Omega$, $C_m = 1\,\mu$F, $L_m = 50\,\mu$H, $i_{0m} = 7.155\,\mu$A, and $Q = 1 \times 10^{-5}\,\mu$A.

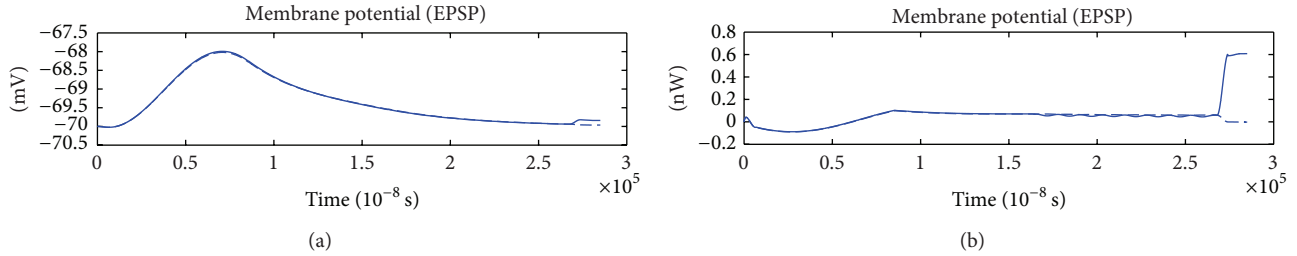

FIGURE 13: The EPSP and the corresponding energy function. $r_{0m} = 0.0001\,\Omega$, $r_{1m} = 0.1\,\Omega$, $r_{2m} = 1000\,\Omega$, $r_{3m} = 0.1\,\Omega$, $r_m = 1000\,\Omega$, $C_m = 1\,\mu$F, $L_m = 50\,\mu$H, $i_{0m} = 7.155\,\mu$A, and $Q = 1 \times 10^{-6}\,\mu$A.

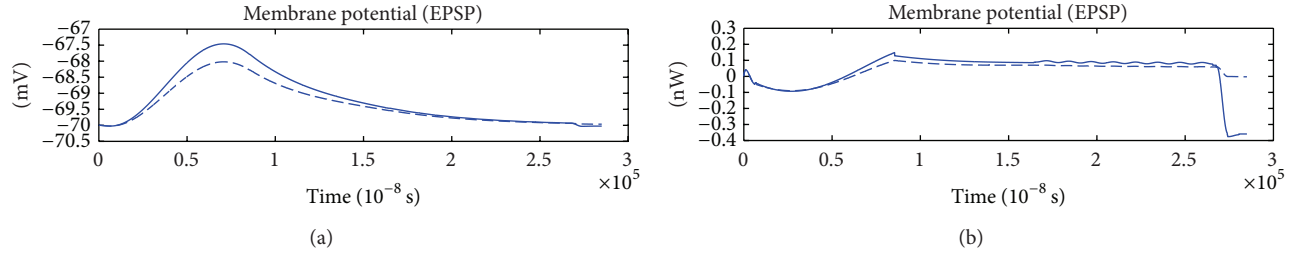

FIGURE 14: The EPSP and the corresponding energy function. $r_{0m} = 0.0001\,\Omega$, $r_{1m} = 0.1\,\Omega$, $r_{2m} = 1000\,\Omega$, $r_{3m} = 0.1\,\Omega$, $r_m = 1000\,\Omega$, $C_m = 1\,\mu$F, $L_m = 50\,\mu$H, $i_{0m} = 7.155\,\mu$A, and $Q = 2 \times 10^{-6}\,\mu$A.

As shown in Figures 8–10, when the noise intensity Q is $6\times10^{-6}\,\mu$A, the fluctuation of the membrane potential and the energy function turns out to be very large. The peak of the action potential fluctuates between 10 mV and 40 mV, while that of the energy function fluctuates from 10 nW to 15 nW. Such noise intensity has great influence on the membrane potential and the energy function, and as a result, the critical value of the noise intensity Q can be assessed at $6 \times 10^{-6}\,\mu$A (error $\pm\ 0.5 \times 10^{-6}\,\mu$A).

3.2. Subthreshold Membrane Potential and Its Neuronal Energy. According to the calculated results of Wang et al. [21], we obtained the EPSP and the corresponding energy waveform as well as the IPSP and the corresponding energy waveform by adding noise (Figures 11, 12, 13, 14, 15, 16, 17, 18, 19, 20, 21, 22, 23, 24, and 25).

When the level of noise intensity Q reached $1\times10^{-4}\,\mu$A, it had a great effect on the EPSP and the corresponding energy waveform. Without the effect of noise, we found that the EPSP

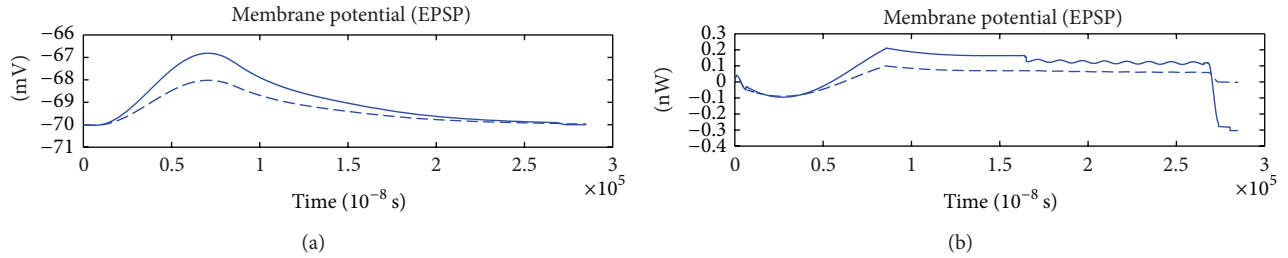

FIGURE 15: The EPSP and the corresponding energy function. $r_{0m} = 0.0001\,\Omega$, $r_{1m} = 0.1\,\Omega$, $r_{2m} = 1000\,\Omega$, $r_{3m} = 0.1\,\Omega$, $r_m = 1000\,\Omega$, $C_m = 1\,\mu F$, $L_m = 50\,\mu H$, $i_{0m} = 7.155\,\mu$A, and $Q = 3 \times 10^{-6}\,\mu$A.

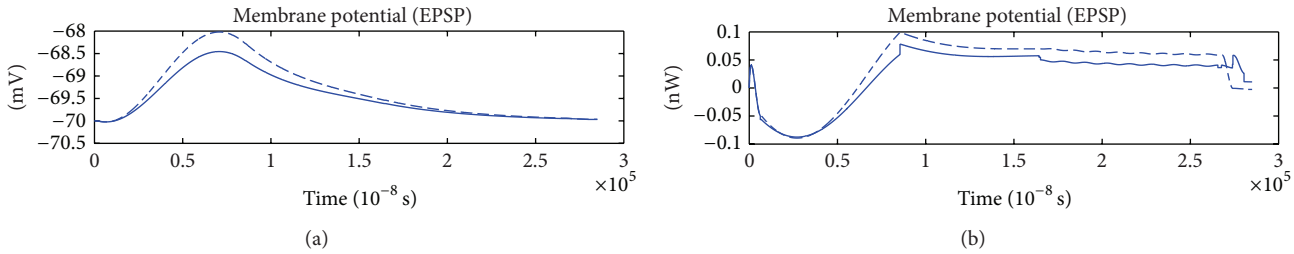

FIGURE 16: The EPSP and the corresponding energy function. $r_{0m} = 0.0001\,\Omega$, $r_{1m} = 0.1\,\Omega$, $r_{2m} = 1000\,\Omega$, $r_{3m} = 0.1\,\Omega$, $r_m = 1000\,\Omega$, $C_m = 1\,\mu$F, $L_m = 50\,\mu$H, $i_{0m} = 7.155\,\mu$A, and $Q = 3 \times 10^{-6}\,\mu$A.

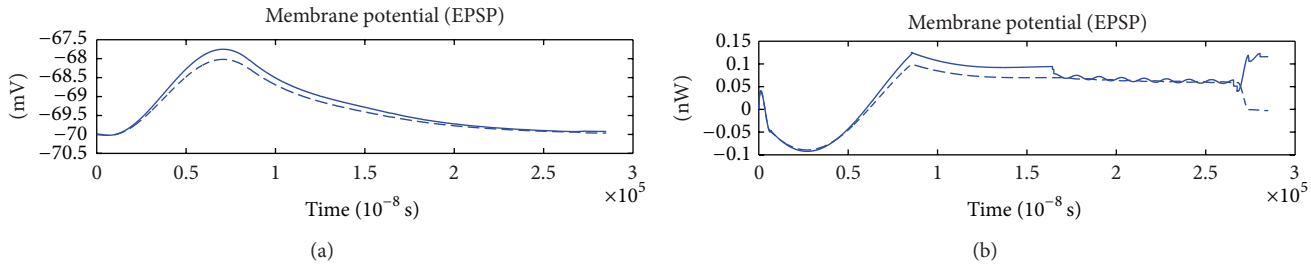

FIGURE 17: The EPSP and the corresponding energy function. $r_{0m} = 0.0001\,\Omega$, $r_{1m} = 0.1\,\Omega$, $r_{2m} = 1000\,\Omega$, $r_{3m} = 0.1\,\Omega$, $r_m = 1000\,\Omega$, $C_m = 1\,\mu$F, $L_m = 50\,\mu$H, $i_{0m} = 7.155\,\mu$A, and $Q = 3 \times 10^{-6}\,\mu$A.

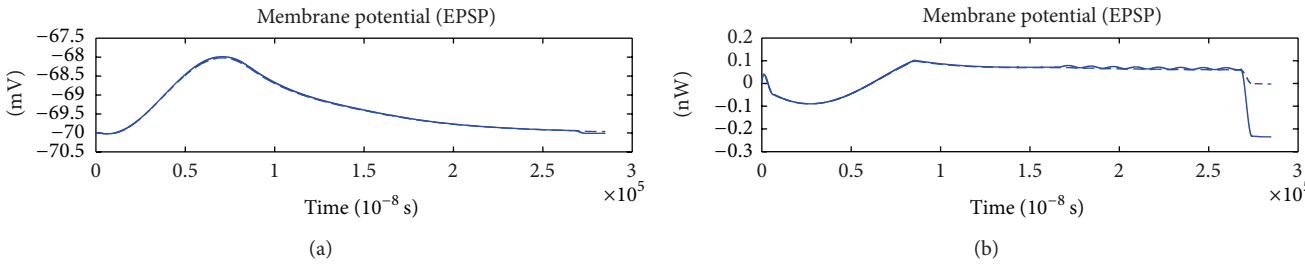

FIGURE 18: The EPSP and the corresponding energy function. $r_{0m} = 0.0001\,\Omega$, $r_{1m} = 0.1\,\Omega$, $r_{2m} = 1000\,\Omega$, $r_{3m} = 0.1\,\Omega$, $r_m = 1000\,\Omega$, $C_m = 1\,\mu$F, $L_m = 50\,\mu$H, $i_{0m} = 7.155\,\mu$A, and $Q = 1 \times 10^{-7}\,\mu$A.

curve increased first and then decreases with a maximum of −68 mV and a minimum of −70 mV. The energy function fell first and then rose towards stability, fluctuating in the range of −0.1 to 0.1 nW. After adding noise, we found that the EPSP curve fell first and then rose towards a minimum of −95 mV, while the energy function increased first and then decreased towards stability, fluctuating in the range of −10 to −80 nW.

When the level of noise intensity Q reached $1 \times 10^{-5}\,\mu$A, it also had a great effect on the EPSP and the corresponding energy waveform. Under an ideal condition without noise, we know that the maximum of the EPSP is about −68 mV and the peak of the energy function is about 0.1 nW. After adding noise, the peak of the EPSP hardly changed, but the oscillatory curve changed sharply in the period from 2.5 ms to 3 ms.

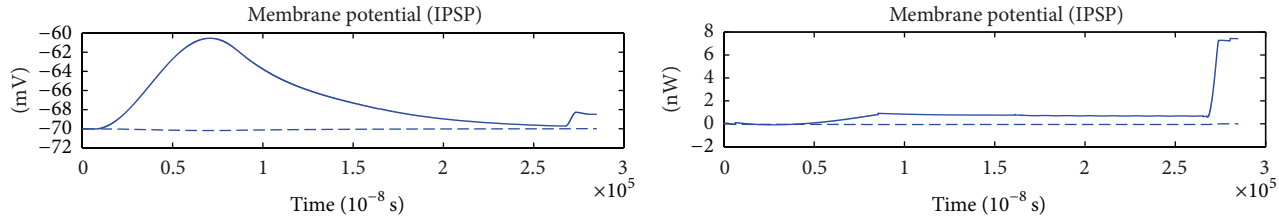

FIGURE 19: The IPSP and the corresponding energy function. $r_{0m} = 0.0001\,\Omega$, $r_{1m} = 0.1\,\Omega$, $r_{2m} = 1000\,\Omega$, $r_{3m} = 0.1\,\Omega$, $r_m = 1000\,\Omega$, $C_m = 1\,\mu$F, $L_m = 50\,\mu$H, $i_{0m} = -0.7\,\mu$A, and $Q = 1 \times 10^{-4}\,\mu$A.

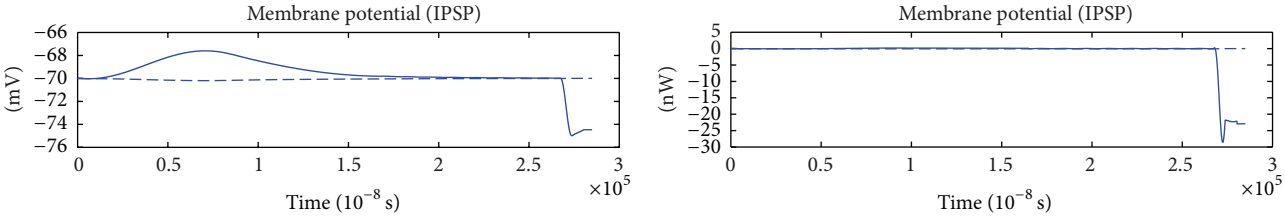

FIGURE 20: The IPSP and the corresponding energy function. $r_{0m} = 0.0001\,\Omega$, $r_{1m} = 0.1\,\Omega$, $r_{2m} = 1000\,\Omega$, $r_{3m} = 0.1\,\Omega$, $r_m = 1000\,\Omega$, $C_m = 1\,\mu$F, $L_m = 50\,\mu$H, $i_{0m} = -0.7\,\mu$A, and $Q = 1 \times 10^{-5}\,\mu$A.

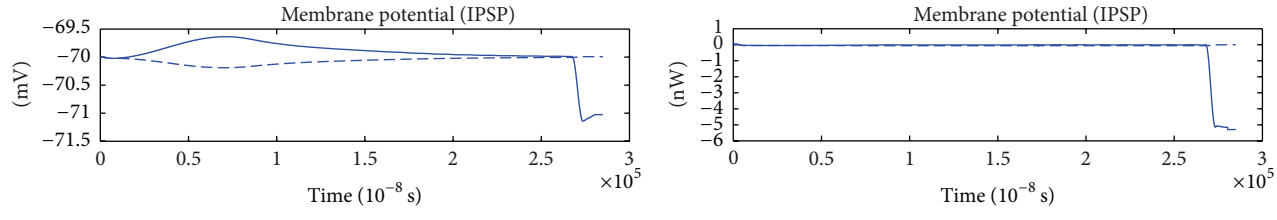

FIGURE 21: The IPSP and the corresponding energy function. $r_{0m} = 0.0001\,\Omega$, $r_{1m} = 0.1\,\Omega$, $r_{2m} = 1000\,\Omega$, $r_{3m} = 0.1\,\Omega$, $r_m = 1000\,\Omega$, $C_m = 1\,\mu$F, $L_m = 50\,\mu$H, $i_{0m} = -0.7\,\mu$A, and $Q = 1 \times 10^{-6}\,\mu$A.

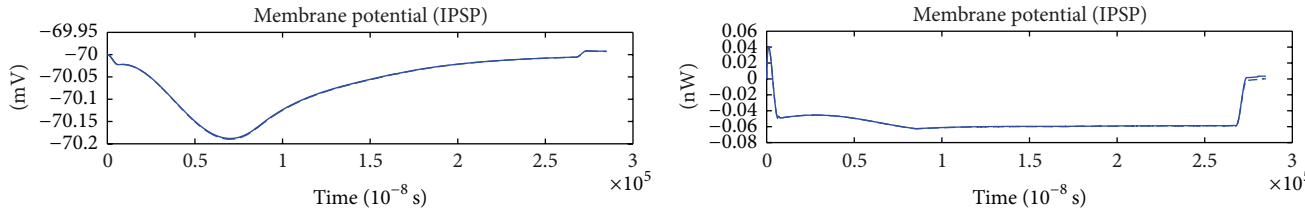

FIGURE 22: The IPSP and the corresponding energy function. $r_{0m} = 0.0001\,\Omega$, $r_{1m} = 0.1\,\Omega$, $r_{2m} = 1000\,\Omega$, $r_{3m} = 0.1\,\Omega$, $r_m = 1000\,\Omega$, $C_m = 1\,\mu$F, $L_m = 50\,\mu$H, $i_{0m} = -0.7\,\mu$A, and $Q = 1 \times 10^{-7}\,\mu$A.

The oscillatory amplitude of the energy function with noise was more intense than that without noise, varying between 1.5 ms and 2.5 ms.

When the noise intensity Q reached $1 \times 10^{-6}\,\mu$A, it had little effect on the EPSP and the corresponding energy waveform. This figure showing the EPSP and energy function with noise is almost the same with one without noise. We could not estimate the range of the noise intensity, which affects the EPSP's corresponding energy function according to the results shown in Figures 11–13. As a solution, we addressed the problem by adjusting the coefficient of the noise level.

When the level of noise intensity Q reached $2 \times 10^{-6}\,\mu$A, it did not have an obvious effect on the EPSP and the corresponding energy waveform. This figure shows the EPSP and energy function with noise is almost the same as one

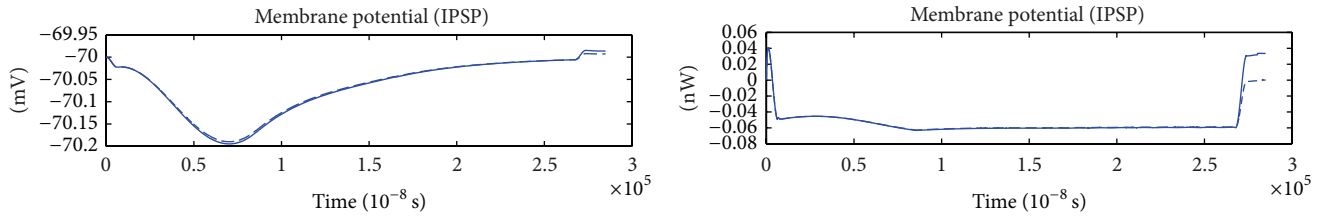

FIGURE 23: The IPSP and the corresponding energy function. $r_{0m} = 0.0001\,\Omega$, $r_{1m} = 0.1\,\Omega$, $r_{2m} = 1000\,\Omega$, $r_{3m} = 0.1\,\Omega$, $r_m = 1000\,\Omega$, $C_m = 1\,\mu$F, $L_m = 50\,\mu$H, $i_{0m} = -0.7\,\mu$A, and $Q = 2 \times 10^{-7}\,\mu$A.

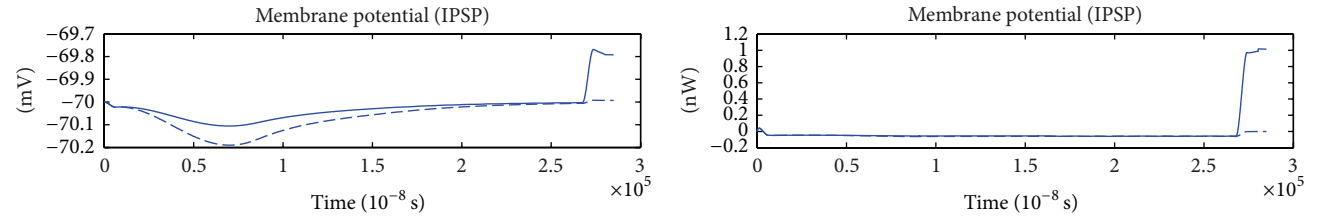

FIGURE 24: The IPSP and the corresponding energy function. $r_{0m} = 0.0001\,\Omega$, $r_{1m} = 0.1\,\Omega$, $r_{2m} = 1000\,\Omega$, $r_{3m} = 0.1\,\Omega$, $r_m = 1000\,\Omega$, $C_m = 1\,\mu$F, $L_m = 50\,\mu$H, $i_{0m} = -0.7\,\mu$A, and $Q = 3 \times 10^{-7}\,\mu$A.

without noise. But the energy function with noise is slightly different from that without noise ranging between 1.5 ms and 2.5 ms.

When the noise intensity Q reached $3 \times 10^{-6}\,\mu$A, it had a great effect on the EPSP and the corresponding energy waveform. Taking the noise into account, we found that the EPSP fluctuated in a small interval from −67 mV to −69 mV, while in the period from 1.5 ms to 2.5 ms, the energy function with noise had greater fluctuations than that without noise.

When the level of noise Q reached $1 \times 10^{-7}\,\mu$A, it had a little effect on the EPSP and the corresponding energy waveform. The figures of the EPSP and energy function with noise are almost the same as those without noise.

In summary, when the noise intensity Q was about $3 \times 10^{-6}\,\mu$A (error $\pm\, 0.5 \times 10^{-6}\,\mu$A), the noise begins to have a significant influence on EPSP and its corresponding energy waveform. As a result, the critical value of the noise was assessed at $3 \times 10^{-6}\,\mu$A (error $\pm\, 0.5 \times 10^{-6}\,\mu$A).

When the noise intensity Q reached $1 \times 10^{-4}\,\mu$A, it had a great effect on the IPSP and the corresponding energy waveform. Without the effect of noise, we found that the IPSP curve fell first and then rose and the energy function curve was almost in the stable state of −0.04 nW. However, after adding noise, we found that the IPSP curve rose first and then fell, while most of the energy function curve was above 0 and there were huge fluctuations of the energy function between 1.5 ms and 2.5 ms.

When the noise intensity Q reached $1 \times 10^{-5}\,\mu$A, it had a critical effect on the IPSP and the corresponding energy waveform. Without the effect of noise, we observed that the IPSP curve fell initially and then rose and the energy function curve was almost in a stable state of −0.04 nW. However, after adding noise, the IPSP curve rose first and then fell and there were huge fluctuations of the energy function between 2.5 ms and 3 ms.

When the noise intensity$Q$ reached $1 \times 10^{-6}\,\mu$A, it had a relatively great effect on the IPSP and the corresponding energy waveform. Without the effect of noise, the IPSP curve fell initially and then rose, while the energy function curve was almost in a stable state of −0.04 nW. After adding noise, the IPSP curve rose first and then fell and there were also huge fluctuations of the energy function from 2.5 ms to 3 ms.

When the noise intensity$Q$ reached $1 \times 10^{-7}\,\mu$A, it had a little effect on the IPSP and the corresponding energy waveform. The figures of the IPSP and energy function with noise are almost the same as those without noise.

We still could not estimate the range of the noise that affects the energy function of the IPSP according to the results shown in Figures 19–22. So as a solution, we addressed it by adjusting the coefficient of the level of noise intensity.

When the noise intensity$Q$ reached $2 \times 10^{-7}\,\mu$A, it had a little effect on the IPSP and the corresponding energy waveform. The figures of the IPSP and energy function with noise are almost the same as those without noise.

When the level of noise intensity$Q$ reached $3 \times 10^{-7}\,\mu$A, it had a little effect on the IPSP and the corresponding energy waveform. The figures of the IPSP and energy function with noise are almost the same as those without noise.

When the level of noise intensity$Q$ reached about $4 \times 10^{-7}\,\mu$A (error $\pm\, 0.5 \times 10^{-7}\,\mu$A), the noise began to significantly influence the IPSP and its corresponding energy waveform. Without the effect of noise, the IPSP curve initially fell and then rose; however, with the effect of noise, the IPSP curve did not monotonically decrease in the time interval

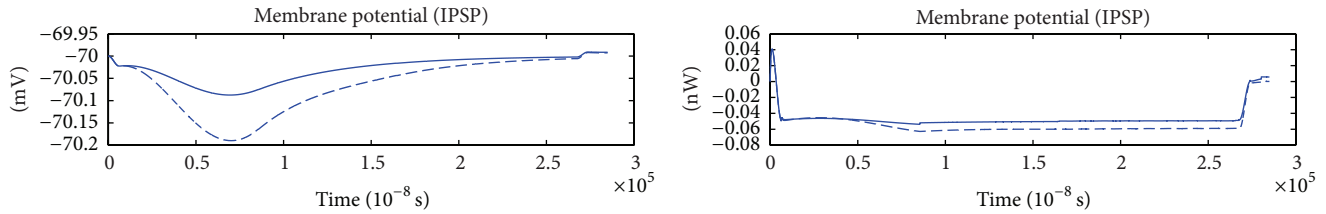

FIGURE 25: The IPSP and the corresponding energy function. $r_{0m} = 0.0001\,\Omega$, $r_{1m} = 0.1\,\Omega$, $r_{2m} = 1000\,\Omega$, $r_{3m} = 0.1\,\Omega$, $r_m = 1000\,\Omega$, $C_m = 1\,\mu$F, $L_m = 50\,\mu$H, $i_{0m} = -0.7\,\mu$A, and $Q = 4 \times 10^{-7}\,\mu$A.

from 0 ms to 1.5 ms, while the energy function began to appear to fluctuate within the interval from 2.5 ms to 3 ms.

In summary, when the level of noise intensity Q reached about $4 \times 10^{-7}\,\mu$A (error $\pm\ 0.5 \times 10^{-7}\,\mu$A), the noise began to have significant influence on the IPSP and its corresponding energy waveform. As a consequence, its critical value was assessed at $4 \times 10^{-7}\,\mu$A (error $\pm\ 0.5 \times 10^{-7}\,\mu$A).

4. Discussion

In this study, we obtained the action potential, EPSP, IPSP, and their corresponding energy waveforms with thermal noise added to the current. By changing the thermal noise intensity, we found the estimated range of the critical value of thermal noise that can significantly influence the neuronal membrane potential and the corresponding energy waveform. When the thermal noise intensity$Q$ reached about $6 \times 10^{-6}\,\mu$A (error $\pm\ 0.5 \times 10^{-6}\,\mu$A), it had a great influence on the action potential and its corresponding energy waveform. When the thermal noise intensity Q reached about $3\times10^{-6}\,\mu A$ (error $\pm\ 0.5 \times 10^{-6}\,\mu$A), it had a great influence on the EPSP and its corresponding energy waveform. When the thermal noise intensity$Q$ reached about $4 \times 10^{-7}\,\mu$A (error $\pm\ 0.5 \times 10^{-7}\,\mu$A), it had a great influence on the IPSP and its corresponding energy waveform. Based on these results, we conclude that noise has less effect on the action potential and its energy waveform than on the EPSP, IPSP, and their energy waveforms, and the thermal noise has less effect on the EPSP and its energy waveform than the IPSP and its waveform. By numerical calculation, we have also obtained the estimated range of the critical value of the noise that has a great effect on the action potential, EPSP, IPSP, and their corresponding energy waveforms. As a result, when we again establish a neural dynamic model in the future, such an estimation of noise intensity will enable us to avoid being subjective in considering the influence of noise on neural firing, so that the calculated results and experimental data will be more consistent. Therefore, the estimation of the thermal noise intensity provides a scientific basis for research on neural information coding in a noisy environment.

The physical model which we used in this paper was proposed by Wang et al. [20, 21] from the viewpoint of energy. Compared with other models, the biggest advantage of this model is that it simplifies the calculation of activity of neuronal firing. Due to the energy coding model's ability to describe mechanisms of brain information processing in biophysical terms, this idea and method can be applied to future research of information encoding in neural ensembles as well as cognitive functioning.

Conflict of Interests

The authors declare that there is no conflict of interests regarding the publication of this paper.

Acknowledgments

This work was supported by the National Natural Science Foundation of China (11232005) and the Ministry of Education Doctoral Foundation (20120074110020).

References

[1] A. A. Faisal, L. P. J. Selen, and D. M. Wolpert, "Noise in the nervous system," *Nature Reviews Neuroscience*, vol. 9, no. 4, pp. 292–303, 2008.

[2] E. T. Rolls and G. Deco, *The Noisy Brain: Stochastic Dynamics as a Principle of Brain Function*, Oxford University Press, 2010.

[3] F. Bernasconi, M. de Lucia, A. Tzovara, A. L. Manuel, M. M. Murray, and L. Spierer, "Noise in brain activity engenders perception and influences discrimination sensitivity," *The Journal of Neuroscience*, vol. 31, no. 49, pp. 17971–17981, 2011.

[4] T. Mori and S. Kai, "Noise-induced entrainment and stochastic resonance in human brain waves," *Physical Review Letters*, vol. 88, no. 21, Article ID 218101, 4 pages, 2002.

[5] T. Wennekers and G. Palm, "Syntactic sequencing in Hebbian cell assemblies," *Cognitive Neurodynamics*, vol. 3, no. 4, pp. 429–441, 2009.

[6] G. Werner, "From brain states to mental phenomena via phase space transitions and renormalization group transformation: proposal of a theory," *Cognitive Neurodynamics*, vol. 6, no. 2, pp. 203–209, 2012.

[7] G. K. Rohde, A. S. Barnett, P. J. Basser, and C. Pierpaoli, "Estimating intensity variance due to noise in registered images: applications to diffusion tensor MRI," *NeuroImage*, vol. 26, no. 3, pp. 673–684, 2005.

[8] D. Hunt, G. Korniss, and B. K. Szymanski, "Network synchronization in a noisy environment with time delays: fundamental limits and trade-offs," *Physical Review Letters*, vol. 105, no. 6, Article ID 068701, 2010.

[9] G. Deco, V. Jirs, A. R. McIntosh, O. Sporns, and R. Kötter, "Key role of coupling, delay, and noise in resting brain fluctuations,"

Proceedings of the National Academy of Sciences of the United States of America, vol. 106, no. 25, pp. 10302–10307, 2009.

[10] R. Wang, Z. Zhang, J. Qu, and J. Cao, "Phase synchronization motion and neural coding in dynamic transmission of neural information," *IEEE Transactions on Neural Networks*, vol. 22, no. 7, pp. 1097–1106, 2011.

[11] X. Zhang, R. Wang, Z. Zhang, J. Qu, J. Cao, and X. Jiao, "Dynamic phase synchronization characteristics of variable high-order coupled neuronal oscillator population," *Neurocomputing*, vol. 73, no. 13–15, pp. 2665–2670, 2010.

[12] X. Jiao and R. Wang, "Synchronous firing patterns of neuronal population with excitatory and inhibitory connections," *International Journal of Non-Linear Mechanics*, vol. 45, no. 6, pp. 647–651, 2010.

[13] J. Gao, J. Hu, and W. Tung, "Complexity measures of brain wave dynamics," *Cognitive Neurodynamics*, vol. 5, no. 2, pp. 171–182, 2011.

[14] Y. Liu, R. Wang, Z. Zhang, and X. Jiao, "Analysis of stability of neural network with inhibitory neurons," *Cognitive Neurodynamics*, vol. 4, no. 1, pp. 61–68, 2010.

[15] M. Hu and H. Liang, "Noise-assisted instantaneous coherence analysis of brain connectivity," *Computational Intelligence and Neuroscience*, vol. 2012, Article ID 275073, 12 pages, 2012.

[16] P. A. Tass, *Phase Resetting in Medicine and Biology*, Springer, 1999.

[17] A. Ghosh, Y. Rho, A. R. McIntosh, R. Kötter, and V. K. Jirsa, "Noise during rest enables the exploration of the brain's dynamic repertoire," *PLoS Computational Biology*, vol. 4, no. 10, Article ID e1000196, 2008.

[18] A. Maye, C. Hsieh, G. Sugihara, and B. Brembs, "Order in spontaneous behavior," *PLoS ONE*, vol. 2, no. 5, article e443, 2007.

[19] R. Wang, Z. Zhang, and X. Jiao, "Mechanism on brain information processing: energy coding," *Applied Physics Letters*, vol. 89, no. 12, Article ID 123903, 2006.

[20] R. Wang and Z. Zhang, "Energy coding in biological neural networks," *Cognitive Neurodynamics*, vol. 1, no. 3, pp. 203–212, 2007.

[21] R. Wang, Z. Zhang, and G. Chen, "Energy coding and energy functions for local activities of the brain," *Neurocomputing*, vol. 73, no. 1–3, pp. 139–150, 2009.

[22] E. R. Marcus and A. G. Debra, "Appraising the brain's energy budget," *Proceedings of the National Academy of Sciences of the United States of America*, vol. 99, no. 16, pp. 10237–10239, 2002.

Hindawi Publishing Corporation
Abstract and Applied Analysis
Volume 2014, Article ID 167623, 6 pages
http://dx.doi.org/10.1155/2014/167623

Research Article

Some Properties on Estrada Index of Folded Hypercubes Networks

Jia-Bao Liu,[1,2,3] Xiang-Feng Pan,[1] and Jinde Cao[2,4]

[1] *School of Mathematics Science, Anhui University, Hefei 230601, China*
[2] *Department of Mathematics, Southeast University, Nanjing 210096, China*
[3] *Anhui Xinhua University, Hefei 230088, China*
[4] *Department of Mathematics, Faculty of Science, King Abdulaziz University, Jeddah 21589, Saudi Arabia*

Correspondence should be addressed to Jinde Cao; jdcao@seu.edu.cn

Received 24 November 2013; Accepted 19 December 2013; Published 5 February 2014

Academic Editor: Qiankun Song

Let G be a simple graph with n vertices and let $\lambda_1, \lambda_2, \ldots, \lambda_n$ be the eigenvalues of its adjacency matrix; the Estrada index $EE(G)$ of the graph G is defined as the sum of the terms e^{λ_i}, $i = 1, 2, \ldots, n$. The n-dimensional folded hypercube networks FQ_n are an important and attractive variant of the n-dimensional hypercube networks Q_n, which are obtained from Q_n by adding an edge between any pair of vertices complementary edges. In this paper, we establish the explicit formulae for calculating the Estrada index of the folded hypercubes networks FQ_n by deducing the characteristic polynomial of the adjacency matrix in spectral graph theory. Moreover, some lower and upper bounds for the Estrada index of the folded hypercubes networks FQ_n are proposed.

1. Introduction

Complex networks have become an important area of multidisciplinary research involving mathematics, physics, social sciences, biology, and other theoretical and applied sciences. It is well known that interconnection networks play an important role in parallel communication systems. An interconnection network is usually modelled by a connected graph $G = (V, E)$, where V denotes the set of processors and E denotes the set of communication links between processors in networks. Let G be a graph with vertices labelled $1, 2, \ldots, n$. The adjacency matrix $A(G)$ of G is an $n \times n$ matrix with the (i, j)-entry equal to 1 if vertices i and j are adjacent and 0 otherwise. The spectrum of G is the spectrum of its adjacency matrix and consists of the numbers $\lambda_1 \geq \lambda_2 \geq \cdots \geq \lambda_n$. In this work we are concerned with finite undirected connected simple graphs (networks). For the underlying graph theoretical definitions and notations we follow [1].

The energy of the graph G [2] is defined as

$$E(G) = \sum_{i=1}^{n} |\lambda_i|. \tag{1}$$

Another graph-spectrum-based invariant, recently put forward by Ernesto Estrada, is defined as

$$EE = EE(G) = \sum_{i=1}^{n} e^{\lambda_i}. \tag{2}$$

This graph invariant appeared for the first time in the year 2000, in a paper by Estrada [3], dealing with the folding of protein molecules. Estrada and Rodríguez-Velázquez showed that EE provides a measure of the centrality of complex (communication, social, metabolic, etc.) networks [4, 5].

Denote by $M_k = M_k(G) = \sum_{i=1}^{n} (\lambda_i)^k$ the kth spectral moment of the graph G. From the Taylor expansion of e^x, we have the following important relation between the Estrada index and the spectral moments of G:

$$EE(G) = \sum_{k=0}^{\infty} \frac{M_k(G)}{k!}. \tag{3}$$

At this point one should recall [4] that $M_k(G)$ is equal to the number of self-returning walks of length k of the graph

G. The first few spectral moments of an (n, m)-graph with m edges and t triangles satisfy the following relations [4]:

$$M_0 = \sum_{i=1}^{n} (\lambda_i)^0 = n; \qquad M_1 = \sum_{i=1}^{n} (\lambda_i)^1 = 0;$$
$$M_2 = \sum_{i=1}^{n} (\lambda_i)^2 = 2m; \qquad M_3 = \sum_{i=1}^{n} (\lambda_i)^3 = 6t. \tag{4}$$

For $1 \le i \le n$, let d_i be the degree of vertex v_i in G. The first Zagreb index [6] of the graph G is defined as $Zg(G) = \sum_{i=1}^{n} d_i^2$:

$$M_4 = \sum_{i=1}^{n} (\lambda_i)^4 = 2Zg(G) - 2m + 8q;$$
$$M_5 = \sum_{i=1}^{n} (\lambda_i)^5 = 30t + 10p + 10r, \tag{5}$$

where p and q are the numbers of pentagons and quadrangles in G, and r is the number of subgraphs consisting of a triangle with a pendent vertex attached [7].

The hypercubes Q_n is one of the most popular and efficient interconnection networks due to its many excellent performances for some practical applications. There is a large amount of literature on the properties of hypercubes networks [8–11]. As an important variant of Q_n, the folded hypercubes networks FQ_n, proposed by Amawy and Latifi [8], are the graphs obtained from Q_n by adding an edge between any pair of vertices complementary addresses. The folded hypercubes FQ_n obtained considerable attention due to its perfect properties, such as symmetry, regular structure, strong connectivity, small diameter, and many of its properties which have been explored [12–19].

The remainder of the present paper is organized as follows. In Section 2, we present some basic notations and some preliminaries in our discussion. The proofs of our main results are in Section 3 and some conclusions are given in Section 4, respectively.

2. Notations and Some Preliminaries

In this section, we introduce some basic properties which will be used in the proofs of our main results.

Let $P_{FQ_n}(x)$ be the characteristic polynomial of the adjacency matrix of the folded hypercube FQ_n; the following results were shown in [12].

Lemma 1 (see [12]). *The characteristic polynomial of the adjacency matrix of the FQ_n ($n \ge 3$) is*

$$P(FQ_n; \lambda) = [\lambda - (n-7)][\lambda - (n-3)]^3 P(FQ_{n-1}; \lambda - 1) \times \prod_{i=2}^{n-2} P(FQ_{n-i}; \lambda - (i-4)). \tag{6}$$

Lemma 2 (see [12]). *For FQ_n with $n \ge 3$, the spectrum of adjacency matrix is as follows:*

(1) *If $n \equiv 0 \pmod 2$,*

$$Spec(FQ_n) = \begin{pmatrix} -n+1 & -n+5 & -n+9 & \cdots & n-7 & n-3 & n+1 \\ C_n^0 + C_n^1 & C_n^2 + C_n^3 & C_n^4 + C_n^5 & \cdots & C_n^{n-4} + C_n^{n-3} & C_n^{n-2} + C_n^{n-1} & C_n^n \end{pmatrix}, \tag{7}$$

(2) *if $n \equiv 1 \pmod 2$,*

$$Spec(FQ_n) = \begin{pmatrix} -n-1 & -n+3 & -n+7 & \cdots & n-7 & n-3 & n+1 \\ C_n^0 & C_n^1 + C_n^2 & C_n^3 + C_n^4 & \cdots & C_n^{n-4} + C_n^{n-3} & C_n^{n-2} + C_n^{n-1} & C_n^n \end{pmatrix}, \tag{8}$$

where C_n^i are the binomial coefficients and the elements in the first and second rows are the eigenvalues of the adjacency matrix of FQ_n and the corresponding multiplicities, respectively.

Lemma 3 (see [20]). *The eigenvalues of a bipartite graph satisfy the pairing property: $\lambda_{n-i+1} = \lambda_i$, $i = 1, 2, \ldots, n$. Therefore, if the graph G is bipartite and if η_0 is nullity (the multiplicity of its eigenvalue zero), then*

$$EE(G) = \eta_0 + 2\sum_{+} \cosh(i), \tag{9}$$

where cosh *stands for the hyperbolic cosine* $\cosh(x) = (e^x + e^{-x})/2$, *whereas* $\sum_+$ *denotes summation over all positive eigenvalues of the corresponding graph.*

Lemma 4 (see [21]). *Let G be a graph with m edges. For $k \ge 4$,*

$$M_{k+2} \ge M_k, \tag{10}$$

with equality for all even $k \ge 4$ if and only if G consists of m copies of K_2 and possibly isolated vertices and with equality for all odd $k \ge 5$ if and only if G is a bipartite graph.

The following lemma is an immediate result of the previous lemma.

Lemma 5 (see [22]). *Let G be an (n,m) graph with m edges. For $k \geq 4$,*

$$\sum_{i=1}^{n}(2\lambda_i)^{k+2} \geq 4\sum_{i=1}^{n}(2\lambda_i)^{k}, \tag{11}$$

with equality for all even $k \geq 4$ if and only if G consists of m copies of K_2 and possibly isolated vertices and with equality for all odd $k \geq 5$ if and only if G is a bipartite graph.

Lemma 6 (see [23]). *Let G be a regular graph of degree $r \neq 0$ and of order n. Then its Estrada index is bounded by*

$$e^{r} + (n-1)\,e^{-r/(n-1)} \leq EE(G) < n - 2 + e^{r} + e^{\sqrt{r(n-r)-1}}. \tag{12}$$

Equality holds if and only if $\lambda_2 = \lambda_3 = \cdots = \lambda_n = -r/(n-1)$.

Lemma 7 (see [23]). *The Estrada index $EE(G)$ and the graph energy $E(G)$ satisfy the following inequality:*

$$\frac{1}{2}E(G)(e-1) + n - n_{+} \leq EE(G) \leq n - 1 + e^{E(G)/2}, \tag{13}$$

and equalities on both sides hold if and only if $E(G) = 0$.

3. Main Results

3.1. The Estrada Index of Folded Hypercubes Networks FQ_n. In this section, we present some explicit formulae for calculating the Estrada index of FQ_n. For convenience, we assume that $C_n^i = 0$ if $i < 0$ or $i > n$.

Theorem 8. *For any FQ_n with $n \geq 3$, then*

(1) $EE(FQ_n) = \sum_{i=0}^{n/2}(C_n^{2i} + C_n^{2i+1})e^{4i-n+1}$, $i = 0, 1, \ldots, n/2$, *if* $n \equiv 0 \pmod 2$;

(2) $EE(FQ_n) = \sum_{i=0}^{n/2}(C_n^{2i-1} + C_n^{2i})e^{4i-n-1}$, $i = 0, 1, \ldots, (n+1)/2$, *if* $n \equiv 1 \pmod 2$,

where the $4i - n + 1$ and $4i - n - 1$ ($i = 0, 1, \ldots, n/2$ or $(n+1)/2$) are the eigenvalues of the adjacent matrix of FQ_n and C_n^i denotes the binomial coefficients.

Proof. By Lemma 1, the characteristic polynomial of the adjacent matrix of FQ_n is

$$P(FQ_n;\lambda) = [\lambda - (n-7)]\,[\lambda - (n-3)]^3 P(FQ_{n-1};\lambda - 1) \times \prod_{i=2}^{n-2} P(FQ_{n-i};\lambda - (i-4)). \tag{14}$$

Through calculating eigenvalues of characteristic polynomial and its multiplicities, we obtained that

(1) if $n \equiv 0 \pmod 2$, FQ_n have $n/2 + 1$ different eigenvalues $4i - n + 1$, with the multiplicities $C_n^{2i} + C_n^{2i+1}$, where $i = 0, 1, \ldots, n/2$;

(2) if $n \equiv 1 \pmod 2$, FQ_n have $(n+1)/2$ different eigenvalues $4i - n - 1$, with the multiplicities $C_n^{2i-1} + C_n^{2i}$, where $i = 0, 1, \ldots, (n+1)/2$.

Combining with the definition of the Estrada index, we derived the result of Theorem 8. □

3.2. Some Bounds for the Estrada Index of Folded Hypercubes Networks FQ_n. It is well known that FQ_n have 2^n vertices. Let $\lambda_1 \geq \lambda_2 \geq \cdots \geq \lambda_n \geq \lambda_{n+1} \geq \cdots \geq \lambda_{2^n}$ be the eigenvalues of FQ_n with nonincreasing order. In order to obtain the bounds for the Estrada index of FQ_n, we prove some results by utilizing the arithmetic and geometric mean inequality; in our proof, some techniques in [22] are referred to.

Theorem 9. *For any FQ_n with $n \geq 2$, one has*

$$\sqrt{4^n + (n+1)\,2^{n+1} + 8t + [\cos(2) - 3]\,M_4 + \left[\cos(2) - \frac{10}{3}\right]M_5} < EE(FQ_n), \tag{15}$$

where $M_4 = 2Zg(G) - 2m + 8q$, $M_5 = 30t + 10p + 10r$, p and q are the numbers of pentagons and quadrangles in FQ_n, and r is the number of subgraphs consisting of a triangle with a pendent vertex attached.

Proof. In order to obtain the lower bounds for the Estrada index, consider that

$$EE^2(FQ_n) = \sum_{i=1}^{2^n} e^{2\lambda_i} + 2\sum_{i<j} e^{\lambda_i}e^{\lambda_j}. \tag{16}$$

Noting that $M_0 = 2^n$, $M_1 = 0$, $M_2 = (n+1)2^{n-1}$, and $M_3 = 6t$, we obtain

$$\begin{aligned}\sum_{i=1}^{2^n} e^{2\lambda_i} &= \sum_{i=1}^{2^n}\sum_{k\geq 0}\frac{(2\lambda_i)^k}{k!} \\ &= 2^n + (n+1)\,2^{n+1} + 8t + \sum_{i=1}^{2^n}\sum_{k\geq 4}\frac{(2\lambda_i)^k}{k!} \\ &= 2^n + (n+1)\,2^{n+1} + 8t + \sum_{k\geq 2}\frac{1}{(2k)!}\sum_{i=1}^{2^n}(2\lambda_i)^{2k} \\ &\quad + \sum_{k\geq 2}\frac{1}{(2k+1)!}\sum_{i=1}^{2^n}(2\lambda_i)^{2k+1}.\end{aligned} \tag{17}$$

By Lemma 5,

$$\sum_{i=1}^{n}(2\lambda_i)^{k+2} \geq 4\sum_{i=1}^{n}(2\lambda_i)^{k}, \tag{18}$$

we can get that

$$\begin{aligned}\sum_{i=1}^{2^n} e^{2\lambda_i} &\geq 2^n + (n+1)\,2^{n+1} + 8t \\ &\quad + \sum_{k\geq 2} \frac{1}{(2k)!} \sum_{i=1}^{2^n} 2^{2k-4} (2\lambda_i)^4 \\ &\quad + \sum_{k\geq 2} \frac{1}{(2k+1)!} \sum_{i=1}^{2^n} 2^{2k-4} (2\lambda_i)^5 \\ &= 2^n + (n+1)\,2^{n+1} + 8t + [\cosh(2) - 3]\, M_4 \\ &\quad + \left[\cosh(2) - \frac{10}{3}\right] M_5,\end{aligned} \tag{19}$$

where $M_4 = 2Zg(G) - 2m + 8q$, $M_5 = 30t + 10p + 10r$, p and q are the numbers of pentagons and quadrangles in FQ_n, and r is the number of subgraphs consisting of a triangle with a pendent vertex attached.

As for the terms $2\sum_{i<j} e^{\lambda_i} e^{\lambda_j}$, by the arithmetic and geometric mean inequality and the fact that $M_1 = 0$,

$$\begin{aligned}2\sum_{i<j} e^{\lambda_i} e^{\lambda_j} &\geq 2^n (2^n - 1) \left(\prod_{i<j} e^{\lambda_i} e^{\lambda_j} \right)^{2/2^n(2^n-1)} \\ &= 2^n (2^n - 1) \left[\left(\prod_{i=1} e^{\lambda_i} \right)^{2^n - 1} \right]^{2/2^n(2^n-1)} \\ &= 2^n (2^n - 1) \left(e^{M_1} \right)^{2/2^n} \\ &= 2^n (2^n - 1),\end{aligned} \tag{20}$$

where the equality holds if and only if $\lambda_1 = \cdots = \lambda_{2^n}$.

Combining with equalities (19) and (20),

$$\begin{aligned}&\sqrt{4^n + (n+1)\,2^{n+1} + 8t + [\cosh(2) - 3]\, M_4 + \left[\cosh(2) - \frac{10}{3}\right] M_5} \\ &\quad \leq EE\left(FQ_n\right),\end{aligned} \tag{21}$$

where $M_4 = 2Zg(G) - 2m + 8q$, $M_5 = 30t + 10p + 10r$, p and q are the numbers of pentagons and quadrangles in FQ_n, and r is the number of subgraphs consisting of a triangle with a pendent vertex attached.

Notice that the equality of (21) holds if and only if the equalities of (19) and (20) hold; that is, the equality holds if and only if $\lambda_1 = \cdots = \lambda_{2^n}$, which is impossible for any FQ_n with $n \geq 2$. Therefore, this implies the results of Theorem 9. □

We now consider the upper bound for the Estrada index of FQ_n as follows.

Theorem 10. *For any FQ_n with $n \geq 2$, one has*

$$EE\left(FQ_n\right) < 2^n - 1 + e^{\sqrt{(n+1)2^n}}. \tag{22}$$

Proof. According to the definition of Estrada index we get

$$\begin{aligned}EE\left(FQ_n\right) &= 2^n + \sum_{i=1}^{2^n} \sum_{k\geq 1} \frac{\lambda_i^k}{k!} \leq 2^n + \sum_{i=1}^{2^n} \sum_{k\geq 1} \frac{|\lambda_i|^k}{k!} \\ &= 2^n + \sum_{k\geq 1} \frac{1}{k!} \sum_{i=1}^{2^n} \left[(\lambda_i)^2\right]^{k/2}.\end{aligned} \tag{23}$$

Notice the inequality

$$\sum_{i=1}^{2^n} \left[(\lambda_i)^2\right]^{k/2} \leq \left[\sum_{i=1}^{2^n} (\lambda_i)^2 \right]^{k/2}; \tag{24}$$

substituting inequality (24) into (23) we obtain that

$$\begin{aligned}EE\left(FQ_n\right) &\leq 2^n + \sum_{k\geq 1} \frac{1}{k!} \left[\sum_{i=1}^{2^n} (\lambda_i)^2 \right]^{k/2} \\ &= 2^n - 1 + \sum_{k\geq 0} \frac{1}{k!} \left[\sum_{i=1}^{2^n} (\lambda_i)^2 \right]^{k/2}.\end{aligned} \tag{25}$$

Since the equality holds in FQ_n,

$$\sum_{i=1}^{2^n} (\lambda_i)^2 = (n+1)\,2^n. \tag{26}$$

Hence,

$$\begin{aligned}EE\left(FQ_n\right) &\leq 2^n - 1 + \sum_{k\geq 0} \frac{1}{k!} \left[(n+1)\,2^n\right]^{k/2} \\ &= 2^n - 1 + \sum_{k\geq 0} \frac{\sqrt{(n+1)2^n}^k}{k!} \\ &= 2^n - 1 + e^{\sqrt{(n+1)2^n}}.\end{aligned} \tag{27}$$

It is evident that equality of (25) will be attained if and only if the graph FQ_n has no nonzero eigenvalues, which, in turn, happens only in the case of the edgeless graph $\overline{K_n}$; it is impossible for any FQ_n with $n \geq 2$ that directly leads to the inequality in (27).

Hence, we can obtain the upper bound for the Estrada index of FQ_n:

$$EE\left(FQ_n\right) < 2^n - 1 + e^{\sqrt{(n+1)2^n}}. \tag{28}$$

The proof of Theorem 10 is completed. □

Remark 11. In [23], it was proved that

$$e^r + (n-1)\,e^{-r/(n-1)} \leq EE(G) < n - 2 + e^r + e^{\sqrt{r(n-r)-1}}, \tag{29}$$

with equality, holds if and only if $\lambda_2 = \lambda_3 = \cdots = \lambda_n = -r/(n-1)$.

Notice that the spectral radius of FQ_n is $\lambda_1 = n+1$ and $r = n+1$; applying Lemma 6, we also give the lower and upper bounds connecting $EE(FQ_n)$ and its spectral radius by simple computations, where the equality is impossible for any FQ_n; hence

$$e^{n+1} + (2^n - 1)\, e^{(-n-1)/(2^n-1)} < EE(FQ_n) < 2^n - 2 + e^{n+1} + e^{\sqrt{(n+1)[2^n-(n+1)]-1}}. \tag{30}$$

3.3. Some Properties on Estrada Index Involving Energy of FQ_n. In this section, we investigate the relations between the Estrada index and the energy of FQ_n. We firstly prove the lower bounds involving energy for the Estrada index of FQ_n; in Theorem 12 proof, some techniques in [23] are referred to.

Theorem 12. *For any FQ_n with $n \geq 2$, one has*

$$\frac{1}{2}(e-1)\, E(FQ_n) + (2^n - n_i) < EE(FQ_n). \tag{31}$$

Proof. Assume that n_i denote the number of positive eigenvalues; we begin with the definition of Estrada index $EE(FQ_n)$:

$$EE(FQ_n) = \sum_{i=1}^{2^n} e_i^{\lambda} = \sum_{\lambda_i \leq 0} e_i^{\lambda} + \sum_{\lambda_i > 0} e_i^{\lambda}. \tag{32}$$

Since $e^x \geq 1 + x$, with equality, holds if and only if $x = 0$, we have

$$\sum_{\lambda_i \leq 0} e_i^{\lambda} \geq \sum_{\lambda_i \leq 0} (1 + \lambda_i) = (2^n - n_i) + \left(\lambda_{n_i+1} + \cdots + \lambda_n\right). \tag{33}$$

The other underlying inequality is $e^x \geq ex$ and equality holds if and only if $x = 1$; we get

$$\sum_{\lambda_i > 0} e_i^{\lambda} \geq \sum_{\lambda_i > 0} e\lambda_i = e\left(\lambda_1 + \lambda_2 \cdots + \lambda_{n_i}\right). \tag{34}$$

Substituting the inequalities (33) and (34) into (32),

$$\begin{aligned} EE(FQ_n) &\geq (2^n - n_i) + \left(\lambda_{n_i+1} + \cdots + \lambda_n\right) \\ &\quad + e\left(\lambda_1 + \lambda_2 \cdots + \lambda_{n_i}\right) \\ &= (2^n - n_i) + \left(\lambda_1 + \lambda_2 \cdots + \lambda_{n_i} + \lambda_{n_i+1} + \cdots + \lambda_n\right) \\ &\quad + (e-1)\left(\lambda_1 + \lambda_2 \cdots + \lambda_{n_i}\right) \\ &= (2^n - n_i) + (e-1)\left(\lambda_1 + \lambda_2 \cdots + \lambda_{n_i}\right). \end{aligned} \tag{35}$$

Note that

$$\lambda_1 + \lambda_2 \cdots + \lambda_{n_i} = \frac{1}{2} E(FQ_n). \tag{36}$$

From the above inequalities (35) and (36), we arrive at

$$\frac{1}{2}(e-1)\, E(FQ_n) + (2^n - n_i) \leq EE(FQ_n), \tag{37}$$

with equality if and only if FQ_n is an empty graph with 2^n vertices, which is impossible.

Hence,

$$\frac{1}{2}(e-1)\, E(FQ_n) + (2^n - n_i) < EE(FQ_n), \tag{38}$$

as desired. □

We now derive the upper bounds involving energy for the Estrada index of FQ_n.

Theorem 13. *For any FQ_n with $n \geq 2$, one has*

$$EE(FQ_n) < E(FQ_n) + 2^n - 1 - \sqrt{(n+1)\, 2^n} + e^{\sqrt{(n+1)2^n}}. \tag{39}$$

Proof. We consider that

$$\begin{aligned} EE(FQ_n) &= \sum_{i=1}^{n} e_i^{\lambda} = 2^n + \sum_{i=1}^{2^n} \sum_{k \geq 1} \frac{\lambda_i^k}{k!} \\ &\leq 2^n + \sum_{i=1}^{2^n} \sum_{k \geq 1} \frac{|\lambda_i|^k}{k!}. \end{aligned} \tag{40}$$

Taking into account the definition of graph energy equation (1), we obtain

$$\begin{aligned} EE(FQ_n) &\leq 2^n + E(FQ_n) + \sum_{i=1}^{2^n} \sum_{k \geq 2} \frac{|\lambda_i|^k}{k!} \\ &= 2^n + E(FQ_n) + \sum_{k \geq 2} \frac{1}{k!} \sum_{i=1}^{2^n} \left[(\lambda_i)^2\right]^{k/2}. \end{aligned} \tag{41}$$

In light of the inequality (24) holds for integer $k \geq 2$, we obtain that

$$\begin{aligned} EE(FQ_n) &\leq 2^n + E(FQ_n) + \sum_{k \geq 2} \frac{1}{k!} \left[\sum_{i=1}^{2^n} (\lambda_i)^2\right]^{k/2} \\ &= 2^n + E(FQ_n) - 1 - \sqrt{(n+1)\, 2^n} \\ &\quad + \sum_{k \geq 0} \frac{1}{k!} \left[\sum_{i=1}^{2^n} (\lambda_i)^2\right]^{k/2}. \end{aligned} \tag{42}$$

Substituting (26) into (42), we get

$$\begin{aligned} EE(FQ_n) &\leq 2^n + E(FQ_n) - 1 - \sqrt{(n+1)\, 2^n} \\ &\quad + \sum_{k \geq 0} \frac{1}{k!} \left[(n+1)\, 2^n\right]^{k/2} \\ &= 2^n + E(FQ_n) - 1 - \sqrt{(n+1)\, 2^n} + e^{\sqrt{(n+1)2^n}}, \end{aligned} \tag{43}$$

with equality if and only if FQ_n is an empty graph with 2^n vertices, which is impossible.

From the above argument, we get the result of Theorem 13. □

4. Conclusions

The main purpose of this paper is to investigate the Estrada index of FQ_n with $n \geq 2$; we established the explicit formulae for calculating the Estrada index of FQ_n by deducing the characteristic polynomial of the adjacency matrix in spectral graph theory.

Moreover, some lower and upper bounds for Estrada index of FQ_n were proposed by utilizing the arithmetic and geometric mean inequality. The lower and upper bounds for the Estrada index involving energy of FQ_n were also obtained.

Conflict of Interests

The authors declare that there is no conflict of interests regarding the publication of this paper.

Acknowledgments

The work of Jia Bao Liu was supported by the Natural Science Foundation of Anhui Province of China under Grant no. KJ2013B105; the work of Xiang-Feng Pan was supported by the National Science Foundation of China under Grants 10901001, 11171097, and 11371028.

References

[1] J. M. Xu, *Topological Strucure and Analysis of Interconnction Networks*, Kluwer Academic, Dordrecht, The Netherlands, 2001.

[2] I. Gutman, "The energy of a graph," *Berichte der Mathematisch-Statistischen Sektion im Forschungszentrum Graz*, vol. 103, no. 22, pp. 100–105, 1978.

[3] E. Estrada, "Characterization of 3D molecular structure," *Chemical Physics Letters*, vol. 319, no. 5, pp. 713–718, 2000.

[4] E. Estrada and J. A. Rodríguez-Velázquez, "Subgraph centrality in complex networks," *Physical Review E*, vol. 71, no. 5, Article ID 056103, 9 pages, 2005.

[5] E. Estrada and J. A. Rodríguez-Velázquez, "Spectral measures of bipartivity in complex networks," *Physical Review E*, vol. 72, no. 4, Article ID 046105, 6 pages, 2005.

[6] K. C. Das, I. Gutman, and B. Zhou, "New upper bounds on Zagreb indices," *Journal of Mathematical Chemistry*, vol. 46, no. 2, pp. 514–521, 2009.

[7] D. M. Cvetković, M. Doob, I. Gutman, and A. Torgašev, *Recent Results in the Theory of Graph Spectra*, vol. 36 of *Annals of Discrete Mathematics*, North-Holland, Amsterdam, The Netherlands, 1988.

[8] E. A. Amawy and S. Latifi, "Properties and performance of folded hypercubes," *IEEE Transactions on Parallel and Distributed Systems*, vol. 2, no. 1, pp. 31–42, 1991.

[9] R. Indhumathi and S. A. Choudum, "Embedding certain height-balanced trees and complete p^m-ary trees into hypercubes," *Journal of Discrete Algorithms*, vol. 22, pp. 53–65, 2013.

[10] J. Fink, "Perfect matchings extend to Hamilton cycles in hypercubes," *Journal of Combinatorial Theory B*, vol. 97, no. 6, pp. 1074–1076, 2007.

[11] J. B. Liu, J. D. Cao, X. F. Pan, and A. Elaiw, "The Kirchhoff index of hypercubes and related complex networks," *Discrete Dynamics in Nature and Society*, vol. 2013, Article ID 543189, 7 pages, 2013.

[12] M. Chen and B. X. Chen, "Spectra of folded hypercubes," *Journal of East China Normal University (Nature Science)*, vol. 2, pp. 39–46, 2011.

[13] X. He, H. Liu, and Q. Liu, "Cycle embedding in faulty folded hypercube," *International Journal of Applied Mathematics & Statistics*, vol. 37, no. 7, pp. 97–109, 2013.

[14] S. Cao, H. Liu, and X. He, "On constraint fault-free cycles in folded hypercube," *International Journal of Applied Mathematics & Statistics*, vol. 42, no. 12, pp. 38–44, 2013.

[15] Y. Zhang, H. Liu, and M. Liu, "Cycles embedding on folded hypercubes with vertex faults," *International Journal of Applied Mathematics & Statistics*, vol. 41, no. 11, pp. 58–70, 2013.

[16] X. B. Chen, "Construction of optimal independent spanning trees on folded hypercubes," *Information Sciences*, vol. 253, pp. 147–156, 2013.

[17] M. Chen, X. Guo, and S. Zhai, "Total chromatic number of folded hypercubes," *Ars Combinatoria*, vol. 111, pp. 265–272, 2013.

[18] G. H. Wen, Z. S. Duan, W. W. Yu, and G. R. Chen, "Consensus in multi-agent systems with communication constraints," *International Journal of Robust and Nonlinear Control*, vol. 22, no. 2, pp. 170–182, 2012.

[19] J. B. Liu, X. F. Pan, Y. Wang, and J. D. Cao, "The Kirchhoff index of folded hypercubes and some variant networks," *Mathematical Problems in Engineering*, vol. 2014, Article ID 380874, 9 pages, 2014.

[20] E. Estrada, J. A. Rodríguez-Velázquez, and M. Randić, "Atomic branching in molecules," *International Journal of Quantum Chemistry*, vol. 106, no. 4, pp. 823–832, 2006.

[21] B. Zhou and Z. Du, "Some lower bounds for Estrada index," *Iranian Journal of Mathematical Chemistry*, vol. 1, no. 2, pp. 67–72, 2010.

[22] Y. Shang, "Lower bounds for the Estrada index of graphs," *Electronic Journal of Linear Algebra*, vol. 23, pp. 664–668, 2012.

[23] J. P. Liu and B. L. Liu, "Bounds of the Estrada index of graphs," *Applied Mathematics*, vol. 25, no. 3, pp. 325–330, 2010.

Hindawi Publishing Corporation
Abstract and Applied Analysis
Volume 2014, Article ID 631071, 8 pages
http://dx.doi.org/10.1155/2014/631071

Research Article

Robust H_∞ Control for a Class of Nonlinear Distributed Parameter Systems via Proportional-Spatial Derivative Control Approach

Cheng-Dong Yang,[1] Jianlong Qiu,[2] and Jun-Wei Wang[3]

[1] *School of Informatics, Linyi University, Linyi 276005, China*
[2] *School of Science, Linyi University, Linyi 276005, China*
[3] *School of Automation and Electrical Engineering, University of Science and Technology Beijing, Beijing 100083, China*

Correspondence should be addressed to Jun-Wei Wang; wangjunwei-1984@163.com

Received 25 September 2013; Accepted 5 November 2013; Published 12 January 2014

Academic Editor: Qiankun Song

This paper addresses the problem of robust H_∞ control design via the proportional-spatial derivative (P-sD) control approach for a class of nonlinear distributed parameter systems modeled by semilinear parabolic partial differential equations (PDEs). By using the Lyapunov direct method and the technique of integration by parts, a simple linear matrix inequality (LMI) based design method of the robust H_∞ P-sD controller is developed such that the closed-loop PDE system is exponentially stable with a given decay rate and a prescribed H_∞ performance of disturbance attenuation. Moreover, a suboptimal H_∞ controller is proposed to minimize the attenuation level for a given decay rate. The proposed method is successfully employed to address the control problem of the FitzHugh-Nagumo (FHN) equation, and the achieved simulation results show its effectiveness.

1. Introduction

A significant research area that has received a lot of attention over the past few decades is the control design for distributed parameter systems (DPSs) modeled by parabolic partial differential equations (PDEs). These DPSs can be applied to describe many industrial processes, such as thermal diffusion processes, fluid, and heat exchangers [1–4]. The key characteristic of DPSs is space distribution, which causes their outputs, inputs, process states, and parameters to be spatially varying. On the other hand, external disturbances and nonlinear phenomena appear in most real systems. In this situation, the study of robust H_∞ control design for nonlinear parabolic PDE systems is of theoretical and practical importance.

Significant research results have been reported in the past few decades for DPSs [1–3, 5–18]. The most interesting results within these research activities are those developed on the basis of PDE model [9–18]. For example, Krstic and Smyshlyaev have developed nonadaptive and adaptive kernel-based backstepping methods for linear boundary control PDE systems [9–11]. Fridman and Orlov [12] have presented exponential stabilization with H_∞ performance in terms of linear matrix inequalities (LMIs) for uncertain semilinear parabolic and hyperbolic systems via a robust collocated static output feedback boundary controller. These results [9–12] are only applicable for boundary control PDE systems. Motivated by significant recent advances in actuation and sensing technology, particularly the advances of microelectromechanical systems, it is possible to manufacture large arrays of microsensors and actuators with integrated control circuitry (for control applications of such devices, see [13] and the references therein). Hence, the problems on distributed control theory and design for PDE systems have received a great deal of attention [1–3, 14–18]. For example, Orlov et al. have developed state feedback tracking control design [3] for an uncertain heat diffusion process and exponential stabilization [14] for an uncertain wave equation via distributed dynamic input extension. Wang, Wu, and Li have established sufficient conditions of distributed exponential stabilization via simple fuzzy

proportional state feedback controllers for first-order hyperbolic PDE systems [15–17] and via a fuzzy proportional-spatial derivative (P-sD) for semi-linear parabolic PDE system [18]. Wu, Wang, and Li [19] have proposed a Lyapunov-based distributed H_∞ fuzzy controller design with constraint for semi-linear first-order hyperbolic PDE systems. Notice that the results reported in [15–19] are presented in terms of spatial differential linear matrix inequalities (SDLMIs), which can be only approximately solved on the basis of standard finite difference method and the existing convex optimization techniques [20, 21]. Despite these efforts, to the best of the authors' knowledge, there are still few results on the robust H_∞ control design via the original PDE model of semi-linear parabolic PDE systems with external disturbances, which motivates this study.

In this study, we will deal with the problem of robust H_∞ control design for a class of semi-linear parabolic PDE systems with external disturbances via P-sD control approach. Based on the Lyapunov direct method and integration by parts, a sufficient condition for the exponential stabilization with a given decay rate and a prescribed H_∞ performance of disturbance attenuation is presented in terms of standard LMIs. Moreover, a suboptimal H_∞ controller is proposed to minimize the attenuation level for a given decay rate. Finally, the simulation study on the robust H_∞ control of a semi-linear parabolic PDE system represented by FitzHugh-Nagumo (FHN) equation is provided to show the effectiveness of the proposed method.

The remainder of this paper is organized as follows. The problem formulation and preliminaries are given in Section 2. The robust H_∞ P-sD control design is provided in Section 3. Section 4 presents an example to illustrate the effectiveness of the proposed method. Finally, Section 5 offers some conclusions.

Notations. The notations used throughout the paper are given as follows. $\mathfrak{R}$, $\mathfrak{R}^n$, and $\mathfrak{R}^{m\times n}$ denote the set of all real numbers, n-dimensional Euclidean space, and the set of all real $m \times n$ matrices, respectively. Identity matrix, of appropriate dimension, will be denoted by $\mathbf{I}$. For a symmetric matrix $\mathbf{M}$, $\mathbf{M} > (\geq, <, \leq)\ 0$ means that it is positive definite (semipositive definite, negative definite, and seminegative definite, resp.). $\mathscr{H}^n \triangleq \mathscr{L}_2([l_1, l_2]; \mathfrak{R}^n)$ is a Hilbert space of n-dimensional square integrable vector functions $\boldsymbol{\vartheta}(x,t) \in \mathfrak{R}^n$, $x \in [l_1, l_2] \subset \mathfrak{R}$, $\forall t \geq 0$ with the inner product and norm:

$$\begin{aligned} \left\langle \boldsymbol{\vartheta}_1(\cdot,t), \boldsymbol{\vartheta}_2(\cdot,t) \right\rangle &= \int_{l_1}^{l_2} \boldsymbol{\vartheta}_1^T(x,t)\, \boldsymbol{\vartheta}_2(x,t)\, dx, \\ \left\| \boldsymbol{\vartheta}_1(\cdot,t) \right\|_2 &= \left\langle \boldsymbol{\vartheta}_1(\cdot,t), \boldsymbol{\vartheta}_1(\cdot,t) \right\rangle^{1/2}, \end{aligned} \tag{1}$$

where $\boldsymbol{\vartheta}_1(\cdot,t) \in \mathscr{H}^n$ and $\boldsymbol{\vartheta}_2(\cdot,t) \in \mathscr{H}^n$. The superscript "$T$" is used for the transpose of a vector or a matrix. The symbol "$*$" is used as an ellipsis in matrix expressions that are induced by symmetry; for example,

$$\begin{bmatrix} \mathbf{S} + [\mathbf{M} + \mathbf{N} + *] & \mathbf{X} \\ * & \mathbf{Y} \end{bmatrix} \triangleq \begin{bmatrix} \mathbf{S} + \left[\mathbf{M} + \mathbf{N} + \mathbf{M}^T + \mathbf{N}^T\right] & \mathbf{X} \\ \mathbf{X}^T & \mathbf{Y} \end{bmatrix}. \tag{2}$$

2. Preliminaries and Problem Formulation

Consider the following nonlinear DPSs modeled by semi-linear parabolic PDEs:

$$\begin{aligned} \mathbf{y}_t(x,t) &= \boldsymbol{\Theta}_1 \mathbf{y}_{xx}(x,t) + \boldsymbol{\Theta}_2 \mathbf{y}_x(x,t) + \mathbf{A}\mathbf{y}(x,t) \\ &\quad + \mathbf{f}\left(\mathbf{y}(x,t), x, t\right) + \mathbf{G}_u \mathbf{u}(x,t) + \mathbf{G}_w \mathbf{w}(x,t), \end{aligned} \tag{3}$$

$$\mathbf{z}(x,t) = \mathbf{C}\mathbf{y}(x,t) + \mathbf{D}\mathbf{u}(x,t) \tag{4}$$

subject to the homogeneous Neumann boundary conditions:

$$\mathbf{y}_x(x,t)\big|_{x=l_1} = \mathbf{y}_x(x,t)\big|_{x=l_2} = 0 \tag{5}$$

and the initial condition:

$$\mathbf{y}(x,0) = \mathbf{y}_0(x), \tag{6}$$

where $\mathbf{y}(x,t) \triangleq [y_1(x,t) \ \cdots \ y_n(x,t)] \in \mathfrak{R}^n$ is the state, the subscripts x and t stand for the partial derivatives with respect to x, t, respectively, $x \in [l_1, l_2] \subset \mathfrak{R}$ and $t \in [0, \infty)$ denote the position and time, respectively, and $\mathbf{u}(x,t) \triangleq [u_1(x,t) \ \cdots \ u_m(x,t)] \in \mathfrak{R}^m$ is the control input. $\mathbf{z}(x,t) \in \mathfrak{R}^q$ is the controlled output. $\mathbf{w}(x,t) \in \mathfrak{R}^p$ is the exogenous disturbance satisfying $\int_0^\infty \|\mathbf{w}(\cdot,t)\|_2^2 dt < \infty$. $\mathbf{f}(\mathbf{y}(x,t), x, t) \in \mathfrak{R}^n$ is the nonlinear part in the system, which is a locally Lipschitz continuous function on $\mathbf{y}(x,t)$ and satisfies $\mathbf{f}(0,x,t) = 0$ for all $x \in [l_1, l_2]$ and $t \geq 0$. $\boldsymbol{\Theta}_1$, $\boldsymbol{\Theta}_2$, $\mathbf{A}$, $\mathbf{G}_u$, $\mathbf{G}_w$, $\mathbf{C}$, and $\mathbf{D}$ are real-known matrices with appropriate dimensions.

This study considers the following P-sD state feedback controller:

$$\mathbf{u}(x,t) = \mathbf{K}_1 \mathbf{y}(x,t) + \mathbf{K}_2 \mathbf{y}_x(x,t), \tag{7}$$

where $\mathbf{K}_1 \in \mathfrak{R}^{m\times n}$ and $\mathbf{K}_2 \in \mathfrak{R}^{m\times n}$ are control gain matrices to be determined. The controller structure is shown in Figure 1, in which the notation "$\partial/\partial x$" means a first-order spatial differentiator.

Remark 1. It must be stressed that the implementation of the controller (7) requires distributed sensing and actuation. Although this is normally recognized as a critical drawback, with recent advances in technological developments of microelectromechanical systems, it becomes feasible to manufacture large arrays of microsensors and actuators with integrated control circuitry, which can be used for the implementation of distributed feedback control loops in some practical applications (see [13] and the references therein). The signal $\mathbf{y}_x(x,t)$ can be obtained using the finite difference method. In addition, it has been pointed out in [18] that the controller (7) can provide more convenient spatial performance.

Substituting (7) into (3) and (4) leads to the following PDE:

$$\begin{aligned} \mathbf{y}_t(x,t) &= \boldsymbol{\Theta}_1 \mathbf{y}_{xx}(x,t) + \left[\boldsymbol{\Theta}_2 + \mathbf{G}_u \mathbf{K}_2\right] \mathbf{y}_x(x,t) + \mathbf{A}_c \mathbf{y}(x,t) \\ &\quad + \mathbf{f}\left(\mathbf{y}(x,t), x, t\right) + \mathbf{G}_w \mathbf{w}(x,t), \\ \mathbf{z}(x,t) &= \mathbf{C}_c \mathbf{y}(x,t) + \mathbf{D}\mathbf{K}_2 \mathbf{y}_x(x,t), \end{aligned} \tag{8}$$

where $\mathbf{A}_c \triangleq \mathbf{A} + \mathbf{G}_u \mathbf{K}_1$ and $\mathbf{C}_c \triangleq \mathbf{C} + \mathbf{D}\mathbf{K}_1$.

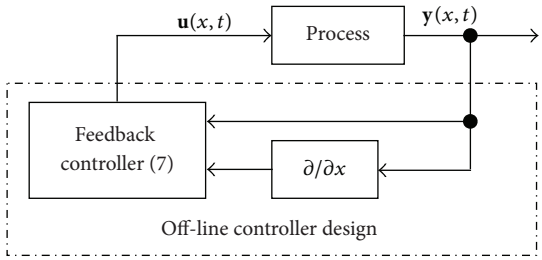

Figure 1: The structure of distributed P-sD state-feedback controller.

In order to attenuate the effect of $\mathbf{w}(x,t)$, robust H_∞ control will be employed in this paper to deal with the disturbance attenuation problem. Let us consider the following H_∞ control performance for the closed-loop PDE system of the form (5), (6), and (8):

$$\int_0^\infty \|\mathbf{z}(\cdot,t)\|_2^2 dt \le \langle \mathbf{y}_0(\cdot), \mathbf{P}\mathbf{y}_0(\cdot)\rangle + \gamma^2 \int_0^\infty \|\mathbf{w}(\cdot,t)\|_2^2 dt, \quad (9)$$

where $\mathbf{P} > 0$ is a real $n \times n$ matrix and $\gamma > 0$ is a prescribed level of disturbance attenuation. In general, it is desirable to make the attenuation level as small as possible to achieve the optimal disturbance attenuation performance.

For simplicity, when $\mathbf{u}(x,t) \equiv 0$, the PDE system (3)–(6) is referred to as an *unforced* PDE system, while when $\mathbf{w}(x,t) \equiv 0$, it is referred to as a *disturbance-free* PDE system. We introduce the following definitions.

Definition 2. Given a constant $\rho > 0$, the unforced disturbance-free PDE system of (5), (6), and (8) (i.e., $\mathbf{u}(x,t) \equiv 0$ and $\mathbf{w}(x,t) \equiv 0$) is said to be *exponentially stable with a given decay rate* ρ, if there exists a constant $\sigma > 0$ such that the following inequality holds:

$$\|\mathbf{y}(\cdot,t)\|_2^2 \le \sigma \exp(-2\rho t) \|\mathbf{y}_0(\cdot)\|_2^2, \quad \forall t \ge 0. \quad (10)$$

Definition 3. Given constants $\rho > 0$ and $\gamma > 0$, the unforced PDE system of (5), (6), and (8) is said to be *exponentially stable with a given decay rate* ρ *and* γ*-disturbance attenuation* if the response $\mathbf{z}(x,t)$ satisfies (9) and the disturbance-free system is *exponentially stable with a given decay rate* ρ.

Therefore, the objective of this study is to find a robust P-sD controller of the form (7) such that the resulting closed-loop system is exponentially stable and the H_∞ performance is ensured for a prescribed disturbance attenuation level $\gamma > 0$. To do this, the following assumption and lemma are useful for the development of the main results.

Assumption 4. There exists a scalar $\chi > 0$ such that the following inequality holds for any $\mathbf{y}(x,t) \in \Omega$:

$$\int_{l_1}^{l_2} \mathbf{f}^T(\mathbf{y}(x,t),x,t)\,\mathbf{f}(\mathbf{y}(x,t),x,t)\,dx \le \chi \int_{l_1}^{l_2} \mathbf{y}^T(x,t)\,\mathbf{y}(x,t)\,dx, \quad (11)$$

where $\Omega \triangleq \{\mathbf{y}(x,t) \mid \sigma_1(x) \le \mathbf{y}(x,t) \le \sigma_2(x),\ x \in [l_1,l_2],\ t \ge 0\}$.

Lemma 5. *For any two square integrable vector functions* $\mathbf{a}(x) \in \mathfrak{R}^n$, $\mathbf{b}(x) \in \mathfrak{R}^n$, $x \in [l_1,l_2]$, *the following inequality holds for any positive scalar* $\alpha \in \mathfrak{R}$, $x \in [l_1,l_2]$:

$$2\langle \mathbf{a},\mathbf{b}\rangle \le \langle \mathbf{a}, \alpha\mathbf{a}\rangle + \left\langle \mathbf{b}, \alpha^{-1}\mathbf{b}\right\rangle. \quad (12)$$

Proof. It is easily verified that $[\alpha\mathbf{a}(x)-\mathbf{b}(x)]^T[\alpha\mathbf{a}(x)-\mathbf{b}(x)] \ge 0$ holds for any $x \in [l_1,l_2]$ and any positive scalar α. Therefore,

$$\begin{aligned} 0 &\le [\alpha\mathbf{a}(x) - \mathbf{b}(x)]^T [\alpha\mathbf{a}(x) - \mathbf{b}(x)] \\ &= \alpha^2 \mathbf{a}^T(x)\,\mathbf{a}(x) - 2\alpha\mathbf{a}^T(x)\,\mathbf{b}(x) + \mathbf{b}^T(x)\,\mathbf{b}(x), \end{aligned} \quad (13)$$

which implies

$$\begin{aligned} 2\mathbf{a}^{\mathbf{T}}(x)\,\mathbf{b}(x) &\le \alpha\mathbf{a}^T(x)\,\mathbf{a}(x) \\ &\quad + \alpha^{-1}\mathbf{b}^T(x)\,\mathbf{b}(x), \quad x \in [l_1,l_2]. \end{aligned} \quad (14)$$

Integrating both sides of (14) from l_1 to l_2, we can obtain that

$$\begin{aligned} 2\int_{l_1}^{l_2} \mathbf{a}^T(x)\,\mathbf{b}(x)\,dx \le & \int_{l_1}^{l_2} \alpha\mathbf{a}^T(x)\,\mathbf{a}(x)\,dx \\ & + \int_{l_1}^{l_2} \alpha^{-1}\mathbf{b}^T(x)\,\mathbf{b}(x)\,dx, \end{aligned} \quad (15)$$

which implies that the inequality (12) holds. The proof is complete. □

3. Robust H_∞ P-sD Control Design

The aim of this section is to develop a robust H_∞ P-sD state feedback controller to not only exponentially stabilize the semi-linear PDE system (3)–(6) but also achieve the H_∞ performance with a prescribed disturbance attenuation level $\gamma > 0$.

Consider the following Lyapunov functional for the system (5), (6), and (8):

$$V(t) = \int_{l_1}^{l_2} \mathbf{y}^T(x,t)\,\mathbf{P}\mathbf{y}(x,t)\,dx, \quad (16)$$

where $\mathbf{P} > 0$ is a real $n \times n$ gain matrix to be determined. The time derivative of $V(t)$ along the solution of the system (5), (6), and (8) is given by

$$\begin{aligned}\dot{V}(t) &= 2\int_{l_1}^{l_2} \mathbf{y}^T(x,t)\,\mathbf{P}\mathbf{y}_t(x,t)\,dx \\ &= 2\int_{l_1}^{l_2} \mathbf{y}^T(x,t)\,\mathbf{P}\boldsymbol{\Theta}_1\mathbf{y}_{xx}(x,t)\,dx \\ &\quad + 2\int_{l_1}^{l_2} \mathbf{y}^T(x,t)\,\mathbf{P}\left[\boldsymbol{\Theta}_2 + \mathbf{G}_u\mathbf{K}_2\right]\mathbf{y}_x(x,t)\,dx \\ &\quad + \int_{l_1}^{l_2} \mathbf{y}^T(x,t)\left[\mathbf{P}\mathbf{A}_c + *\right]\mathbf{y}(x,t)\,dx \\ &\quad + 2\int_{l_1}^{l_2} \mathbf{y}^T(x,t)\,\mathbf{P}\mathbf{f}\left(\mathbf{y}(x,t),x,t\right)dx \\ &\quad + 2\int_{l_1}^{l_2} \mathbf{y}^T(x,t)\,\mathbf{P}\mathbf{G}_w\mathbf{w}(x,t)\,dx.\end{aligned} \tag{17}$$

Integrating by parts and taking into account (5) yield

$$\begin{aligned}&\int_{l_1}^{l_2} \mathbf{y}^T(x,t)\,\mathbf{P}\boldsymbol{\Theta}_1\mathbf{y}_{xx}(x,t)\,dx \\ &\quad = \mathbf{y}^T(x,t)\,\mathbf{P}\boldsymbol{\Theta}_1\mathbf{y}_x(x,t)\Big|_{x=l_1}^{x=l_2} \\ &\qquad - \int_{l_1}^{l_2} \mathbf{y}_x^T(x,t)\,\mathbf{P}\boldsymbol{\Theta}_1\mathbf{y}_x(x,t)\,dx \\ &\quad = -\int_{l_1}^{l_2} \mathbf{y}_x^T(x,t)\,\mathbf{P}\boldsymbol{\Theta}_1\mathbf{y}_x(x,t)\,dx.\end{aligned} \tag{18}$$

Applying Assumption 4, for any scalar $\alpha > 0$,

$$\begin{aligned}&2\int_{z_1}^{z_2} \mathbf{y}^T(x,t)\,\mathbf{P}\mathbf{f}\left(\mathbf{y}(x,t),x,t\right)dx \\ &\le \alpha\int_{l_1}^{l_2} \mathbf{y}^T(x,t)\,\mathbf{P}\mathbf{P}\mathbf{y}(x,t)\,dx \\ &\quad + \alpha^{-1}\int_{l_1}^{l_2} \mathbf{f}^T\left(\mathbf{y}(x,t),x,t\right)\mathbf{f}\left(\mathbf{y}(x,t),x,t\right)dx \\ &\le \alpha\int_{l_1}^{l_2} \mathbf{y}^T(x,t)\,\mathbf{P}\mathbf{P}\mathbf{y}(x,t)\,dx \\ &\quad + \alpha^{-1}\chi\int_{l_1}^{l_2} \mathbf{y}^T(x,t)\,\mathbf{y}(x,t)\,dx \\ &= \int_{l_1}^{l_2} \mathbf{y}^T(x,t)\left[\alpha\mathbf{P}\mathbf{P} + \alpha^{-1}\chi\mathbf{I}\right]\mathbf{y}(x,t)\,dx.\end{aligned} \tag{19}$$

Substitution of (18) and (19) into (17) implies

$$\begin{aligned}&\dot{V}(t) + 2\rho V(t) \\ &\le \int_{l_1}^{l_2} \mathbf{y}^T(x,t)\left[\left[\mathbf{P}\mathbf{A}_c + *\right] + \alpha\mathbf{P}\mathbf{P} + \alpha^{-1}\chi\mathbf{I} + 2\rho\mathbf{P}\right]\mathbf{y}(x,t)\,dx \\ &\quad + 2\int_{l_1}^{l_2} \mathbf{y}^T(x,t)\,\mathbf{P}\left[\boldsymbol{\Theta}_2 + \mathbf{G}_u\mathbf{K}_2\right]\mathbf{y}_x(x,t)\,dx \\ &\quad - \int_{l_1}^{l_2} \mathbf{y}_x^T(x,t)\left[\mathbf{P}\boldsymbol{\Theta}_1 + *\right]\mathbf{y}_x(x,t)\,dx \\ &\le \int_{l_1}^{l_2} \widetilde{\mathbf{y}}^T(x,t)\,\overline{\Psi}\widetilde{\mathbf{y}}(x,t)\,dx \\ &\quad + 2\int_{l_1}^{l_2} \mathbf{y}^T(x,t)\,\mathbf{P}\mathbf{G}_w\mathbf{w}(x,t)\,dx,\end{aligned} \tag{20}$$

where $\widetilde{\mathbf{y}}(x,t) \triangleq \left[\mathbf{y}^T(x,t)\ \ \mathbf{y}_x^T(x,t)\right]^T$ and

$$\overline{\Psi} \triangleq \begin{bmatrix} \left[\mathbf{P}\mathbf{A}_c + *\right] + \alpha\mathbf{P}\mathbf{P} + \alpha^{-1}\chi\mathbf{I} + 2\rho\mathbf{P} & \mathbf{P}\left[\boldsymbol{\Theta}_2 + \mathbf{G}_u\mathbf{K}_2\right] \\ * & -\left[\mathbf{P}\boldsymbol{\Theta}_1 + *\right] \end{bmatrix}. \tag{21}$$

Combining (4) and (20) gives

$$\begin{aligned}&\dot{V}(t) + 2\rho V(t) + \|\mathbf{z}(\cdot,t)\|_2^2 - \gamma^2\|\mathbf{w}(\cdot,t)\|_2^2 \\ &\quad \le \int_{l_1}^{l_2} \widetilde{\mathbf{y}}^T(x,t)\left[\overline{\Psi} + \begin{bmatrix}\mathbf{C}_c & \mathbf{D}\mathbf{K}_2\end{bmatrix}^T\begin{bmatrix}\mathbf{C}_c & \mathbf{D}\mathbf{K}_2\end{bmatrix}\right]\widetilde{\mathbf{y}}(x,t)\,dx \\ &\qquad + 2\int_{l_1}^{l_2} \mathbf{y}^T(x,t)\,\mathbf{P}\mathbf{G}_w\mathbf{w}(x,t)\,dx \\ &\qquad - \gamma^2\int_{l_1}^{l_2} \mathbf{w}^T(x,t)\,\mathbf{w}(x,t)\,dx \\ &\quad = \int_{l_1}^{l_2} \widehat{\mathbf{y}}^T(x,t)\,\widehat{\Psi}\widehat{\mathbf{y}}(x,t)\,dx,\end{aligned} \tag{22}$$

where $\widehat{\mathbf{y}}(x,t) \triangleq \left[\widetilde{\mathbf{y}}^T(x,t)\ \ \mathbf{w}^T(x,t)\right]^T$ and

$$\begin{aligned}\widehat{\Psi} &\triangleq \begin{bmatrix} \left[\mathbf{P}\mathbf{A}_c + *\right] + \alpha\mathbf{P}\mathbf{P} + \alpha^{-1}\chi\mathbf{I} + 2\rho\mathbf{P} & \mathbf{P}\left[\boldsymbol{\Theta}_2 + \mathbf{G}_u\mathbf{K}_2\right] & \\ & & \mathbf{P}\mathbf{G}_w \\ * & -\left[\mathbf{P}\boldsymbol{\Theta}_1 + *\right] & 0 \\ * & * & -\gamma^2\mathbf{I} \end{bmatrix} \\ &\quad + \begin{bmatrix} \mathbf{C}_c^T \\ \mathbf{K}_2^T\mathbf{D}^T \\ 0 \end{bmatrix}\begin{bmatrix} \mathbf{C}_c^T \\ \mathbf{K}_2^T\mathbf{D}^T \\ 0 \end{bmatrix}^T.\end{aligned} \tag{23}$$

From the above analysis, we have the following theorem.

Theorem 6. *Consider the semi-linear PDE system* (3)–(6) *with the P-sD controller* (7)*. For some given scalar* $\rho > 0$ *and* $\gamma > 0$*, the closed-loop PDE system is exponentially stable with a decay rate* ρ *and the* γ*-disturbance attenuation, if there exist a* $n \times n$ *matrix* $\mathbf{Q} > 0$*,* $m \times n$ *matrices* $\mathbf{Z}_i$*,* $i \in \{1, 2\}$*, and a positive scalar* α *satisfying the following LMI:*

$$\Xi \triangleq \begin{bmatrix} \Xi_{11} & \boldsymbol{\Theta}_2\mathbf{Q} + \mathbf{G}_u\mathbf{Z}_2 & \mathbf{G}_w & \mathbf{Q} & \widetilde{\mathbf{C}}^T \\ * & -\left[\boldsymbol{\Theta}_1\mathbf{Q} + *\right] & 0 & 0 & \mathbf{Z}_2^T\mathbf{D}^T \\ * & * & -\gamma^2\mathbf{I} & 0 & 0 \\ * & * & * & -\alpha\chi^{-1}\mathbf{I} & 0 \\ * & * & * & * & -\mathbf{I} \end{bmatrix} < 0, \quad (24)$$

where $\Xi_{11} \triangleq [\mathbf{A}\mathbf{Q} + \mathbf{G}_u\mathbf{Z}_1 + *] + 2\rho\mathbf{Q} + \alpha\mathbf{I}$ *and* $\widetilde{\mathbf{C}} \triangleq \mathbf{C}\mathbf{Q} + \mathbf{D}\mathbf{Z}_1$*. In this case, the gain matrices* $\mathbf{K}_i$*,* $i \in \{1, 2\}$ *can be constructed as*

$$\mathbf{K}_i = \mathbf{Z}_i\mathbf{Q}^{-1}, \quad i \in \{1, 2\}. \quad (25)$$

Proof. Set

$$\mathbf{Q} = \mathbf{P}^{-1} > 0, \qquad \mathbf{Z}_i = \mathbf{K}_i\mathbf{Q}, \quad i \in \{1, 2\}. \quad (26)$$

By pre- and post-multiplying the matrix $\widehat{\Psi}$ by the matrix $\mathrm{diag}\{\mathbf{Q}, \mathbf{Q}, \mathbf{I}\}$, respectively, we get

$$\overline{\Xi} \triangleq \begin{bmatrix} \Xi_{11} + \alpha^{-1}\chi\mathbf{Q}\mathbf{Q} & \boldsymbol{\Theta}_2\mathbf{Q} + \mathbf{G}_u\mathbf{Z}_2 & \mathbf{G}_w \\ * & -\left[\boldsymbol{\Theta}_1\mathbf{Q} + *\right] & 0 \\ * & * & -\gamma^2\mathbf{I} \end{bmatrix} + \begin{bmatrix} \widetilde{\mathbf{C}}^T \\ \mathbf{Z}_2^T\mathbf{D}^T \\ 0 \end{bmatrix} \begin{bmatrix} \widetilde{\mathbf{C}}^T \\ \mathbf{Z}_2^T\mathbf{D}^T \\ 0 \end{bmatrix}^T. \quad (27)$$

Using the Schur complement two times, LMI (24) is equivalent to the inequality $\overline{\Xi} < 0$. Since $\mathrm{diag}\{\mathbf{Q}, \mathbf{Q}, \mathbf{I}\} > 0$ and $\overline{\Xi} < 0$, we can get the inequality $\widehat{\Psi} < 0$.

From the inequality $\widehat{\Psi} < 0$ and (22), we can drive

$$\dot{V}(t) + 2\rho V(t) + \|\mathbf{z}(\cdot, t)\|_2^2 - \gamma^2\|\mathbf{w}(\cdot, t)\|_2^2 \le 0. \quad (28)$$

Since $\rho V(t) \ge 0$, we can obtain from (28) that

$$\dot{V}(t) + \|\mathbf{z}(\cdot, t)\|_2^2 - \gamma^2\|\mathbf{w}(\cdot, t)\|_2^2 \le 0. \quad (29)$$

Integrating (29) from $t = 0$ to $t = \infty$ yields

$$\int_0^\infty \dot{V}(t)\, dt + \int_0^\infty \left(\|\mathbf{z}(\cdot, t)\|_2^2 - \gamma^2\|\mathbf{w}(\cdot, t)\|_2^2\right) dt \le 0, \quad (30)$$

which implies

$$V(\infty) - V(0) + \int_0^\infty \left(\|\mathbf{z}(\cdot, t)\|_2^2 - \gamma^2\|\mathbf{w}(\cdot, t)\|_2^2\right) dt \le 0. \quad (31)$$

Since $V(\infty) \ge 0$, we obtain (9) from (31).

Next, we will show the exponential stability with a given decay rate ρ of the disturbance-free system of (5), (6), and (8). When $\mathbf{w}(x, t) = 0$, inequality (20) can be rewritten as

$$\dot{V}(t) + 2\rho V(t) \le \int_{l_1}^{l_2} \widetilde{\mathbf{y}}^T(x, t)\, \overline{\Psi}\, \widetilde{\mathbf{y}}(x, t)\, dx. \quad (32)$$

We can easily derive $\overline{\Psi} < 0$ from $\widehat{\Psi} < 0$. Hence, the inequality (32) can be further written as

$$\dot{V}(t) + 2\rho V(t) \le 0. \quad (33)$$

Integration of (33) from 0 to t yields

$$V(t) \le V(0) \exp(-2\rho t). \quad (34)$$

Since $\mathbf{P} > 0$, it is easily observed that $V(t)$ given by (16) satisfies the following inequality:

$$p_m\|\mathbf{y}(\cdot, t)\|_2^2 \le V(t) \le p_M\|\mathbf{y}(\cdot, t)\|_2^2, \quad (35)$$

where $p_m \triangleq \lambda_{\min}(\mathbf{P})$ and $p_M \triangleq \lambda_{\max}(\mathbf{P})$ are two positive scalars. Inequalities (34) and (35) imply

$$\|\mathbf{y}(\cdot, t)\|_2^2 \le p_m^{-1} p_M \|\mathbf{y}(\cdot, 0)\|_2^2 \exp(-2\rho t). \quad (36)$$

Thus, from Definition 2 and (36), the disturbance-free system of (5), (6), and (8) is exponentially stable with a given decay rate ρ. From Definition 3, the closed-loop system (5), (6), and (8) is exponentially stable with a given decay rate ρ and γ-disturbance attenuation. Moreover, from (26), we have (25). The proof is complete. □

From Theorem 6, since the controller (7) has been shown to be an effective control which can attenuate the effect of uncertain external disturbances, it is appealing to eliminate the influence brought by external disturbances as possible, that is, making the attenuation level as small as possible. To achieve this goal, for a given decay rate ρ, setting $\vartheta = \gamma^2$, we consider the following minimization optimization problem:

$$\min_{\{\vartheta, \mathbf{Q} > 0, \mathbf{Z}_1, \mathbf{Z}_2, \alpha > 0\}} \vartheta \quad (37)$$

subject to the following LMI

$$\begin{bmatrix} \Xi_{11} & \boldsymbol{\Theta}_2\mathbf{Q} + \mathbf{G}_u\mathbf{Z}_2 & \mathbf{G}_w & \mathbf{Q} & \widetilde{\mathbf{C}}^T \\ * & -\left[\boldsymbol{\Theta}_1\mathbf{Q} + *\right] & 0 & 0 & \mathbf{Z}_2^T\mathbf{D}^T \\ * & * & -\vartheta\mathbf{I} & 0 & 0 \\ * & * & * & -\alpha\chi^{-1}\mathbf{I} & 0 \\ * & * & * & * & -\mathbf{I} \end{bmatrix} < 0. \quad (38)$$

Remark 7. Notice that the control design proposed in this paper is different from the results reported in [18, 19]. The result in [18] only considers simple exponential stabilization for a class of semi-linear parabolic PDE systems. The main difference between the result in this study and [19] is that the system under consideration in the latter one is a class of semi-linear first-order hyperbolic PDE systems, whereas the system addressed in this study is a class of semi-linear parabolic PDE systems. On the other hand, different from the SDLMI-based control designs in [18, 19], the main result of this study is presented in terms of standard LMI, which can be directly verified via the existing convex optimization techniques [20, 21].

4. Simulation Study on the FHN Equation

To illustrate the effectiveness of the proposed methods, the control problem of the FHN equation is considered, which is a wavy behavior model extensively applied to excitable media in biology [22] and chemistry [23]. The FHN equation has the following closed-form description:

$$\begin{aligned} y_{1,t}(x,t) &= y_{1,xx}(x,t) - 0.5y_{1,x}(x,t) + y_1(x,t) \\ &\quad - 0.9y_2(x,t) - 0.1y_1^3(x,t) \\ &\quad + u(x,t) + 0.5w(x,t), \\ y_{2,t}(x,t) &= 4y_{2,xx}(x,t) - 0.5y_{2,x}(x,t) + 0.2y_1(x,t) \\ &\quad - y_2(x,t) + 0.2w(x,t) \end{aligned} \tag{39}$$

subject to the boundary conditions

$$\begin{aligned} y_{1,x}(x,t)\big|_{x=0} &= y_{1,x}(x,t)\big|_{x=L} = 0, \\ y_{2,x}(x,t)\big|_{x=0} &= y_{2,x}(x,t)\big|_{x=L} = 0 \end{aligned} \tag{40}$$

and the initial conditions

$$y_1(x,0) = y_{1,0}(x), \qquad y_2(x,0) = y_{2,0}(x), \tag{41}$$

where $y_1(x,t)$ and $y_2(x,t)$ are the state variables and $u(x,t)$ is the manipulated input. t, x, and L denote the independent time, space variables, and the length of the spatial domain, respectively. $y_{1,0}(x)$ and $y_{2,0}(x)$ are the initial conditions.

To more intuitively illustrate the effectiveness of the proposed design method, for the above values, we first verify through simulation that the operating steady states $y_1(x,t) = 0$ and $y_2(x,t) = 0$ of the system (39)–(41) are unstable ones. The initial conditions in (41) are assumed to be $y_{1,0}(x) = 0.6\cos(\pi x/L)$ and $y_{2,0}(x) = 0.1$. The length of spatial domain is set to be 20; that is, $L = 20$. The disturbance input is chosen as $w(x,t) = \cos(x)\exp(-0.5t)$. Figure 2 shows the open-loop profiles of the evolution of $y_1(x,t)$ and $y_2(x,t)$ starting from the initial conditions. It is easily observed from Figure 2 that the equilibria $y_1(x,t) = 0$ and $y_2(x,t) = 0$ of the system (39)–(41) are unstable ones and $-1 \le y_i(x,t) \le 1$, $x \in [0,L]$, $t \ge 0$, $i \in \{1,2\}$.

Equations (39) can be rewritten as the form of PDE (3) with the following parameters:

$$\begin{aligned} \mathbf{\Theta}_1 &= \begin{bmatrix} 1 & 0 \\ 0 & 4 \end{bmatrix}, \qquad \mathbf{\Theta}_2 = \begin{bmatrix} -0.1 & 0 \\ 0 & -0.1 \end{bmatrix}, \qquad \mathbf{A} = \begin{bmatrix} 1 & 5 \\ 0.2 & -1 \end{bmatrix}, \\ \mathbf{G_u} &= \begin{bmatrix} 1 \\ 0 \end{bmatrix}, \qquad \mathbf{G_w} = \begin{bmatrix} 0.5 \\ 0.2 \end{bmatrix}, \\ \mathbf{f}(\mathbf{y}(x,t), x, t) &= \begin{bmatrix} -0.3y_1^3(x,t) & 0 \end{bmatrix}^T, \end{aligned} \tag{42}$$

where $\mathbf{y}(x,t) \triangleq [y_1(x,t) \;\; y_2(x,t)]^T$ and $y_1^3(x,t)$ is a nonlinear term. The controlled output $\mathbf{z}(x,t)$ is chosen as $\mathbf{z}(x,t) = y_1(x,t)$. Hence, the parameter matrices in (4) are chosen as $\mathbf{C} = [1 \;\; 0]$ and $\mathbf{D} = 0$.

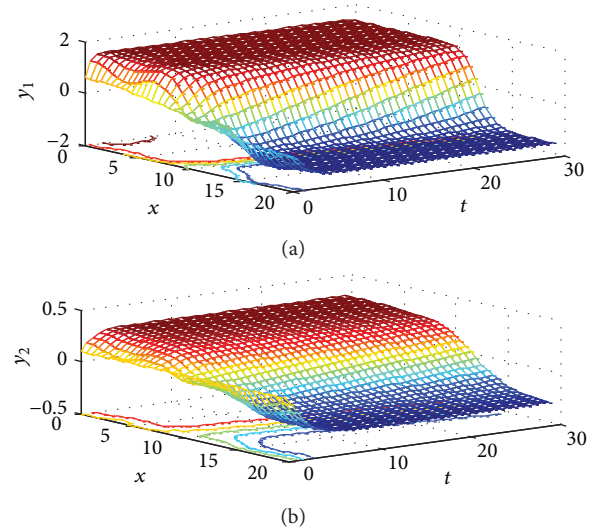

Figure 2: Open-loop profiles of evolution of $y_1(x,t)$ and $y_2(x,t)$.

From Figure 2, we can easily observe that $-1 \le y_i(x,t) \le 1$, $x \in [0,L]$, $t \ge 0$, $i \in \{1,2\}$. Let $\Omega \triangleq \{\mathbf{y}(x,t) \mid -1.0 \le y_i(x,t) \le 1.0, x \in [0,L], t \ge 0, i \in \{1,2\}\}$. The parameter χ satisfying Assumption 4 is chosen as

$$\begin{aligned} \chi &\triangleq \max_{\mathbf{y}(x,t)} \left\{ \sum_{i=1}^{2} \sum_{j=1}^{2} \frac{\partial f_i(\mathbf{y}(x,t))}{\partial y_j(x,t)} \right\} \\ &= 0.09 \max_{\mathbf{y}(x,t)} \left\{ 9y_1^4(x,t) \right\} = 0.81. \end{aligned} \tag{43}$$

We first show the effectiveness of the proposed design method. Set $\rho = 0.04$. Solving the optimization problem (37), we can get the optimized level of attenuation γ as $\gamma^* = \sqrt{\vartheta} = 4.3435 \times 10^{-5}$. Setting $\gamma = 0.8$ and solving LMI (24), the control gain matrices in (7) can be derived as follows:

$$\begin{aligned} \mathbf{K}_1 &= \begin{bmatrix} -5.2143 & -5.2365 \end{bmatrix}^T, \\ \mathbf{K}_2 &= \begin{bmatrix} 0.0999 & -0.0002 \end{bmatrix}^T. \end{aligned} \tag{44}$$

Applying the P-sD controller (7) with the control gain matrices given in (44) to the semi-linear PDE system (39)–(41), the closed-loop profiles of evolution of $y_1(x,t)$ and $y_2(x,t)$ are shown in Figure 3, which implies that the proposed P-sD controller (7) with the control gain matrices given in (44) can stabilize the semi-linear PDE system (39)–(41). Moreover, profile of evolution of $\mathbf{u}(x,t)$ is shown in Figure 4.

Define the function $\eta(t)$ as

$$\begin{aligned} \eta(t) &\triangleq \int_0^t \|\mathbf{z}(\cdot,\tau)\|_2^2 d\tau - \langle \mathbf{y}_0(\cdot), \mathbf{P}\mathbf{y}_0(\cdot) \rangle \\ &\quad - 0.64 \int_0^t \|\mathbf{w}(\cdot,\tau)\|_2^2 d\tau. \end{aligned} \tag{45}$$

Figure 5 shows the value of $\eta(t)$. From this figure, we can see that $\eta(t) < 0$ for all time $t \ge 0$, which implies that the H_∞ control performance in (9) is ensured.

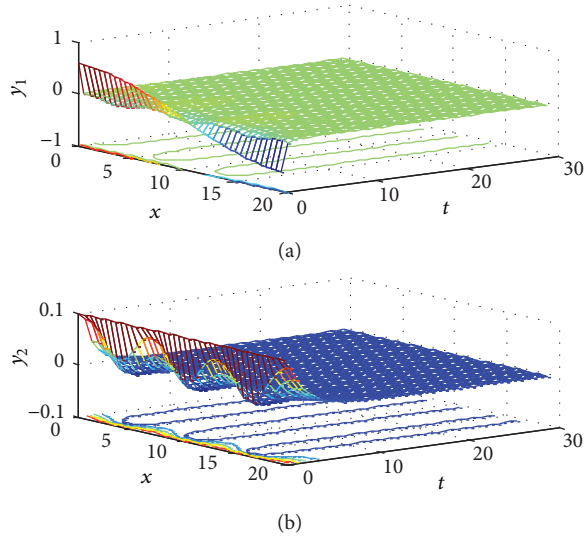

Figure 3: Closed-loop profiles of evolution of $y_1(x,t)$ and $y_2(x,t)$.

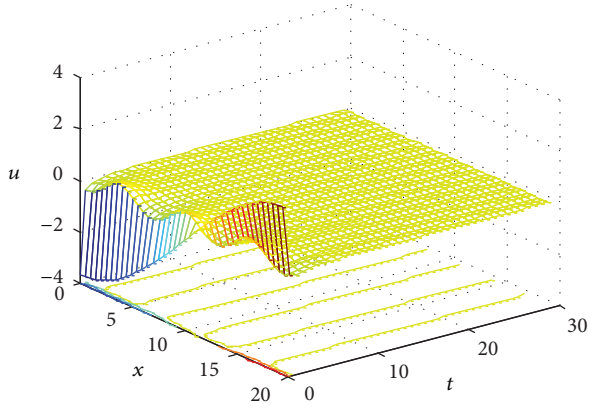

Figure 4: Profile of evolution of $u(x,t)$.

5. Conclusions

In this paper, we have addressed the problem of robust H_∞ P-sD state-feedback controller design for a class of semi-linear parabolic PDE systems with external disturbances. Based on the Lyapunov technique, the robust H_∞ P-sD state-feedback controller design is formulated as a standard LMI optimization problem. The proposed controller can not only exponentially stabilize the semi-linear PDE system but also satisfy the H_∞ performance in (9). The influence caused by external disturbances is eliminated as possible by the minimization optimization problem. Finally, the developed design method is successfully applied to the control of the FHN equation, and the achieved simulation results illustrate its effectiveness. Compared to one node in the paper, it is interesting to study the collective control in a coupled network with multiple nodes described by nonlinear parabolic PDEs in the future work.

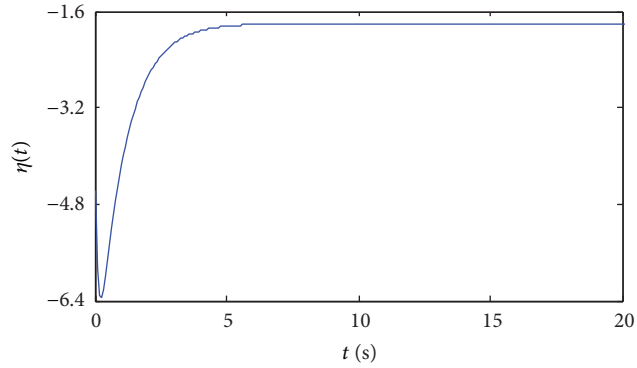

Figure 5: Trajectory of $\eta(t)$.

Conflict of Interests

The authors declare that there is no conflict of interests regarding the publication of this paper.

Acknowledgments

This work was supported in part by the National Natural Science Foundation of China under Grant 61273012, in part by the College Science and Technology Plan Project of Shandong Province under Grants J12LN91 and J13LN84, in part by the Science and Technology Development Plan Project of Shandong Province under Grant 2012YD01052, and in part by the Applied Mathematics Enhancement Program of Linyi University. The authors gratefully acknowledge the insightful comments and suggestions of the Associate Editor and anonymous reviewers, which helped improve the quality of this study.

References

[1] W. H. Ray, *Advanced Process Control*, McGraw-Hill, New York, NY, USA, 1981.

[2] P. D. Christofides, *Nonlinear and Robust Control of PDE Systems: Methods and Applications to Transport-Reaction Processes*, Birkhäauser, Boston, Mass, USA, 2001.

[3] Y. Orlov, A. Pisano, and E. Usai, "Continuous state-feedback tracking of an uncertain heat diffusion process," *Systems and Control Letters*, vol. 59, no. 12, pp. 754–759, 2010.

[4] H.-X. Li and C. Qi, "Modeling of distributed parameter systems for applications—a synthesized review from time-space separation," *Journal of Process Control*, vol. 20, no. 8, pp. 891–901, 2010.

[5] R. Padhi and S. F. Ali, "An account of chronological developments in control of distributed parameter systems," *Annual Reviews in Control*, vol. 33, no. 1, pp. 59–68, 2009.

[6] R. F. Curtain and H. J. Zwart, *An Introduction to Infinite-Dimensional Linear Systems Theory*, Springer, New York, NY, USA, 1995.

[7] H.-N. Wu and H.-X. Li, "H_∞ fuzzy observer-based control for a class of nonlinear distributed parameter systems with control constraints," *IEEE Transactions on Fuzzy Systems*, vol. 16, no. 2, pp. 502–516, 2008.

[8] H. N. Wu and H. X. Li, "A multi-objective optimization based fuzzy control for nonlinear spatially distributed processes with

application to a catalytic rod," *IEEE Transactions on Industrial Informatics*, vol. 8, no. 4, pp. 860–868, 2012.

[9] M. Krstic and A. Smyshlyaev, *Boundary Control of PDEs-A Course on Backstepping Designs*, SIAM, Philadelphia, Pa, USA, 2008.

[10] M. Krstic and A. Smyshlyaev, "Adaptive control of PDEs," *Annual Reviews in Control*, vol. 32, no. 2, pp. 149–160, 2008.

[11] M. Krstic, *Delay Compensation for Nonlinear, Adaptive, and PDE Systems*, Birkhäauser, Boston, Mass, USA, 2009.

[12] E. Fridman and Y. Orlov, "An LMI approach to H_∞boundary control of semilinear parabolic and hyperbolic systems," *Automatica*, vol. 45, no. 9, pp. 2060–2066, 2009.

[13] B. Bamieh, F. Paganini, and M. A. Dahleh, "Distributed control of spatially invariant systems," *IEEE Transactions on Automatic Control*, vol. 47, no. 7, pp. 1091–1107, 2002.

[14] Y. Orlov, A. Pisano, and E. Usai, "Exponential stabilization of the uncertain wave equation via distributed dynamic input extension," *IEEE Transactions on Automatic Control*, vol. 56, no. 1, pp. 212–217, 2011.

[15] J.-W. Wang, H.-N. Wu, and H.-X. Li, "Stochastically exponential stability and stabilization of uncertain linear hyperbolic PDE systems with Markov jumping parameters," *Automatica*, vol. 48, no. 3, pp. 569–576, 2012.

[16] J. W. Wang and H. N. Wu, "Guaranteed cost distributed fuzzy control design for a class of nonlinear first-order hyperbolic PDE systems," in *Proceedings of the American Control Conference (ACC '12)*, pp. 4375–4380, Montréal, Canada, 2012.

[17] J. W. Wang, H. N. Wu, and H. X. Li, "Guaranteed cost distributed fuzzy observer-based control for a class of nonlinear spatially distributed processes," *AIChE Journal*, vol. 59, no. 7, pp. 2366–2378, 2013.

[18] J. W. Wang, H. N. Wu, and H. X. Li, "Distributed proportional-spatial derivative control of nonlinear parabolic systems," *IEEE Transactions on Systems, Man, and Cybernetics B*, vol. 42, no. 3, pp. 927–938, 2012.

[19] H. N. Wu, J. W. Wang, and H. X. Li, "Design of distributed H_∞ fuzzy controllers with constraint for nonlinear hyperbolic PDE systems," *Automatica*, vol. 48, no. 10, pp. 2535–2543, 2012.

[20] S. Boyd, L. EI Ghaoui, E. Feron, and V. Balakrishnan, *Linear Matrix Inequalities in System and Control Theory*, SIAM, Philadelphia, Pa, USA, 1994.

[21] P. Gahinet, A. Nemirovskii, A. J. Laub, and M. Chilali, *LMI Control Toolbox for Use with Matlab*, The MathWorks, Natick, Mass, USA, 1995.

[22] J. Keener and J. Sneyd, *Mathematical Physiology*, Springer, New York, NY, USA, 1998.

[23] C. Theodoropoulos, Y.-H. Qian, and I. G. Kevrekidis, ""Coarse" stability and bifurcation analysis using time-steppers: a reaction-diffusion example," *Proceedings of the National Academy of Sciences of the United States of America*, vol. 97, no. 18, pp. 9840–9843, 2000.

Hindawi Publishing Corporation
Abstract and Applied Analysis
Volume 2013, Article ID 486178, 9 pages
http://dx.doi.org/10.1155/2013/486178

Research Article

Neurodynamics of up and down Transitions in Network Model

Xuying Xu[1] and Rubin Wang[2]

[1] *Institute for Cognitive Neurodynamics, School of Science, East China University of Science and Technology, Shanghai 200237, China*
[2] *Institute for Cognitive Neurodynamics, School of Science, School of Information Science and Engineering, East China University of Science and Technology, Shanghai 200237, China*

Correspondence should be addressed to Rubin Wang; rbwang@163.com

Received 20 November 2013; Accepted 27 November 2013

Academic Editor: Jinde Cao

This paper focuses on the neurodynamical research of a small neural network that consists of 25 neurons. We study the periodic spontaneous activity and transitions between up and down states without synaptic input. The results demonstrate that these transitions are bidirectional or unidirectional with the parameters changing, which not only reveals the function of the cortex, but also cohere with the experiment results.

1. Introduction

Different patterns of brain activity can give rise to different behavioral states of the animals. Neural electrophysiology experiments show that during slow-wave sleep in the primary visual cortex of anesthetized animals [1–3] and during quiet wakefulness in the somatosensory cortex of unanesthetized animals [4, 5], the membrane potentials make spontaneous transitions between two different levels called up and down states [6]. Transitions between up and down states can also be evoked by sensory stimulation [1, 4, 7–11]. An interesting result of these transitions is that sensory-evoked activity patterns are similar to those produced spontaneously. A hallmark of this subthreshold activity is a bimodal distribution of the membrane potential [12]. However, why these transitions occur or whether this spontaneous activity engages in brain functions or not remains unclear. In fact, we know little about expressions of neuron membrane potentials and interactions between neural networks, especially the relationship between neural coding modes and cognitive behaviors. So our purpose is to try to understand the inner connection between the up and down transitions of a single neuron and that of neural network.

Recent findings show that activation of a single cortical neuron can significantly modulate sensory and motor outputs [13, 14]. Furthermore, repetitive high frequency burst spiking of a single rat cortical neuron could trigger a switch between the cortical states resembling slow-wave and rapid-eye-movement sleep [15]. This is reflected in the switching of membrane potential of the stimulated neuron from high frequency and low amplitude oscillations to low frequency and high amplitude ones or vice versa. At the same time, cortical local field potential (LFP) changes over time. Here we use local field potential (LFP) to describe the state of the whole cortex [16–19]. Therefore, the up and down states of single neuron reflect distinct global cortical states, which resemble slow-wave and rapid-eye-movement sleep, respectively [20–22]. All of these results point to the power of single cortical neurons in modulating the behavior state of animals [15]. Here, one single neuron affects the whole network status by impacting other coupling neurons.

We have started our research on a single neuron, studied the electrophysiological phenomenon of status transitions, and obtained the bistability and spontaneity that is similar to experiment observation. In addition, we found that these up and down transitions show unidirectional or bidirectional changing with different parameters. Bistability means that the neuron stays in one state before stimulation and turn to another state after stimulation. These two states are called up state and down state, respectively. That is to say, the neuron can switch between up and down states. And directivity refers to the fact that it is not arbitrary to switch from one state to another. In some cases, transition can only occur from up state to down state, while it occurs from down state to up state

in other cases. Spontaneity, the periodic spontaneous activity of neural membrane potential, is the most significant feature of the transition.

This paper tries to further explore neural dynamic mechanism of up and down transitions in a neural network based on the above results. This work will lay a foundation for studying the relationship between neural coding and cognitive behavior. We focus on the dynamic process of the average membrane potential of a small neural network that consists of 25 neurons and switches between up and down states. And we observe the difference and distinguish between transitions in network and one single neuron by numerical simulation and theoretical analysis. Then we try to know what happened to the appearance of behavior states and the inducement of brain cognition. What we want to highlight is that how great the effect of the emerged relationship between behavior states and cognition and the ratio of activated neurons on up and down transitions is. This is also the subject for our further study.

2. Network Model

There are different kinds of complicated connection between neurons. According to the topology, some scholars proposed chain link, ring link, grid link, and so forth [23]. However, the internal connections between neurons are much more complicated than those above connections. This paper constructs a dynamical network model that consists of 25 neurons based on previous study [24]. In this network, any one neuron connects to any other neurons in the network. That means every two neurons in the network are coupled with the connection strength asymmetrically and obeying standard uniform distribution [25].

The coupling strength between neurons can be expressed with matrix variable, denoted by G. Then we have

$$G = \begin{bmatrix} g_{1,1} & g_{1,2} & \cdots & g_{1,n} \\ g_{2,1} & \ddots & & g_{2,n} \\ \vdots & & \ddots & \vdots \\ g_{n,1} & g_{n,2} & \cdots & g_{n,n} \end{bmatrix} = \begin{bmatrix} 0 & g_{1,2} & \cdots & g_{1,n} \\ g_{2,1} & 0 & \cdots & g_{2,n} \\ \vdots & \vdots & \ddots & \vdots \\ g_{n,1} & g_{n,2} & \cdots & 0 \end{bmatrix}, \quad (1)$$

where $g_{i,j}$ represents the coupling strength form neuron i to neuron j. Absolutely, neurons do not couple with themselves, so these coupling strength denoted by $g_{i,j}$ equals to zero.

To illustrate the state changing of the whole network, we use the changing of average membrane potential to describe the changing of local field potential (LFP), which means that we average membrane potentials of every neuron in the network to express LFP.

The dynamic model of one neuron in the neural network is based on H-H equations and is described by (2) to (8). This dynamic model consists of three ionic currents and synaptic currents which come from surrounding neurons. The ionic currents contain an instantaneous, inward current (sodium current), a slow h-like current [26, 27], and an outward current (a potassium current and a leak current). Two types of persistent inward, persistent sodium, and persistent calcium have been characterized in Purkinje cells [28, 29]. Somatic Purkinje cell bistability has been associated with persistent sodium whereas dendritic bistability has been shown to result from persistent calcium conductance. Here we use persistent sodium in our model for simplicity but it is likely that it is the combination of these two currents that enables the bistability [30].

On the basis of previous research, we propose the following neural network model to study the characteristics, bistability, directivity, and spontaneity, of the up and down transitions that have been observed in electrophysiology experiments. Thus, we clarify the neural dynamic mechanism of the up and down transitions in neural network. The current equation for the model is

$$C\frac{dV_i}{dt} = -\left(I^i_{\mathrm{Na}} + I^i_h + I^i_K + I^i_l + I^i_{\mathrm{syn}}\right). \quad (2)$$

Here, the ionic currents are as follows:

$$I^i_{\mathrm{Na}} = g_{\mathrm{Na}} m_\infty \left(V_i - V_{\mathrm{Na}}\right), \quad (3)$$

$$I^i_h = g_h h_i \left(V_i - V_h\right), \quad (4)$$

$$I^i_K = g_K b_i \left(V_i - V_K\right), \quad (5)$$

$$I^i_l = g_l \left(V_i - V_l\right), \quad (6)$$

where

$$m_\infty = \left(1 + e^{-(V_i - T_m)/\sigma_m}\right)^{-1}. \quad (7)$$

The synaptic current is

$$I^i_{\mathrm{syn}} = \sum_{j \neq i} g_{ji}\left(V_i - V_j\right). \quad (8)$$

The synaptic current of the ith neuron is a sum of effects from all the other neurons in the network, so this kind of current plays a key role in coupling every two neurons in the whole network. The changing activity of one neuron affects the whole network states changing through this way.

There are two dynamic variables: membrane potential V_i and the inactivation term of the h-current h_i, when we discuss the bistability and directivity. But when studying the spontaneity, we need another variable called the inactivation term of potassium current b_i. The dynamics of the inactivation terms of h-current and potassium current are

$$\frac{dh_i}{dt} = \frac{h_\infty - h_i}{\tau_h}, \qquad \frac{db_i}{dt} = \frac{b_\infty - b_i}{\tau_b}, \quad (9)$$

where

$$h_\infty = \left(1 + e^{(V_i - T_h)/\sigma_h}\right)^{-1},$$

$$\tau_h = \frac{1}{\alpha + \beta},$$

$$\alpha = \frac{a_\alpha \cdot V_i + b_\alpha}{1 - e^{((V_i + b_\alpha)/a_\alpha)/k_\alpha}},$$

$$\beta = \frac{a_\beta \cdot V_i + b_\beta}{1 - e^{((V_i + b_\beta)/a_\beta)/k_\beta}}, \quad (10)$$

$$b_\infty = \left(1 + e^{-(V_i - T_b)/\sigma_b}\right)^{-1},$$

$$\tau_b = \tau_b^0 \cdot \sec\left(h_i \frac{V_i - T_b}{4 \cdot \sigma_b}\right).$$

In these equations, V_i represents membrane potential of the ith neuron, while I_h^i, I_K^i, I_l^i replace a sodium current, a slow h-like current, and a potassium current and a leak current of the ith neuron, respectively. Similarly, g_{Na}, g_h, g_K, g_l, respectively, represent the sodium conductance, the slow h-like conductance, the potassium conductance, and the leak conductance, and V_{Na}, V_h, V_K, V_l are the corresponding reversal potentials. The inactivation term of the sodium current, the h-like current, and the potassium current are described by $m_\infty, h_\infty, b_\infty$, and dynamic variables h_i, b_i, with the synaptic time constant τ_h, τ_b. And T_m, σ_m, T_h, σ_h, T_b, σ_b, τ_b^0, a_α, b_α,k_α, a_β,b_β, k_β are constants.

3. Results

3.1. Bistability. When we studied the single neuron model, we found that transitions between up and down states can be induced by two different kinds of stimulus. One is to add brief outward current pulses; another is to improve the sodium conductance to a certain value instantaneously. Now, we research the neural network in the same way to try to find out that there exist the similar phenomenon or not which agrees with electrophysiology experiment results.

In the period of 10 seconds, we add a pulse current which lasts 0.1 second every two seconds, with the current intensity 7.2 μA/cm^2. The results are shown in Figure 1. We find that the average membrane potential switches between the up state (about −45 mV) and the down state (about −65 mV).

In the period of 10 seconds, we add the stimulation that lasts 4 ms every one or two seconds, leading to the intensity of sodium conductance changing from 0.06 mS/cm^2 to 1.2 mS/cm^2 instantaneously. The results are shown in Figure 2. We find that the average membrane potential switches between the up state (about −45 mV) and the down state (about −65 mV) when adding the same stimulation. And these transitions are a little bit complex: the membrane potential rises up to 0 mV instantaneously but then drops quickly.

So from the above two results, we find that this dynamic model can describe the bistability of up and down transitions of neural membrane potential in the neural network. That means there are two stable states for neural network, with other states unstable. The network can stay in one of these two stable states without any input. When the neuron in the network is stimulated, which destroys its original stability, it can switch its state from one to another to adjust itself to a new balance. These two states are called the up state and the down state, respectively. That is to say, the up and down transitions can be modulated by external stimulations. The ionic movement between inside and outside of the membrane may be the mechanism of the transitions. When sodium conductance increases to a certain level, it causes slight depolarization, activating the sodium channel with sodium move into cells, which increases the range of the polarization. In return, the larger the range of depolarization occurs, the more the sodium channels are activated and the more the sodium moves into cells. When it arrives to the peak of membrane potential, the sodium channel is inactivated and the h-like channel is activated, which leads to repolarization of the membrane potential. When the membrane potential reduces to about −45 mV, h-like channel is inactivated. At this point, a new balance between the outflow of potassium and the inflow of sodium begins. Namely, membrane potential stays in a stable state. According to the different extent of the

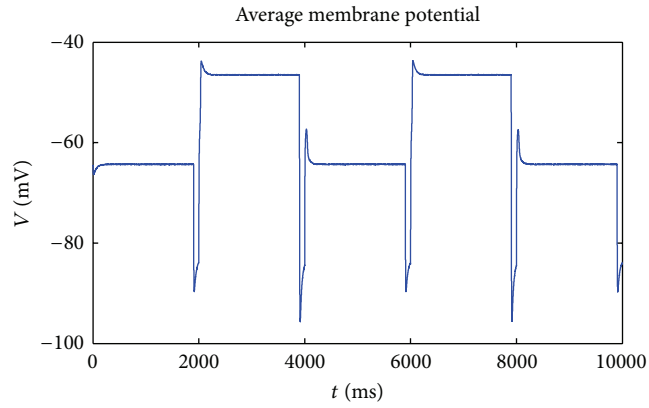

Figure 1: Add brief outward current pulses (lasts 0.1 s, every 2 s, 7.2 μA/cm^2).

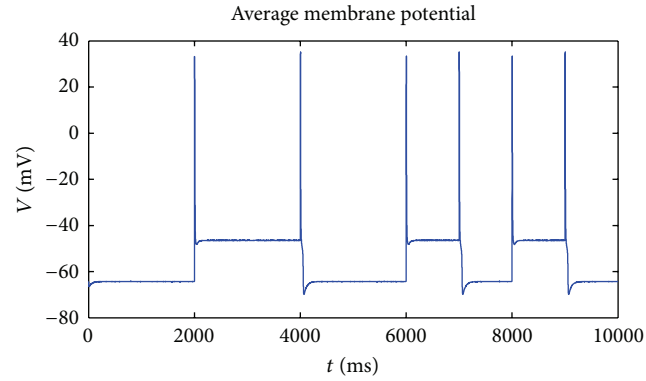

Figure 2: Increase the sodium conductance instantaneously (0.06 mS/cm^2 to 1.2 mS/cm^2).

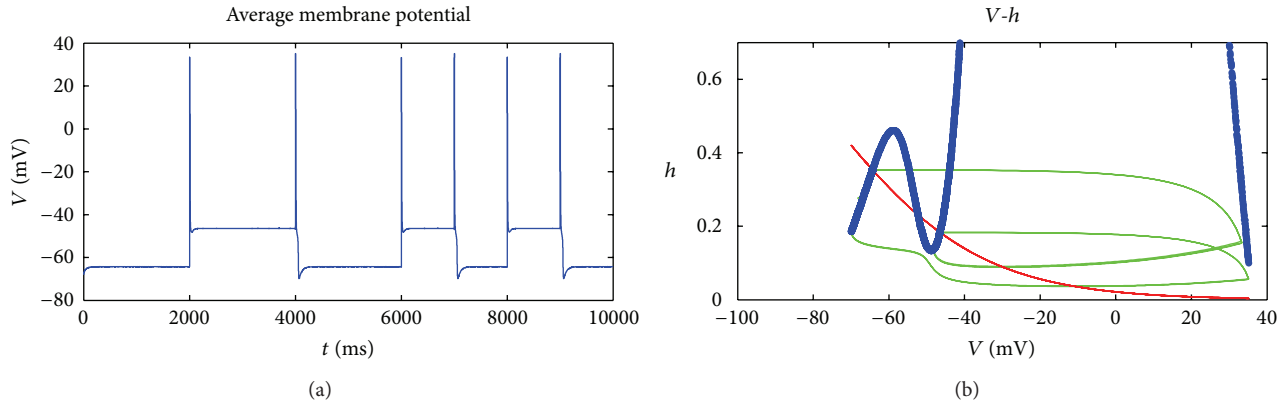

Figure 3: Average membrane potential V and h-V phase plane when $g_k = 0.1\,\text{mS/cm}^2$ and $g_{\text{Na}} = 1.2\,\text{mS/cm}^2$.

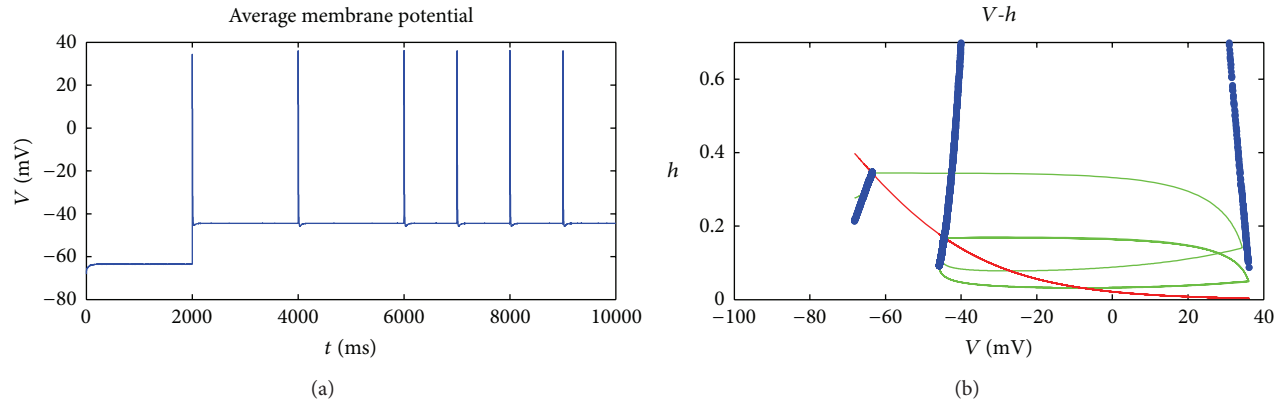

Figure 4: Average membrane potential V and h-V phase plane when $g_k = 0.09\,\text{mS/cm}^2$ and $g_{\text{Na}} = 1.2\,\text{mS/cm}^2$.

h-like channel inhibition, the membrane potential stays in the up state (about −45 mV) or the down state (about −65 mV).

3.2. Directivity. In the model of a single neuron, directivity of the transition is modulated by potassium conductance. We found that when $g_k = 0.1\,\text{mS/cm}^2$, membrane potential can transit both from the down state to the up state and from the up state to the down state, when $g_k = 0.09\,\text{mS/cm}^2$, membrane potential can only transit from the down state to the up state, and when $g_k = 0.105\,\text{mS/cm}^2$, membrane potential can only transit from the up state to the down state.

In the model of neural network of this paper, we also do research on the directivity. And we find that the changing of sodium conductance can modulate the directivity of the transitions as well as potassium conductance. Figures 3–7 describe different transition modes adjusted by different values of potassium conductance and sodium conductance. The tops of Figures 3–7 are average membrane potential V of the neural network, namely, up and down transitions, while the bottoms are phase plane for the mean of two kinds of dynamic variables h and V in the model, denoted by $V_{\text{mean}}, h_{\text{mean}}$. V_{mean} is average membrane potential of all the neurons in the network. h_{mean} is average inactivation rate of all the h-like channel in the network. The red solid line shows all the points that $h' = 0$, the blue dot line shows all the points that $V' = 0$, and the intersection of these two lines is stable point of the system. In other words, the two points are stable states of the network, and other points in the plane are unstable. That means, the system will stay in any one of the two stable points after a long run. The green solid line in the figure presents the transit process from one stable point to another.

Figure 3 shows that when $g_k = 0.1\,\text{mS/cm}^2$, membrane potential can transit from the down state to the up state by adding a stimulation that increase sodium conductance to $g_{\text{Na}} = 1.2\,\text{mS/cm}^2$ instantaneously. With the same stimulation, it also can transit from the up state to the down state. So the transitions are bidirectional on condition that $g_k = 0.1\,\text{mS/cm}^2$ and $g_{\text{Na}} = 1.2\,\text{mS/cm}^2$. The h-V phase plane further shows that the system transmits between the two stable states.

We can observe the changing of up and down transitions of the whole network by making some changes on the potassium conductance while keeping sodium conductance unchanged; namely, $g_{\text{Na}} = 1.2\,\text{mS/cm}^2$. The results are shown in Figures 4-5.

Figure 4 represents that when $g_k = 0.09\,\text{mS/cm}^2$, the average membrane potential can transit from the down state

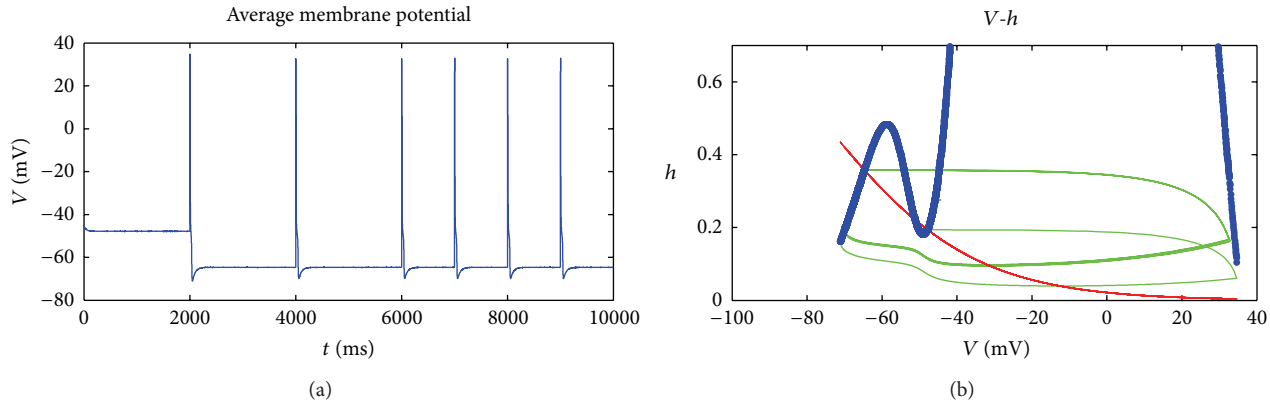

FIGURE 5: Average membrane potential V and h-V phase plane when $g_k = 0.105\,\text{mS/cm}^2$ and $g_{\text{Na}} = 1.2\,\text{mS/cm}^2$.

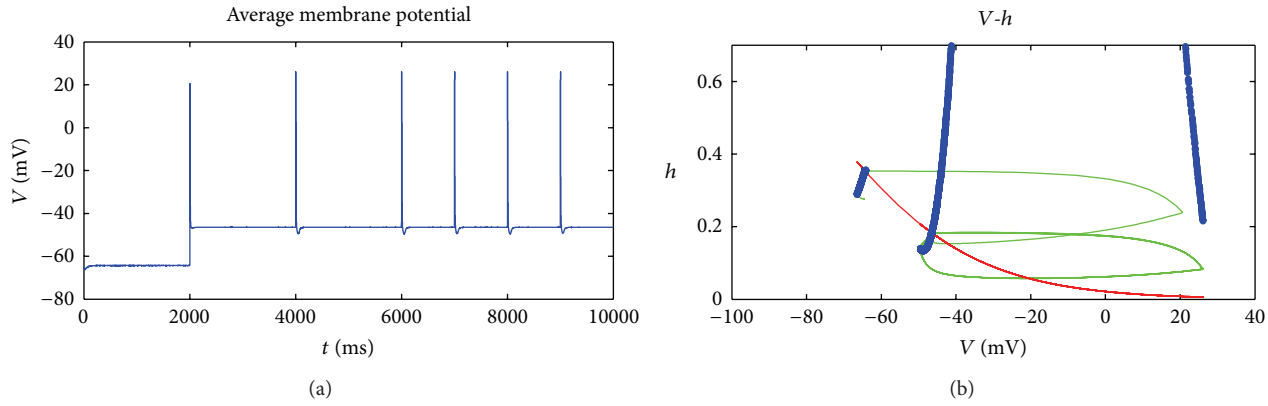

FIGURE 6: Average membrane potential V and h-V phase plane when $g_k = 0.1\,\text{mS/cm}^2$ and $g_{\text{Na}} = 0.8\,\text{mS/cm}^2$.

to the up state by adding a stimulation that increase sodium conductance instantaneously. But with the same stimulation, the average membrane potential always stays in the up state without any change. In other words, the transitions that are unidirectional vary from the down state to the up state in the circumstances that $g_k = 0.09\,\text{mS/cm}^2$. The h-V phase plane also shows that the system can only vary from the lower membrane potential stable point to higher one and then move around the higher one periodically.

Figure 5 reveals that when $g_k = 0.105\,\text{mS/cm}^2$, the average membrane potential can transit from the up state to the down state by adding a stimulation that increase sodium conductance instantaneously. However, with the same stimulation, the average membrane potential always stays in the down state without any change. In other words, the transitions that are unidirectional vary from the up state to the down state under the circumstances that $g_k = 0.105\,\text{mS/cm}^2$. The h-V phase plane also presents that the system can only vary from the higher membrane potential stable point to lower one and then move around the lower one periodically.

Accordingly, we can also observe the changing of up and down transitions of the whole network by making some changes on the sodium conductance while keeping potassium conductance unchanged; namely, $g_k = 0.1\,\text{mS/cm}^2$. The results are shown in Figures 6-7.

Figure 6 presents that when $g_{\text{Na}} = 0.8\,\text{mS/cm}^2$, the average membrane potential can transit from the down state to the up state by adding a stimulation that increase sodium conductance instantaneously. But with the same stimulation, the average membrane potential always stays in the up state without any change. In other words, the transitions that are unidirectional vary from the down state to the up state in the circumstances that $g_{\text{Na}} = 0.8\,\text{mS/cm}^2$. The h-V phase plane also shows that the system can only vary from the lower membrane potential stable point to higher one and then move around the higher one periodically.

Figure 7 reveals that when $g_{\text{Na}} = 2\,\text{mS/cm}^2$, the average membrane potential can transit from the up state to the down state by adding a stimulation that increase sodium conductance instantaneously. However, with the same stimulation, the average membrane potential always stays in the down state without any change. In other words, the transitions that are unidirectional vary from the up state to the down state under the circumstances that $g_{\text{Na}} = 2\,\text{mS/cm}^2$. The h-V phase plane also presents that the system can only vary from the higher membrane potential stable point to lower one and then move around the lower one periodically.

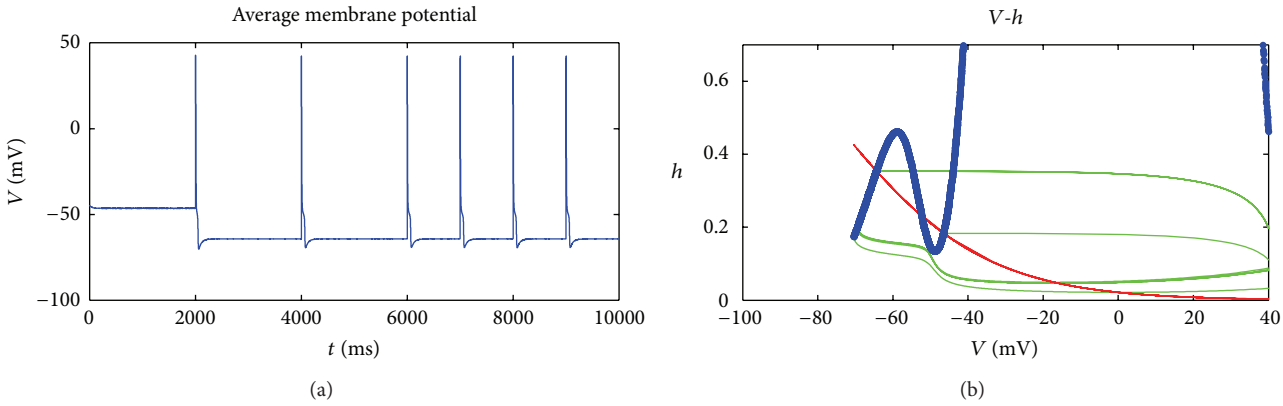

FIGURE 7: Average membrane potential V and h-V phase plane when $g_k = 0.1\ \text{mS/cm}^2$ and $g_{\text{Na}} = 2\ \text{mS/cm}^2$.

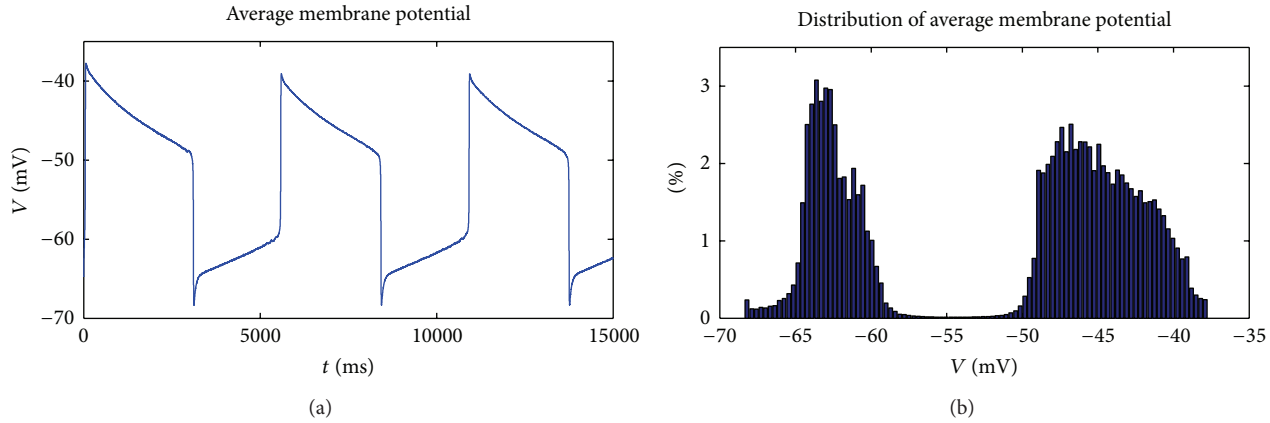

FIGURE 8: The average membrane potential of spontaneous transitions and its distribution.

The above results reveal that this dynamic model can well describe the bidirectional or unidirectional characteristic of up and down transitions of neural network when stimulated by certain stimulus. These results accord with the results of a single neuron model. Transitions in the network can be bidirection from the up state to the down one and vice versa. And also may be single direction from the up state to the down one, or only from down state to the up one according to the different level of conductance.

3.3. Spontaneity. In the discussion of bistability and direction of the model of a single neuron, we should introduce the input of synapse to generate the up and down transitions. Is a neuron still able to up and down transit, if there is no input of synapse? Virtually, *in vivo* or *in vitro* experiments of animals show that the potential of neural membrane can transit between up state and down state spontaneously and periodically. By increasing the variable of the inactivation of a potassium conductance rate in the original model, we can obtain the result that is identical to the experimental result.

In this paper, we introduce the dynamic variable b, the inactivation rate of potassium conductance of each neuron, to study the spontaneous transitions of neural networks.

The calculated results shown in Figure 8, are case without external stimuli showing that the average membrane potential transit spontaneously and periodically, while the distribution graph illustrates the distribution of the average membrane potential, a two-peak distribution, indicating the two stable state of up and down transitions of membrane potential.

By adding the interval of 1 or 2 seconds and lasting time of 4 ms stimuli on this spontaneous network model, the intensity of sodium conductance increases rapidly from $0.06\ \text{mS/cm}^2$ to $1.2\ \text{mS/cm}^2$; the computed results are shown in Figures 9–11.

The tops of Figures 9(a) and 10(a) show the changes of membrane potentials after adding stimuli, respectively, and the bottoms show the corresponding distributions of membrane potentials.

The simulating results of each neuron stimulated in the network are shown in Figure 9. Compared with the case without stimuli, after adding stimuli, the spontaneous transition of the whole network stops. Because of the disruption brought by the outer stimuli, the neurons, which should have been able to transit or transfer to another stable state

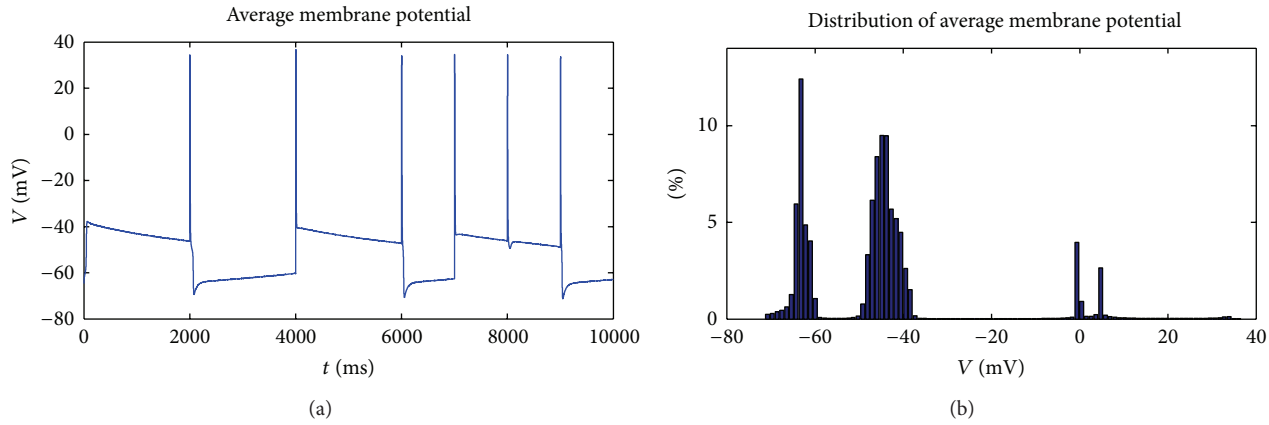

Figure 9: Adding stimuli on each neuron of the spontaneous model to rapidly increase the sodium conductance.

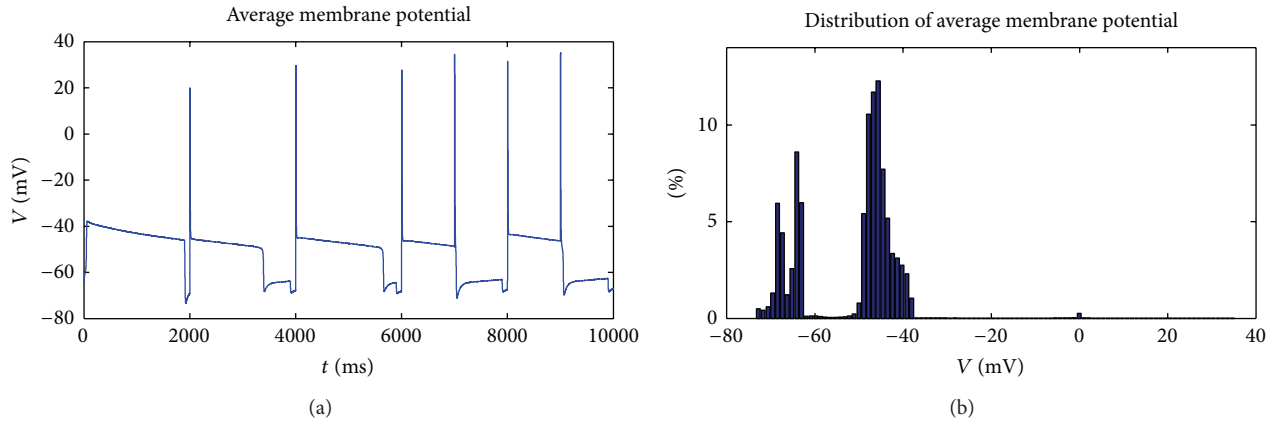

Figure 10: Adding stimuli on some neurons of the spontaneous model to rapidly increase the sodium conductance.

or to the original stable state of itself. However, for the whole network, the instant time for transition is different for each neuron, so the ability of network transition is not well obtained just by averaging the membrane potential. As a result, all the transitions we could see are caused by external stimuli, on the contrary, not all the stimuli can generate transition. For instance, the stimulus at 8 s fails to generate the state transition, which indicates that these transitions have something to do with the state of neural network. The network in a down state is more susceptible to external stimuli and transits, while in the up state it is not susceptible to external stimuli, since the network has a strong self-stability.

The simulating results of some neurons stimulated in the network are shown in Figure 10. Compared with the results in Figure 9, this network maintains its spontaneous transition ability; that is to say, it transits at the moment without any stimulus. On the other hand, the input of synapse is also able to let the state of the network transit and each stimulus leads to a state transition. Because there is coupling among the neurons, when a neuron is stimulated, such stimulus is certainly transmitted to everywhere else in the network by coupling, so as to change the state of the whole network.

To observe this transmission, Figure 11 shows the membrane potential of a neuron that is directly and indirectly stimulated, respectively. The results of the their potential are similar, since when a neuron is directly stimulated, its membrane potential changes correspondingly, and according to (8), this change transmits to others without delay. This is one of the aspects for our further improvement in the future.

The obtained results illustrate that this dynamical model dose can depict the phenomenon of the spontaneous and periodical transitions. By adjusting the number of the stimulated neurons, the situation of transition of a network differs. When every neuron is stimulated, the spontaneous transition of a network disappears, and the external stimuli play an important role on transitions. When a stimulus is added to a single neuron, besides the spontaneous transitions, the network is also able to respond to the external stimuli and transit. Such transmission between the coupling neurons is very fast and has no delay.

4. Conclusion

This paper constructs a dynamical network model that consists of 25 neurons which can show the up and down

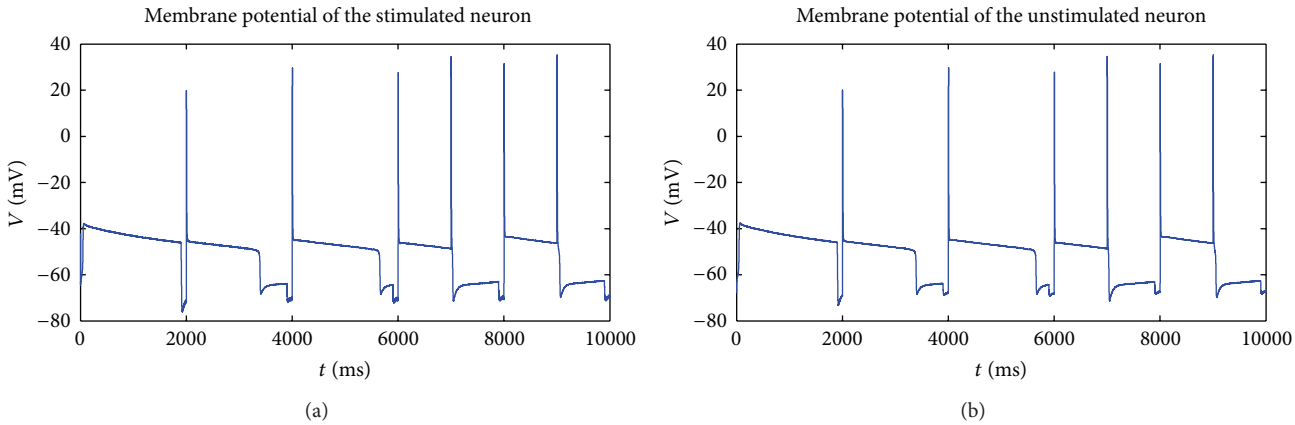

(a) (b)

Figure 11: Membrane potential of a neuron is stimulated directly or indirectly, respectively.

transitions, describing three characteristics, bistability, directivity, and spontaneity, of up and down transitions. The main conclusions are as follows.

(1) This dynamic model can describe the bistalility of up and down transitions of the neural network modulated by external stimulations and sodium conductance.

(2) The dynamic model can describe the bidirectional or unidirectional characteristic of up and down transitions of the neural network controlled by potassium conductance and potassium conductance.

(3) The dynamic model can describe periodic spontaneous transitions between the up and down states in absence of input and transitions will become complex when adding synaptic input.

The above conclusions are similar to the results of up and down transitions of a single neuron, since the characteristic of a single neuron's bursting dominates the real activities of the neural networks and the dynamic of a single neuron represents the behavior of the whole networks. In this paper, the study of up and down transitions is proposed as a preparation for the further scope of large-scale neural population and up and down transitions of network behaviors, so as to understand the effect of a single neuron's transitions on network behaviors under the condition of coupling of neural population as a sort of foundation of the research of the dynamical mechanism of neural spikes between a single neuron and the networks behaviors.

Acknowledgments

This work was supported by the Key Project of National Natural Science Foundation of China (NSFC) (11232005) and was supported by the Fundamental Research Funds for the Central Universities of China.

References

[1] J. Anderson, I. Lampl, I. Reichova, M. Carandini, and D. Ferster, "Stimulus dependence of two-state fluctuations of membrane potential in cat visual cortex," *Nature Neuroscience*, vol. 3, no. 6, pp. 617–621, 2000.

[2] I. Lampl, I. Reichova, and D. Ferster, "Synchronous membrane potential fluctuations in neurons of the cat visual cortex," *Neuron*, vol. 22, no. 2, pp. 361–374, 1999.

[3] M. Steriade, A. Nunez, and F. Amzica, "Intracellular analysis of relations between the slow (<1 Hz) neocortical oscillation and other sleep rhythms of the electroencephalogram," *The Journal of Neuroscience*, vol. 13, no. 8, pp. 3266–3283, 1993.

[4] C. C. H. Petersen, T. T. G. Hahn, M. Mehta, A. Grinvald, and B. Sakmann, "Interaction of sensory responses with spontaneous depolarization in layer 2/3 barrel cortex," *Proceedings of the National Academy of Sciences of the United States of America*, vol. 100, no. 23, pp. 13638–13643, 2003.

[5] N. Parga and L. F. Abbott, "Network model of spontaneous activity exhibiting synchronous transitions between up and down states," *Neuroscience*, vol. 1, no. 1, pp. 57–66, 2007.

[6] I. Timofeev, F. Grenier, and M. Steriade, "Disfacilitation and active inhibition in the neocortex during the natural sleep-wake cycle: an intracellular study," *Proceedings of the National Academy of Sciences of the United States of America*, vol. 98, no. 4, pp. 1924–1929, 2001.

[7] R. N. S. Sachdev, F. F. Ebner, and C. J. Wilson, "Effect of subthreshold up and down states on the whisker evoked response in somatosensory cortex," *Journal of Neurophysiology*, vol. 92, no. 6, pp. 3511–3521, 2004.

[8] B. Haider, A. Duque, A. R. Hasenstaub, Y. Yu, and D. A. McCormick, "Enhancement of visual responsiveness by spontaneous local network activity in vivo," *Journal of Neurophysiology*, vol. 97, no. 6, pp. 4186–4202, 2007.

[9] I. Timofeev, F. Grenier, M. Bazhenov, T. J. Sejnowski, and M. Steriade, "Origin of slow cortical oscillations in deafferented cortical slabs," *Cerebral Cortex*, vol. 10, no. 12, pp. 1185–1199, 2000.

[10] F. B. Vialatte, J. Dauwels, M. Maurice, Y. Yamaguchi, and A. Cichocki, "On the synchrony of steady state visual evoked potentials and oscillatory burst events," *Congnitive Neurodynamics*, vol. 3, no. 3, pp. 251–261, 2009.

[11] D. M. Alexander and C. van Leeuwen, "Mapping of contextual modulation in the population response of primary visual cortex," *Congnitive Neurodynamics*, vol. 4, no. 1, pp. 1–24, 2010.

[12] E. A. Stern, D. Jaeger, and C. J. Wilson, "Membrane potential synchrony of simultaneously recorded striatal spiny neurons in vivo," *Nature*, vol. 394, no. 6692, pp. 475–478, 1998.

[13] M. Brecht, M. Schneider, B. Sakmann, and T. W. Margrie, "Hisker movements evoked by stimulation of single pyramidal cells in rat motor cortex," *Nature*, vol. 427, pp. 704–710, 2004.

[14] R. Houweling and M. Brecht, "Behavioural report of single neuron stimulation in somatosensory cortex," *Nature*, vol. 451, no. 7174, pp. 65–68, 2008.

[15] C. T. Li, M. Poo, and Y. Dan, "Burst spiking of a single cortical neuron modifies global brain state," *Science*, vol. 324, no. 5927, pp. 643–646, 2009.

[16] R. Wang, Z. Zhang, and G. Chen, "Energy coding and energy functions for local activities of brain," *Neurocomputing*, vol. 73, no. 1–3, pp. 139–150, 2009.

[17] R. Wang, Z. Zhang, and G. Chen, "Energy function and energy evolution on neural population," *IEEE Transactions on Neural Networks*, vol. 19, no. 3, pp. 535–538, 2008.

[18] R. Wang and Z. Zhang, "Energy coding in biological neural network," *Cognitive Neurodynamics*, vol. 1, no. 3, pp. 203–212, 2007.

[19] Y. Liu, R. Wang, Z. Zhang, and X. Jiao, "Analysis on stability of neural network in the presence of inhibitory neurons," *Congnitive Neurodynamics*, vol. 4, no. 1, pp. 61–68, 2010.

[20] M. Steriade, D. McCormick, and T. Sejnowski, "Thalamocortical oscillations in the sleeping and aroused brain," *Science*, vol. 262, no. 5134, pp. 679–685, 1993.

[21] A. Destexhe, D. Contreras, and M. Steriade, "Spatiotemporal analysis of local field potentials and unit discharges in cat cerebral cortex during natural wake and sleep states," *The Journal of Neuroscience*, vol. 19, no. 11, pp. 4595–4608, 1999.

[22] D. Gervasoni, S.-C. Lin, S. Ribeiro, E. S. Soares, J. Pantoja, and M. A. L. Nicolelis, "Global forebrain dynamics predict rat behavioral states and their transitions," *The Journal of Neuroscience*, vol. 24, no. 49, pp. 11137–11147, 2004.

[23] J. Qu, R. Wang, Y. Du, and J. Cao, "Synchronization study ring-like and grid-like neuronal networks," *Congnitive Neurodynamics*, vol. 6, no. 1, pp. 21–31, 2012.

[24] X. Xu and R. Wang, "Neurodynamics of transitions between up and down states," . In press.

[25] M. Rubinov, O. Sporns, J.-P. Thivierge, and M. Breakspear, "Neurobiologically realistic determinants of self-organized criticality in networks of spiking neurons," *PLoS Computational Biology*, vol. 7, no. 6, Article ID e1002038, 2011.

[26] S. R. Williams, S. R. Christensen, G. J. Stuart, M. Häusser, and M. Membrane, "Potential bistability is controlled by the hyperpolarization activated current I(H) in rat cerebellar Purkinje neurons in vitro," *The Journal of Physiology*, vol. 1, part 2, no. 539, pp. 469–483, 2002.

[27] A. Roth and M. Häusser, "Compartmental models of rat cerebellar Purkinje cells based on simultaneous somatic and dendritic patchclamp recordings," *The Journal of Physiology*, vol. 535, pp. 445–472, 2001.

[28] R. Llinas and M. Sugimori, "Electrophysiological properties of in vitro Purkinje cell somata in mammalian cerebellar slices," *The Journal of Physiology*, vol. 305, pp. 171–195, 1980.

[29] R. Llinas and M. Sugimori, "Electrophysiological properties of in vitro Purkinje cell dendrites in mammalian cerebellar slices," *The Journal of Physiology*, vol. 305, pp. 197–213, 1980.

[30] Y. Loewenstein, S. Mahon, P. Chadderton et al., "Bistability of cerebellar Purkinje cells modulated by sensory stimulation," *Neuroscience*, vol. 8, no. 2, pp. 202–211, 2005.

Hindawi Publishing Corporation
Abstract and Applied Analysis
Volume 2013, Article ID 175068, 10 pages
http://dx.doi.org/10.1155/2013/175068

Research Article

Entrained Collective Rhythms of Multicellular Systems: Partial Impulsive Control Strategy

Lifei Chen,[1] Yonghui Sun,[2] and Qingli Yang[2]

[1] *School of Economics and Management, Nanjing University of Information Science & Technology, Nanjing 210044, China*
[2] *College of Energy and Electrical Engineering, Hohai University, Nanjing 210098, China*

Correspondence should be addressed to Lifei Chen; chenlifei2188@126.com

Received 26 September 2013; Accepted 13 November 2013

Academic Editor: Jinde Cao

This paper is concerned with the study of entrained collective rhythms of multicellular systems by using partial impulsive control strategy. The objective is to design an impulsive controller based on only those partially available cell states, so that the entrained collective rhythms are guaranteed for the multicellular systems with cell-to-cell communication mechanism. By using the newly developed impulsive integrodifferential inequality, the sufficient conditions are derived to achieve the entrained collective rhythms of multicellular systems. A synthetic multicellular system with simulation results is finally given to illustrate the usefulness of the developed results.

1. Introduction

Complex physiological rhythms are ubiquitous in living organisms, which are central to life, such as our daily cycle of waking and sleeping and the beating of our hearts. Collective rhythms are normally generated by thousands of divers clock cells which manage to function in a coherent oscillatory state [1, 2]. In fields ranging from circadian biology to endocrinology, however, it remains an exciting challenge to understand how collective rhythms emerge in multicellular structures [3–7].

Elucidating the collective dynamics of multicellular systems not only is essential for the understanding of the rhythmic phenomena of living organisms at both molecular and cellular levels but also has many potential applications in bioengineering areas. For example, in cancer chemotherapy, treatments could be based on the circadian rhythm of cell division [8]. Over the past decade or so, many researchers have paid a great deal of attention to study the collective dynamics of multicellular systems. For instance, in [9–12], the authors considered stability of genetic networks and neural networks. In [3], the authors pointed out that intercell signaling mechanism does lead to synchronous behavior across a population of cells. In [13], after making real-time analysis of the gene expression, the authors showed the synchronized rhythms of clock gene transcription across hundreds of neurons within the mammalian suprachiasmatic nucleus (SCN) in organotypic slice culture. In addition, based on the Lyapunov stability theory, the collective rhythms of multicellular systems were further studied in [14]. For the other relevant results, please see [15–17].

Although there are significant advances on elucidating the collective behaviors of biological organisms in recent years, the essential mechanisms from which the collective rhythms arise remain to be fully understood. It is well known that coupling among cells is not sufficient to achieve collective rhythms. In fact, the collective rhythms of multicellular systems are far away from being well understood and warrant further and insightful study.

On the other hand, experimental results have already shown that external stimuli play an important role in achieving the collective rhythms. In [18], physiological rhythms were induced by regular or periodic inputs occurring in the context of medical devices. In [19], an external voltage

was applied to enhance the synchronization of electronic synthetic genetic networks. In [20], it was shown that a specific collective behavior could be realized by changing the frequency and amplitude of the periodic stimuli. Another well-known example is that organisms usually display a circadian rhythm, where the key processes show a 24-hour periodicity entrained to the light-dark cycle [21]. In [22], the authors studied the rhythmic process of the circadian oscillators under the effect of the daily light-dark cycle. Furthermore, from the view of impulsive control systems, collective behaviors of coupled systems were investigated and some interesting results have been obtained in [23–27], and, for the other relevant results, please refer to [28–32] and the references therein.

However, in the above-mentioned results, one basic assumption is that the external stimuli are applied to all the cells in the community, that is very expensive or unrealistic in practice. Actually, in many practical medical cases, only partial specific cells could be detected and utilized. In these situations, the external stimuli are applied to only those cells in the community. To the best of our knowledge, there are few results in the open literature on the entrained collective rhythms of multicellular systems by applying impulsive control based on the partially available cell states.

This paper is to study the entrained collective rhythms of multicellular systems with only partially available cell states. By using the newly developed impulsive integrodifferential inequality, a new criterion is derived to ensure the entrained collective rhythms of multicellular systems. It is shown that when the spontaneous synchrony cannot be achieved, an appropriate periodic stimulus could achieve a collective rhythm even only with partially available cell states. It is noted that the proposed partial impulsive control method can be also easily extended to study other complex systems.

The rest of the paper is organized as follows. Section 2 formulates the problem of the entrained collective rhythms and provides some useful lemmas. Section 3 presents the main results for entrained collective rhythms of multicellular systems. A synthetic multicellular system will be employed to illustrate the effectiveness of the developed results in Section 4, which is followed by conclusions in Section 5.

2. Model Description and Problem Formulation

To make it easy for the readers, let us start from a single cell model of the form

$$\dot{x}(t) = -Ax(t) + f(x(t)), \tag{1}$$

where $x(t) \in \mathbb{R}^{n+}$ represents the concentrations of proteins, RNAs, and other chemical complexes, A is the positive diagonal matrix denoting the degradation and dilution rate, and $f(x(t))$ is the complex regulatory function, which usually is of the Michaelis-Menten or Hill form.

Remark 1. It is known that many biological models can be represented by (1), such as the Goodwin model [33] and the toggle switch [34]. Furthermore, the regulatory function $f(x)$ in model (1) is usually monotonically increasing or decreasing.

Without loss of generality, the regulatory function is always assumed to satisfy the following assumption.

Assumption 2. The regulatory function $f(x)$ in (1) satisfies

$$\left(f_i(a) - f_i(b)\right)\left[f_i(a) - f_i(b) - l_i(a-b)\right] \le 0, \tag{2}$$

for all $a, b \in R$, $a \neq b$, and $l_i > 0$.

Consider multicellular systems with cell-to-cell communication mechanism described as follows:

$$\begin{aligned}\dot{x}_i(t) = {} & -Ax_i(t) + f\left(x_i(t)\right) \\ & + c\sum_{j=1}^{N} G_{ij}\Gamma x_j(t), \quad i = 1, \ldots, N,\end{aligned} \tag{3}$$

where $x_i(t) \in \mathbb{R}^{n+}$ is the state of the ith cell, denoting the concentrations of chemical complexes in this cell, and N is the total cell number of the entire community. The third term in model (3) describes the capability of cells to communicate with each other in order to coordinate the behavior of the entire community. $G = (G_{ij})_{N\times N}$ is the coupling structure matrix that represents the communications between different cells, and Γ is the inner coupling structure that represents the connections of different chemical complexes in one cell. G satisfies the diffusive coupling condition

$$\begin{aligned}& G_{ij} \ge 0, \quad \text{for } i \neq j, \\ & G_{ii} = -\sum_{j=1, j\neq i}^{N} G_{ij}, \quad i = 1, 2, \ldots, N.\end{aligned} \tag{4}$$

It can be noted that such coupling is biologically plausible in many biological systems, such as the quorum sensing mechanism in bacteria [2, 35].

Suppose only l cell states in the community are measurable for the multicellular systems (3). Consider the following linear impulsive controller based on those l measurable cell states:

$$u_i = \sum_{k=1}^{\infty} E_{ik}\left(x_i - x\right)\delta\left(t - t_k\right), \quad i = 1, 2, \ldots, l,\ k \in \mathbb{N}, \tag{5}$$

where x is the state of the isolated cell described in (1), l is the number of the measurable cell states, E_{ik} is the gain matrix, and $\delta(t - t_k)$ is the Dirac impulse function with discontinuity points $t_1 < t_2 < \cdots < t_k < \cdots$, $\lim_{k\to\infty} t_k = \infty$.

Then the impulsive-controlled multicellular systems with partial states can be described by the following impulsive differential equation:

$$\begin{aligned}
\dot{x}_i(t) &= -Ax_i(t) + f\left(x_i(t)\right) \\
&\quad + c\sum_{j=1}^{N} G_{ij}\Gamma x_j(t), \quad t \in \left(t_{k-1}, t_k\right], \\
\Delta x_i\left(t_k\right) &= x_i\left(t_k^+\right) - x_i\left(t_k^-\right) = E_{ik}\left(x_i - x\right), \\
&\quad k = 1, 2, \ldots, \quad t = t_k, \\
&\quad i = 1, \ldots, l, \\
\dot{x}_i(t) &= -Ax_i(t) + f\left(x_i(t)\right) \\
&\quad + c\sum_{j=1}^{N} G_{ij}\Gamma x_j(t), \quad i = l+1, \ldots, N.
\end{aligned} \tag{6}$$

Defining $e_i(t) = x_i(t) - x(t)$, one can obtain the following error system:

$$\begin{aligned}
\dot{e}_i(t) &= -Ae_i(t) + f\left(x_i(t)\right) - f\left(x(t)\right) \\
&\quad + c\sum_{j=1}^{N} G_{ij}\Gamma e_j(t), \quad t \in \left(t_{k-1}, t_k\right], \\
e_i\left(t_k^+\right) &= \left(I + E_{ik}\right)e_i\left(t_k\right), \quad k = 1, 2, \ldots, \\
&\quad t = t_k, \quad i = 1, \ldots, l, \\
\dot{e}_i(t) &= -Ae_i(t) + f\left(x_i(t)\right) - f\left(x(t)\right) \\
&\quad + c\sum_{j=1}^{N} G_{ij}\Gamma e_j(t), \quad i = l+1, \ldots, N.
\end{aligned} \tag{7}$$

Then the problem of entrained collective rhythms is to design the partial impulsive controller (5) such that the stability of the error system (7) is guaranteed. Before presenting the main results, some useful lemmas are introduced in advance.

Lemma 3 (see [36]). *If $P \in \mathbb{R}^{n\times n}$ is a positive definite matrix and $Q \in \mathbb{R}^{n\times n}$ is a symmetric matrix, then*

$$\begin{aligned}
&\lambda_{\min}\left(P^{-1}Q\right)x^{\mathrm{T}}Px \le x^{\mathrm{T}}Qx \\
&\quad \le \lambda_{\max}\left(P^{-1}Q\right)x^{\mathrm{T}}Px, \quad \forall x \in \mathbb{R}^n,
\end{aligned} \tag{8}$$

where $\lambda_{\min}(\cdot)$ and $\lambda_{\max}(\cdot)$ are the minimum and maximum eigenvalues of the matrix, respectively.

Lemma 4. *For positive scalars $\delta > 0$, $\mu > 0$, and $\rho > 0$, if $u(t)$ satisfies*

$$\begin{aligned}
\dot{u}(t) &\le h\left(t, u(t)\right) + \delta\int_0^t e^{-\rho(t-s)}u(s)\,ds, \quad t \ne t_k, \\
u\left(t_k^+\right) &\le \mu u\left(t_k\right), \quad t = t_k, \\
u(0) &\le u_0,
\end{aligned} \tag{9}$$

where $h(t, u(t))$ is a continuous function, then one has $u(t) \le u_\epsilon(t)$, $t \ge 0$ for $\epsilon \ge 0$, where $u_\epsilon(t)$ is the solution to the following impulsive integrodifferential equation:

$$\begin{aligned}
\dot{u}_\epsilon(t) &= h\left(t, u_\epsilon(t)\right) + \delta\int_0^t e^{-\rho(t-s)}u_\epsilon(s)\,ds + \epsilon, \quad t \ne t_k, \\
u_\epsilon\left(t_k^+\right) &= \mu u_\epsilon\left(t_k\right), \quad t = t_k, \\
u_\epsilon(0) &= u_0.
\end{aligned} \tag{10}$$

Proof. Firstly, we prove

$$u(t) \le u_\epsilon(t), \quad t \in \left(0, t_1\right]. \tag{11}$$

If argument (11) is not right, then there exists $\tilde{t} \in (0, t_1)$ such that

$$u\left(\tilde{t}\right) > u_\epsilon\left(\tilde{t}\right). \tag{12}$$

Considering the continuity of $u(t)$, $u_\epsilon(t)$ on $(0, t_1]$, there must exist $t^* \in (0, \tilde{t})$ such that

$$\begin{aligned}
u\left(t^*\right) &= u_\epsilon\left(t^*\right), \qquad \dot{u}\left(t^*\right) \ge \dot{u}_\epsilon\left(t^*\right), \\
u(t) &\le u_\epsilon(t), \quad \forall t \le t^*;
\end{aligned} \tag{13}$$

then it yields

$$\begin{aligned}
\dot{u}\left(t^*\right) &\le h\left(t^*, u\left(t^*\right)\right) + \delta\int_0^{t^*} e^{-\rho(t^*-s)}u(s)\,ds \\
&< h\left(t^*, u_\epsilon\left(t^*\right)\right) + \delta\int_0^{t^*} e^{-\rho(t^*-s)}u_\epsilon(s)\,ds + \epsilon \\
&= \dot{u}_\epsilon\left(t^*\right),
\end{aligned} \tag{14}$$

which contradicts the condition $\dot{u}(t^*) \ge \dot{u}_\epsilon(t^*)$, so (11) holds.

Suppose $u(t) \le u_\epsilon(t)$, for all $t \in (0, t_k]$; then by $u(t_k^+) = \mu u(t_k) \le \mu u_\epsilon(t_k) = u_\epsilon(t_k^+)$, similarly, one has $u(t) \le u_\epsilon(t)$, for all $t \in (t_k, t_{k+1}]$. By using the mathematical induction method, one can conclude $u(t) \le u_\epsilon(t)$, for all $t \in (0, t_k]$ for any positive integer k. The proof is thus complete. □

Lemma 5 (Grownwall-Bellman Inequality [37]). *Let $\alpha(t)$ be a real value continuous function and $\beta(t)$ a nonnegative continuous function on $[a, b]$. If a continuous function $u(t)$ has the property that*

$$u(t) \le \alpha(t) + \int_a^t \beta(s)\,u(s)\,ds, \quad a \le t \le b, \tag{15}$$

then on $[a, b]$ one has

$$u(t) \le \alpha(t) + \int_a^t \alpha(s)\,\beta(s)\exp\left(\int_s^t \beta(r)\,dr\right)ds. \tag{16}$$

Definition 6. The multicellular system (6) is said to achieve collective rhythms with the designed partial impulsive controller, if there exist scalars $\rho > 0$ and $M > 0$ such that

$$\lim_{t\to\infty}\|X(t)\|^2 \le Me^{-\rho t}\|X(0)\|^2, \tag{17}$$

where $X(t) = [x_1^{\mathrm{T}} - x^{\mathrm{T}}, \ldots, x_N^{\mathrm{T}} - x^{\mathrm{T}}]^{\mathrm{T}}$ and $X(0)$ is the initial condition.

3. Main Results

In this section, by using the proposed impulsive integrodifferential inequality, a sufficient condition guaranteeing the entrained collective rhythms of multicellular systems is derived.

Theorem 7. *For a given scalar $\mu \in (0,1)$, if there exist matrices $P_i > 0$, $i = 1,2,\ldots,l$, $Q_i > 0$, $i = l+1,\ldots,N$, scalars $\lambda_i > 0$, $\mu_i > 0$, $i = 1,2,\ldots,l$, $\eta_i > 0$, $i = l+1,\ldots,N$, and positive scalars ϵ_1, ϵ_2, δ_1, and δ_2 such that*

$$\left(-A^T P_i - P_i A\right) + \lambda_{\max}\left(P_i\right)\left(\epsilon_1 I + \epsilon_1^{-1} L^T L + c\delta_1 \sum_{j=1}^{N} \left|G_{ij}\right|\right) + c\delta_1^{-1} \sum_{j=1}^{l} \lambda_{\max}\left(P_j\right)\left|G_{ji}\right| \Gamma^T \Gamma \le \lambda_i P_i, \tag{18}$$

$$\left(I + E_{ik}\right)^T P_i \left(I + E_{ik}\right) \le \mu_i P_i, \tag{19}$$

for $i = 1,\ldots,l$, and

$$\left(-A^T Q_i - Q_i A\right) + \lambda_{\max}\left(Q_i\right)\left(\epsilon_2 I + \epsilon_2^{-1} L^T L + c\delta_2 \sum_{j=1}^{N} \left|G_{ij}\right|\right) + c\delta_2^{-1} \sum_{j=l+1}^{N} \lambda_{\max}\left(Q_j\right)\left|G_{ji}\right| \Gamma^T \Gamma \le -\eta_i Q_i, \tag{20}$$

for $i = l+1,\ldots,N$, and, for any impulsive time sequence $\{t_k\}$ satisfying

$$\delta := \sup_k \{t_{k+1} - t_k\} < \frac{\ln\left(1/\mu\right)}{\eta + \lambda + (\beta\gamma)/(\eta\mu)}, \tag{21}$$

for $k = 0,1,2,\ldots$, where $\mu = \max(\mu_i)$, $\lambda = \max(\lambda_i)$, $i = 1,\ldots,l$, and $\eta = \min(\eta_i)$, $i = l+1,\ldots,N$, then the entrained collective rhythms of multicellular systems (6) *are achieved.*

Proof. Consider the following Lyapunov function:

$$V(t) = V_1(t) + V_2(t), \tag{22}$$

where

$$V_1(t) := \sum_{i=1}^{l} e_i^{\mathrm{T}}(t) P_i e_i(t), \qquad V_2(t) := \sum_{i=l+1}^{N} e_i^{\mathrm{T}}(t) Q_i e_i(t), \tag{23}$$

where P_i, $i = 1,2,\ldots,l$ and Q_i, $i = l+1,\ldots,N$ are positive definite matrices to be determined.

For any $t \in (t_k, t_{k+1}]$, $k \in \mathbb{N}$, taking the Dini derivative along the trajectories of (7), we have

$$\begin{aligned} D^+V_1(t) &= \sum_{i=1}^{l}\left(\dot{e}_i^{\mathrm{T}}(t) P_i e_i(t) + e_i^{\mathrm{T}}(t) P_i \dot{e}_i(t)\right) \\ &= \sum_{i=1}^{l}\Bigg(e_i^{\mathrm{T}}(t)\left(-A^{\mathrm{T}}P_i - P_i A\right)e_i(t) \\ &\qquad + 2e_i^{\mathrm{T}}(t) P_i\left(f\left(x_i(t)\right) - f\left(x(t)\right)\right) \\ &\qquad + 2c\sum_{j=1}^{N} e_i^{\mathrm{T}}(t) P_i G_{ij} \Gamma e_j(t)\Bigg). \end{aligned} \tag{24}$$

It follows from Assumption 2 that

$$\begin{aligned} &2e_i^{\mathrm{T}}(t) P_i\left(f\left(x_i(t)\right) - f\left(x(t)\right)\right) \\ &\quad \le \lambda_{\max}\left(P_i\right)\left(\epsilon_1 e_i^{\mathrm{T}}(t) e_i(t) + \epsilon_1^{-1} e_i^{\mathrm{T}}(t) L^{\mathrm{T}} L e_i(t)\right), \\ &2c\sum_{j=1}^{N} e_i^{\mathrm{T}}(t) P_i G_{ij} \Gamma e_j(t) \\ &\quad \le c\lambda_{\max}\left(P_i\right)\sum_{j=1}^{N}\left|G_{ij}\right| \\ &\qquad \times\left(\delta_1 e_i^{\mathrm{T}}(t) e_i(t) + \delta_1^{-1} e_j^{\mathrm{T}}(t) \Gamma^{\mathrm{T}}\Gamma e_j(t)\right), \end{aligned} \tag{25}$$

where $\epsilon_1 > 0$, $\delta_1 > 0$ and $L = \mathrm{diag}(l_1,\ldots,l_n)$. One also has

$$\begin{aligned} &c\delta_1^{-1}\sum_{i=1}^{l}\sum_{j=1}^{N}\lambda_{\max}\left(P_i\right)\left|G_{ij}\right| e_j^{\mathrm{T}}(t) \Gamma^{\mathrm{T}}\Gamma e_j(t) \\ &\quad = c\delta_1^{-1}\sum_{i=1}^{N}\sum_{j=1}^{l}\lambda_{\max}\left(P_j\right)\left|G_{ji}\right| e_i^{\mathrm{T}}(t) \Gamma^{\mathrm{T}}\Gamma e_i(t) \\ &\quad = c\delta_1^{-1}\sum_{i=1}^{l}\sum_{j=1}^{l}\lambda_{\max}\left(P_j\right)\left|G_{ji}\right| e_i^{\mathrm{T}}(t) \Gamma^{\mathrm{T}}\Gamma e_i(t) \\ &\qquad + c\delta_1^{-1}\sum_{i=l+1}^{N}\sum_{j=1}^{l}\lambda_{\max}\left(P_j\right)\left|G_{ji}\right| e_i^{\mathrm{T}}(t) \Gamma^{\mathrm{T}}\Gamma e_i(t). \end{aligned} \tag{26}$$

Substituting (25)–(26) into (24) yields

$$\begin{aligned}
D^+V_1(t) \le & \sum_{i=1}^{l}\Bigg(e_i^{\mathrm{T}}(t)\left(-A^{\mathrm{T}}P_i - P_iA\right)e_i(t) + \lambda_{\max}\left(P_i\right)e_i^{\mathrm{T}}(t) \\
& \times\left(\epsilon_1 I + \epsilon_1^{-1}L^{\mathrm{T}}L + c\delta_1\sum_{j=1}^{N}\left|G_{ij}\right|\right)e_i(t) \\
& + c\delta_1^{-1}\sum_{i=1}^{l}\sum_{j=1}^{l}\lambda_{\max}\left(P_j\right)\left|G_{ji}\right|e_i^{\mathrm{T}}(t)\,\Gamma^{\mathrm{T}}\Gamma e_i(t)\Bigg) \\
& + c\delta_1^{-1}\sum_{i=l+1}^{N}\sum_{j=1}^{l}\lambda_{\max}\left(P_j\right)\left|G_{ji}\right|e_i^{\mathrm{T}}(t)\,\Gamma^{\mathrm{T}}\Gamma e_i(t) \\
= & \sum_{i=1}^{l}e_i^{\mathrm{T}}(t)\Bigg(\left(-A^{\mathrm{T}}P_i - P_iA\right) + \lambda_{\max}\left(P_i\right) \\
& \times\left(\epsilon_1 I + \epsilon_1^{-1}L^{\mathrm{T}}L + c\delta_1\sum_{j=1}^{N}\left|G_{ij}\right|\right) \\
& + c\delta_1^{-1}\sum_{j=1}^{l}\lambda_{\max}\left(P_j\right)\left|G_{ji}\right|\Gamma^{\mathrm{T}}\Gamma\Bigg)e_i(t) \\
& + c\delta_1^{-1}\sum_{i=l+1}^{N}\sum_{j=1}^{l}\lambda_{\max}\left(P_j\right)\left|G_{ji}\right|e_i^{\mathrm{T}}(t)\,\Gamma^{\mathrm{T}}\Gamma e_i(t).
\end{aligned} \tag{27}$$

Define $\beta_i = c\delta_1^{-1}\sum_{j=1}^{l}\lambda_{\max}(P_j)|G_{ji}|$. Then it follows from condition (18) and Lemma 3 that

$$\begin{aligned}
D^+V_1(t) &\le \sum_{i=1}^{l}e_i^{\mathrm{T}}(t)\,\lambda_i P_i e_i(t) + \sum_{i=l+1}^{N}\beta_i e_i^{\mathrm{T}}(t)\,e_i(t) \\
&\le \lambda V_1(t) + \beta V_2(t),
\end{aligned} \tag{28}$$

where $\lambda = \max(\lambda_i)$ and $\beta = \max(\beta_i\lambda_{\max}(Q_i^{-1}))$.

Furthermore, for any $t \ge 0$, one can also get

$$\begin{aligned}
D^+V_2(t) = & \sum_{i=l+1}^{N}\left(\dot{e}_i^{\mathrm{T}}(t)\,Q_i e_i(t) + e_i^{\mathrm{T}}(t)\,Q_i\dot{e}_i(t)\right) \\
= & \sum_{i=l+1}^{N}\Bigg(e_i^{\mathrm{T}}(t)\left(-A^{\mathrm{T}}Q_i - Q_iA\right)e_i(t) \\
& + 2e_i^{\mathrm{T}}(t)\,Q_i\left(f\left(x_i(t)\right) - f\left(x(t)\right)\right) \\
& + 2c\sum_{j=1}^{N}e_i^{\mathrm{T}}(t)\,Q_iG_{ij}\Gamma e_j(t)\Bigg) \\
\le & \sum_{i=l+1}^{N}\Bigg(e_i^{\mathrm{T}}(t)\left(-A^{\mathrm{T}}Q_i - Q_iA\right)e_i(t) \\
& + \lambda_{\max}\left(Q_i\right)e_i^{\mathrm{T}}(t) \\
& \times\left(\epsilon_2 I + \epsilon_2^{-1}L^{\mathrm{T}}L + c\delta_2\sum_{j=1}^{N}\left|G_{ij}\right|\right)e_i(t) \\
& + c\delta_2^{-1}\sum_{j=l+1}^{N}\lambda_{\max}\left(Q_j\right)\left|G_{ji}\right|e_i^{\mathrm{T}}(t)\,\Gamma^{\mathrm{T}}\Gamma e_i(t)\Bigg) \\
& + c\delta_2^{-1}\sum_{i=1}^{l}\sum_{j=l+1}^{N}\lambda_{\max}\left(Q_j\right)\left|G_{ji}\right|e_i^{\mathrm{T}}(t)\,\Gamma^{\mathrm{T}}\Gamma e_i(t) \\
= & \sum_{i=l+1}^{N}e_i^{\mathrm{T}}(t) \\
& \times\Bigg(\left(-A^{\mathrm{T}}Q_i - Q_iA\right) + \lambda_{\max}\left(Q_i\right) \\
& \times\left(\epsilon_2 I + \epsilon_2^{-1}L^{\mathrm{T}}L + c\delta_2\sum_{j=1}^{N}\left|G_{ij}\right|\right) \\
& + c\delta_2^{-1}\sum_{j=l+1}^{N}\lambda_{\max}\left(Q_j\right)\left|G_{ji}\right|\Gamma^{\mathrm{T}}\Gamma\Bigg)e_i(t) \\
& + c\delta_2^{-1}\sum_{i=1}^{l}\sum_{j=l+1}^{N}\lambda_{\max}\left(Q_j\right)\left|G_{ji}\right|e_i^{\mathrm{T}}(t)\,\Gamma^{\mathrm{T}}\Gamma e_i(t),
\end{aligned} \tag{29}$$

where $\epsilon_2 > 0$, $\delta_2 > 0$.

Defining $\gamma_i = c\delta_2^{-1}\sum_{j=l+1}^{N}\lambda_{\max}(Q_j)|G_{ji}|$, it follows from (20) and (29) that

$$\begin{aligned}
D^+V_2(t) \le & -\sum_{i=l+1}^{N}\eta_i e_i^{\mathrm{T}}(t)\,Q_i e_i(t) \\
& + \sum_{i=1}^{l}\gamma_i e_i^{\mathrm{T}}(t)\,e_i(t) \\
\le & -\eta V_2(t) + \gamma V_1(t),
\end{aligned} \tag{30}$$

where $\eta = \min(\eta_i)$ and $\gamma = \max(\gamma_i\lambda_{\max}(P_i^{-1}))$, which implies

$$V_2(t) \le e^{-\eta t}V_2(0) + \gamma\int_0^t e^{-\eta(t-\alpha)}V_1(\alpha)\,d\alpha. \tag{31}$$

Then substituting (31) into (28) yields

$$\begin{aligned}
D^+V_1(t) \le & \lambda V_1(t) + \beta e^{-\eta t}V_2(0) \\
& + \beta\gamma\int_0^t e^{-\eta(t-\alpha)}V_1(\alpha)\,d\alpha, \quad t \in \left(t_k, t_{k+1}\right].
\end{aligned} \tag{32}$$

On the other hand, when $t = t_k^+$, it follows from (19) that

$$\begin{aligned} V_1(t_k^+) &= \sum_{i=1}^{l} e_i^{\mathrm{T}}(t_k)(I+E_{ik})^{\mathrm{T}} P_i (I+E_{ik}) e_i(t_k) \\ &\le \sum_{i=1}^{l} e_i^{\mathrm{T}}(t_k)\mu_i P_i e_i(t_k) \\ &\le \mu V_1(t_k), \end{aligned} \tag{33}$$

where $\mu = \max(\mu_i)$, $i = 1, \ldots, l$.

For any scalar $\epsilon > 0$, define the following impulsive integrodifferential equation:

$$\begin{aligned} \dot{V}_\epsilon(t) &= \lambda V_\epsilon(t) + \beta e^{-\eta t} V_2(0) \\ &\quad + \beta\gamma \int_0^t e^{-\eta(t-\alpha)} V_\epsilon(\alpha)\, d\alpha \\ &\quad + \epsilon, \quad t \in (t_{k-1}, t_k], \\ V_\epsilon(t_k^+) &= \mu V_\epsilon(t_k), \quad t = t_k, \\ V_\epsilon(0) &= V_1(0). \end{aligned} \tag{34}$$

It then follows from Lemma 4 that $V_1(t) \le V_\epsilon(t)$, for all $t \in (0, t_k]$.

The solution to (34) can be expressed as follows:

$$\begin{aligned} V_\epsilon(t) &= W(t,0) V_\epsilon(0) + \int_0^t W(t,s) \\ &\quad \times \left\{ \epsilon + \beta e^{-\eta s} V_2(0) \right. \\ &\quad \left. + \beta\gamma \int_0^s e^{-\eta(s-\alpha)} V_\epsilon(\alpha)\, d\alpha \right\} ds, \end{aligned} \tag{35}$$

where $W(t,s)\,(t,s \ge 0)$ is the Cauchy matrix of the linear impulsive system

$$\begin{aligned} \dot{u}(t) &= \lambda u(t), \quad t \in (t_{k-1}, t_k], \\ u(t_k^+) &= \mu u(t_k), \quad k = 1, 2, \ldots, \ t = t_k. \end{aligned} \tag{36}$$

Furthermore, noting that $\mu < 1$ and $t_{k+1} - t_k \le \delta$, it follows from condition (21) that $W(t,s)$ could be estimated as

$$\begin{aligned} W(t,s) &= e^{\lambda(t-s)} \prod_{s<t_k\le t} \mu \le e^{\lambda(t-s)} \mu^{((t-s)/\delta)-1} \\ &= \frac{1}{\mu} e^{-((1/\delta)\ln(1/\mu)-\lambda)(t-s)}. \end{aligned} \tag{37}$$

Defining $\widehat{\lambda} = (1/\delta)\ln(1/\mu) - \lambda$, one has

$$\begin{aligned} V_\epsilon(t) &\le \frac{1}{\mu} e^{-\widehat{\lambda} t} V_\epsilon(0) \\ &\quad + \frac{1}{\mu} \int_0^t e^{-\widehat{\lambda}(t-s)} \left(\epsilon + \beta e^{-\eta s} V_2(0)\right) ds \\ &\quad + \frac{\beta\gamma}{\mu} \int_0^t e^{-\widehat{\lambda}(t-s)} \int_0^s e^{-\eta(s-\alpha)} V_\epsilon(\alpha)\, d\alpha\, ds \\ &= \frac{1}{\mu} e^{-\widehat{\lambda} t} V_\epsilon(0) + \frac{\epsilon}{\mu\widehat{\lambda}} \left(1 - e^{-\widehat{\lambda} t}\right) \\ &\quad + \frac{\beta V_2(0)}{\mu\left(\widehat{\lambda} - \eta\right)} \left(e^{-\eta t} - e^{-\widehat{\lambda} t}\right) \\ &\quad + \frac{\beta\gamma}{\mu} \int_0^t \int_\alpha^t e^{-\widehat{\lambda}(t-s)} e^{-\eta(s-\alpha)} V_\epsilon(\alpha)\, ds\, d\alpha \\ &= \frac{1}{\mu} e^{-\widehat{\lambda} t} V_\epsilon(0) + \frac{\epsilon}{\mu\widehat{\lambda}} \left(1 - e^{-\widehat{\lambda} t}\right) \\ &\quad + \frac{\beta V_2(0)}{\mu\left(\widehat{\lambda} - \eta\right)} \left(e^{-\eta t} - e^{-\widehat{\lambda} t}\right) + \frac{\beta\gamma}{\mu\left(\widehat{\lambda} - \eta\right)} \\ &\quad \times \int_0^t \left(e^{-\eta(t-\alpha)} - e^{-\widehat{\lambda}(t-\alpha)}\right) V_\epsilon(\alpha)\, d\alpha. \end{aligned} \tag{38}$$

Noting from condition (21) that $\widehat{\lambda} > \eta$, then one gets

$$\begin{aligned} V_\epsilon(t) &\le \frac{1}{\mu} e^{-\widehat{\lambda} t} V_\epsilon(0) + \frac{\epsilon}{\mu\widehat{\lambda}} + \frac{\beta V_2(0)}{\mu\left(\widehat{\lambda} - \eta\right)} e^{-\eta t} \\ &\quad + \frac{\beta\gamma}{\mu\left(\widehat{\lambda} - \eta\right)} \int_0^t e^{-\eta(t-\alpha)} V_\epsilon(\alpha)\, d\alpha. \end{aligned} \tag{39}$$

Defining $u(t) = e^{\eta t} V_\epsilon(t)$, $\alpha(t) = (V_\epsilon(0)/\mu) + (\beta V_2(0)/\mu(\widehat{\lambda} - \eta)) + (\epsilon/\mu\widehat{\lambda}) e^{\eta t}$, and $\beta(t) = (\beta\gamma/\mu(\widehat{\lambda} - \eta)) = \rho$, one obtains

$$u(t) \le \alpha(t) + \int_0^t \beta(s)\, u(s)\, ds, \quad t \ge 0. \tag{40}$$

Then by using Lemma 5, it is easy to get

$$u(t) \le \left(\frac{V_\epsilon(0)}{\mu} + \frac{\beta V_2(0)}{\mu\left(\widehat{\lambda} - \eta\right)}\right) e^{\rho t} + \frac{\epsilon\eta}{\mu\widehat{\lambda}\,(\eta - \rho)} e^{\eta t}, \quad t \ge 0, \tag{41}$$

which implies

$$V_\epsilon(t) \le \left(\frac{V_\epsilon(0)}{\mu} + \frac{\beta V_2(0)}{\mu\left(\widehat{\lambda} - \eta\right)}\right) e^{-(\eta-\rho)t} + \frac{\epsilon\eta}{\mu\widehat{\lambda}\,(\eta - \rho)}, \quad t \ge 0. \tag{42}$$

Let $\epsilon \to 0^+$, one can get

$$V_1(t) \le e^{-(\eta-\rho)t} \left(\frac{V_1(0)}{\mu} + \frac{\beta V_2(0)}{\mu\left(\widehat{\lambda} - \eta\right)}\right). \tag{43}$$

Then it follows from (31) that

$$V_2(t) \le e^{-\eta t} V_2(0) + e^{-(\eta-\rho)t}\left(\frac{V_1(0)}{\mu} + \frac{\beta V_2(0)}{\mu\left(\widehat{\lambda}-\eta\right)}\right)\frac{\gamma}{\rho}. \quad (44)$$

Furthermore, it follows from condition (21) that $\eta > \rho$. Therefore together with (43) and (44), one can conclude that condition (17) is satisfied; that is, the entrained collective rhythms of multicellular systems (6) are achieved. The proof is thus completed. □

Remark 8. The obtained result not only provides a new prospective to understand the interactions between the external stimuli and intrinsic physiological rhythms but also is potentially useful for the development of some medical devices. The result presented here is more effective in comparison with those in [38–41], where it is assumed that all the states are available for feedback purpose.

As a special case, if the positive matrices P_i and Q_i in the Lyapunov function (22) are chosen as the identity matrix, the following simplified result could be readily obtained.

Corollary 9. *For a given scalar $\mu \in (0,1)$, if there exist scalars $\lambda_i > 0$, $\mu_i > 0$, $i = 1,2,\ldots,l, \eta_i > 0$, $i = l+1,\ldots,N$, and positive scalars ϵ_1, ϵ_2, δ_1, and δ_2 such that*

$$\begin{aligned} &-A^T - A + \epsilon_1 I + \epsilon_1^{-1} L^T L + c\delta_1 \sum_{j=1}^{N} \left|G_{ij}\right| \\ &+ c\delta_1^{-1} \sum_{j=1}^{l} \left|G_{ji}\right| \Gamma^T \Gamma \le \lambda_i, \\ &\left(I + E_{ik}\right)^T \left(I + E_{ik}\right) \le \mu_i, \end{aligned} \quad (45)$$

for $i = 1,\ldots,l$ and

$$\begin{aligned} &-A^T - A + \epsilon_2 I + \epsilon_2^{-1} L^T L + c\delta_2 \sum_{j=1}^{N} \left|G_{ij}\right| \\ &+ c\delta_2^{-1} \sum_{j=l+1}^{N} \left|G_{ji}\right| \Gamma^T \Gamma \le -\eta_i, \end{aligned} \quad (46)$$

for $i = l+1,\ldots,N$, and, for any impulsive time sequence $\{t_k\}$ satisfying

$$\delta := \sup_k \{t_{k+1} - t_k\} < \frac{\ln(1/\mu)}{\eta + \lambda + (\beta\gamma)/(\eta\mu)}, \quad (47)$$

for $k = 0,1,2,\ldots$, where $\mu = \max(\mu_i)$, $\lambda = \max(\lambda_i)$, $i = 1,\ldots,l$, and $\eta = \min(\eta_i)$, $i = l+1,\ldots,N$, then the entrained collective rhythms of multicellular systems (6) *are achieved.*

4. Numerical Example

In this section, a synthetic multicellular system composed of N Goodwin oscillators [33] is employed to illustrate the effectiveness of the proposed control strategy.

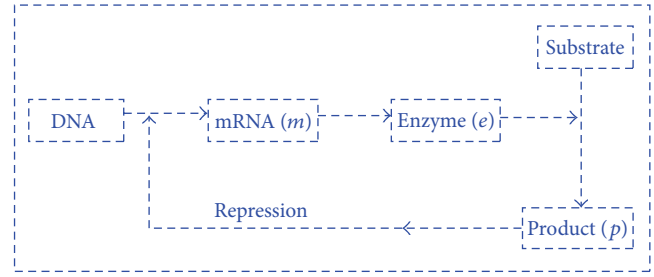

Figure 1: Regulatory scheme of the Goodwin oscillator.

4.1. Goodwin Oscillators. The Goodwin oscillator is a genetic network with negative feedback formed in a cyclic way [33], where metabolites repress the enzymes which are essential for their own synthesis by inhibiting the transcription of the molecule DNA to messenger RNA (mRNA) (see [42] for more details). The regulatory scheme of the Goodwin oscillator can be shown in Figure 1.

A modified model reflecting the above regulation process is given by

$$\begin{aligned} \frac{dm}{dt} &= \frac{u}{k_1 + p^\alpha} - am, \\ \frac{de}{dt} &= vm - be, \\ \frac{dp}{dt} &= we - \frac{cp}{k_2 + p}, \end{aligned} \quad (48)$$

where m, e, and p are the concentrations of mRNA, the enzyme, and the product of the reaction of the enzyme and a substrate, respectively. a, b, and c are the degradation rates of each component, respectively. u, v, and w denote the rates of transcription, translation, and catalysis, respectively. k_1 and k_2 are two positive constants. α is the Hill coefficient denoting the cooperativity of the end product repression. It should be pointed out that model (46) is slightly different from the model in [33]. By changing the linear degradation form of the product to Michaelis-Menten form, the limit cycle oscillations can occur for a lower value of the Hill coefficient α (see [42] for details).

The parameters are chosen as $a = b = c = v = w = 0.1$, $u = 1$, and $k_1 = k_2 = 0.1$, and the Hill coefficient α is taken as $\alpha = 4$. Given 4 random initial conditions, the simulation results are recorded in Figures 2 and 3. Figure 2 shows the time response of every products, and Figure 3 shows the limit cycle of the oscillators in phase space.

4.2. Multicellular System Model. Without loss of generality, we perform the simulation study on the scale-free network structure, which is assumed to obey the scale-free distribution of the Barabási-Albert (BA) model [43]. The parameters are given as $m_0 = m = 5$ and $N = 60$. Figure 4 is the generated BA network graph.

The inner coupling matrix Γ is given by $\Gamma = \mathrm{diag}(1, 1.2, 1)$, and the regulation function in Michaelis-Menten form satisfies condition (2). Assume that only the first 20 nodes are

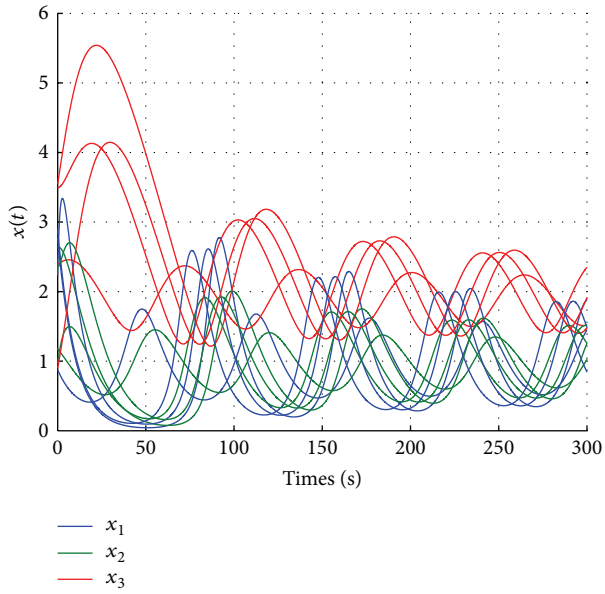

Figure 2: Time response of four oscillators.

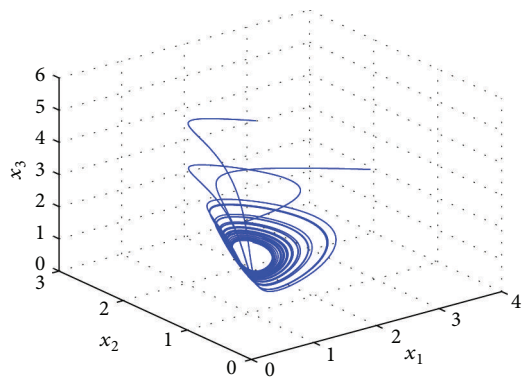

Figure 3: Limit cycle of the oscillators in phase space.

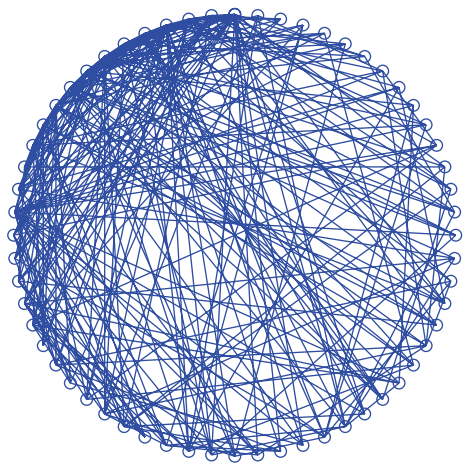

Figure 4: BA scale-free network graph.

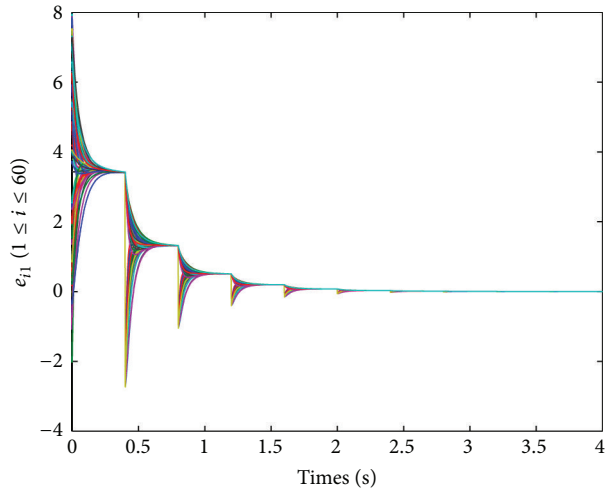

Figure 5: Rhythmic errors e_{i1} in BA network.

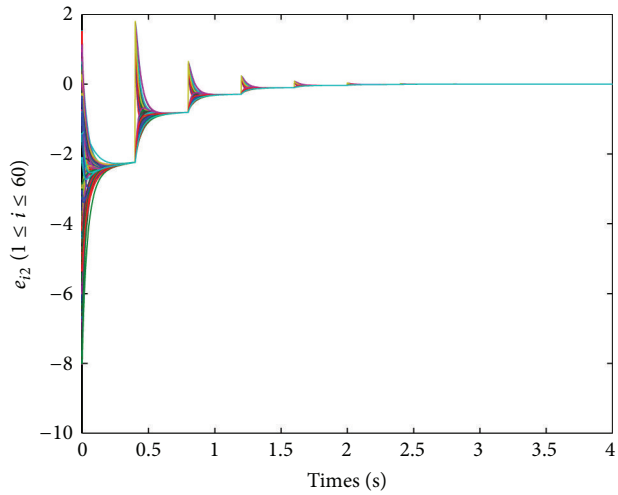

Figure 6: Rhythmic errors e_{i2} in BA network.

able to accept the external inputs. The parameters are chosen as $c = 4$, $\epsilon_1 = 0.03$, and $\epsilon_2 = 0.01$. The impulse magnitude is given as $E_{ik} = -1.8$, and impulse interval is chosen as $\delta = 0.4$. It follows from Corollary 9 that the entrained collective behaviors can be achieved. Figures 5, 6, and 7 show the rhythmic errors of the multicellular systems.

It is noted that since only 20 measurable cells in the network are subject to the external stimuli, the approaches in [38–41], which need the information of all the states, cannot be applied in this case.

5. Conclusion

In this paper, the entrained collective rhythms of multicellular systems have been investigated. It is shown that the entrained collective behavior can be achieved via impulsive control even when only partial states of multicellular systems are available. With the help of the newly developed impulsive integrod-ifferential inequality, the sufficient conditions are derived

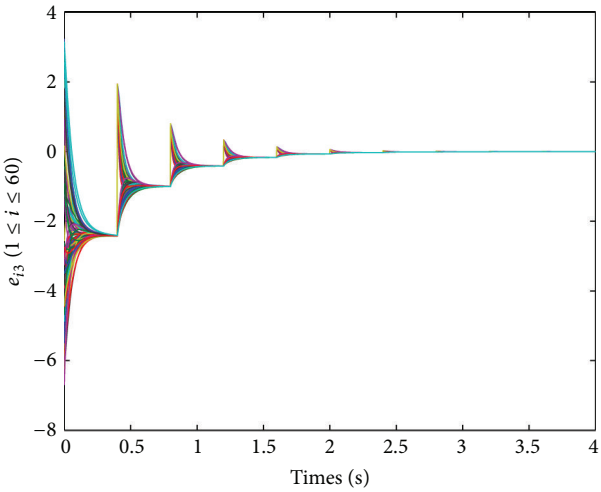

FIGURE 7: Rhythmic errors e_{i3} in BA network.

to ensure the entrained collective rhythms of multicellular systems. A synthetic multicellular system is finally used to illustrate the effectiveness of the developed impulsive control strategy.

Acknowledgments

The work was supported in part by the National Natural Science Foundation of China under Grant 61104045, in part by Technology Foundation for Selected Overseas Chinese Scholar, Ministry of Personnel of China, and in part by the Fundamental Research Funds for the Central Universities of China under Grant 2012B03514.

References

[1] L. Glass, "Synchronization and rhythmic processes in physiology," *Nature*, vol. 410, no. 6825, pp. 277–284, 2001.

[2] J. Garcia-Ojalvo, M. B. Elowitz, and S. H. Strogatz, "Modeling a synthetic multicellular clock: repressilators coupled by quorum sensing," *Proceedings of the National Academy of Sciences of the United States of America*, vol. 101, no. 30, pp. 10955–10960, 2004.

[3] D. McMillen, N. Kopell, J. Hasty, and J. J. Collins, "Synchronizing genetic relaxation oscillators by intercell signaling," *Proceedings of the National Academy of Sciences of the United States of America*, vol. 99, no. 2, pp. 679–684, 2002.

[4] T. Zhou, L. Chen, and R. Wang, "A mechanism of synchronization in interacting multi-cell genetic systems," *Physica D*, vol. 211, no. 1-2, pp. 107–127, 2005.

[5] E. Ullner, A. Koseska, J. Kurths, E. Volkov, H. Kantz, and J. García-Ojalvo, "Multistability of synthetic genetic networks with repressive cell-to-cell communication," *Physical Review E*, vol. 78, no. 3, Article ID 031904, 8 pages, 2008.

[6] T. Zhou, J. Zhang, Z. Yuan, and L. Chen, "Synchronization of genetic oscillators," *Chaos*, vol. 18, no. 3, Article ID 037126, 20 pages, 2008.

[7] Y. Sun, G. Feng, and J. Cao, "A new approach to dynamic fuzzy modeling of genetic regulatory networks," *IEEE Transactions on Nanobioscience*, vol. 9, no. 4, pp. 263–272, 2010.

[8] M. Mormont and F. Lévi, "Circadian-system alterations during cancer processes: a review," *International Journal of Cancer*, vol. 70, no. 2, pp. 241–247, 1997.

[9] J. Cao and F. Ren, "Exponential stability of discrete-time genetic regulatory networks with delays," *IEEE Transactions on Neural Networks*, vol. 19, no. 3, pp. 520–523, 2008.

[10] L. Pan and J. Cao, "Anti-periodic solution for delayed cellular neural networks with impulsive effects," *Nonlinear Analysis: Real World Applications*, vol. 12, no. 6, pp. 3014–3027, 2011.

[11] Y. Sun, G. Feng, and J. Cao, "Robust stochastic stability analysis of genetic regulatory networks with disturbance attenuation," *Neurocomputing*, vol. 79, pp. 39–49, 2012.

[12] Q. Zhu and J. Cao, "Stability analysis of Markovian jump stochastic BAM neural networks with impulse control and mixed time delays," *IEEE Transactions on Neural Networks and Learning Systems*, vol. 23, no. 3, pp. 467–479, 2012.

[13] S. Yamaguchi, H. Isejima, T. Matsuo et al., "Synchronization of cellular clocks in the suprachiasmatic nucleus," *Science*, vol. 302, no. 5649, pp. 1408–1412, 2003.

[14] R. Wang and L. Chen, "Synchronizing genetic oscillators by signaling molecules," *Journal of Biological Rhythms*, vol. 20, no. 3, pp. 257–269, 2005.

[15] C. Li, L. Chen, and K. Aihara, "Synchronization of coupled nonidentical genetic oscillators," *Physical Biology*, vol. 3, no. 1, pp. 37–44, 2006.

[16] C. Li, L. Chen, and K. Aihara, "Stochastic synchronization of genetic oscillator networks," *BMC Systems Biology*, vol. 1, article 6, 2007.

[17] J. Qiu and J. Cao, "Global synchronization of delay-coupled genetic oscillators," *Neurocomputing*, vol. 72, no. 16–18, pp. 3845–3850, 2009.

[18] P. M. Simon, A. M. Habel, J. A. Daubenspeck, and J. C. Leiter, "Vagal feedback in the entrainment of respiration to mechanical ventilation in sleeping humans," *Journal of Applied Physiology*, vol. 89, no. 2, pp. 760–769, 2000.

[19] A. Wagemakers, J. Buldu, J. Garcia-Ojalvo, and M. Sanjuan, "Synchronization of electronic genetic networks," *Chaos*, vol. 16, no. 1, Article ID 013127, 8 pages, 2006.

[20] R. Wang, L. Chen, and K. Aihara, "Synchronizing a multicellular system by external input: an artificial control strategy," *Bioinformatics*, vol. 22, no. 14, pp. 1775–1781, 2006.

[21] T. F. Schultz and S. A. Kay, "Circadian clocks in daily and seasonal control of development," *Science*, vol. 301, no. 5631, pp. 326–328, 2003.

[22] Y. Li, Z. Liu, J. Zhang, R. Wang, and L. Chen, "Synchronisation mechanisms of circadian rhythms in the suprachiasmatic nucleus," *IET Systems Biology*, vol. 3, no. 2, pp. 100–112, 2009.

[23] J. Cao and L. Li, "Cluster synchronization in an array of hybrid coupled neural networks with delay," *Neural Networks*, vol. 22, no. 4, pp. 335–342, 2009.

[24] W. Yu et al., "Local synchronization of a complex network model," *IEEE Transactions on Systems, Man, and Cybernetics B*, vol. 39, no. 1, pp. 230–241, 2009.

[25] J. Lu, D. W. C. Ho, and J. Cao, "A unified synchronization criterion for impulsive dynamical networks," *Automatica*, vol. 46, no. 7, pp. 1215–1221, 2010.

[26] J. Lu, D. W. C. Ho, J. Cao, and J. Kurths, "Exponential synchronization of linearly coupled neural networks with impulsive disturbances," *IEEE Transactions on Neural Networks*, vol. 22, no. 2, pp. 329–335, 2011.

[27] X. Yang, J. Cao, and J. Lu, "Stochastic synchronization of complex networks with nonidentical nodes via hybrid adaptive and impulsive control," *IEEE Transactions on Circuits and Systems*, vol. 59, no. 2, pp. 371–384, 2012.

[28] D. T. Kaplan, J. R. Clay, T. Manning, L. Glass, M. R. Guevara, and A. Shrier, "Subthreshold dynamics in periodically stimulated squid giant axons," *Physical Review Letters*, vol. 76, no. 21, pp. 4074–4077, 1996.

[29] T. Zhou, J. Zhang, Z. Yuan, and A. Xu, "External stimuli mediate collective rhythms: artificial control strategies," *PLoS ONE*, vol. 2, no. 2, article e231, 2007.

[30] G. Feng and J. Cao, "Master-slave synchronization of chaotic systems with a modified impulsive controller," *Advances in Difference Equations*, vol. 2013, article 24, 2013.

[31] X. Yang, J. Cao, and Z. Yang, "Synchronization of coupled reaction-diffusion neural networks with time-varying delays via pinning-impulsive controller," *SIAM Journal on Control and Optimization*, vol. 51, no. 5, pp. 3486–3510, 2013.

[32] J. Lu, D. W. C. Ho, J. Cao, and J. Kurths, "Single impulsive controller for globally exponential synchronization of dynamical networks," *Nonlinear Analysis: Real World Applications*, vol. 14, no. 1, pp. 581–593, 2013.

[33] B. C. Goodwin, "Oscillatory behavior in enzymatic control processes," *Advances in Enzyme Regulation*, vol. 3, pp. 425–438, 1965.

[34] T. S. Gardner, C. R. Cantor, and J. J. Collins, "Construction of a genetic toggle switch in *Escherichia coli*," *Nature*, vol. 403, no. 6767, pp. 339–342, 2000.

[35] M. B. Miller and B. L. Bassler, "Quorum sensing in bacteria," *Annual Review of Microbiology*, vol. 55, pp. 165–199, 2001.

[36] L. Huang, *Linear Algebra in Systems and Control Theory*, Science Press, Beijing, China, 1984.

[37] R. Bellman, "The stability of solutions of linear differential equations," *Duke Mathematical Journal*, vol. 10, pp. 643–647, 1943.

[38] W. Wang and J. Cao, "Synchronization in an array of linearly coupled networks with time-varying delay," *Physica A*, vol. 366, pp. 197–211, 2006.

[39] P. Li, J. Cao, and Z. Wang, "Robust impulsive synchronization of coupled delayed neural networks with uncertainties," *Physica A*, vol. 373, pp. 261–272, 2007.

[40] J. Cao, D. W. C. Ho, and Y. Yang, "Projective synchronization of a class of delayed chaotic systems via impulsive control," *Physics Letters A*, vol. 373, no. 35, pp. 3128–3133, 2009.

[41] Y. Yang and J. Cao, "Exponential synchronization of the complex dynamical networks with a coupling delay and impulsive effects," *Nonlinear Analysis: Real World Applications*, vol. 11, no. 3, pp. 1650–1659, 2010.

[42] C. P. Fall, E. S. Marland, J. M. Wagner, and J. J. Tyson, Eds., *Computational Cell Biology*, vol. 20 of *Interdisciplinary Applied Mathematics*, Springer, New York, NY, USA, 2005.

[43] A.-L. Barabási and R. Albert, "Emergence of scaling in random networks," *Science*, vol. 286, no. 5439, pp. 509–512, 1999.

Hindawi Publishing Corporation
Abstract and Applied Analysis
Volume 2013, Article ID 795682, 5 pages
http://dx.doi.org/10.1155/2013/795682

Research Article

A New Class of the Planar Networks with High Clustering and High Entropy

Guona Hu,[1] Yuzhi Xiao,[2,3] Huanshen Jia,[1] and Haixing Zhao[2,3]

[1] *Department of Mathematics, Qinghai Normal University, Xining, Qinghai 810008, China*
[2] *School of Computer Science, Shaanxi Normal University, Xi'an, Shaanxi 710062, China*
[3] *Department of Computer Science, Qinghai Normal University, Xining, Qinghai 810008, China*

Correspondence should be addressed to Haixing Zhao; h.x.zhao@163.com

Received 27 September 2013; Accepted 16 November 2013

Academic Editor: Jinde Cao

Small-world networks are ubiquitous in real-life systems, such as the World Wide Web, communication networks, and electric power grids, and most of them are stochastic. In this paper, we present a model that generates a small-world network in a simple deterministic way and analyze the relevant topological properties of the model, such as the degree distribution, clustering coefficient, and diameter. Meanwhile, according to the special structure of the model, we derive analytically the exact numbers of spanning trees in the planar networks. The results show that the model has a discrete exponential degree distribution, high clustering coefficient, short diameter, and high entropy.

1. Introduction

Over the past decade, a lot of authors in different scientific communities have made a concerted effort toward unveiling and understanding the generic properties of complex networked systems in nature and society [1–5]. One of the most important things is the network modeling. Its importance lies in the fact that it cannot only capture correctly the processes that assembled the networks that we see today, but also help to know how various microscopic processes influence the network topology [6]. At present, many papers related to complex network models are stochastic [7–9]. But the randomness, while in line with the major features of real-life networks, makes it harder to gain a visual understanding of how networks are shaped and how do different nodes relate to each other [10]. Therefore, it would be not only of major theoretical interest but also of great practical significance to construct models that lead to small-world networks in deterministic fashions.

The first successful attempt to generate networks with high clustering coefficients and small average path length (APL) is the model introduced by Watts and Strogatz (WS model) [11]. This pioneering work of Watts and Strogatz started an avalanche of research on the properties of small-world networks and the Watts-Strogatz (WS) model [12]. A much-studied variant of the WS model was proposed by Newman and Watts [13, 14]. In 1999, Kasturirangan proposed an alternative model to WS small-world network [15]. Actually, small-world networks are characterized by three main properties. First, their APL does not increase linearly with the system size, but grows logarithmically with the number of nodes or slower. Second, average node degree of the network is small. Third, the network has a strong average clustering [11] compared to an Erdös-Rényi (ER) random network [16, 17] of equal size and average node degree.

In this paper, we propose a generation algorithm of a deterministic planar network model. And we analyze its topological properties; the results show that our model has a discrete exponential degree distribution, high clustering, and small diameter, which appears small-world effect. In addition, it is known to us that the number of spanning trees is an important quantity characterizing the reliability of a network. Generally, the number of spanning trees in a network can be obtained by directly calculating a related determinant

corresponding to the network. However, for a large network, evaluating the relevant determinant is intractable [18]. Therefore, we propose a generic linear algorithm to count the number of spanning trees of the general planar networks. Using the algorithm, we derive analytically the exact numbers of spanning trees in the planar networks. Based on the number of spanning trees, we determine the entropy of its spanning trees.

2. Network Construction

The studied network is constructed in an iterative way. We denote the network after t steps by $M(t)$. Then, the network at step t is built as follows. For $t = 1$, $M(1)$ is a complete graph with 4 nodes. For $t \geq 2$, $M(t)$ is obtained from $M(t-1)$ by replacing each existing iterative edge in $M(t-1)$ with $M(1)$. The process is repeated till the desired graph order is reached; see Figure 1.

Now, we compute the order and size of $M(t)$. Let $L_v(t)$, $L_e(t)$, and $L_i(t)$ denote, respectively, the set of vertices, edges, and iterative edges introduced at step t, while $V(t)$ and $E(t)$ are the set of vertices and edges of the graph $M(t)$. Notice that, at each iteration, an iterative edge is replaced by two new iterative edges and three noniterative edges. Therefore, $|L_i(t)| = 2|L_i(t-1)|$, and $|L_i(t)| = 3 \cdot 2^{t-1}$ $(t \geq 1)$. As each iterative edge introduces at the next iteration two new vertices and five new edges, we have $|L_v(t)| = 2|L_i(t-1)| = 3 \cdot 2^{t-1}$ $(t \geq 2)$ and $|L_e(t)| = 5|L_i(t-1)| = 15 \cdot 2^{t-2}$ $(t \geq 2)$. As $L_i(1) = 3$, $|L_v(t)| = 4$ and $|L_e(t)| = 6$. Thus,

$$|V(t)| = \sum_{i=0}^{n} |L_v(t)| = 3 \cdot 2^t - 2 \quad (t \geq 1) \tag{1}$$

$$|E(t)| = \sum_{i=0}^{n} |L_e(t)| = 15 \cdot 2^{t-1} - 9 \quad (t \geq 1). \tag{2}$$

The average degree is then

$$\langle k \rangle = \frac{2|E(t)|}{|V(t)|} = \frac{15 \cdot 2^{t-1} - 9}{3 \cdot 2^{t-1} - 1}. \tag{3}$$

Obviously, for large t, it is approximately equal to 5.

3. Relevant Characteristics of the Deterministic Small-World Network

In the following, we concentrate on the degree distribution, clustering coefficient, and diameter.

3.1. Degree Distribution. The degree is the simplest and the most intensively studied characteristic of an individual node. The degree of a node i is the number of edges in the whole network connected to i. The degree distribution $P(k)$ is defined as the probability that a randomly selected node has exactly k edges.

Let $k_i(t)$ be the degree of node i at step t. All nodes can be divided into two categories. (i) Interior nodes; for those nodes that only connect to noniterative edges, their degree

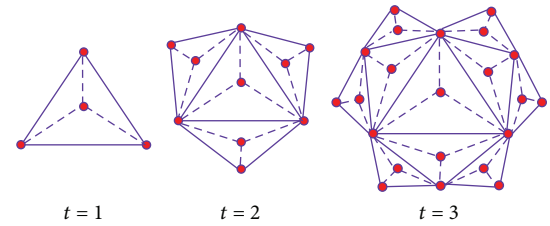

Figure 1: (Color online) construction of the deterministic planar network $M(t)$, showing three steps of the iterative progress. The solid links are iterated links; the dashed links are noniterated links.

is always equal to 3. (ii) Noninterior nodes; one can see that at any iteration, a iterative edge is replaced by two new iterative edges and three new noniterative edges, so the degree of noninterior nodes is added 4 at each iteration. Thus, the degree $k_i(t)$ of a node i satisfies the relation $k_i(t+1) = k_i(t)+4$. Then, $k_i(t) = 4t - 1$. And we have

$$k_i(t) = \begin{cases} 3, & \text{if the node } i \text{ is interior node,} \\ 4t-1 & \text{if the node } i \text{ is noninterior node.} \end{cases} \tag{4}$$

Let t_i be the step at which a node i is created, then $k_i(t_i) = 3$, and hence, for noninterior nodes, we have

$$k_i(t) = 3 + 4(t - t_i). \tag{5}$$

Therefore, the degree spectrum of the present network is a series of discrete values: at step t, the number of nodes of degree $k = 3, 7, 11, \ldots, 4t-9, 4t-5, 4t-1$, equals $9 \cdot 2^{t-2} - 2, |L(t-2)|, |L(t-3)|, \ldots, |L(2)|, |L(1)|, |L(1)|$, respectively. Other values of degree are absent in the spectrum. Due to the discreteness of this degree spectrum, it is convenient to obtain its cumulative degree distribution [18]; that is,

$$P_{\text{cum}}(k) = \sum_{k'=k}^{\infty} P(k'). \tag{6}$$

Using (5), we have $P_{\text{cum}}(k) = \sum_{k'=k}^{\infty} P(k') = P(t' \leq \tau = (3 + 4t - k)/4)$. Hence,

$$P_{\text{cum}}(k) = \sum_{t'=0}^{\tau} \frac{|n(t')|}{|V(t)|} = \frac{3 \cdot 2^{(3/4)+t-(k/4)}}{3 \cdot 2^t - 2}. \tag{7}$$

Obviously, when the size of the network is large, the degree distribution $P_{\text{cum}}(k) = 2^{(3/4)-(k/4)}$ is an exponential of a power of degree k.

3.2. Clustering Coefficient. Clustering coefficient is another significant property of a network, which provides a measure of the local structure within the network. The most immediate measure of clustering is the clustering coefficient C_i for every node i. By definition, clustering coefficient C_i of a node i is the ratio of the total number E_i of edges that actually exist between all k_i its nearest neighbors and the number $k_i(k_i-1)/2$ of all possible edges between them; that is, $C_i = 2E_i/[k_i(k_i-1)]$. The clustering coefficient C_t of the

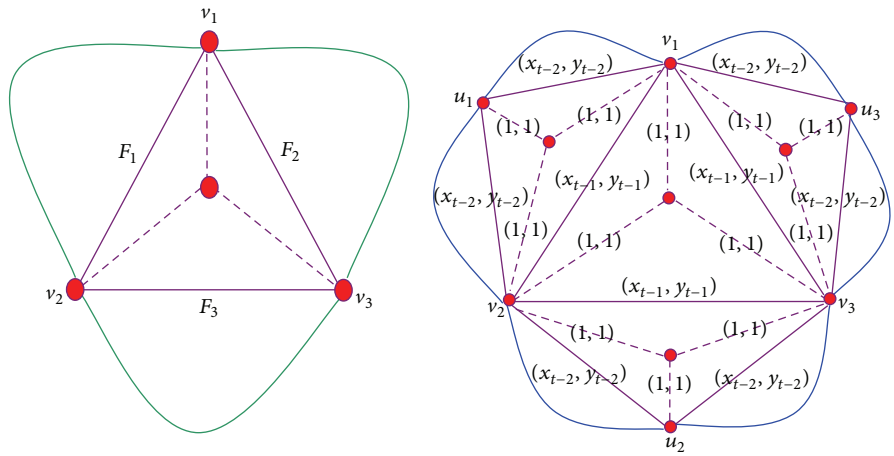

Figure 2: (Color online) the network $M(t)$. The solid links are iterated links, the dashed links are noniterated links.

whole network is the average of all individual C_i's. For this network, we can obtain the exact expression of the clustering coefficient C_t. By construction, for any given node u having a degree k, there are $E_u = 3 \cdot (k-1)/2$ links that actually exist among the neighbor nodes. So, one can see that there is a one-to-one corresponding relation between the coefficient $C(k)$ of the node and its degree k: $C(k) = 3/k$. This expression indicates that the local clustering scales as $C(k) \sim k^{-1}$.

Clearly, the number of nodes of degree $k = 3, 7, 11, \ldots, 4t-9, 4t-5, 4t-1$, equals $9 \cdot 2^{t-2} - 2, |L(t-2)|, |L(t-3)|, \ldots, |L(2)|, |L(1)|, |L(1)|$, respectively. The clustering coefficient C_t is given by the following:

$$C_t = \frac{9 \cdot 2^{t-2} - 2 + 9 \cdot \sum_{i=2}^{t-1} \left(\left(2^{t-1-i} / (4i-1) \right) + (9/(4t-1)) \right)}{3 \cdot 2^t - 2}. \tag{8}$$

For infinite t, C_t approaches to a constant value of 0.8309, so the clustering is high.

3.3. Diameter. Besides degree distribution and clustering coefficient, average path length (APL) is another important parameter to characterize a network. APL is defined as the average number of edges along the shortest paths for all possible pairs of network nodes. People have found the small-world phenomenon in most real-life networks that behave with a short APL. For most network models, it is hard to obtain the analytic solution of APL. To demonstrate the short distance between any pair of nodes, we can adopt another parameter that is defined as the maximal communication delay in the network. If a network has a small diameter, then this network is undoubtedly with a short APL [19]. For the network proposed, we denote the diameter at iteration t as $D(t)$. According to Figure 1, we can clearly know that $D(1) = 1$ and $D(2) = 2$. At each iteration, one can see that the diameter always lies between a pair of newly created nodes at this iteration because at each iterative edge we paste a complete graph $M(1)$, so the diameter for the network proposed has the following simple formula, $D(t) = t$.

Notice that the logarithm value of total number of nodes $|V(t)|$ is approximately equal to $t \ln 2$ for large t. Thus, the diameter grows logarithmically with the number of nodes and the average path length increases more slowly than $\ln |V(t)|$.

Based on the above discussions, our model is a deterministic small-world network because it is a sparse one with high clustering and short diameter, which satisfies the necessary property for small-world network.

4. Spanning Trees in the Network

In this section, we investigate the number of spanning trees in this network. Our aim is to derive the exact formula for the number of spanning trees and determine its entropy.

Let $M(t)$ be a planar graph generated by t steps. Since $M(t)$ is symmetry, suppose that the edges v_1v_2, v_1v_3, and v_2v_3 are weighted by (x_{t-1}, y_{t-1}), where x_{t-1} denote the number of spanning trees of the subgraph F_1 and y_{t-1} denote the number of spanning forests of the subgraph F_1 with two components such v_1 and v_2 belong to distinct components. Let $N_{ST}(t)$ be the number of spanning trees of $M(t)$. Figure 3 gives all spanning trees of $M(1)$ and Figure 4 gives all spanning forests with two components. Then, by Figure 2, we have

$$N_{ST}(t) = 9x_{t-1}^2 y_{t-1} + 6x_{t-1} y_{t-1}^2 + y_{t-1}^3. \tag{9}$$

According to Figures 2, 3, and 4, we obtain the recursion relations between x_{t-1} and x_{t-2} as follows:

$$\begin{aligned} x_{t-1} &= 3x_{t-2}^2 + 3y_{t-2}^2 + 10x_{t-2}y_{t-2}, \\ y_{t-1} &= 2y_{t-2}^2 + 6x_{t-2}y_{t-2}. \end{aligned} \tag{10}$$

Let $a_{t-1} = x_{t-1}/y_{t-1}$, by (10) it follows that

$$a_{t-1} = \frac{3 \cdot 2^{t-1} - 2}{2^{t-1}}, \tag{11}$$

with the initial condition $a_0 = 1$. So, we get

$$y_t = \prod_{i=0}^{t-2} \left(20 - \frac{3}{2^{i-2}} \right)^{2^{t-i-2}}. \tag{12}$$

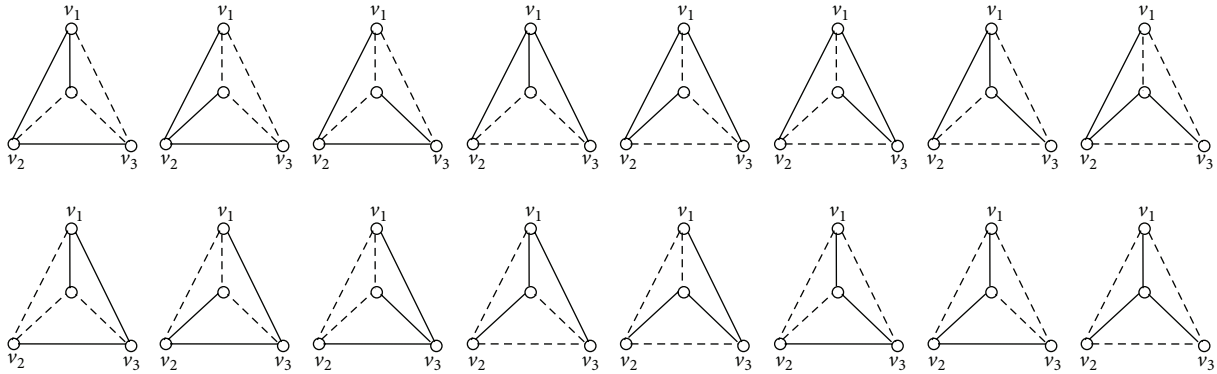

Figure 3: The number of spanning trees of $M(1)$ is 16. The solid link indicates that one node is connected to another node; the dashed link indicates that one node is not connected to another node.

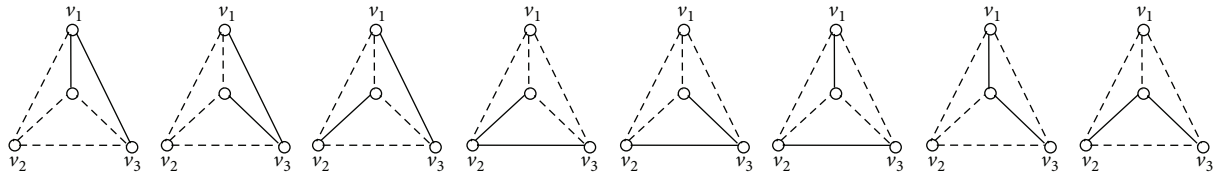

Figure 4: The number of spanning forests with two components of $M(1)$ is 8. The solid link indicates that one node is connected to another node; the dashed link indicates that one node is not connected to another node.

By (9),

$$N_{\mathrm{ST}}(t) = 9x_{t-1}^2 y_{t-1} + 6x_{t-1} y_{t-1}^2 + y_{t-1}^3. \tag{13}$$

Substituting (11) and (12) with (13), we have

$$N_{\mathrm{ST}}(t) = \left(10 - \frac{3}{2^{t-2}}\right) \prod_{i=0}^{2^{t-2}} \left(20 - \frac{3}{2^{i-2}}\right)^{3\cdot 2^{t-i-2}}. \tag{14}$$

From (14), together with (1), we determine the entropy of the number of spanning trees—an important quantity characterizing network structure—for $M(t)$ as the limiting value [20, 21]:

$$E_{\mathrm{ST}}(t) = \lim_{|V_t| \to \infty} \frac{\ln N_{\mathrm{ST}}(t)}{|V_t|} \approx 1.2109. \tag{15}$$

The obtained entropy of spanning trees in $M(t)$ can be compared to those found in other networks. In the pseudofractal fractal web [22], the entropy is 0.8959, a value less than 1, for the square lattice [23] and the two-dimensional Sierpinski gasket [24], their entropy of spanning trees is 1.16624 and 1.0486, respectively, and for the fractal scale-free lattice [25], the entropy is 1.0397. And all of them have the same average degree of 4. While in Apollonian network [26] having the average degree of 6, the entropy is 1.3540, the entropy of our model with average degree of 5 is between them.

5. Conclusion

In conclusion, we have investigated a simple model, which is constructed in a deterministic way. Then, we have presented an exhaustive analysis of many properties of the considered model and obtained the analytic solutions for most of the topological features, including degree distributions, clustering coefficient, and diameter. Finally, according to the special structure, we give a general algorithm to count the number of spanning trees of this model. Using the algorithm, we obtained entropies of spanning trees.

Conflict of Interests

The authors declare that there is no conflict of interests regarding the publication of this paper.

Acknowledgments

This research supported by the National Science Foundation of China (nos. 61164005 and 60863006), the National Basic Research Program of China (no. 2010CB334708), and Program for Changjiang Scholars and Innovative Research Team in University (no. IRT1068).

References

[1] R. Albert and A. L. Barabási, "Statistical mechanics of complex networks," *Reviews of Modern Physics*, vol. 74, no. 1, pp. 47–97, 2002.

[2] S. N. Dorogovtsev and J. F. F. Mendes, "Evolution of networks," *Advances in Physics*, vol. 51, no. 4, pp. 1079–1187, 2002.

[3] M. E. J. Newman, "The structure and function of complex networks," *SIAM Review*, vol. 45, no. 2, pp. 167–256, 2003.

[4] S. Boccaletti, V. Latora, Y. Moreno, M. Chavez, and D.-U. Hwang, "Complex networks: structure and dynamics," *Physics Reports*, vol. 424, no. 4-5, pp. 175–308, 2006.

[5] Z. Zhang, Y. Lin, S. Gao, S. Zhou, and J. Guan, "Average distance in a hierarchical scale-free network: an exact solution," *Journal of Statistical Mechanics*, vol. 2009, no. 10, Article ID P10022, 2009.

[6] Z. Z. Zhang, S. G. Zhou, and J. Q. Fang, "Recent progess of deterministic models of complex networks," *Complex Systems and Complexity Science*, Article ID 16723813, 2008.

[7] S. N. Dorogovtsev and J. F. F. Mendes, "Scalling behavior of developing and decaying networks," *Europhysics Letters*, vol. 52, no. 1, 2000.

[8] J. M. Kleinberg, "Navigation in a small world," *Nature*, vol. 406, no. 6798, p. 845, 2000.

[9] J. Ozik, B. R. Hunt, and E. Ott, "Growing networks with geographical attachment preference: emergence of small worlds," *Physical Review E*, vol. 69, no. 2, Article ID 026108, pp. 026108–5, 2004.

[10] A.-L. Barabási, E. Ravasz, and T. Vicsek, "Deterministic scale-free networks," *Physica A*, vol. 299, no. 3-4, pp. 559–564, 2001.

[11] D. J. Watts and S. H. Strogatz, "Collective dynamics of small world network," *Nature*, vol. 393, no. 6684, pp. 440–442, 1998.

[12] Z. Zhang, L. Rong, and C. Guo, "A deterministic small-world network created by edge iterations," *Physica A*, vol. 363, no. 2, pp. 567–572, 2006.

[13] M. E. J. Newman and D. J. Watts, "Renormalization group analysis of the small-world network model," *Physics Letters A*, vol. 263, no. 4–6, pp. 341–346, 1999.

[14] M. E. J. Newman and D. J. Watts, "Scaling and percolation in the small-world network model," *Physical Review E*, vol. 60, no. 6, pp. 7332–7342, 1999.

[15] R. Kasturirangan, Multiple Scales in Small-World Graphs AI Lab Memo. 1663, Massachusetts Institute of Technology, 1999.

[16] P. Erdös and A. R. Rényi, "On random graphs I," *Publicationes Mathematicae*, vol. 6, pp. 290–297, 1959.

[17] P. Erdös and A. R. Rényi, "On the evolution of random graphs," *Publication of the Mathematical Institute of the Hungarian Academy of Sciences*, vol. 5, pp. 17–61, 1960.

[18] Y. Z. Xiao and H. X. Zhao, "New method for counting the numberof spanning trees in a two-tree network," *Physica A*, vol. 392, pp. 4576–4583, 2013.

[19] Z.-M. Lu and S.-Z. Guo, "A small-world network derived from the deterministic uniform recursive tree," *Physica A*, vol. 391, no. 1-2, pp. 87–92, 2012.

[20] R. Burton and R. Pemantle, "Local characteristics, entropy-and limit theorems for spanning trees and domino tilingsvia transfer-impedances," *Annals of Probability*, vol. 21, p. 1329, 1993.

[21] R. Lyons, "Asymptotic enumeration of spanning trees," *Combinatorics Probability and Computing*, vol. 14, no. 4, pp. 491–522, 2005.

[22] Z. Z. Zhang, H. X. Liu, B. Wu, and S. G. Zhou, "Enumeration of spanning trees in a pseudofractal scale-free web," *Europhysics Letters*, vol. 90, no. 6, Article ID 680029, 2010.

[23] F. Y. Wu, "Number of spanning trees on a lattice," *Journal of Physics A*, vol. 10, no. 6, article 4, pp. L113–L115, 1977.

[24] S.-C. Chang, L.-C. Chen, and W.-S. Yang, "Spanning trees on the Sierpinski gasket," *Journal of Statistical Physics*, vol. 126, no. 3, pp. 649–667, 2007.

[25] Z. Zhang, H. Liu, B. Wu, and T. Zou, "Spanning trees in a fractal scale-free lattice," *Physical Review E*, vol. 83, no. 1, Article ID 016116, 2011.

[26] Y. Lin, B. Wu, Z. Zhang, and G. Chen, "Counting spanning trees in self-similar networks by evaluating determinants," *Journal of Mathematical Physics*, vol. 52, no. 11, Article ID 113303, 2011.

Hindawi Publishing Corporation
Abstract and Applied Analysis
Volume 2013, Article ID 521812, 5 pages
http://dx.doi.org/10.1155/2013/521812

Research Article

Scaling-Base Drive Function Projective Synchronization between Different Fractional-Order Chaotic Systems

Ping Zhou[1,2] and Kun Huang[1,2]

[1] *Center of System Theory and Its Applications, Chongqing University of Posts and Telecommunications, Chongqing 400065, China*
[2] *Key Laboratory of Industrial Internet of Things & Networked Control, Ministry of Education, Chongqing University of Posts and Telecommunications, Chongqing 400065, China*

Correspondence should be addressed to Ping Zhou; zhouping@cqupt.edu.cn

Received 14 September 2013; Accepted 11 November 2013

Academic Editor: Jianquan Lu

A new function projective synchronization scheme between different fractional-order chaotic systems, called scaling-base drive function projective synchronization (SBDFPS), is discussed. In this SBDFPS scheme, one fractional-order chaotic system is chosen as scaling drive system, one fractional-order chaotic system is chosen as base drive systems, and another fractional-order chaotic system is chosen as response system. The SBDFPS technique scheme is based on the stability theory of nonlinear fractional-order systems, and the synchronization technique is theoretically rigorous. Numerical experiments are presented and show the effectiveness of the SBDFPS scheme.

1. Introduction

In the past twenty years, many synchronization schemes for chaotic systems have been presented [1–9]. However, the function projective synchronization (FPS) scheme for chaotic systems is extensively considered due to its potential applications in secure communication. Because the drive and response systems could be synchronized with a scaling function matrix in FPS, the unpredictability of the scaling function matrix in FPS scheme can enhance the security in secure communication. In FPS, only two chaotic systems (one drive system and one response system) are considered, and the function matrix comes from one drive system. Therefore, more than one drive system (two or three drive systems or four drive systems, etc.) and one response system in FPS, and the scaling function matrix coming from multidrive systems, are general case. Moreover, multidrive systems in FPS scheme can additionally enhance the security of communication; this is due to the fact that the transmitted signals can be split into several parts, and each part can be loaded in different drive systems, or the transmitted signals can be divided time into different intervals, and the signals in different intervals can be loaded in different drive systems [8].

Motivated by the previous part, we demonstrated a new function projective synchronization scheme between different fractional-order chaotic systems in this paper, which is called scaling-base drive function projective synchronization (briefly denoted by SBDFPS). In SBDFPS scheme, there are two drive systems, which are called the *scaling drive system* and the *base drive system*, respectively. The proposed SBDFPS technique is based on the stability theory of nonlinear fractional-order systems and is theoretically rigorous. The SBDFPS between two-driver chaotic systems (fractional-order Lorenz chaotic system as *scaling drive system* and fractional-order Lu chaotic system as *base drive system*) and one response chaotic system (fractional-order Chen chaotic system) is achieved. Numerical experiments show the effectiveness of the SBDFPS scheme.

This paper is organized as follows. In Section 2, the SBDFPS scheme between different fractional-order chaotic systems is demonstrated. In Section 3, some examples are considered and show the effectiveness of the SBDFPS scheme. Finally, the conclusion ends the paper in Section 4.

2. The Scaling-Base Drive Function Projective Synchronization (SBDFPS) between Different Fractional-Order Chaotic Systems

The Caputo definition of the fractional derivative is used, which is

$$D^q f(t) = \frac{1}{\Gamma(m-q)} \int_0^t \frac{f^{(m)}(\tau)}{(t-\tau)^{q+1-m}} d\tau, \quad m-1 < q < m, \tag{1}$$

where D^q is called the Caputo operator, m is the first integer which is not less than q, and $f^{(m)}(t)$ is the m-order derivative for $f(t)$; that is, $f^{(m)}(t) = d^m f(t)/dt^m$.

Now, the SBDFPS scheme between different fractional-order chaotic systems will be established. Consider the fractional-order scaling drive chaotic system and base drive chaotic system and one response chaotic system described by systems (2), (3), and (4), respectively as follows:

$$D^{q_{d1}} x_1 = f_{d1}(x_1), \tag{2}$$

$$D^{q_{d2}} x_2 = f_{d2}(x_2), \tag{3}$$

$$D^{q_r} y = f_r(y) + M(x_1, x_2, y), \tag{4}$$

where $0 < q_{di} < 1$ $(i = 1, 2)$ and $0 < q_r < 1$ are fractional-order. $x_1 = (x_{11}, x_{12}, \ldots, x_{1n})^T$, $x_2 = (x_{21}, x_{22}, \ldots, x_{2n})^T$, and $y = (y_1, y_2, \ldots y_n)^T$ are state vectors of fractional-order chaotic systems (2)–(4). f_{di} $(i = 1, 2) : R^n \to R^n$ and $f_r : R^n \to R^n$ are differential nonlinear functions. $M(x_1, x_2, y) \in R^{n\times 1}$ is a vector controller and will be designed.

Definition 1. Give the scaling drive system (2), the base drive systems (3), and the response system (4). It is said to scaling-base drive function projective synchronization (SBDFPS) if there exist real nonzero constant matrix $C_i \in R^{n\times n}$ $(i = 1, 2)$ and nonzero scaling function matrix $S_i(x_i) \in R^{n\times n}$ $(i = 1, 2)$ such that

$$\lim_{t\to+\infty} \|e\| = \lim_{t\to+\infty} \left\| [C_1 S_1(x_1) + C_2 S_2(x_2)] x_1 - y \right\| = 0, \tag{5}$$

where $\|\cdot\|$ represents the Euclidean norm.

Remark 2. If $C_1 \neq 0, C_2 = 0$, then the SBDFPS scheme will be turned into FPS. If $C_i = 0$ $(i = 1, 2)$, then the SBDFPS scheme will be turned into a chaos control problem.

Remark 3. System (2) and systems (3) in SBDFPS scheme may be integer order systems. So, the SBDFPS between integer order chaotic system and fractional-order can be achieved.

Let the SBDFPS error between the scaling drive system (2), base drive systems (3), and response system (4) be defined as

$$e = y - [C_1 S_1(x_1) + C_2 S_2(x_2)] x_1, \tag{6}$$

where $e = (e_1, e_2, \ldots, e_n)^T$.

Now, choose vector controller $M(x_1, x_2, y) \in R^{n\times 1}$ as

$$\begin{aligned} M(x_1, x_2, y) &= D^{q_r} \{[C_1 S_1(x_1) + C_2 S_2(x_2)] x_1\} \\ &\quad - f_r \{[C_1 S_1(x_1) + C_2 S_2(x_2)] x_1\} + M_1(x_1, x_2, y) e, \end{aligned} \tag{7}$$

where feedback controller $M_1(x_1, x_2, y) \in R^{n\times n}$ will be designed later.

By (6) and (7), system (4) can be changed as follows:

$$\begin{aligned} D^{q_r} e &= f_r(y) - f_r \{[C_1 S_1(x_1) + C_2 S_2(x_2)] x_1\} + M_1(x_1, x_2, y) e. \end{aligned} \tag{8}$$

In this paper, we assume that

$$f_r(y) - f_r \{[C_1 S_1(x_1) + C_2 S_2(x_2)] x_1\} = M_2(x_1, x_2, y) e, \tag{9}$$

where $M_2(x_1, x_2, y) \in R^{n\times n}$. In fact, many fractional-order chaotic (hyperchaotic) systems satisfy this assumption.

By (9), system (8) can be rewritten as

$$D^{q_r} e = [M_1(x_1, x_2, y) + M_2(x_1, x_2, y)] e. \tag{10}$$

By (10), the SBDFPS between the scaling drive system (2), base drive systems (3), and response system (4) is turned into the following problem: select suitable $M_1(x_1, x_2, y) \in R^{n\times n}$ such that the system (10) asymptotically converges to zero.

Theorem 4. *Select suitable matrix $M_1(x_1, x_2, y) \in R^{n\times n}$ such that $M_1(x_1, x_2, y) + M_2(x_1, x_2, y)$ satisfy the following conditions:*

(1) $M_{ij} = -M_{ji}$ $(i \neq j)$

(2) $M_{ii} \leq 0$ (all M_{ii} are not equal to zero),

where M_{ij} $(i, j = 1, 2, \ldots n, \forall M_{ij} \in R)$ are the entries of $M_1(x_1, x_2, y) + M_2(x_1, x_2, y)$. Then the SBDFPS between the scaling drive system (2)*, base drive systems* (3)*, and response system* (4) *can be reached.*

Proof. Let λ be one of the eigenvalues of matrix $M_1(x_1, x_2, y) + M_2(x_1, x_2, y)$ and ρ the corresponding nonzero eigenvector. So, we have

$$[M_1(x_1, x_2, y) + M_2(x_1, x_2, y)] \rho = \lambda \rho. \tag{11}$$

By (11), taking conjugate transpose on both sides of (11), one can obtain

$$\overline{\{[M_1(x_1, x_2, y) + M_2(x_1, x_2, y)] \rho\}^{\mathbf{T}}} = \overline{\lambda} \rho^{\mathbf{H}}, \tag{12}$$

where $\mathbf{H}$ denotes conjugate transpose.

Now, (12) multiplied right by ρ plus (11) multiplied left by $\rho^{\mathbf{H}}$. Thus

$$\begin{aligned} &\rho^{\mathbf{H}} \left\{ [M_1(x_1, x_2, y) + M_2(x_1, x_2, y)] \right. \\ &\qquad \left. + [M_1(x_1, x_2, y) + M_2(x_1, x_2, y)]^{\mathbf{H}} \right\} \rho \\ &\qquad = \rho^{\mathbf{H}} \rho \left(\lambda + \overline{\lambda}\right). \end{aligned} \tag{13}$$

Thus

$$\lambda + \overline{\lambda} = \rho^{\mathbf{H}} \left\{ \left[M_1 (x_1, x_2, y) + M_2 (x_1, x_2, y) \right] + \left[M_1 (x_1, x_2, y) + M_2 (x_1, x_2, y) \right]^{\mathbf{H}} \right\} \frac{\rho}{\rho^{\mathbf{H}} \rho}. \tag{14}$$

Using $M_{ij} = -M_{ji}$ $(i \neq j, \forall b_{ij} \in R)$, so

$$\lambda + \overline{\lambda} = \rho^{\mathbf{H}} \begin{pmatrix} 2M_{11} & 0 & \cdots & 0 \\ 0 & 2M_{22} & \cdots & 0 \\ 0 & 0 & \cdots & 0 \\ 0 & 0 & 0 & 2M_{nn} \end{pmatrix} \frac{\rho}{\rho^{\mathbf{H}} \rho}. \tag{15}$$

Because $M_{ii} \leq 0$ (all M_{ii} are not equal to zero), we have

$$\lambda + \overline{\lambda} \leq 0. \tag{16}$$

That is,

$$\left| \arg \lambda \left[M_1 (x_1, x_2, y) + M_2 (x_1, x_2, y) \right] \right| \geq 0.5\pi. \tag{17}$$

Therefore,

$$\left| \arg \lambda \left[M_1 (x_1, x_2, y) + M_2 (x_1, x_2, y) \right] \right| \geq q_r \frac{\pi}{2}. \tag{18}$$

According to the stability theorem for nonlinear fractional-order systems [9–11], (18) indicates that the equilibrium point $e = (0, 0, \ldots, 0)^T$ in system (10) is asymp-totically stable; that is,

$$\lim_{t \to +\infty} \|e\| = \lim_{t \to +\infty} \left\| \left[C_1 S_1 (x_1) + C_2 S_2 (x_2) \right] x_1 - y \right\| = 0. \tag{19}$$

Equation (19) demonstrates that the SBDFPS between the scaling drive system (2), base drive systems (3), and response system (4) can be received. The proof is completed. □

3. Illustrative Examples

To illustrate the effectiveness of the proposed synchronization scheme, some examples are given and the numerical simulations are yielded.

First, the improved version of Adams-Bashforth-Moulton numerical algorithm [12] for fractional-order nonlinear systems is introduced. Now, consider the nonlinear fractional-order system

$$\begin{aligned} \frac{d^{q_1} z_1}{dt^{q_1}} &= h_1 (z_1, z_2), \\ \frac{d^{q_2} z_2}{dt^{q_2}} &= h_2 (z_1, z_2), \end{aligned} \tag{20}$$

with initial condition $(z_1(0), z_2(0))$. Let $\tau = T/N$ and $t_n = n\tau$ $(n = 0, 1, 2 \ldots, N)$. Then, nonlinear fractional-order system (20) is discretized as follows:

$$\begin{aligned} z_1 (n+1) &= z_1 (0) + \frac{\tau^{q_1}}{\Gamma (q_1 + 2)} \\ &\quad \times \left[h_1 \left(z_1^p (n+1), z_2^p (n+1) \right) + \sum_{j=0}^{n} \alpha_{1,j,n+1} h_1 (z_1 (j), z_2 (j)) \right], \\ z_2 (n+1) &= z_2 (0) + \frac{\tau^{q_2}}{\Gamma (q_2 + 2)} \\ &\quad \times \left[h_2 \left(z_1^p (n+1), z_2^p (n+1) \right) + \sum_{j=0}^{n} \alpha_{2,j,n+1} h_2 (z_1 (j), z_2 (j)) \right], \end{aligned} \tag{21}$$

where

$$z_1^p (n+1) = z_1 (0) + \frac{1}{\Gamma (q_1)} \sum_{j=0}^{n} \beta_{1,j,n+1} h_1 (z_1 (j), z_2 (j)),$$

$$z_2^p (n+1) = z_2 (0) + \frac{1}{\Gamma (q_2)} \sum_{j=0}^{n} \beta_{2,j,n+1} h_2 (z_1 (j), z_2 (j)),$$

$$\alpha_{i,j,n+1} = \begin{cases} n^{q_i+1} - (n - q_i)(n+1)^{q_i}, & j = 0 \\ (n-j+2)^{q_i+1} + (n-j)^{q_i+1} - 2(n-j+1)^{q_i+1}, & 1 \leq j \leq n \\ 1, & j = n+1, \end{cases} \quad (i = 1, 2), \tag{22}$$

$$\beta_{i,j,n+1} = \frac{\tau^{q_i}}{q_i} \left[(n-j+1)^{q_i} - (n-j)^{q_i} \right], \quad 0 \leq j \leq n \ (i = 1, 2). \tag{23}$$

The error of this approximation is

$$\left| z_i (t_n) - z_i (n) \right| = o \left(\tau^{p_i} \right), \quad p_i = \min (2, 1 + q_i) \quad (i = 1, 2). \tag{24}$$

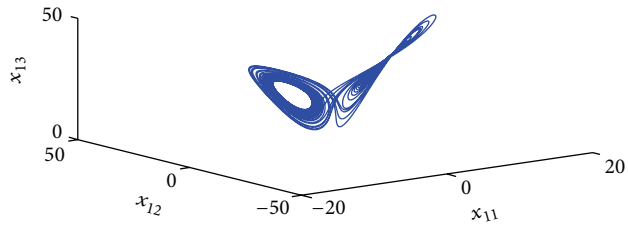

Figure 1: Chaotic attractors of fractional-order Lorenz system (25) for $q_{d1} = 0.994$.

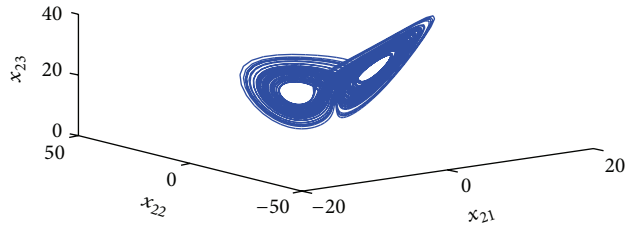

Figure 2: Chaotic attractors of fractional-order Lu system (26) for $q_{d2} = 0.95$.

The fractional-order Lorenz chaotic system [7] is depicted as

$$\begin{aligned} D^{q_{d1}} x_{11} &= 10\left(x_{12} - x_{11}\right), \\ D^{q_{d1}} x_{12} &= 28x_{11} - x_{12} - x_{11}x_{13}, \\ D^{q_{d1}} x_{13} &= x_{11}x_{12} - \frac{8x_{13}}{3}. \end{aligned} \tag{25}$$

The fractional-order Lorenz system (25) exhibits chaotic behavior for fractional-order $q \geq 0.993$. The chaotic attractor for $q_{d1} = 0.994$ is shown in Figure 1.

The fractional-order Lu chaotic system [13] is described as

$$\begin{aligned} D^{q_{d2}} x_{21} &= 36\left(x_{22} - x_{21}\right), \\ D^{q_{d2}} x_{22} &= 20x_{22} - x_{21}x_{23}, \\ D^{q_{d2}} x_{23} &= x_{21}x_{22} - 3x_{23}. \end{aligned} \tag{26}$$

Its chaotic attractor for $q_{d2} = 0.95$ is illustrated in Figure 2.

The fractional-order Chen chaotic system [7] is

$$\begin{aligned} D^{q_r} y_1 &= 35\left(y_2 - y_1\right), \\ D^{q_r} y_2 &= -7y_1 + 28y_2 - y_1y_3, \\ D^{q_r} y_3 &= y_1y_2 - 3y_3. \end{aligned} \tag{27}$$

The fractional-order Chen system (27) exhibits chaotic behavior for fractional-order $q_r \geq 0.83$. The chaotic attractor of fractional-order Chen system (27) for $q_r = 0.85$ is displayed in Figure 3.

Now, the fractional-order Lorenz chaotic system (25) is selected as the scaling drive system, the fractional-order Lu chaotic system (26) is selected as the base drive system, and the fractional-order Chen chaotic system (27) is selected as

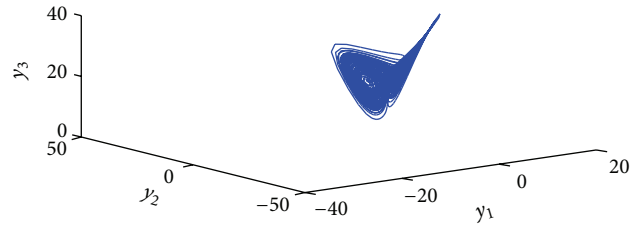

Figure 3: Chaotic attractors of fractional-order Chen system (27) for $q_r = 0.85$.

response system. Our goal is to realize the SBDFPS between the scaling drive system (25), the base drive system (26), and response system (27).

According to the results in Section 2, we derive that

$$M_2\left(x_1, x_2, y\right) = \begin{pmatrix} -35 & 35 & 0 \\ -7 - y_3 & 28 & -\beta \\ y_2 & \beta & -3 \end{pmatrix}, \tag{28}$$

where $\beta = x_{11}[\sum_{i=1}^{2} C_i S_i(x_i)]_{11} + x_{12}[\sum_{i=1}^{2} C_i S_i(x_i)]_{12} + x_{13}[\sum_{i=1}^{2} C_i S_i(x_i)]_{13}$, $[\sum_{i=1}^{2} C_i S_i(x_i)]_{1j}$ $(j = 1, 2)$ are the elements of matrix $[\sum_{i=1}^{2} C_i S_i(x_i)]$. $C_i \in R^{3\times 3}$ $(i = 1, 2)$ are real nonzero constant matrix.

Now, we select matrix $M_1(x_1, x_2, y)$ as follows:

$$M_1\left(x_1, x_2, y\right) = \begin{pmatrix} 0 & -28 + y_3 & -y_2 \\ 0 & -30 & 0 \\ 0 & 0 & 0 \end{pmatrix}. \tag{29}$$

Then,

$$M_1\left(x_1, x_2, y\right) + M_2\left(x_1, x_2, y\right) = \begin{pmatrix} -35 & 7 + y_3 & -y_2 \\ -7 - y_3 & -2 & -\beta \\ y_2 & \beta & -3 \end{pmatrix}. \tag{30}$$

According to Theorem 4, we can obtain the following:

$$\left|\arg\lambda\left[M_1\left(x_1, x_2, y\right) + M_2\left(x_1, x_2, y\right)\right]\right| \geq q_r\frac{\pi}{2}. \tag{31}$$

This result means that

$$\lim_{t\to+\infty}\|e\| = \lim_{t\to+\infty}\left\|\left[C_1S_1\left(x_1\right) + C_2S_2\left(x_2\right)\right]x_1 - y\right\| = 0. \tag{32}$$

Equation (32) implies that the SBDFPS between the scaling drive system (25), base drive systems (26), and response system (27) can be received.

For example, let

$$\begin{aligned} C_i &= \mathrm{diag}\left(1, 1, 1\right) \quad (i = 1, 2), \\ S_1\left(x_1\right) &= \mathrm{diag}\left[35\left(x_{12} - x_{11}\right), -7x_{11} - x_{11}x_{13}, x_{11}x_{12}\right], \\ S_2\left(x_2\right) &= \mathrm{diag}\left[10\left(x_{22} - x_{21}\right), -x_{22} - x_{21}x_{23}, x_{21}x_{22} - x_{23}\right]. \end{aligned} \tag{33}$$

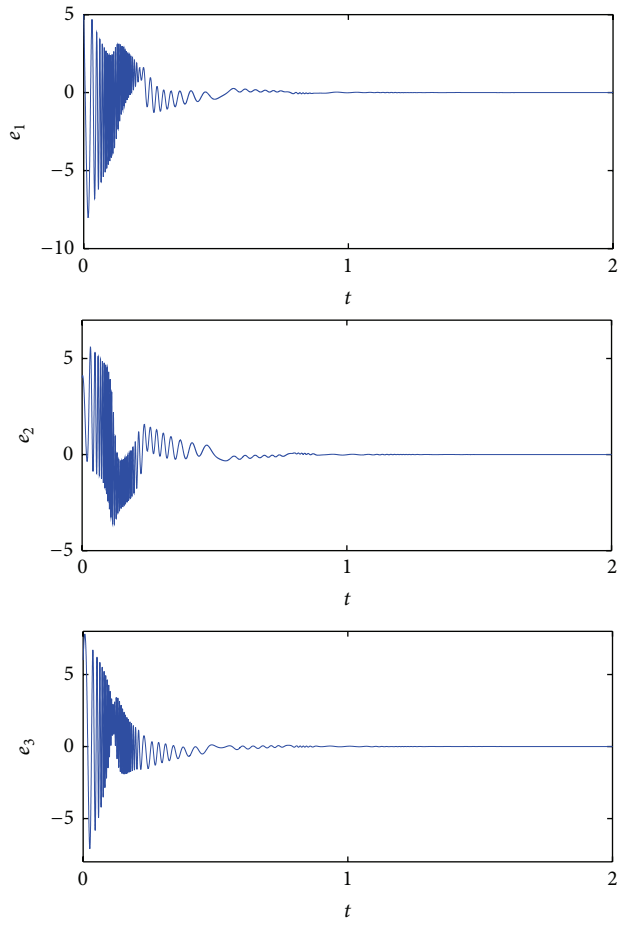

FIGURE 4: The SBDFPS errors between the scaling drive system (25), base drive systems (26), and response system (27).

The initial conditions are $(x_{11}, x_{12}, x_{13}) = (2, 2, 2)$, $(x_{21}, x_{22}, x_{23}) = (1, 1, 1)$, and $(y_1, y_2, y_3) = (5, -24, 8)$, respectively. The numerical experiments are illustrated in Figure 4.

4. Conclusions

In this paper, the scaling-base drive function projective synchronization (SBDFPS) is presented. The SBDFPS scheme is different from the FPS scheme because the scaling function matrix comes from more than one chaotic system (the scaling drive system and the base drive system). The SBDFPS between the fractional-order Lorenz chaotic system (scaling drive system), the fractional-order Lu chaotic system (base drive system), and the fractional-order Chen chaotic system (response system) is taken for example. Numerical experiments show the effectiveness of the SBDFPS scheme.

Conflict of Interests

The authors declare that there is no conflict of interests regarding the publication of this paper.

References

[1] L. M. Pecora and T. L. Carroll, "Synchronization in chaotic systems," *Physical Review Letters*, vol. 64, no. 8, pp. 821–824, 1990.

[2] T. L. Carroll and L. M. Pecora, "Synchronizing chaotic circuits," *IEEE Transactions on Circuits and Systems I*, vol. 38, pp. 453–456, 1991.

[3] L. Kacarev and U. Parlitz, "Generalized synchronization, predictability, and equivalence of unidirectionally coupled dynamical systems," *Physical Review Letters*, vol. 76, pp. 1816–1819, 1996.

[4] L. Kacarev and U. Parlitz, "General approach for chaotic synchronization, with application to communication," *Physical Review Letters*, vol. 74, pp. 5028–5031, 1996.

[5] R. Mainieri and J. Rehacek, "Projective synchronization in the three-dimensional chaotic systems," *Physical Review Letters*, vol. 82, pp. 3042–3045, 1999.

[6] H. Y. Du, Q. S. Zeng, C. H. Wang, and M. X. Ling, "Function projective synchronization in coupled chaotic systems," *Nonlinear Analysis. Real World Applications*, vol. 11, no. 2, pp. 705–712, 2010.

[7] P. Zhou and W. Zhu, "Function projective synchronization for fractional-order chaotic systems," *Nonlinear Analysis. Real World Applications*, vol. 12, no. 2, pp. 811–816, 2011.

[8] J. W. Sun, Y. Shen, Q. Yin, and C. J. Xu, "Compound synchronization of four memristor chaotic oscillator systems and secure communication," *Chaos*, vol. 23, no. 1, Article ID 013140, 2013.

[9] E. Ahmed, A. M. A. El-Sayed, and H. A. A. El-Saka, "Equilibrium points, stability and numerical solutions of fractional-order predator-prey and rabies models," *Journal of Mathematical Analysis and Applications*, vol. 325, no. 1, pp. 542–553, 2007.

[10] Z. Odibat, "A note on phase synchronization in coupled chaotic fractional order systems," *Nonlinear Analysis. Real World Applications*, vol. 13, no. 2, pp. 779–789, 2012.

[11] A. S. Hegazi, E. Ahmed, and A. E. Matouk, "On chaos control and synchronization of the commensurate fractional order Liu system," *Communications in Nonlinear Science and Numerical Simulation*, vol. 18, no. 5, pp. 1193–1202, 2013.

[12] C. P. Li and G. J. Peng, "Chaos in Chen's system with a fractional order," *Chaos, Solitons & Fractals*, vol. 22, no. 2, pp. 443–450, 2004.

[13] W. H. Deng and C. P. Li, "Chaos synchronization of the fractional Lu system," *Physica A*, vol. 353, pp. 61–72, 2005.

Hindawi Publishing Corporation
Abstract and Applied Analysis
Volume 2013, Article ID 689495, 6 pages
http://dx.doi.org/10.1155/2013/689495

Research Article

Influential Node Control Strategy for Opinion Evolution on Social Networks

Cheng Ju,[1] Jinde Cao,[1,2] Weiqi Zhang,[3] and Mengxin Ji[4]

[1] *Department of Mathematics, Southeast University, Nanjing 210096, China*
[2] *Department of Mathematics, Faculty of Science, King Abdulaziz University, Jeddah 21589, Saudi Arabia*
[3] *School of Computer and Science and Engineering, Southeast University, Nanjing 210096, China*
[4] *College of Economics, Zhejiang University, Hangzhou 310058, China*

Correspondence should be addressed to Jinde Cao; jdcao@seu.edu.cn

Received 16 October 2013; Accepted 17 November 2013

Academic Editor: Qiankun Song

We study opinion dynamics in social networks and present a new strategy to control the invasive opinion. A developed continuous-opinion evolution model is proposed to describe the mechanism of making decision in closed community. Two basic strategies of evolution are determined, and some basic features of our new model are analyzed. We study the different invasive strategies. It is shown via using Monte Carlo simulations that our new model shows different invulnerability with traditional model. Node degree and cohesion in invasive small-world community plays less significant role when the evolution of opinion is continuous rather than dichotomous. Using simulation, we find one kind of Influential Nodes that can affect the outcome dramatically, while these Influential Nodes are sensitive to their node degree and the evolution weight. Thus, we develop invasive control strategy based on these features.

1. Introduction

There is long history in social science to learn social phenomenon such as opinion cluster and invasion. Some simple mathematic models are helpful tools to simulate such phenomenon. Recently the mathematic models learning the invasion and spread of new opinion have received a lot of attention [1–3]. At present, the spread rumors in real world become easier and can make huge influence on our daily life [4, 5]. Thus, the study of the dynamics of different opinions and rumors has gradually become one of the most popular fields in the study of complex networks [6, 7].

Some other questions come out with gradually deepening the study of rumors spread. It is known that some rumors and ideas seem harmless at first while they can do great harm to the health of the network if they are not controlled. To deal with such problem, many researches developed lots of strategies [8–12]. Community structure appears to be essential for the evolution of invasive opinion [13, 14]. Some researches focus on a few nodes which have large connective like Targeted immunization [11]. Furthermore, some researches also use real world data and cases to develop and evaluate their control strategy [15–17].

In order to understand the role of the Influential Node and the different strategies of opinion evolutions in the opinions dynamics, for simplicity, a continuous-opinion model is proposed in this paper, including two strategies of opinion evolution. It does not aim at an exact description of reality. However, it focuses on discovering some essential and fundamental features of an otherwise very complex and multiple phenomena by doing some crude approximations. Therefore, we use Monte Carlo method to simulate the reality and determine the sensitivity of the model and our new strategy in the different situation.

In this paper, to understand the difference between traditional dichotomous model and our new continues model and the mechanism of the Influential Node in the opinions dynamics, we focus on the following four questions. First of all, how can the different evolution strategies affect the dynamic of the model? Are there any transition points where the model is very sensitive? The answer can help us better understanding the dynamic of this continues-opinion

evolution model. Then we would like to know how the size of the invasive community and its node degree can contribute to the outcome of the model when the proportion of the strategies is fixed. Some feature of network in former study [18] may not be suitable for continues model. It is also known that the community structure can affect the evolution. So could the community structure affect the evolution of the network? If so, is the effect the same as that in the traditional dichotomous model? Last, in order to know the role it plays in the evolution, it is critical to know how Influential Node can contribute to the evolution of the network and are such nodes sensitive to some factors such as node degree. If we have better understanding of this kind of nodes, we could develop new strategy to control the spread of invasive rumor.

In the first part, we investigate the outcome of the model with different proportion of the opinion evolution strategy. The first strategy of evolution is the change of the topology structure of the network, and the second strategy is the intersecting opinion of the different points in the network. The different proportion of two basic strategies will lead to the different outcome of the dynamic model. If the model only uses the first way, the opinion of every node will not change, while the topology structure of the network will change all the time. Hence, the entire network will evolute into several small communities, and there should be no intersects between two different networks in certain time. When the model only uses the second way, the opinion of different nodes will change while the topology structure will remain the same. In this situation, the model will develop into single connected network where the structure remains the same. We define the term "consensus": if the value of every node in the network converge to a certan interval, it means this model makes "consensus". Using Monte Carlo method, we simulate the situation for different length of time. We count the probability of consensus for every 1% change of the proportion of the two strategies.

In the second part, we focus on some other questions. At first, we assign the same value of opinion to all the nodes in the network. Then we develop two major kinds of invasion for the contrary opinion. The first way is invasion with small-world community. Some former studies show that the size of community and the node degree are two major factors for the outcome. Therefore, we simulate the outcome with different size of invasive small-world and its node degree. We define Influential Node in opinion invasion. This kind of nodes has more node degree and better stability. Then we study the different factors which can affect the power of Influential Node and develop new control strategy to impede the spread of invasive opinion.

2. Model Description

2.1. Symbol Description of Network. We develop our continues-opinion model based on our former discrete multiopinion model [19].

2.2. Two Strategies of the Evolution. For the first strategy, the opinion of every node will not change, while the topology structure of the network will change every step. Hence, if the node i connects with the node j and their opinions are different, the node i will remove the edge to the j and randomly choose. And the node i will then find a note which has the same opinion to develop a new edge.

Table 1: Symbols table.

Symbol	Description
N	The number of nodes in the entire network
n	The number of Influential Nodes
M	The proportion of the invasive nodes
MN	The number of invasive nodes
K	The average number of edges for every node (average node degree)
m	The average number of extra edges for the Influential Nodes
k	The average number of extra edges for the nodes in the invasive community
P	The proportion of the first way of process
t	Time (or the number of the steps)
T	The length of experiment
w	The evolution weight
$d_{ij}(t)$	If nodes i and j connect at time t $d_{ij}(t) = 1$. Otherwise $d_{ij}(t) = 0$
$\sigma_i(t)$	The opinion value of node i at time t

For the second strategy, the opinions are intersected with the different connected nodes in the network. In some former work, the network is dichotomous. Therefore, the process of this strategy can be expressed as a differential equation as follows (see Table 1 for the description of the symbols):

$$\sigma_i(t+1) = \operatorname{sign}\left[\sum_{j=1}^{N} d_{ij}\sigma_i(t)\,\xi_{ij}(t) + h_i(t)\right]. \quad (1)$$

However, in real world, new kind of invasive opinion may intersect with traditional opinion and therefore develop new kind of opinion. For example, some people would have neutralized opinion when facing two extreme opinions. Therefore, we propose our continues-opinion model as follows:

$$\sigma_i(t+1) = (1-w)\left[\sum_{j=1}^{N} d_{ij}\sigma_j(t)\right] + w\left[\sigma_i(t)\right]. \quad (2)$$

It reflects the fact that for every node, its own opinion and the opinion of its connected nodes can contribute to its opinion in the future. The difference is that, in this paper, extreme opinions can be neutralized and develop to new opinion.

3. The Sensitivity of the Model to the Proportion of Two Strategies

In order to determine how the proportion of two strategies can affect the evolution, we stimulate by using Monte Carlo method.

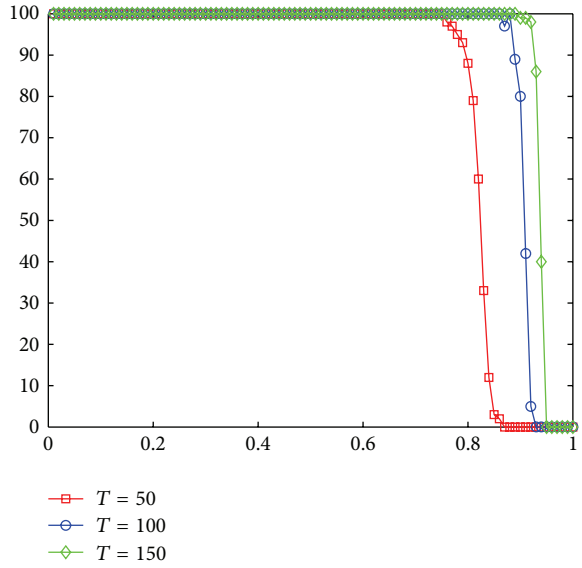

Figure 1: The y-axis represents the number of win in 100 experiments. The x-axis represents the proportion of two strategies.

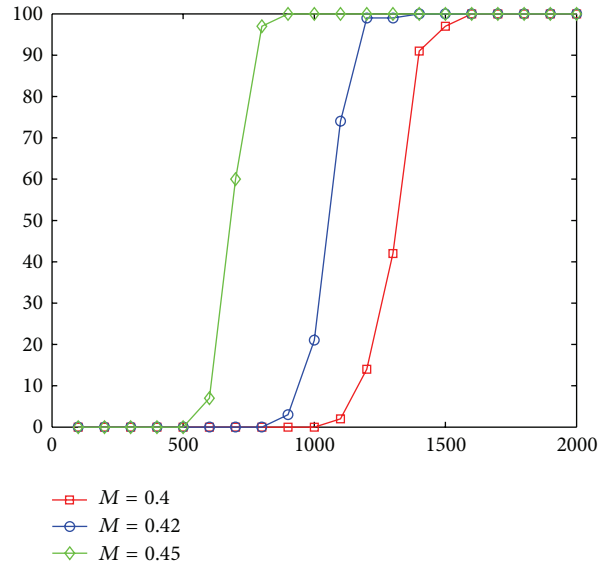

Figure 2: The y-axis represents the number of weak win in 100 experiments. The x-axis represents k.

First of all, we define "consensus" that if at the end of experiment, every in the network converges to an interval and the range of this interval is less than 0.2. We consider the situation that $N = 1000$ and the initial value of every node is obeying uniform distribution on $[-1, 1]$. We simulated the probability of consensus with different proportion of two strategies.

Figure 1 shows that, compared with traditional model, nodes in continues-model are more likely to make consensus. We can see that the probability for consensus is high when the proportion of first strategy is little. The probability for consensus decreased sharply by the increase of the proportion after $P > 0.8$. Hence, in conclusion, we determine that the phase transition point is around 0.85 when $T = 50$ and will increase a little with the increase of T.

4. Evolution under Small-World Invasive Strategy

Some researches study some features of small-world community. Connection of the community can make the node in it prefer grouping together and therefore make critical impact on opinion evolution in the entire network [18].

First, we construct a scale-free network and the value of every node is 1. Then the invasive nodes become −1. In order to define the outcome of the invasion, we define the term "strong win" if all values of the nodes in the network converge to $[-1, -0.75]$ and "weak win" if all the values of the nodes are smaller than 0.

We consider the situation that $N = 1000$ and $M = 0.4$, 0.42, and 0.45. Then we randomly add some extra nodes into invasive community. Therefore, we can have a small-world invasive community.

Figure 2 shows the probability of weak win for different node degree in invasive community. When $M = 0.45$ in new model, if invasive community wants to have "weak win," it should have greater average node degree compared with traditional model. Although node degree still can help minority succeed, the effect is much smaller.

Remark 1. In continues-opinion evolution model, small-world communities are less likely to success. They need much dense of connection to maintain their impact on the network. Moreover, size of community plays more significant role in evolution. In other word, the communities with large size are more likely to success.

5. Evolution under Influential Node Invasive Strategy

It is known that in the real network, some celebrities can make far more impact to the opinion evolution compared with normal people. Therefore, we present a kind of node to simulate such people. This kind of node has two main characteristics.

(1) They have much more node degrees compared with other nodes.

(2) They are less likely to change their own opinion value compared with ordinary nodes.

In order to have better understanding of this kind of nodes, we investigate three factors of such nodes:

(1) quantity: n

(2) Their influence (their node degree): m

(3) how can they be influenced by other nodes: w.

Therefore, we simulate with different parameters to find out how these three factors can affect the success rate for the invasive community.

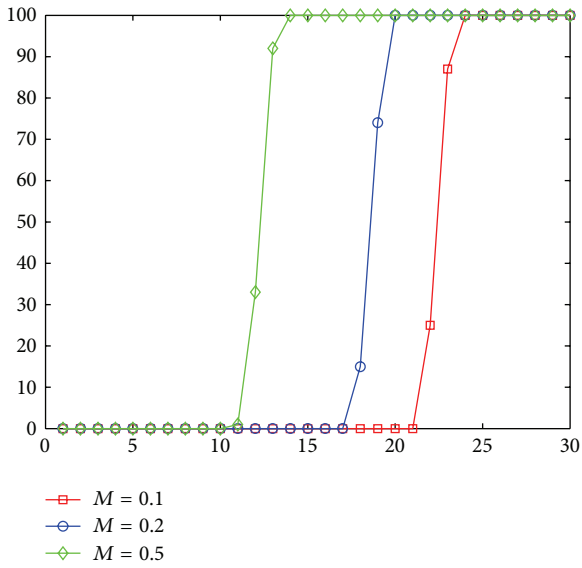

Figure 3: The y-axis represents the number of strong win in 100 experiments. The x-axis represents n, when $m = 50$.

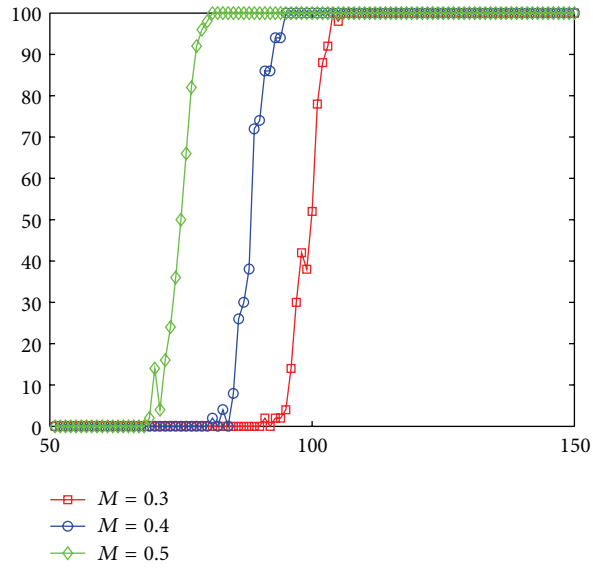

Figure 4: The y-axis represents the number of strong win in 100 experiments. The x-axis represents m, when $n = 10$.

5.1. The Effect of the Number of Influential Nodes. We consider the situation that $N = 1000$, $w = 1$, $m = 50$, and $M = 0.1$, 0.2, and 0.5. Then we randomly choose NM nodes in invasive nodes and n invasive nodes as Influential Nodes. We do 100 experiments at different n and find the probability for invasive community to win.

Figure 3 shows the probability for invasive community to win with different number of Influential Nodes. It shows that the outcome is sensitive to the number of Influential Nodes. When $M = 0.1$, $n < 10$, there seems to be no chance for invasive community to win. However, the probability increases abruptly around $n = 12$. The community with smaller size may need more Influential Nodes to keep success. Hence, near the transition point, controlling the number of the Influential Nodes is an economic and efficient way to control the invasive opinion.

Remark 2. The spread power of invasive opinion is sensitive to the number of Influential Nodes. To control the spread of invasive opinion, controlling the number of Influential Nodes is an economic and efficient strategy when n is not large.

5.2. The Effect of the Degree of Influential Nodes. We consider the situation that $N = 1000$, $w = 1$, $n = 10$, and $M = 0.3$, 0.4, and 0.5. Then we randomly choose NM nodes in invasive nodes and n invasive nodes as Influential Nodes. We do 100 experiments with different node degree and find the probability for invasive community to win.

Figure 4 shows the probability for invasive community to win with different node degree. It is known that the celebrities with more influence and more followers can better influence the opinion evolution. In our model, we define the influence as node degree. In this simulation we find that the model is also sensitive to the node degree of Influential Nodes. With low degree, invasive community still has very small chance to win. However, with the increase of degree, Influential Nodes can play much greater impact on evolution.

Remark 3. The spread power of invasive opinion is sensitive to the degree of Influential Nodes. To control the spread of invasive opinion, controlling the degree of Influential Nodes is an economic and efficient strategy when n cannot be controlled.

5.3. The Effect of the Evolution Weight of Influential Nodes. In real world social network, evolution weight for every single point can be considered as the influence of this individual. The nodes with great weight can make more impact on the opinion evolution.

We consider the situation that $N = 1000$, $w = 1$, $n = 15$, and $M = 0.45$. Then we randomly choose NM nodes in invasive nodes and n invasive nodes as Influential Nodes. We do 100 experiments with different evolution weight w.

In our pretreatment, we find that if $w < 1$, the nodes in entire network would never converge to the interval $[-1, -0.75]$. Therefore, we try to use Convergence Interval Midpoint to evaluate the impact of Influential Nodes on the evolution.

Figure 5 shows the Convergence Interval Midpoint for every experiment. It shows that with the decrease of w, the Convergence Interval Midpoint approaches to 0 abruptly. Though it still can make negative influence on the entire network, the loss would be reduced a lot. Even a little reduction of w can contribute a lot to control the harm of the invasion.

Remark 4. The opinion evolution is sensitive to the evolution weight of Influential Nodes. Although reducing w cannot control the spread of invasive opinion, it can reduce the negative impact on the entire network. Therefore it can help the entire network recover much easier.

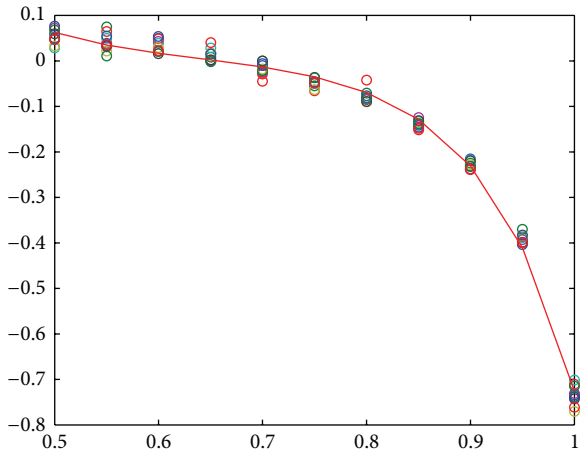

Figure 5: The y-axis represents the Convergence Interval Midpoint for every experiment. The x-axis represents w when $n = 15$, $m = 50$, and $M = 0.45$.

6. Conclusions

In conclusion, we have investigated a developed continues-opinion evolution model. Two basic strategies of evolution are determined, and some basic features of our new model are analyzed. Then we analyze Influential Node and its impact on entire network. Different invasive opinion control strategies are also considered. By analyzing the phase transition point, we find that our new model is more likely to make consensus compared with the discrete traditional model. Our model can better characterize the process of the opinion neutralization. In continues model, invasive small-world community is less likely to achieve success. In other words, community size is much more significant in this new model. Further analysis shows that one kind of nodes can play critical role in invasion. With a little proportion of Influential Nodes, invasive community can achieve success even if the size is small. Hence we investigate three factors which may affect the outcome: quantity, node degree, and evolution weight. It has been observed that Influential Nodes are sensitive to their population and node degree. Though the evolution weight cannot contribute to controlling the spread of invasion, it can reduce the negative impact of invasion. Therefore, controlling these three parameters of Influential Nodes can be an effective method to impede the invasion and reduce the potential loss.

Conflict of Interests

The authors declare that there is no conflict of interests regarding the publication of this paper.

Acknowledgments

This work was jointly supported by the National Natural Science Foundation of China under Grants nos. 61272530 and 11072059, the Natural Science Foundation of Jiangsu Province of China under Grant no. BK2012741, and the Specialized Research Fund for the Doctoral Program of Higher Education under Grant nos. 20110092110017 and 20130092110017.

References

[1] N. Crokidakis and F. L. Forgerini, "Consequence of reputation in the Sznajd consensus model," *Physics Letters A*, vol. 374, no. 34, pp. 3380–3383, 2010.

[2] P. Holme and M. E. J. Newman, "Nonequilibrium phase transition in the coevolution of networks and opinions," *Physical Review E*, vol. 74, no. 5, Article ID 056108, 5 pages, 2006.

[3] R. Lambiotte, M. Ausloos, and J. A. Hołyst, "Majority model on a network with communities," *Physical Review E*, vol. 75, no. 3, Article ID 030101, 4 pages, 2007.

[4] F. Radicchi and S. Fortunato, "Explosive percolation: a numerical analysis," *Physical Review E*, vol. 81, no. 3, Article ID 036110, 10 pages, 2010.

[5] M. Girvan and M. E. J. Newman, "Community structure in social and biological networks," *Proceedings of the National Academy of Sciences of the United States of America*, vol. 99, no. 12, pp. 7821–7826, 2002.

[6] P. L. Krapivsky and S. Redner, "Dynamics of majority rule in two-state interacting spin systems," *Physical Review Letters*, vol. 90, no. 23, Article ID 238701, 4 pages, 2003.

[7] M. Lewenstein, A. Nowak, and B. Latané, "Statistical mechanics of social impact," *Physical Review A*, vol. 45, no. 2, pp. 763–776, 1992.

[8] Y. Chen, G. Paul, S. Havlin, F. Liljeros, and H. E. Stanley, "Finding a better immunization strategy," *Physical Review Letters*, vol. 101, no. 5, Article ID 058701, 4 pages, 2008.

[9] R. Cohen, K. Erez, D. Ben-Avraham, and S. Havlin, "Resilience of the Internet to random breakdowns," *Physical Review Letters*, vol. 85, no. 21, pp. 4626–4628, 2000.

[10] R. Cohen, K. Erez, D. Ben-Avraham, and S. Havlin, "Breakdown of the internet under intentional attack," *Physical Review Letters*, vol. 86, no. 16, pp. 3682–3685, 2001.

[11] P. Holme, B. J. Kim, C. N. Yoon, and S. K. Han, "Attack vulnerability of complex networks," *Physical Review E*, vol. 65, no. 5, Article ID 056109, 14 pages, 2002.

[12] L. K. Gallos, F. Liljeros, P. Argyrakis, A. Bunde, and S. Havlin, "Improving immunization strategies," *Physical Review E*, vol. 75, no. 4, Article ID 045104, 4 pages, 2007.

[13] M. E. J. Newman, "Scientific collaboration networks. I. Network construction and fundamental results," *Physical Review E*, vol. 64, no. 1, Article ID 016131, 8 pages, 2001.

[14] M. E. J. Newman, "Scientific collaboration networks. II. Shortest paths, weighted networks, and centrality," *Physical Review E*, vol. 64, no. 1, Article ID 016132, 7 pages, 2001.

[15] R. M. Tripathy, A. Bagchi, and S. Mehta, "A study of rumor control strategies on social networks," in *Proceedings of the ACM 19th International Conference on Information and Knowledge Management (CIKM '10)*, pp. 1817–1820, ACM, October 2010.

[16] A. J. Kimmel and A. Audrain-Pontevia, "Analysis of commercial rumors from the perspective of marketing managers: rumor prevalence, effects, and control tactics," *Journal of Marketing Communications*, vol. 16, no. 4, pp. 239–253, 2010.

[17] L. Zhao, Q. Wang, J. Cheng, Y. Chen, J. Wang, and W. Huang, "Rumor spreading model with consideration of forgetting mechanism: a case of online blogging LiveJournal," *Physica A*, vol. 390, no. 13, pp. 2619–2625, 2011.

[18] G. Huang, J. Cao, and Y. Qu, "The minority's success under majority rule," *Physica A*, vol. 388, no. 18, pp. 3911–3916, 2009.

[19] C. Ju, Y. Cao, and P. Zhou, "The effect of different strategies and the structure on opinion formation," *Discrete Dynamics in Nature and Society*, vol. 2013, Article ID 705318, 6 pages, 2013.

Hindawi Publishing Corporation
Abstract and Applied Analysis
Volume 2013, Article ID 105724, 6 pages
http://dx.doi.org/10.1155/2013/105724

Research Article

Mechanism of Stochastic Resonance in a Quorum Sensing Network Regulated by Small RNAs

Ya-nan Zhu,[1,2] Jianwei Shen,[1] and Yong Xu[2]

[1] *Institute of Applied Mathematics, Xuchang University, Xuchang, Henan 461000, China*
[2] *Department of Applied Mathematics, Northwestern Polytechnical University, Xi'an 710072, China*

Correspondence should be addressed to Jianwei Shen; xcjwshen@gmail.com

Received 27 September 2013; Accepted 24 October 2013

Academic Editor: Jinde Cao

Bacterial quorum sensing (QS) is an important process of cell communication and more and more attention is paid to it. Moreover, the noises are ubiquitous in nature and often play positive role. In this paper, we investigate how the noise enhances the QS though the stochastic resonance (SR) and explain the mechanism of SR in this quorum sensing network. In addition, we also discuss the interaction between the small RNA and the other genes in this network and discover the biological importance.

1. Introduction

In each cell, the survival of bacteria depends mainly on the regulatory networks involved in quorum sensing, which is a mechanism of cell communication that enable bacteria to track population density by secreting and detecting extracellular signaling molecules called autoinducers (AIs) [1, 2]. QS can regulate the concentration of AIs and alter the expression of genes to transmit information and carry out task. Recently, the experiments [3, 4] show that the small RNAs play an important role in QS network of the bacterium *Vibrio harveyi* and indicate that there is a feedback loop between small RNAs and QS master regulatory protein.

In order to investigate qualitatively the QS, we hope to model the network by the use of mathematical tool. Shen [5] constructs a mathematical model according to Michaelis-Menten kinetics and mass action law and shows the oscillatory dynamics of the QS network regulated by small RNA and obtains some theoretical results. As we know, there are noises when the genes interact in cell, and the movement of genes abides by Gaussian distribution. In this paper, we will investigate how the noise enhances the QS though the stochastic resonance (SR) and explain the mechanism of SR in this quorum sensing network. Stochastic resonance is said to be observed when increases in levels of unpredictable fluctuations take place. for example, random noises cause an increase in the metric of the quality of signal transmission or detection performance rather than a decrease.

Hobert [6, 7] discussed common principles and conceptual differences between transcription factor and microRNA regarding how these factors control gene expression. Shimoni et al. [8], showed quantitatively that regulation by sRNA is advantageous when fast responses to external signals are needed, which is consistent with experimental data about its involvement in stress responses.

Moreover, the studies show that noises often play the constructive role, enhancing the response of a nonlinear system and emerging the type of stochastic resonance (SR). SR can be realized in a wide variety of systems, including monostable systems [9], excitable systems [10], and bistable-well systems [11, 12]. The effect of SR has equally been examined in physical systems [13, 14] and chemical systems [15, 16], as well as biological systems [17, 18]. These SR phenomena are typically driven by periodic forces or noise signals. Especially, Hou and Xin [19] found that noises can induce circadian oscillations, when the corresponding deterministic system does not oscillate; that is, stochastic resonance occurs when circadian oscillation undergoes to maximum at a certain noise level. However, it is worth noting that noises can enhance the performance of oscillation when the corresponding deterministic system does oscillate, which suggests that stochastic resonance will occur for a particular

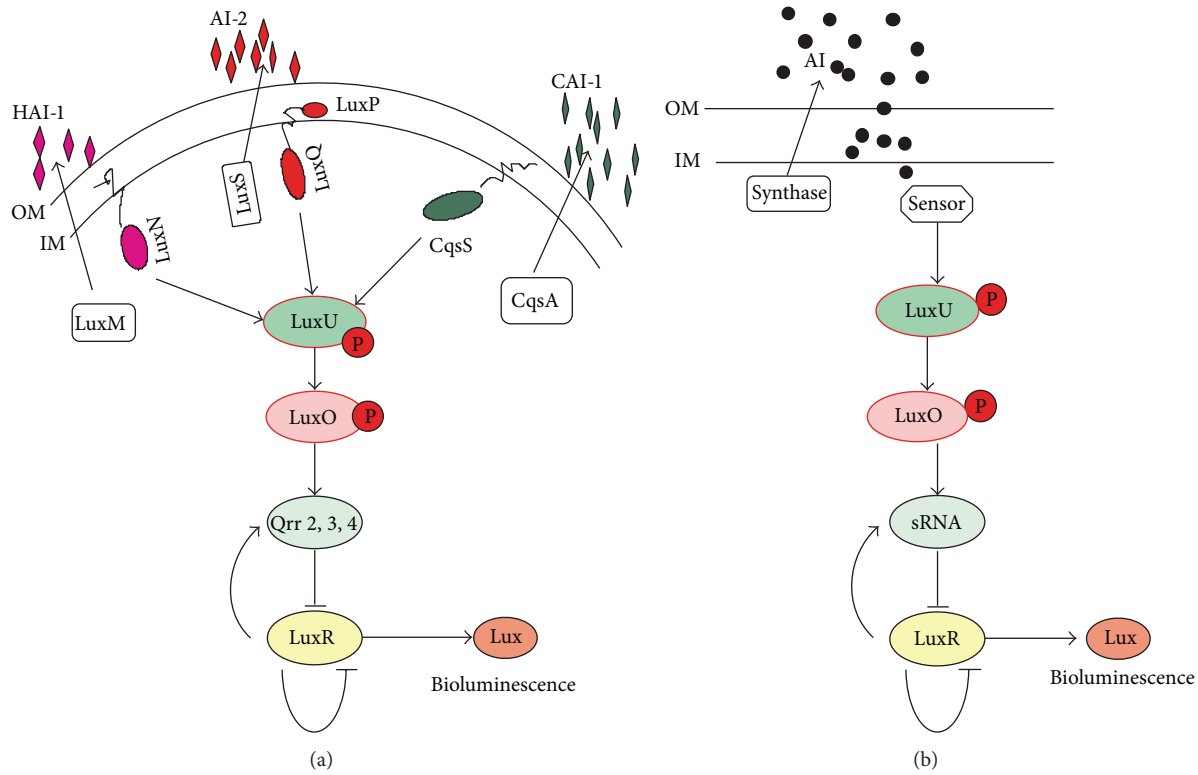

Figure 1: Schematic diagram showing the gene regulation mediated by sRNA with a negative feedback loop. (a) Original model; (b) abstract model.

noise intensity. Here, we also consider the QS network driven by noises.

The rest of the paper is organized as follows. In Section 2, we give the model description. In Section 3, we describe the method of how to investigate the noises on this network. In Section 4, we give some results and discuss the dynamics and the mechanism of SR on QS network.

2. Model Description

Bacteria quorum sensing regulated by small RNA in *Vibrio harveyi* was descripted by Miller an Bassler [1], Waters and Bassler [2]; they descripted the network as in Figure 1.

For the quorum sensing network in *Vibrio harveyi*, the phosphorylation of regulator protein LuxO can be controlled by the interaction between AIs and sensors. At negligible concentrations of AIs, that is, at low cell density (LCD), these sensors act as kinases that transfer phosphate through LuxU to LuxO [3, 4]. LuxO-P activates the expression of genes encoding small RNAs which in turn posttranscriptionally repress the QS master regulatory protein LuxR. At the high cell density (HCD), AIs accumulate and bind to their cognate sensors and the sensors act as phosphatases, reversing the phosphate flow through the QS circuit. This results in dephosphorylation and inactivation of LuxO, so that the expression of genes encoding the small RNAs is terminated. To understand the dynamics of this network, Shen [5] abstracted Figure 1(b) from Figure 1(a) and investigated the dynamics of the quorum sensing network regulated by Small RNAs for some fixed parameters and found that Hopf bifurcation occurred in this system when control parameter undergo a critical value τ_0. However, we know that signal recognized by living organisms is often noisy, and it is not typically ignored. To further characterize the dynamics of quorum sensing network, it is essential to consider the effect of noise on Quorum Sensing network [5]. When noise is taken into account, we can describe the dynamics of the model using stochastic differential equations as follows:

$$\frac{d\,[\mathrm{LuxM}]}{dt} = a_1 - k_1\,[\mathrm{LuxM}]\,,$$

$$\frac{d\,[\mathrm{AI}]}{dt} = k_1\,[\mathrm{LuxM}] - d_1\,[\mathrm{AI}]\,,$$

$$\frac{d\left[\mathrm{LuxU_p}\right]}{dt} = k_4\,[S_k]\left(\mathrm{U_0} - \left[\mathrm{LuxU_p}\right]\right) - k_5\left[S_p\right]\left[\mathrm{LuxU_p}\right] - d_3\left[\mathrm{LuxU_p}\right],$$

$$\frac{d\,[\mathrm{sRNA}]}{dt} = \frac{1 + k_7[\mathrm{protein}]^m\,(t-\tau_1) + \delta_1\left[\mathrm{LuxO_p}\right]}{1 + [\mathrm{protein}]^m\,(t-\tau_1) + \delta_2\left[\mathrm{LuxO_p}\right]} - r\,[\mathrm{sRNA}]\,[\mathrm{mRNA}] - d_4\,[\mathrm{sRNA}] + D\xi\,(t)\,,$$

$$\begin{aligned}
&\frac{d\,[\mathrm{mRNA}]}{dt} \\
&\quad = \frac{k_8}{1+[\mathrm{protein}]^m\,(t-\tau_1)} \\
&\qquad - r\,[\mathrm{sRNA}]\,[\mathrm{mRNA}] - d_5\,[\mathrm{mRNA}]\,, \\
&\frac{d\,[\mathrm{protein}]}{dt} \\
&\quad = k_9\,[\mathrm{mRNA}]\,(t-\tau_2) - d_6\,[\mathrm{protein}]\,, \\
&\frac{d\,[\mathrm{Lux}]}{dt} = \frac{k_{10}[\mathrm{protein}]^m\,(t-\tau_1)}{1+[\mathrm{protein}]^m\,(t-\tau_1)} - d_7\,[\mathrm{Lux}]\,,
\end{aligned} \tag{1}$$

where

$$\begin{aligned}
&[\mathrm{O_0}] = [\mathrm{LuxO}] + \left[\mathrm{LuxO_p}\right]\left[\mathrm{LuxO_p}\right] \\
&\quad = \frac{\left[\mathrm{LuxO_p}\right]\mathrm{O_1}}{k\left[\mathrm{U_0}\right] + (1-k)\left[\mathrm{LuxO_p}\right]}, \\
&S_0 = S_k + S_p, \qquad k = \frac{k_{-5}}{k_5}, \\
&\mathrm{U_0} = [\mathrm{LuxU}] + \left[\mathrm{LuxU_p}\right], \qquad S_p = \frac{[\mathrm{AI}]^n\,[S_0]}{k_0^n + [\mathrm{AI}]^n}, \\
&S_k = \frac{k_0^n\,[S_0]}{k_0^n + [\mathrm{AI}]^n}, \qquad k_0 = \left(\frac{k_{-2}k_{-3}}{k_2k_3}\right)^{1/n}.
\end{aligned} \tag{2}$$

In the above equations, [LuxM], [AI], [LuxU], [sRNA], [mRNA], [protein], and [Lux] represent the concentrations of LuxM, AI, $\mathrm{LuxU_p}$, sRNA, mRNA, protein, and Lux, respectively. S_k represents sensor corresponding to the kinase state and S_p represents the sensor corresponding to the phosphatase state. LuxO is a kind of regulator protein. LuxO represents phosphorylated $\mathrm{LuxO_p}$. $k_1 \sim k_6$ represent the reaction rate and the $k_{-1} \sim k_{-3}$, $k_{-5} \sim k_{-6}$ represent the dissociation constant. $k_7 \sim k_{10}$ and $\delta_1 \sim \delta_2$ are the basal rate of transcription in the absence of transcription. $d_1 \sim d_7$ represent the degradation rate. r is a rate for small RNA base pairs with the target mRNA. m and n are Hill coefficients. τ_1 and τ_2 are the time delays. The noise $\xi(t)$ is assumed as Gaussian noise with zero mean and delta-correlated: $\langle \xi(t)\xi(t')\rangle = \delta(t-t')$; $\langle\cdot\rangle$ denote an ensemble average and D is noise intensity.

3. Methods

Quorum sensing makes the concentration of protein circulate from HCD to LCD and transmits the information. In real world, the noises are ubiquitous and play an important role; they can increase the periodical oscillation from HCD to LCD and emerge the phenomena of stochastic resonance. As we all know, the measures characterizing SR are present widely in nonlinear system, including amplification factor, signal-to-noise ratio, the degrees of coherence and of order. For example, Fauve and Heslot used SNR (signal-to-noise ratio) as a measure for characterizing SR phenomenon in the Schmitt trigger system [20] subjected to a weak periodic signal. Jung and Hänggi described SR phenomenon using the measure of spectral power amplification (SPA) in the standard double-well system [11] subjected to periodic forces and noise signal. Although these measures showed some differences in definition, they measure have a common feature which undergo to the maximum for a certain optimal noise intensity. Here we adopt SNR as a method for describing SR phenomenon in the context of a Quorum Sensing network with time delay regulated by small RNAs, where SNR [21] is defined as the ratio between the peak of the power spectrum of a signal and the width of frequency corresponding to height $h_1 = e^{-1/2} * \text{peak}$. The formula of SNR is as follows:

$$\mathrm{SNR} = \frac{H * \omega_p}{\Delta\omega}, \tag{3}$$

where H is the maximum of the power spectrum of a signal, ω_p is the internal signal frequency, and $\Delta\omega$ is the width of frequency corresponding to height $h_1 = e^{-1/2} * H$. Additionally, the spectral estimate [22] at a given frequency for a single discrete signal series x_t is

$$C_{xx}(f) = 2\Delta\left\{c_{xx}(0) + 2\sum_{k=1}^{L-1} c_{xx}(k)\,w(k)\cos(2\pi f k\Delta)\right\}. \tag{4}$$

In the above equation, $c_{xx}(k)$ is the autocovariance function evaluated at the lag k, Δ is the distance between adjacent time series values, L is the length of signal series, and f is the frequency. The $w(k)$ is the window function; here, we adopt Welch window [23] as window function. The autoamplitude spectral estimate (power spectrum) is defined as $P(f) = |C_{xx}(f)|^2$. In the following, we will make use of the above method to discuss the QS network.

4. Results and Discussion

In the previous work, we know that there are periodical oscillations when control parameter $\tau(\tau_1+\tau_2)$ is larger than critical value. Now, we mainly focus on the effect of noise when τ is larger than threshold value; that is, the corresponding deterministic system is oscillatory. In order to investigate the effect of noise, firstly, we integrate the corresponding deterministic system and stochastic differential system (1) for control parameter $\tau = 10.5$ which is on the right of critical value. Figure 2 shows the tendency for time history diagram of small RNA concentration when $D = 0$. These oscillations of small RNA caused by different noise levels are presented in Figure 3. Here, the parameter values that remain unchanged during simulation are as follows: $a_1 = 1$, $s_0 = 2$, $u_0 = 2$, $k = 0.8$, $m = 2$, $n = 2$, $O_0 = 2$, $r = 1$, $k_0 = 0.8$, $k_1 = 0.2$, $k_4 = 0.3$, $k_5 = 0.3$, $k_6 = 1$, $k_7 = 0.5$, $k_8 = 2$, $k_9 = 1$, $k_{10} = 1$, $d_1 = 0.5$, $d_2 = 0.6$, $d_3 = 0.5$, $d_4 = 0.3$, $d_5 = 0.2$, $d_6 = 0.1$, $a_1 = 1$, $d_7 = 0.8$, $\delta_1 = 1$, $\delta_2 = 1.1$, $\tau_1 = 3.5$, and $\tau_2 = 7$.

Comparing Figures 2 and 3, we clearly see that the periodical oscillation of small RNA is not explicitly improved

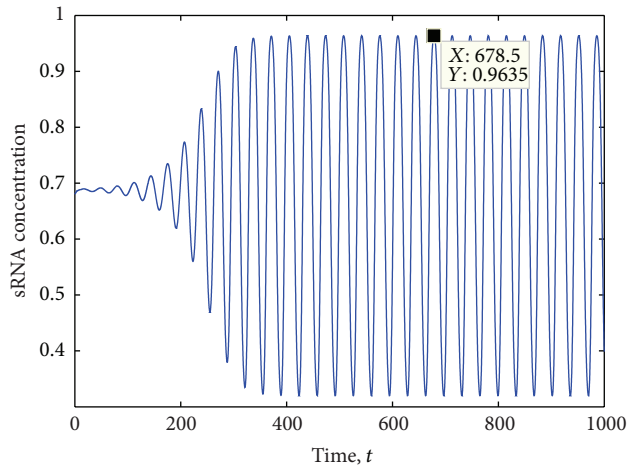

Figure 2: Time history diagram of small RNA concentration when $D = 0$.

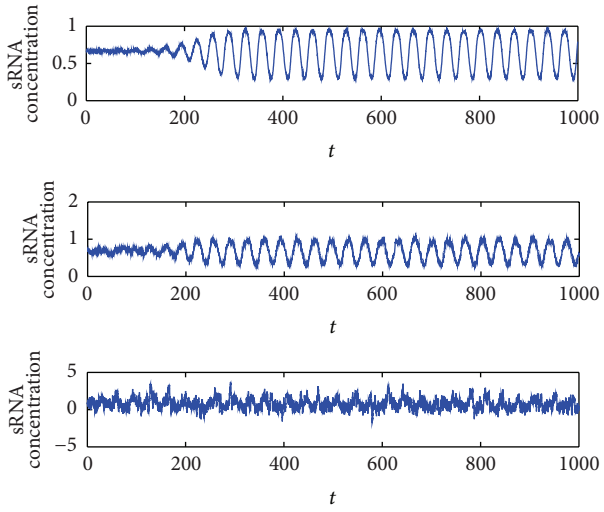

Figure 3: The dynamics of system (1) for different noise intensities: From bottom to top, $D = 0.8$, $D = 0.05$, and $D = 0.01$.

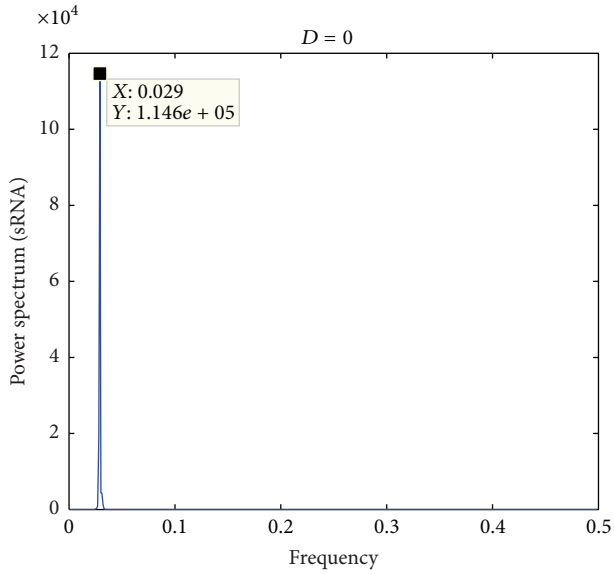

Figure 4: The power spectrum of small RNA presented in Figure 2.

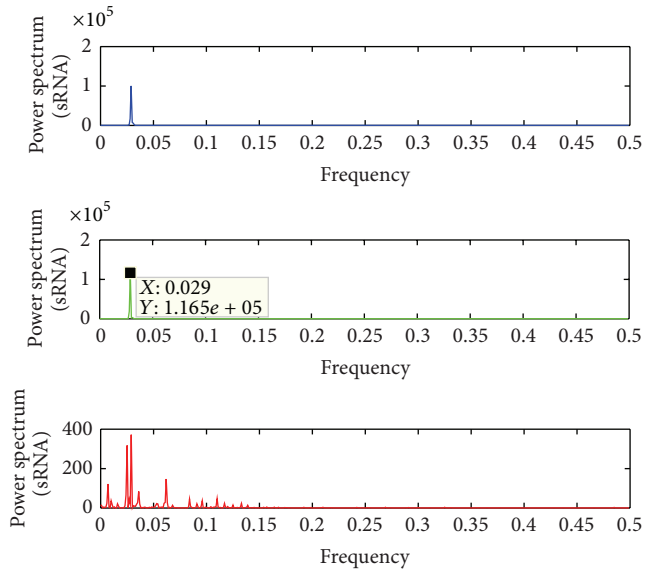

Figure 5: The power spectrum of small RNA presented in Figure 3.

when small noise intensity is added in the system (1), while the periodic oscillation of small RNA is almost completely disturbed by strong noise amplitude; that is, the strong noise-induced oscillations appear to be rather irregular. However, we surprisingly find that the periodical oscillation of small RNA is largely improved at a particular noise intensity. Meanwhile, we can also illustrate the above results in terms of power spectrum.

We know that the frequency of period oscillation is about 0.029 as shown in Figure 2. The corresponding power spectrum performs an obvious peak in the foundational frequency, which can be seen in Figure 4. Additionally, the power spectrum diagrams of small RNA that caused different noise amplitudes are depicted in Figure 5. It is easy to find that the peak values at the internal signal frequency (0.029) for both the small and large noise amplitudes are smaller than of the corresponding deterministic system. However, the peak value in the second diagram in Figure 5 is larger than that in the second diagram in Figure 4, showing that the oscillation amplitude of small RNA is improved to a large extent, which suggests that explicit internal stochastic resonance occurs at a certain optimal noise intensity. This means that the amplitude of these peaks will increase up to a certain critical noise level when the noise intensity is increased. After this point, information on the output signal will degrade, so the performance of quorum sensing on the network will be increased at the optimized noise and will be propitious to communicate between intracelluar and extracelluar.

Finally, to qualitatively characterize stochastic resonance, here, we use SNR defined in Section 3 to illustrate this phenomenon. The SNR versus noise intensity is presented

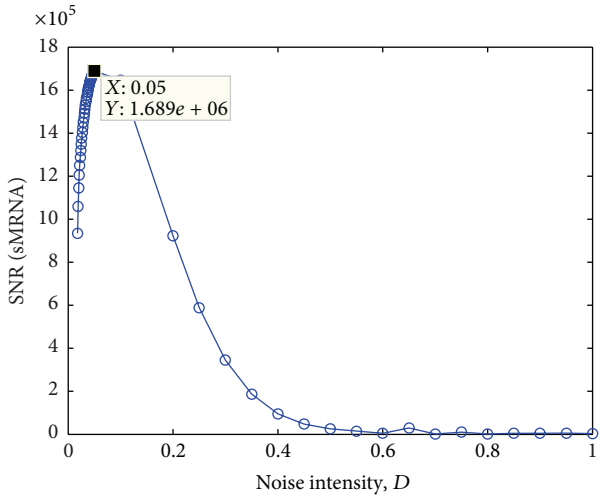

Figure 6: SNR as functions of the noise amplitude D.

in Figure 6. It is clear to show that the rapid rise of SNR to a peak with varying noise amplitude, which implies that explicit internal stochastic resonance appears at the peak value. This means that the performance of such sustained oscillation undergoes the maximum with the increment of internal noise and reaches the optimal condition at the maximum of peak. Previous studies on biological networks often view noise as a nuisance, so the regulatory mechanisms need to show robustness or resistance to random noise. In our work, we show that noise can play constructive roles via SR. It was well known that many biological systems can take advantage of the benefits of noise for nonlinear transmission and amplification of feeble information and increase the information communication via quorum sensing in *Vibrio Harveyi*.

5. Conclusions

In this work, we only focus on the dynamics of small RNA and study the influence of noises on a Quorum Sensing network regulated by small RNAs in *Vibrio Harveyi*. We demonstrate that noise can enhance the performance of oscillation when the corresponding deterministic system stays in the oscillatory region; that is, explicit internal stochastic resonance appears at an optimal noise intensity. Such phenomenon implies that explicit internal stochastic resonance might be widely appeared in biological regulatory networks and can speed up the information between intracellular and extracellular in the quorum sensing network and also improve the performance of small RNAs which regulate the quorum sensing network.

Conflict of Interests

The authors declare that there is no conflict of interests.

Acknowledgments

This work is supported by the National Natural Science Foundation of China (11272277), the Program for New Century Excellent Talents in University (NCET-10-0238), the Key Project of Chinese Ministry of Education (211105), the Innovation Scientists and Technicians Troop Construction Projects of Henan Province (134100510013), and the Innovative Research Team in University of Henan Province (13IRTSTHN019).

References

[1] M. B. Miller and B. L. Bassler, "Quorum sensing in bacteria," *Annual Review of Microbiology*, vol. 55, pp. 165–199, 2001.

[2] C. M. Waters and B. L. Bassler, "Quorum sensing: cell-to-cell communication in bacteria," *Annual Review of Cell and Developmental Biology*, vol. 21, no. 6, pp. 319–346, 2005.

[3] K. C. Tu, C. M. Waters, S. L. Svenningsen, and B. L. Bassler, "A small-RNA-mediated negative feedback loop controls quorum-sensing dynamics in *Vibrio harveyi*," *Molecular Microbiology*, vol. 70, no. 4, pp. 896–907, 2008.

[4] I.-H. Lee and U.-I. Cho, "Pattern formations with Turing and Hopf oscillating pattern in a discrete reaction-diffusion system," *Bulletin of the Korean Chemical Society*, vol. 21, no. 12, pp. 1213–1216, 2000.

[5] J. W. Shen, "Dynamics and mechanism of A quorum sensing network regulated by small RNAs in *Vibrio harveyi*," *Communications in Theoretical Physics*, vol. 52, no. 2, 2009.

[6] O. Hobert, "Common logic of transcription factor and microRNA action," *Trends in Biochemical Sciences*, vol. 29, no. 9, pp. 462–468, 2004.

[7] O. Hobert, "Gene regulation by transcription factors and MicroRNAs," *Science*, vol. 319, no. 5871, pp. 1785–1786, 2008.

[8] Y. Shimoni, G. Friedlander, G. Hetzroni et al., "Regulation of gene expression by small non-coding RNAs: a quantitative view," *Molecular Systems Biology*, vol. 3, article 138, pp. 1–9, 2007.

[9] N. G. Stocks, N. D. Stein, and P. V. E. McClintock, "Stochastic resonance in monostable systems," *Journal of Physics A*, vol. 26, no. 7, article 007, pp. L385–L390, 1993.

[10] A. S. Pikovsky and J. Kurths, "Coherence resonance in a noise-driven excitable system," *Physical Review Letters*, vol. 78, no. 5, pp. 775–778, 1997.

[11] P. Jung and P. Hänggi, "Amplification of small signals via stochastic resonance," *Physical Review A*, vol. 44, no. 12, pp. 8032–8042, 1991.

[12] A. Neiman and L. Schimansky-Geier, "Stochastic resonance in bistable systems driven by harmonic noise," *Physical Review Letters*, vol. 72, no. 19, pp. 2988–2991, 1994.

[13] B. McNamara, K. Wiesenfeld, and R. Roy, "Observation of stochastic resonance in a ring laser," *Physical Review Letters*, vol. 60, no. 25, pp. 2626–2629, 1988.

[14] A. N. Grigorenko, P. I. Nikitin, A. N. Slavin, and P. Y. Zhou, "Experimental observation of magnetostochastic resonance," *Journal of Applied Physics*, vol. 76, no. 10, pp. 6335–6337, 1994.

[15] M. I. Dykman, T. Horita, and J. Ross, "Statistical distribution and stochastic resonance in a periodically driven chemical system," *The Journal of Chemical Physics*, vol. 103, no. 3, pp. 966–972, 1995.

[16] D. S. Leonard and L. E. Reichl, "Stochastic resonance in a chemical reaction," *Physical Review E*, vol. 49, no. 2, pp. 1734–1737, 1994.

[17] A. Longtin, A. Bulsara, and F. Moss, "Time-interval sequences in bistable systems and the noise-induced transmission of information by sensory neurons," *Physical Review Letters*, vol. 67, no. 5, pp. 656–659, 1991.

[18] S. M. Bezrukov and I. Vodyanoy, "Noise-induced enhancement of signal transduction across voltage-dependent ion channels," *Nature*, vol. 378, no. 6555, pp. 362–364, 1995.

[19] Z. Hou and H. Xin, "Internal noise stochastic resonance in a circadian clock system," *Journal of Chemical Physics*, vol. 119, no. 22, pp. 11508–11512, 2003.

[20] S. Fauve and F. Heslot, "Stochastic resonance in a bistable system," *Physics Letters A*, vol. 97, no. 1-2, pp. 5–7, 1983.

[21] H. Gang, T. Ditzinger, C. Z. Ning, and H. Haken, "Stochastic resonance without external periodic force," *Physical Review Letters*, vol. 71, no. 6, pp. 807–810, 1993.

[22] A. Heckert and J. J. Filliben, *NIST Handbook 148: Data Plot Reference Manual*, 1996.

[23] W. H. Press, B. P. Flannery, S. A. Teukolsky, and W. T. Vetterling, *Numerical Recipes in C*, 1993.

Hindawi Publishing Corporation
Abstract and Applied Analysis
Volume 2013, Article ID 290574, 10 pages
http://dx.doi.org/10.1155/2013/290574

Research Article

Synchronization of Chaotic Neural Networks with Leakage Delay and Mixed Time-Varying Delays via Sampled-Data Control

Ting Lei,[1] Qiankun Song,[1] Zhenjiang Zhao,[2] and Jianxi Yang[3]

[1] *Department of Mathematics, Chongqing Jiaotong University, Chongqing 400074, China*
[2] *Department of Mathematics, Huzhou Teachers College, Huzhou 313000, China*
[3] *College of Information Science and Engineering, Chongqing Jiaotong University, Chongqing 400074, China*

Correspondence should be addressed to Qiankun Song; qiankunsong@gmail.com

Received 26 September 2013; Accepted 30 October 2013

Academic Editor: Xinsong Yang

This paper investigates the synchronization problem for neural networks with leakage delay and both discrete and distributed time-varying delays under sampled-data control. By employing the Lyapunov functional method and using the matrix inequality techniques, a delay-dependent LMIs criterion is given to ensure that the master systems and the slave systems are synchronous. An example with simulations is given to show the effectiveness of the proposed criterion.

1. Introduction

Since the pioneering works of Pecora and Carroll [1], the synchronization of chaotic systems has received considerable attention due to its potential applications in biology, chemistry, secret communication, cryptography, nonlinear oscillation synchronization, and some other nonlinear fields [2]. It has been shown that the neural networks can exhibit chaotic behavior [3]. Therefore, it has a wider significance to study the problem on the synchronization of chaotic neural networks.

In the past decades, some works dealing with the synchronization of neural networks have also appeared; for example, see [4–22] and references therein. In [4], authors discussed the synchronization and computation in a chaotic neural network. In [7], the local synchronization and global exponential stability for an array of linearly coupled identical connected neural networks with delays were investigated without assuming that the coupling matrix is symmetric or irreducible; the linear matrix inequality approach was used to judge synchronization with global convergence property. In [8], authors presented an adaptive synchronization scheme between two different kinds of delayed chaotic neural networks with partly unknown parameters. An adaptive controller was designed to guarantee the global asymptotic synchronization of state trajectories for two different chaotic neural networks with time delay. In [9], the concept of μ-synchronization was introduced; some sufficient conditions were derived for the global μ-synchronization for the linearly coupled neural networks with delayed couplings, where the intrinsic systems are recurrently connected neural networks with unbounded time-varying delays, and the couplings include instant couplings and unbounded delayed couplings. In [10], authors proposed a general array model of coupled delayed neural networks with hybrid coupling, which is composed of constant coupling, discrete-delay coupling, and distributed-delay coupling. Based on the Lyapunov functional method and Kronecker product properties, several sufficient conditions were established to ensure global exponential synchronization based on the design of the coupling matrices, the inner linking matrices, and/or some free matrices representing the relationships between the system matrices. The conditions are expressed within the framework of linear matrix inequalities, which can be easily computed by the interior-point method. In addition, a typical chaotic cellular neural network was used as the node in the array to illustrate the effectiveness and advantages of the theoretical results. In [11], the globally robust synchronization problem was investigated for an array of coupled neural networks with uncertain parameters and

time delays. Both the cases of linear coupling and nonlinear coupling were simultaneously taken into account. Several criteria for checking the robust exponential synchronization were given for the considered coupled neural networks. In [12], authors presented a new linear matrix inequality-based approach to an H^∞ output feedback control problem of master-slave synchronization of artificial neural networks with uncertain time delay. In [13], the problem of feedback controller design to achieve synchronization for neural network of neutral type with stochastic perturbation was considered. Based on Lyapunov method and LMI framework, a criterion for master-slave synchronization was obtained. In [16], authors investigated the globally exponential synchronization for linearly coupled neural networks with time-varying delay and impulsive disturbances. Since the impulsive effects discussed were regarded as disturbances, the impulses should not happen too frequently. The concept of average impulsive interval was used to formalize this phenomenon. By referring to an impulsive delay differential inequality, a criterion for the globally exponential synchronization of linearly coupled neural networks with impulsive disturbances was given. In [18], the projective synchronization between two continuous-time delayed neural systems with time-varying delay was investigated. A sufficient condition for synchronization of the coupled systems with modulated delay was presented analytically with the help of the Krasovskii-Lyapunov approach. In [19], the problem of guaranteed cost control for exponential synchronization of cellular neural networks with interval nondifferentiable and distributed time-varying delays via hybrid feedback control was considered. Several delay-dependent sufficient conditions for the exponential synchronization were obtained. In [20], authors studied the synchronization in an array of coupled neural networks with Markovian jumping and random coupling strength. By designing a novel Lyapunov function and using inequality techniques and the properties of random variables, several delay-dependent synchronization criteria were derived for the coupled networks of continuous-time version. Discrete-time analogues of the continuous-time networks were also formulated and studied. In [21], authors considered adaptive synchronization of chaotic Cohen-Grossberg neural networks with mixed time delays. In [22], pth moment exponential synchronization for stochastic delayed Cohen-Grossberg neural networks with Markovian switching was investigated.

On the other hand, with the development of networked control systems, sampled-data control in the presence of a constant input delay has been an important research area in recent years, because networked control systems are usually modeled as sampled-data systems under variable sampling with an additional network-induced delay [23]. There are some results dealing with the synchronization problem using sampled-data control; for example, see [23–38] and references therein. In [23], a new approach, the input delay approach, has been proposed that can deal well with the sampled-data control problems. The main idea of this approach is to convert the considered sampling period into a time-varying but bounded delay and then accomplish the sampled-data control or state estimation tasks by using the existing theory of time-delayed systems. In [24], the synchronization of chaotic system using a sampled-data fuzzy controller was studied. In [25–27], the synchronization for chaotic Lur'e systems using sampled-data control was investigated; several criteria were given to ensure that the master systems synchronize with the slave systems by using Lyapunov-Krasovskii functional and LMI approach. In [28–35], authors discussed the synchronization of chaotic system and complex networks by using sampled-data control. In [36–38], the synchronization of neural networks with time-varying delays was considered; by using sampled-data control method, several criteria for checking the synchronization were obtained. To the best of the authors knowledge, there is no results on the problem of the synchronization for neural networks with leakage delay and both discrete and distributed time-varying delays [38]. Therefore, there is a need to further extend the synchronization results reported in [38].

Motivated by the previous discussions, the objective of this paper is to study the synchronization for neural networks with leakage delay and both discrete and distributed time-varying delays by using sampled-data control approach. The obtained sufficient conditions do not require the differentiability of time-varying delays and are expressed in terms of linear matrix inequalities, which can be checked numerically using the effective LMI toolbox in MATLAB. An example is given to show the effectiveness and less conservatism of the proposed criterion.

Notations. The notations are quite standard. Throughout this paper, $\mathbb{R}^n$ and $\mathbb{R}^{n\times m}$ denote, respectively, the n-dimensional Euclidean space and the set of all $n\times m$ real matrices. $\|\cdot\|$ refers to the Euclidean vector norm. A^T represents the transpose of matrix A and the asterisk "$*$" in a matrix is used to represent the term which is induced by symmetry. I is the identity matrix with compatible dimension. $X > Y$ means that X and Y are symmetric matrices and that $X - Y$ is positive definite. Matrices, if not explicitly specified, are assumed to have compatible dimensions.

2. Model Description and Preliminaries

Consider the following neural networks with leakage delay and mixed time-varying delays:

$$\begin{aligned}\dot{x}(t) = &-Dx(t-\delta) + Af(x(t)) + Bf(x(t-\tau(t))) \\ &+ C\int_{t-\sigma(t)}^{t} f(x(s))\,ds + J(t),\end{aligned} \tag{1}$$

for $t \geq 0$, where $x(t) = (x_1(t), x_2(t), \ldots, x_n(t))^T \in \mathbb{R}^n$ is the state vector of the network at time t, n corresponds to the number of neurons, $D \in \mathbb{R}^{n\times n}$ is a positive diagonal matrix, $A \in \mathbb{R}^{n\times n}$, $B \in \mathbb{R}^{n\times n}$, and $C \in \mathbb{R}^{n\times n}$ are the connection weight matrix, the discretely delayed connection weight matrix, and the distributively delayed connection weight matrix, respectively, $f(x(t)) = (f_1(x_1(t)), f_2(x_2(t)), \ldots, f_n(x_n(t)))^T \in \mathbb{R}^n$ denotes the neuron activation at time t, $J(t) = (J_1(t), J_2(t), \ldots, J_n(t))^T \in \mathbb{R}^n$ is an external input vector, and δ, $\tau(t)$, and $\sigma(t)$ denote the

leakage delay, discrete time-varying delay and the distributed time-varying delay, respectively.

In this paper, system (1) is regarded as the master system and a slave system for (1) can be described by the following equation:

$$\dot{y}(t) = -Dy(t-\delta) + Af(y(t)) + Bf(y(t-\tau(t))) + C\int_{t-\sigma(t)}^{t} f(y(s))\,ds + u(t) + J(t), \tag{2}$$

where $u(t) \in \mathbb{R}^n$ is the appropriate control input that will be designed in order to obtain a certain control objective.

Throughout this paper, we make the following assumptions.

(H1) For any $j \in \{1, 2, \ldots, n\}$, there exist constants F_j^- and F_j^+ such that

$$F_j^- \le \frac{f_j(\alpha_1) - f_j(\alpha_2)}{\alpha_1 - \alpha_2} \le F_j^+, \tag{3}$$

for all $\alpha_1 \ne \alpha_2$.

(H2) The leakage delay δ, the discrete time-varying delays $\tau(t)$, and the distributed time-varying delay $\sigma(t)$ satisfy the following conditions:

$$0 \le \delta, \qquad 0 \le \tau(t) \le \tau, \qquad 0 \le \sigma(t) \le \sigma, \tag{4}$$

where δ, τ, and σ are constants.

By defining the error signal as $e(t) = y(t) - x(t)$, the error system for (1) and (2) can be represented as follows:

$$\dot{e}(t) = -De(t-\delta) + Ag(e(t)) + Bg(e(t-\tau(t))) + C\int_{t-\sigma(t)}^{t} g(e(s))\,ds + u(t), \tag{5}$$

where $g(e(t)) = f(y(t)) - f(x(t))$.

In many real-world applications, it is difficult to guarantee that the state variables transmitted to controllers are continuous. In addition, in order to make full use of modern computer technique, the sampled-data feedback control is applied to synchronize delayed neural networks [36]. In this paper, the following sampled-data controller is adopted [38]:

$$u(t) = Ke(t_k), \quad t_k \le t < t_{k+1}, \tag{6}$$

where K is sampled-data feedback controller gain matrix to be determined, t_k denotes the sampling instant and satisfies $0 = t_0 < t_1 < t_2 < \cdots < t_k < \cdots$, $\lim_{k\to+\infty} t_k = +\infty$. Moreover, the sampling period under consideration is assumed to be bounded by a known constant h; that is,

$$t_{k+1} - t_k \le h, \tag{7}$$

for any integer $k \ge 0$, where h is a positive scalar and represents the largest sampling interval.

Substituting control law (6) into the error system (5) yields

$$\dot{e}(t) = -De(t-\delta) + Ag(e(t)) + Bg(e(t-\tau(t))) + C\int_{t-\sigma(t)}^{t} g(e(s))\,ds + Ke(t_k). \tag{8}$$

Clearly, it is difficult to analyze the synchronization of neural networks based on error system (8) because of the discrete term $e(t_k)$. Therefore, the input delay approach [23] is applied; that is, a sawtooth function is defined as follows:

$$\gamma(t) = t - t_k, \quad t_k \le t < t_{k+1}. \tag{9}$$

It can be found from (7) and (9) that $0 \le \gamma(t) < h$ and $\dot{\gamma}(t) = 1$ for $t \ne t_k$.

By substituting (9) into (8), we get that

$$\dot{e}(t) = -De(t-\delta) + Ag(e(t)) + Bg(e(t-\tau(t))) + C\int_{t-\sigma(t)}^{t} g(e(s))\,ds + Ke(t-\gamma(t)). \tag{10}$$

The main purpose of this paper is to design controller with the form (6) to ensure that master system (1) synchronizes with slave system (2). In other words, we are interested in finding a feedback gain matrix K such that error system (10) is stable.

To prove our result, the following lemmas that can be found in [39] are necessary.

Lemma 1 (see [39]). *For any constant matrix $W \in \mathbb{R}^{m\times m}$, $W > 0$, scalar $0 < h(t) < h$, and vector function $\omega(\cdot) : [0, h] \to \mathbb{R}^m$ such that the integrations concerned are well defined; then*

$$\left(\int_0^{h(t)} \omega(s)\,ds\right)^T W \left(\int_0^{h(t)} \omega(s)\,ds\right) \le h(t)\int_0^{h(t)} \omega^T(s) W \omega(s)\,ds. \tag{11}$$

Lemma 2 (see [39]). *Given constant matrices P, Q, and R, where $P^T = P$, $Q^T = Q$, then*

$$\begin{bmatrix} P & R \\ R^T & -Q \end{bmatrix} < 0 \tag{12}$$

is equivalent to the following conditions:

$$Q > 0, \quad P + RQ^{-1}R^T < 0. \tag{13}$$

3. Main Results

Theorem 3. *Suppose that (H1) and (H2) hold. If there exist seven symmetric positive definite matrices P_i ($i = 1, 2, 3, 4, 5, 6, 7$), four positive diagonal matrices W_1, W_2, R_1, and R_2, and nine matrices X_{11}, X_{12}, X_{22}, Q_1, Q_2, Q_3, Q_4, Q_5, and Z such that the following LMIs hold:*

$$X = \begin{bmatrix} X_{11} & X_{12} \\ * & X_{22} \end{bmatrix} > 0, \tag{14}$$

$$\Omega = \begin{bmatrix} \Omega_1 & \Omega_2 \\ * & \Omega_3 \end{bmatrix} < 0, \tag{15}$$

where

$$\Omega_1 = \begin{bmatrix} \Omega_{11} & \Omega_{12} & \Omega_{13} & X_{22} & Q_3 & 0 & \Omega_{17} & 0 & \Omega_{19} & Q_1B & Q_1C \\ * & \Omega_{22} & -Q_1D & X_{12} & 0 & 0 & Z & 0 & \Omega_{29} & Q_1B & Q_1C \\ * & * & -P_1 & -X_{12} & 0 & 0 & 0 & 0 & 0 & 0 & 0 \\ * & * & * & -P_2 & 0 & 0 & 0 & 0 & 0 & 0 & 0 \\ * & * & * & * & \Omega_{55} & Q_2 & 0 & 0 & 0 & F_4R_2 & 0 \\ * & * & * & * & * & -P_3 & 0 & 0 & 0 & 0 & 0 \\ * & * & * & * & * & * & \Omega_{77} & Q_2 & 0 & 0 & 0 \\ * & * & * & * & * & * & * & -P_5 & 0 & 0 & 0 \\ * & * & * & * & * & * & * & * & \Omega_{99} & 0 & 0 \\ * & * & * & * & * & * & * & * & * & -R_2 & 0 \\ * & * & * & * & * & * & * & * & * & * & -P_7 \end{bmatrix}, \tag{16}$$

$$\Omega_2 = \begin{bmatrix} Q_3 & Q_5 & 0 & 0 \\ 0 & 0 & 0 & 0 \\ 0 & 0 & 0 & 0 \\ 0 & 0 & 0 & 0 \\ 0 & 0 & Q_2 & 0 \\ 0 & 0 & 0 & 0 \\ 0 & 0 & 0 & Q_4 \\ 0 & 0 & 0 & 0 \\ 0 & 0 & 0 & 0 \\ 0 & 0 & 0 & 0 \\ 0 & 0 & 0 & 0 \end{bmatrix}, \qquad \Omega_3 = \begin{bmatrix} -\frac{1}{\tau}P_4 & 0 & 0 & 0 \\ 0 & -\frac{1}{h}P_6 & 0 & 0 \\ 0 & 0 & -\frac{1}{\tau}P_4 & 0 \\ 0 & 0 & 0 & -\frac{1}{h}P_6 \end{bmatrix},$$

in which $\Omega_{11} = X_{12}+X_{12}^T+P_1+\delta^2P_2+P_3+P_5-Q_3-Q_3^T-Q_5-Q_5^T-F_3R_1$, $\Omega_{12} = X_{11}-F_1W_1+F_2W_2-Q_1$, $\Omega_{13} = -X_{12}-Q_1D$, $\Omega_{17} = Z+Q_5$, $\Omega_{19} = Q_1A+F_4R_1$, $\Omega_{22} = \tau P_4+hP_6-Q_1-Q_1^T$, $\Omega_{29} = W_1-W_2+Q_1A$, $\Omega_{55} = -Q_2-Q_2^T-F_3R_2$, $\Omega_{77} = -Q_4-Q_4^T$, *and* $\Omega_{99} = \sigma^2P_7-R_1$, *then master system* (1) *and slave system* (2) *are synchronous. Moreover, the desired controller gain matrix* K *in* (6) *can be given by*

$$K = Q_1^{-1}Z. \tag{17}$$

Proof. From assumption (H1), we know that

$$\begin{aligned} &\int_0^{e_i(t)} \left(g_i(s) - F_i^- s\right) ds \geq 0, \\ &\int_0^{e_i(t)} \left(F_i^+ s - g_i(s)\right) ds \geq 0, \quad i = 1, 2, \ldots, n. \end{aligned} \tag{18}$$

Let $W_1 = \mathrm{diag}(w_{11}, w_{12}, \ldots, w_{1n})$ and $W_2 = \mathrm{diag}(w_{21}, w_{22}, \ldots, w_{2n})$, and consider the following Lyapunov-Krasovskii functional:

$$V(t) = V_1(t) + V_2(t) + V_3(t) + V_4(t) + V_5(t) + V_6(t), \tag{19}$$

where

$$\begin{aligned} V_1(t) &= \begin{bmatrix} e(t) \\ \int_{t-\delta}^t e(s)\, ds \end{bmatrix}^T \begin{bmatrix} X_{11} & X_{12} \\ * & X_{22} \end{bmatrix} \begin{bmatrix} e(t) \\ \int_{t-\delta}^t e(s)\, ds \end{bmatrix}, \\ V_2(t) &= 2\sum_{i=1}^n w_{1i} \int_0^{e_i(t)} \left(g_i(s) - F_i^- s\right) ds \\ &\quad + 2\sum_{i=1}^n w_{2i} \int_0^{e_i(t)} \left(F_i^+ s - g_i(s)\right) ds, \\ V_3(t) &= \int_{t-\delta}^t e^T(s) P_1 e(s)\, ds \\ &\quad + \delta \int_{-\delta}^0 \int_{t+\xi}^t e^T(s) P_2 e(s)\, ds d\xi, \\ V_4(t) &= \int_{t-\tau}^t e^T(s) P_3 e(s)\, ds \\ &\quad + \int_{-\tau}^0 \int_{t+\xi}^t \dot{e}^T(s) P_4 \dot{e}(s)\, ds d\xi, \\ V_5(t) &= \int_{t-h}^t e^T(s) P_5 e(s)\, ds \\ &\quad + \int_{-h}^0 \int_{t+\xi}^t \dot{e}^T(s) P_6 \dot{e}(s)\, ds d\xi, \\ V_6(t) &= \sigma \int_{-\sigma}^0 \int_{t+\xi}^t g^T(e(s)) P_7 g(e(s))\, ds d\xi. \end{aligned} \tag{20}$$

Calculating the time derivative of $V_i(t)$ $(i = 1, 2, 3, 4, 5, 6)$, we obtain

$$\begin{aligned}\dot{V}_1(t) &= 2\begin{bmatrix} e(t) \\ \int_{t-\delta}^{t} e(s)\,ds \end{bmatrix}^T \begin{bmatrix} X_{11} & X_{12} \\ * & X_{22} \end{bmatrix} \begin{bmatrix} \dot{e}(t) \\ e(t) - e(t-\delta) \end{bmatrix} \\ &= e^T(t)\left(X_{12} + X_{12}^T\right)e(t) + 2e^T(t)X_{11}\dot{e}(t) \\ &\quad - 2e^T(t)X_{12}e(t-\delta) + 2e^T(t)X_{22}\int_{t-\delta}^{t} e(s)\,ds \\ &\quad + 2\dot{e}^T(t)X_{12}\int_{t-\delta}^{t} e(s)\,ds \\ &\quad - 2e^T(t-\delta)X_{22}\int_{t-\delta}^{t} e(s)\,ds, \end{aligned} \tag{21}$$

$$\begin{aligned}\dot{V}_2(t) &= 2\dot{e}^T(t)W_1\left(g(e(t)) - F_1e(t)\right) \\ &\quad + 2\dot{e}^T(t)W_2\left(F_2e(t) - g(e(t))\right) \\ &= 2e^T(t)\left(-F_1W_1 + F_2W_2\right)\dot{e}(t) \\ &\quad + 2\dot{e}^T(t)\left(W_1 - W_2\right)g(e(t)), \end{aligned} \tag{22}$$

$$\begin{aligned}\dot{V}_3(t) &= e^T(t)\left(P_1 + \delta^2P_2\right)e(t) - e^T(t-\delta)P_1e(t-\delta) \\ &\quad - \delta\int_{t-\delta}^{t} e^T(s)P_2e(s)\,ds \\ &\le e^T(t)\left(P_1 + \delta^2P_2\right)e(t) - e^T(t-\delta)P_1e(t-\delta) \\ &\quad - \left(\int_{t-\delta}^{t} e(s)\,ds\right)^T P_2\left(\int_{t-\delta}^{t} e(s)\,ds\right), \end{aligned} \tag{23}$$

$$\begin{aligned}\dot{V}_4(t) &= e^T(t)P_3e(t) - e^T(t-\tau)P_3e(t-\tau) \\ &\quad + \tau\dot{e}^T(t)P_4\dot{e}(t) - \int_{t-\tau}^{t}\dot{e}^T(s)P_4\dot{e}(s)\,ds, \end{aligned} \tag{24}$$

$$\begin{aligned}\dot{V}_5(t) &= e^T(t)P_5e(t) - e^T(t-h)P_5e(t-h) \\ &\quad + h\dot{e}^T(t)P_6\dot{e}(t) - \int_{t-h}^{t}\dot{e}^T(s)P_6\dot{e}(s)\,ds. \end{aligned} \tag{25}$$

$$\begin{aligned}\dot{V}_6(t) &= \sigma^2g^T(e(t))P_7g(e(t)) \\ &\quad - \sigma\int_{t-\sigma}^{t} g^T(e(s))P_7g(e(s))\,ds \\ &\le \sigma^2g^T(e(t))P_7g(e(t)) \\ &\quad - \sigma(t)\int_{t-\sigma(t)}^{t} g^T(e(s))P_7g(e(s))\,ds \\ &\le \sigma^2g^T(e(t))P_7g(e(t)) \\ &\quad - \left(\int_{t-\sigma(t)}^{t} g(e(s))\,ds\right)^T P_7\left(\int_{t-\sigma(t)}^{t} g(e(s))\,ds\right). \end{aligned} \tag{26}$$

In deriving inequalities (23) and (26), we have made use of Lemma 1. It follows from inequalities (21)–(26) that

$$\begin{aligned}\dot{V}(t) &\le e^T(t)\left(X_{12} + X_{12}^T + P_1 + \delta^2P_2 + P_3 + P_5\right)e(t) \\ &\quad + 2e^T(t)\left(X_{11} - F_1W_1 + F_2W_2\right)\dot{e}(t) \\ &\quad - 2e^T(t)X_{12}e(t-\delta) + 2e^T(t)X_{22} \\ &\quad \times \int_{t-\delta}^{t} e(s)\,ds + \dot{e}^T(t)\left(\tau P_4 + hP_6\right)\dot{e}(t) + 2\dot{e}^T(t) \\ &\quad \times X_{12}\int_{t-\delta}^{t} e(s)\,ds + 2\dot{e}^T(t)\left(W_1 - W_2\right)g(e(t)) \\ &\quad - e^T(t-\delta)P_1e(t-\delta) - 2e^T(t-\delta)X_{22} \\ &\quad \times \int_{t-\delta}^{t} e(s)\,ds - e^T(t-\tau)P_3e(t-\tau) \\ &\quad - \left(\int_{t-\delta}^{t} e(s)\,ds\right)^T P_2\left(\int_{t-\delta}^{t} e(s)\,ds\right) \\ &\quad - e^T(t-h)P_5e(t-h) \\ &\quad - \int_{t-\tau}^{t}\dot{e}^T(s)P_4\dot{e}(s)\,ds - \int_{t-h}^{t}\dot{e}^T(s)P_6\dot{e}(s)\,ds \\ &\quad + \sigma^2g^T(e(t))P_7g(e(t)) \\ &\quad - \left(\int_{t-\sigma(t)}^{t} g(e(s))\,ds\right)^T P_7\left(\int_{t-\sigma(t)}^{t} g(e(s))\,ds\right). \end{aligned} \tag{27}$$

From model (10), we have

$$\begin{aligned} 0 &= 2\left(e^T(t) + \dot{e}^T(t)\right)Q_1 \\ &\quad \times \Big[-\dot{e}(t) - De(t-\delta) + Ag(e(t)) + Bg(e(t-\tau(t))) \\ &\quad + C\int_{t-\sigma(t)}^{t} g(e(s))\,ds + Ke\left(t-\gamma(t)\right)\Big]. \end{aligned} \tag{28}$$

From Newton-Leibniz formulation and assumption (H2), we have

$$\begin{aligned} 0 &= -2e^T(t-\tau(t)) \\ &\quad \times Q_2\left(e(t-\tau(t)) - e(t-\tau) - \int_{t-\tau}^{t-\tau(t)}\dot{e}(s)\,ds\right) \\ &\le -2e^T(t-\tau(t))Q_2e(t-\tau(t)) \\ &\quad + 2e^T(t-\tau(t))Q_2e(t-\tau) + \tau e^T(t-\tau(t)) \\ &\quad \times Q_2P_4^{-1}Q_2^Te(t-\tau(t)) + \int_{t-\tau}^{t-\tau(t)}\dot{e}^T(s)P_4\dot{e}(s)\,ds, \end{aligned}$$

$$
\begin{aligned}
0 &= -2e^T(t)Q_3\left(e(t)-e(t-\tau(t))-\int_{t-\tau(t)}^{t}\dot{e}(s)\,ds\right)\\
&\le -2e^T(t)Q_3e(t)+2e^T(t)Q_3e(t-\tau(t))\\
&\quad+\tau e^T(t)Q_3P_4^{-1}Q_3^Te(t)+\int_{t-\tau(t)}^{t}\dot{e}^T(s)P_4\dot{e}(s)\,ds,\\
0 &= -2e^T(t-\gamma(t))\\
&\quad\times Q_4\left(e(t-\gamma(t))-e(t-h)-\int_{t-h}^{t-\gamma(t)}\dot{e}(s)\,ds\right)\\
&\le -2e^T(t-\gamma(t))Q_4e(t-\gamma(t))\\
&\quad+2e^T(t-\gamma(t))Q_2e(t-h)\\
&\quad+he^T(t-\gamma(t))Q_4P_6^{-1}Q_4^Te(t-\gamma(t))\\
&\quad+\int_{t-h}^{t-\gamma(t)}\dot{e}^T(s)P_6\dot{e}(s)\,ds,\\
0 &= -2e^T(t)Q_5\left(e(t)-e(t-\gamma(t))-\int_{t-\gamma(t)}^{t}\dot{e}(s)\,ds\right)\\
&\le -2e^T(t)Q_5e(t)+2e^T(t)Q_5e(t-\gamma(t))\\
&\quad+he^T(t)Q_5P_6^{-1}Q_5^Te(t)+\int_{t-\gamma(t)}^{t}\dot{e}^T(s)P_6\dot{e}(s)\,ds.
\end{aligned}
\tag{29}
$$

In addition, for positive diagonal matrices $R_1 > 0$ and $R_2 > 0$, we can get from assumption (H1) that [40]

$$
\begin{bmatrix} e(t)\\ g(e(t))\end{bmatrix}^T\begin{bmatrix} F_3R_1 & -F_4R_1\\ -F_4R_1 & R_1\end{bmatrix}\begin{bmatrix} e(t)\\ g(e(t))\end{bmatrix}\le 0, \tag{30}
$$

$$
\begin{aligned}
&\begin{bmatrix} e(t-\tau(t))\\ g(e(t-\tau(t)))\end{bmatrix}^T\begin{bmatrix} F_3R_2 & -F_4R_2\\ -F_4R_2 & R_2\end{bmatrix}\\
&\quad\times\begin{bmatrix} e(t-\tau(t))\\ g(e(t-\tau(t)))\end{bmatrix}\le 0.
\end{aligned}
\tag{31}
$$

It follows from (27)–(31) that

$$
\begin{aligned}
\dot{V}(t) &\le e^T(t)\Big(2X_{12}+P_1+\delta^2P_2+P_3+P_5\\
&\qquad-2Q_3+\tau Q_3P_4^{-1}Q_3^T-2Q_5\\
&\qquad+hQ_5P_6^{-1}Q_5^T-F_3R_1\Big)e(t)\\
&\quad+2e^T(t)\left(X_{11}-F_1W_1+F_2W_2-Q_1\right)\dot{e}(t)\\
&\quad-2e^T(t)\left(X_{12}+Q_1D\right)e(t-\delta)\\
&\quad+2e^T(t)X_{22}\int_{t-\delta}^{t}e(s)\,ds+2e^T(t)Q_3e(t-\tau(t))\\
&\quad+2e^T(t)\left(Q_1K+Q_5\right)e(t-\gamma(t))\\
&\quad+2e^T(t)\left(Q_1A+F_4R_1\right)g(e(t))\\
&\quad+2e^T(t)Q_1Bg(e(t-\tau(t)))\\
&\quad+2e^T(t)Q_1C\int_{t-\sigma(t)}^{t}g(e(s))\,ds\\
&\quad+\dot{e}^T(t)\left(\tau P_4+hP_6-2Q_1\right)\dot{e}(t)\\
&\quad-2\dot{e}^T(t)Q_1De(t-\delta)+2\dot{e}^T(t)X_{12}\\
&\quad\times\int_{t-\delta}^{t}e(s)\,ds+2\dot{e}^T(t)Q_1Ke(t-\gamma(t))\\
&\quad+2\dot{e}^T(t)\left(W_1-W_2+Q_1A\right)g(e(t))\\
&\quad+2\dot{e}^T(t)Q_1Bg(e(t-\tau(t)))+2\dot{e}^T(t)Q_1C\\
&\quad\times\int_{t-\sigma(t)}^{t}g(e(s))\,ds-e^T(t-\delta)P_1e(t-\delta)\\
&\quad-2e^T(t-\delta)X_{22}\int_{t-\delta}^{t}e(s)\,ds-\left(\int_{t-\delta}^{t}e(s)\,ds\right)^T\\
&\quad\times P_2\left(\int_{t-\delta}^{t}e(s)\,ds\right)+e^T(t-\tau(t))\\
&\quad\times\left(-2Q_2+\tau Q_2P_4^{-1}Q_2^T-F_3R_2\right)e(t-\tau(t))\\
&\quad+2e^T(t-\tau(t))Q_2e(t-\tau)+2e^T(t-\tau(t))\\
&\quad\times F_4R_2g(e(t-\tau(t)))-e^T(t-\tau)P_3e(t-\tau)\\
&\quad+e^T(t-\gamma(t))\left(-2Q_4+hQ_4P_6^{-1}Q_4^T\right)e(t-\gamma(t))\\
&\quad+2e^T(t-\gamma(t))Q_2e(t-h)-e^T(t-h)P_5e(t-h)\\
&\quad+g^T(e(t))\left(\sigma^2P_7-R_1\right)g(e(t))\\
&\quad-g^T(e(t-\tau(t)))R_2g(e(t-\tau(t)))\\
&\quad-\left(\int_{t-\sigma(t)}^{t}g(e(s))\,ds\right)^TP_7\left(\int_{t-\sigma(t)}^{t}g(e(s))\,ds\right)\\
&=\xi^T(t)\Pi\xi(t),
\end{aligned}
\tag{32}
$$

where $\xi(t) = (e^T(t), \dot{e}^T(t), e^T(t-\delta), \int_{t-\delta}^{t}e^T(s)ds, e^T(t-\tau(t)), e^T(t-\tau), e^T(t-\gamma(t)), e^T(t-h), g^T(e(t)), g^T(e(t-\tau(t))), \int_{t-\sigma(t)}^{t}g^T(e(s))ds)^T$ and

$$\Pi = \begin{bmatrix} \Pi_{11} & \Omega_{12} & \Omega_{13} & X_{22} & Q_3 & 0 & \Omega_{17} & 0 & \Omega_{19} & Q_1B & Q_1C \\ * & \Omega_{22} & -Q_1D & X_{12} & 0 & 0 & Q_1K & 0 & \Omega_{29} & Q_1B & Q_1C \\ * & * & -P_1 & -X_{12} & 0 & 0 & 0 & 0 & 0 & 0 & 0 \\ * & * & * & -P_2 & 0 & 0 & 0 & 0 & 0 & 0 & 0 \\ * & * & * & * & \Pi_{55} & Q_2 & 0 & 0 & 0 & F_4R_2 & 0 \\ * & * & * & * & * & -P_3 & 0 & 0 & 0 & 0 & 0 \\ * & * & * & * & * & * & \Pi_{77} & Q_2 & 0 & 0 & 0 \\ * & * & * & * & * & * & * & -P_5 & 0 & 0 & 0 \\ * & * & * & * & * & * & * & * & \Omega_{99} & 0 & 0 \\ * & * & * & * & * & * & * & * & * & -R_2 & 0 \\ * & * & * & * & * & * & * & * & * & * & -P_7 \end{bmatrix}, \tag{33}$$

with $\Pi_{11} = X_{12} + X_{12}^T + P_1 + \delta^2 P_2 + P_3 + P_5 - Q_3 - Q_3^T + \tau Q_3 P_4^{-1} Q_3^T - Q_5 - Q_5^T + hQ_5 P_6^{-1} Q_5^T - F_3 R_1$, $\Pi_{55} = -Q_2 - Q_2^T + \tau Q_2 P_4^{-1} Q_2^T - F_3 R_2$, $\Pi_{77} = -Q_4 - Q_4^T + hQ_4 P_6^{-1} Q_4^T$.

By using Lemma 2 and noting $K = Q_1^{-1} Z$, it is easy to verify the equivalence of $\Pi < 0$ and $\Omega < 0$. Thus, one can derive from (15) and (32) that

$$\dot{V}(t) \leq 0, \tag{34}$$

which implies that error-state system (10) is global and asymptotically stable; that is, master system (1) and slave system (2) are synchronous. The proof is completed. □

4. Numerical Example

To verify the effectiveness of the theoretical result of this paper, consider the following example.

Example 1. Consider master system (1) and slave system (2) with the following parameters:

$$D = \begin{pmatrix} 1 & 0 \\ 0 & 1 \end{pmatrix}, \qquad A = \begin{pmatrix} 1.8 & 0.1 \\ -4.3 & 2.9 \end{pmatrix},$$

$$B = \begin{pmatrix} -1.6 & -0.1 \\ -0.2 & -2.7 \end{pmatrix}, \qquad C = \begin{pmatrix} -0.3 & 0.1 \\ 0.1 & -0.2 \end{pmatrix},$$

$$f_1(\alpha) = f_2(\alpha) = \tanh(\alpha), \qquad J_1(t) = J_2(t) = 0,$$

$$\delta = 0.3, \qquad \tau(t) = 0.5\,|\sin t|, \qquad \sigma(t) = 0.2\,|\cos(2t)|. \tag{35}$$

The chaotic behaviors of master system (1) and slave system (2) with $u(t) = 0$ are given in Figure 1 and Figure 2, respectively, with the initial states chosen as $x(s) = (-0.1, 0.1)^T$, $y(s) = (-0.5\sin(23t), -0.6\cos(5t))^T$, and $s \in [-0.5, 0]$.

It can be verified that assumptions (H1) and (H2) are satisfied, and $F_1 = 0$, $F_2 = I$, $F_3 = 0$, $F_4 = \mathrm{diag}\{0.5, 0.5\}$, $\tau = 0.5$, and $\sigma = 0.2$.

Further, the sampling period is taken as $h = 0.7$; by using the MATLAB LMI Control Toolbox, a solution to the LMIs in (14)-(15) is found as follows:

$$P_1 = 10^{-8} \begin{bmatrix} 0.5575 & -0.0458 \\ -0.0458 & 0.0813 \end{bmatrix},$$

$$P_2 = 10^{-7} \begin{bmatrix} 0.1589 & -0.0521 \\ -0.0521 & 0.1440 \end{bmatrix},$$

$$P_3 = 10^{-8} \begin{bmatrix} 0.7818 & -0.0275 \\ -0.0275 & 0.0804 \end{bmatrix},$$

$$P_4 = 10^{-9} \begin{bmatrix} 0.5382 & -0.0061 \\ -0.0061 & 0.0069 \end{bmatrix},$$

$$P_5 = 10^{-8} \begin{bmatrix} 0.1046 & -0.0257 \\ -0.0257 & 0.0731 \end{bmatrix},$$

$$P_6 = 10^{-8} \begin{bmatrix} 0.2393 & -0.0215 \\ -0.0215 & 0.0690 \end{bmatrix},$$

$$P_7 = 10^{-7} \begin{bmatrix} 0.3430 & -0.0452 \\ -0.0452 & 0.3334 \end{bmatrix},$$

$$Q_1 = 10^{-9} \begin{bmatrix} 0.3710 & -0.0167 \\ -0.0064 & 0.0142 \end{bmatrix},$$

$$Q_2 = 10^{-9} \begin{bmatrix} 0.9695 & -0.0121 \\ -0.0121 & 0.0465 \end{bmatrix},$$

$$Q_3 = 10^{-8} \begin{bmatrix} 0.1136 & -0.0020 \\ -0.0013 & 0.0066 \end{bmatrix},$$

$$Q_4 = 10^{-7} \begin{bmatrix} 0.4169 & -0.0372 \\ -0.0403 & 0.1167 \end{bmatrix},$$

$$Q_5 = 10^{-7} \begin{bmatrix} 0.2032 & -0.0197 \\ -0.0199 & 0.0622 \end{bmatrix},$$

$$Z = 10^{-9} \begin{bmatrix} -0.3765 & 0.0456 \\ 0.0973 & -0.1631 \end{bmatrix},$$

$$W_1 = 10^{-10} \begin{bmatrix} 0.3365 & 0 \\ 0 & 0.3390 \end{bmatrix},$$

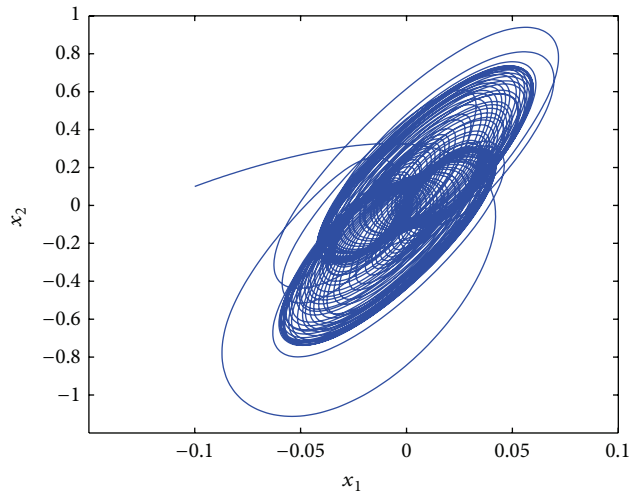

FIGURE 1: The chaotic behavior of master system (1).

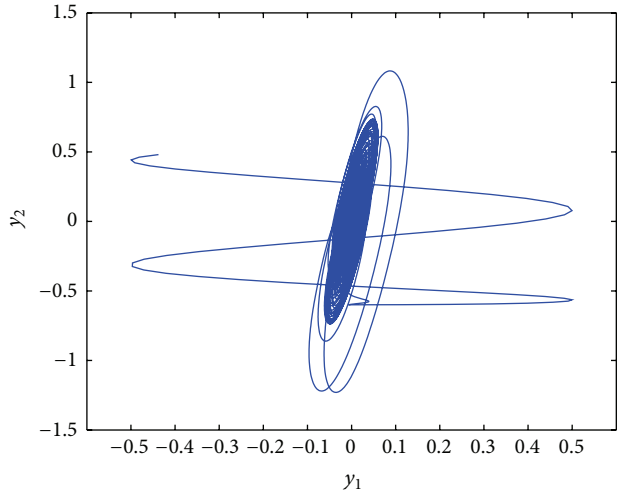

FIGURE 2: The chaotic behavior of slave system (2) with $u(t) = 0$.

$$W_2 = 10^{-9}\begin{bmatrix} 0.7363 & 0 \\ 0 & 0.0811 \end{bmatrix},$$

$$R_1 = 10^{-8}\begin{bmatrix} 0.6542 & 0 \\ 0 & 0.4249 \end{bmatrix},$$

$$R_2 = 10^{-8}\begin{bmatrix} 0.2055 & 0 \\ 0 & 0.0173 \end{bmatrix},$$

$$X_{11} = 10^{-10}\begin{bmatrix} 0.9837 & -0.2378 \\ -0.2378 & 0.5765 \end{bmatrix},$$

$$X_{12} = 10^{-9}\begin{bmatrix} -0.0813 & 0.0340 \\ 0.0424 & -0.1056 \end{bmatrix},$$

$$X_{22} = 10^{-8}\begin{bmatrix} 0.2687 & -0.0933 \\ -0.0933 & 0.2625 \end{bmatrix}. \quad (36)$$

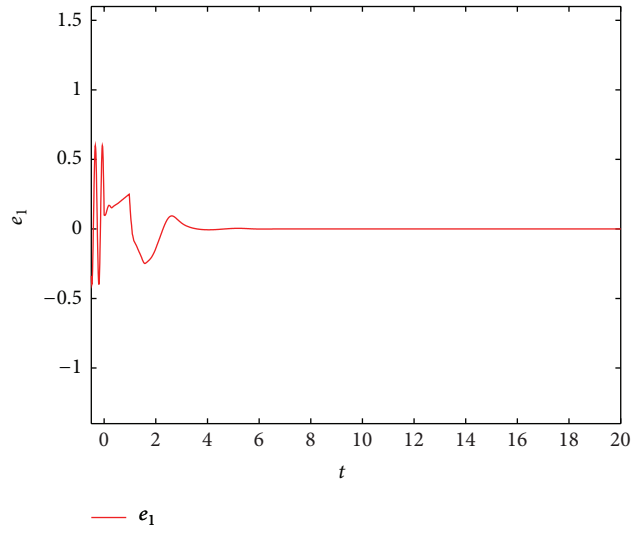

(a)

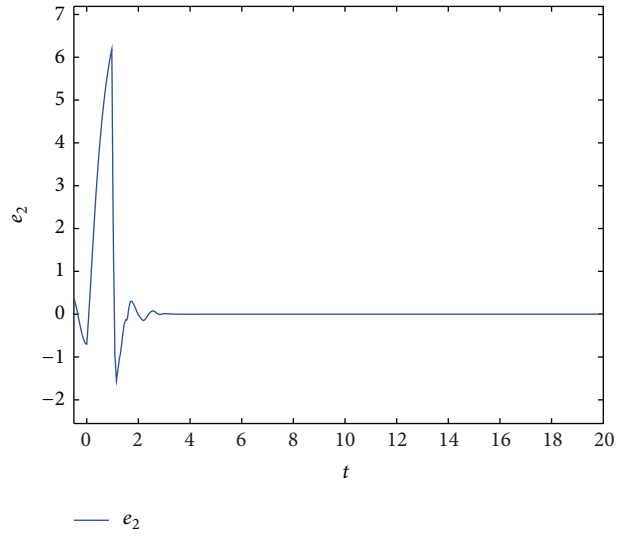

(b)

FIGURE 3: State trajectory of $e_1(t)$ and $e_2(t)$ of error system (8).

Subsequently, we can obtain from $K = Q_1^{-1}Z$ that

$$K = \begin{bmatrix} -0.7228 & -0.3994 \\ 6.5033 & -11.6367 \end{bmatrix}. \quad (37)$$

According to Theorem 3, master system (1) and slave system (2) are synchronous under sampled-data controller (6). Figure 3 depicts the synchronization errors of state variables between master system (1) and slave system (2). The numerical simulations clearly verify the effectiveness of the developed sampled-data control approach in the synchronization of two chaotic neural networks with discrete and distributed time-varying delays as well as leakage delay.

5. Conclusions

In this paper, we have dealt with the synchronization problems for chaotic neural networks with leakage delay and both

discrete and distributed time-varying delays. Based on the sampled-data control techniques, Lyapunov stability theory, and the matrix inequality techniques, a delay-dependent criterion sufficient condition has been developed to guarantee synchronization of the considered coupled neural networks. An example has been provided to demonstrate the effectiveness of the proposed criterion since the feasible solutions to the given LMIs criterion in this paper have been found.

Conflict of Interests

The authors declare that there is no conflict of interests regarding the publication of this paper.

Acknowledgments

The authors would like to thank the editor and the anonymous reviewers for their valuable suggestions and comments which have led to a much improved paper. This work was supported by the National Natural Science Foundation of China under Grants 61273021, 60974132, 11172247, and 51208538 and in part by the Natural Science Foundation Project of CQ cstc2013jjB40008.

References

[1] L. M. Pecora and T. L. Carroll, "Synchronization in chaotic systems," *Physical Review Letters*, vol. 64, no. 8, pp. 821–824, 1990.

[2] Z. Wang, Y. Wang, and Y. Liu, "Global synchronization for discrete-time stochastic complex networks with randomly occurred nonlinearities and mixed time delays," *IEEE Transactions on Neural Networks*, vol. 21, no. 1, pp. 11–25, 2010.

[3] F. Zou and J. A. Nossek, "A chaotic attractor with cellular neural networks," *IEEE Transactions on Circuits and Systems I*, vol. 38, no. 7, pp. 811–812, 1991.

[4] D. Hansel and H. Sompolinsky, "Synchronization and computation in a chaotic neural network," *Physical Review Letters*, vol. 68, no. 5, pp. 718–721, 1992.

[5] T. B. Luzyanina, "Synchronization in an oscillator neural network model with time-delayed coupling," *Network*, vol. 6, no. 1, pp. 43–59, 1995.

[6] J. Karbowski and N. Kopell, "Multispikes and synchronization in a large neural network with temporal delays," *Neural Computation*, vol. 12, no. 7, pp. 1573–1606, 2000.

[7] W. Lu and T. Chen, "Synchronization of coupled connected neural networks with delays," *IEEE Transactions on Circuits and Systems I*, vol. 51, no. 12, pp. 2491–2503, 2004.

[8] H. Zhang, Y. Xie, Z. Wang, and C. Zheng, "Adaptive synchronization between two different chaotic neural networks with time delay," *IEEE Transactions on Neural Networks*, vol. 18, no. 6, pp. 1841–1845, 2007.

[9] T. Chen, W. Wu, and W. Zhou, "Global μ-synchronization of linearly coupled unbounded time-varying delayed neural networks with unbounded delayed coupling," *IEEE Transactions on Neural Networks*, vol. 19, no. 10, pp. 1809–1816, 2008.

[10] J. Cao, G. Chen, and P. Li, "Global synchronization in an array of delayed neural networks with hybrid coupling," *IEEE Transactions on Systems, Man, and Cybernetics B*, vol. 38, no. 2, pp. 488–498, 2008.

[11] J. Liang, Z. Wang, and P. Li, "Robust synchronisation of delayed neural networks with both linear and non-linear couplings," *International Journal of Systems Science*, vol. 40, no. 9, pp. 973–984, 2009.

[12] F. O. Souza and R. M. Palhares, "Synchronisation of chaotic delayed artificial neural networks: an H_∞ control approach," *International Journal of Systems Science*, vol. 40, no. 9, pp. 937–944, 2009.

[13] J. H. Park and O. M. Kwon, "Synchronization of neural networks of neutral type with stochastic perturbation," *Modern Physics Letters B*, vol. 23, no. 14, pp. 1743–1751, 2009.

[14] H. R. Karimi and H. Gao, "New delay-dependent exponential H_∞ synchronization for uncertain neural networks with mixed time delays," *IEEE Transactions on Systems, Man, and Cybernetics B*, vol. 40, no. 1, pp. 173–185, 2010.

[15] H. Wang and Q. Song, "Synchronization for an array of coupled stochastic discrete-time neural networks with mixed delays," *Neurocomputing*, vol. 74, no. 10, pp. 1572–1584, 2011.

[16] J. Lu, D. W. C. Ho, J. Cao, and J. Kurths, "Exponential synchronization of linearly coupled neural networks with impulsive disturbances," *IEEE Transactions on Neural Networks*, vol. 22, no. 2, pp. 329–335, 2011.

[17] P. Balasubramaniam and V. Vembarasan, "Synchronization of recurrent neural networks with mixed time-delays via output coupling with delayed feedback," *Nonlinear Dynamics*, vol. 70, no. 1, pp. 677–691, 2012.

[18] D. Ghosh and S. Banerjee, "Projective synchronization of time-varying delayed neural network with adaptive scaling factors," *Chaos, Solitons & Fractals*, vol. 53, pp. 1–9, 2013.

[19] T. Botmart and W. Weera, "Guaranteed cost control for exponential synchronization of cellular neural networks with mixed time-varying delays via hybrid feedback control," *Abstract and Applied Analysis*, vol. 2013, Article ID 175796, 12 pages, 2013.

[20] X. Yang, J. Cao, and J. Lu, "Synchronization of randomly coupled neural networks with Markovian jumping and time-delay," *IEEE Transactions on Circuits and Systems I*, vol. 60, no. 2, pp. 363–376, 2013.

[21] Q. Zhu and J. Cao, "Adaptive synchronization of chaotic Cohen-Crossberg neural networks with mixed time delays," *Nonlinear Dynamics*, vol. 61, no. 3, pp. 517–534, 2010.

[22] Q. Zhu and J. Cao, "pth moment exponential synchronization for stochastic delayed Cohen-Grossberg neural networks with Markovian switching," *Nonlinear Dynamics*, vol. 67, no. 1, pp. 829–845, 2012.

[23] E. Fridman, A. Seuret, and J.-P. Richard, "Robust sampled-data stabilization of linear systems: an input delay approach," *Automatica*, vol. 40, no. 8, pp. 1441–1446, 2004.

[24] H. K. Lam and L. D. Seneviratne, "Chaotic synchronization using sampled-data fuzzy controller based on fuzzy-model-based approach," *IEEE Transactions on Circuits and Systems I*, vol. 55, no. 3, pp. 883–892, 2008.

[25] J.-G. Lu and D. J. Hill, "Global asymptotical synchronization of chaotic Lur'e systems using sampled data: a linear matrix inequality approach," *IEEE Transactions on Circuits and Systems II*, vol. 55, no. 6, pp. 586–590, 2008.

[26] C.-K. Zhang, Y. He, and M. Wu, "Improved global asymptotical synchronization of chaotic lur'e systems with sampled-data control," *IEEE Transactions on Circuits and Systems II*, vol. 56, no. 4, pp. 320–324, 2009.

[27] W. Chen, Z. Wang, and X. Lu, "On sampled-data control for master-slave synchronization of chaotic Lur'e systems," *IEEE*

Transactions on Circuits and Systems II, vol. 59, no. 8, pp. 515–519, 2012.

[28] N. Li, Y. Zhang, J. Hu, and Z. Nie, "Synchronization for general complex dynamical networks with sampled-data," *Neurocomputing*, vol. 74, no. 5, pp. 805–811, 2011.

[29] T. H. Lee, J. H. Park, O. M. Kwon, and S. M. Lee, "Synchronization of chaos systems via sampled-data control," *Transactions of the Korean Institute of Electrical Engineers*, vol. 61, no. 4, pp. 617–621, 2012.

[30] B. Shen, Z. Wang, and X. Liu, "Sampled-data synchronization control of dynamical networks with stochastic sampling," *Institute of Electrical and Electronics Engineers*, vol. 57, no. 10, pp. 2644–2650, 2012.

[31] T. H. Lee, Z.-G. Wu, and J. H. Park, "Synchronization of a complex dynamical network with coupling time-varying delays via sampled-data control," *Applied Mathematics and Computation*, vol. 219, no. 3, pp. 1354–1366, 2012.

[32] S. J. S. Theesar, S. Banerjee, and P. Balasubramaniam, "Synchronization of chaotic systems under sampled-data control," *Nonlinear Dynamics*, vol. 70, no. 3, pp. 1977–1987, 2012.

[33] Z.-G. Wu, J. H. Park, H. Su, B. Song, and J. Chu, "Exponential synchronization for complex dynamical networks with sampled-data," *Journal of the Franklin Institute*, vol. 349, no. 9, pp. 2735–2749, 2012.

[34] H. Zhang and J. Zhou, "Synchronization of sampled-data coupled harmonic oscillators with control inputs missing," *Systems & Control Letters*, vol. 61, no. 12, pp. 1277–1285, 2012.

[35] Z. Wu, P. Shi, H. Su, and J. Chu, "Sampled-data exponential synchronization of complex dynamical networks with time-varying coupling delay," *IEEE Transactions on Neural Networks and Learning Systems*, vol. 24, no. 8, pp. 1177–1187, 2013.

[36] C.-K. Zhang, Y. He, and M. Wu, "Exponential synchronization of neural networks with time-varying mixed delays and sampled-data," *Neurocomputing*, vol. 74, no. 1–3, pp. 265–273, 2010.

[37] Z.-G. Wu, J. H. Park, H. Su, and J. Chu, "Discontinuous Lyapunov functional approach to synchronization of time-delay neural networks using sampled-data," *Nonlinear Dynamics*, vol. 69, no. 4, pp. 2021–2030, 2012.

[38] Q. Gan and Y. Liang, "Synchronization of chaotic neural networks with time delay in the leakage term and parametric uncertainties based on sampled-data control," *Journal of the Franklin Institute*, vol. 349, no. 6, pp. 1955–1971, 2012.

[39] K. Gu, V. L. Kharitonov, and J. Chen, *Stability of Time-Delay Systems*, Birkhauser, Boston, Mass, USA, 2003.

[40] Y. Liu, Z. Wang, and X. Liu, "Global exponential stability of generalized recurrent neural networks with discrete and distributed delays," *Neural Networks*, vol. 19, no. 5, pp. 667–675, 2006.

Hindawi Publishing Corporation
Abstract and Applied Analysis
Volume 2013, Article ID 167198, 6 pages
http://dx.doi.org/10.1155/2013/167198

Research Article

Synchronization between Two Discrete-Time Networks with Mutual Couplings

Meng Xiao, Weigang Sun, and Fangyue Chen

Institute of Applied Mathematics and Engineering Computations, Hangzhou Dianzi University, Hangzhou 310018, China

Correspondence should be addressed to Weigang Sun; wgsun@hdu.edu.cn

Received 22 September 2013; Accepted 4 November 2013

Academic Editor: Jianquan Lu

We investigate synchronization between two discrete-time networks with mutual couplings, including inner synchronization inside each network and outer synchronization between two networks. We then obtain a synchronized criterion for the inner synchronization inside each network by the method of linear matrix inequality and derive a relationship between the inner and outer synchronization. Finally, we show numerical examples to verify our theoretical analysis and discuss the effect of coupling strengths, node dynamics, and topological structures on the inner and outer synchronization. Compared to the inner synchronization inside each network, the outer synchronization between two networks is difficult to achieve.

1. Introduction

Network synchronization, as a collective behavior existing inside a network, has been widely studied since the birth of small-world and scale-free networks [1–3]. The main focus is to investigate the interplay between the complexity in the overall topology and the local dynamics of the coupled nodes [4–6]. The topological structures may be globally connected, random, small-world, and scale-free. There are many applications using the synchronization of networks [7], for instance, secure communication and multirobot coordination control. Apart from the complete synchronization appearing inside a network, there are some other types of synchronization, such as phase synchronization, generalized synchronization, lag synchronization, and cluster synchronization [8–12].

Generally, we refer to synchronization happening between two networks as outer synchronization [13], which is distinguished from inner synchronization inside a network. Compared to the inner synchronization, outer synchronization of two networks is more complex, which involves more system parameters. In 2007, Li et al. first proposed the concept of outer synchronization and applied the open-plus-closed-loop method to realize the outer synchronization between two networks with identical topologies [13]. Shortly later, using the adaptive control method, Tang et al. achieved the outer synchronization between two networks with different topological structures [14]. In [15], Wu et al. studied the generalized outer synchronization between two networks with different dimensions of node dynamics. In addition, there are many works on the outer synchronization, that is, introducing the noise, time delay, fractional order node dynamics, and unknown parameters [16–21].

In the above-mentioned works on the outer synchronization, the researchers usually applied the control methods to realize the outer synchronization and did not study the inner synchronization inside a network. In reality, the mutual coupling forms between two networks are colorful; for instance, Wu et al. investigated the outer synchronization between two networks with two active forms nonlinear signals and reciprocity [22]; however, these two coupling forms do not make the outer synchronization happen. In addition, the inner synchronization inside each network was not considered. In [23], Sorrentino and Ott provided a method to study the inner synchronization of two groups. The problem of collective behaviors inside a network and between two networks is of broad interest. For example, in subway systems, when the trains reach the platform, the outer and inner doors simultaneously open or close, showing that both inner and outer synchronization happen [24]. It is also found

that present studies on the synchronization between two networks with various couplings are much less, then studying the effect of various couplings on the synchronization is interesting and meaningful.

Inspired by the above discussions, we study synchronization between two discrete-time networks with mutual couplings, including inner synchronization inside each network and outer synchronization between them. By the Lyapunov stability theory and linear matrix inequality, we obtain a synchronous theorem on the inner synchronization inside each network and a relationship between the inner and outer synchronization. Numerical simulations show that the inner synchronization is easier to achieve than the outer synchronization. In addition, given the mutual coupling matrices and appropriate node dynamics, we can adjust coupling strengths to realize the inner and outer synchronization simultaneously. In Section 2, network models and synchronization analysis are presented, and numerical examples are shown in Section 3. Finally, the discussions are included in the last section.

2. Model Presentation and Synchronization Analysis

In this paper, we investigate the synchronization between two discrete-time networks with mutual couplings. The dynamical equations are described as follows:

$$\begin{aligned} x_i(t+1) &= f\left(x_i(t)\right) + m_x \sum_{j=1}^{N} a_{ij}\left(y_j(t) - x_j(t)\right), \\ &\qquad i = 1, 2, \ldots, N, \\ y_i(t+1) &= g\left(y_i(t)\right) + m_y \sum_{j=1}^{N} b_{ij}\left(x_j(t) - y_j(t)\right), \\ &\qquad i = 1, 2, \ldots, N, \end{aligned} \tag{1}$$

where the node dynamical equations are $x_i(t+1) = f(x_i(t))$ and $y_i(t+1) = g(y_i(t)), i = 1, \ldots, N$. $f(\cdot) : R^n \to R^n$ and $g(\cdot) : R^n \to R^n$ are continuously differential functions. $x_i(y_i)$ is an n-dimensional state vector. N is the number of network nodes. m_x and m_y are the coupling strengths. $A = (a_{ij})_{N\times N}$ and $B = (b_{ij})_{N\times N}$ represent the mutual coupling matrices between these two networks, whose entries a_{ij} denote the intensity from i in network X to j in network Y; analogously, the entries of B are the same defined as A.

Let us now consider the possibility whether the individual networks achieve inner synchronization; that is, $\lim_{t\to+\infty} \|x_i(t) - x_s(t)\| = 0$ and $\lim_{t\to+\infty} \|y_i(t) - y_s(t)\| = 0, i = 1 \ldots, N$, where $\|\cdot\|$ denotes the Euclidean norm of a vector. If there exist such synchronous states, satisfying

$$\begin{aligned} \sum_{j=1}^{N} a_{ij} &= \gamma_x, \quad \forall i \in X, \\ \sum_{j=1}^{N} b_{ij} &= \gamma_y, \quad \forall i \in Y, \end{aligned} \tag{2}$$

without loss of generality, we set $\gamma_x = \gamma_y = 1$.

Thus the synchronized state equations are

$$\begin{aligned} x_s(t+1) &= f\left(x_s(t)\right) + m_x\left(y_s(t) - x_s(t)\right), \\ y_s(t+1) &= g\left(y_s(t)\right) + m_y\left(x_s(t) - y_s(t)\right). \end{aligned} \tag{3}$$

Linearizing the synchronous states around x_s and y_s, we obtain

$$\begin{aligned} \delta x_i(t+1) &= Df\left(x_s(t)\right)\delta x_i(t) \\ &\quad + m_x \sum_{j=1}^{N} a_{ij}\left(\delta y_j(t) - \delta x_j(t)\right), \quad i = 1, 2, \ldots, N, \\ \delta y_i(t+1) &= Dg\left(y_s(t)\right)\delta y_i(t) \\ &\quad + m_y \sum_{j=1}^{N} b_{ij}\left(\delta x_j(t) - \delta y_j(t)\right), \quad i = 1, 2, \ldots, N, \end{aligned} \tag{4}$$

where $\delta x_i(t) = x_i(t) - x_s(t)$, $\delta y_i(t) = y_i(t) - y_s(t)$, $Df(x_s(t))$, and $Dg(y_s(t))$ are the Jacobians of $f(x(t)), g(y(t))$ at x_s and y_s, respectively. Assume $A = B$ and let $\delta x(t) = \in R^{n\times N}$ and $\delta y(t) = [\delta y_1(t), \ldots, \delta y_N(t)] \in R^{n\times N}$. Then (4) is rewritten as

$$\begin{aligned} \delta x(t+1) &= Df\left(x_s(t)\right)\delta x(t) + m_x\left(\delta y(t) - \delta x(t)\right)A^T, \\ \delta y(t+1) &= Dg\left(y_s(t)\right)\delta y(t) + m_y\left(\delta x(t) - \delta y(t)\right)A^T. \end{aligned} \tag{5}$$

Further, let $\delta(t) = \begin{bmatrix} \delta x(t) \\ \delta y(t) \end{bmatrix} \in R^{2n\times N}$; then (5) reads

$$\delta(t+1) = \mathscr{D}\delta(t) + \mathscr{W}\delta(t)A^T, \tag{6}$$

where $\mathscr{D} = \begin{bmatrix} Df(x_s(t)) & 0 \\ 0 & Dg(y_s(t)) \end{bmatrix}$ and $\mathscr{W} = \begin{bmatrix} -m_x I_n & m_x I_n \\ m_y I_n & -m_y I_n \end{bmatrix}$, where I_n is an identity matrix of size n and A^T denotes the transpose of A. Generally, the coupling matrix can be decomposed into $A^T = \Phi J \Phi^{-1}$, where J is the Jordan canonical form with complex eigenvalues $\lambda \in C$ and Φ contains the corresponding eigenvectors ϕ. Denote $\eta(t) = \delta(t)\Phi$; we obtain

$$\eta(t+1) = \mathscr{D}\eta(t) + \mathscr{W}\eta(t)J, \tag{7}$$

where J is a block diagonal matrix; that is,

$$J = \begin{bmatrix} J_1 & & \\ & \ddots & \\ & & J_h \end{bmatrix}, \tag{8}$$

and J_k is the block corresponding to the N_k multiple eigenvalue λ_k of A^T; that is,

$$J_k = \begin{bmatrix} \lambda_k & 1 & 0 & \cdots & 0 \\ 0 & \lambda_k & 1 & \cdots & 0 \\ \vdots & \vdots & \ddots & \ddots & \vdots \\ 0 & 0 & \cdots & \lambda_k & 1 \\ 0 & 0 & \cdots & 0 & \lambda_k \end{bmatrix}. \tag{9}$$

Let $\eta(t) = [\eta_1(t), \eta_2(t), \ldots, \eta_h(t)]$ and $\eta_k(t) = [\eta_{k,1}(t), \eta_{k,2}(t), \ldots, \eta_{k,N_k}(t)]$. We can rewrite (7) in a component form as

$$\eta_{k,1}(t+1) = (\mathscr{D} + \lambda_k \mathscr{W})\,\eta_{k,1}(t), \tag{10}$$

$$\eta_{k,p+1}(t+1) = (\mathscr{D} + \lambda_k \mathscr{W})\,\eta_{k,p+1}(t) + \mathscr{W}\eta_{k,p}(t), \quad 1 \le p \le N_k - 1, \tag{11}$$

where $k = 1, 2, \ldots, h$.

Firstly, we study the system of (10). Let $\eta_{k,1}(t) = \mu_{k,1}(t) + j\nu_{k,1}(t)$, $\lambda_k = \alpha_k + j\beta_k$, where $\alpha_k, \beta_k \in R$, $\mu_{k,1}, \nu_{k,1} \in R^{2n}$, j is and the imaginary unit. Then (10) reads

$$\begin{aligned}\mu_{k,1}(t+1) &= (\mathscr{D} + \alpha_k \mathscr{W})\,\mu_{k,1}(t) - \beta_k \mathscr{W}\nu_{k,1}(t),\\ \nu_{k,1}(t+1) &= (\mathscr{D} + \alpha_k \mathscr{W})\,\nu_{k,1}(t) + \beta_k \mathscr{W}\mu_{k,1}(t).\end{aligned} \tag{12}$$

Construct the Lyapunov function as

$$V(t) = \mu_{k,1}^T(t)\,\mu_{k,1}(t) + \nu_{k,1}^T(t)\,\nu_{k,1}(t). \tag{13}$$

Then,

$$\begin{aligned}\Delta V(t) &= V(t+1) - V(t)\\ &= \mu_{k,1}^T(t+1)\,\mu_{k,1}(t+1) + \nu_{k,1}^T(t+1)\,\nu_{k,1}(t+1)\\ &\quad - \mu_{k,1}^T(t)\,\mu_{k,1}(t) - \nu_{k,1}^T(t)\,\nu_{k,1}(t)\\ &= \begin{bmatrix}\mu_{k,1}(t)\\ \nu_{k,1}(t)\end{bmatrix}^T M_k \begin{bmatrix}\mu_{k,1}(t)\\ \nu_{k,1}(t)\end{bmatrix},\end{aligned} \tag{14}$$

where $M_k = P_k^T P_k - \mathrm{diag}\{I_{2n}, I_{2n}\}$ with $P_k = \begin{bmatrix}\mathscr{D}+\alpha_k\mathscr{W} & -\beta_k\mathscr{W}\\ \beta_k\mathscr{W} & \mathscr{D}+\alpha_k\mathscr{W}\end{bmatrix}$, $k = 1, 2, \ldots, h$. If $M_k < 0, k = 1, 2, \ldots, h$, that is, these matrices are negative definite, then the zero solution of (10) is asymptotically stable.

Secondly, we study the stability of (11). Let $\eta_{k,p+1}(t) = \mu_{k,p+1}(t) + j\nu_{k,p+1}(t)$; then

$$\begin{aligned}\mu_{k,p+1}(t+1) &= (\mathscr{D} + \alpha_k \mathscr{W})\,\mu_{k,p+1}(t)\\ &\quad - \beta_k \mathscr{W}\nu_{k,p+1}(t) + \mathscr{W}\mu_{k,p}(t), \quad 1 \le p \le N_k - 1,\\ \nu_{k,p+1}(t+1) &= (\mathscr{D} + \alpha_k \mathscr{W})\,\nu_{k,p+1}(t)\\ &\quad + \beta_k \mathscr{W}\mu_{k,p+1}(t) + \mathscr{W}\nu_{k,p}(t), \quad 1 \le p \le N_k - 1.\end{aligned} \tag{15}$$

Choose the Lyapunov function as

$$\overline{V}(t) = \mu_{k,p+1}^T(t)\,\mu_{k,p+1}(t) + \nu_{k,p+1}^T(t)\,\nu_{k,p+1}(t). \tag{16}$$

Then we obtain

$$\begin{aligned}\Delta\overline{V}(t) &= \overline{V}(t+1) - \overline{V}(t)\\ &= \begin{bmatrix}u_{k,p}(t)\\ v_{k,p}(t)\\ u_{k,p+1}(t)\\ v_{k,p+1}(t)\end{bmatrix}^T L_k \begin{bmatrix}u_{k,p}(t)\\ v_{k,p}(t)\\ u_{k,p+1}(t)\\ v_{k,p+1}(t)\end{bmatrix},\end{aligned} \tag{17}$$

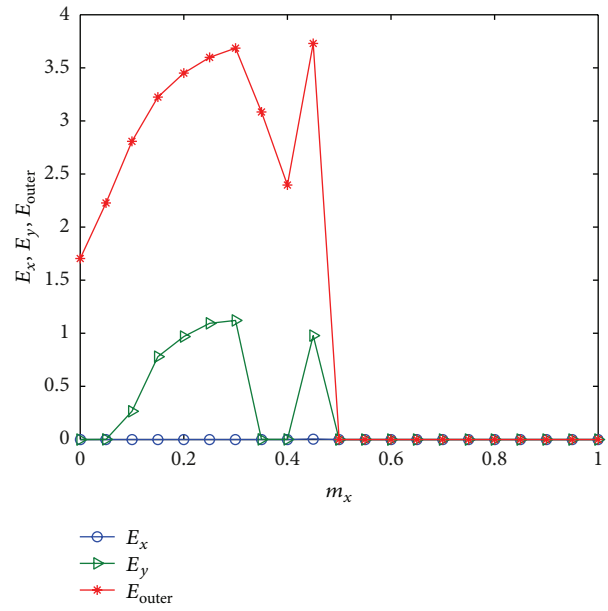

FIGURE 1: The panels exhibit E_x, E_y, and E_{outer} at $t = 400$ with regard to m_x for $N = 10$ and $m_y = 0.2$. The bottom one shows that the inner synchronization inside network X is easily achieved. When $m_x \ge 0.5$, the inner and outer synchronization simultaneously appear.

where $L_k = Q_k^T Q_k - \mathrm{diag}\{0, 0, \mathscr{W}^T\mathscr{W} + I_{2n}, \mathscr{W}^T\mathscr{W} + I_{2n}\}$ with

$$Q_k = \begin{bmatrix}0 & 0 & \mathscr{W} & 0\\ 0 & 0 & 0 & \mathscr{W}\\ \mathscr{W} & 0 & \mathscr{D} + \alpha_k\mathscr{W} & -\beta_k\mathscr{W}\\ 0 & \mathscr{W} & \beta_k\mathscr{W} & \mathscr{D} + \alpha_k\mathscr{W}\end{bmatrix}. \tag{18}$$

If $L_k < 0, k = 1, 2, \ldots, h$, then the zero solution of (11) is asymptotically stable. Hence we obtain a synchronized theorem for networks (1).

Theorem 1. *Consider network systems* (1). *Assume the mutual coupling matrices* $A = B$. *Let* $\lambda_k = \alpha_k + j\beta_k$ *be the eigenvalues of* A, *where* $\alpha_k, \beta_k \in R$. *If these matrices* $M_k, L_k < 0, k = 1, 2, \ldots, h$, *then the networks* (1) *will achieve inner synchronization inside each network.*

Remark 2. Note that Theorem 1 only gives a feasibility of the inner synchronization inside each network. When the inner synchronization inside networks X and Y happens, and the synchronized states $\|x_s(t) - y_s(t)\| \to 0$ for a large time, then the outer synchronization between networks X and Y will be achieved.

3. Numerical Examples

In this section, we will give some examples to illustrate our theoretical results obtained in the previous section. We mainly investigate the effect of coupling strengths, node dynamics, and mutual coupling forms on the inner and outer

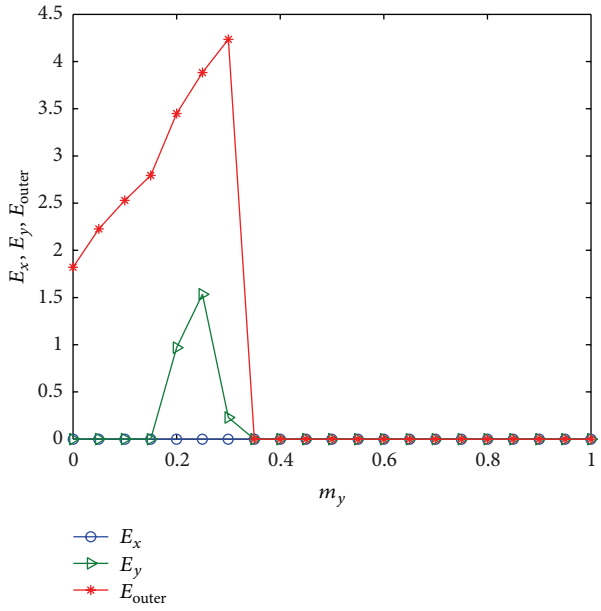

FIGURE 2: The plots show E_x, E_y, and E_{outer} at $t = 400$ on m_y for $N = 10$ and $m_x = 0.3$. When $m_y \geq 0.35$, the inner and outer synchronization simultaneously happen.

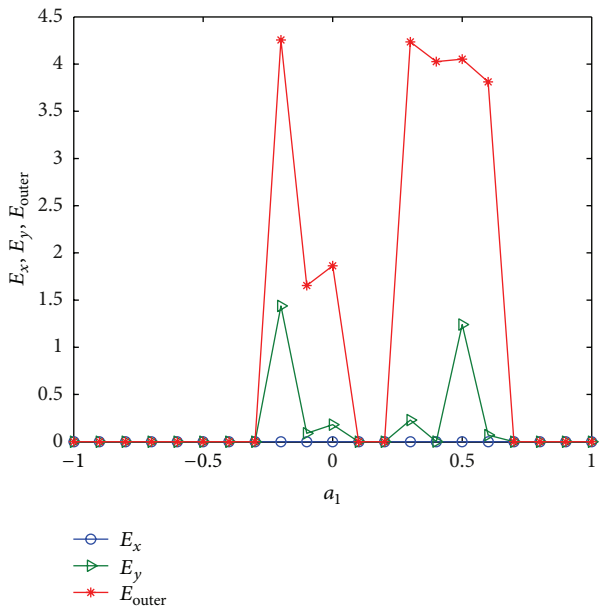

FIGURE 3: The curves of E_x, E_y, and E_{outer} at $t = 400$ concerning a_1 with $b_1 = 0.2, a_2 = 0.5$, and $b_2 = 0.3$ and $N = 10, m_x = 0.2$, and $m_y = 0.3$.

synchronization. We consider the following coupled discrete-time networks, which are in the form of (1):

$$x_{i1}(t+1) = 1 + x_{i2}(t) - a_1 x_{i1}(t)^2 + m_x \sum_{j=1}^{N} a_{ij}\left(y_{j1}(t) - x_{j1}(t)\right),$$

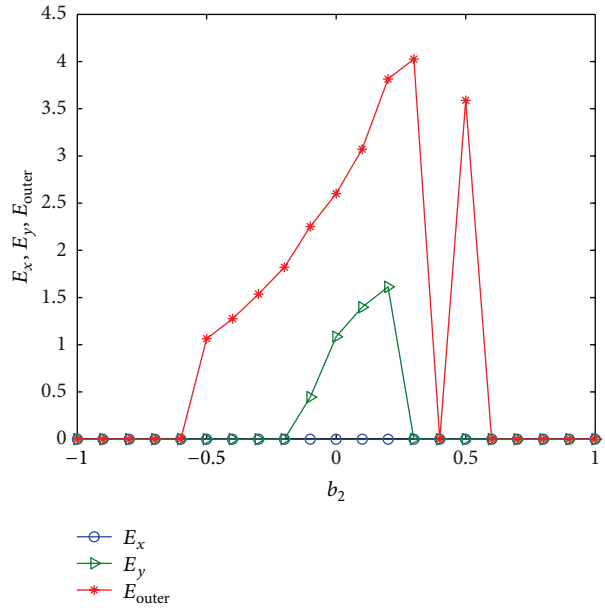

FIGURE 4: The trajectories of E_x, E_y, and E_{outer} at $t = 400$ regarding b_2 with $a_1 = 0.3, b_1 = 0.2$, and $a_2 = 0.5$ and $N = 10, m_x = 0.2$, and $m_y = 0.3$.

$$\begin{aligned}
x_{i2}(t+1) &= b_1 x_{i1}(t) + m_x \sum_{j=1}^{N} a_{ij}\left(y_{j2}(t) - x_{j2}(t)\right), \quad i = 1, 2, \ldots, N, \\
y_{i1}(t+1) &= 1 + y_{i2}(t) - a_2 y_{i1}(t)^2 + m_y \sum_{j=1}^{N} b_{ij}\left(x_{j1}(t) - y_{j1}(t)\right), \\
y_{i2}(t+1) &= b_2 y_{i1}(t) + m_y \sum_{j=1}^{N} b_{ij}\left(x_{j2}(t) - y_{j2}(t)\right), \\
& \qquad i = 1, 2, \ldots, N, \qquad (19)
\end{aligned}$$

where the node equations in (19) are both Henön maps, which have colorful dynamical properties, for instance, $a_1 = 0.5$ and $b_1 = 0.3$; it has a periodic solution. Since the sum of each row of mutual matrices is one, for simplicity, we take $a_{ij} = b_{ij} = 1/N$ for $i, j = 1, \ldots, N$. To measure the extent to which inner synchronization is achieved, we introduce two quantities, $E_x = \|x_i(t) - x_s(t)\|$ and $E_y = \|y_i(t) - y_s(t)\|, i = 1, \ldots, N$. In addition, we denote another quantity $E_{\text{outer}} = \|x_i(t) - y_i(t)\|$ for $i = 1, \ldots, N$ to demonstrate whether outer synchronization happens. Given the values of $a_1 = 0.3, b_1 = 0.2, a_2 = 0.5$, and $b_2 = 0.3$, we first study the effect of coupling strengths m_x and m_y on the inner and outer synchronization. Figure 1 shows that the outer synchronization does not happen when the coupling strength is $m_x < 0.5$, while the inner synchronization inside network X always appears. In the same way, considering the effect of coupling strength m_y, the details are shown in Figure 2.

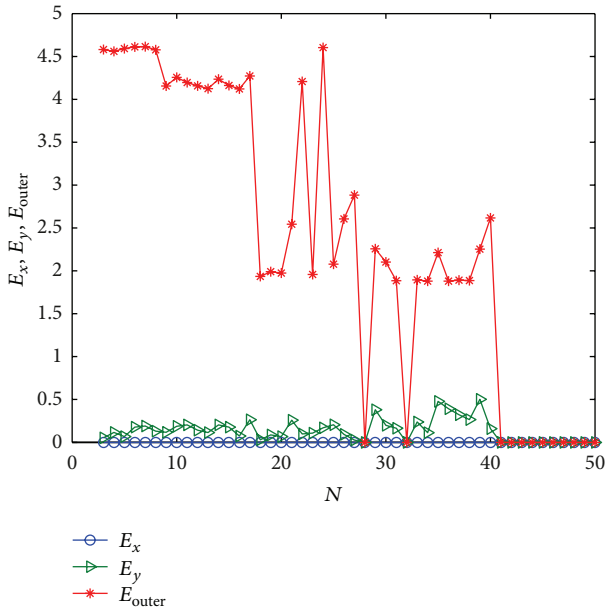

FIGURE 5: The plots show E_x, E_y, and E_{outer} at $t = 400$ on N with $a_1 = 0.3, b_1 = 0.2, a_2 = 0.5$, and $b_2 = 0.3$ and $m_x = 0.2$ and $m_y = 0.3$. The topologies are $a_{ij} = b_{ij} = 1/N, i, j = 1, \ldots, N$. Obviously the inner synchronization inside network Y and outer synchronization do not happen for the network size $N < 40$ except some values of N.

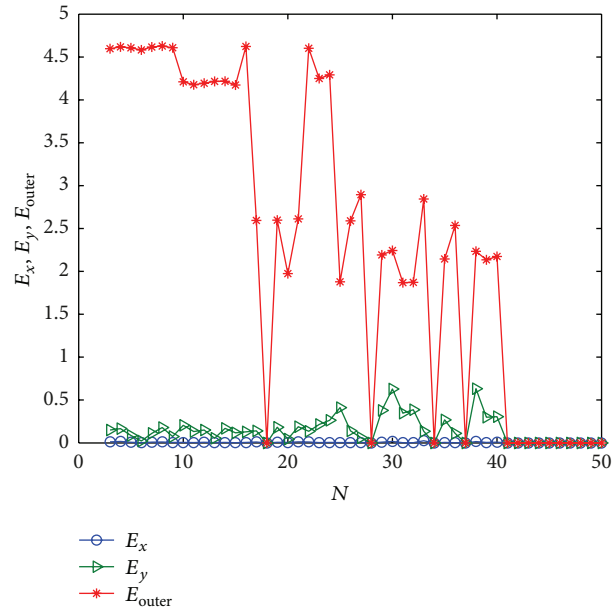

FIGURE 6: The curves of E_x, E_y, and E_{outer} at $t = 400$ regarding N with $a_1 = 0.3, b_1 = 0.2, a_2 = 0.5$, and $b_2 = 0.3$ and $m_x = 0.2$, and $m_y = 0.3$. The coupling matrix $A(B)$ is a random matrix satisfying the sum of each row being one.

Next, we discuss the effect of node dynamics on the inner and outer synchronization and take $b_1 = 0.2$, $a_2 = 0.5$, and $b_2 = 0.3$ and $N = 10$, $m_x = 0.2$, and $m_y = 0.3$. We then investigate the effect of parameter a_1 on the inner and outer synchronization. Similarly, given $a_1 = 0.3$, $b_1 = 0.2$, and $a_2 = 0.5$ and $N = 10$, $m_x = 0.2$, and $m_y = 0.3$, we study the influence of b_2. The numerical simulations are summarized in Figures 3 and 4, showing that the inner synchronization inside network X always happens, while the inner synchronization inside network Y and the outer synchronization only appear for some values of a_1 or b_2.

Finally, we discuss the effect of network size N on the inner and outer synchronization with $a_{ij} = b_{ij} = 1/N, i, j = 1, \ldots, N$. Taking the values of $a_1 = 0.3, b_1 = 0.2, a_2 = 0.5$, and $b_2 = 0.3$ and $m_x = 0.2$ and $m_y = 0.3$, we plot the curves of E_x, E_y, and E_{outer} in Figure 5. In the following, we change the topological structures of mutual coupling matrices and choose $A = B$ as a random matrix; the numerics are shown in Figure 6. It is found that the globally connected and random topological structures have similar effect on the inner and outer synchronization. It is noted that the inner synchronization inside network X always happens. A possible reason is the effect of node dynamics. Furthermore, when the Henön map behaves chaotically, no synchronization appears.

4. Conclusions

The current study investigated the synchronization between two discrete-time networks with mutual couplings and mainly studied inner synchronization inside each network and outer synchronization between them. We then obtained a synchronous theorem on the inner synchronization inside each network in terms of linear matrix inequality, for the lack of a criterion on the outer synchronization. When the inner synchronization is achieved inside each network and the synchronized states x_s and y_s are same for a large time, then the outer synchronization will happen. From the numerical simulations, we see that the inner and outer synchronization simultaneously happen when we adjust the values of coupling strengths and parameters in the node dynamics. The globally connected and random topologies have similar effect on the inner and outer synchronization. In addition, outer synchronization is more difficult to achieve than the inner synchronization, meaning that the outer synchronization needs a strong coupling form. Because of the diversity of coupling forms between two networks, deriving the criteria on the inner and outer synchronization simultaneously is a technical challenge, which would be discussed in the future.

Conflict of Interests

The authors declare that there is no conflict of interests regarding the publication of this paper.

Acknowledgments

This work was supported by the National Natural Science Foundation of China (nos. 61203155 and 11171084) and Zhejiang Provincial Natural Science Foundation of China under Grant no. LQ12F03003.

References

[1] D. J. Watts and S. H. Strogatz, "Collective dynamics of small-world networks," *Nature*, vol. 393, no. 6684, pp. 440–442, 1998.

[2] A.-L. Barabási and R. Albert, "Emergence of scaling in random networks," *Science*, vol. 286, no. 5439, pp. 509–512, 1999.

[3] S. Boccaletti, V. Latora, Y. Moreno, M. Chavez, and D.-U. Hwang, "Complex networks: structure and dynamics," *Physics Reports*, vol. 424, no. 4-5, pp. 175–308, 2006.

[4] A. Arenas, A. Díaz-Guilera, J. Kurths, Y. Moreno, and C. Zhou, "Synchronization in complex networks," *Physics Reports*, vol. 469, no. 3, pp. 93–153, 2008.

[5] Q. Wang, Z. Duan, G. Chen, and Z. Feng, "Synchronization in a class of weighted complex networks with coupling delays," *Physica A*, vol. 387, no. 22, pp. 5616–5622, 2008.

[6] W. Yu, G. Chen, J. Lü, and J. Kurths, "Synchronization via pinning control on general complex networks," *SIAM Journal on Control and Optimization*, vol. 51, no. 2, pp. 1395–1416, 2013.

[7] M. Sheikhan, R. Shahnazi, and S. Garoucy, "Synchronization of general chaotic systems using neural controllers with application to secure communication," *Neural Computing and Applications*, vol. 22, no. 2, pp. 361–373, 2013.

[8] X. Li, "Phase synchronization in complex networks with decayed long-range interactions," *Physica D*, vol. 223, no. 2, pp. 242–247, 2006.

[9] M. Sun, C. Zeng, and L. Tian, "Linear generalized synchronization between two complex networks," *Communications in Nonlinear Science and Numerical Simulation*, vol. 15, no. 8, pp. 2162–2167, 2010.

[10] D. H. Ji, S. C. Jeong, J. H. Park, S. M. Lee, and S. C. Won, "Adaptive lag synchronization for uncertain complex dynamical network with delayed coupling," *Applied Mathematics and Computation*, vol. 218, no. 9, pp. 4872–4880, 2012.

[11] W. L. Lu, B. Liu, and T. Chen, "Cluster synchronization in networks of distinct groups of maps," *European Physical Journal B*, vol. 77, no. 2, pp. 257–264, 2010.

[12] Z. Ma, Z. Liu, and G. Zhang, "A new method to realize cluster synchronization in connected chaotic networks," *Chaos*, vol. 16, no. 2, Article ID 023103, 2006.

[13] C. Li, W. Sun, and J. Kurths, "Synchronization between two coupled complex networks," *Physical Review E*, vol. 76, no. 4, Article ID 046204, 2007.

[14] H. Tang, L. Chen, J.-A. Lu, and C. K. Tse, "Adaptive synchronization between two complex networks with nonidentical topological structures," *Physica A*, vol. 387, no. 22, pp. 5623–5630, 2008.

[15] X. Wu, W. X. Zheng, and J. Zhou, "Generalized outer synchronization between complex dynamical networks," *Chaos*, vol. 19, no. 1, Article ID 013109, 2009.

[16] G. Wang, J. Cao, and J. Lu, "Outer synchronization between two nonidentical networks with circumstance noise," *Physica A*, vol. 389, no. 7, pp. 1480–1488, 2010.

[17] Y. Z. Sun and D. H. Zhao, "Effects of noise on the outer synchronization of two unidirectionally coupled complex dynamical networks," *Chaos*, vol. 22, no. 2, Article ID 023131, 2012.

[18] S. Zheng, S. Wang, G. Dong, and Q. Bi, "Adaptive synchronization of two nonlinearly coupled complex dynamical networks with delayed coupling," *Communications in Nonlinear Science and Numerical Simulation*, vol. 17, no. 1, pp. 284–291, 2012.

[19] M. M. Asheghan, J. Míguez, M. T. Hamidi-Beheshti, and M. S. Tavazoei, "Robust outer synchronization between two complex networks with fractional order dynamics," *Chaos*, vol. 21, no. 3, Article ID 033121, 2011.

[20] Z. Wu and X. Fu, "Outer synchronization between drive-response networks with nonidentical nodes and unknown parameters," *Nonlinear Dynamics*, vol. 69, no. 1-2, pp. 685–692, 2012.

[21] X. Wu and H. Lu, "Outer synchronization of uncertain general complex delayed networks with adaptive coupling," *Neurocomputing*, vol. 82, pp. 157–166, 2012.

[22] Y.-Q. Wu, W.-G. Sun, and S.-S. Li, "Anti-synchronization between coupled networks with two active forms," *Communications in Theoretical Physics*, vol. 55, no. 5, pp. 835–840, 2011.

[23] F. Sorrentino and E. Ott, "Network synchronization of groups," *Physical Review E*, vol. 76, no. 5, Article ID 056114, 2007.

[24] W. Sun, J. Zhang, and C. Li, "Synchronization analysis of two coupled complex networks with time delays," *Discrete Dynamics in Nature and Society*, vol. 2011, Article ID 209321, 12 pages, 2011.

Hindawi Publishing Corporation
Abstract and Applied Analysis
Volume 2013, Article ID 503659, 5 pages
http://dx.doi.org/10.1155/2013/503659

Research Article

Projective Lag Synchronization of Delayed Neural Networks Using Intermittent Linear State Feedback

Junjian Huang,[1,2] Chuandong Li,[1,3] Tingwen Huang,[4] Huaqing Li,[1] and Mei Peng[5]

[1] *College of Computer Science, Chongqing University, Chongqing 400030, China*
[2] *Department of Computer Science, Chongqing University of Education, Chongqing 400067, China*
[3] *School of Electronics and Information Engineering, Southwest University, Chongqing 400715, China*
[4] *Texas A&M University at Qatar, P.O. Box 23874, Doha, Qatar*
[5] *College of Mathematical and Computer Science, Yangtze Normal University, Chongqing 400084, China*

Correspondence should be addressed to Chuandong Li; licd@cqu.edu.cn

Received 12 August 2013; Accepted 10 September 2013

Academic Editor: Jinde Cao

The problem of projective lag synchronization of coupled neural networks with time delay is investigated. By means of the Lyapunov stability theory, an intermittent controller is designed for achieving projective lag synchronization between two delayed neural networks systems. Numerical simulations on coupled Lu neural systems illustrate the effectiveness of the results.

1. Introduction

In the past few years, synchronization of neural networks has been extensively investigated due to their successful application in many areas, such as communication, modeling brain activity, signal processing, and combinatorial optimization. There are several different synchronization schemes including complete, lag, projective, generalized, phase, and anticipated synchronization [1–9]. In projective synchronization, the master-slave systems can be synchronized up to a scaling factor. Due to the potential applications in secure communication, projective synchronization has attracted increasing attention [10–13]. In [10], the authors study the projective synchronization for different chaotic delayed neural networks via sliding mode control approach. Function projective synchronization of two-cell Quantum-CNN chaotic oscillators using adaptive method is investigated in [11]. It is worth noting that the propagation delay may exist in remote communication systems. However, to the best of the authors' knowledge, few results (if any) for the projective lag synchronization of neural networks with time delay have been reported in the literature.

In this paper, we will deal with the analysis issue for projective lag synchronization of neural networks with time delay by intermittent control approach. Recently, we have employed this method to stabilize and synchronize chaotic systems [14–16]. In this paper, by using Lyapunov stability theory and intermittent control technique, the intermittent controllers and corresponding parameter update rules are designed to obtain projective lag synchronization of neural networks. The rest of the paper is organized as follows. In Section 2, we formulate the problem of projective lag synchronization of coupled neural networks. In Section 3, a general scheme for the projective lag synchronization is presented. Numerical simulations are given in Section 4. Finally, conclusions are given in Section 5.

2. Problem Formulation and Preliminaries

In this paper, we consider the chaotic cellular neural networks described by

$$\begin{aligned} \dot{x}_i(t) &= -c_i x(t) + \sum_{j=1}^{n} a_{ij} f_i(x(t)) + \sum_{j=1}^{n} b_{ij} g_i(x(t-\tau)), \\ &\qquad i = 1, 2, 3, \ldots, n;\ t > 0, \\ x(t) &= \varphi(t), \quad -\tau \le t \le 0, \end{aligned} \tag{1}$$

or, in a compact form,

$$\begin{aligned} \dot{x}(t) &= Cx(t) + Af(x(t)) + Bg(x(t-\tau)), \quad t > 0, \\ x(t) &= \varphi(t), \quad -\tau \le t \le 0, \end{aligned} \tag{2}$$

where $x(t) = [x_1(t), x_2(t), \ldots, x_n(t)] \in R^n$ denotes the state vector, C, A, and $B \in R^{m\times m}$ are constant matrices, τ is the time delay, and $f, g : R^m \to R^m$ are nonlinear functions satisfying the Lipschitz condition, namely; there exist positive constants L_f, L_g such that, for all $x, y \in R^n$,

$$\begin{aligned} |f(x) - f(y)| &\le L_f |x - y|, \\ |g(\alpha) - g(\beta)| &\le L_g |\alpha - \beta|. \end{aligned} \tag{3}$$

Consider the corresponding slave system given in the following form:

$$\begin{aligned} \dot{y}(t) &= Cy(t) + Af(y(t)) + Bg(y(t-\tau)) + u(t), \\ & \qquad t > 0, \\ y(t) &= \psi(t), \quad -\tau \le t \le 0, \end{aligned} \tag{4}$$

where $y(t) \in R^n$ denotes the state vector, C, A, and $B \in R^{n\times n}$ are constant matrices, and $u(t)$ denotes the intermittent feedback control defined as follows:

$$u(t) = \begin{cases} H(t) + K(t), & nT \le t < nT + \sigma T, \\ H(t), & nT + \sigma T \le t < (n+1)T, \end{cases} \tag{5}$$

where k denotes the control strength, $0 < \sigma < 1$ denotes the switching rate, T denotes the control period, and $H(t)$ and $K(t)$ are the active control functions.

Let θ be the transmittal delay. Defining the projective lag synchronization error between systems (2) and (4) as $e(t) = y(t) - \alpha x(t-\theta)$, where α denotes projective scaling factor, we have the following error dynamical system:

$$\begin{aligned} \dot{e}(t) &= \dot{y}(t) - \alpha \dot{x}(t-\theta) \\ &= Cy(t) + Af(y(t)) + Bg(y(t-\tau)) + u(t) \\ &\quad - \alpha \big(Cx(t-\theta) + Af(x(t-\theta)) \\ &\qquad + Bg(x(t-\tau-\theta))\big). \end{aligned} \tag{6}$$

Under the control of the form (5), the system (6) can be rewritten as

$$\begin{aligned} \dot{e}(t) &= Cy(t) + Af(y(t)) + Bg(y(t-\tau)) + H(t) + K(t) \\ &\quad - \alpha \big(Cx(t-\theta) + Af(x(t-\theta)) + Bg(x(t-\tau-\theta))\big), \\ &\qquad nT \le t < nT + \sigma T, \\ \dot{e}(t) &= Cy(t) + Af(y(t)) + Bg(y(t-\tau)) + H(t) \\ &\quad - \alpha \big(Cx(t-\theta) + Af(x(t-\theta)) + Bg(x(t-\tau-\theta))\big), \\ &\qquad nT + \sigma T \le t < (n+1)T. \end{aligned} \tag{7}$$

Definition 1. The master system (2) and the slave system (4) are said to be projective lag synchronization if there exist a compact set α, σ and delay time θ such that, for any initial values $\varphi(t_0), \psi(t_0) \in \Omega$, $t_0 \in [-\tau, 0]$, the error system is exponentially stable; that is,

$$\lim_{t\to\infty} \|e(t)\| = \lim_{t\to\infty} \|y(t) - \alpha x(t-\theta)\| \le \|e(0)\| e^{-\sigma t}, \quad \forall t \ge 0. \tag{8}$$

3. Main Results

This section addresses the projective lag synchronization problem of coupled neural networks.

Theorem 2. *Suppose that there exist constants α, the coupling strength k, time delay θ, and the functions $H(t)$, $K(t)$ such that*

(i) $C + C^T - 2kI + g_1 I \le 0$;

(ii) $C + C^T - g_2 I \le 0$;

(iii) $H(t) = -Af(y(t)) - Bg(y(t-\tau)) + \alpha Af(x(t-\theta)) + \alpha Bg(x(t-\tau-\theta))$;

(iv) $K(t) = -k(y(t) - \alpha x(t-\theta))$;

(v) $g_1\sigma - (1-\sigma)g_2 > 0$.

Then, the projective lag synchronization error system (7) *is globally exponentially stable, that is; the projective lag synchronization between the master system* (2) *and the slave system* (4) *under intermittent control* (5) *is achieved.*

Proof. Consider the following Lyapunov function:

$$V(t) = e(t)^T e(t). \tag{9}$$

When $nT \le t < nT + \sigma T$, the derivative of (9) with respect to time t along the trajectories of the first subsystem of the system (7) is calculated and estimated as follows:

$$\begin{aligned} \dot{V}(t) &= 2e(t)^T \dot{e}(t) \\ &= 2e(t)^T \big[Cy(t) + Af(y(t)) + Bg(y(t-\tau)) \\ &\qquad + H(t) + K(t) \\ &\qquad - \alpha \big(Cx(t-\theta) + Af(x(t-\theta)) \\ &\qquad\quad + Bg(x(t-\tau-\theta))\big)\big] \\ &= e(t)^T \left[C + C^T - 2kI + g_1 I\right] e(t) - g_1 e(t)^T e(t) \\ &\le -g_1 e(t)^T e(t). \end{aligned} \tag{10}$$

Similarly, when $nT + \sigma T \le t < (n+1)T$, one obtains

$$\begin{aligned} \dot{V}(t) &= 2e(t)^T \dot{e}(t) = 2e(t)^T \\ &\quad \times \big[Cy(t) + Af(y(t)) + Bg(y(t-\tau)) + H(t) \\ &\qquad - \alpha \big(Cx(t-\theta) + Af(x(t-\theta)) + Bg(x(t-\tau-\theta))\big)\big] \\ &= e(t)^T \left[C + C^T - g_2 I\right] e(t) + g_2 e(t)^T e(t) \\ &\le g_2 e(t)^T e(t). \end{aligned} \tag{11}$$

Therefore,

$$\begin{aligned} \dot{V}(t) &\le -g_1 V(t), \qquad nT \le t < nT + \sigma T, \\ \dot{V}(t) &\le g_2 V(t), \qquad nT + \sigma T \le t < (n+1)T. \end{aligned} \tag{12}$$

Then, one observes that

$$\begin{aligned} V(t) &\le \|V(nT)\| \exp\left(-g_1 (t - nT)\right), \\ &\qquad nT \le t < nT + \sigma T, \\ V(t) &\le \|V(nT + \sigma T)\| \exp\left(g_2 (t - nT - \sigma T)\right), \\ &\qquad nT + \sigma T \le t < (n+1)T. \end{aligned} \tag{13}$$

By (12) and (13), we can obtain the following.

(1) For $0 \le t < \sigma T$,

$$\begin{aligned} V(t) &\le \|V(t_0)\| \exp\left(-g_1 t\right), \\ V(\sigma T) &\le \|V(t_0)\| \exp\left(-g_1 \sigma T\right). \end{aligned} \tag{14}$$

(2) For $\sigma T \le t < T$,

$$\begin{aligned} V(t) &\le (\|V(\sigma T)\|) \exp\left(g_2 (t - \sigma T)\right) \\ &\le \left(\|V(t_0)\|\right) \exp\left(-g_1 \sigma T + g_2 (t - \sigma T)\right), \\ V(T) &\le \left(\|V(t_0)\|\right) \exp\left(-g_1 \sigma T + g_2 (T - \sigma T)\right). \end{aligned} \tag{15}$$

(3) For $T \le t < T + \sigma T$,

$$\begin{aligned} V(t) &\le (\|V(T)\|) \exp\left(-g_1 (t - T)\right) \\ &\le \left(\|V(t_0)\|\right) \exp\left(-g_1 \sigma T + g_2 (T - \sigma T) - g_1 (t - T)\right), \\ V(T + \sigma T) &\le \left(\|V(t_0)\|\right) \\ &\quad \times \exp\left(-g_1 \sigma T + g_2 (T - \sigma T) - g_1 (T + \sigma T - T)\right) \\ &\le \left(\|V(t_0)\|\right) \exp\left(-2 g_1 \sigma T + g_2 (T - \sigma T)\right). \end{aligned} \tag{16}$$

(4) For $T + \sigma T \le t < 2T$,

$$\begin{aligned} V(t) &\le \left(\|V(t_0)\|\right) \\ &\quad \times \exp\left(-2 g_1 \sigma T + g_2 (T - \sigma T) + g_2 (t - T - \sigma T)\right), \\ V(2T) &\le \left(\|V(t_0)\|\right) \exp\left(-2 g_1 \sigma T + 2 g_2 (T - \sigma T)\right). \end{aligned} \tag{17}$$

By induction, we have the following.

(5) For $nT \le t < nT + \sigma T$,

$$\begin{aligned} V(t) &\le (\|V(nT)\|) \exp\left(-g_1 (t - nT)\right) \\ &\le \left(\|V(t_0)\|\right) \exp\left(-g_1 (t - nT)\right) \\ &\quad \times \exp\left(-n g_1 \sigma T + n g_2 (T - \sigma T)\right) \\ &\le \left(\|V(t_0)\|\right) \exp\left(-n g_1 \sigma T + n g_2 (T - \sigma T)\right). \end{aligned} \tag{18}$$

Note that $(t - \sigma T)/T \le n < t/T$; in this case, we can obtain

$$\begin{aligned} V(t) &\le \left(\|V(t_0)\|\right) \\ &\quad \times \exp\left(-\frac{\left(g_1 \sigma T - g_2 (T - \sigma T)\right)(t - \sigma T)}{T}\right) \\ &\le \left(\|V(t_0)\|\right) \exp\left(-\left(g_1 \sigma - g_2 (1 - \sigma)\right)(t - \sigma T)\right). \end{aligned} \tag{19}$$

(6) For $nT + \sigma T \le t < (n+1)T$

$$\begin{aligned} V(t) &\le (\|V(nT + \sigma T)\|) \exp\left(-g_2 (t - nT - \sigma T)\right) \\ &\le \left(\|V(t_0)\|\right) \exp\left(-g_2 (t - nT - \sigma T)\right) \\ &\quad \times \exp\left(-(n+1) g_1 \sigma T + g_2 (n+1)(T - \sigma T)\right) \\ &\le \left(\|V(t_0)\|\right) \\ &\quad \times \exp\left(-(n+1) g_1 \sigma T + g_2 (n+1)(T - \sigma T)\right). \end{aligned} \tag{20}$$

Note that $t/T \le n + 1 < (t + T - \sigma T)/T$; in this case, we can obtain

$$\begin{aligned} V(t) &\le \left(\|V(t_0)\|\right) \\ &\quad \times \exp\left(-(n+1) g_1 \sigma T + g_2 (n+1)(T - \sigma T)\right) \\ &\le \left(\|V(t_0)\|\right) \exp\left(-\left(g_1 \sigma - g_2 (1 - \sigma)\right)(t - \sigma T)\right). \end{aligned} \tag{21}$$

Therefore, for any $t \ge 0$,

$$\begin{aligned} \|e(t)\|^2 &= V(t) \\ &\le \left(\|V(t_0)\|\right) \exp\left(-\left(g_1 \sigma - g_2 (1 - \sigma)\right)(t - \sigma T)\right). \end{aligned} \tag{22}$$

This implies that the projective lag synchronization error system (7) is globally exponentially stable, and the following estimate holds:

$$\|e(t)\| \le \left(\sqrt{\|V(t_0)\|}\right) \exp\left(-\frac{\left(g_1 \sigma - g_2 (1 - \sigma)\right)(t - \sigma T)}{2}\right). \tag{23}$$

This implies that the projective lag synchronization between the master system (2) and slave system (4) is achieved. □

Let ${g_1}^* = -\lambda_{\max}(C + C^T) + 2k$ and ${g_2}^* = \lambda_{\max}(C + C^T)$, where ${g_1}^* \ge g_1$, ${g_2}^* \le g_2$. If we replace the first condition in Theorem 2 with ${g_1}^*$, ${g_2}^*$, then Theorem 2 also can hold. In addition, one can obtain the following corollary from Theorem 2.

Corollary 3. *Suppose that there exist positive scalars k and σ satisfying $0 < \sigma < 1$ such that*

$$ {g_1}^* \sigma - (1 - \sigma) {g_2}^* > 0, \tag{24}$$

where ${g_1}^* = -\lambda_{\max}(C + C^T) + 2k$ and ${g_2}^* = \lambda_{\max}(C + C^T)$. Then, the system (7) *is exponentially stable, and the projective lag synchronization between the master system* (2) *and the slave system* (4) *under intermittent control* (5) *is achieved.*

Remark 4. If $\alpha = 1$, it is clear that the lag synchronization between the system (2) and system (4) will occur.

Remark 5. It is clear that when the time delay vanishes, that is, $\theta = 0$, we have $e(t) = y(t) - \alpha x(t)$, which implies that the projective synchronization between master system (2) without delay and system (4) without delay will occur.

Remark 6. From Corollary 3, one observes that the control strength k can be estimated as follows:

$$k > k^* = \frac{\lambda_{\max}\left(C + C^T\right)}{2\sigma} > 0. \tag{25}$$

Note that C are determined only by the system itself, and σ is control parameter. Then, we can estimate the feasible region D of control parameters (k, σ) as follows:

$$D = \left\{(k,\sigma) \mid k > k^* = \frac{\lambda_{\max}\left(C + C^T\right)}{2\sigma} > 0, 0 < \sigma < 1\right\}. \tag{26}$$

4. Numerical Example

In this section, Lu neural oscillator [17] is presented as an example to verify the effectiveness of Theorem 2. The programs DDE23 in MATLAB are used to solve numerically the delay differential equations.

Example 1. Consider the Lu neural oscillator [17]

$$\dot{x}(t) = -Cx(t) + Af(x(t)) + Bg(x(t-1)), \tag{27}$$

where

$$C = \begin{pmatrix} 1 & 0 \\ 0 & 1 \end{pmatrix}, \quad A = \begin{pmatrix} 3.0 & 5.0 \\ 0.1 & 2.0 \end{pmatrix}, \quad B = \begin{pmatrix} -2.5 & 0.2 \\ 0.1 & -1.5 \end{pmatrix}, \tag{28}$$

and $f(x(t)) = g(x(t)) = \tanh(x(t))$.

This model was investigated by Lu in [17] where it was shown to be chaotic, as shown in Figure 1. The corresponding slave system is given by

$$\dot{y}(t) = -Cy(t) + Af(y(t)) + Bg(y(t-1)) + u(t). \tag{29}$$

From Theorem 2, the controller can be obtained as follows:

$$u(t) = \begin{cases} -Af(y(t)) - Bg(y(t-1)) + \alpha Af(x(t-\theta)) \\ +\alpha Bg(x(t-1-\theta)) - k(y(t) - \alpha x(t-\theta)), \\ nT \le t < nT + \sigma T, \\ -Af(y(t)) - Bg(y(t-1)) + \alpha Af(x(t-\theta)) \\ +\alpha Bg(x(t-1-\theta)), \\ nT \le t < nT + \sigma T. \end{cases} \tag{30}$$

So, when $nT \le t < nT + \sigma T$, we have

$$\begin{aligned} y(t) &= -Cy(t) + Af(y(t)) + Bg(y(t-1)) \\ &\quad - Af(y(t)) - Bg(y(t-1)) \\ &\quad + \alpha Af(x(t-\theta)) + \alpha Bg(x(t-1-\theta)) - ke(t) \\ &= -Cy(t) + \alpha Af(x(t-\theta)) \\ &\quad + \alpha Bg(x(t-1-\theta)) - ke(t). \end{aligned} \tag{31}$$

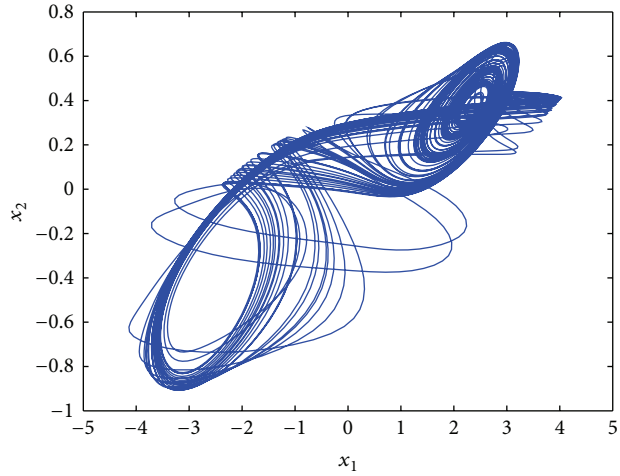

Figure 1: The chaotic attractor of the Lu oscillator described by (7) with initial value $x_1(\theta) = 0.2$, $x_2(\theta) = -0.5$, for $\theta \in [-1, 0]$.

When $nT + \sigma T \le t < (n+1)T$, we have

$$\begin{aligned} y(t) &= -Cy(t) + Af(y(t)) + Bg(y(t-1)) \\ &\quad - Af(y(t)) - Bg(y(t-1)) \\ &\quad + \alpha Af(x(t-\theta)) + \alpha Bg(x(t-1-\theta)) \\ &= -Cy(t) + \alpha Af(x(t-\theta)) + \alpha Bg(x(t-1-\theta)). \end{aligned} \tag{32}$$

Noting that $\lambda_{\max}(C + C^T) = 2$, the feasible region of control parameters (k, σ) is $D = \{(k, \sigma) \mid k < k^* = -1/\sigma, 0 < \sigma < 1\}$, as shown in Figure 2. For numerical simulation, we select $\alpha = 2$, $\theta = 0.01$, $\sigma = 0.1$, and $k = 10$ and plot the norm of projective lag synchronization errors curve, as shown in Figure 3. As the time t goes to infinity, the projective lag synchronization error system is stable. Hence, the projective lag synchronization between system (27) and system (29) is achieved.

5. Conclusions

This paper addressed projective lag synchronization of coupled neural networks with time delay. Based on Lyapunov stability theory and adaptive control techniques, several criteria for projective lag synchronization of identical neural networks with time delay have been established. With the proposed method, the simulations of projective lag between coupled Lu systems have showed the effectiveness of theoretical result.

Acknowledgments

This publication was made possible by NPRP Grant no. NPRP 4-1162-1-181 from the Qatar National Research Fund (a member of Qatar Foundation). The statements made herein are solely the responsibility of the authors. This work was also supported by Natural Science Foundation of China (Grant

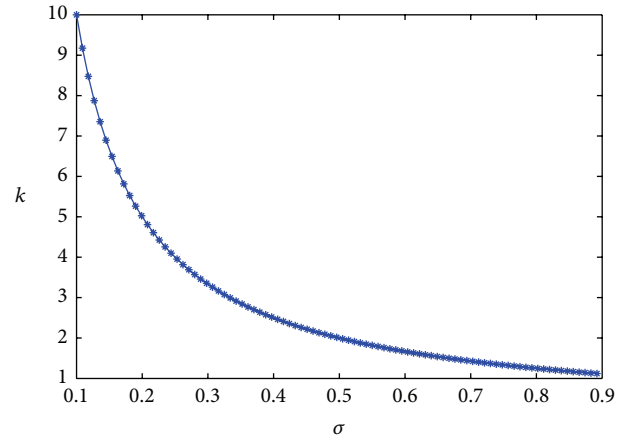

Figure 2: The relationship between k and σ.

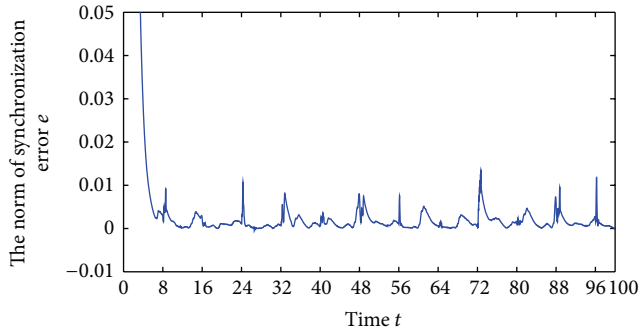

Figure 3: The norm of synchronization error curve with $\alpha = 2$, $\theta = 0.01$, $\sigma = 0.1$ and $k = 10$.

no. 61374078), the Scientific and Technological Research Program of Chongqing Municipal Education Commission (Grant no. KJ121505), the Natural Science Foundation Project of Chongqing CSTC (Grant no. cstc2011jjA40005).

References

[1] L. M. Pecora and T. L. Carroll, "Synchronization in chaotic systems," *Physical Review Letters*, vol. 64, no. 8, pp. 821–824, 1990.

[2] L. M. Pecora and T. L. Carroll, "Driving systems with chaotic signals," *Physical Review A*, vol. 44, no. 4, pp. 2374–2383, 1991.

[3] N. F. Rulkov, M. M. Sushchik, L. S. Tsimring, and H. D. I. Abarbanel, "Generalized synchronization of chaos in directionally coupled chaotic systems," *Physical Review E*, vol. 51, no. 2, pp. 980–994, 1995.

[4] R. Mainieri and J. Rehacek, "Projective synchronization in three-dimensional chaotic systems," *Physical Review Letters*, vol. 82, no. 15, pp. 3042–3045, 1999.

[5] M. G. Rosenblum, A. S. Pikovsky, and J. Kurths, "Phase synchronization of chaotic oscillators," *Physical Review Letters*, vol. 76, no. 11, pp. 1804–1807, 1996.

[6] M. G. Rosenblum, A. S. Pikovsky, and J. Kurths, "From phase to lag synchronization in coupled chaotic oscillators," *Physical Review Letters*, vol. 78, no. 22, pp. 4193–4196, 1997.

[7] C. Masoller and D. H. Zanette, "Anticipated synchronization in coupled chaotic maps with delays," *Physica A*, vol. 300, no. 3-4, pp. 359–366, 2001.

[8] X. Li, C. Ding, and Q. Zhu, "Synchronization of stochastic perturbed chaotic neural networks with mixed delays," *Journal of the Franklin Institute*, vol. 347, no. 7, pp. 1266–1280, 2010.

[9] H. Huang, G. Feng, and J. Cao, "Exponential synchronization of chaotic Lur'e systems with delayed feedback control," *Nonlinear Dynamics*, vol. 57, no. 3, pp. 441–453, 2009.

[10] D. Zhang and J. Xu, "Projective synchronization of different chaotic time-delayed neural networks based on integral sliding mode controller," *Applied Mathematics and Computation*, vol. 217, no. 1, pp. 164–174, 2010.

[11] K. S. Sudheer and M. Sabir, "Adaptive function projective synchronization of two-cell Quantum-CNN chaotic oscillators with uncertain parameters," *Physics Letters A*, vol. 373, no. 21, pp. 1847–1851, 2009.

[12] S. Chen and J. Cao, "Projective synchronization of neural networks with mixed time-varying delays and parameter mismatch," *Nonlinear Dynamics*, vol. 67, no. 2, pp. 1397–1406, 2012.

[13] L. Chen, Y. Chai, and R. Wu, "Modified function projective synchronization of chaotic neural networks with delays based on observer," *International Journal of Modern Physics C*, vol. 22, no. 2, pp. 169–180, 2011.

[14] C. Li, X. Liao, and T. Huang, "Exponential stabilization of chaotic systems with delay by periodically intermittent control," *Chaos*, vol. 17, no. 1, Article ID 013103, 2007.

[15] J. Huang, C. Li, and Q. Han, "Stabilization of delayed chaotic neural networks by periodically intermittent control," *Circuits, Systems, and Signal Processing*, vol. 28, no. 4, pp. 567–579, 2009.

[16] J. Huang, C. Li, T. Huang, and Q. Han, "Lag quasisynchronization of coupled delayed systems with parameter mismatch by periodically intermittent control," *Nonlinear Dynamics*, vol. 71, no. 3, pp. 469–478, 2013.

[17] H. Lu, "Chaotic attractors in delayed neural networks," *Physics Letters A*, vol. 298, no. 2-3, pp. 109–116, 2002.

Hindawi Publishing Corporation
Abstract and Applied Analysis
Volume 2013, Article ID 120849, 10 pages
http://dx.doi.org/10.1155/2013/120849

Research Article

Combined Heat and Power Dynamic Economic Dispatch with Emission Limitations Using Hybrid DE-SQP Method

A. M. Elaiw,[1,2] X. Xia,[3] and A. M. Shehata[2]

[1] *Department of Mathematics, Faculty of Science, King Abdulaziz University, P.O. Box 80203, Jeddah 21589, Saudi Arabia*
[2] *Department of Mathematics, Faculty of Science, Al-Azhar University, Assiut 71511, Egypt*
[3] *Centre of New Energy Systems, Department of Electrical, Electronic and Computer Engineering, University of Pretoria, Pretoria 0002, South Africa*

Correspondence should be addressed to A. M. Elaiw; a_m_elaiw@yahoo.com

Received 28 August 2013; Accepted 1 October 2013

Academic Editor: Jinde Cao

Combined heat and power dynamic economic emission dispatch (CHPDEED) problem is a complicated nonlinear constrained multiobjective optimization problem with nonconvex characteristics. CHPDEED determines the optimal heat and power schedule of committed generating units by minimizing both fuel cost and emission simultaneously under ramp rate constraints and other constraints. This paper proposes hybrid differential evolution (DE) and sequential quadratic programming (SQP) to solve the CHPDEED problem with nonsmooth and nonconvex cost function due to valve point effects. DE is used as a global optimizer, and SQP is used as a fine tuning to determine the optimal solution at the final. The proposed hybrid DE-SQP method has been tested and compared to demonstrate its effectiveness.

1. Introduction

Recently, combined heat and power (CHP) units, known as cogeneration or distributed generation, have played an increasingly important role in the utility industry. CHP units can provide not only electrical power but also heat to the customers. While the efficiency of the normal power generation is between 50% and 60%, the power and heat cogeneration increases the efficiency to around 90% [1]. Besides thier high efficiency, CHP units reduce the emission of gaseous pollutants (SO_2, NO_x, CO, and) by about 13–18% [2].

In order to utilize the integrated CHP system more CO_2 economically, combined heat and power economic dispatch (CHPED) problem is applied. The objective of the CHPED problem is to determine both power generation and heat production from units by minimizing the fuel cost such that both heat and power demands are met, while the combined heat and power units are operated in a bounded heat versus power plane. For most CHP units the heat production capacities depend on the power generation. This mutual dependency of the CHP units introduces a complication to the problem [3]. In addition, considering valve point effects in the CHPED problem makes the problem nonsmooth with multiple local optimal point which makes finding the global optimal challenging.

In the literature, several optimization techniques have been used to solve the CHPED problem with complex objective functions or constraints such as Lagrangian relaxation (LR) [4, 5], semidefinite programming (SDP) [6], augmented Lagrange combined with Hopfield neural network [7], harmony search (HS) algorithm [1, 8], genetic algorithm (GA) [9], ant colony search algorithm (ACSA) [10], mesh adaptive direct search (MADS) algorithm [11], self adaptive real-coded genetic algorithm (SARGA) [3], particle swarm optimization (PSO) [2, 12], artificial immune system (AIS) [13], bee colony optimization (BCO) [14], differential evolution [15], and evolutionary programming (EP) [16]. In [2, 13–15], the valve point effects and the transmission line losses are incorporated into the CHPED problem.

In the CHPED formulation the ramp rate limits of the units are neglected. Plant operators, to avoid life-shortening of the turbines and boilers, try to keep thermal stress on the equipments within the safe limits. This mechanical

constraint is usually transformed into a limit on the rate of change of the electrical output of generators. Such ramp rate constraints link the generator operation in two consecutive time intervals. Combined heat and power dynamic economic dispatch (CHPDED) problem is an extension of CHPED problem where the ramp rate constraint is considered. The primary objective of the CHPDED problem is to determine the heat and power schedule of the committed units so as to meet the predicted heat and electricity load demands over a time horizon at minimum operating cost under ramp rate constraints and other constraints [17]. Since the ramp rate constraints couple the time intervals, the CHPDED problem is a difficult optimization problem. If the ramp rate constraints are not included in the optimization problem, the CHPDED problem is reduced to a set of uncoupled CHPED problems that can easily be solved. In the literature an overwhelming number of reported works deal with CHPED problem; however, the CHPDED problem has only been considered in [17].

The traditional dynamic economic dispatch (DED) problem which considers only thermal units that provide only electric power has been studied by several authors (see the review paper [18]). The emission has been taken into the traditional (DED) formulation in three main approaches. The first approach is to minimize the fuel cost and treat the emission as a constraint with a permissible limit (see, e.g., [19–21]). This formulation, however, has a severe difficulty in getting the trade-off relations between cost and emission [22]. The second approach handles both fuel cost and emission simultaneously as competing objectives [23–25]. The third approach treats the emission as another objective in addition to fuel cost objective. However, the multiobjective optimization problem is converted to a single-objective optimization problem by linear combination of both objectives [19, 26–30]. In the second and third approaches, the dynamic dispatch problem is referred to as dynamic economic emission dispatch (DEED) which is a multiobjective optimization problem, which minimizes both fuel cost and emission simultaneously under ramp rate constraint and other constraints [19, 24]. In this paper, we incoroporate the CHP units into the DEED problem. Combined heat and power dynamic economic emission dispatch (CHPDEED) is formulated with the objective to determine the unit power and heat production so that the system's production cost and emission are simultaneously minimized, while the power and heat demands and other constraints are met [17]. The emission has been taken into consideration in the CHPED and CHPDED in [17, 31], respectively. In [17], both fuel cost and emission are simultaneously handled as competing objectives and the multiobjective problem is solved using an enhanced firefly algorithm (FA). In the present paper, the multiobjective optimization problem is converted into a single-objective optimization using the weighting method. This approach yields meaningful result to the decision maker when solved many times for different values of the weighting factor. In [17], the simulation results for test system are shown, but the data of the heat demand is not explicitly tabulated; instead it is expressed graphically (see Figure 12 in [17]). In this case a comparison of our proposed method and FA cannot be performed. In our paper, all the data and the solutions of the test system are available for comparison.

Differential evolution algorithm (DE), which was proposed by Storn and Price [32] is a population based stochastic parallel search technique. DE uses a rather greedy and less stochastic approach to problem solving compared to other evolutionary algorithms. DE has the ability to handle optimization problems with nonsmooth/nonconvex objective functions [32]. Moreover, it has a simple structure and a good convergence property, and it requires a few robust control parameters [32]. DE has been applied to the CHPED and CHPDED problems with non-smooth and non-convex cost functions in [15, 33], respectively.

The DE shares many similarities with evolutionary computation techniques such as genetic algorithms (GA) techniques. The system is initialized with a population of random solutions and searches for optima by updating generations. DE has evolution operators such as crossover and mutation. Although DE seem to be good methods to solve the CHPDEED problem with non-smooth and non-convex cost functions, solutions obtained are just near global optimum with long computation time. Therefore, hybrid methods such as DE-SQP can be effective in solving the CHPDEED problems with valve point effects.

The main contributions of the paper are as follows. (1) A multi-objective optimization problem is formulated using CHPDEED approach. The multi-objective optimization problem is converted into a single-objective optimization using the weighting method. (2) Hybrid DE-SQP method is proposed and validated for solving the CHPDEED problem with nonsmooth and nonconvex objective function. DE is used as a base level search for global exploration and SQP is used as a local search to fine-tune the solution obtained from DE. (3) The effectiveness of the proposed method is shown for test systems.

2. Problem Formulation

In this section we formulate the CHPDEED problem. The system under consideration has three types of generating units, conventional thermal units (TU), CHP units, and heat-only units (H). The power is generated by conventional thermal units and CHP units, while the heat is generated by CHP units and heat-only units. The objective of the CHPDEED problem is to simultaneously minimize the system's production cost and emission so as to meet the predicted heat and power load demands over a time horizon under ramp rate and other constraints. The following objectives and constraints are taken into account in the formulation of the CHPDEED problem.

2.1. Objective Functions. In this section, we introduce the cost and emission functions of three types of generating units, conventional thermal units which produce power only, CHP units which produce both heat and power, and heat-only units which produce heat only.

2.1.1. Conventional Thermal Units

Cost. The cost function curve of a conventional thermal unit can be approximated by a quadratic function [35]. Power plants commonly have multiple valves which are used to control the power output of the unit. When steam admission valves in conventional thermal units are first open, a sudden increase in losses is registered which results in ripples in the cost function [18, 36]. This phenomenon is called as valve-point effects. The generator with valve-point effects has very different input-output curve compared with smooth cost function. Taking the valve-point effects into consideration, the fuel cost is expressed as the sum of a quadratic and sinusoidal functions [17, 24, 25, 37]. Therefore, the fuel cost function of the conventional thermal units is given by

$$C_i^{\mathrm{TU}}\left(P_{i,t}^{\mathrm{TU}}\right) = a_i + b_i P_{i,t}^{\mathrm{TU}} + c_i\left(P_{i,t}^{\mathrm{TU}}\right)^2 + \left|e_i \sin\left(f_i\left(P_{i,\min}^{\mathrm{TU}} - P_{i,t}^{\mathrm{TU}}\right)\right)\right|, \tag{1}$$

where a_i, b_i, and c_i are positive constants, e_i and f_i are the coefficients of conventional thermal unit i reflecting valve-point effects, $P_{i,t}^{\mathrm{TU}}$ is the power generation of conventional thermal unit i during the tth time interval $[t-1, t)$, $P_{i,\min}^{\mathrm{TU}}$ is the minimum capacity of conventional thermal unit i, and $C_i^{\mathrm{TU}}(P_{i,t}^{\mathrm{TU}})$ is the fuel cost of conventional thermal unit i to produce $P_{i,t}^{\mathrm{TU}}$.

Emission. The amount of emission of gaseous pollutants from conventional thermal units can be expressed as a combination of quadratic function and exponential function of the unit's active power output [21]. The emission function is given by

$$E_i^{\mathrm{TU}}\left(P_{i,t}^{\mathrm{TU}}\right) = \alpha_i + \beta_i P_{i,t}^{\mathrm{TU}} + \gamma_i\left(P_{i,t}^{\mathrm{TU}}\right)^2 + \eta_i \exp\left(\delta_i P_{i,t}^{\mathrm{TU}}\right), \tag{2}$$

where $E_i^{\mathrm{TU}}(P_{i,t}^{\mathrm{TU}})$ is the amount of emission from unit i from producing power $P_{i,t}^{\mathrm{TU}}$. Constants α_i, β_i, γ_i, η_i, and δ_i are the coefficients of the ith unit emission characteristics [24].

2.1.2. CHP Units

Cost. A CHP unit has a convex cost function in both power and heat. The form of the fuel cost function of CHP units can be given by [6, 17] the following:

$$C_j^{\mathrm{CHP}}\left(P_{j,t}^{\mathrm{CHP}}, H_{j,t}^{\mathrm{CHP}}\right) = \overline{a}_j + \overline{b}_j P_{j,t}^{\mathrm{CHP}} + \overline{c}_j\left(P_{j,t}^{\mathrm{CHP}}\right)^2 + \overline{d}_j H_{j,t}^{\mathrm{CHP}} + \overline{e}_j\left(H_{j,t}^{\mathrm{CHP}}\right)^2 + \overline{f}_j P_{j,t}^{\mathrm{CHP}} H_{j,t}^{\mathrm{CHP}}, \tag{3}$$

where $C_j^{\mathrm{CHP}}(P_{j,t}^{\mathrm{CHP}}, H_{j,t}^{\mathrm{CHP}})$ is the generation fuel cost of CHP unit i to produce power $P_{j,t}^{\mathrm{CHP}}$and heat $H_{j,t}^{\mathrm{CHP}}$. Constants $\overline{a}_j$, $\overline{b}_j$, $\overline{c}_j$, $\overline{d}_j$, $\overline{e}_j$, and $\overline{f}_j$ are the fuel cost coefficients of CHP unit j.

Emission. The emission of gaseous pollutants from CHP units is proportional to their active power output [17, 31]:

$$E_j^{\mathrm{CHP}}\left(P_{j,t}^{\mathrm{CHP}}\right) = \left(\overline{\alpha}_j + \overline{\beta}_j\right) P_{j,t}^{\mathrm{CHP}}, \tag{4}$$

where $\overline{\alpha}_j$ and $\overline{\beta}_j$ are the emission coefficients of CHP unit j.

2.1.3. Heat-Only Units

Cost. The cost function of heat-only units can take the following form [6, 17]:

$$C_k^H\left(H_{k,t}^H\right) = \widetilde{a}_k + \widetilde{b}_k H_{k,t}^H + \widetilde{c}_k\left(H_{k,t}^H\right)^2, \tag{5}$$

where $\widetilde{a}_k$, $\widetilde{b}_k$, and $\widetilde{c}_k$ are the fuel cost coefficients of heat-only unit k and they are constants.

Emission. The emission of gaseous pollutants from CHP units is proportional to their heat output [17, 31]:

$$E_k^H\left(H_t^H\right) = \left(\widetilde{\alpha}_k + \widetilde{\beta}_k\right) H_{k,t}^H, \tag{6}$$

where $\widetilde{\alpha}_k$ and $\widetilde{\beta}_k$ are the emission coefficients of heat-only unit k.

Let N be the number of dispatch intervals and $N_p + N_c + N_h$ the number of committed units, where N_p is the number of conventional thermal units, N_c is the number of the CHP units, and N_h is the number of the heat-only units. Then the total fuel cost and amount of emission over the dispatch period $[0, N]$ are given, respectively, by

$$\begin{aligned} C(\mathbf{PH}) &= \sum_{t=1}^{N}\left(\sum_{i=1}^{N_p} C_i^{\mathrm{TU}}\left(P_{i,t}^{\mathrm{TU}}\right) + \sum_{j=1}^{N_c} C_j^{\mathrm{CHP}}\left(P_{j,t}^{\mathrm{CHP}}, H_{j,t}^{\mathrm{CHP}}\right) + \sum_{k=1}^{N_h} C_k^H\left(H_{k,t}^H\right)\right), \\ E(\mathbf{PH}) &= \sum_{t=1}^{N}\left(\sum_{i=1}^{N_p} E_i^{\mathrm{TU}}\left(P_{i,t}^{\mathrm{TU}}\right) + \sum_{j=1}^{N_c} E_j^{\mathrm{CHP}}\left(P_{j,t}^{\mathrm{CHP}}\right) + \sum_{k=1}^{N_h} E_k^H\left(H_{k,t}^H\right)\right), \end{aligned} \tag{7}$$

where $\mathbf{PH} = (\mathbf{PH}_1, \mathbf{PH}_2, \ldots, \mathbf{PH}_t, \ldots, \mathbf{PH}_N)'$, $\mathbf{PH}_t = (\mathbf{P}_t^{\mathrm{TU}}, \mathbf{P}_t^{\mathrm{CHP}}, \mathbf{H}_t^{\mathrm{CHP}}, \mathbf{H}_t^H)'$, $\mathbf{P}_t^{\mathrm{TU}} = (P_{1,t}^{\mathrm{TU}}, P_{2,t}^{\mathrm{TU}}, \ldots, P_{N_p,t}^{\mathrm{TU}})'$, $\mathbf{P}_t^{\mathrm{CHP}} = (P_{1,t}^{\mathrm{CHP}}, P_{2,t}^{\mathrm{CHP}}, \ldots, P_{N_c,t}^{\mathrm{CHP}})'$, $\mathbf{H}_t^{\mathrm{CHP}} = (H_{1,t}^{\mathrm{CHP}}, H_{2,t}^{\mathrm{CHP}}, \ldots, H_{N_c,t}^{\mathrm{CHP}})'$, and $\mathbf{H}_t^H = (H_{1,t}^H, H_{2,t}^H, \ldots, H_{N_h,t}^H)'$.

2.2. Constraints. There are three kinds of constraints considered in the CHPDEED problem, that is, the equilibrium constraints of power and heat production, the capacity limits of each unit, and the ramp rate limits.

(i) Power Production and Demand Balance

$$\sum_{i=1}^{N_p} P_{i,t}^{\mathrm{TU}} + \sum_{j=1}^{N_c} P_{j,t}^{\mathrm{CHP}} = P_{D,t} + \mathrm{Loss}_t, \qquad t = 1, \ldots, N, \tag{8}$$

Table 1: Hourly generation (MW) schedule obtained from DED using DE-SQP for 10-unit system.

H	P_1^{TU}	P_2^{TU}	P_3^{TU}	P_4^{TU}	P_5^{TU}	P_6^{TU}	P_7^{TU}	P_8^{TU}	P_9^{TU}	P_{10}^{TU}	Loss
1	150.0000	135.0000	73.0000	70.3333	222.9974	155.1682	99.2918	120.0000	20.0000	10.0000	19.7912
2	150.0000	135.0000	101.9485	120.3333	222.6154	123.7029	129.2918	90.0000	48.7980	10.7150	22.4058
3	150.0000	135.0000	181.9485	170.3333	174.2621	130.9190	129.6896	120.0000	53.5785	40.7150	28.4468
4	150.0000	135.0000	183.1516	218.2899	223.5485	160.0000	129.3947	120.0000	80.0000	42.0564	35.4415
5	150.0000	135.0000	258.8414	249.7412	224.0147	160.0000	128.5373	120.0000	80.0000	13.2136	39.3484
6	150.0000	135.0000	315.1962	299.7412	243.0000	160.0000	129.8624	120.0000	80.0000	43.2136	48.0136
7	150.0000	176.9470	340.0000	300.0000	243.0000	160.0000	130.0000	120.0000	80.0000	55.0000	52.9470
8	178.2448	228.3049	340.0000	300.0000	243.0000	160.0000	129.9436	120.0000	80.0000	54.9118	58.4054
9	258.2448	308.3049	340.0000	300.0000	243.0000	160.0000	130.0000	120.0000	80.0000	55.0000	70.5500
10	289.0490	384.5331	340.0000	300.0000	243.0000	160.0000	130.0000	120.0000	80.0000	55.0000	79.5821
11	368.7363	397.1230	340.0000	300.0000	243.0000	160.0000	130.0000	120.0000	80.0000	55.0000	87.8595
12	374.8564	439.5807	340.0000	300.0000	243.0000	160.0000	130.0000	120.0000	80.0000	55.0000	92.4378
13	342.1737	386.2429	340.0000	300.0000	243.0000	160.0000	130.0000	120.0000	80.0000	55.0000	84.4166
14	262.1737	306.2429	340.0000	300.0000	243.0000	160.0000	130.0000	120.0000	80.0000	53.1527	70.5693
15	182.1737	226.2429	340.0000	299.9639	243.0000	160.0000	130.0000	120.0000	80.0000	53.0342	58.4148
16	150.0000	146.2429	294.7660	249.9639	223.6700	160.0000	129.6353	120.0000	80.0000	43.3613	43.6398
17	150.0000	135.0000	258.1720	249.5279	223.9121	160.0000	128.8682	120.0000	80.0000	13.8650	39.3459
18	150.0000	151.6366	298.4749	299.5279	243.0000	160.0000	129.7933	120.0000	80.0000	43.6183	48.0511
19	227.2425	231.6366	299.3393	300.0000	243.0000	160.0000	130.0000	120.0000	80.0000	43.5728	58.7914
20	307.2425	311.6366	340.0000	300.0000	243.0000	160.0000	130.0000	120.0000	80.0000	55.0000	74.8793
21	265.4293	301.1183	340.0000	300.0000	243.0000	160.0000	130.0000	120.0000	80.0000	55.0000	70.5476
22	185.4293	221.1183	263.3759	250.0000	225.8767	160.0000	129.8685	120.0000	80.0000	41.1109	48.7801
23	150.0000	141.1183	183.3759	200.0000	223.4887	155.9437	128.7427	120.0000	50.0000	11.1109	31.7806
24	150.0000	135.0000	173.1056	180.5739	173.7249	118.1382	128.6826	120.0000	20.0000	10.0000	25.2260

Table 2: Comparison results of 10-thermal-unit system (cost $\times 10^6$ \$) for the DED problem.

Method	EP [34]	PSO [34]	AIS [34]	NSGA-II [24]	IBFA [30]	DE-SQP
cost (\$)	2.5854	2.5722	2.5197	2.5168	2.4817	2.4659

Table 3: Data of the CHP units and heat-only unit system.

CHP units	$\overline{a}_j$	$\overline{b}_j$	$\overline{c}_j$	$\overline{d}_j$	$\overline{e}_j$	$\overline{f}_j$	$\overline{\alpha}_j$	$\overline{\beta}_j$	$DR_j^{CHP} = UR_j^{CHP}$
$j = 1$	2650	14.5	0.0345	4.2	0.030	0.031	0.00015	0.0015	70
$j = 2$	1250	36	0.0435	0.6	0.027	0.011	0.00015	0.0015	50
Heat-only units		$H_{k,\max}^H$	$H_{k,\min}^H$	$\widetilde{a}_k$	$\widetilde{b}_k$	$\widetilde{c}_k$	$\widetilde{\alpha}_j$	$\widetilde{\beta}_j$	
$k = 1$		2695.2	0	950	2.0109	0.038	0.0008	0.0010	

where $P_{D,t}$ and Loss_t are the system power demand and transmission line losses at time t (i.e., the tth time interval), respectively. The B-coefficient method is one of the most commonly used by power utility industry to calculate the network losses. In this method the network losses are expressed as a quadratic function of the unit's power outputs that can be approximated in the following:

$$\text{Loss}_t = \sum_{i=1}^{N_p+N_c} \sum_{j=1}^{N_p+N_c} \mathbf{PL}_{i,t} B_{ij} \mathbf{PL}_{j,t}, \quad t = 1, \ldots, N, \tag{9}$$

where

$$\mathbf{PL}_{i,t} = \begin{cases} P_{i,t}^{TU}, & i = 1, \ldots, N_p, \\ P_{i-N_p,t}^{CHP}, & i = N_p + 1, \ldots, N_p + N_c, \end{cases} \tag{10}$$

and B_{ij} is the ijth element of the loss coefficient square matrix of size $N_p + N_c$.

(ii) Heat Production and Demand Balance

$$\sum_{j=1}^{N_c} H_{j,t}^{CHP} + \sum_{k=1}^{N_h} H_{k,t}^{H} = H_{D,t}, \quad t = 1, \ldots, N, \tag{11}$$

where $H_{D,t}$ is the system heat demand at time t.

(iii) Capacity Limits of Conventional Thermal Units

$$P_{i,\min}^{TU} \le P_{i,t}^{TU} \le P_{i,\max}^{TU}, \quad i = 1, \ldots, N_p, \ t = 1, \ldots, N, \tag{12}$$

Table 4: Heat load demand of the three-unit system for 24 hours.

Time (h)	Demand (MWth)
1	390
2	400
3	410
4	420
5	440
6	450
7	450
8	455
9	460
10	460
11	470
12	480
13	470
14	460
15	450
16	450
17	420
18	435
19	445
20	450
21	445
22	435
23	400
24	400

where $P_{i,\min}^{\mathrm{TU}}$ and $P_{i,\max}^{\mathrm{TU}}$ are the minimum and maximum power capacity of conventional thermal unit i, respectively.

(iv) Capacity Limits of CHP Units

$$\begin{aligned} P_{j,\min}^{\mathrm{CHP}}\left(H_{j,t}^{\mathrm{CHP}}\right) \le P_{j,t}^{\mathrm{CHP}} \le P_{j,\max}^{\mathrm{CHP}}\left(H_{j,t}^{\mathrm{CHP}}\right), \\ j = 1,\ldots,N_c, \quad t = 1,\ldots,N, \\ H_{j,\min}^{\mathrm{CHP}}\left(P_{j,t}^{\mathrm{CHP}}\right) \le H_{j,t}^{\mathrm{CHP}} \le H_{j,\max}^{\mathrm{CHP}}\left(P_{j,t}^{\mathrm{CHP}}\right), \\ j = 1,\ldots,N_c, \quad t = 1,\ldots,N, \end{aligned} \tag{13}$$

where $P_{j,\min}^{\mathrm{CHP}}(H_{j,t}^{\mathrm{CHP}})$ and $P_{i,\max}^{\mathrm{CHP}}(H_{j,t}^{\mathrm{CHP}})$ are the minimum and maximum power limit of CHP unit j, respectively, and they are functions of generated heat ($H_{j,t}^{\mathrm{CHP}}$). $H_{j,\min}^{\mathrm{CHP}}(P_{j,t}^{\mathrm{CHP}})$ and $H_{j,\max}^{\mathrm{CHP}}(P_{j,t}^{\mathrm{CHP}})$ are the heat generation limits of CHP unit j which are functions of generated power ($P_{j,t}^{\mathrm{CHP}}$).

(v) Capacity Limits of Heat-Only Units

$$H_{k,\min}^{H} \le H_{k,t}^{H} \le H_{k,\max}^{H}, \quad k = 1,\ldots,N_h, \ t = 1,\ldots,N, \tag{14}$$

where $H_{k,\min}^{H}$ and $H_{k,\max}^{H}$ are the minimum and maximum heat capacity of heat-only unit k, respectively.

(vi) Upper/Down Ramp Rate Limits of Conventional Thermal Units

$$\begin{aligned} -DR_i^{\mathrm{TU}} \le P_{i,t+1}^{\mathrm{TU}} - P_{i,t}^{\mathrm{TU}} \le UR_i^{\mathrm{TU}}, \\ i = 1,\ldots,N_p, \quad t = 1,\ldots,N-1, \end{aligned} \tag{15}$$

where UR_i^{TU} and DR_i^{TU} are the maximum ramp up/down rates for conventional thermal unit i [18].

(vii) Upper/Down Ramp Rate Limits of CHP Units

$$\begin{aligned} -DR_j^{\mathrm{CHP}} \le P_{j,t+1}^{\mathrm{CHP}} - P_{j,t}^{\mathrm{CHP}} \le UR_j^{\mathrm{CHP}}, \\ j = 1,\ldots,N_c, \quad t = 1,\ldots,N-1, \end{aligned} \tag{16}$$

where UR_j^{CHP} and DR_j^{CHP} are the maximum ramp up/down rates for CHP unit j [17].

2.3. The Optimization Problem. Aggregating the objectives and constraints, the CHPDEED problem can be mathematically formulated as a nonlinear constrained multi-objective optimization problem which can be converted into a single-objective optimization using the weighting method as

$$\begin{aligned} \min_{\mathbf{PH}} \quad & F(\mathbf{PH}) = wC(\mathbf{PH}) + (1-w)E(\mathbf{PH}), \\ \text{subject to} \quad & \text{constraints (8)–(16)}, \end{aligned} \tag{17}$$

where $w \in [0,1]$ is a weighting factor. It will be noted that, when $w = 1$, problem (17) determines the optimal amount of the generated heat and power by minimizing the fuel cost regardless of emission and the problem will be referred to as combined heat and power dynamic economic dispatch (CHPDED) problem. If $w = 0$, then problem (17) determines the optimal amount of the generated power by minimizing the emission regardless of cost and the problem will be referred to as combined heat and power pure dynamic emission dispatch (CHPPDED).

3. Differential Evolution Method

DE is a simple yet powerful heuristic method for solving nonlinear, nonconvex, and nonsmooth optimization problems. DE algorithm is a population based algorithm using three operators; mutation, crossover, and selection to evolve from randomly generated initial population to final individual solution [32]. In the initialization a population of NP target vectors (parents) $X_i = \{x_{1i}, x_{2i}, \ldots, x_{Di}\}$, $i = 1, 2, \ldots, \mathrm{NP}$, is randomly generated within user-defined bounds, where D is the dimension of the optimization problem. Let $X_i^G = \{x_{1i}^G, x_{2i}^G, \ldots, x_{Di}^G\}$ be the individual i at the current generation G. A mutant vector $V_i^{G+1} = (v_{1i}^{G+1}, v_{2i}^{G+1}, \ldots, v_{Di}^{G+1})$ is generated according to

$$\begin{aligned} V_i^{G+1} = X_{r_1}^G + \mathscr{F} \times \left(X_{r_2}^G - X_{r_3}^G\right), \\ r_1 \ne r_2 \ne r_3 \ne i, \quad i = 1, 2, \ldots, \mathrm{NP}, \end{aligned} \tag{18}$$

Table 5: Hourly heat and power schedule obtained from CHPDED.

H	P_1^{TU}	P_2^{TU}	P_3^{TU}	P_4^{TU}	P_5^{TU}	P_6^{TU}	P_7^{TU}	P_8^{TU}	P_1^{CHP}	P_2^{CHP}	Loss	H_1^{CHP}	H_2^{CHP}	H_1^{H}
1	150.0000	135.0000	74.5372	72.0784	124.5129	124.4302	20.0000	10.0000	236.8041	110.1974	21.5630	57.3450	135.5994	197.0556
2	150.0000	135.0000	98.1135	122.0784	122.2113	101.6179	48.2025	10.0000	236.8011	110.1974	24.2248	57.3614	135.5994	207.0392
3	150.0000	135.0000	178.1135	172.0784	120.7640	98.7468	78.2025	10.0000	235.3275	110.1974	30.4319	65.6496	135.5994	208.7509
4	150.0000	135.0000	188.0106	218.5077	160.0000	126.3142	80.0000	40.0000	235.2182	110.1974	37.2496	66.2643	135.5994	218.1363
5	150.0000	135.0000	268.0106	244.7145	128.0292	129.9179	80.0000	42.2707	233.2313	110.1974	41.3736	77.4390	135.5994	226.9616
6	150.0000	135.0000	334.4706	294.7145	160.0000	130.0000	80.0000	48.0931	235.6609	110.1974	50.1383	63.7746	135.5994	250.6260
7	150.0000	199.1593	340.0000	300.0000	160.0000	130.0000	80.0000	49.7990	238.0991	110.1974	55.2549	50.0614	135.5994	264.3392
8	189.7336	229.5497	340.0000	300.0000	160.0000	130.0000	80.0000	55.0000	242.2569	110.1974	60.7377	26.6766	135.5994	292.7240
9	265.3596	309.5497	340.0000	300.0000	160.0000	130.0000	80.0000	55.0000	247.0000	110.1974	73.1068	0.0	135.5994	324.4006
10	303.6024	378.5162	340.0000	300.0000	160.0000	130.0000	80.0000	55.0000	246.9410	110.1974	82.2580	0.3317	135.5994	324.0689
11	368.8317	405.6648	340.0000	300.0000	160.0000	130.0000	80.0000	55.0000	247.0000	110.1974	90.6945	0.0	135.5994	334.4006
12	367.7179	455.4472	340.0000	300.0000	160.0000	130.0000	80.0000	55.0000	247.0000	110.1974	95.3624	0.0	135.5994	344.4006
13	352.0071	385.0034	340.0000	300.0000	160.0000	130.0000	80.0000	55.0000	247.0000	110.1974	87.2079	0.0	135.5994	334.4006
14	272.0071	305.0034	340.0000	300.0000	160.0000	130.0000	80.0000	55.0000	244.9090	110.1974	73.1169	11.7604	135.5994	312.6402
15	193.6233	225.0034	340.0000	300.0000	160.0000	130.0000	80.0000	55.0000	242.9121	110.1974	60.7362	22.9917	135.5994	291.4089
16	150.0000	145.0034	296.8330	250.8703	160.0000	129.9573	80.0000	43.4626	233.2660	110.1974	45.5900	77.2439	135.5994	237.1567
17	150.0000	135.0000	260.0109	250.0000	160.0000	100.0000	80.0000	40.9143	235.3888	110.1974	41.5121	65.3046	135.5994	219.0959
18	150.0000	151.0646	319.4485	300.0000	160.0000	130.0000	80.0000	40.0577	237.4722	110.1974	50.2419	53.5869	135.5994	245.8137
19	229.4141	231.0646	313.3779	300.0000	160.0000	130.0000	80.0000	46.0360	237.0065	110.1974	61.0988	56.2062	135.5994	253.1943
20	309.4141	311.0646	340.0000	300.0000	160.0000	130.0000	80.0000	55.0000	247.0000	116.9757	77.4552	0.0	90.7694	359.2306
21	272.4577	300.8037	340.0000	300.0000	160.0000	130.0000	80.0000	55.0000	247.0000	111.8344	73.0959	0.0	124.7723	320.2277
22	192.4577	220.8037	260.6669	250.0000	160.0000	124.1397	80.0000	45.9763	234.6724	110.1974	50.9154	69.3338	135.5994	230.0668
23	150.0000	140.8037	180.6669	200.0000	127.6584	130.0000	50.0000	40.0000	236.4213	110.1974	33.7482	59.4980	135.5994	204.9026
24	150.0000	135.0000	100.6669	177.0362	123.2649	128.6636	42.3316	10.0000	234.6572	109.5624	27.1834	69.4196	135.0513	195.5291

Cost ($) = 2.5257×10^6. Emission (lb) = 2.8287×10^5. Total loss (MW) = 1.3443×10^3.

Table 6: Hourly heat and power schedule obtained from CHPDEED ($w = 0.5$).

t	P_1^{TU}	P_2^{TU}	P_3^{TU}	P_4^{TU}	P_5^{TU}	P_6^{TU}	P_7^{TU}	P_8^{TU}	P_1^{CHP}	P_2^{CHP}	Loss	H_1^{CHP}	H_2^{CHP}	H_1^{H}
1	150.0000	135.0000	77.5875	65.0188	122.5177	129.0996	20.0000	10.0000	238.1722	110.1974	21.5935	49.6499	135.5994	204.7506
2	150.0000	135.0000	73.0000	115.0188	123.4971	126.6027	50.0000	13.3209	237.5744	110.1974	24.2115	53.0122	135.5994	211.3884
3	150.0000	135.0000	135.6390	143.2389	123.5028	130.0000	80.0000	43.3209	237.2689	110.1974	30.1680	54.7308	135.5994	219.6698
4	150.0000	135.0000	197.2495	193.2389	160.0000	130.0000	80.0000	46.3828	241.1942	110.1974	37.2630	32.6533	135.5994	251.7473
5	150.0000	135.0000	227.7945	243.2389	160.0000	130.0000	80.0000	46.9362	238.0276	110.1974	41.1946	50.4634	135.5994	253.9371
6	150.0000	148.0006	307.4622	293.2389	160.0000	130.0000	80.0000	55.0000	244.2131	110.1974	50.1122	15.6745	135.5994	298.7261
7	153.7715	216.0682	309.3974	300.0000	160.0000	130.0000	80.0000	55.0000	242.8740	110.1974	55.3090	23.2061	135.5994	291.1945
8	204.6091	224.9723	327.2185	300.0000	160.0000	130.0000	80.0000	55.0000	244.8130	110.1974	60.8102	12.3003	135.5994	307.1003
9	269.9376	304.9723	340.0000	300.0000	160.0000	130.0000	80.0000	55.0000	247.0000	110.1974	73.1072	0.0	135.5994	324.4006
10	302.8816	379.1708	340.0000	300.0000	160.0000	130.0000	80.0000	55.0000	247.0000	110.2066	82.2590	0.0	135.5384	324.4616
11	374.8455	398.1777	340.0000	300.0000	160.0000	130.0000	80.0000	55.0000	247.0000	111.6628	90.6861	0.0	125.9076	344.0924
12	396.3649	416.9874	340.0000	300.0000	160.0000	130.0000	80.0000	55.0000	247.0000	119.8750	95.2273	0.0	71.5941	408.4059
13	353.1036	382.7187	340.0000	300.0000	160.0000	130.0000	80.0000	55.0000	247.0000	111.3732	87.1956	0.0	127.8228	342.1772
14	273.1036	302.7187	339.8378	300.0000	160.0000	130.0000	80.0000	55.0000	246.2562	110.1974	73.1138	4.1831	135.5994	320.2175
15	213.0095	222.7187	321.3321	300.0000	160.0000	130.0000	80.0000	55.0000	244.5974	110.1974	60.8552	13.5127	135.5994	300.8879
16	150.0000	142.7187	291.8181	250.0000	160.0000	130.0000	80.0000	46.1485	238.7061	110.1974	45.5889	46.6476	135.5994	267.7530
17	150.0000	135.0000	228.5656	240.9760	160.0000	130.0000	80.0000	45.7659	240.7225	110.1974	41.2275	35.3065	135.5994	249.0941
18	150.0000	207.5152	294.3486	250.0000	160.0000	130.0000	80.0000	55.0000	241.3976	110.1974	50.4588	31.5093	135.5994	267.8913
19	227.0251	235.5649	297.1019	300.0000	160.0000	130.0000	80.0000	55.0000	242.1587	110.1974	61.0481	27.2289	135.5994	282.1716
20	307.0251	315.5649	340.0000	300.0000	160.0000	130.0000	80.0000	55.0000	247.0000	114.8749	77.4649	0.00	104.6636	345.3364
21	270.9950	301.2766	340.0000	300.0000	160.0000	130.0000	80.0000	55.0000	247.0000	112.8155	73.0871	0.00	118.2834	326.7166
22	190.9950	221.2766	260.0000	250.0000	157.3134	126.2505	80.0000	43.7439	239.1773	110.1974	50.9541	43.9973	135.5994	255.4033
23	150.0000	141.2766	180.0000	200.0000	154.2635	126.4607	51.1156	13.7439	238.8386	110.1974	33.8966	45.9019	135.5994	218.4987
24	150.0000	135.0000	100.0000	150.0000	118.3525	129.7054	78.8178	10.0000	235.4040	103.7586	27.0385	65.2191	130.0411	204.7398

Cost ($) = 2.5295×10^6. Emission (lb) = 2.7209×10^5. Total loss (MW) = 1.3439×10^3.

Table 7: Hourly heat and power schedule obtained from CHPPDED.

H	P_1^{TU}	P_2^{TU}	P_3^{TU}	P_4^{TU}	P_5^{TU}	P_6^{TU}	P_7^{TU}	P_8^{TU}	P_1^{CHP}	P_2^{CHP}	Loss	H_1^{CHP}	H_2^{CHP}	H_1^H
1	150.0000	135.0000	73.0000	60.0000	84.3406	63.6438	64.0384	55	247	125.8	21.8228	0.0	31.4722	358.5278
2	150.0000	135.0000	75.2831	75.5559	107.4058	83.4606	80.0000	55	247	125.8	24.5054	0.0	32.4074	367.5926
3	150.0000	146.7217	108.1787	108.2058	154.2362	113.4606	80.0000	55	247	125.8	30.6030	0.0	18.2661	391.7339
4	187.3290	187.7229	135.7677	135.7127	160.0000	130.0000	80.0000	55	247	125.8	38.3323	0.0	32.4074	387.5926
5	209.9448	210.5929	152.0706	152.2866	160.0000	130.0000	80.0000	55	247	125.8	42.6949	0.0	32.4074	407.5926
6	252.6588	252.9491	188.3610	188.4287	160.0000	130.0000	80.0000	55	247	125.8	52.1977	0.0	25.5244	424.4756
7	272.2261	272.7171	208.2382	208.3486	160.0000	130.0000	80.0000	55	247	125.8	57.3300	0.0	26.7637	423.2363
8	290.5854	291.0583	229.5277	229.7367	160.0000	130.0000	80.0000	55	247	125.8	62.7082	0.0	32.4074	422.5926
9	323.8400	324.1415	276.1324	276.3023	160.0000	130.0000	80.0000	55	247	125.8	74.2162	0.0	25.5487	434.4513
10	346.7105	346.8973	313.1106	300.0000	160.0000	130.0000	80.0000	55	247	125.8	82.5184	0.0	32.4074	427.5926
11	379.2210	379.5185	340.0000	300.0000	160.0000	130.0000	80.0000	55	247	125.8	90.5395	0.0	29.4012	440.5988
12	403.5504	403.8291	340.0000	300.0000	160.0000	130.0000	80.0000	55	247	125.8	95.1796	0.0	31.9845	448.0155
13	361.7512	362.0812	337.4700	300.0000	160.0000	130.0000	80.0000	55	247	125.8	87.1023	0.0	32.0189	437.9811
14	323.7805	324.1252	276.7607	275.7492	160.0000	130.0000	80.0000	55	247	125.8	74.2157	0.0	25.5863	434.4137
15	291.7264	292.3796	231.0966	225.7492	160.0000	130.0000	80.0000	55	247	125.8	62.7519	0.0	31.8710	418.1290
16	229.7976	230.1379	167.7688	175.7492	160.0000	130.0000	80.0000	55	247	125.8	47.2535	0.0	31.3306	418.6694
17	210.0699	210.4074	152.1822	152.2351	160.0000	130.0000	80.0000	55	247	125.8	42.6946	0.0	32.3578	387.6422
18	252.7542	253.2318	188.2091	188.2081	160.0000	130.0000	80.0000	55	247	125.8	52.2031	0.0	29.7791	405.2209
19	288.2429	288.7410	226.6332	237.2113	160.0000	130.0000	80.0000	55	247	125.8	62.6285	0.0	27.4724	417.5276
20	335.1319	335.4397	294.6392	287.2113	160.0000	130.0000	80.0000	55	247	125.8	78.2222	0.0	31.3390	418.6610
21	332.6192	333.0535	282.3523	252.7233	160.0000	130.0000	80.0000	55	247	125.8	74.5483	0.0	32.3100	412.6900
22	252.6192	253.0535	202.3523	202.7233	149.4115	112.3565	80.0000	55	247	125.8	52.3163	0.0	27.3503	407.6497
23	172.6192	173.0535	122.3523	152.7233	135.8629	102.0552	80.0000	55	247	125.8	34.4664	0.0	25.1547	374.8453
24	150.0000	135.0000	90.3380	102.7233	128.7354	96.7805	80.0000	55	247	125.8	27.3771	0..0	31.5331	368.4669

Cost ($) = 2.6945×10^6. Emission (lb) = 2.4195×10^5. Total loss (MW) = 1.3684×10^3.

with randomly chosen integer indexes $r_1, r_2, r_3 \in \{1, 2, \ldots, \mathrm{NP}\}$. Here $\mathcal{F}$ is the mutation factor.

According to the target vector X_i^G and the mutant vector V_i^{G+1}, a new trial vector (offspring) $U_i^{G+1} = \{u_{1i}^{G+1}, u_{2i}^{G+1}, \ldots, u_{Di}^{G+1}\}$ is created with

$$u_{ji}^{G+1} = \begin{cases} v_{ji}^{G+1}, & \text{if } \left(\text{rand}\left(j\right) \le \text{CR}\right) \text{ or } j = rnb\left(i\right), \\ x_{ji}^{G}, & \text{otherwise,} \end{cases} \tag{19}$$

where $j = 1, 2, \ldots, D$, $i = 1, 2, \ldots, \mathrm{NP}$ and rand(j) is the jth evaluation of a uniform random number between [0, 1]. CR $\in$ [0, 1] is the crossover constant which has to be determined by the user. $rnb(i)$ is a randomly chosen index from $1, 2, \ldots, D$ which ensures that U_i^{G+1} gets at least one parameter from V_i^{G+1} [32].

The selection process determines which of the vectors will be chosen for the next generation by implementing one-to-one competition between the offsprings and their corresponding parents. If f denotes the function to be minimized, then

$$X_i^{G+1} = \begin{cases} U_i^{G+1} & \text{if } f\left(U_i^{G+1}\right) \le f\left(X_i^G\right), \\ X_i^G & \text{otherwise,} \end{cases} \tag{20}$$

where $i = 1, 2, \ldots, \mathrm{NP}$. The value of f of each trial vector U_i^{G+1} is compared with that of its parent target vector X_i^G. The above iteration process of reproduction and selection will continue until a user-specified stopping criteria is met.

In this paper, we define the evaluation function for evaluating the fitness of each individual in the population in DE algorithm as follows:

$$\begin{aligned} f = F &+ \lambda_1 \sum_{t=1}^{N} \left(\sum_{i=1}^{N_p} P_{i,t}^{\mathrm{TU}} + \sum_{j=1}^{N_c} P_{j,t}^{\mathrm{CHP}} - \left(P_{D,t} + \mathrm{Loss}_t\right) \right)^2 \\ &+ \lambda_2 \sum_{t=1}^{N} \left(\sum_{j=1}^{N_c} H_{j,t}^{\mathrm{CHP}} + \sum_{k=1}^{N_h} H_{k,t}^{H} - H_{D,t} \right)^2, \end{aligned} \tag{21}$$

where λ_1 and λ_2 are penalty values. Then the objective is to find $f_{\min}$, the minimum evaluation value of all the individuals in all iterations. The penalty term reflects the violation of the equality constraints. Once the minimum of f is reached, the equality constraints are satisfied.

4. Sequential Quadratic Programming Method

SQP method can be considered as one of the best nonlinear programming methods for constrained optimization problems [38]. It outperforms every other nonlinear programming method in terms of efficiency, accuracy, and percentage of successful solutions over a large number of test problems. The method closely resembles Newton's method for

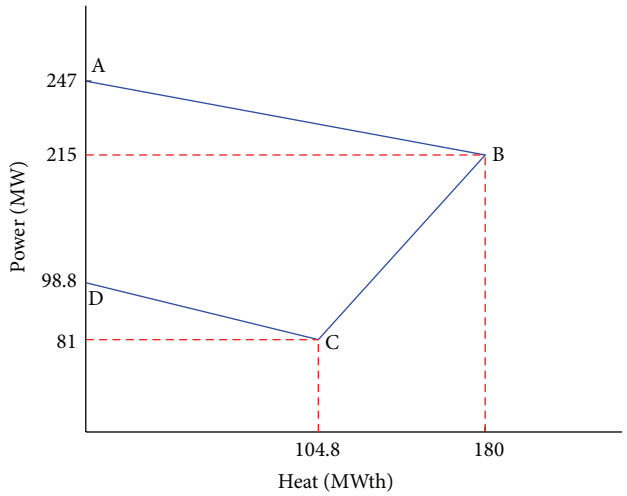

Figure 1: Heat-power feasible operating region for CHP unit 1.

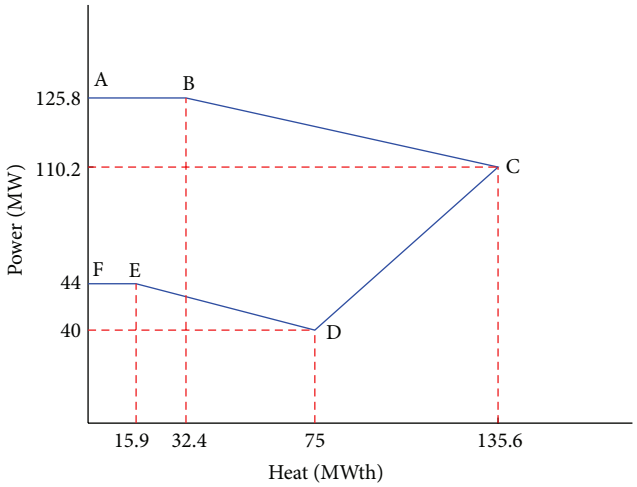

Figure 2: Heat-power feasible operating region for CHP unit 2.

constrained optimization, just as is done for unconstrained optimization. At each iteration, an approximation is made of the Hessian of the Lagrangian function using Broyden-Fletcher-Goldfarb-Shanno (BFGS) quasi-Newton updating method. The result of the approximation is then used to generate a quadratic programming (QP) subproblem whose solution is used to form a search direction for a line search procedure. Since the objective function of the CHPDEED problem is non-convex and non-smooth, SQP ensures a local minimum for an initial solution. In this paper, DE is used as a global search and finally the best solution obtained from DE is given as initial condition for SQP method as a local search to fine-tune the solution. SQP simulations can be computed by the `fmincon` code of the MATLAB Optimization Toolbox.

5. Simulation Results

In this section we present two examples. The first example shows the efficiency of the proposed DE-SQP method for the DED problem. In the second example, the hybrid DE-SQP method is applied to the CHPDEED problem. In DE-SQP method, the control parameters are chosen as NP = 80, $\mathcal{F}$ = 0.423 and CR = 0.885. The maximum number of iterations are selected as 20, 000. The results represent the average of 30 runs of the proposed method. All computations are carried out by MATLAB program.

Example 1. This example consists of ten conventional thermal units to investigate the effectiveness of the proposed DE-SQP technique in solving the DED problem with valve point effects and transmission line losses. The technical data of the units as well as the demand for the 10-unit system are taken from [24]. The best solution of the DED problem is given in Table 1. Comparison between our proposed method (DE-SQP) and other methods is given in Table 2. It is observed that the proposed method reduces the total generation cost better than the other methods reported in the literature.

Example 2. This example is 11-unit system (eight conventional thermal units, two CHP units, and one heat-only unit) for solving the CHPDED, CHPDEED, and CHPPDED problems using DE-SQP method. We shall solve the CHPDEED problem when $w = 0.5$, in addition to the CHPDED and CHPPDED problems which correspond to $w = 1$ and $w = 0$, respectively. The technical data of conventional thermal units, the matrix B, and the demand are taken from the 10-unit system presented in [24]. The 5th and 8th conventional units in [24] were replaced by two CHP units. The technical data of the two CHP units and the heat-only unit are taken from [17] and are given in Table 3. The heat demand for 24 hours is given in Table 4. The feasible operating regions of the two CHP units are given in Figures 1 and 2 (see [4, 14]).

The best solutions of the CHPDED, CHPDEED, and CHPPDED problems for DE-SQP algorithm are given in Tables 5, 6, and 7, respectively. The best cost, the amount of emission, and the transmission line losses are also given in Tables 5–7. It is seen that the cost is 2.5257×10^6 \$ under CHPDED, but it increases to 2.6945×10^6 \$ under CHPPDED. The emission obtained from CHPDED is 2.8287×10^5 lb, but it decreases to 2.4195×10^5 lb under CHPPDED. Under the CHPDEED problem, the cost is 2.5295×10^6 \$ which is more than 2.5257×10^6 \$ and less than 2.6945×10^6 \$. Moreover, the emission is 2.7209×10^5 lb which is less than 2.8287×10^5 lb and more than 2.4195×10^5 lb.

6. Conclusion

This paper presents a hybrid method combining differential evolution (DE) and sequential quadratic programming (SQP) for solving dynamic dispatch (CHPDED, CHPDEED, and CHPPDED) problems with valve-point effects including generator ramp rate limits. In this paper, DE is first applied to find the best solution. This best solution is given to SQP as an initial condition that fine tunes the optimal solution at the final. The feasibility and efficiency of the DE-SQP were illustrated by conducting case studies with system consisting of eight conventional thermal units, two CHP units, and one heat-only unit.

Conflict of Interests

The authors declare that there is no conflict of interests regarding the publication of this paper.

Acknowledgment

This work was funded by the Deanship of Scientific Research (DSR), King Abdulaziz University, Jeddah, under Grant no. (130-107-D1434). The authors, therefore, acknowledge with thanks DSR technical and financial support.

References

[1] A. Vasebi, M. Fesanghary, and S. M. T. Bathaee, "Combined heat and power economic dispatch by harmony search algorithm," *International Journal of Electrical Power and Energy Systems*, vol. 29, no. 10, pp. 713–719, 2007.

[2] M. Behnam, M. Mohammad, and R. Abbas, "Combined heat and power economic dispatch problem solution using particle swarm optimization with time varying acceleration coefficients," *Electric Power Systems Research*, vol. 95, pp. 9–18, 2013.

[3] P. Subbaraj, R. Rengaraj, and S. Salivahanan, "Enhancement of combined heat and power economic dispatch using self adaptive real-coded genetic algorithm," *Applied Energy*, vol. 86, no. 6, pp. 915–921, 2009.

[4] T. Guo, M. I. Henwood, and M. van Ooijen, "An algorithm for combined heat and power economic dispatch," *IEEE Transactions on Power Systems*, vol. 11, no. 4, pp. 1778–1784, 1996.

[5] A. Sashirekha, J. Pasupuleti, N. H. Moin, and C. S. Tan, "Combined heat and power (CHP) economic dispatch solved using Lagrangian relaxation with surrogate subgradient multiplier updates," *Electrical Power and Energy Systems*, vol. 44, pp. 421–430, 2013.

[6] A. M. Jubril, A. O. Adediji, and O. A. Olaniyan, "Solving the combined heat and power dispatch problem: a semidefinite programming approach," *Electric Power Components and Systems*, vol. 40, pp. 1362–1376, 2012.

[7] V. N. Dieu and W. Ongsakul, "Augmented lagrangehopfield network for economic load dispatch with combined heat and power," *Electric Power Components and Systems*, vol. 37, no. 12, pp. 1289–1304, 2009.

[8] E. Khorram and M. Jaberipour, "Harmony search algorithm for solving combined heat and power economic dispatch problems," *Energy Conversion and Management*, vol. 52, no. 2, pp. 1550–1554, 2011.

[9] C. Su and C. Chiang, "An incorporated algorithm for combined heat and power economic dispatch," *Electric Power Systems Research*, vol. 69, no. 2-3, pp. 187–195, 2004.

[10] Y. H. Song, C. S. Chou, and T. J. Stonham, "Combined heat and power economic dispatch by improved ant colony search algorithm," *Electric Power Systems Research*, vol. 52, no. 2, pp. 115–121, 1999.

[11] S. S. Sadat Hosseini, A. Jafarnejad, A. H. Behrooz, and A. H. Gandomi, "Combined heat and power economic dispatch by mesh adaptive direct search algorithm," *Expert Systems with Applications*, vol. 38, no. 6, pp. 6556–6564, 2011.

[12] V. Ramesh, T. Jayabarathi, N. Shrivastava, and A. Baska, "A novel selective particle swarm optimization approach for combined heat and power economic dispatch," *Electric Power Components and Systems*, vol. 37, no. 11, pp. 1231–1240, 2009.

[13] M. Basu, "Artificial immune system for combined heat and power economic dispatch," *Electrical Power and Energy Systems*, vol. 43, pp. 1–5, 2012.

[14] M. Basu, "Bee colony optimization for combined heat and power economic dispatch," *Expert Systems with Applications*, vol. 38, no. 11, pp. 13527–13531, 2011.

[15] M. Basu, "Combined heat and power economic dispatch by using differential evolution," *Electric Power Components and Systems*, vol. 38, no. 8, pp. 996–1004, 2010.

[16] K. P. Wong and C. Algie, "Evolutionary programming approach for combined heat and power dispatch," *Electric Power Systems Research*, vol. 61, no. 3, pp. 227–232, 2002.

[17] N. Taher, A. A. Rasoul, R. Alireza, and A. Babak, "A new multi-objective reserve constrained combined heat and power dynamic economic emission dispatch," *Energy*, vol. 42, pp. 530–545, 2012.

[18] X. Xia and A. M. Elaiw, "Optimal dynamic economic dispatch of generation: a review," *Electric Power Systems Research*, vol. 80, no. 8, pp. 975–986, 2010.

[19] A. M. Elaiw, X. Xia, and A. M. Shehata, "Application of model predictive control to optimal dynamic dispatch of generation with emission limitations," *Electric Power Systems Research*, vol. 84, no. 1, pp. 31–44, 2012.

[20] G. P. Granelli, M. Montagna, G. L. Pasini, and P. Marannino, "Emission constrained dynamic dispatch," *Electric Power Systems Research*, vol. 24, no. 1, pp. 55–64, 1992.

[21] Y. H. Song and I. Yu, "Dynamic load dispatch with voltage security and environmental constraints," *Electric Power Systems Research*, vol. 43, no. 1, pp. 53–60, 1997.

[22] M. A. Abido, "Environmental/economic power dispatch using multiobjective evolutionary algorithms," *IEEE Transactions on Power Systems*, vol. 18, no. 4, pp. 1529–1537, 2003.

[23] M. Basu, "Dynamic economic emission dispatch using evolutionary programming and fuzzy satisfied method," *International Journal of Emerging Electric Power Systems*, vol. 8, pp. 1–15, 2007.

[24] M. Basu, "Dynamic economic emission dispatch using nondominated sorting genetic algorithm-II," *International Journal of Electrical Power and Energy Systems*, vol. 30, no. 2, pp. 140–149, 2008.

[25] C. X. Guo, J. P. Zhan, and Q. H. Wu, "Dynamic economic emission dispatch based on group search optimizer with multiple producers," *Electric Power Systems Research*, vol. 86, pp. 8–16, 2012.

[26] A. M. Elaiw, X. Xia, and A. M. Shehata, "Hybrid DE-SQP and hybrid PSO-SQP methods for solving dynamic economic emission dispatch problem with valve-point effects," *Electric Power Systems Research*, vol. 84, pp. 192–200, 2013.

[27] A. M. Elaiw, X. Xia, and A. M. Shehata, "Minimization of fuel costs and gaseous emissions of electric power generation by model predictive control," *Mathematical Problems in Engineering*, vol. 2013, Article ID 906958, 15 pages, 2013.

[28] J. S. Alsumait, M. Qasem, J. K. Sykulski, and A. K. Al-Othman, "An improved Pattern Search based algorithm to solve the Dynamic Economic Dispatch problem with valve-point effect," *Energy Conversion and Management*, vol. 51, no. 10, pp. 2062–2067, 2010.

[29] M. Basu, "Particle swarm optimization based goal-attainment method for dynamic economic emission dispatch," *Electric Power Components and Systems*, vol. 34, no. 9, pp. 1015–1025, 2006.

[30] P. Nicole, T. Anshul, T. Shashikala, and P. Manjaree, "An improved bacterial foraging algorithm for combined static/dynamic environmental economic dispatch," *Applied Soft Computing*, vol. 12, pp. 3500–3513, 2012.

[31] G. S. Piperagkas, A. G. Anastasiadis, and N. D. Hatziargyriou, "Stochastic PSO-based heat and power dispatch under environmental constraints incorporating CHP and wind power units," *Electric Power Systems Research*, vol. 81, no. 1, pp. 209–218, 2011.

[32] R. Storn and K. Price, "Differential Evolution—a simple and efficient adaptive scheme for global optimization over continuous spaces," *Journal of Global Optimization*, vol. 11, no. 4, pp. 341–359, 1997.

[33] A. M. Elaiw, X. Xia, and A. M. Shehata, "Hybrid DE-SQP method for solving combined heat and power dynamic economic dispatch problem," *Mathematical Problems in Engineering*, vol. 2013, Article ID 982305, 7 pages, 2013.

[34] M. Basu, "Artificial immune system for dynamic economic dispatch," *International Journal of Electrical Power and Energy Systems*, vol. 33, no. 1, pp. 131–136, 2011.

[35] X. Xia, J. Zhang, and A. Elaiw, "An application of model predictive control to the dynamic economic dispatch of power generation," *Control Engineering Practice*, vol. 19, no. 6, pp. 638–648, 2011.

[36] C. K. Panigrahi, P. K. Chattopadhyay, R. N. Chakrabarti, and M. Basu, "Simulated annealing technique for dynamic economic dispatch," *Electric Power Components and Systems*, vol. 34, no. 5, pp. 577–586, 2006.

[37] P. Attaviriyanupap, H. Kita, E. Tanaka, and J. Hasegawa, "A hybrid EP and SQP for dynamic economic dispatch with nonsmooth fuel cost function," *IEEE Transactions on Power Systems*, vol. 17, no. 2, pp. 411–416, 2002.

[38] P. T. Boggs and J. W. Tolle, "Sequential quadratic programming," *Acta Numerica*, vol. 3, no. 4, pp. 1–52, 1995.

Hindawi Publishing Corporation
Abstract and Applied Analysis
Volume 2013, Article ID 513871, 8 pages
http://dx.doi.org/10.1155/2013/513871

Research Article

Criterion for Unbounded Synchronous Region in Complex Networks

Jin Zhou

School of Mathematics and Statistics, State Key Lab of Software Engineering, Wuhan University, Wuhan 430072, China

Correspondence should be addressed to Jin Zhou; jzhou@whu.edu.cn

Received 20 August 2013; Accepted 18 September 2013

Academic Editor: Jinde Cao

Synchronization of complex networks has been extensively studied in many fields, where intensive efforts have been devoted to the understanding of its mechanisms. As for discriminating network synchronizability by Master Stability Function method, a dilemma usually encountered is that we have no prior knowledge of the network type that the synchronous region belongs to. In this paper, we investigate a sufficient condition for a general complex dynamical network in the absence of control. A main result is that, when the coupling strength is sufficiently strong, the dynamical network achieves synchronization provided that the symmetric part of the inner-coupling matrix is positive definite. According to our results, synchronous region of the network with positive definite inner-coupling matrix belongs to the unbounded one, and then the eigenvalue of the outer-coupling matrix nearest 0 can be used for judging synchronizability. Even though we cannot gain the necessary and sufficient conditions for synchronizing a network so far, our results constitute a first step toward a better understanding of network synchronization.

1. Introduction

Complex dynamical networks have received increasing attention from different fields in the past two decades. So far, the dynamics of complex networks has been extensively investigated, in which synchronization is a typical topic which has attracted lots of concern [1–17].

As an interesting phenomenon that enables coherent behavior in networks as a result of coupling, synchronization and the discussion upon its sufficient or necessary condition are fundamental and valuable. Pecora and his colleagues used the so-called Master Stability Function (MSF) approach to determine the synchronous region in coupled systems [18, 19], in which the negativeness of Lyapunov Exponent for master stability equation ensures synchronization. Combining MSF approach with Gershörin disk theory, Chen et al. imposed constraints on the coupling strengths to guarantee stability of the synchronous states in coupled dynamical network [20]. These methods, however, obtain just necessary conditions for synchronization due to the fact that Lyapunov Exponent is employed to judge the stability of system.

Zhou et al. and Li and Chen investigated synchronization in general dynamical networks by integrating network models and an adaptive technique and proved that strong enough couplings will synchronize an array of identical cells [11, 12]. To overcome the difficulties caused by too many controllers in large scale complex networks, pinning mechanism is further applied to analyze network synchronization criteria in the works by Zhou et al. and Chen et al. [13, 14]. Research studies on network synchronization mentioned above focused on sufficient conditions, but all of them are gained by introducing controllers.

For general complex dynamical networks in the absence of control, we investigate their sufficient conditions for achieving network synchronization in the current work. Using Lyapunov direct method [21, 22] and matrix theory [23–27], a criterion for synchronization in generally coupled identical systems is proposed. We conclude that network synchronization will be reached when the coupling strength is larger than a threshold, given that the symmetric part of the inner-coupling matrix is positive definite. It is analytically derived in our paper that a network belongs to *Type I* with respect to synchronized region [28], provided with a positive definite inner-coupling matrix.

For discriminating network synchronizability, it is well known that a dilemma is usually encountered in the process

of applying MSF method. That is, we have no prior knowledge of the network type that the synchronous region belongs to. Stemmed from our results, the eigenvalue of the outer-coupling matrix nearest 0 can be used for judging synchronizability of a dynamical network with positive definite inner-coupling matrix. Even though we cannot gain the necessary and sufficient conditions for synchronizing a network so far, our results constitute a first step toward a better understanding of network synchronization.

The rest of the paper is organized as follows. In Section 2, a general complex dynamical network model and some mathematical preliminaries are introduced. A sufficient condition for achieving synchronization in the network and detailed discussion are presented in Section 3. Section 4 gives some numerical simulations to show the effectiveness of the proposed synchronization criterion and further illustrates the relationship between synchronous region and our main results. Conclusions are finally drawn in Section 5.

2. Preliminaries

To begin with, we introduce a complex network model describing the dynamical evolution of node states, which is formulated as

$$\dot{\mathbf{x}}_i(t) = \mathbf{f}\left(\mathbf{x}_i(t)\right) + c\sum_{j\in\mathcal{N}_i} a_{ij}\,\mathbf{H}\mathbf{x}_j(t), \tag{1}$$

where $1 \le i \le N$, $\mathcal{N}_i$ represents the neighborhood of the ith node, the state vector of the ith node $\mathbf{x}_i(t) = (x_{i1}(t), x_{i2}(t), \ldots, x_{in}(t))^\top \in \mathbb{R}^n$ is a continuous function, $\mathbf{f}: \mathbb{R}^n \to \mathbb{R}^n$ is a smooth nonlinear vector function, individual node dynamics is $\dot{\mathbf{x}}(t) = \mathbf{f}(\mathbf{x}(t))$, and $\mathbf{H} \in \mathbb{R}^{n\times n}$ is the inner-coupling matrix. The outer-coupling weight configuration matrix $\mathbf{A} = (a_{ij}) \in \mathbb{R}^{N\times N}$ ($a_{ij} \in \{0, 1\}$, $j \ne i$) is symmetric and diffusive satisfying $\sum_{j=1}^{N} a_{ij} = 0$. If there is a link between node i and node j ($j \ne i$), then $a_{ij} = a_{ji} = 1$; otherwise, $a_{ij} = a_{ji} = 0$. In addition, $a_{ii} = -\sum_{j=1, j\ne i} a_{ij}$. It is clear that $0 = \lambda_1 > \lambda_2 \ge \lambda_3 \ge \cdots \ge \lambda_N$ due to the diffusion, with λ_i ($1 \le i \le N$) being the eigenvalues of $\mathbf{A}$.

Definition 1. Let $\mathbf{X}(\mathbf{X}_0; t) = (\mathbf{x}_1^\top(\mathbf{X}_0; t), \mathbf{x}_2^\top(\mathbf{X}_0; t), \ldots, \mathbf{x}_N^\top(\mathbf{X}_0; t))^\top$ be a solution of the complex dynamical network (1) with initial state $\mathbf{X}_0 = (\mathbf{x}_1^\top(t_0), \mathbf{x}_2^\top(t_0), \ldots, \mathbf{x}_N^\top(t_0))^\top$. Assume that $\mathbf{f}: \Omega \to \mathbf{R}^n$ is continuously differentiable, where $\Omega \subseteq \mathbf{R}^n$. If there is a nonempty subset $E \subseteq \Omega$, with $\mathbf{x}_i(t_0) \in E$ ($1 \le i \le N$), such that $\mathbf{x}_i(\mathbf{X}_0; t) \in \Omega$ for all $t \ge t_0$, $1 \le i \le N$ and that

$$\lim_{t\to\infty} \left\|\mathbf{x}_i(\mathbf{X}_0; t) - \mathbf{x}_j(\mathbf{X}_0; t)\right\| = 0 \quad (1 \le i, j \le N), \tag{2}$$

where $\|\cdot\|$ denotes any norm of a vector or a matrix, then the complex dynamical network (1) is said to achieve *synchronization*.

To develop the main results, a useful hypothesis on the inner-coupling matrix $\mathbf{H}$ is introduced.

Assumption 2. Suppose that $\mu_i > 0$ ($1 \le i \le n$), with $\mu_1, \mu_2, \ldots, \mu_n$ being eigenvalues of the symmetric part of the inner-coupling matrix $\mathbf{H}^s \triangleq (\mathbf{H} + \mathbf{H}^\top)/2$.

It suggests that $\mathbf{H}^s$ should be a positive definite matrix. This is common for the inner-coupling matrix $\mathbf{H}$ to satisfy $\mu_i > 0$ ($1 \le i \le n$); for instance, the symmetric part $\mathbf{H}^s$ is strictly diagonally dominant.

Since $\mathbf{A}$ and $\mathbf{H}^s$ are symmetric, there exist orthogonal matrices $\mathbf{P} \in \mathbb{R}^{N\times N}$ and $\mathbf{Q} \in \mathbb{R}^{n\times n}$, such that

$$\begin{aligned}\mathbf{P}^{-1}\mathbf{A}\mathbf{P} &= \operatorname{diag}\{\lambda_1, \lambda_2, \ldots, \lambda_N\} \triangleq \Lambda,\\ \mathbf{Q}^{-1}\mathbf{H}^s\mathbf{Q} &= \operatorname{diag}\{\mu_1, \mu_2, \ldots, \mu_n\} \triangleq \overline{\Lambda},\end{aligned} \tag{3}$$

where $\lambda_1, \lambda_2, \ldots, \lambda_N$ are real numbers and the denotation $\operatorname{diag}\{*, **, \ldots, * * *\}$ represents a diagonal matrix whose elements are $*, **, \ldots, * * *$.

Let $\xi = (\xi_1, \xi_2, \ldots, \xi_N)^\top$ be the left eigenvector of the coupling configuration matrix $\mathbf{A}$ corresponding to the eigenvalue $\lambda_1 = 0$, in which $\sum_{j=1}^{N} \xi_j = 1$. It is obvious that $\xi^\top\mathbf{A} = \mathbf{0}$. Then introducing a weighted mean state of all nodes

$$\overline{\mathbf{x}}(t) = \sum_{j=1}^{N} \xi_j \mathbf{x}_j(t), \tag{4}$$

one has the following Lemma.

Lemma 3. *For any initial state* $\mathbf{X}_0$ *of model* (1)*, network synchronization* $\lim_{t\to\infty}\|\mathbf{x}_i(t) - \mathbf{x}_j(t)\| = 0$ ($1 \le i, j \le N$) *is equivalent to* $\lim_{t\to\infty}\|\mathbf{x}_i(t) - \overline{\mathbf{x}}(t)\| = 0$ ($1 \le i \le N$).

Proof. On one hand, provided with $\lim_{t\to\infty}\|\mathbf{x}_i(t) - \mathbf{x}_j(t)\| = 0$ ($1 \le i, j \le N$), one obtains

$$\begin{aligned}0 \le{}& \left\|\mathbf{x}_i(t) - \overline{\mathbf{x}}(t)\right\|\\ ={}& \left\|\mathbf{x}_i(t) - \sum_{j=1}^{N}\xi_j\mathbf{x}_j(t)\right\|\\ ={}& \left\|\sum_{j=1}^{N}\xi_j\mathbf{x}_i(t) - \sum_{j=1}^{N}\xi_j\mathbf{x}_j(t)\right\|\\ ={}& \left\|\sum_{j=1}^{N}\xi_j\left(\mathbf{x}_i(t) - \mathbf{x}_j(t)\right)\right\|\\ \le{}& \sum_{j=1}^{N}\left|\xi_j\right|\left\|\mathbf{x}_i(t) - \mathbf{x}_j(t)\right\|.\end{aligned} \tag{5}$$

Thus $\lim_{t\to\infty}\|\mathbf{x}_i(t) - \mathbf{x}_j(t)\| = 0$ ($1 \le i, j \le N$) results in $\lim_{t\to\infty}\|\mathbf{x}_i(t) - \overline{\mathbf{x}}(t)\| = 0$ ($1 \le i \le N$).

On the other hand, if $\lim_{t\to\infty}\|\mathbf{x}_i(t) - \overline{\mathbf{x}}(t)\| = 0$ ($1 \le i \le N$), one has $\lim_{t\to\infty}\max_{1\le i\le N}\|\mathbf{x}_i(t) - \overline{\mathbf{x}}(t)\| = 0$ ($1 \le i \le N$). Owing to the fact that

$$\begin{aligned}0 \le{}& \left\|\mathbf{x}_i(t) - \mathbf{x}_j(t)\right\|\\ ={}& \left\|\mathbf{x}_i(t) - \overline{\mathbf{x}}(t) + \overline{\mathbf{x}}(t) - \mathbf{x}_j(t)\right\|\\ \le{}& \left\|\mathbf{x}_i(t) - \overline{\mathbf{x}}(t)\right\| + \left\|\overline{\mathbf{x}}(t) - \mathbf{x}_j(t)\right\|\\ \le{}& 2\max_{1\le i\le N}\left\|\mathbf{x}_i(t) - \overline{\mathbf{x}}(t)\right\|,\end{aligned} \tag{6}$$

one gets $\lim_{t\to\infty}\|\mathbf{x}_i(t) - \mathbf{x}_j(t)\| = 0$ ($1 \le i, j \le N$). □

Remark 4. Lemma 3 has proved that $\lim_{t\to\infty}\|\mathbf{x}_i(t)-\overline{\mathbf{x}}(t)\|=0$ $(1\le i\le N)$ is a sufficient and necessary condition for network synchronization. In other words, the dynamics of all nodes in the complex network (1) would approach $\overline{\mathbf{x}}(t)$ when network synchronization is reached.

Recently, it has been mathematically proved that $\overline{\mathbf{x}}(t)$ is a solution of single node dynamical system in the sense of positive limit set [29]

$$\dot{\mathbf{x}}(t)=\mathbf{f}(\mathbf{x}(t)). \tag{7}$$

Namely, the synchronous state can be an equilibrium point, a periodic orbit, an aperiodic orbit, or even a chaotic orbit in the phase space.

Define the state error vectors as $\widetilde{\mathbf{x}}_i(t)=\mathbf{x}_i(t)-\overline{\mathbf{x}}(t)$ $(1\le i\le N)$ for all nodes in the network.

Then the error system is given by

$$\dot{\widetilde{\mathbf{x}}}_i=\mathbf{f}(\mathbf{x}_i)-\mathbf{f}(\overline{\mathbf{x}})+c\sum_{j=1}^{N}a_{ij}\mathbf{H}\widetilde{\mathbf{x}}_j, \tag{8}$$

according to systems (1) and (4), where $1\le i\le N$.

Denote $\widetilde{\mathbf{X}}=(\widetilde{\mathbf{x}}_1^\top,\widetilde{\mathbf{x}}_2^\top,\ldots,\widetilde{\mathbf{x}}_N^\top)^\top$, $\overline{\mathbf{X}}=(\overline{\mathbf{x}}_1^\top,\overline{\mathbf{x}}_2^\top,\ldots,\overline{\mathbf{x}}_N^\top)^\top$, $\mathbf{F}(\mathbf{X})=(\mathbf{f}(\mathbf{x}_1)^\top,\mathbf{f}(\mathbf{x}_2)^\top,\ldots,\mathbf{f}(\mathbf{x}_N)^\top)^\top$, and $\mathbf{F}(\overline{\mathbf{X}})=(\mathbf{f}(\overline{\mathbf{x}})^\top,\mathbf{f}(\overline{\mathbf{x}})^\top,\ldots,\mathbf{f}(\overline{\mathbf{x}})^\top)^\top$. Then one has

$$\dot{\widetilde{\mathbf{X}}}=\mathbf{F}(\mathbf{X})-\mathbf{F}\left(\overline{\mathbf{X}}\right)+c(\mathbf{A}\otimes\mathbf{H})\widetilde{\mathbf{X}}, \tag{9}$$

where $\otimes$ represents the direct product of matrices.

3. Main Results

In this section, a sufficient condition for reaching synchronization in a general complex dynamical network (1) is presented based on Lyapunov direct method and some related matrix theory. Further discussion of the synchronization criterion in detail is also included.

Linearizing the state equation (1) at trajectory $\overline{\mathbf{x}}(t)$, one obtains the variational equation as follows:

$$\dot{\widetilde{\mathbf{X}}}=\left(\mathbf{I}_N\otimes\mathbf{Df}(\overline{\mathbf{x}})+c\mathbf{A}\otimes\mathbf{H}\right)\widetilde{\mathbf{X}}, \tag{10}$$

where $\mathbf{Df}(\overline{\mathbf{x}})$ is the Jacobian matrix of $\mathbf{f}(\overline{\mathbf{x}})$ evaluated at trajectory $\overline{\mathbf{x}}(t)$. Letting $\eta=(\mathbf{P}\otimes\mathbf{I}_n)^{-1}\widetilde{\mathbf{X}}$, one has

$$\begin{aligned}\dot{\eta}&=(\mathbf{P}\otimes\mathbf{I}_n)^{-1}\left(\mathbf{I}_N\otimes\mathbf{DF}(\overline{\mathbf{x}})+c\mathbf{A}\otimes\mathbf{H}\right)(\mathbf{P}\otimes\mathbf{I}_n)\eta\\&=\left(\mathbf{I}_N\otimes\mathbf{DF}(\overline{\mathbf{x}})+c\left(\mathbf{P}^{-1}\mathbf{AP}\right)\otimes\mathbf{H}\right)\eta\\&=\left(\mathbf{I}_N\otimes\mathbf{DF}(\overline{\mathbf{x}})+c\Lambda\otimes\mathbf{H}\right)\eta.\end{aligned} \tag{11}$$

Denote η as the form $\eta=(\eta_1^\top,\eta_2^\top,\ldots,\eta_N^\top)^\top$, where $\eta_i=(\eta_{i1},\eta_{i2},\ldots,\eta_{in})^\top\in\mathbb{R}^n$. Equation (11) can be rewritten as follows:

$$\dot{\eta}_i=\left(\mathbf{DF}(\overline{\mathbf{x}})+c\lambda_i\mathbf{H}\right)\eta_i, \tag{12}$$

where $1\le i\le N$.

For $\lambda_1=0$ $(i=1)$, one gets the variational equation for the synchronization manifold. Thus one has succeeded in separating $i=1$ from the transverse directions $i=2,3,\ldots,N$. All the $i=2,3,\ldots,N$ correspond to the transverse eigenvectors. Therefore, the synchronous solution of dynamical network (1) is asymptotically stable if the following system is stable:

$$\dot{\eta}_i=\left(\mathbf{DF}(\overline{\mathbf{x}})+c\lambda_i\mathbf{H}\right)\eta_i, \tag{13}$$

where $2\le i\le N$.

To deduce the sufficient condition for stability of system (13), the following assumption is one of the basic prerequisites.

Assumption 5. Suppose that there exists a positive constant $\mathscr{L}>0$ satisfying $\|\mathbf{Df}(\cdot)\|\le\mathscr{L}$.

This hypothesis is achievable for a large class of systems depicted by $\dot{\mathbf{x}}(t)=\mathbf{f}(\mathbf{x}(t))$, including linear systems, piecewise linear systems, and numerous chaotic systems (e.g., Chua's circuit [30], Lorenz family [31–33], etc.).

Theorem 6. *Suppose that Assumptions 2 and 5 hold. The synchronous solution of network* (1) *is asymptotically stable provided that c is larger than* c_0, *where* $c_0=-\mathscr{L}/\lambda_2\min_{1\le k\le n}\{\mu_k\}$.

Proof. According to Lemma 3 and the previous discussion, asymptotical stability of synchronous solution $\overline{\mathbf{X}}$ of network model (1) can be analyzed by investigating the stability of system (13). Consider a positive semidefinite function as

$$V=\sum_{i=2}^{N}\frac{1}{2}\eta_i^\top\eta_i \tag{14}$$

and regard V as a Lyapunov candidate. Then the derivation of V along the trajectories of (13) is

$$\begin{aligned}\dot{V}&=\sum_{i=2}^{N}\frac{1}{2}\left(\dot{\eta}_i^\top\eta_i+\eta_i^\top\dot{\eta}_i\right)\\&=\sum_{i=2}^{N}\eta_i^\top\dot{\eta}_i\\&=\sum_{i=2}^{N}\eta_i^\top\left(\mathbf{DF}(\overline{\mathbf{x}})+c\lambda_i\mathbf{H}\right)\eta_i\\&=\sum_{i=2}^{N}\left(\eta_i^\top\mathbf{DF}(\overline{\mathbf{x}})\eta_i+c\lambda_i\eta_i^\top\mathbf{H}^s\eta_i\right).\end{aligned} \tag{15}$$

Introducing the denotation $\zeta_i\triangleq\mathbf{Q}^{-1}\eta_i$ $(2\le i\le N)$, one has $\eta_i^\top\eta_i=\zeta_i^\top\zeta_i$ and $\eta_i^\top\mathbf{H}^s\eta_i=\zeta_i^\top\mathbf{Q}^\top\mathbf{H}^s\mathbf{Q}\zeta_i=\zeta_i^\top\overline{\Lambda}\zeta_i$; thus one obtains

$$\begin{aligned}\dot{V}&=\sum_{i=2}^{N}\left(\eta_i^\top\mathbf{DF}(\overline{\mathbf{x}})\eta_i+c\lambda_i\zeta_i^\top\overline{\Lambda}\zeta_i\right)\\&\le\sum_{i=2}^{N}\left(\mathscr{L}\eta_i^\top\eta_i+c\lambda_i\min_{1\le k\le n}\{\mu_k\}\zeta_i^\top\zeta_i\right)\end{aligned}$$

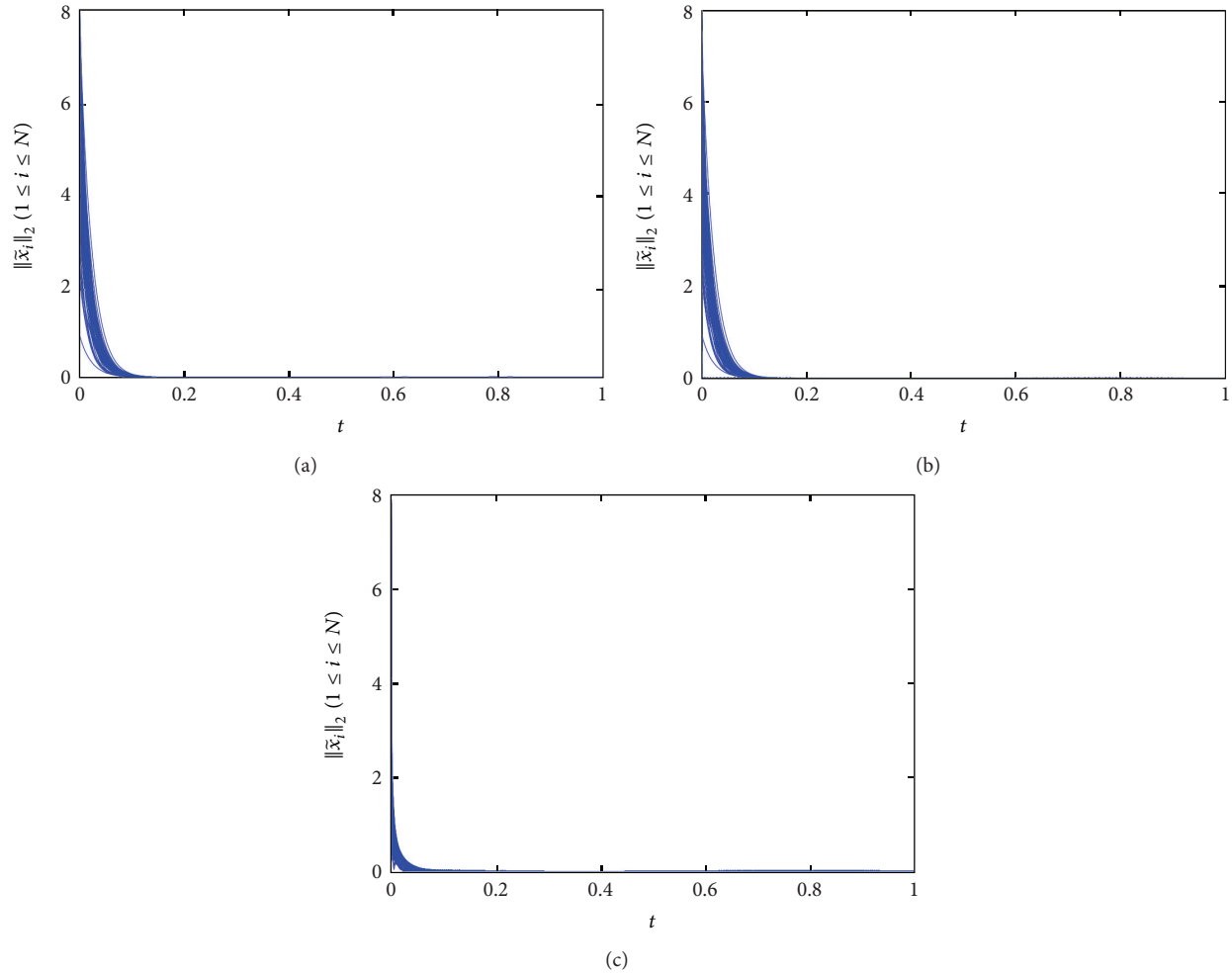

FIGURE 1: Synchronization errors $\|\tilde{\mathbf{x}}_i\|_2$ $(1 \le i \le 50)$ for globally coupled network (GCN) with $c = 1$, $\mathbf{H} = \mathbf{I}$ (a); $\|\tilde{\mathbf{x}}_i\|_2$ $(1 \le i \le 50)$ for star network (SN) with $c = 50$, $\mathbf{H} = \mathbf{I}$ (b); $\|\tilde{\mathbf{x}}_i\|_2$ $(1 \le i \le 50)$ for loop network (LN) with $c = 3040$, $\mathbf{H} = \mathbf{I}$ (c).

$$= \sum_{i=2}^{N} \left(\mathscr{L} + c\lambda_i \min_{1 \le k \le n} \{\mu_k\} \right) \zeta_i^\top \zeta_i$$

$$\le \left(\mathscr{L} + c\lambda_2 \min_{1 \le k \le n} \{\mu_k\} \right) \sum_{i=2}^{N} \zeta_i^\top \zeta_i. \tag{16}$$

In view of $\lambda_i < 0$ $(2 \le i \le N)$ and $\mu_k > 0$ $(1 \le k \le n)$, the derivation of the Lyapunov candidate $\dot{V}$ would be nonpositive given $c > -\mathscr{L}/\lambda_2 \min_{1 \le k \le n}\{\mu_k\}$. The largest invariant set of $\{\dot{V} = 0\}$ is $\Xi = \{\zeta_i = 0, 2 \le i \le N\}$. According to LaSalle's invariance principle [21], all the trajectories of system (13) will converge to Ξ asymptotically for any initial values. In this set, it is plain to see that $\eta_i = 0$ for $2 \le i \le N$. That means system (13) is stable, and accordingly the synchronous solution $\overline{\mathbf{X}}$ of dynamical network (1) is asymptotically stable. □

From Theorem 6, we conclude that whether can synchronization of a general complex dynamical network (1) be achieved depends on the relationship between the coupling strength c and the constant c_0. The term $c_0 = -\mathscr{L}/\lambda_2 \min_{1 \le k \le n}\{\mu_k\}$ is associated with individual node dynamics $(\mathscr{L})$, inner coupling $(\min_{1 \le k \le n}\{\mu_k\})$, and topology structure (λ_2) of the whole network.

Remark 7. The smaller the c_0 is, the larger the coupling strength c which leads to network synchronization is. In detail, smaller $\mathscr{L}$ of single node dynamics or larger $\min_{1 \le k \le n} \{\mu_k\}$ of inner-coupling matrix brings about better synchronizability for particular network topology.

Remark 8. It is worth noticing that although the previous result assumes that $c > c_0 = -\mathscr{L}/\lambda_2 \min_{1 \le k \le n} \{\mu_k\}$, the threshold of c may be much smaller than c_0 in reality. In other words, the synchronization criterion for dynamical network (1) is just a sufficient condition.

Remark 9. Theorem 6 reveals that for any topology structure, synchronization of network (1) can be achieved when the coupling strength c is strong enough, provided that Assumptions 2 and 5 hold. Further, it is seen that the synchronous region of dynamical network (1) belongs to *Type I* from the angle of Master Stability Function method [28] (see Section 4). Accordingly, the eigenvalue λ_2 of the

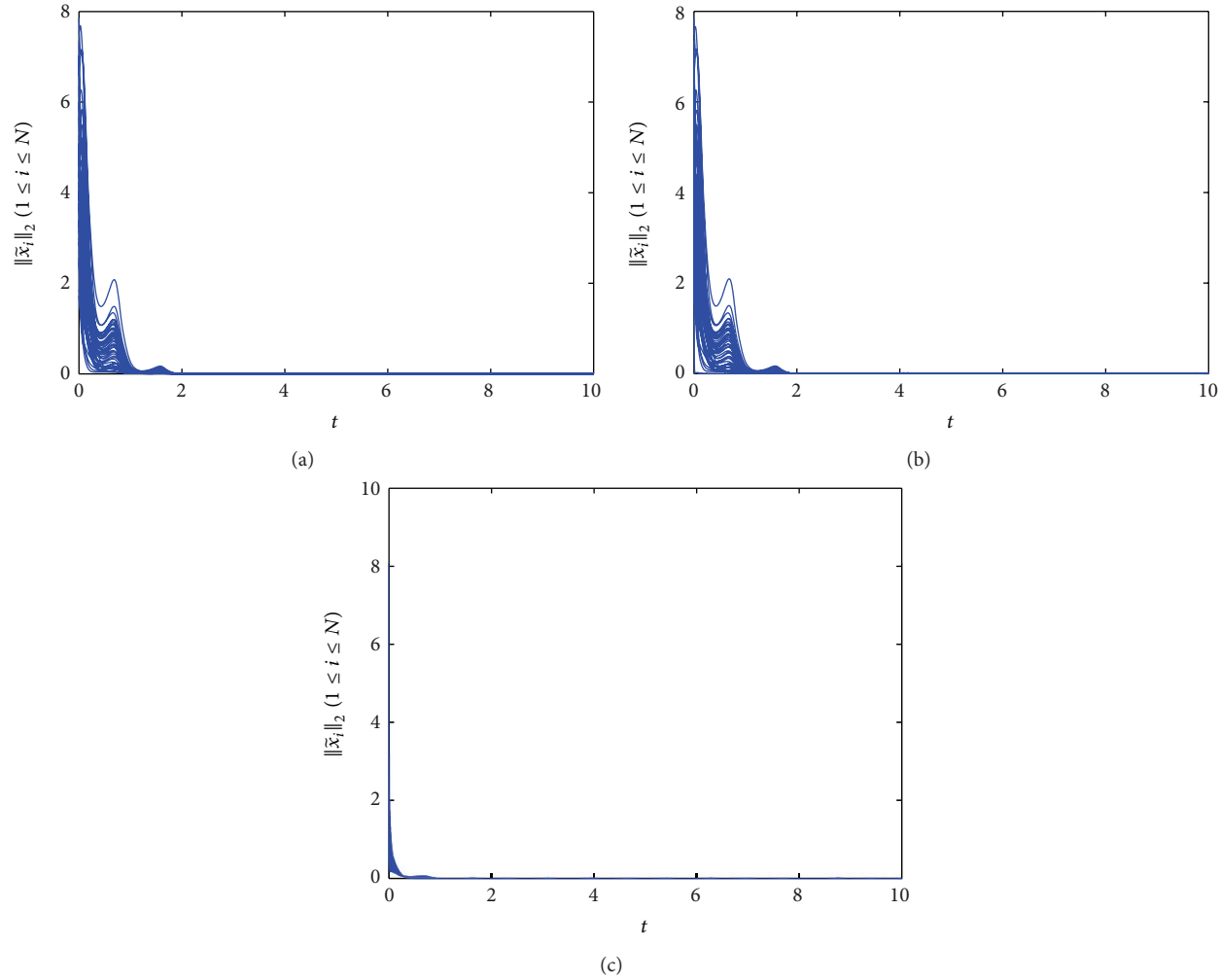

FIGURE 2: Synchronization errors $\|\tilde{\mathbf{x}}_i\|_2$ $(1 \le i \le 50)$ for globally coupled network (GCN) with $c = 0.1$, $\mathbf{H} = \mathbf{I}$ (a); $\|\tilde{\mathbf{x}}_i\|_2$ $(1 \le i \le 50)$ for star network (SN) with $c = 5$, $\mathbf{H} = \mathbf{I}$ (b); $\|\tilde{\mathbf{x}}_i\|_2$ $(1 \le i \le 50)$ for loop network (LN) with $c = 310$, $\mathbf{H} = \mathbf{I}$ (c).

outer-coupling matrix nearest 0 can be used for judging synchronizability of networks.

Remark 10. Although our analysis is founded on a basic hypothesis that the complex network is bidirectionally coupled (the outer-coupling matrix $\mathbf{A}$ is symmetric), similar conclusions can be drawn for the case in which this hypothesis is relaxed to unidirectional network.

4. Numerical Simulations

To verify the effectiveness of our main results, we choose the node dynamics as Lorenz system and the inner-coupling matrix as $\mathbf{I}$ in model (1), where $\mathbf{I}$ represents identity matrix. Topology structures selected in the network are globally coupled network (GCN), star network (SN), and loop network (LN). Then the outer-coupling matrices are $\mathbf{A}_{\mathrm{GCN}}$, $\mathbf{A}_{\mathrm{SN}}$, and $\mathbf{A}_{\mathrm{LN}}$, respectively, where

$$\mathbf{A}_{\mathrm{GCN}} = \begin{pmatrix} -49 & 1 & 1 & \cdots & 1 \\ 1 & -49 & 1 & \cdots & 1 \\ 1 & 1 & -49 & \cdots & 1 \\ & & & \cdots & \\ 1 & 1 & 1 & \cdots & -49 \end{pmatrix},$$

$$\mathbf{A}_{\mathrm{SN}} = \begin{pmatrix} -49 & 1 & 1 & \cdots & 1 \\ 1 & -1 & 0 & \cdots & 0 \\ 1 & 0 & -1 & \cdots & 0 \\ & & & \cdots & \\ 1 & 0 & 0 & \cdots & -1 \end{pmatrix},$$

$$\mathbf{A}_{\mathrm{LN}} = \begin{pmatrix} -2 & 1 & 0 & \cdots & 0 & 1 \\ 1 & -2 & 1 & \cdots & 0 & 0 \\ 0 & 1 & -2 & \cdots & 0 & 0 \\ & & & \cdots & & \\ 1 & 0 & 0 & \cdots & 1 & -2 \end{pmatrix}. \tag{17}$$

Lorenz system is a typical benchmark chaotic system, which is a simplified mathematical model first developed by Lorenz in 1963 to describe atmospheric convection. The model is a system of three ordinary differential equations now known as the Lorenz equations [31]:

$$\dot{\mathbf{x}} = \begin{pmatrix} -a & a & 0 \\ c & -1 & 0 \\ 0 & 0 & -b \end{pmatrix} \begin{pmatrix} x_1 \\ x_2 \\ x_3 \end{pmatrix} + \begin{pmatrix} 0 \\ -x_1 x_3 \\ x_1 x_2 \end{pmatrix}, \tag{18}$$

which is chaotic when $a = 10$, $b = 8/3$, and $c = 28$.

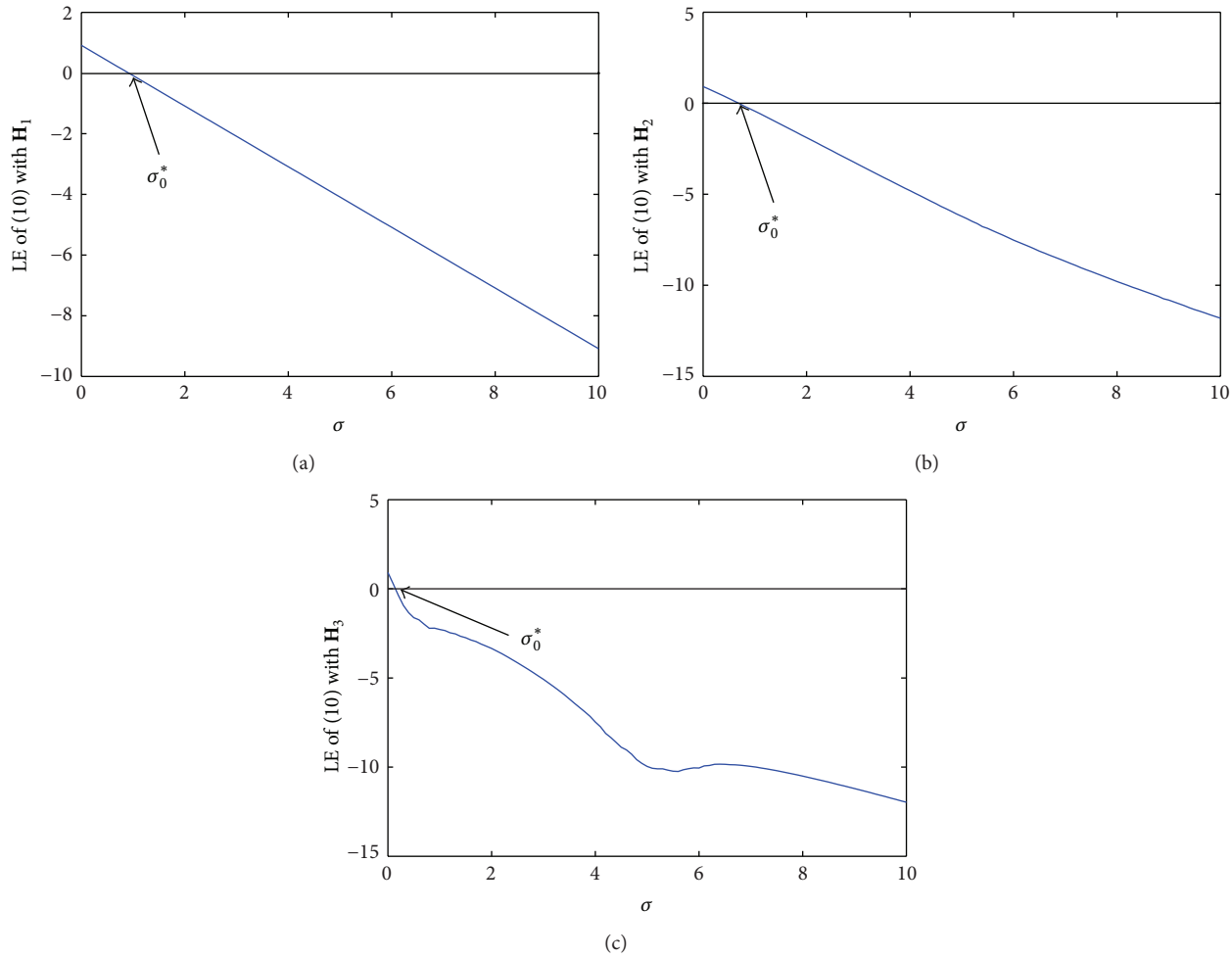

FIGURE 3: X label: $\sigma = -c\lambda$, Y label: Lyapunov Exponent of network (13), single node dynamics: Lorenz system, inner-coupling matrix: $\mathbf{H}_1$ (a); $\mathbf{H}_2$ (b); $\mathbf{H}_3$ (c). The cross point σ_0^* represents the lower bound of synchronous region in each subgraph.

It is easy to get that $\mathscr{L}$ of Lorenz system is 48 and $\min_{1\le k\le n}\{\mu_k\}$ of the inner-coupling matrix $\mathbf{I}$ is 1. For dynamical network (1) coupled with 50 nodes, a direct result is

$$\lambda_2\,(\mathrm{GCN}) = -50, \qquad \lambda_2\,(\mathrm{SN}) = -1, \qquad \lambda_2\,(\mathrm{LN}) = -0.0158. \tag{19}$$

Accordingly, because of $c_0 = -\mathscr{L}/\lambda_2 \min_{1\le k\le n}\{\mu_k\}$, one has

$$c_0\,(\mathrm{GCN}) = 0.96, \qquad c_0\,(\mathrm{SN}) = 48, \qquad c_0\,(\mathrm{LN}) = 3038. \tag{20}$$

Then selecting $c(\mathrm{GCN}) = 1 > c_0(\mathrm{GCN})$, $c(\mathrm{SN}) = 50 > c_0(\mathrm{SN})$, and $c(\mathrm{LN}) = 3040 > c_0(\mathrm{LN})$, we have the following error figure to picture the synchronization errors $\|\tilde{\mathbf{x}}_i\|_2$ ($1 \le i \le 50$) in dynamical network (1), in which topology structures are chosen as GCN, SN, and LN. See Figure 1.

From Figure 1, three networks have all reached synchronization in the condition of $c > c_0$, which are consistent with Theorem 6.

According to Remark 8, the condition $c > c_0$ for network synchronization is just sufficient. To illustrate, let c be about 10% of the original coupling strength; say, $c(\mathrm{GCN}) = 0.1$, $c(\mathrm{SN}) = 5$, and $c(\mathrm{LN}) = 310$. It is seen from Figure 2 that synchronization of three networks is achieved as well even if the synchronization criterion $c > c_0$ is not guaranteed.

Theorem 6 reveals that if Assumptions 2 and 5 hold, synchronization of network (1) can be achieved provided that c is sufficiently large. In the case of network synchronization, the real number $\sigma = -c\,\lambda$ falls into the synchronous region [28], where λ is any eigenvalue of the outer-coupling matrix $\mathbf{A}$ except $\lambda_1 = 0$. Furthermore, in view of Theorem 6, the synchronous region of the network is unbounded, which belongs to *Type I*. If the network belongs to one of the other three types of synchronous region, the coupling strength c which leads to synchronization may be upper bounded or even nonexistent. To clarify the unboundedness of synchronous region for the qualified network, three inner-coupling matrices which satisfy Assumption 2 are employed. We choose Lorenz systems as the nodes in dynamical network (1) and coupled them through $\mathbf{H}_1$, $\mathbf{H}_2$, and $\mathbf{H}_3$. Let $\mathbf{H}_1 = \mathbf{I}$, $\mathbf{H}_2 = \begin{pmatrix} 2 & 1 & 0 \\ 1 & 1 & 0 \\ 0 & 0 & 1 \end{pmatrix}$, and $\mathbf{H}_3 = \begin{pmatrix} 5 & 0 & 0 \\ 1 & 1 & 1 \\ 0 & 1 & 8 \end{pmatrix}$. It is easy to verify that the symmetric part of the inner-coupling matrices $\mathbf{H}_1^s$, $\mathbf{H}_2^s$, and $\mathbf{H}_3^s$ is positive definite. Figure 3 shows the relationship between Lyapunov

Exponents (LEs) of system (13) and $\sigma = -c\lambda$. During the growth of σ, LE of system (13) becomes negative when σ crosses a threshold σ_0^*, and accordingly system (13) is stable. In other words, if synchronization of network (1) is reached, the coupling strength c should be larger than a threshold $c_0^* = \sigma_0^*/-\lambda_2$. Predictably, c_0^* is much weaker than c_0 got from Theorem 6. Given coupling configuration structure of a dynamical network, the eigenvalues λ_i $(1 \le i \le N)$ would be certain, and thus network (1) synchronization would ensure $c > c_0^* = \sigma_0^*/-\lambda_2$. This is in agreement with Remark 9. On the one hand, the exact threshold of coupling strength c_0^{th} for network synchronization is smaller than c_0 according to Theorem 6. On the other hand, c_0^{th} that is larger than c_0^* lies in the fact that $c < c_0^*$ leads to asynchronization. Although we cannot gain the exact value of c_0^{th} so far, our results pave the way for exploring in depth the necessary and sufficient conditions of network synchronization.

5. Conclusions

In conclusion, we have developed a sufficient condition for a general complex dynamical network in the absence of control. We have concluded that if the coupling strength c is larger than $c_0 = -\mathscr{L}/\lambda_2 \min_{1\le k\le n}\{\mu_k\}$, synchronization will be reached in the network, where the symmetric part of the inner-coupling matrix $\mathbf{H}^s$ is positive definite. In the sense of Master Stability Function method, we have further illustrated that positive eigenvalues of $\mathbf{H}^s$ lead to *Type I* network with which synchronous region is unbounded. The findings show that the eigenvalue λ_2 of the outer-coupling matrix nearest 0 can be used for exploring synchronizability of a dynamical network with positive definite inner-coupling matrix.

Conflict of Interests

The author declares that there is no conflict of interests regarding the publication of this paper.

Acknowledgment

This work is supported by the National Natural Science Foundation of China under Grants 61004096, 61374173, and 11172215.

References

[1] A. Arenas, A. Díaz-Guilera, and C. J. Pérez-Vicente, "Synchronization reveals topological scales in complex networks," *Physical Review Letters*, vol. 96, Article ID 114102, 2006.

[2] I. Leyva, A. Navas, I. Sendina-Nadal et al., "Explosive transitions to synchronization in networks of phase oscillators," *Scientific Reports*, vol. 3, article 1281, 2013.

[3] R. M. Szmoski, R. F. Pereira, and S. E. de Souza Pinto, "Effective dynamics for chaos synchronization in networks with time-varying topology," *Communications in Nonlinear Science and Numerical Simulation*, vol. 18, no. 6, pp. 1491–1498, 2013.

[4] Y. Wu, C. Li, Y. Wu, and J. Kurths, "Generalized synchronization between two different complex networks," *Communications in Nonlinear Science and Numerical Simulation*, vol. 17, no. 1, pp. 349–355, 2012.

[5] L. M. Pecora and T. L. Carroll, "Synchronization in chaotic systems," *Physical Review Letters*, vol. 64, no. 8, pp. 821–824, 1990.

[6] C. W. Wu and L. O. Chua, "Synchronization in an array of linearly coupled dynamical systems," *IEEE Transactions on Circuits and Systems I*, vol. 42, no. 8, pp. 430–447, 1995.

[7] X. F. Wang and G. Chen, "Synchronization in scale-free dynamical networks: robustness and fragility," *IEEE Transactions on Circuits and System I*, vol. 49, no. 1, pp. 54–62, 2002.

[8] A. E. Motter, C. Zhou, and J. Kurths, "Network synchronization, diffusion, and the paradox of heterogeneity," *Physical Review E*, vol. 71, no. 1, Article ID 016116, 2005.

[9] J. Cao and F. Ren, "Exponential stability of discrete-time genetic regulatory networks with delays," *IEEE Transactions on Neural Networks*, vol. 19, no. 3, pp. 520–523, 2008.

[10] T. Nishikawa and A. E. Motter, "Maximum performance at minimum cost in network synchronization," *Physica D*, vol. 224, no. 1-2, pp. 77–89, 2006.

[11] J. Zhou, J.-a. Lu, and J. Lü, "Adaptive synchronization of an uncertain complex dynamical network," *IEEE Transactions on Automatic Control*, vol. 51, no. 4, pp. 652–656, 2006.

[12] Z. Li and G. Chen, "Robust adaptive synchronization of uncertain dynamical networks," *Physics Letters A*, vol. 324, no. 2-3, pp. 166–178, 2004.

[13] J. Zhou, J.-a. Lu, and J. Lü, "Pinning adaptive synchronization of a general complex dynamical network," *Automatica*, vol. 44, no. 4, pp. 996–1003, 2008.

[14] T. Chen, X. Liu, and W. Lu, "Pinning complex networks by a single controller," *IEEE Transactions on Circuits and Systems I*, vol. 54, no. 6, pp. 1317–1326, 2007.

[15] W. Yu, J. Cao, and J. Lü, "Global synchronization of linearly hybrid coupled networks with time-varying delay," *SIAM Journal on Applied Dynamical Systems*, vol. 7, no. 1, pp. 108–133, 2008.

[16] W. Yu, G. Chen, and J. Lü, "On pinning synchronization of complex dynamical networks," *Automatica*, vol. 45, no. 2, pp. 429–435, 2009.

[17] W. Yu, G. Chen, J. Lü, and J. Kurths, "Synchronization via pinning control on general complex networks," *SIAM Journal on Control and Optimization*, vol. 51, no. 2, pp. 1395–1416, 2013.

[18] L. M. Pecora and T. L. Carroll, "Master stability functions for synchronized coupled systems," *Physical Review Letters*, vol. 80, no. 10, pp. 2109–2112, 1998.

[19] M. Barahona and L. M. Pecora, "Synchronization in small-world systems," *Physical Review Letters*, vol. 89, no. 5, Article ID 054101, 4 pages, 2002.

[20] Y. Chen, G. Rangarajan, and M. Ding, "General stability analysis of synchronized dynamics in coupled systems," *Physical Review E*, vol. 67, no. 2, Article ID 026209, 4 pages, 2003.

[21] K. K. Hassan, *Nonlinear Systems*, Prentice Hall, 3rd edition, 2002.

[22] A. Isidori, *Nonlinear Control Systems II*, Electronic Industry Press, 1st edition, 2012 (Chinese).

[23] C. Godsil and G. Royle, *Algebraic Graph Theory*, vol. 207, Springer, New York, NY, USA, 2001.

[24] R. A. Horn and C. R. Johnson, *Matrix Analysis*, Cambridge University Press, New York, NY, USA, 1985.

[25] R. Olfati-Saber and R. M. Murray, "Consensus problems in networks of agents with switching topology and time-delays,"

IEEE Transactions on Automatic Control, vol. 49, no. 9, pp. 1520–1533, 2004.

[26] C. W. Wu, "Synchronization in networks of nonlinear dynamical systems coupled via a directed graph," *Nonlinearity*, vol. 18, no. 3, pp. 1057–1064, 2005.

[27] W. Lu and T. Chen, "New approach to synchronization analysis of linearly coupled ordinary differential systems," *Physica D*, vol. 213, no. 2, pp. 214–230, 2006.

[28] G. R. Chen, X. F. Wang, and X. Li, *Introduction to Complex Networks: Models, Structures and Dynamics*, Higher Education Press, 1st edition, 2012.

[29] J. A. Lu, J. Chen, and J. Zhou, "On relations between synchronousstate and solution of single node in complex networks," *Acta Automatica Sinica*. In press.

[30] T. Matsumoto, L. O. Chua, and M. Komuro, "The double scroll," *IEEE Transactions on Circuits and Systems*, vol. 32, no. 8, pp. 797–818, 1985.

[31] E. N. Lorenz, "Deterministic non-periodic flow," *Journal of the Atmospheric Sciences*, vol. 20, pp. 130–141, 1963.

[32] J. Lü and G. Chen, "A new chaotic attractor coined," *International Journal of Bifurcation and Chaos in Applied Sciences and Engineering*, vol. 12, no. 3, pp. 659–661, 2002.

[33] J. Lü, G. Chen, D. Cheng, and S. Celikovsky, "Bridge the gap between the Lorenz system and the Chen system," *International Journal of Bifurcation and Chaos in Applied Sciences and Engineering*, vol. 12, no. 12, pp. 2917–2926, 2002.

Hindawi Publishing Corporation
Abstract and Applied Analysis
Volume 2013, Article ID 289526, 9 pages
http://dx.doi.org/10.1155/2013/289526

Research Article

State Estimation for Neural Networks with Leakage Delay and Time-Varying Delays

Jing Liang,[1] Zengshun Chen,[2] and Qiankun Song[1]

[1] *Department of Mathematics, Chongqing Jiaotong University, Chongqing 400074, China*
[2] *School of Civil Engineering & Architecture, Chongqing Jiaotong University, Chongqing 400074, China*

Correspondence should be addressed to Qiankun Song; qiankunsong@gmail.com

Received 31 July 2013; Accepted 1 September 2013

Academic Editor: Jinde Cao

The state estimation problem is investigated for neural networks with leakage delay and time-varying delay as well as for general activation functions. By constructing appropriate Lyapunov-Krasovskii functionals and employing matrix inequality techniques, a delay-dependent linear matrix inequalities (LMIs) condition is developed to estimate the neuron state with some observed output measurements such that the error-state system is globally asymptotically stable. An example is given to show the effectiveness of the proposed criterion.

1. Introduction

In the past few years, neural networks have been extensively studied and successfully applied in many areas such as combinatorial optimization, signal processing, associative memory, affine invariant matching, and pattern recognition [1]. In such applications, the stability analysis is a necessary step for the practical design of neural networks [2]. In hardware implementation, time delays occur due to finite switching speed of the amplifiers and communication time. The existence of time delay may lead to some complex dynamic behaviors such as oscillation, divergence, chaos, instability, or other poor performance of the neural networks [3]. Therefore, the issue of stability analysis of neural networks with time delay attracts many researchers, and a number of remarkable results have been built up in the open literature; for example, see [2–5] and references therein.

When a neural network is designed to handle complex nonlinear problems, a great number of neurons with tremendous connections are often required. In such relatively large-scale neural networks, it may be very difficult and expensive (or even impossible) to obtain the complete information of the neuron states. On the other hand, in many practical applications, one needs to know the neuron states and then use them to achieve certain objectives. For instance, a recurrent neural network was presented in [6] to model an unknown nonlinear system, and the neuron states were utilized to implement a control law. Therefore, it is of great importance to study the state estimation problem of neural networks.

Recently, some results related to the state estimation problem for neural networks have been reported; for example, see [7–38] and references therein. In [7], authors initially studied the state estimation problem of delayed neural networks, where a delay-independent condition was obtained in terms of a linear matrix inequality (LMI). In [8], authors proposed a free-weighting matrix approach to discuss the state estimation problem for neural networks with time-varying delay. By using the Newton-Leibniz formula, some slack variables were introduced to derive a less conservative condition. In [11], attention was focused on the design of a state estimator to estimate the neuron states by using the delay-fractioning technique to reduce the possible conservatism. The authors in [13] first investigated the robust state estimator problem of delayed neural networks with parameter uncertainties. Delay-dependent conditions were presented to guarantee the global asymptotical stability of the error system. In [16], a further result on design problem of state estimator for a class of neural networks of neutral type was presented. A delay-dependent LMI criterion for existence of the estimator was derived. In [20], the state estimation problem for discrete

neural networks with partially unknown transition probabilities and time-varying delays was discussed. By utilizing a novel Lyapunov functional integrating both lower and upper time-delay bounds and some new techniques, some delay-range-dependent sufficient conditions under which the estimation error dynamics were stochastically stable are established. In [22], authors investigated the state estimation problem for neural networks with discrete time-varying delay and distributed time-varying delay; a delay-interval-dependent condition is developed to estimate the neuron state with some observed output measurements such that the error-state system was globally asymptotically stable. In [25], leakage delay in the leakage term was used to destabilize the neuron states. By constructing the Lyapunov-Krasovskii functional which contains a triple-integral term, an improved delay-dependent stability criterion was derived in terms of LMIs. In [27], the state estimation problem for a class of discrete-time stochastic neural networks with random delays was considered. By employing a Lyapunov-Krasovskii functional, sufficient delay distribution- dependent conditions were established in terms of LMIs that guarantee the existence of the state estimator. In [33], authors discussed the state estimation problem for Takagi-Sugeno (T-S) fuzzy Hopfield neural networks via strict output passivation of the error system. In [36–38], authors investigated the distributed state estimation problem for sensor networks and presented several new sufficient conditions to guarantee the convergence of the estimation error systems. To the best of the author's knowledge, there are no results on the problem of state estimation for neural networks with leakage delay and time-varying delays. As pointed out in [39], neural networks with leakage delay are a class of important neural networks; time delay in the leakage term also has great impact on the dynamics of neural networks since time delay in the stabilizing negative feedback term has a tendency to destabilize a system. Therefore, it is necessary to investigate the state estimation problem for neural networks with leakage delay [25].

Motivated by the previous discussions, the objective of this paper is to study the state estimation for neural networks with leakage delay and time-varying delays by employing new Lyapunov-Krasovskii functionals and using matrix inequality techniques. The obtained sufficient condition does not require the differentiability of time-varying delays and is expressed in terms of linear matrix inequalities, which can be checked numerically using the effective LMI toolbox in Matlab. An example is given to show the effectiveness of the proposed criterion.

Notations. The notations are quite standard. Throughout this paper, $\mathbb{R}^n$ and $\mathbb{R}^{n\times m}$ denote, respectively, the n-dimensional Euclidean space and the set of all $n \times m$ real matrices. $\|\cdot\|$ refers to the Euclidean vector norm. A^T represents the transpose of matrix A, and the asterisk "$*$" in a matrix is used to represent the term which is induced by symmetry. I is the identity matrix with compatible dimension. $X > Y$ means that X and Y are symmetric matrices and that $X - Y$ is positive definite. Matrices, if not explicitly specified, are assumed to have compatible dimensions.

2. Model Description and Preliminaries

Consider the following neural networks with leakage delay and time-varying delays:

$$\dot{x}(t) = -Cx(t-\delta) + Af(x(t)) + Bf(x(t-\tau(t))) + J(t) \tag{1}$$

for $t \geq 0$, where $x(t) = (x_1(t), x_2(t), \ldots, x_n(t))^T \in \mathbb{R}^n$ is the state vector of the network at time t, and n corresponds to the number of neurons; $C \in \mathbb{R}^{n\times n}$ is a positive diagonal matrix, and $A \in \mathbb{R}^{n\times n}$ and $B \in \mathbb{R}^{n\times n}$ are the connection weight matrix and the delayed connection weight matrix, respectively; $f(x(t)) = (f_1(x_1(t)), f_2(x_2(t)), \ldots, f_n(x_n(t)))^T \in \mathbb{R}^n$ denotes the neuron activation at time t; $J(t) \in \mathbb{R}^n$ is an external input vector; δ and $\tau(t)$ denote the leakage delay and time-varying delay, respectively.

Throughout this paper, we make the following assumptions.

(H1) (see [40]) For any $j \in \{1, 2, \ldots, n\}$ there exist constants F_j^- and F_j^+ such that

$$F_j^- \leq \frac{f_j(\alpha_1) - f_j(\alpha_2)}{\alpha_1 - \alpha_2} \leq F_j^+ \tag{2}$$

for all $\alpha_1 \neq \alpha_2$.

(H2) (see [25]) The leakage delay δ and time-varying delays $\tau(t)$ satisfy the following conditions:

$$0 \leq \delta, \quad 0 \leq \tau(t) \leq \tau, \tag{3}$$

where δ and τ are constants.

As is well known, information about the neuron states is often incomplete from the network measurements (outputs) in applications, and the network measurements are subject to nonlinear disturbances. Similar to [7], we assume that the network measurements satisfy

$$y(t) = Dx(t) + g(t, x(t)), \tag{4}$$

where $y(t) \in \mathbb{R}^m$ is the measurement output, and $D \in \mathbb{R}^{m\times n}$ is a known constant matrix with appropriate dimension. $g : \mathbb{R} \times \mathbb{R}^n \to \mathbb{R}^m$ is the neuron-dependent nonlinear disturbances on the network outputs and satisfies the following condition.

(H3) (see [22]) For any $j \in \{1, 2, \ldots, m\}$ there exist constants G_j^- and G_j^+ such that

$$G_j^- \leq \frac{g_j(t, \alpha_1(t)) - g_j(t, \alpha_2(t))}{\alpha_1(t) - \alpha_2(t)} \leq G_j^+ \tag{5}$$

for $t \geq 0$ and all $\alpha_1(t) \neq \alpha_2(t)$.

Remark 1. As pointed out in [40], the constants F_j^- and F_j^+ in assumption (H1) of this paper are allowed to be positive, negative, or zero. Hence, assumption (H1), first proposed by Liu et al. in [40], is weaker than the Lipschitz condition.

For the delay neural networks (1), we construct the full-order state estimation as follows:

$$\begin{aligned}\dot{u}(t) = &-Cu(t-\delta) + Af(u(t)) \\ &+ Bf(u(t-\tau(t))) + J(t) + K\left(y(t) - v(t)\right)\end{aligned} \tag{6}$$

$$v(t) = Du(t) + g(t, u(t)), \tag{7}$$

where $u(t) \in \mathbb{R}^n$ is an estimation of the state $x(t)$ of (1), and $K \in \mathbb{R}^{n\times m}$, to be determined, is a gain matrix of the state estimator.

Let the error state be $e(t) = x(t) - u(t)$ then it follows from (1), (4), (6), and (7) that

$$\begin{aligned}\dot{e}(t) = &-KDe(t) - Ce(t-\delta) + Ah(e(t)) \\ &+ Bh(e(t-\tau(t))) - Kr(t, e(t)),\end{aligned} \tag{8}$$

where $h(e(t)) = f(x(t)) - f(u(t))$, $r(t, e(t)) = g(t, x(t)) - g(t, u(t))$.

The problem to be addressed in this study is to find out the gain matrix K such that the system (8) is globally asymptotically stable.

To prove our results, the following lemmas that can be found in [22] are necessary.

Lemma 2 (see [22]). *For any constant matrix $W \in \mathbb{R}^{m\times m}$, $W > 0$, scalar $0 < h(t) < h$, and vector function $\omega(\cdot) : [0, h] \to \mathbb{R}^m$ such that the integrations concerned are well defined, then*

$$\begin{aligned}&\left(\int_0^{h(t)} \omega(s)\, ds\right)^T W \left(\int_0^{h(t)} \omega(s)\, ds\right) \\ &\quad \le h(t) \int_0^{h(t)} \omega^T(s) W \omega(s)\, ds.\end{aligned} \tag{9}$$

Lemma 3 (see [22]). *Given constant matrices P, Q, and R, where $P^T = P$, $Q^T = Q$, then*

$$\begin{bmatrix} P & R \\ R^T & -Q \end{bmatrix} < 0 \tag{10}$$

is equivalent to the following conditions:

$$Q > 0, \quad P + RQ^{-1}R^T < 0. \tag{11}$$

3. Main Results

For presentation convenience, in the following, we denote

$$\begin{aligned}F_1 &= \operatorname{diag}\left(F_1^-, F_2^-, \ldots, F_n^-\right), \\ F_2 &= \operatorname{diag}\left(F_1^+, F_2^+, \ldots, F_n^+\right), \\ F_3 &= \operatorname{diag}\left(F_1^- F_1^+, F_2^- F_2^+, \ldots, F_n^- F_n^+\right), \\ F_4 &= \operatorname{diag}\left(\frac{F_1^- + F_1^+}{2}, \frac{F_2^- + F_2^+}{2}, \ldots, \frac{F_n^- + F_n^+}{2}\right), \\ G_1 &= \operatorname{diag}\left(G_1^- G_1^+, G_2^- G_2^+, \ldots, G_n^- G_n^+\right), \\ G_2 &= \operatorname{diag}\left(\frac{G_1^- + G_1^+}{2}, \frac{G_2^- + G_2^+}{2}, \ldots, \frac{G_n^- + G_n^+}{2}\right).\end{aligned} \tag{12}$$

Theorem 4. *Assume that the assumptions* (H1)–(H3) *hold. If there exist four symmetric positive definite matrices P_i ($i = 1, 2, 3, 4$), five positive diagonal matrices W_1, W_2, R_1, R_2, and R_3, and seven matrices Q_1, Q_2, Q_3, X_{11}, X_{12}, X_{22}, and Z, such that the following LMIs hold:*

$$X = \begin{bmatrix} X_{11} & X_{12} \\ * & X_{22} \end{bmatrix} > 0, \tag{13}$$

$$\Omega = \begin{bmatrix} \Omega_{11} & \Omega_{12} & Q_3 & 0 & \Omega_{15} & X_{22} & \Omega_{17} & Q_1B & \Omega_{19} & Q_3 & 0 \\ * & \Omega_{22} & 0 & 0 & -Q_1C & X_{12} & \Omega_{27} & Q_1B & -Z & 0 & 0 \\ * & * & \Omega_{33} & Q_2 & 0 & 0 & F_4R_2 & 0 & 0 & 0 & Q_2 \\ * & * & * & -P_3 & 0 & 0 & 0 & 0 & 0 & 0 & 0 \\ * & * & * & * & -P_1 & -X_{22} & 0 & 0 & 0 & 0 & 0 \\ * & * & * & * & * & -P_2 & 0 & 0 & 0 & 0 & 0 \\ * & * & * & * & * & * & -R_1 & 0 & 0 & 0 & 0 \\ * & * & * & * & * & * & * & -R_2 & 0 & 0 & 0 \\ * & * & * & * & * & * & * & * & -R_3 & 0 & 0 \\ * & * & * & * & * & * & * & * & * & -\frac{1}{\tau}P_4 & 0 \\ * & * & * & * & * & * & * & * & * & 0 & -\frac{1}{\tau}P_4 \end{bmatrix} < 0, \tag{14}$$

where $\Omega_{11} = X_{12} + X_{12}^T + P_1 + \delta^2 P_2 + P_3 - ZD - D^T Z^T - Q_3 - Q_3^T - F_3R_1 - G_1R_3$, $= X_{11} - F_1W_1 + F_2W_2 - Q_1 - D^T Z^T$, $\Omega_{15} = -X_{12} - Q_1C$, $\Omega_{17} = Q_1A + F_4R_1$, $\Omega_{19} = -Z + G_2R_3$, $\Omega_{22} = -Q_1 - Q_1^T + \tau P_4$, $\Omega_{27} = W_1 - W_2 + Q_1A$, $\Omega_{33} = -Q_2 - Q_2^T -$

F_3R_2, then error-state system (8) *of the delayed neural network described by* (1) *and* (6) *is globally asymptotically stable, and the estimator gain matrix K can be designed as $K = Q_1^{-1}Z$.*

Proof. From assumption (H1), we know that

$$\int_0^{e_i(t)} \left(h_i(s) - F_i^- s\right) ds \geq 0, \tag{15}$$

$$\int_0^{e_i(t)} \left(F_i^+ s - h_i(s)\right) ds \geq 0, \quad i = 1, 2, \ldots, n. \tag{16}$$

Let $W_1 = \mathrm{diag}(w_{11}, w_{12}, \ldots, w_{1n})$, $W_2 = \mathrm{diag}(w_{21}, w_{22}, \ldots, w_{2n})$, and consider the following Lyapunov-Krasovskii functional as

$$V(t) = V_1(t) + V_2(t) + V_3(t) + V_4(t), \tag{17}$$

where

$$\begin{aligned}
V_1(t) &= \begin{bmatrix} e(t) \\ \int_{t-\delta}^{t} e(s)ds \end{bmatrix}^T \begin{bmatrix} X_{11} & X_{12} \\ * & X_{22} \end{bmatrix} \begin{bmatrix} e(t) \\ \int_{t-\delta}^{t} e(s)\,ds \end{bmatrix}, \\
V_2(t) &= 2\sum_{i=1}^{n} w_{1i} \int_0^{e_i(t)} \left(h_i(s) - F_i^- s\right) ds \\
&\quad + 2\sum_{i=1}^{n} w_{2i} \int_0^{e_i(t)} \left(F_i^+ s - h_i(s)\right) ds, \\
V_3(t) &= \int_{t-\delta}^{t} e^T(s) P_1 e(s)\,ds + \delta \int_{-\delta}^{0} \int_{t+\xi}^{t} e^T(s) P_2 e(s)\,ds\,d\xi, \\
V_4(t) &= \int_{t-\tau}^{t} e^T(s) P_3 e(s)\,ds + \int_{-\tau}^{0} \int_{t+\xi}^{t} \dot{e}^T(s) P_4 \dot{e}(s)\,ds\,d\xi.
\end{aligned} \tag{18}$$

Calculating the time derivative of $V_i(t)$ $(i = 1, 2, 3, 4)$, we obtain

$$\begin{aligned}
\dot{V}_1(t) &= 2\begin{bmatrix} e(t) \\ \int_{t-\delta}^{t} e(s)ds \end{bmatrix}^T \begin{bmatrix} X_{11} & X_{12} \\ * & X_{22} \end{bmatrix} \begin{bmatrix} \dot{e}(t) \\ e(t) - e(t-\delta) \end{bmatrix} \\
&= e^T(t)\left(X_{12} + X_{12}^T\right) e(t) + 2e^T(t) X_{11} \dot{e}(t) \\
&\quad - 2e^T(t) X_{12} e(t-\delta) + 2e^T(t) X_{22} \int_{t-\delta}^{t} e(s)\,ds \\
&\quad + 2\dot{e}^T(t) X_{12} \int_{t-\delta}^{t} e(s)\,ds \\
&\quad - 2e^T(t-\delta) X_{22} \int_{t-\delta}^{t} e(s)\,ds,
\end{aligned} \tag{19}$$

$$\begin{aligned}
\dot{V}_2(t) &= 2\dot{e}^T(t) W_1 \left(h(e(t)) - F_1 e(t)\right) \\
&\quad + 2\dot{e}^T(t) W_2 \left(F_2 e(t) - h(e(t))\right) \\
&= 2e^T(t)\left(-F_1 W_1 + F_2 W_2\right) \dot{e}(t) \\
&\quad + 2\dot{e}^T(t)\left(W_1 - W_2\right) h(e(t)),
\end{aligned} \tag{20}$$

$$\begin{aligned}
\dot{V}_3(t) &= e^T(t)\left(P_1 + \delta^2 P_2\right) e(t) \\
&\quad - e^T(t-\delta) P_1 e(t-\delta) - \delta \int_{t-\delta}^{t} e^T(s) P_2 e(s)\,ds \\
&\leq e^T(t)\left(P_1 + \delta^2 P_2\right) e(t) - e^T(t-\delta) P_1 e(t-\delta) \\
&\quad - \left(\int_{t-\delta}^{t} e(s)\,ds\right)^T P_2 \left(\int_{t-\delta}^{t} e(s)\,ds\right),
\end{aligned} \tag{21}$$

$$\begin{aligned}
\dot{V}_4(t) &= e^T(t) P_3 e(t) - e^T(t-\tau) P_3 e(t-\tau) \\
&\quad + \tau \dot{e}^T(t) P_4 \dot{e}(t) - \int_{t-\tau}^{t} \dot{e}^T(s) P_4 \dot{e}(s)\,ds.
\end{aligned} \tag{22}$$

In deriving inequality (21), we have made use of Lemma 2. It follows from inequalities (19)–(22) that

$$\begin{aligned}
\dot{V}(t) &\leq e^T(t)\left(X_{12} + X_{12}^T + P_1 + \delta^2 P_2 + P_3\right) e(t) \\
&\quad + 2e^T(t)\left(X_{11} - F_1 W_1 + F_2 W_2\right) \dot{e}(t) \\
&\quad - 2e^T(t) X_{12} e(t-\delta) \\
&\quad + 2e^T(t) X_{22} \int_{t-\delta}^{t} e(s)\,ds \\
&\quad + \tau \dot{e}^T(t) P_4 \dot{e}(t) + 2\dot{e}^T(t) X_{12} \int_{t-\delta}^{t} e(s)\,ds \\
&\quad + 2\dot{e}^T(t)\left(W_1 - W_2\right) h(e(t)) \\
&\quad - e^T(t-\delta) P_1 e(t-\delta) \\
&\quad - 2e^T(t-\delta) X_{22} \int_{t-\delta}^{t} e(s)\,ds \\
&\quad - e^T(t-\tau) P_3 e(t-\tau) \\
&\quad - \left(\int_{t-\delta}^{t} e(s)\,ds\right)^T P_2 \left(\int_{t-\delta}^{t} e(s)\,ds\right) \\
&\quad - \int_{t-\tau}^{t} \dot{e}^T(s) P_4 \dot{e}(s)\,ds.
\end{aligned} \tag{23}$$

From model (8), we have

$$\begin{aligned}
0 &= 2\left(e^T(t)+\dot{e}^T(t)\right)Q_1 \\
&\quad\times[-\dot{e}(t)-KDe(t)-Ce(t-\delta)+Ah(e(t)) \\
&\qquad +Bh(e(t-\tau(t)))-Kr(t,e(t))] \\
&= -e^T(t)\left(Q_1KD+D^TK^TQ_1^T\right)e(t) \\
&\quad -2e^T(t)Q_1\dot{e}(t)-2e^T(t)Q_1Ce(t-\delta) \\
&\quad +2e^T(t)Q_1Ah(e(t))+2e^T(t)Q_1Bh \\
&\quad\times(e(t-\tau(t)))-2e^T(t)Q_1Kr(t,e(t)) \\
&\quad -\dot{e}^T(t)\left(Q_1+Q_1^T\right)\dot{e}(t)-2e^T(t)D^TK^TQ_1^T\dot{e}(t) \\
&\quad -2\dot{e}^T(t)Q_1Ce(t-\delta)+2\dot{e}^T(t)Q_1Ah(e(t)) \\
&\quad +2\dot{e}^T(t)Q_1Bh(e(t-\tau(t))) \\
&\quad -2\dot{e}^T(t)Q_1Kr(t,e(t)).
\end{aligned} \tag{24}$$

By Newton-Leibniz formulation and assumption (H2), we have

$$\begin{aligned}
0 &= -2e^T(t-\tau(t))Q_2 \\
&\quad\times\left(e(t-\tau(t))-e(t-\tau)-\int_{t-\tau}^{t-\tau(t)}\dot{e}(s)\,ds\right) \\
&\le -2e^T(t-\tau(t))Q_2e(t-\tau(t)) \\
&\quad +2e^T(t-\tau(t))Q_2e(t-\tau) \\
&\quad +\tau e^T(t-\tau(t))Q_2P_4^{-1}Q_2^Te(t-\tau(t)) \\
&\quad +\int_{t-\tau}^{t-\tau(t)}\dot{e}^T(s)P_4\dot{e}(s)\,ds, \\
0 &= -2e^T(t)Q_3 \\
&\quad\times\left(e(t)-e(t-\tau(t))-\int_{t-\tau(t)}^{t}\dot{e}(s)\,ds\right) \\
&\le -2e^T(t)Q_3e(t)+2e^T(t)Q_3e(t-\tau(t)) \\
&\quad +\tau e^T(t)Q_3P_4^{-1}Q_3^Te(t) \\
&\quad +\int_{t-\tau(t)}^{t}\dot{e}^T(s)P_4\dot{e}(s)\,ds.
\end{aligned} \tag{25}$$

In addition, for positive diagonal matrices $R_i > 0$ ($i = 1,2,3$), we can get from assumption (H1) and assumption (H3) that [15]

$$\begin{aligned}
&\begin{bmatrix} e(t) \\ h(e(t)) \end{bmatrix}^T \begin{bmatrix} F_3R_1 & -F_4R_1 \\ -F_4R_1 & R_1 \end{bmatrix} \begin{bmatrix} e(t) \\ h(e(t)) \end{bmatrix} \le 0, \\
&\begin{bmatrix} e(t-\tau(t)) \\ h(e(t-\tau(t))) \end{bmatrix}^T \begin{bmatrix} F_3R_2 & -F_4R_2 \\ -F_4R_2 & R_2 \end{bmatrix} \\
&\quad\times \begin{bmatrix} e(t-\tau(t)) \\ h(e(t-\tau(t))) \end{bmatrix} \le 0, \\
&\begin{bmatrix} e(t) \\ r(t,e(t)) \end{bmatrix}^T \begin{bmatrix} G_1R_3 & -G_2R_3 \\ -G_2R_3 & R_3 \end{bmatrix} \begin{bmatrix} e(t) \\ r(t,e(t)) \end{bmatrix} \le 0.
\end{aligned} \tag{26}$$

It follows from (23)–(26) that

$$\begin{aligned}
\dot{V}(t) &\le e^T(t)\left(X_{12}+X_{12}^T+P_1+\delta^2P_2+P_3\right. \\
&\qquad -Q_1KD-D^TK^TQ_1^T-Q_3-Q_3^T \\
&\qquad \left.+\tau Q_3P_4^{-1}Q_3^T-F_3R_1-G_1R_3\right)e(t) \\
&\quad +2e^T(t)\left(X_{11}-F_1W_1+F_2W_2\right. \\
&\qquad \left.-Q_1-D^TK^TQ_1^T\right)\dot{e}(t) \\
&\quad +2e^T(t)Q_3e(t-\tau(t)) \\
&\quad -2e^T(t)\left(X_{12}+Q_1C\right)e(t-\delta) \\
&\quad +2e^T(t)X_{22}\int_{t-\delta}^{t}e(s)\,ds \\
&\quad +2e^T(t)\left(Q_1A+F_4R_1\right)h(e(t)) \\
&\quad +2e^T(t)Q_1Bh(e(t-\tau(t))) \\
&\quad +2e^T(t)\left(-Q_1K+G_2R_3\right)r(t,e(t)) \\
&\quad +\dot{e}^T(t)\left(-Q_1-Q_1^T+\tau P_4\right)\dot{e}(t) \\
&\quad -2\dot{e}^T(t)Q_1Ce(t-\delta) \\
&\quad +2\dot{e}^T(t)X_{12}\int_{t-\delta}^{t}e(s)\,ds \\
&\quad +2\dot{e}^T(t)\left(W_1-W_2+Q_1A\right)h(e(t)) \\
&\quad +2\dot{e}^T(t)Q_1Bh(e(t-\tau(t))) \\
&\quad -2\dot{e}^T(t)Q_1Kr(t,e(t)+e^T(t-\tau(t)) \\
&\quad\times\left(-Q_2-Q_2^T+\tau Q_2P_4^{-1}Q_2^T\right. \\
&\qquad \left.-F_3R_2\right)e(t-\tau(t)) \\
&\quad +2e^T(t-\tau(t))Q_2e(t-\tau) \\
&\quad +2e^T(t-\tau(t))F_4R_2h(e(t-\tau(t)))
\end{aligned}$$

$$
\begin{aligned}
&- e^T(t-\tau) P_3 e(t-\tau) - e^T(t-\delta) P_1 e \\
&\times (t-\delta) - 2e^T(t-\delta) X_{22} \int_{t-\delta}^{t} e(s)\, ds \\
&- \left(\int_{t-\delta}^{t} e(s)\, ds \right)^T P_2 \left(\int_{t-\delta}^{t} e(s)\, ds \right) \\
&- h^T(e(t)) R_1 h(e(t)) \\
&- h^T(e(t-\tau(t))) R_2 h(e(t-\tau(t))) \\
&- r^T(t, e(t)) R_3 r(t, e(t)) = \xi^T(t) \Pi \xi(t),
\end{aligned} \tag{27}
$$

where $\xi(t) = (e^T(t), \dot{e}^T(t), e^T(t-\tau(t)), e^T(t-\tau), e^T(t-\delta), \int_{t-\delta}^{t} e^T(s)ds, h^T(e(t)), h^T(e(t-\tau(t))), r^T(t, e(t)))^T$,

$$
\Pi = \begin{bmatrix}
\Pi_{11} & \Pi_{12} & Q_3 & 0 & -X_{12} - Q_1 C & X_{22} & Q_1 A + F_4 R_1 & Q_1 B & -Q_1 K + G_2 R_3 \\
* & \Pi_{22} & 0 & 0 & -Q_1 C & X_{12} & W_1 - W_2 + Q_1 A & Q_1 B & -Q_1 K \\
* & * & \Pi_{33} & Q_2 & 0 & 0 & F_4 R_2 & 0 & 0 \\
* & * & * & -P_3 & 0 & 0 & 0 & 0 & 0 \\
* & * & * & * & -P_1 & -X_{22} & 0 & 0 & 0 \\
* & * & * & * & * & -P_2 & 0 & 0 & 0 \\
* & * & * & * & * & * & -R_1 & 0 & 0 \\
* & * & * & * & * & * & * & -R_2 & 0 \\
* & * & * & * & * & * & * & * & -R_3
\end{bmatrix} \tag{28}
$$

with $\Pi_{11} = X_{12} + X_{12}^T + P_1 + \delta^2 P_2 + P_3 - Q_1 K D - D^T K^T Q_1^T - Q_3 - Q_3^T + \tau Q_3 P_4^{-1} Q_3^T - F_3 R_1 - G_1 R_3$, $\Pi_{12} = X_{11} - F_1 W_1 + F_2 W_2 - Q_1 - D^T K^T Q_1^T$, $\Pi_{22} = -Q_1 - Q_1^T + \tau P_4$, $\Pi_{33} = -Q_2 - Q_2^T + \tau Q_2 P_4^{-1} Q_2^T - F_3 R_2$.

By using Lemma 3, and noting $K = Q_1^{-1} Z$, it is easy to verify the equivalence of $\Pi < 0$ and $\Omega < 0$. Thus, one can derive from (14) and (27) that

$$
\dot{V}(t) \le 0, \tag{29}
$$

which implies that the error-state system (8) of the delayed neural networks described by (1) and (6) is globally asymptotically stable. The proof is completed. □

4. Numerical Example

To verify the effectiveness of the theoretical result of this paper, consider the following example.

Example 1. Consider a two-neuron neural network (1), where

$$
\begin{aligned}
C &= \begin{bmatrix} 1.3 & 0 \\ 0 & 0.9 \end{bmatrix}, \qquad A = \begin{bmatrix} 0.5 & -0.2 \\ 0.7 & 0.5 \end{bmatrix}, \\
B &= \begin{bmatrix} 0.6 & -0.1 \\ -1.2 & -0.8 \end{bmatrix}, \qquad J(t) = \begin{bmatrix} 1.6\cos(21t) \\ -1.3\sin(1.1t) \end{bmatrix}, \\
f_1(x) &= f_2(x) = \tanh(x), \\
\delta &= 0.1, \qquad \tau(t) = 0.27\,|\sin(7t)|.
\end{aligned} \tag{30}
$$

Figure 1 shows that the considered neural network has a chaotic attractor, where the initial condition is $x_1(t) = 0.5\cos(0.5t)$, $x_2(t) = -0.2\sin(18t)$, and $t \in [-0.27, 0]$.

It can be verified that assumptions (H1) and (H2) are satisfied, and $F_1 = 0$, $F_2 = I$, $F_3 = 0$, $F_4 = \mathrm{diag}\{0.5, 0.5\}$, $\tau = 0.27$.

Choose network measurement (4), where

$$
D = \begin{bmatrix} 0.7 & -0.2 \\ 0.1 & 0.5 \end{bmatrix}, \qquad g(t, x(t)) = 0.1\cos x(t) + 0.3. \tag{31}
$$

It is obvious that assumption (H3) is satisfied with $G_1 = -0.01I$ and $G_2 = 0$. By the Matlab LMI Control Toolbox, we find a solution to the LMIs in (13) and (14) as follows:

$$
\begin{aligned}
P_1 &= \begin{bmatrix} 0.5042 & 0.0068 \\ 0.0068 & 0.1895 \end{bmatrix}, \qquad P_2 = \begin{bmatrix} 2.7464 & 0.0896 \\ 0.0896 & 2.0468 \end{bmatrix}, \\
P_3 &= \begin{bmatrix} 0.3288 & -0.0027 \\ -0.0027 & 0.1564 \end{bmatrix}, \qquad P_4 = \begin{bmatrix} 0.1907 & 0.0138 \\ 0.0138 & 0.1027 \end{bmatrix}, \\
W_1 &= \begin{bmatrix} 0.1184 & 0 \\ 0 & 0.0779 \end{bmatrix}, \qquad W_2 = \begin{bmatrix} 0.2313 & 0 \\ 0 & 0.1183 \end{bmatrix}, \\
R_1 &= \begin{bmatrix} 0.9466 & 0 \\ 0 & 0.4360 \end{bmatrix}, \qquad R_2 = \begin{bmatrix} 0.4704 & 0 \\ 0 & 0.2050 \end{bmatrix}, \\
R_3 &= \begin{bmatrix} 2.9274 & 0 \\ 0 & 3.4376 \end{bmatrix}, \qquad Q_1 = \begin{bmatrix} 0.2168 & 0.0134 \\ 0.0144 & 0.0812 \end{bmatrix}, \\
Q_2 &= \begin{bmatrix} 0.2025 & 0.0032 \\ 0.0032 & 0.1054 \end{bmatrix}, \qquad Q_3 = \begin{bmatrix} -0.0134 & 0.0159 \\ -0.0162 & 0.0155 \end{bmatrix}, \\
X_{11} &= \begin{bmatrix} 0.4753 & 0.0123 \\ 0.0123 & 0.1554 \end{bmatrix}, \qquad X_{12} = \begin{bmatrix} -0.5667 & -0.0378 \\ -0.0362 & -0.2141 \end{bmatrix}, \\
X_{22} &= \begin{bmatrix} 0.8376 & 0.0508 \\ 0.0508 & 0.4503 \end{bmatrix}, \qquad Z = \begin{bmatrix} 0.5858 & 0.1452 \\ -0.0249 & 0.4239 \end{bmatrix}.
\end{aligned} \tag{32}
$$

Subsequently, we can obtain from $K = Q_1^{-1} Z$ that

$$
K = \begin{bmatrix} 2.7511 & 0.3508 \\ -0.7949 & 5.1560 \end{bmatrix}. \tag{33}
$$

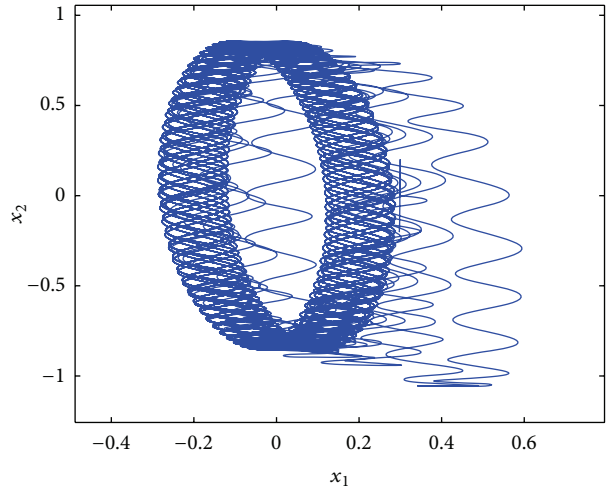

Figure 1: Phase trajectory of model (1).

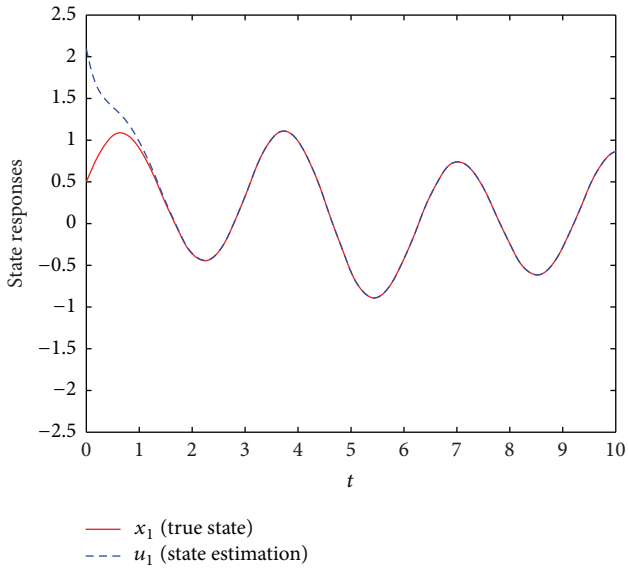

Figure 2: The responses of the true state $x_1(t)$ (solid line) and its estimation $u_1(t)$ (dash line).

Therefore, we know from Theorem 4 that error-state system (8) of the delayed neural network described by (1) and (6) is globally asymptotically stable. The simulation results are shown in Figures 2 and 3, which demonstrate the effectiveness of the developed approach for the design of the state estimator for neural networks with leakage delay and time-varying delay.

5. Conclusions

In this paper, the state estimation problem has been investigated for neural networks with leakage delay and time-varying delay as well as general activation functions. By employing Lyapunov functional method and the matrix inequality techniques, a delay-dependent LMIs condition has been established to estimate the neuron state with some

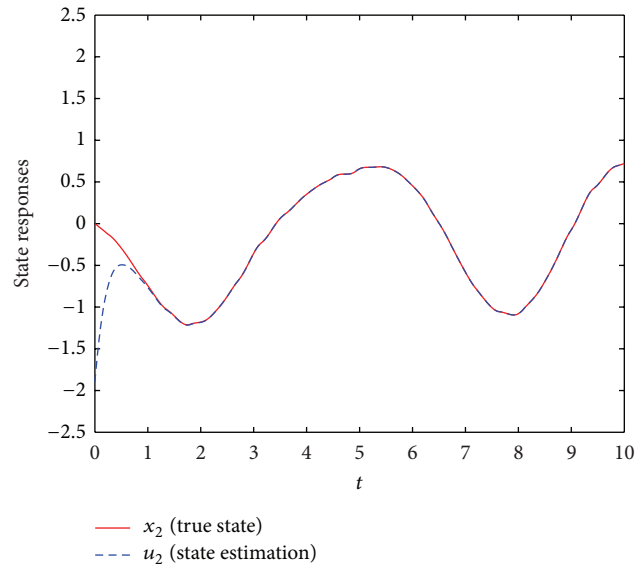

Figure 3: The responses of the true state $x_2(t)$ (solid line) and its estimation $u_2(t)$ (dash line).

observed output measurements such that the error-state system is globally asymptotically stable. An example has been provided to show the effectiveness of the proposed criterion.

Acknowledgments

The authors would like to thank the reviewers and the editor for their valuable suggestions and comments which have led to a much improved paper. This work was supported by the National Natural Science Foundation of China under Grants 61273021, 60974132, 11172247, and 51208538 and in part by the Natural Science Foundation Project of CQ cstc2013jjB40008.

References

[1] X. Yang, J. Cao, and J. Lu, "Synchronization of markovian coupled neural networks with nonidentical node-delays and random coupling strengths," *IEEE Transactions on Neural Networks and Learning Systems*, vol. 23, no. 1, pp. 60–71, 2012.

[2] T. Chen, W. Lu, and G. Chen, "Dynamical behaviors of a large class of general delayed neural networks," *Neural Computation*, vol. 17, no. 4, pp. 949–968, 2005.

[3] J. Cao and Q. Song, "Stability in Cohen-Grossberg-type bidirectional associative memory neural networks with time-varying delays," *Nonlinearity*, vol. 19, no. 7, pp. 1601–1617, 2006.

[4] Z. Zeng and W. Zheng, "Multistability of neural networks with time-varying delays and concave-convex characteristics," *IEEE Transactions on Neural Networks and Learning Systems*, vol. 23, no. 2, pp. 293–305, 2012.

[5] H. Zhang, F. Yang, X. Liu, and Q. Zhang, "Stability analysis for neural networks with time-varying delay based on quadratic convex combination," *IEEE Transactions on Neural Networks and Learning Systems*, vol. 24, no. 2, pp. 513–521, 2013.

[6] L. Jin, P. N. Nikiforuk, and M. M. Gupta, "Adaptive control of discrete-time nonlinear systems using recurrent neural networks," *IEE Proceedings*, vol. 141, no. 3, pp. 169–176, 1994.

[7] Z. Wang, D. W. C. Ho, and X. Liu, "State estimation for delayed neural networks," *IEEE Transactions on Neural Networks*, vol. 16, no. 1, pp. 279–284, 2005.

[8] Y. He, Q. Wang, M. Wu, and C. Lin, "Delay-dependent state estimation for delayed neural networks," *IEEE Transactions on Neural Networks*, vol. 17, no. 4, pp. 1077–1081, 2006.

[9] T. Li and S. Fei, "Exponential state estimation for recurrent neural networks with distributed delays," *Neurocomputing*, vol. 71, no. 1–3, pp. 428–438, 2007.

[10] Z. Wang, Y. Liu, and X. Liu, "State estimation for discrete-time Markovian jumping neural networks with mixed mode-dependent delays," *Physics Letters A*, vol. 372, no. 48, pp. 7147–7155, 2008.

[11] S. Mou, H. Gao, W. Qiang, and Z. Fei, "State estimation for discrete-time neural networks with time-varying delays," *Neurocomputing*, vol. 72, no. 1–3, pp. 643–647, 2008.

[12] J. H. Park, O. M. Kwon, and S. M. Lee, "State estimation for neural networks of neutral-type with interval time-varying delays," *Applied Mathematics and Computation*, vol. 203, no. 1, pp. 217–223, 2008.

[13] H. Huang, G. Feng, and J. Cao, "Robust state estimation for uncertain neural networks with time-varying delay," *IEEE Transactions on Neural Networks*, vol. 19, no. 8, pp. 1329–1339, 2008.

[14] M. S. Mahmoud, "New exponentially convergent state estimation method for delayed neural networks," *Neurocomputing*, vol. 72, no. 16–18, pp. 3935–3942, 2009.

[15] Y. Liu, Z. Wang, and X. Liu, "State estimation for jumping recurrent neural networks with discrete and distributed delays," *Neural Networks*, vol. 22, no. 1, pp. 41–48, 2009.

[16] J. H. Park and O. M. Kwon, "Further results on state estimation for neural networks of neutral-type with time-varying delay," *Applied Mathematics and Computation*, vol. 208, no. 1, pp. 69–75, 2009.

[17] H. Huang, G. Feng, and J. Cao, "State estimation for static neural networks with time-varying delay," *Neural Networks*, vol. 23, no. 10, pp. 1202–1207, 2010.

[18] Z. Wang, Y. Liu, X. Liu, and Y. Shi, "Robust state estimation for discrete-time stochastic neural networks with probabilistic measurement delays," *Neurocomputing*, vol. 74, no. 1–3, pp. 256–264, 2010.

[19] C. K. Ahn, "Delay-dependent state estimation of T-S fuzzy delayed Hopfield neural networks," *Nonlinear Dynamics*, vol. 61, no. 3, pp. 483–489, 2010.

[20] Z. Wu, H. Su, and J. Chu, "State estimation for discrete Markovian jumping neural networks with time delay," *Neurocomputing*, vol. 73, no. 10–12, pp. 2247–2254, 2010.

[21] P. Balasubramaniam, S. Lakshmanan, and S. J. S. Theesar, "State estimation for Markovian jumping recurrent neural networks with interval time-varying delays," *Nonlinear Dynamics*, vol. 60, no. 4, pp. 661–675, 2010.

[22] H. Wang and Q. Song, "State estimation for neural networks with mixed interval time-varying delays," *Neurocomputing*, vol. 73, no. 7–9, pp. 1281–1288, 2010.

[23] H. Huang and G. Feng, "A scaling parameter approach to delay-dependent state estimation of delayed neural networks," *IEEE Transactions on Circuits and Systems II*, vol. 57, no. 1, pp. 36–40, 2010.

[24] X. Li and R. Rakkiyappan, "Robust asymptotic state estimation of Takagi-Sugeno fuzzy Markovian jumping Hopfield neural networks with mixed interval time-varying delays," *Mathematical Methods in the Applied Sciences*, vol. 34, no. 17, pp. 2197–2207, 2011.

[25] P. Balasubramaniam, M. Kalpana, and R. Rakkiyappan, "State estimation for fuzzy cellular neural networks with time delay in the leakage term, discrete and unbounded distributed delays," *Computers & Mathematics with Applications*, vol. 62, no. 10, pp. 3959–3972, 2011.

[26] P. Balasubramaniam, V. Vembarasan, and R. Rakkiyappan, "Delay-dependent robust exponential state estimation of Markovian jumping fuzzy Hopfield neural networks with mixed random time-varying delays," *Communications in Nonlinear Science and Numerical Simulation*, vol. 16, no. 4, pp. 2109–2129, 2011.

[27] H. Bao and J. Cao, "Delay-distribution-dependent state estimation for discrete-time stochastic neural networks with random delay," *Neural Networks*, vol. 24, no. 1, pp. 19–28, 2011.

[28] D. Zhang and L. Yu, "Exponential state estimation for Markovian jumping neural networks with time-varying discrete and distributed delays," *Neural Networks*, vol. 35, pp. 103–111, 2012.

[29] S. Lakshmanan, J. H. Park, D. H. Ji, H. Y. Jung, and G. Nagamani, "State estimation of neural networks with time-varying delays and Markovian jumping parameter based on passivity theory," *Nonlinear Dynamics*, vol. 70, no. 2, pp. 1421–1434, 2012.

[30] Y. Chen and W. X. Zheng, "Stochastic state estimation for neural networks with distributed delays and Markovian jump," *Neural Networks*, vol. 25, pp. 14–20, 2012.

[31] X. Kan, Z. Wang, and H. Shu, "State estimation for discrete-time delayed neural networks with fractional uncertainties and sensor saturations," *Neurocomputing*, vol. 117, pp. 64–71, 2013.

[32] T. H. Lee, J. H. Park, O. M. Kwon, and S. M. Lee, "Stochastic sampled-data control for state estimation of time-varying delayed neural networks," *Neural Networks*, vol. 46, pp. 99–108, 2013.

[33] C. K. Ahn, "State estimation for T-S fuzzy Hopfield neural networks via strict output passivation of the error system," *International Journal of General Systems*, vol. 42, no. 5, pp. 503–518, 2013.

[34] H. Huang, T. Huang, and X. Chen, "Guaranteed H_∞ performance state estimation of delayed static neural networks," *IEEE Transactions on Circuits and Systems II*, vol. 60, no. 6, pp. 371–375, 2013.

[35] S. Lakshmanan, V. Vembarasan, and P. Balasubramaniam, "Delay decomposition approach to state estimation of neural networks with mixed time-varying delays and Markovian jumping parameters," *Mathematical Methods in the Applied Sciences*, vol. 36, no. 4, pp. 395–412, 2013.

[36] J. Liang, Z. Wang, B. Shen, and X. Liu, "Distributed state estimation in sensor networks with randomly occurring nonlinearities subject to time-delays," *ACM Transactions on Sensor Networks*, vol. 9, no. 1, article 4, 2012.

[37] J. Liang, Z. Wang, and X. Liu, "Distributed state estimation for uncertain Markov-type sensor networks with mode-dependent distributed delays," *International Journal of Robust and Nonlinear Control*, vol. 22, no. 3, pp. 331–346, 2012.

[38] J. Liang, Z. Wang, and X. Liu, "Distributed state estimation for discrete-time sensor networks with randomly varying nonlinearities and missing measurements," *IEEE Transactions on Neural Networks*, vol. 22, no. 3, pp. 486–496, 2011.

[39] K. Gopalsamy, "Leakage delays in BAM," *Journal of Mathematical Analysis and Applications*, vol. 325, no. 2, pp. 1117–1132, 2007.

[40] Y. Liu, Z. Wang, and X. Liu, "Global exponential stability of generalized recurrent neural networks with discrete and distributed delays," *Neural Networks*, vol. 19, no. 5, pp. 667–675, 2006.

Hindawi Publishing Corporation
Abstract and Applied Analysis
Volume 2013, Article ID 524028, 9 pages
http://dx.doi.org/10.1155/2013/524028

Research Article

Passivity Analysis and Passive Control for T-S Fuzzy Systems with Leakage Delay and Mixed Time-Varying Delays

Ting Lei,[1] Zengshun Chen,[2] Qiankun Song,[1] and Zhenjiang Zhao[3]

[1] *Department of Mathematics, Chongqing Jiaotong University, Chongqing 400074, China*
[2] *School of Civil Engineering & Architecture, Chongqing Jiaotong University, Chongqing 400074, China*
[3] *Department of Mathematics, Huzhou Teachers College, Huzhou 313000, China*

Correspondence should be addressed to Qiankun Song; qiankunsong@gmail.com

Received 17 July 2013; Accepted 24 August 2013

Academic Editor: Xinsong Yang

The passivity and passification for Takagi-Sugeno (T-S) fuzzy systems with leakage delay and both discrete and distributed time-varying delays are investigated. By employing the Lyapunov functional method and using the matrix inequality techniques, several delay-dependent criteria to ensure the passivity and passification of the considered T-S fuzzy systems are established in terms of linear matrix inequalities (LMIs) that can be easily checked by using the standard numerical software. The obtained results generalize some previous results. Two examples are given to show the effectiveness of the proposed criteria.

1. Introduction

The Takagi-Sugeno (T-S) fuzzy system, initially proposed and studied by Takagi and Sugeno [1], has attracted increasing interest due to the fact that it provides a general framework to represent a nonlinear plant by using a set of local linear models which are smoothly connected through nonlinear fuzzy membership functions [2]. In practice, time delays often occur in many dynamic systems such as chemical processes, metallurgical processes, biological systems, and neural networks [3]. The existence of time delays is usually a source of instability and poor performance [4]. Therefore, the study of stability with consideration of time delays becomes extremely important [5]. Recently, the stability and stabilization of T-S fuzzy systems with delays have been extensively studied; for example, see [3–13] and references therein.

On the other hand, the passivity theory is another effective tool to the stability analysis of the system [14]. The main idea of passivity theory is that the passive properties of the system can keep the system internal stability [15]. For these reasons, the passivity and passification problems have been an active area of research recently. The passification problem, which is also called the passive control problem, is formulated as the problem of finding a suitable controller such that the resulting closed-loop system is passive. Recently, some authors have studied the passivity of some systems and obtained sufficient conditions for checking the passivity of the systems that include linear systems with delays [14–16], delayed neural networks [17, 18], networked control systems [19], nonlinear discrete-time systems with direct input-output link [20], and T-S fuzzy systems [21–25]. In [21], the stability of fuzzy control loops is proven with the unique condition that the controlled plant can be made passive by zero shifting. For linear time-invariant plants, this approach leads to frequency response conditions similar to the previous results in the literature, but which are more general and can include robust stability considerations. In [23], the passivity and feedback passification of T-S fuzzy systems with time delays are considered. Both delay-independent and delay-dependent results are presented, and the theoretical results are given in terms of LMIs. In [24], discrete-time T-S fuzzy systems with delays were considered, and several sufficient conditions for checking passivity and passification were obtained. In [25], the contiguous-time T-S fuzzy systems with time-varying delays were investigated, and several criteria to ensure the passivity and feedback passification were given. In [22], the passivity and feedback passification of T-S fuzzy systems with both discrete and distributed time-varying

delays were investigated without assuming the differentiability of the time-varying delays. By employing appropriate Lyapunov-Krasovskii functionals, several delay-dependent criteria for the passivity of the considered T-S fuzzy systems were established in terms of LMIs.

Recently, Gopalsamy initially investigated the bidirectional associative memory (BAM) neural networks with constant delays in the leakage terms and derived several sufficient conditions for the existence of a unique equilibrium as well as its asymptotic and exponential stability [26]. Inspired by this work, authors considered the T-S fuzzy systems with constant leakage delay and investigated their stability problem [7]. As pointed out in [7], T-S fuzzy systems with leakage delay are a class of important T-S fuzzy systems: time delay in the leakage term also has great impact on the dynamics of T-S fuzzy systems since time delay in the stabilizing negative feedback term has a tendency to destabilize a system. To the best of the authors knowledge, there is no results on the problem of passivity for T-S fuzzy systems with leakage delay. Therefore, there is a need to further extend the passivity results reported in [22].

Motivated by the above discussions, the objective of this paper is to study the passivity and feedback passification of T-S fuzzy systems with leakage delay and mixed time-varying delays by employing new Lyapunov-Krasovskii functionals and using matrix inequality techniques. The obtained sufficient conditions do not require the differentiability of time-varying delays and are expressed in terms of linear matrix inequalities, which can be checked numerically using the effective LMI toolbox in MATLAB. Two examples are given to show the effectiveness and less conservatism of the proposed criteria.

Notations. The notations are quite standard. Throughout this paper, $\mathbb{R}^n$ and $\mathbb{R}^{n\times m}$ denote, respectively, the n-dimensional Euclidean space and the set of all $n\times m$ real matrices. $\|\cdot\|$ refers to the Euclidean vector norm. A^T represents the transpose of matrix A, and the asterisk "$*$" in a matrix is used to represent the term which is induced by symmetry. I is the identity matrix with compatible dimension. $X > Y$ means that X and Y are symmetric matrices and that $X - Y$ is positive definite. Matrices, if not explicitly specified, are assumed to have compatible dimensions.

2. Model Description and Preliminaries

Consider a continuous time T-S fuzzy system with discrete and distributed time-varying delays as well as leakage delay, and the ith rule of the model is of the following form.

Plant Rule i. If $z_1(t)$ is M_{i1} and...and $z_p(t)$ is M_{ip}, then

$$\begin{aligned}\dot{x}(t) &= A_i x(t-\delta) + B_i x(t-\tau(t)) \\ &\quad + W_i \int_{t-d(t)}^{t} x(s)\,ds + U_i w(t), \\ y(t) &= C_i x(t-\delta) + D_i x(t-\tau(t)) \\ &\quad + H_i \int_{t-d(t)}^{t} x(s)\,ds + V_i w(t), \\ x(s) &= \phi(s), \quad s \in [-\rho, 0],\end{aligned} \tag{1}$$

where $t \geq 0$, $i = 1, 2, \ldots, r$, and r is the number of If-then rules; $z_1(t), z_2(t), \ldots, z_p(t)$ are the premise variables; each M_{ij} ($j = 1, 2, \ldots, p$) is a fuzzy set; $x(t) = (x_1(t), x_2(t), \ldots, x_n(t))^T \in \mathbb{R}^n$ is the state vector of the system at time t; $w(t) = (w_1(t), w_2(t), \ldots, w_q(t))^T \in \mathbb{R}^q$ is the square integrable exogenous input; $y(t) = (y_1(t), y_2(t), \ldots, y_q(t))^T \in \mathbb{R}^q$ is the output vector of the system; δ, $\tau(t)$, and $d(t)$ denote the leakage delay, the discrete time-varying delay, and the distributed time-varying delay, respectively, and satisfy $0 \leq \tau(t) \leq \tau$, $0 \leq d(t) \leq d$, where τ and d are constants; $\phi(s)$ is bounded and continuously differentiable on $[-\rho, 0]$, where $\rho = \max\{\delta, \tau, d\}$; A_i, B_i, W_i, U_i, C_i, D_i, H_i, and V_i are some given constant matrices with appropriate dimensions.

Let $\mu_i(t)$ be the normalized membership function of the inferred fuzzy set $\gamma_i(t)$; that is,

$$\mu_i(t) = \frac{\gamma_i(t)}{\sum_{i=1}^{r} \gamma_i(t)}, \tag{2}$$

where $\gamma_i(t) = \prod_{j=1}^{p} M_{ij}(z_j(t))$ with $M_{ij}(z_j(t))$ being the grade of membership function of $z_j(t)$ in $M_{ij}(t)$. It is assumed that $\gamma_i(t) \geq 0$ ($i = 1, 2, \ldots, r$) and $\sum_{i=1}^{r} \gamma_i(t) > 0$ for all t. Thus, $\mu_i(t) \geq 0$ and $\sum_{i=1}^{r} \mu_i(t) = 1$ for all t. And the T-S fuzzy model (1) can be defuzzied as

$$\begin{aligned}\dot{x}(t) &= \sum_{i=1}^{r} \mu_i(t) \Big[A_i x(t-\delta) + B_i x(t-\tau(t)) \\ &\quad + W_i \int_{t-d(t)}^{t} x(s)\,ds + U_i w(t) \Big], \\ y(t) &= \sum_{i=1}^{r} \mu_i(t) \Big[C_i x(t-\delta) + D_i x(t-\tau(t)) \\ &\quad + H_i \int_{t-d(t)}^{t} x(s)\,ds + V_i w(t) \Big], \\ x(s) &= \phi(s), \quad s \in [-\rho, 0].\end{aligned} \tag{3}$$

In the literature, there are different definitions of passivity. In this paper, we adopt the following widely accepted definition of passivity, which can been found in [22].

Definition 1. System (1) is called passive if there exists a scalar $\gamma > 0$ such that

$$2\int_0^{t_p} y^T(s)\, w(s)\, ds \geq -\gamma \int_0^{t_p} w^T(s)\, w(s)\, ds \tag{4}$$

for all $t_p \geq 0$ and for the solution of (1) with $\phi(\cdot) \equiv 0$.

To prove our results, the following lemma that can be found in [27] is necessary.

Lemma 2 (see [27]). *For any constant matrix $W \in \mathbb{R}^{m\times m}$, $W > 0$, scalar $0 < h(t) < h$, vector function $\omega(\cdot) : [0,h] \to \mathbb{R}^m$ such that the integrations concerned are well defined; then,*

$$\left(\int_0^{h(t)} \omega(s)\,ds\right)^T W \left(\int_0^{h(t)} \omega(s)\,ds\right) \le h(t)\int_0^{h(t)} \omega^T(s) W \omega(s)\,ds. \tag{5}$$

3. Main Results

Theorem 3. *Model* (1) *is passive in the sense of Definition 1 if there exist a scalar $\gamma > 0$, three symmetric positive definite matrices P_1, P_2, and P_3, and eleven matrices Q_1, Q_2, X_{11}, X_{12}, X_{22}, Y_{ij} $(i, j = 1, 2, 3, i \le j)$ such that the following LMIs hold for $i = 1, 2, \ldots, r$:*

$$X = \begin{bmatrix} X_{11} & X_{12} \\ * & X_{22} \end{bmatrix} > 0, \tag{6}$$

$$Y = \begin{bmatrix} Y_{11} & Y_{12} & Y_{13} \\ * & Y_{22} & Y_{23} \\ * & * & Y_{33} \end{bmatrix} > 0, \tag{7}$$

$$\Pi_i = \begin{bmatrix} \Pi_{11} & X_{11}-Q_1 & -X_{12}+Q_1A_i & \Pi_{14,i} & X_{22} & Q_1W_i & Q_1U_i \\ * & \Pi_{22} & Q_2A_i & Q_2B_i & X_{12} & Q_2W_i & Q_1U_i \\ * & * & -P_1 & 0 & -X_{22} & 0 & -C_i^T \\ * & * & * & \Pi_{44} & 0 & 0 & -D_i^T \\ * & * & * & * & -P_2 & 0 & 0 \\ * & * & * & * & * & -P_3 & -H_i^T \\ * & * & * & * & * & * & \Pi_{77,i} \end{bmatrix} < 0, \tag{8}$$

where $\Pi_{11} = P_1 + \delta^2 P_2 + d^2 P_3 + X_{12} + X_{12}^T + \tau Y_{11} + Y_{13} + Y_{13}^T$, $\Pi_{14,i} = \tau Y_{12} - Y_{13} + Y_{23}^T + Q_1 B_i$, $\Pi_{22} = \tau Y_{33} - Q_2 - Q_2^T$, $\Pi_{44} = \tau Y_{22} - Y_{23} - Y_{23}^T$, *and* $\Pi_{77,i} = -V_i - V_i^T - \gamma I$.

Proof. From condition (7), we know that $Y_{33} > 0$. Consider the following Lyapunov-Krasovskii functional as

$$V(t) = V_1(t) + V_2(t) + V_3(t) + V_4(t), \tag{9}$$

where

$$\begin{aligned} V_1(t) &= \int_{t-\delta}^{t} x^T(s) P_1 x(s)\,ds + \delta \int_{-\delta}^{0}\int_{t+\xi}^{t} x^T(s) P_2 x(s)\,ds\,d\xi \\ &\quad + d\int_{-d}^{0}\int_{t+\xi}^{t} x^T(s) P_3 x(s)\,ds\,d\xi, \\ V_2(t) &= \begin{bmatrix} x(t) \\ \int_{t-\delta}^{t} x(s)ds \end{bmatrix}^T \begin{bmatrix} X_{11} & X_{12} \\ * & X_{22} \end{bmatrix} \begin{bmatrix} x(t) \\ \int_{t-\delta}^{t} x(s)\,ds \end{bmatrix}, \\ V_3(t) &= \int_{t-\tau}^{t}\int_{\xi}^{t} \dot{x}^T(s) Y_{33} \dot{x}(s)\,ds\,d\xi, \\ V_4(t) &= \int_0^t \int_{\xi-\tau(\xi)}^{\xi} u^T(\xi,s) Y u(\xi,s)\,ds\,d\xi, \end{aligned} \tag{10}$$

and $u(\xi,s) = (x^T(\xi), x^T(\xi-\tau(\xi)), \dot{x}^T(s))^T$.

Calculating the time derivative of $V(t)$ and using Lemma 2, we obtain that

$$\begin{aligned} \dot{V}_1(t) &= x^T(t)\left(P_1 + \delta^2 P_2 + d^2 P_3\right) x(t) \\ &\quad - x^T(t-\delta) P_1 x(t-\delta) \\ &\quad - \delta\int_{t-\delta}^{t} x^T(s) P_2 x(s)\,ds - d\int_{t-d}^{t} x^T(s) P_3 x(s)\,ds \\ &\le x^T(t)\left(P_1 + \delta^2 P_2 + d^2 P_3\right) x(t) \\ &\quad - x^T(t-\delta) P_1 x(t-\delta) \\ &\quad - \left(\int_{t-\delta}^{t} x(s)\,ds\right)^T P_2 \left(\int_{t-\delta}^{t} x(s)\,ds\right) \\ &\quad - \left(\int_{t-d(t)}^{t} x(s)\,ds\right)^T P_3 \left(\int_{t-d(t)}^{t} x(s)\,ds\right), \\ \dot{V}_2(t) &= 2\begin{bmatrix} x(t) \\ \int_{t-\delta}^{t} x(s)ds \end{bmatrix}^T \begin{bmatrix} X_{11} & X_{12} \\ * & X_{22} \end{bmatrix} \begin{bmatrix} \dot{x}(t) \\ x(t) - x(t-\delta) \end{bmatrix} \\ &= x^T(t)\left(X_{12} + X_{12}^T\right) x(t) + 2x^T(t) X_{11} \dot{x}(t) \\ &\quad - 2x^T(t) X_{12} x(t-\delta) + 2x^T(t) X_{22} \int_{t-\delta}^{t} x(s)\,ds \\ &\quad + 2\dot{x}^T(t) X_{12} \int_{t-\delta}^{t} x(s)\,ds \\ &\quad - 2x^T(t-\delta) X_{22} \int_{t-\delta}^{t} x(s)\,ds, \\ \dot{V}_3(t) &= \tau \dot{x}^T(t) Y_{33} \dot{x}(t) - \int_{t-\tau}^{t} \dot{x}^T(s) Y_{33} \dot{x}(s)\,ds, \\ \dot{V}_4(t) &= \int_{t-\tau(t)}^{t} \left(x^T(t), x^T(t-\tau(t)), \dot{x}^T(s)\right) Y \\ &\quad \times \left(x^T(t), x^T(t-\tau(t)), \dot{x}^T(s)\right)^T ds \\ &= \tau(t) \begin{bmatrix} x(t) \\ x(t-\tau(t)) \end{bmatrix}^T \begin{bmatrix} Y_{11} & Y_{12} \\ Y_{12}^T & Y_{22} \end{bmatrix} \begin{bmatrix} x(t) \\ x(t-\tau(t)) \end{bmatrix} \\ &\quad + 2x^T(t) Y_{13} x(t) - 2x^T(t) Y_{13} x(t-\tau(t)) \\ &\quad + 2x^T(t-\tau(t)) Y_{23} x(t) \\ &\quad - 2x^T(t-\tau(t)) Y_{23} x(t-\tau(t)) \\ &\quad + \int_{t-\tau(t)}^{t} \dot{x}^T(s) Y_{33} \dot{x}(s)\,ds \\ &\le x^T(t)\left(\tau Y_{11} + Y_{13} + Y_{13}^T\right) x(t) \\ &\quad + 2x^T(t)\left(\tau Y_{12} - Y_{13} + Y_{23}^T\right) x(t-\tau(t)) \end{aligned}$$

$$+x^T(t-\tau(t))\left(\tau Y_{22}-Y_{23}-Y_{23}^T\right)x(t-\tau(t))+\int_{t-\tau}^{t}\dot{x}^T(s)Y_{33}\dot{x}(s)\,ds. \tag{11}$$

It follows from (11) that

$$\begin{aligned}\dot{V}(t)\le{}& x^T(t)\left(P_1+\delta^2P_2+d^2P_3+X_{12}+X_{12}^T+\tau Y_{11}+Y_{13}+Y_{13}^T\right)x(t)\\&+2x^T(t)X_{11}\dot{x}(t)-2x^T(t)X_{12}x(t-\delta)\\&+2x^T(t)\left(\tau Y_{12}-Y_{13}+Y_{23}^T\right)x(t-\tau(t))\\&+2x^T(t)X_{22}\int_{t-\delta}^{t}x(s)\,ds+\tau\dot{x}^T(t)Y_{33}\dot{x}(t)\\&+2\dot{x}^T(t)X_{12}\int_{t-\delta}^{t}x(s)\,ds\\&+x^T(t-\tau(t))\left(\tau Y_{22}-Y_{23}-Y_{23}^T\right)x(t-\tau(t))\\&-x^T(t-\delta)P_1x(t-\delta)\\&-2x^T(t-\delta)X_{22}\int_{t-\delta}^{t}x(s)\,ds\\&-\left(\int_{t-\delta}^{t}x(s)\,ds\right)^TP_2\left(\int_{t-\delta}^{t}x(s)\,ds\right)\\&-\left(\int_{t-d(t)}^{t}x(s)\,ds\right)^TP_3\left(\int_{t-d(t)}^{t}x(s)\,ds\right).\end{aligned} \tag{12}$$

From the first equation of (3), we have

$$\begin{aligned}0={}&2\left(x^T(t)Q_1+\dot{x}^T(t)Q_2\right)\\&\times\sum_{i=1}^{r}\mu_i(t)\Big[-\dot{x}(t)+A_ix(t-\delta)+B_ix(t-\tau(t))\\&\qquad+W_i\int_{t-d(t)}^{t}x(s)\,ds+U_iw(t)\Big]\\={}&\sum_{i=1}^{r}\mu_i(t)\Big(-2x^T(t)Q_1\dot{x}(t)+2x^T(t)Q_1A_ix(t-\delta)\\&\qquad+2x^T(t)Q_1B_ix(t-\tau(t))\\&\qquad+2x^T(t)Q_1W_i\int_{t-d(t)}^{t}x(s)\,ds\\&\qquad+2x^T(t)Q_1U_iw(t)\\&\qquad-2\dot{x}^T(t)Q_2\dot{x}(t)+2\dot{x}^T(t)Q_2A_ix(t-\delta)\\&\qquad+2\dot{x}^T(t)Q_2B_ix(t-\tau(t))\\&\qquad+2\dot{x}^T(t)Q_2W_i\int_{t-d(t)}^{t}x(s)\,ds\\&\qquad+2\dot{x}^T(t)Q_2U_iw(t)\Big).\end{aligned} \tag{13}$$

It follows from (12) and (13) that

$$\begin{aligned}&\dot{V}(t)-2w^T(t)y(t)-\gamma w^T(t)w(t)\\&\le\sum_{i=1}^{r}\mu_i(t)\Big[x^T(t)\left(P_1+\delta^2P_2+d^2P_3+X_{12}+X_{12}^T+\tau Y_{11}+Y_{13}+Y_{13}^T\right)x(t)\\&\quad+2x^T(t)\left(X_{11}-Q_1\right)\dot{x}(t)\\&\quad+2x^T(t)\left(-X_{12}+Q_1A_i\right)x(t-\delta)\\&\quad+2x^T(t)\left(\tau Y_{12}-Y_{13}+Y_{23}^T+Q_1B_i\right)\\&\quad\times x(t-\tau(t))\\&\quad+2x^T(t)X_{22}\int_{t-\delta}^{t}x(s)\,ds\\&\quad+2x^T(t)Q_1W_i\int_{t-d(t)}^{t}x(s)\,ds\\&\quad+2x^T(t)Q_1U_iw(t)\\&\quad+\dot{x}^T(t)\left(\tau Y_{33}-Q_2-Q_2^T\right)\dot{x}(t)\\&\quad+2\dot{x}^T(t)Q_2A_ix(t-\delta)\\&\quad+2\dot{x}^T(t)Q_2B_ix(t-\tau(t))\\&\quad+2\dot{x}^T(t)X_{12}\int_{t-\delta}^{t}x(s)\,ds\\&\quad+2\dot{x}^T(t)Q_2W_i\int_{t-d(t)}^{t}x(s)\,ds\\&\quad+2\dot{x}^T(t)Q_2U_iw(t)\\&\quad-x^T(t-\delta)P_1x(t-\delta)\\&\quad-2x^T(t-\delta)X_{22}\int_{t-\delta}^{t}x(s)\,ds\\&\quad-2x^T(t-\delta)C_i^Tw(t)\\&\quad+x^T(t-\tau(t))\left(\tau Y_{22}-Y_{23}-Y_{23}^T\right)\\&\quad\times x(t-\tau(t))-2x^T(t-\tau(t))D_i^Tw(t)\end{aligned}$$

$$
\begin{aligned}
&- \left(\int_{t-\delta}^{t} x(s)\, ds \right)^T P_2 \left(\int_{t-\delta}^{t} x(s)\, ds \right) \\
&- \left(\int_{t-d(t)}^{t} x(s)\, ds \right)^T P_3 \left(\int_{t-d(t)}^{t} x(s)\, ds \right) \\
&- 2\left(\int_{t-d(t)}^{t} x(s)\, ds \right)^T H_i^T w(t) \\
&+ w^T(t) \left(-V_i - V_i^T - \gamma I \right) w(t) \Bigg] \\
&= \sum_{i=1}^{r} \mu_i(t)\, z^T(t)\, \Pi_i z(t),
\end{aligned} \tag{14}
$$

where $z(t) = (x^T(t), \dot{x}^T(t), x^T(t-\delta), x^T(t-\tau(t)), \int_{t-\delta}^{t} x^T(s)ds, \int_{t-d(t)}^{t} x^T(s)ds, w^T(t))^T$. Thus, one can derive from (8) and (14) that

$$
\dot{V}(t) - 2w^T(t)\, y(t) - \gamma w^T(t)\, w(t) \le 0. \tag{15}
$$

By integrating (15) with respect to t from 0 to t_p, we obtain

$$
\begin{aligned}
2\int_0^{t_p} w^T(s)\, y(s)\, ds &\ge V\left(x\left(t_p \right) \right) \\
&- V(x(0)) - \gamma \int_0^{t_p} w^T(s)\, w(s)\, ds.
\end{aligned} \tag{16}
$$

From the definition of $V(x(t))$, we have $V(x(t_p)) \ge 0$ and $V(x(0) = 0$ when $\phi(\cdot) \equiv 0$. Thus,

$$
2\int_0^{t_p} w^T(s)\, y(s)\, ds \ge -\gamma \int_0^{t_p} w^T(s)\, w(s)\, ds \tag{17}
$$

holds for all $t_p \ge 0$. The proof is completed. □

Next, we consider the passification problem; that is, a state feedback controller is to be designed to make the closed-loop fuzzy system passive. Extending on system (1), we consider the following T-S fuzzy system with control input.

Plant Rule i. If $z_1(t)$ is M_{i1} and ... and $z_p(t)$ is M_{ip}, then

$$
\begin{aligned}
\dot{x}(t) &= A_i x(t-\delta) + B_i x(t-\tau(t)) \\
&+ W_i \int_{t-d(t)}^{t} x(s)\, ds + U_i w(t) + R_i u(t), \\
y(t) &= C_i x(t-\delta) + D_i x(t-\tau(t)) \\
&+ H_i \int_{t-d(t)}^{t} x(s)\, ds + V_i w(t), \\
x(s) &= \phi(s), \quad s \in [-\rho, 0],
\end{aligned} \tag{18}
$$

where $u(t) \in R^l$ is the control input, R_i is a constant matrix with appropriate dimension.

Controller Rule i. If $z_1(t)$ is M_{i1} and ... and $z_p(t)$ is M_{ip}, then

$$
u(t) = K_i x(t), \quad i = 1, 2, \ldots, r. \tag{19}
$$

And the overall state feedback controller is presented by

$$
u(t) = \sum_{j=1}^{r} \mu_j(t)\, K_j x(t), \tag{20}
$$

where $\mu_j(t)$ is defined as before. The closed-loop fuzzy system can be represented as

$$
\begin{aligned}
\dot{x}(t) &= \sum_{i=1}^{r} \sum_{j=1}^{r} \mu_i(t)\, \mu_j(t) \\
&\times \Bigg[R_i K_j x(t) + A_i x(t-\delta) + B_i x(t-\tau(t)) \\
&+ W_i \int_{t-\sigma(t)}^{t} x(s)\, ds + U_i w(t) \Bigg], \\
y(t) &= \sum_{i=1}^{r} \mu_i(t) \\
&\times \Bigg[C_i x(t) + D_i x(t-\tau(t)) \\
&+ H_i \int_{t-\sigma(t)}^{t} x(s)\, ds + V_i w(t) \Bigg], \\
x(s) &= \phi(s), \quad s \in [-\rho, 0].
\end{aligned} \tag{21}
$$

The following theorem establishes the main result of the state feedback passification.

Theorem 4. *The closed-loop fuzzy system* (21) *is passive in the sense of Definition 1 if there exist a scalar $\gamma > 0$, four symmetric positive definite matrices E_1, E_2, E_3, and S, and matrices F_{11}, F_{12}, F_{22}, G_{ij} $(i, j = 1, 2, 3, i \le j)$, and Z_j $(j = 1, 2, \ldots, r)$ such that the following LMIs hold for $i, j = 1, 2, \ldots, r$:*

$$
X = \begin{bmatrix} X_{11} & X_{12} \\ * & X_{22} \end{bmatrix} > 0, \tag{22}
$$

$$
Y = \begin{bmatrix} Y_{11} & Y_{12} & Y_{13} \\ * & Y_{22} & Y_{23} \\ * & * & Y_{33} \end{bmatrix} > 0, \tag{23}
$$

$$
\Omega_{ij} = \begin{bmatrix}
\Omega_{11,ij} & \Omega_{12,ij} & -F_{12} + A_i S & \Omega_{14,i} & F_{22} & W_i S & U_i \\
* & \Omega_{22} & A_i S & B_i S & F_{12} & W_i S & U_i \\
* & * & -E_1 & 0 & -F_{22} & 0 & -SC_i^T \\
* & * & * & \Omega_{44} & 0 & 0 & -SD_i^T \\
* & * & * & * & -E_2 & 0 & 0 \\
* & * & * & * & * & -E_3 & -SH_i^T \\
* & * & * & * & * & * & \Omega_{77,i}
\end{bmatrix} < 0, \tag{24}
$$

where $\Omega_{11,ij} = E_1 + \delta^2 E_2 + d^2 E_3 + F_{12} + F_{12}^T + \tau G_{11} + G_{13} + G_{13}^T + R_i Z_j + Z_j^T R_i^T$, $\Omega_{12,ij} = F_{11} - S + Z_j^T R_i^T$, $\Omega_{14,i} = \tau G_{12} - G_{13} + G_{23}^T + B_i S$, $\Omega_{22} = \tau G_{33} - 2S$, $\Omega_{44} = \tau G_{22} - G_{23} - G_{23}^T$, and $\Omega_{77,i} = -V_i - V_i^T - \gamma I$.

Moreover, the state feedback gains can be constructed as

$$
K_j = Z_j S^{-1}, \quad j = 1, 2, \ldots, r. \tag{25}
$$

Proof. Structure Lyapunov-Krasovskii functional (9), where $P_1 = S^{-1}E_1S^{-1}$, $P_2 = S^{-1}E_2S^{-1}$, $P_3 = S^{-1}E_3S^{-1}$, $X_{ij} = S^{-1}F_{ij}S^{-1}$ ($i = 1, 2, i \le j$), and $Y_{ij} = S^{-1}G_{ij}S^{-1}$ ($i = 1, 2, 3, i \le j$).

From the first equation of (21), we have

$$\begin{aligned}
0 &= 2\left(x^T(t) + \dot{x}^T(t)\right)S^{-1} \\
&\quad \times \sum_{i=1}^{r}\sum_{j=1}^{r}\mu_i(t)\mu_j(t) \\
&\quad \times \Bigg[-\dot{x}(t) + R_iK_jx(t) + A_ix(t-\delta) \\
&\qquad + B_ix(t-\tau(t)) + W_i\int_{t-\sigma(t)}^{t} x(s)\,ds + U_iw(t) \Bigg] \\
&= \sum_{i=1}^{r}\sum_{j=1}^{r}\mu_i(t)\mu_j(t) \\
&\quad \times \Bigg(2x^T(t)S^{-1}R_iK_jx(t) \\
&\qquad + x^T(t)\left(-2S^{-1} + 2K_j^TR_i^TS^{-1}\right)\dot{x}(t) \\
&\qquad + 2x^T(t)S^{-1}A_ix(t-\delta) \\
&\qquad + 2x^T(t)S^{-1}B_ix(t-\tau(t)) \\
&\qquad + 2x^T(t)S^{-1}W_i\int_{t-d(t)}^{t} x(s)\,ds \\
&\qquad + 2x^T(t)S^{-1}U_iw(t) - 2\dot{x}^T(t)S^{-1}\dot{x}(t) \\
&\qquad + 2\dot{x}^T(t)S^{-1}A_ix(t-\delta) \\
&\qquad + 2\dot{x}^T(t)S^{-1}B_ix(t-\tau(t)) \\
&\qquad + 2\dot{x}^T(t)S^{-1}W_i\int_{t-d(t)}^{t} x(s)\,ds \\
&\qquad + 2\dot{x}^T(t)S^{-1}U_iw(t) \Bigg).
\end{aligned} \tag{26}$$

It follows from (12) and (26) that

$$\begin{aligned}
&\dot{V}(t) - 2w^T(t)y(t) - \gamma w^T(t)w(t) \\
&\quad \le \sum_{i=1}^{r}\sum_{j=1}^{r}\mu_i(t)\mu_j(t) \\
&\qquad \times \Bigg[x^T(t)\Big(P_1 + \delta^2P_2 + d^2P_3 + X_{12} + X_{12}^T \\
&\qquad\qquad + \tau Y_{11} + Y_{13} + Y_{13}^T + S^{-1}R_iK_j \\
&\qquad\qquad + K_j^TR_i^TS^{-1}\Big)x(t) \\
&\qquad + 2x^T(t)\left(X_{11} - S^{-1} + K_j^TR_i^TS^{-1}\right)\dot{x}(t) \\
&\qquad + 2x^T(t)\left(-X_{12} + S^{-1}A_i\right)x(t-\delta) \\
&\qquad + 2x^T(t)\left(\tau Y_{12} - Y_{13} + Y_{23}^T + S^{-1}B_i\right) \\
&\qquad \times x(t-\tau(t)) \\
&\qquad + 2x^T(t)X_{22}\int_{t-\delta}^{t} x(s)\,ds \\
&\qquad + 2x^T(t)S^{-1}W_i\int_{t-d(t)}^{t} x(s)\,ds \\
&\qquad + 2x^T(t)S^{-1}U_iw(t) \\
&\qquad + \dot{x}^T(t)\left(\tau Y_{33} - 2S^{-1}\right)\dot{x}(t) \\
&\qquad + 2\dot{x}^T(t)S^{-1}A_ix(t-\delta) \\
&\qquad + 2\dot{x}^T(t)S^{-1}B_ix(t-\tau(t)) \\
&\qquad + 2\dot{x}^T(t)X_{12}\int_{t-\delta}^{t} x(s)\,ds \\
&\qquad + 2\dot{x}^T(t)S^{-1}W_i\int_{t-d(t)}^{t} x(s)\,ds \\
&\qquad + 2\dot{x}^T(t)S^{-1}U_iw(t) \\
&\qquad - x^T(t-\delta)P_1x(t-\delta) \\
&\qquad - 2x^T(t-\delta)X_{22}\int_{t-\delta}^{t} x(s)\,ds \\
&\qquad - 2x^T(t-\delta)C_i^Tw(t) \\
&\qquad + x^T(t-\tau(t))\left(\tau Y_{22} - Y_{23} - Y_{23}^T\right) \\
&\qquad \times x(t-\tau(t)) \\
&\qquad - 2x^T(t-\tau(t))D_i^Tw(t) \\
&\qquad - \left(\int_{t-\delta}^{t} x(s)\,ds\right)^T P_2\left(\int_{t-\delta}^{t} x(s)\,ds\right) \\
&\qquad - \left(\int_{t-d(t)}^{t} x(s)\,ds\right)^T P_3\left(\int_{t-d(t)}^{t} x(s)\,ds\right) \\
&\qquad - 2\left(\int_{t-d(t)}^{t} x(s)\,ds\right)^T H_i^Tw(t) \\
&\qquad + w^T(t)\left(-V_i - V_i^T - \gamma I\right)w(t) \Bigg] \\
&\quad = \sum_{i=1}^{r}\sum_{j=1}^{r}\mu_i(t)\mu_j(t)\,z^T(t)\,\Xi_{ij}z(t),
\end{aligned} \tag{27}$$

where $z(t) = (x^T(t), \dot{x}^T(t), x^T(t-\delta), x^T(t-\tau(t)), \int_{t-\delta}^{t} x^T(s)ds, \int_{t-d(t)}^{t} x^T(s)ds, w^T(t))^T$, and

$$\Xi_{ij} = \begin{bmatrix} \Xi_{11,ij} & \Xi_{12,ij} & -S^{-1}F_{12}S^{-1} + S^{-1}A_i & \Xi_{14,i} & S^{-1}F_{22}S^{-1} & S^{-1}W_i & S^{-1}U_i \\ * & \Xi_{22} & S^{-1}A_i & S^{-1}B_i & S^{-1}F_{12}S^{-1} & S^{-1}W_i & S^{-1}U_i \\ * & * & -S^{-1}E_1S^{-1} & 0 & -S^{-1}F_{22}S^{-1} & 0 & -C_i^T \\ * & * & * & \Xi_{44} & 0 & 0 & -D_i^T \\ * & * & * & * & -S^{-1}E_2S^{-1} & 0 & 0 \\ * & * & * & * & * & -S^{-1}E_3S^{-1} & -H_i^T \\ * & * & * & * & * & * & \Xi_{77,i} \end{bmatrix} \tag{28}$$

with $\Xi_{11,ij} = S^{-1}(E_1 + \delta^2 E_2 + d^2 E_3 + F_{12} + F_{12}^T + \tau G_{11} + G_{13} + G_{13}^T)S^{-1} + S^{-1}R_iK_j + K_j^T R_i^T S^{-1}$, $\Xi_{12,ij} = S^{-1}F_{11}S^{-1} - S^{-1} + K_j^T R_i^T S^{-1}$, $\Xi_{14,i} = S^{-1}(\tau G_{12} - G_{13} + G_{23}^T + B_iS)S^{-1}$, $\Xi_{22} = \tau S^{-1}G_{33}S^{-1} - 2S^{-1}$, $\Xi_{44} = S^{-1}(\tau G_{22} - G_{23} - G_{23}^T)S^{-1}$, $\Xi_{77,i} = -V_i - V_i^T - \gamma I$.

Pre- and postmultiply Ξ_{ij} by matrix $\mathrm{diag}(S, S, S, S, S, S, I)$, we get that

$$\Pi_{ij} = \begin{bmatrix} \Pi_{11,ij} & \Pi_{12,ij} & -F_{12} + A_iS & \Pi_{14,i} & F_{22} & W_iS & U_i \\ * & \Pi_{22} & A_iS & B_iS & F_{12} & W_iS & U_i \\ * & * & -E_1 & 0 & -F_{22} & 0 & -SC_i^T \\ * & * & * & \Pi_{44} & 0 & 0 & -SD_i^T \\ * & * & * & * & -E_2 & 0 & 0 \\ * & * & * & * & * & -E_3 & -SH_i^T \\ * & * & * & * & * & * & \Pi_{77,i} \end{bmatrix} \tag{29}$$

with $\Pi_{11,ij} = E_1 + \delta^2 E_2 + d^2 E_3 + F_{12} + F_{12}^T + \tau G_{11} + G_{13} + G_{13}^T + R_iK_jS + SK_j^T R_i^T$, $\Pi_{12,ij} = F_{11} - S + SK_j^T R_i^T$, $\Pi_{14,i} = \tau G_{12} - G_{13} + G_{23}^T + B_iS$, $\Pi_{22} = \tau G_{33} - 2S$, $\Pi_{44} = \tau G_{22} - G_{23} - G_{23}^T$, and $\Pi_{77,i} = -V_i - V_i^T - \gamma I$.

Obviously, $\Xi_{ij} < 0$ and $\Pi_{ij} < 0$ are equivalent. And we get from condition (25) that $\Pi_{ij} = \Omega_{ij}$.

It follows from condition (24) and inequality (27) that

$$\dot{V}(t) - 2y^T(x(t))w(t) - \gamma w^T(t)w(t) \le 0, \tag{30}$$

which means

$$2\int_0^{t_p} y^T(x(s))u(s)ds \ge -\gamma \int_0^{t_p} u^T(s)u(s)ds. \tag{31}$$

From Definition 1, we know that the stochastic T-S fuzzy system (1) is passive in the sense of expectation. The proof is completed. □

4. Numerical Examples

To verify the effectiveness of the theoretical results of this paper, consider the following two examples.

Example 1. Consider a T-S fuzzy system (1) with $r = 2$, where $\delta = 0.2$, $\tau(t) = 0.5|\cos t|$, and $d(t) = 0.1|\cos(2t)|$,

$$A_1 = \begin{bmatrix} 0.8 & -0.2 \\ 0 & 0.6 \end{bmatrix}, \quad B_1 = \begin{bmatrix} 0.2 & -0.9 \\ -0.1 & 0.2 \end{bmatrix},$$

$$W_1 = \begin{bmatrix} -1.6 & 0.4 \\ 1.2 & 0.3 \end{bmatrix}, \quad U_1 = \begin{bmatrix} 0.1 & -0.2 \\ 0.1 & -0.1 \end{bmatrix},$$

$$C_1 = \begin{bmatrix} 0.2 & 0 \\ 0.1 & 0.1 \end{bmatrix}, \quad D_1 = \begin{bmatrix} 0 & -0.1 \\ 0.2 & 0.1 \end{bmatrix},$$

$$H_1 = \begin{bmatrix} 0.2 & -0.1 \\ -0.2 & -0.1 \end{bmatrix}, \quad V_1 = \begin{bmatrix} 0.1 & 0.2 \\ 0 & -0.1 \end{bmatrix},$$

$$A_2 = \begin{bmatrix} -0.7 & -0.6 \\ 1.1 & -0.1 \end{bmatrix}, \quad B_2 = \begin{bmatrix} -0.1 & -0.4 \\ -0.3 & -0.2 \end{bmatrix},$$

$$W_2 = \begin{bmatrix} 0.2 & 0.9 \\ -0.1 & 0.4 \end{bmatrix}, \quad U_2 = \begin{bmatrix} -0.6 & -0.2 \\ 0.5 & 0 \end{bmatrix},$$

$$C_2 = \begin{bmatrix} 0.1 & 0.5 \\ 0.2 & -0.4 \end{bmatrix}, \quad D_2 = \begin{bmatrix} 0.6 & -0.1 \\ -0.2 & 0.1 \end{bmatrix},$$

$$H_2 = \begin{bmatrix} -0.1 & 0.3 \\ -0.7 & -0.6 \end{bmatrix}, \quad V_2 = \begin{bmatrix} -0.1 & -0.2 \\ 0.8 & -0.3 \end{bmatrix}. \tag{32}$$

It can be verified that $\tau = 0.5$, $d = 0.1$. By using the MATLAB LMI Control Toolbox, a solution to the LMIs in (6)–(8) is found as follows:

$$P_1 = 10^{-9}\begin{bmatrix} 0.1318 & 0.0174 \\ 0.0174 & 0.1795 \end{bmatrix},$$

$$P_2 = 10^{-8}\begin{bmatrix} 0.1126 & -0.0105 \\ -0.0105 & 0.1813 \end{bmatrix},$$

$$P_3 = 10^{-8}\begin{bmatrix} 0.3237 & -0.0297 \\ -0.0297 & 0.4519 \end{bmatrix},$$

$$Q_1 = 10^{-10}\begin{bmatrix} 0.0548 & 0.0458 \\ 0.7636 & 0.5797 \end{bmatrix},$$

$$Q_2 = 10^{-9}\begin{bmatrix} 0.1094 & 0.0750 \\ 0.0967 & 0.1859 \end{bmatrix},$$

$$X_{11} = 10^{-10}\begin{bmatrix} 0.3230 & 0.3149 \\ 0.3149 & 0.6926 \end{bmatrix},$$

$$X_{12} = 10^{-9}\begin{bmatrix} -0.0972 & 0.0056 \\ -0.0134 & -0.1477 \end{bmatrix},$$

$$X_{22} = 10^{-9}\begin{bmatrix} 0.1644 & -0.0150 \\ -0.0150 & 0.2929 \end{bmatrix},$$

$$Y_{11} = 10^{-8}\begin{bmatrix} 0.1105 & 0.0483 \\ 0.0483 & 0.1743 \end{bmatrix},$$

$$Y_{12} = 10^{-8}\begin{bmatrix} -0.1175 & -0.0473 \\ -0.0510 & -0.1812 \end{bmatrix},$$

$$Y_{13} = 10^{-9}\begin{bmatrix} -0.4500 & -0.1940 \\ -0.1940 & -0.6933 \end{bmatrix},$$

$$Y_{22} = 10^{-8}\begin{bmatrix} 0.1157 & 0.0497 \\ 0.0497 & 0.1815 \end{bmatrix},$$

$$Y_{23} = 10^{-9}\begin{bmatrix} 0.4500 & 0.1940 \\ 0.1940 & 0.6933 \end{bmatrix},$$

$$Y_{33} = 10^{-9}\begin{bmatrix} 0.1618 & 0.0970 \\ 0.0970 & 0.2835 \end{bmatrix},$$

$$\gamma = 6.9261 \times 10^{9}. \tag{33}$$

According to Theorem 3, the considered model (1) is passive in the sense of Definition 1.

Example 2. We use the data of Example 1 in addition to

$$R_1 = \begin{bmatrix} 0.3 & 0.1 \\ 0.7 & -0.2 \end{bmatrix}, \qquad R_2 = \begin{bmatrix} -0.3 & 0.1 \\ -0.4 & -0.1 \end{bmatrix}. \tag{34}$$

By using the MATLAB LMI Control Toolbox, a solution to the LMIs in (22)–(24) is found as follows:

$$E_1 = \begin{bmatrix} 176.3972 & -120.7648 \\ -120.7648 & 318.6006 \end{bmatrix},$$

$$E_2 = \begin{bmatrix} 330.6365 & 13.3938 \\ 13.3938 & 485.5898 \end{bmatrix},$$

$$E_3 = \begin{bmatrix} 534.8304 & -124.7740 \\ -124.7740 & 945.8976 \end{bmatrix},$$

$$S = \begin{bmatrix} 49.8112 & 1.0593 \\ 1.0593 & 115.3239 \end{bmatrix},$$

$$F_{11} = \begin{bmatrix} 236.7653 & -230.2321 \\ -230.2321 & 436.0261 \end{bmatrix},$$

$$F_{12} = \begin{bmatrix} -44.4016 & -52.5502 \\ -14.9764 & -39.8274 \end{bmatrix},$$

$$F_{22} = \begin{bmatrix} 54.2464 & 7.9191 \\ 7.9191 & 96.0467 \end{bmatrix},$$

$$G_{11} = \begin{bmatrix} 226.1583 & -23.8308 \\ -23.8308 & 253.3605 \end{bmatrix},$$

$$G_{12} = \begin{bmatrix} -92.2107 & -144.1195 \\ -27.1469 & -174.7165 \end{bmatrix},$$

$$G_{13} = \begin{bmatrix} -46.2910 & -140.9230 \\ -15.2074 & -83.4028 \end{bmatrix},$$

$$G_{22} = \begin{bmatrix} 115.7710 & -1.7962 \\ -1.7962 & 362.7980 \end{bmatrix},$$

$$G_{23} = \begin{bmatrix} 52.3927 & -9.2251 \\ 5.1656 & 258.7547 \end{bmatrix},$$

$$G_{33} = \begin{bmatrix} 29.6087 & 5.0408 \\ 5.0408 & 240.9688 \end{bmatrix},$$

$$Z_1 = 10^{3}\begin{bmatrix} -0.1547 & 0.1479 \\ -2.0308 & 2.9733 \end{bmatrix},$$

$$Z_2 = 10^{3}\begin{bmatrix} -0.1547 & 0.1479 \\ -2.0308 & 2.9733 \end{bmatrix},$$

$$\gamma = 405.7666. \tag{35}$$

Subsequently, we can obtain from (25) that

$$K_1 = \begin{bmatrix} -3.1335 & 1.3116 \\ -41.3262 & 26.1620 \end{bmatrix},$$

$$K_2 = \begin{bmatrix} -3.1335 & 1.3116 \\ -41.3262 & 26.1620 \end{bmatrix}. \tag{36}$$

Thus, a fuzzy controller (20) with feedback gains K_1 and K_2 can be constructed to make the closed-loop T-S fuzzy system (21) passive.

5. Conclusions

In this paper, the passivity and passification for T-S fuzzy systems with both discrete and distributed time-varying delays have been investigated without assuming the differentiability of the time-varying delays. By utilizing the Lyapunov functional method and the matrix inequality techniques, several delay-dependent criteria to ensure the passivity of the considered T-S fuzzy systems have been established in terms of linear matrix inequalities (LMIs) that can be easily checked by using the standard numerical software. Two examples have been provided to demonstrate the effectiveness of the proposed criteria since the feasible solutions to the given LMIs criteria in this paper have been found.

Acknowledgments

The authors would like to thank the editor and the anonymous reviewers for their valuable suggestions and comments which have led to a much improved paper. This work was supported by the National Natural Science Foundation of China under Grants 61273021, 60974132, 11172247 and 51208538 and in part by the Natural Science Foundation Project of CQ cstc2013jjB40008.

References

[1] T. Takagi and M. Sugeno, "Fuzzy identification of systems and its applications to modeling and control," *IEEE Transactions on Systems, Man and Cybernetics*, vol. 15, no. 1, pp. 116–132, 1985.

[2] S. Xu, B. Song, J. Lu, and J. Lam, "Robust stability of uncertain discrete-time singular fuzzy systems," *Fuzzy Sets and Systems*, vol. 158, no. 20, pp. 2306–2316, 2007.

[3] C.-L. Chen, G. Feng, and X.-P. Guan, "Delay-dependent stability analysis and controller synthesis for discrete-time T-S fuzzy systems with time delays," *IEEE Transactions on Fuzzy Systems*, vol. 13, no. 5, pp. 630–643, 2005.

[4] X. Liu and H. Zhang, "Delay-dependent robust stability of uncertain fuzzy large-scale systems with time-varying delays," *Automatica*, vol. 44, no. 1, pp. 193–198, 2008.

[5] F. Liu, M. Wu, Y. He, and R. Yokoyama, "New delay-dependent stability criteria for T-S fuzzy systems with time-varying delay," *Fuzzy Sets and Systems*, vol. 161, no. 15, pp. 2033–2042, 2010.

[6] C. Peng and M.-R. Fei, "An improved result on the stability of uncertain T-S fuzzy systems with interval time-varying delay," *Fuzzy Sets and Systems*, vol. 212, pp. 97–109, 2013.

[7] S. Lakshmanan, R. Rakkiyappan, and P. Balasubramaniam, "Global robust stability criteria for T-S fuzzy systems with distributed delays and time delay in the leakage term," *Iranian Journal of Fuzzy Systems*, vol. 9, no. 2, pp. 127–146, 2012.

[8] J. An and G. Wen, "Improved stability criteria for time-varying delayed T-S fuzzy systems via delay partitioning approach," *Fuzzy Sets and Systems*, vol. 185, pp. 83–94, 2011.

[9] L. Wu, X. Su, P. Shi, and J. Qiu, "A new approach to stability analysis and stabilization of discrete-time T-S fuzzy time-varying delay systems," *IEEE Transactions on Systems, Man, and Cybernetics B*, vol. 41, no. 1, pp. 273–286, 2011.

[10] J. Liu and D. Yue, "Asymptotic and robust stability of T-S fuzzy genetic regulatory networks with time-varying delays," *International Journal of Robust and Nonlinear Control*, vol. 22, no. 8, pp. 827–840, 2012.

[11] O. M. Kwon, M. J. Park, S. M. Lee, and J. H. Park, "Augmented Lyapunov-Krasovskii functional approaches to robust stability criteria for uncertain Takagi-Sugeno fuzzy systems with time-varying delays," *Fuzzy Sets and Systems*, vol. 201, pp. 1–19, 2012.

[12] L. Figueredo, J. Ishihara, G. Borges, and A. Bauchspiess, "Delay-dependent robust stability analysis for time-delay T-S fuzzy systems with nonlinear local models," *Journal of Control, Automation and Electrical Systems*, vol. 24, no. 1-2, pp. 11–21, 2013.

[13] F. Ahmida and E. Tissir, "Exponential stability of uncertain T-S fuzzy switched systems with time delay," *International Journal of Automation and Computing*, vol. 10, no. 1, pp. 32–38, 2013.

[14] S.-I. Niculescu and R. Lozano, "On the passivity of linear delay systems," *IEEE Transactions on Automatic Control*, vol. 46, no. 3, pp. 460–464, 2001.

[15] E. Fridman and U. Shaked, "On delay-dependent passivity," *IEEE Transactions on Automatic Control*, vol. 47, no. 4, pp. 664–669, 2002.

[16] M. S. Mahmoud and A. Ismail, "Passivity and passification of time-delay systems," *Journal of Mathematical Analysis and Applications*, vol. 292, no. 1, pp. 247–258, 2004.

[17] C. Li and X. Liao, "Passivity analysis of neural networks with time delay," *IEEE Transactions on Circuits and Systems II*, vol. 52, no. 8, pp. 471–475, 2005.

[18] J. H. Park, "Further results on passivity analysis of delayed cellular neural networks," *Chaos, Solitons and Fractals*, vol. 34, no. 5, pp. 1546–1551, 2007.

[19] H. Gao, T. Chen, and T. Chai, "Passivity and passification for networked control systems," *SIAM Journal on Control and Optimization*, vol. 46, no. 4, pp. 1299–1322, 2007.

[20] E. M. Navarro-López and E. Fossas-Colet, "Feedback passivity of nonlinear discrete-time systems with direct input-output link," *Automatica*, vol. 40, no. 8, pp. 1423–1428, 2004.

[21] G. Calcev, R. Gorez, and M. De Neyer, "Passivity approach to fuzzy control systems," *Automatica*, vol. 34, no. 3, pp. 339–344, 1998.

[22] Q. Song, Z. Wang, and J. Liang, "Analysis on passivity and passification of T-S fuzzy systems with time-varying delays," *Journal of Intelligent & Fuzzy Systems*, vol. 24, no. 1, pp. 21–30, 2013.

[23] C. Li, H. Zhang, and X. Liao, "Passivity and passification of fuzzy systems with time delays," *Computers & Mathematics with Applications*, vol. 52, no. 6-7, pp. 1067–1078, 2006.

[24] X. Liu, "Passivity and passification analysis of uncertain discrete-time fuzzy systems," *Kybernetes*, vol. 38, no. 3-4, pp. 396–405, 2009.

[25] B. Zhang, W. X. Zheng, and S. Xu, "Passivity analysis and passive control of fuzzy systems with time-varying delays," *Fuzzy Sets and Systems*, vol. 174, pp. 83–98, 2011.

[26] K. Gopalsamy, "Leakage delays in BAM," *Journal of Mathematical Analysis and Applications*, vol. 325, no. 2, pp. 1117–1132, 2007.

[27] K. Gu, V. L. Kharitonov, and J. Chen, *Stability of Time-Delay Systems*, Birkhauser, Boston, Mass, USA, 2003.

Hindawi Publishing Corporation
Abstract and Applied Analysis
Volume 2013, Article ID 352826, 8 pages
http://dx.doi.org/10.1155/2013/352826

Research Article

Full Synchronization Studied by a Set of Partitions Connected Together

Jianbao Zhang,[1] Zhongjun Ma,[2] and Jinde Cao[3,4]

[1] *School of Science, Hangzhou Dianzi University, Hangzhou 310018, China*
[2] *School of Mathematics and Computing Science, Guilin University of Electronic Technology, Guilin 541004, China*
[3] *Department of Mathematics, Southeast University, Nanjing 210096, China*
[4] *Department of Mathematics, King Abdulaziz University, Jeddah 21589, Saudi Arabia*

Correspondence should be addressed to Zhongjun Ma; mzj1234402@163.com

Received 9 July 2013; Accepted 22 August 2013

Academic Editor: Qiankun Song

A novel approach is brought forward for synchronization of a clustered network in this paper, the objective of which is twofold. The first one is to study cluster synchronization by analyzing the inner coupling matrices of the individual clusters instead of the one of the whole network. The other is to show that full synchronization can be ensured by several types of cluster synchronization, the partitions of which are connected together. Compared with the classical method for full synchronization, our approach reduces the network size to the cluster size and additionally obtains the thresholds for different types of cluster synchronization. As a numerical example, cluster and full synchronization in a special clustered network are investigated through our approach. It turns out that we obtain the same threshold for full synchronization as the one obtained by the classical method. Numerical simulations confirm the validity of our approach.

1. Introduction

Collective behavior of complex networks has become a focal subject due to the important and extensive applications in various fields of science and technology. Full and cluster synchronization are two types of typical and fundamental collective behavior. The former means that all oscillators in a network acquire identical behavior, while the latter means that the coupled oscillators split into subgroups called clusters, and all the oscillators in the same cluster behave in the same fashion. Research on cluster and full synchronization has attracted increasing attention in the past decades.

Several effective methods have been applied to study full synchronization, which is also called complete synchronization. Pecora and Carroll proposed the famous master stability function method to study the local stability of the synchronous state [1], while Lyapunov function method was employed to study the global stability of the synchronous state [2–4]. With the help of the two classical methods mentioned above, a great deal of research has been carried out in recent years. By imposing constraints on the coupling strength, local stability of the synchronous states in arbitrarily coupled systems was ensured based on Gershörin disk theory [5]. By analyzing the characters of the network topology, connection graph stability method was put forward [2] and applied to study synchronization in a network with time-dependent on-off coupling, which is also called blinking model [3]. By decomposing the space into a direct sum of the synchronization manifold and the transverse space, criteria were obtained for both local and global stability of the synchronous state [4].

Cluster structures can be found to exist widely in real-world networks such as circles of friends or colleagues in social networks [6], compartments in food webs [7], groups of web pages sharing identical topics in the World Wide Web [8], and functional modules such as proteins having the same function in biological networks [9]. In those clustered networks, cluster synchronization usually occurs firstly before full synchronization occurs. Therefore, research on cluster and full synchronization in clustered networks has very obvious practical significance. Synchronization in a clustered network composed of two BA scale-free subnetworks has

been studied in [10]. Control schemes were proposed for synchronization between two clusters, which is also called outer synchronization [11]. With the help of the method in [4], a criterion for cluster synchronization was obtained in [12]. Based on the criterion, cluster synchronization bifurcations are analyzed in a globally coupled network with a parameter [13].

However, to the best of our knowledge, most of the previous research on cluster and full synchronization focused on the topology of the whole network, which may be very complex. In this paper, the complexity of a clustered network is simplified by partitioning the whole network into clusters under a certain hypothesis. It is proved that cluster synchronization can be ensured by suitable inner couplings of the clusters, and sufficient conditions, which are independent of the outer couplings between different clusters, are obtained theoretically. Based on this result, a novel method for full synchronization is derived. If there exist two or several partitions connected together along some arrangement of all the oscillators, which imply that the intersection of the cluster synchronization manifolds corresponding to those partitions is equal to the full synchronization manifold, then full synchronization occurs if cluster synchronization corresponding to every partition is ensured. The method declares that both cluster and full synchronization can be studied by the inner topologies of the individual clusters. Obviously, the network size reduction provides convenience for the studies on synchronization in clustered networks with great mounts of oscillators.

The rest of the paper is organized as follows. Section 2 is devoted to introducing some concerned concepts such as partitions and cluster synchronization manifolds. Sufficient conditions independent of the outer couplings between different clusters are obtained for cluster synchronization in Section 3. The tedious proof of this result is carried out in the Appendix. The concept of partitions connected together along some arrangement is proposed and employed to study full synchronization in Section 4. In order to confirm the validity of the theoretical results, numerical experiments are carried out in Section 5. The final section is devoted to a brief discussion of the obtained results.

2. Preliminaries

Consider a network composed of m oscillators

$$\dot{x}_i = f(x_i, t) + \varepsilon \sum_{j=1}^{m} a_{ij} \Gamma x_j, \quad i = 1, \ldots, m, \tag{1}$$

where $x_i = (x_i^1, \ldots, x_i^n)^\top$ is the state variable of the ith oscillator, $t \in [0, +\infty)$ is a continuous time, $f : R^n \times [0, +\infty) \to R^n$ is a continuous map, $\varepsilon \geq 0$ is the coupling strength, $\Gamma = \mathrm{diag}(\gamma_1, \ldots, \gamma_n)$ is a nonnegative matrix, $A = (a_{ij})_{m\times m}$ is the coupling matrix with $a_{ij} = a_{ji} \geq 0$ for $i \neq j$, and $\sum_{j=1}^{m} a_{ij} = s$ for $i = 1, \ldots, m$.

Suppose that the index set $\{1, \ldots, m\}$ of the m oscillators is divided into d nonempty subsets called clusters. Let $P = \{P_1, \ldots, P_d\}$ be its partition; that is, $P_i \cap P_j = \phi$ for $i \neq j$ and $\bigcup_{i=1}^{d} P_i = \{1, \ldots, m\}$. The following denotations are introduced for every $l = 1, \ldots, d$.

(D_1) Denote the cardinal number of cluster P_l by p_l, and denote the subscript of the cluster containing i by $\widehat{i}$; that is, $\widehat{i} = l$ if $i \in P_l$.

(D_2) Suppose that all oscillators in the cluster P_l are arranged adjacently; that is, $P_l = \{\sigma_{l-1} + 1, \ldots, \sigma_l\}$, where $\sigma_0 = 0$, $\sigma_l = p_1 + \cdots + p_l$.

(D_3) Suppose that $p_l \geq 2$ for $1 \leq l \leq \overline{d}$ and $p_l = 1$ for $\overline{d} < l \leq d$. It can be seen that for any $\overline{d} < l \leq d$, synchronization of the oscillators corresponding to cluster P_l always occurs for any $\varepsilon \geq 0$ since P_l contains only one oscillator.

We will discuss sufficient conditions for the p_l oscillators corresponding to P_l to synchronize with each other, $l = 1, \ldots, d$. Before that, the following sets should be introduced for every $l = 1, \ldots, d$.

(M_1) The synchronization submanifold of the cluster P_l is as follows:

$$\mathbb{M}(P_l) = \left\{ \left(x_{\sigma_{l-1}+1}^\top, \ldots, x_{\sigma_l}^\top\right)^\top \in R^{p_l n} \mid x_{\sigma_{l-1}+1} = \cdots = x_{\sigma_l} \right\}. \tag{2}$$

(M_2) The cluster synchronization manifold of the partition P is as follows:

$$\mathbb{M}(P) = \mathbb{M}(P_1) \times \mathbb{M}(P_2) \times \cdots \times \mathbb{M}(P_d) \subset R^{mn}. \tag{3}$$

(M_3) The transverse subspace for $\mathbb{M}(P_l)$ is as follows:

$$\mathbb{L}(P_l) = \left\{ \left(x_{\sigma_{l-1}+1}^\top, \ldots, x_{\sigma_l}^\top\right)^\top \in R^{p_l n} \mid \sum_{i=1}^{p_l} x_{\sigma_{l-1}+i} = 0 \right\}. \tag{4}$$

(M_4) The transverse space for $\mathbb{M}(P)$ is as follows:

$$\mathbb{L}(P) = \mathbb{L}(P_1) \times \mathbb{L}(P_2) \times \cdots \times \mathbb{L}(P_d) \subset R^{mn}. \tag{5}$$

In case $d = 1$, the synchronization manifold $\mathbb{M}(P)$ is called a full synchronization manifold. For simplicity, we denote the full synchronization manifold by $\mathbb{M}$ and the corresponding transverse space by $\mathbb{L}$.

Definitions of cluster and full synchronization in the network (1) are listed as follows.

(S_1) The cluster synchronization manifold $\mathbb{M}(P)$ is said to be globally attractive for the network (1), or cluster synchronization of the partition P occurs, if, for any initial condition $(x_1^\top(0), \ldots, x_m^\top(0))^\top$,

$$\lim_{t\to+\infty} \frac{1}{m} \sum_{l=1}^{d} \sum_{i\in P_l} \left\| x_i - x_{\sigma_{l-1}+1} \right\| = 0, \tag{6}$$

where $\|\cdot\|$ denotes 2-norm of vectors.

(S_2) In case of $d = 1$, the full synchronization manifold $\mathbb{M}$ is said to be globally attractive for the network (1); that is, full synchronization occurs.

3. Result on Cluster Synchronization

Before the results on cluster synchronization are carried out, two common hypotheses in previous related research should be introduced.

At first, a synchronization manifold is always supposed to be an invariant manifold in order to discuss its attractiveness. The following lemma gives a sufficient and necessary condition for a cluster synchronization manifold being an invariant manifold.

Lemma 1 (see [12]). *Partition the coupling matrix A according to partition P as follows:*

$$A = \begin{bmatrix} A_{11} & A_{12} & \cdots & A_{1d} \\ A_{21} & A_{22} & \cdots & A_{2d} \\ \cdots & \cdots & \cdots & \cdots \\ A_{d1} & A_{d2} & \cdots & A_{dd} \end{bmatrix}, \tag{7}$$

where $A_{lk} \in R^{p_l \times p_k}$; the synchronization manifold $\mathbb{M}(P)$ is an invariant manifold of the network (1)*, if and only if every submatrix A_{lk} has equal-row-sum s_{lk}, $l, k = 1, \ldots, d$.*

According to Lemma 1, we carry out the first hypothesis (H_1).

(H_1) Every submatrix $A_{lk} \in R^{p_l \times p_k}$ in the partitioned matrix (7) has equal-row-sum s_{lk}; that is, for every $i \in P_l$, there holds $\sum_{j \in P_k} a_{ij} = s_{lk}$, $l, k = 1, \ldots, d$. In addition, suppose that all the principal submatrices A_{ll}, $l = 1, \ldots, d$, are irreducible.

In order to study the inner couplings of the cluster P_l, we put forward the following matrix:

$$\overline{A}(P_l) = A_{ll} + \sum_{k=1, k \neq l}^{d} s_{lk} I_{p_l}, \tag{8}$$

where $I_{p_l} \in R^{p_l \times p_l}$ is an identity matrix. Then the elements of $\overline{A}(P_l)$ satisfy that $\sum_{j \in P_l} \overline{a}_{ij} = s$ for $i \in P_l$, and

$$\overline{a}_{ij} = \begin{cases} a_{ij}, & i \neq j, \\ a_{ij} + \sum_{k=1, k \neq l}^{d} s_{lk}, & i = j, \end{cases} \tag{9}$$

where $i, j \in P_l$, $l = 1, \ldots, d$. We will study the dependence of cluster synchronization on the matrices $\overline{A}(P_l)$, $l = 1, \ldots, d$. Noticing the importance of the matrix $\overline{A}(P_l)$, we call it a principal quasi-submatrix of the cluster P_l since A_{ll} is a principal submatrix, $l = 1, \ldots, d$.

The second crucial hypothesis is the individual oscillator dynamics satisfying QUAD(Δ, Q, R^n) condition as follows [12].

(H_2) There exists a positive-definite diagonal matrix $Q = \mathrm{diag}(q_1, \ldots, q_n)$, with a diagonal matrix $\Delta = \mathrm{diag}(\delta_1, \ldots, \delta_n)$ satisfying $\delta_j \leq 0$ for $j \in \{j : \gamma_j = 0\}$ and a constant $\epsilon > 0$, such that

$$\begin{aligned} &(u - v)^{\top} Q \{[f(u, t) - f(v, t)] - \Delta(u - v)\} \\ &\quad \leq -\epsilon (u - v)^{\top} (u - v) \end{aligned} \tag{10}$$

holds for any $u, v \in R^n$ and all $t \geq 0$.

Hypothesis (H_2) means that the following two coupled oscillators:

$$\begin{aligned} \dot{x}_1 &= f(x_1, t) + \frac{\Delta(x_2 - x_1)}{2}, \\ \dot{x}_2 &= f(x_2, t) + \frac{\Delta(x_1 - x_2)}{2} \end{aligned} \tag{11}$$

can synchronize when the coupling $\Delta/2$ is made sufficiently large. Many chaotic oscillators have been proved to satisfy the hypothesis, such as Chua circuits [14], standard Hopfield neural networks [4], and x-coupled [15, 16] or y-coupled Lorenz systems [17] in an absorbing domain $\mathscr{B}$. However, many other systems are not the case such as a lattice of x-coupled Rössler systems, in which the stability of synchronization regime is lost with the increasing of coupling [18].

Now, the preliminaries above, together with Lyapunov function method, bring us to the following theorem.

Theorem 2. *Suppose that hypotheses (H_1) and (H_2) hold and that*

$$\varepsilon \lambda_2(P_l) \gamma_j + \delta_j \leq 0, \quad j = 1, \ldots, n, \tag{12}$$

where $\lambda_2(P_l)$ is the second-largest eigenvalue of $\overline{A}(P_l)$, $l = 1, \ldots, \overline{d}$, and the synchronization manifold $\mathbb{M}(P)$ is globally attractive for the network (1).

For a rigorous proof of Theorem 2, the reader is referred to the Appendix.

As a special case, if all the row sums of A are equal to zero, then $\overline{A}(P_l)$ also has zero row sums, and $\lambda_2(P_l) < 0$, $l = 1, \ldots, \overline{d}$. Therefore, condition (12) is equivalent to

$$\varepsilon \geq \frac{\max_{j \in \{j : \gamma_j > 0\}} \{0, \delta_j / \gamma_j\}}{\min_{1 \leq l \leq \overline{d}} |\lambda_2(P_l)|}. \tag{13}$$

4. Result on Full Synchronization

Suppose that there are a set of partitions $P(k, \cdot) = \{P(k, 1), \ldots, P(k, d_k)\}$, $k = 1, \ldots, c$, satisfying hypothesis (H_1). The following definition is put forward for the first time to study full synchronization.

Definition 3. Rearrange the numbers $1 \cdots m$ as $i_1 \cdots i_m$. A set of partitions $P(k)$, $k = 1, \ldots, c$, are connected together along the arrangement $i_1 \cdots i_m$, if, for every i_j, $j = 1, \ldots, m-1$, there exists a subset $P(k_j, l_j)$ such that $\{i_j, i_{j+1}\} \subseteq P(k_j, l_j)$.

For example, the set $\{1, 2, 3, 4\}$ has two partitions as follows:

$$P(1) = \{1, 2; 3, 4\}, \qquad P(2) = \{1, 3; 2, 4\}. \tag{14}$$

Since

$$\{1,2\} \subseteq P(1,1), \qquad \{2,4\} \subseteq P(2,2), \qquad \{4,3\} \subseteq P(1,2), \tag{15}$$

$P(1)$ and $P(2)$ form a set of partitions connected together along the arrangement 1243.

From the definition above, we obtain the following lemma.

Lemma 4. *A set of partitions $P(k)$, $k = 1,\ldots,c$, are connected together along some arrangement $i_1 \cdots i_m$, if and only if the cluster synchronization manifolds of those partitions satisfy that*

$$\bigcap_{k=1}^{c} \mathbb{M}(P(k)) = \mathbb{M}. \tag{16}$$

The proof of Lemma 4 is straightforward and will not be given here.

Now, we are in a position to carry out the following theorem on full synchronization of the network (1).

Theorem 5. *There are a set of partitions $P(k)$, $k = 1,\ldots,c$, connected together along some arrangement $i_1 \cdots i_m$ and satisfying hypothesis (H_1). Then under hypothesis (H_2), the full synchronization manifold $\mathbb{M}$ is globally attractive for the network* (1) *if*

$$\varepsilon\gamma_j\lambda_2(P(k,l)) + \delta_j \le 0, \quad j = 1,\ldots,n, \tag{17}$$

where $\lambda_2(P(k,l))$ is the second-largest eigenvalue of $\overline{A}(P(k,l))$, $k = 1,\ldots,c$, $l = 1,\ldots,\overline{d}_k$.

The proof of Theorem 5 can be completed by combining Theorem 2 and Lemma 4, and so it is omitted here.

As a special case, if all the row-sums of A are equal to zero, condition (17) is equivalent to

$$\varepsilon \ge \frac{\max_{j\in\{j:\gamma_j>0\}}\{0,\delta_j/\gamma_j\}}{\min_{1\le k\le c,1\le l\le\overline{d}_k}|\lambda_2(P(k,l))|}. \tag{18}$$

5. Numerical Examples

Consider the system (1) composed of m neural networks

$$\dot{x}_i = -Dx_i + Tg(x_i) + \varepsilon\sum_{j=1}^{m} a_{ij}\Gamma x_j, \quad i = 1,\ldots,m, \tag{19}$$

where $x_i \in R^3$, $D = \Gamma = I_3$, $g(x_i) = (g(x_i^1), g(x_i^2), g(x_i^3))^\top$, $g(s) = (|s+1| - |s-1|)/2$, and

$$T = \begin{pmatrix} 1.25 & -3.2 & -3.2 \\ -3.2 & 1.1 & -4.4 \\ -3.2 & 4.4 & 1.0 \end{pmatrix}. \tag{20}$$

With the help of matlab LMI Control Toolbox, hypothesis (H_2) can be satisfied by taking $Q = I_3$ and $\Delta = \delta I_3$, where $\delta = 5.5685$ [4].

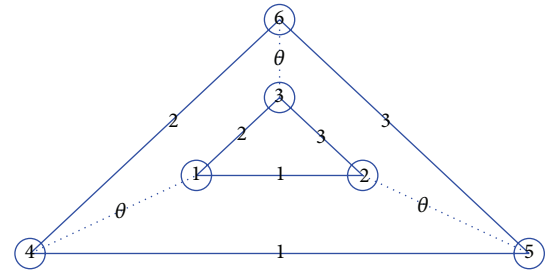

Figure 1: Topology structure corresponding to the coupling matrix (21). The coupling weights of the edges are the values lying on them.

Define the coupling matrix $A = (a_{ij})_{6\times6}$ as follows:

$$A = \begin{pmatrix} A_1 & \theta I_3 \\ \theta I_3 & A_1 \end{pmatrix},$$
$$A_1 = \begin{pmatrix} -3-\theta & 1 & 2 \\ 1 & -4-\theta & 3 \\ 2 & 3 & -5-\theta \end{pmatrix}. \tag{21}$$

The topology structure corresponding to the matrix (21) is shown in Figure 1. It is easy to show that the following partitions satisfy (H_1):

$$P(1) = \{1,2,3;4,5,6\}, \qquad P(2) = \{1,4;2,5;3,6\}, \tag{22}$$

the principal quasi-submatrices of which are

$$\overline{A}(P(1,l_1)) = A_1|_{\theta=0}, \quad l_1 = 1,2,$$
$$\overline{A}(P(2,l_2)) = \begin{pmatrix} -\theta & \theta \\ \theta & -\theta \end{pmatrix}, \quad l_2 = 1,2,3, \tag{23}$$

respectively. Further calculations give rise to the eigenvalues sets of the principal quasi-submatrices mentioned above as follows:

$$\sigma\left(\overline{A}(P(1,l_1))\right) = \left\{0, -6 \pm \sqrt{3}\right\}, \quad l_1 = 1,2,$$
$$\sigma\left(\overline{A}(P(2,l_2))\right) = \{0,-2\theta\}, \quad l_2 = 1,2,3. \tag{24}$$

Obviously, partitions $P(1)$ and $P(2)$ are connected together along the arrangement 123654. According to Theorems 2 and 5, one concludes the following.

(1) If $\varepsilon \ge \delta/(6-\sqrt{3})$, cluster synchronization of partition $P(1)$ occurs.

(2) If $\varepsilon \ge \delta/(2\theta)$, cluster synchronization of partition $P(2)$ occurs.

(3) If $\varepsilon \ge \max\{\delta/(6-\sqrt{3}), \delta/(2\theta)\}$, full synchronization occurs.

These results can be seen more clearly in Figure 2, the red solid lines in which are threshold lines of $\varepsilon - \theta$ for full synchronization.

In order to be compared with the previous classical results on full (complete) synchronization, the second-largest eigenvalue of A should be obtained, and the threshold for full

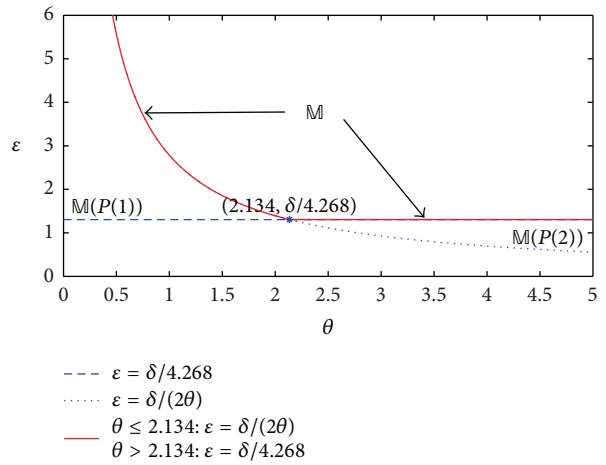

FIGURE 2: Thresholds for the attractiveness of the synchronization manifolds $\mathbb{M}(P(1))$, $\mathbb{M}(P(2))$, and $\mathbb{M}$.

synchronization should be $\varepsilon \geq \delta/|\lambda_2(A)|$ [1, 4]. In fact, the eigenvalues set of A is

$$\sigma(A) = \left\{0, -2\theta, -6 \pm \sqrt{3}, -6 \pm \sqrt{3} - 2\theta\right\}. \tag{25}$$

Therefore, $\lambda_2(A) = \max\{-6 + \sqrt{3}, -2\theta\}$. Obviously, there is a good agreement between our result and the previous classical results.

Define the following cluster errors:

$$e_1(t_0) = \frac{1}{6}\sum_{i=1}^{3}\left\|x_i(t_0) - x_1(t_0)\right\| + \frac{1}{6}\sum_{i=4}^{6}\left\|x_i(t_0) - x_4(t_0)\right\|,$$

$$e_2(t_0) = \frac{1}{6}\sum_{i=1}^{3}\left\|x_{i+3}(t_0) - x_i(t_0)\right\|,$$

$$e(t_0) = \frac{1}{6}\sum_{i=1}^{6}\left\|x_i(t_0) - x_1(t_0)\right\|, \tag{26}$$

where $t_0 = 100$. Take $\theta = 0.1$ and let ε increase from 0 to 1 step by step. Figure 3(a) shows that the cluster error $e_1(t_0)$ reaches zero firstly, while $e_2(t_0)$ and $e(t_0)$ reach zero at the same value of ε. While fixing θ at 3, Figure 3(b) shows that $e_2(t_0)$ reaches zero firstly, while $e_1(t_0)$ and $e(t_0)$ reach zero at the same value of ε.

In fact, these results can be forecasted in Figure 2. If the parameter θ is fixed in $(0, 1.5]$ and if ε increases gradually, synchronization of the partition $P(1)$ will firstly occur, and then synchronization of $P(2)$ and full synchronization occur at the same value of ε since $\mathbb{M}(P(1)) \bigcap \mathbb{M}(P(2)) = \mathbb{M}$. Therefore, the effectiveness of the theoretical results is confirmed.

6. Conclusions

This paper has investigated cluster and full synchronization in a clustered network. In order to study cluster synchronization, we propose the concept of principal quasi-submatrices corresponding to the individual clusters, which represent the inner couplings of the individual clusters. Theoretically, sufficient conditions independent of the outer couplings between different clusters are obtained for cluster synchronization. In order to study full synchronization, we propose the concept of partitions connected together along some arrangement. If all types of cluster synchronization of those partitions are ensured, it is proved that full synchronization occurs. The results are more advantageous than the classical results. Firstly, it allows us to divide a network composed of great amounts of oscillators into some smaller subnetworks. The network size reduction provides convenience to reduce the great amounts of calculations. Secondly, our approach can be applied to study cluster synchronization corresponding to any possible partitions. In summary, this paper has proposed a novel, convenient, and double purpose approach for both cluster and full synchronization in clustered networks.

Appendix

Denoting $\iota_{p_l} = (1, \ldots, 1)^\top \in R^{p_l}$, we define the following cluster errors for $l = 1, \ldots, d$:

(E_1) $\overline{x}_l = (1/p_l)\sum_{i\in P_l} x_i$, $\delta x_i = x_i - \overline{x}_{\widehat{i}}$, $i = 1, \ldots, m$;

(E_2) $X_l = (x_{\sigma_{l-1}+1}^\top, \ldots, x_{\sigma_l}^\top)^\top$, $\overline{X}_l = \iota_{p_l} \otimes \overline{x}_l$, $\delta X_l = X_l - \overline{X}_l$;

(E_3) $x = (x_1^\top, \ldots, x_m^\top)^\top$, $\overline{x} = (\overline{x}_1^\top, \ldots, \overline{x}_{\widehat{m}}^\top)^\top$, $\delta x = (\delta x_1^\top, \ldots, \delta x_m^\top)^\top$.

Proof. Denote $F(X_l, t) = (f(x_{\sigma_{l-1}+1}, t)^\top, \ldots, f(x_{\sigma_l}, t)^\top)^\top$ and rewrite the network (1) as follows:

$$\frac{dX_l}{dt} = F(X_l, t) + \varepsilon\sum_{k=1}^{d}(A_{lk} \otimes \Gamma) X_k. \tag{A.1}$$

Therefore,

$$\begin{aligned}\frac{d\delta X_l}{dt} &= \frac{d\left(X_l - \overline{X}_l\right)}{dt} = \frac{dX_l}{dt} - \iota_{p_l} \otimes \left(\frac{1}{p_l}\sum_{i\in P_l}\frac{dx_i}{dt}\right)\\ &= F(X_l, t) + \varepsilon\sum_{k=1}^{d}(A_{lk} \otimes \Gamma) X_k - \iota_{p_l} \otimes \left(\frac{1}{p_l}\sum_{i\in P_l}\frac{dx_i}{dt}\right)\\ &= F(X_l, t) - F\left(\overline{X}_l, t\right) + \varepsilon\sum_{k=1}^{d}(A_{lk} \otimes \Gamma)\delta X_k + \mathbb{J}_l,\end{aligned} \tag{A.2}$$

where

$$\mathbb{J}_l = F\left(\overline{X}_l, t\right) + \varepsilon\sum_{k=1}^{d}(A_{lk} \otimes \Gamma)\overline{X}_k - \iota_{p_l} \otimes \left(\frac{1}{p_l}\sum_{i\in P_l}\frac{dx_i}{dt}\right). \tag{A.3}$$

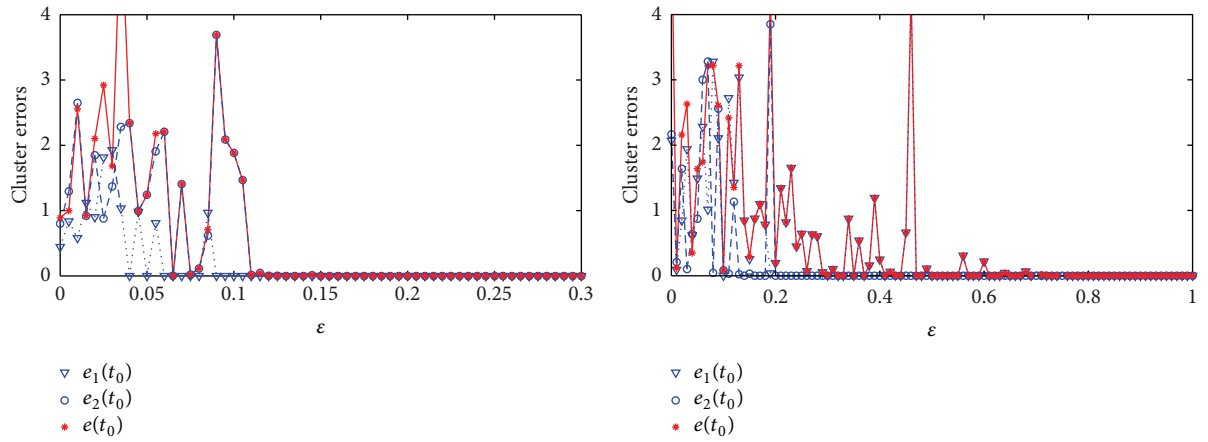

(a) $\theta = 0.1$ (b) $\theta = 3$

FIGURE 3: Dependence of the cluster errors $e_1(t_0)$, $e_2(t_0)$, and $e(t_0)$ on the coupling strength ε for the network (19) with the coupling matrix (21).

Noticing that $F(\overline{X}_l, t) = \iota_{p_l} \otimes f(\overline{x}_l, t)$ and

$$\begin{aligned}\sum_{k=1}^{d} (A_{lk} \otimes \Gamma)\, \overline{X}_k &= \sum_{k=1}^{d} (A_{lk} \otimes \Gamma)\left(\iota_{p_k} \otimes \overline{x}_k\right) = \sum_{k=1}^{d} \left(A_{lk}\iota_{p_k}\right) \otimes (\Gamma \overline{x}_k) \\ &= \sum_{k=1}^{d} s_{lk}\iota_{p_l} \otimes (\Gamma \overline{x}_k) = \iota_{p_l} \otimes \left(\sum_{k=1}^{d} s_{lk} \Gamma \overline{x}_k\right),\end{aligned} \tag{A.4}$$

we have

$$\mathbb{J}_l = \iota_{p_l} \otimes \left(f(\overline{x}_l, t) + \sum_{k=1}^{d} s_{lk}\Gamma \overline{x}_k - \frac{1}{p_l} \sum_{i \in P_l} \frac{dx_i}{dt}\right). \tag{A.5}$$

Let $\mathbb{J}_l = \iota_{p_l} \otimes J_l$; it can be seen that J_l is independent of $i \in P_l$.

In order to utilize the QUAD(Δ, Q, R^n) condition, a Lyapunov function is defined as follows,

$$V(\delta x) = \frac{1}{2} \sum_{l=1}^{d} \delta X_l^{\top} \left(I_{p_l} \otimes Q\right) \delta X_l. \tag{A.6}$$

The derivative of V with respect to time t is as follows:

$$\begin{aligned}\frac{dV(\delta x)}{dt} &= \sum_{l=1}^{d} \delta X_l^{\top} \left(I_{p_l} \otimes Q\right) \frac{d\delta X_l}{dt} \\ &= \sum_{l=1}^{d} \delta X_l^{\top} \left(I_{p_l} \otimes Q\right) \\ &\quad \times \left(F(X_l, t) - F\left(\overline{X}_l, t\right) + \varepsilon \sum_{k=1}^{d} (A_{lk} \otimes \Gamma)\, \delta X_k + \mathbb{J}_l\right).\end{aligned} \tag{A.7}$$

Noticing that $\sum_{i \in P_l} \delta x_i = 0$, we have

$$\begin{aligned}&\sum_{l=1}^{d} \delta X_l^{\top} \left(I_{p_l} \otimes Q\right) \mathbb{J}_l \\ &= \sum_{l=1}^{d} \delta X_l^{\top} \left(I_{p_l} \otimes Q\right) \left(\iota_{p_l} \otimes J_l\right) \\ &= \sum_{l=1}^{d} \delta X_l^{\top} \left(\iota_{p_l} \otimes Q J_l\right) \\ &= \sum_{l=1}^{d} \sum_{i \in P_l} \delta x_i^{\top} Q J_l = \sum_{l=1}^{d} \left(\sum_{i \in P_l} \delta x_i^{\top}\right) Q J_l = 0.\end{aligned} \tag{A.8}$$

which together with hypothesis (H_2) leads to

$$\begin{aligned}\frac{dV(\delta x)}{dt} &= \sum_{l=1}^{d} \delta X_l^{\top} \left(I_{p_l} \otimes Q\right) \\ &\quad \times \Bigg(\left[F(X_l, t) - F\left(\overline{X}_l, t\right) - \left(I_{p_l} \otimes \Delta\right)\left(X_l - \overline{X}_l\right)\right] \\ &\quad + \left[\left(I_{p_l} \otimes \Delta\right)\left(X_l - \overline{X}_l\right) + \varepsilon \sum_{k=1}^{d} (A_{lk} \otimes \Gamma)\, \delta X_k\right]\Bigg)\end{aligned}$$

$$\begin{aligned}
&\leq -\epsilon\sum_{l=1}^{d}\delta X_l^{\top}\delta X_l+\sum_{l=1}^{d}\delta X_l^{\top}\\
&\quad\times\left[\left(I_{p_l}\otimes Q\Delta\right)\delta X_l+\varepsilon\sum_{k=1}^{d}\left(A_{lk}\otimes Q\Gamma\right)\delta X_k\right]\\
&\leq -2\epsilon\frac{V\left(\delta x\left(t\right)\right)}{\max_{1\leq i\leq n}q_i}+\mathbb{S}.
\end{aligned}\tag{A.9}$$

Noticing the equality (8), that is, $A_{ll}=\overline{A}_l-\sum_{k=1,k\neq l}^{d}s_{lk}I_{p_l}$, where $\overline{A}_l=\overline{A}(P_l)$, we have

$$\begin{aligned}
\mathbb{S}&=\sum_{l=1}^{d}\delta X_l^{\top}\left(\left(I_{p_l}\otimes Q\Delta\right)\delta X_l+\varepsilon\left(A_{ll}\otimes Q\Gamma\right)\delta X_l\right.\\
&\qquad\left.+\varepsilon\sum_{k=1,k\neq l}^{d}\left(A_{lk}\otimes Q\Gamma\right)\delta X_k\right)\\
&=\sum_{l=1}^{d}\delta X_l^{\top}\left[I_{p_l}\otimes Q\Delta+\varepsilon\overline{A}_l\otimes Q\Gamma\right]\delta X_l\\
&\quad+\varepsilon\sum_{l=1}^{d}\sum_{k=1,k\neq l}^{d}\delta X_l^{\top}\left[\left(A_{lk}\otimes Q\Gamma\right)\delta X_k-s_{lk}\left(I_{p_l}\otimes Q\Gamma\right)\delta X_l\right]\\
&=\mathbb{S}_1+\mathbb{S}_2.
\end{aligned}\tag{A.10}$$

The proof will be completed by showing that $\mathbb{S}_1\leq 0$ and $\mathbb{S}_2\leq 0$ as follows.

As we know, the symmetric matrix $\overline{A}_l$ has the famous decomposition $\overline{A}_l=U_l\Lambda_l U_l^{\top}$, where $\Lambda_l=\mathrm{diag}\{\lambda_1(P_l),\ldots,\lambda_{p_l}(P_l)\}$ satisfying $s=\lambda_1(P_l)>\lambda_2(P_l)\geq\cdots\geq\lambda_{p_l}(P_l)$, and $U_l\in R^{p_l\times p_l}$ is a unitary matrix; that is, $U_lU_l^{\top}=I_{p_l}$. The ith column of U_l is the eigenvector of $\overline{A}_l$ corresponding to the eigenvalue $\lambda_i(P_l), i=1,\ldots,p_l$. By the substitutions of variables $\delta X_l=(U_l\otimes I_n)\xi_l$, $l=1,\ldots,d$, we have

$$\begin{aligned}
\mathbb{S}_1&=\sum_{l=1}^{d}\xi_l^{\top}\left(U_l\otimes I_n\right)^{\top}\\
&\quad\times\left[I_{p_l}\otimes\left(Q\Delta\right)+\varepsilon\overline{A}_l\otimes\left(Q\Gamma\right)\right]\left(U_l\otimes I_n\right)\xi_l\\
&=\sum_{l=1}^{d}\xi_l^{\top}\left[I_{p_l}\otimes\left(Q\Delta\right)+\varepsilon\left(U_l^{\top}\overline{A}_lU_l\right)\otimes\left(Q\Gamma\right)\right]\xi_l\\
&=\sum_{l=1}^{d}\xi_l^{\top}\left[I_{p_l}\otimes\left(Q\Delta\right)+\varepsilon\Lambda_l\otimes\left(Q\Gamma\right)\right]\xi_l.
\end{aligned}\tag{A.11}$$

Noticing that the matrices Q, Δ, Λ_l, and Γ are all diagonal matrices, we obtain

$$\mathbb{S}_1=\sum_{l=1}^{d}\xi_l^{\top}\,\mathrm{diag}\left(\underbrace{\lambda_{11},\ldots,\lambda_{1n}}_{n},\ldots,\underbrace{\lambda_{p_l1},\ldots,\lambda_{p_ln}}_{n}\right)\xi_l,\tag{A.12}$$

where $\lambda_{ij}=q_j(\varepsilon\lambda_i(P_l)\gamma_j+\delta_j)$, $i=1,\ldots p_l$, $j=1,\ldots,n$. It is well known that the first column of U_l is ι_{p_l}; then one can conclude from the inverse substitutions of variables $\xi_l=(U_l^{\top}\otimes I_n)\delta X_l$ that $\xi_l^j=\sum_{i\in P_l}\delta x_i^j=0$, $j=1,\ldots,n, l=1,\ldots,d$. Therefore, condition (12) is sufficient for $\mathbb{S}_1\leq 0$.

Finally, some techniques in [2, page 164] are employed to show that $\mathbb{S}_2\leq 0$ as follows:

$$\begin{aligned}
\mathbb{S}_2&=\varepsilon\sum_{l=1}^{d}\sum_{k=1,k\neq l}^{d}\delta X_l^{\top}\left[\left(A_{lk}\otimes Q\Gamma\right)\delta X_k-s_{lk}\left(I_{p_l}\otimes Q\Gamma\right)\delta X_l\right]\\
&=\varepsilon\left[\sum_{l=1}^{d-1}\sum_{k=l+1}^{d}+\sum_{k=1}^{d-1}\sum_{l=k+1}^{d}\right]\\
&\quad\times\delta X_l^{\top}\left[\left(A_{lk}\otimes Q\Gamma\right)\delta X_k-s_{lk}\left(I_{p_l}\otimes Q\Gamma\right)\delta X_l\right]\\
&=\varepsilon\sum_{l=1}^{d-1}\sum_{k=l+1}^{d}\delta X_l^{\top}\left[\left(A_{lk}\otimes Q\Gamma\right)\delta X_k-s_{lk}\left(I_{p_l}\otimes Q\Gamma\right)\delta X_l\right]\\
&\quad+\varepsilon\sum_{l=1}^{d-1}\sum_{k=l+1}^{d}\delta X_k^{\top}\left[\left(A_{kl}\otimes Q\Gamma\right)\delta X_l-s_{kl}\left(I_{p_k}\otimes Q\Gamma\right)\delta X_k\right]\\
&=\varepsilon\sum_{l=1}^{d-1}\sum_{k=l+1}^{d}\left(\delta X_l^{\top}\left[\sum_{i\in P_l}\sum_{j\in P_k}\left(a_{ij}E_{ij}^{p_l\times p_k}\otimes Q\Gamma\right)\delta X_k\right.\right.\\
&\qquad\left.-s_{lk}\left(\sum_{i\in P_l}E_{ii}^{p_l\times p_l}\otimes Q\Gamma\right)\delta X_l\right]\\
&\qquad+\delta X_k^{\top}\left[\sum_{i\in P_l}\sum_{j\in P_k}\left(a_{ji}E_{ji}^{p_k\times p_l}\otimes Q\Gamma\right)\delta X_l\right.\\
&\qquad\left.\left.-s_{kl}\left(\sum_{j\in P_k}E_{jj}^{p_k\times p_k}\otimes Q\Gamma\right)\delta X_k\right]\right),
\end{aligned}\tag{A.13}$$

where $E_{ij}^{p_l\times p_k}=e_i^{p_l}\otimes e_j^{p_k\top}$ and $e_i^p\in R^p$ is the ith column of I_p. Substituting s_{lk} and s_{kl} by (9), we have

$$\begin{aligned}
\mathbb{S}_2=\varepsilon\sum_{l=1}^{d-1}\sum_{k=l+1}^{d}\sum_{i\in P_l}\sum_{j\in P_k}a_{ij}&\left(\delta X_l^{\top}\left[\left(E_{ij}^{p_l\times p_k}\otimes Q\Gamma\right)\delta X_k\right.\right.\\
&\left.-\left(E_{ii}^{p_l\times p_l}\otimes Q\Gamma\right)\delta X_l\right]\\
&+\delta X_k^{\top}\left[\left(E_{ji}^{p_k\times p_l}\otimes Q\Gamma\right)\delta X_l\right.\\
&\left.\left.-\left(E_{jj}^{p_k\times p_k}\otimes Q\Gamma\right)\delta X_k\right]\right)
\end{aligned}$$

$$= \varepsilon \sum_{l=1}^{d-1} \sum_{k=l+1}^{d} \sum_{i\in P_l} \sum_{j\in P_k} a_{ij} \left(\delta X_l^{\top} \left[e_i^{p_l} \otimes Q\Gamma \left(\delta x_j - \delta x_i \right) \right] + \delta X_k^{\top} \left[e_j^{p_k} \otimes Q\Gamma \left(\delta x_i - \delta x_j \right) \right] \right)$$

$$= \varepsilon \sum_{l=1}^{d-1} \sum_{k=l+1}^{d} \sum_{i\in P_l} \sum_{j\in P_k} a_{ij} \left(\delta x_i^{\top} Q\Gamma \left(\delta x_j - \delta x_i \right) + \delta x_j^{\top} Q\Gamma \left(\delta x_i - \delta x_j \right) \right)$$

$$= -\varepsilon \sum_{l=1}^{d-1} \sum_{k=l+1}^{d} \sum_{i\in P_l} \sum_{j\in P_k} a_{ij} \left(\delta x_j - \delta x_i \right)^{\top} Q\Gamma \left(\delta x_j - \delta x_i \right) \le 0. \tag{A.14}$$

The proof is completed. □

Acknowledgments

This project was supported the by the National Natural Science Foundation of China (Grant nos. 11162004 and 60964006), Zhejiang Provincial Natural Science Foundation of China (no. LQ12a01003), the Science Foundation of Guangxi Province (no. 2013GXNSFAA019006), and the Deanship of Scientific Research (DSR), King Abdulaziz University, under Grant no. 3-130/1434/HiCi. The authors, therefore, acknowledge the technical and financial support of KAU.

References

[1] L. M. Pecora and T. L. Carroll, "Master stability functions for synchronized coupled systems," *Physical Review Letters*, vol. 80, no. 10, pp. 2109–2112, 1998.

[2] V. N. Belykh, I. V. Belykh, and M. Hasler, "Connection graph stability method for synchronized coupled chaotic systems," *Physica D*, vol. 195, no. 1-2, pp. 159–187, 2004.

[3] I. V. Belykh, V. N. Belykh, and M. Hasler, "Blinking model and synchronization in small-world networks with a time-varying coupling," *Physica D*, vol. 195, no. 1-2, pp. 188–206, 2004.

[4] W. Lu and T. Chen, "New approach to synchronization analysis of linearly coupled ordinary differential systems," *Physica D*, vol. 213, no. 2, pp. 214–230, 2006.

[5] Y. H. Chen, G. Rangarajan, and M. Z. Ding, "Stability analysis of synchronized dynamics in coupled systems," *Physical Review E*, vol. 67, Article ID 026209, 4 pages, 2003.

[6] M. Girvan and M. E. J. Newman, "Community structure in social and biological networks," *Proceedings of the National Academy of Sciences of the United States of America*, vol. 99, no. 12, pp. 7821–7826, 2002.

[7] A. E. Krause, K. A. Frank, D. M. Mason, R. E. Ulanowicz, and W. W. Taylor, "Compartments revealed in food-web structure," *Nature*, vol. 426, no. 6964, pp. 282–285, 2003.

[8] G. W. Flake, S. Lawrence, C. L. Giles, and F. M. Coetzee, "Self-organization of the web and identification of communities," *IEEE Computer*, vol. 35, no. 3, pp. 66–70, 2002.

[9] A. W. Rives and T. Galitski, "Modular organization of cellular networks," *Proceedings of the National Academy of Sciences of the United States of America*, vol. 100, no. 3, pp. 1128–1133, 2003.

[10] C. Feng, Y. L. Zou, and F. Q. Wei, "Synchronization processes in clustered networks with different inter-cluster couplings," *Acta Physica Sinica*, vol. 62, no. 7, Article ID 070506, 7 pages, 2013.

[11] X. Wu, W. X. Zheng, and J. Zhou, "Generalized outer synchronization between complex dynamical networks," *Chaos*, vol. 19, no. 1, article 013109, 9 pages, 2009.

[12] W. Wu and T. Chen, "Partial synchronization in linearly and symmetrically coupled ordinary differential systems," *Physica D*, vol. 238, no. 4, pp. 355–364, 2009.

[13] Z. J. Ma, S. Z. Zhang, and G. R. Jiang, "Effect of the coupling matrix with a weight parameter on synchronization pattern in a globally coupled network," *Nonlinear Dynamics*, 2013.

[14] C. W. Wu and L. O. Chua, "Synchronization in an array of linearly coupled dynamical systems," *IEEE Transactions on Circuits and Systems. I*, vol. 42, no. 8, pp. 430–447, 1995.

[15] I. Belykh, V. Belykh, K. Nevidin, and M. Hasler, "Persistent clusters in lattices of coupled nonidentical chaotic systems," *Chaos*, vol. 13, no. 1, pp. 165–178, 2003.

[16] Z. Ma, Z. Liu, and G. Zhang, "A new method to realize cluster synchronization in connected chaotic networks," *Chaos*, vol. 16, no. 2, aricle 023103, 9 pages, 2006.

[17] X. Liu and T. Chen, "Boundedness and synchronization of y-coupled Lorenz systems with or without controllers," *Physica D*, vol. 237, no. 5, pp. 630–639, 2008.

[18] J. F. Heagy, L. M. Pecora, and T. L. Carroll, "Short wavelength bifurcations and size instabilities in coupled oscillator systems," *Physical Review Letters*, vol. 74, no. 21, pp. 4185–4188, 1995.

Hindawi Publishing Corporation
Abstract and Applied Analysis
Volume 2013, Article ID 680604, 7 pages
http://dx.doi.org/10.1155/2013/680604

Research Article

Synchronization of N Coupled Chaotic Systems with Ring Connection Based on Special Antisymmetric Structure

Xiangyong Chen,[1] Jianlong Qiu,[1] Qiang Song,[2] and Ancai Zhang[3]

[1] *School of Sciences, Linyi University, Linyi 276005, China*
[2] *School of Electronics and Information, Hangzhou Dianzi University, Hangzhou 310018, China*
[3] *School of Automobile Engineering, Linyi University, Linyi 276005, China*

Correspondence should be addressed to Jianlong Qiu; qiujianlong@lyu.edu.cn

Received 15 June 2013; Accepted 20 August 2013

Academic Editor: Xinsong Yang

This paper considers the complete synchronization problem for N coupled chaotic systems with ring connections. First, we use a direct design method to design a synchronization controller. It transforms the error system into a stable system with special antisymmetric structure. And then, we get some simple stability criteria of achieving the complete synchronization. These criteria are not only easily verified but also improve and generalize previous known results. Finally, numerical examples are provided to demonstrate the effectiveness of the theoretical analysis.

1. Introduction

Since the pioneering work of Pecora and Carroll [1], chaotic synchronization has been intensively investigated due to its potential applications in many fields [2–4]. Several types of synchronization phenomena have been reported, such as complete synchronization [5], phase synchronization [6], antisynchronization [7], projective synchronization [8, 9], and generalized synchronization [10]. To solve the problem of chaotic synchronization, many approaches have been developed. That includes a sliding mode control method [11], an impulsive control method [11], an adaptive control method [7, 12], a pinning control method [13], and a sampled-data control method [14]. However, these control algorithms are just suitable to synchronize two identical or nonidentical chaotic systems.

Nowadays, the synchronization of multiple chaotic systems has attracted increasing attention. It has been widely used in secure communication area in order to reduce the synchronizing cost of multiple chaotic communication and make simultaneous multiparty communications possible. Therefore, the synchronization in multiple chaotic systems has more advantages and deserves to be deeply investigated comparing with the conventional chaotic synchronization. Several types of synchronization in an array of chaotic systems have been investigated in the past few years, for example, the global synchronization in [15, 16], and the adaptive coupled synchronization in [17], the projective synchronization in [18]. In [19–21], the synchronization of N chaotic systems of with ring and chain connection was investigated. In addition, Yang and Zhang [22] studied the synchronization of an array of identical chaotic systems and discussed its application for secure communication with noise perturbation.

However, it is notable that the realization of synchronization of N coupled chaotic systems is much more difficult. So, it is necessary to find an easy method that realizes the synchronization of such multiple chaotic systems. Cai et al. [7, 8] investigated the generalized projective synchronization of two different chaotic systems based on a special antisymmetric structure. We studied the problem of synchronization of N different chaotic systems by using a special antisymmetric structure [21]. Inspired by the above discussions, we further discuss the synchronization of N coupled chaotic systems in this paper. First, a synchronization controller that is designed by using a direct design method transforms the error system into a stable system with special antisymmetric structure. And then, we derive some sufficient conditions in order to guarantee the asymptotical stabilization of the error system

at the origin. It means that the synchronization of N coupled chaotic systems is realized.

The paper is organized as follows. In Section 2, the synchronization of N coupled chaotic systems with ring connection is theoretically analyzed. A stability theorem for such systems with special antisymmetric structure is given. In Section 3, the synchronization control schemes are applied to three identical and non-identical coupled chaotic systems. Simulation results demonstrate the effectiveness of proposed schemes. And finally some concluding remarks are given in Section 4.

2. Synchronization of N Chaotic Systems and Controllers Design

Consider N coupled chaotic systems with ring connections described by

$$\begin{aligned}
\dot{x}_1 &= A_1 x_1 + g_1(x_1) + D_1(x_N - x_1),\\
\dot{x}_2 &= A_2 x_2 + g_2(x_2) + D_2(x_1 - x_2),\\
&\vdots\\
\dot{x}_N &= A_N x_N + g_n(x_N) + D_N(x_{N-1} - x_N),
\end{aligned} \tag{1}$$

where $x_1, x_2, \ldots, x_N$ are the state vectors of the chaotic systems; $g_i(x_i)$ $(i = 1, \ldots, N)$ is the continuous nonlinear function; $A_1, A_2, \ldots, A_N$ are constant matrices; $D_i = \mathrm{diag}(d_{1j}, \ldots, d_{Nj})$ and $d_{ij} \geq 0$ are the diagonal matrices which represent the coupled parameters. If

$$\begin{aligned}
&A_i \neq A_j, \quad i = 1, \ldots N,\ j = 1, \ldots N,\ i \neq j,\\
&g_i(\cdot) \neq g_j(\cdot), \quad i = 1, \ldots N,\ j = 1, \ldots N,\ i \neq j,
\end{aligned} \tag{2}$$

then the system (1) is an array of non-identical chaotic systems.

Now the above simple coupling form is applied to investigate the synchronization of N chaotic systems. The systems are

$$\begin{aligned}
\dot{x}_1 &= A_1 x_1 + g_1(x_1) + D_1(x_N - x_1),\\
\dot{x}_2 &= A_2 x_2 + g_2(x_2) + D_2(x_1 - x_2) + u_1,\\
&\vdots\\
\dot{x}_N &= A_N x_N + g_n(x_N) + D_N(x_{N-1} - x_N) + u_{N-1}.
\end{aligned} \tag{3}$$

Let the state error be $e_{i-1} = x_i - x_{i-1}$, $(i = 2, \ldots, N)$. It is not difficult to obtain the following dynamical error system:

$$\begin{aligned}
\dot{e} = &\begin{bmatrix}
A_2 - D_1 - D_2 & -D_1 & -D_1 & \cdots & -D_1\\
D_2 & A_3 - D_3 & 0 & \cdots & 0\\
0 & D_3 & A_4 - D_4 & \cdots & 0\\
\vdots & \vdots & \vdots & \vdots & \vdots\\
0 & 0 & 0 & \cdots & A_N - D_N
\end{bmatrix}
\begin{bmatrix} e_1\\ e_2\\ e_3\\ \vdots\\ e_{N-1} \end{bmatrix}\\
&+ \begin{bmatrix}
(A_2 - A_1)x_1 + g_2(x_2) - g_1(x_1) + u_1\\
(A_3 - A_2)x_2 + g_3(x_3) - g_2(x_2) + u_2 - u_1\\
\vdots\\
(A_N - A_{N-1})x_{N-1} + g_N(x_N) - g_{N-1}(x_{N-1}) + u_{N-1} - u_{N-2}
\end{bmatrix}.
\end{aligned} \tag{4}$$

Our purpose is to design the controllers u_i $(i = 1, \ldots, N-1)$ such that the error system (4) is asymptotically stable at the origin. That is,

$$\lim_{t \to \infty} \|e_{i-1}\| = \lim_{t \to \infty} \|x_i - x_{i-1}\| = 0. \tag{5}$$

This implies that the synchronization of chaotic systems (3) is realized.

Here a direct design control method [7, 8, 21] is used to achieve the objective. This method presents an easy procedure of selecting proper controllers in chaos synchronization. So we adopt this method to transform the error system into a stable system with a special antisymmetric structure. The main results are given below.

First, we choose the control input u_i to eliminate all known items that cannot be shown in the form of the error system e_i. The controllers are given by

$$\begin{aligned}
u_1 &= v_1 - (A_2 - A_1)x_1 - g_2(x_2) + g_1(x_1),\\
u_2 &= v_2 - (A_3 - A_2)x_2 - g_3(x_3) + g_2(x_2) + u_1,\\
&\vdots\\
u_{N-1} &= v_{N-1} - (A_N - A_{N-1})x_{N-1}\\
&\quad - g_N(x_N) + g_{N-1}(x_{N-1}) + u_{N-2},
\end{aligned} \tag{6}$$

where $\begin{bmatrix} v_1 & v_2 & \cdots & v_{N-1} \end{bmatrix}^T = H \begin{bmatrix} e_1 & e_2 & \cdots & e_{N-1} \end{bmatrix}^T$ and H is a coefficient matrix. So, the error systems (4) are rewritten by

$$\dot{e} = L(e)\, e, \tag{7}$$

where

$$L(e) = \begin{bmatrix}
A_2 - D_1 - D_2 & -D_1 & -D_1 & \cdots & -D_1\\
D_2 & A_3 - D_3 & 0 & \cdots & 0\\
0 & D_3 & A_4 - D_4 & \cdots & 0\\
\vdots & \vdots & \vdots & \vdots & \vdots\\
0 & 0 & 0 & \cdots & A_N - D_N
\end{bmatrix} + H. \tag{8}$$

Theorem 1. *Consider the systems* (7) *with the state dependent coefficient* $L(e) = L_1(e) + L_2$. *If* $L_1(e)$ *and* L_2 *satisfy the following assumptions:*

$$\begin{aligned}
&L_1^T(e) = -L_1(e),\\
&L_2 = \mathrm{diag}(l_1, \ldots, l_n), \quad l_i < 0, (i = 1, \ldots, n),
\end{aligned} \tag{9}$$

then the system (7) *is asymptotically stable, which means that the complete synchronization of* N *coupled chaotic systems* (3) *are achieved.*

Proof. Choose a Lyapunov function to be

$$V = \frac{1}{2} e^T e. \tag{10}$$

The derivative of V is

$$\dot{V} = \frac{1}{2}\left(\dot{e}^T e + e^T \dot{e}\right) = \frac{1}{2} e^T \left(L(e)^T + L(e)\right) e. \tag{11}$$

Since $L(e) = L_1(e) + L_2$, $L_1^T(e) = -L_1(e)$ and $L_2 = \mathrm{diag}(l_1, \ldots, l_n)$, $l_i < 0$, $(i = 1, \ldots, n)$, it is easy to get

$$\dot{V} = e^T L_2 e < 0. \tag{12}$$

From Lyapunov stability theory, we know that the equilibrium $e = 0$ of the system (7) is global asymptotically stable. Then the complete synchronization of N chaotic systems (3) is achieved. □

Remark 2. The error dynamic system (4) is transformed into the systems $\dot{e} = L(e)e$ under the control law u_i, where $L(e)$ possesses the antisymmetric structure. Theorem 1 ensures that the error system (4) is asymptotically stable at the origin.

Remark 3. There are many possible choices for H as long as it guarantees the error dynamic system (7) to be asymptotically stable at the origin. Without loss of generality, we define H to be a state dependent coefficient matrix. As a result, the sufficient stability conditions of the systems (7) are given by transforming it into a stable system with a special antisymmetric structure.

Remark 4. The antisymmetric structures in Theorem 1 are the generalization of the tridiagonal structures. The error system constructed with the antisymmetric structure is more convenient than the one with tridiagonal structure when the original system has some zero elements at the tridiagonal position and nonzero elements at other positions.

Since the antisymmetric structure is related to the coefficient matrices and the states of the original system, the selecting of the coefficient matrices with antisymmetric structure is an important and difficult task. In the next section, we will demonstrate the proposed approaches for the special structure through numerical examples.

3. Applications of Synchronization Control Schemes

In this section, we use two simulation examples to illustrate the effectiveness of the proposed schemes. The synchronization is simulated for the non-identical and identical chaotic systems, respectively.

Case 1. When the drive system and response systems are identical chaotic systems, the drive system and response systems are all the Lorenz chaotic system. They are described as follows:

$$\begin{aligned}
\dot{x}_{11} &= -10x_{11} + 10x_{12} + d_{11}(x_{31} - x_{11}),\\
\dot{x}_{12} &= 28x_{11} - x_{12} - x_{11}x_{13} + d_{12}(x_{32} - x_{12}),\\
\dot{x}_{13} &= -\frac{8}{3}x_{13} + x_{11}x_{12} + d_{13}(x_{33} - x_{13}),\\
\dot{x}_{21} &= -10x_{21} + 10x_{22} + d_{21}(x_{11} - x_{21}) + u_{11},\\
\dot{x}_{22} &= 28x_{21} - x_{22} - x_{21}x_{23} + d_{22}(x_{12} - x_{22}) + u_{12},\\
\dot{x}_{23} &= -\frac{8}{3}x_{23} + x_{21}x_{22} + d_{23}(x_{13} - x_{23}) + u_{13},\\
\dot{x}_{31} &= -10x_{31} + 10x_{32} + d_{31}(x_{21} - x_{31}) + u_{21},\\
\dot{x}_{32} &= 28x_{31} - x_{32} - x_{31}x_{33} + d_{32}(x_{22} - x_{32}) + u_{22},\\
\dot{x}_{33} &= -\frac{8}{3}x_{33} + x_{31}x_{32} + d_{33}(x_{23} - x_{33}) + u_{23},
\end{aligned} \tag{13}$$

where

$$\begin{aligned}
A_1 = A_2 = A_3 = A &= \begin{bmatrix} -10 & 10 & 0 \\ 28 & -1 & 0 \\ 0 & 0 & -\frac{8}{3} \end{bmatrix},\\
g_1(x_1) &= \begin{bmatrix} 0 \\ -x_{11}x_{13} \\ x_{11}x_{12} \end{bmatrix}, \qquad g_2(x_2) = \begin{bmatrix} 0 \\ -x_{21}x_{23} \\ x_{21}x_{22} \end{bmatrix},\\
g_3(x_3) &= \begin{bmatrix} 0 \\ -x_{31}x_{33} \\ x_{31}x_{32} \end{bmatrix},
\end{aligned} \tag{14}$$

and $D_1 = \mathrm{diag}(d_{11}, d_{12}, d_{13})$, $D_2 = \mathrm{diag}(d_{21}, d_{22}, d_{23})$, $D_3 = \mathrm{diag}(d_{31}, d_{32}, d_{33})$ are the coupled matrices, and $u_1 = [u_{11}, u_{12}, u_{13}]^T$ and $u_2 = [u_{21}, u_{22}, u_{23}]^T$ are the control inputs.

Let the synchronization error state be $\dot{e}_{i-1} = \dot{x}_i - \dot{x}_{i-1}$, $(i = 2, 3)$. The error dynamical equations are

$$\dot{e} = \begin{bmatrix} \Gamma_1 & \Gamma_2 \\ \Gamma_3 & \Gamma_4 \end{bmatrix} e + \begin{bmatrix} u_{11} \\ -x_{21}x_{23} + x_{11}x_{13} + u_{12} \\ x_{21}x_{22} - x_{11}x_{12} + u_{13} \\ u_{21} - u_{11} \\ -x_{31}x_{33} + x_{21}x_{23} + u_{22} - u_{12} \\ x_{31}x_{32} - x_{21}x_{22} + u_{23} - u_{13} \end{bmatrix}, \tag{15}$$

where

$$\begin{aligned}
\Gamma_1 &= \begin{bmatrix} -10 - d_{11} - d_{21} & 10 & 0 \\ 28 & -1 - d_{12} - d_{22} & 0 \\ 0 & 0 & -\frac{8}{3} - d_{13} - d_{23} \end{bmatrix},\\
\Gamma_2 &= \begin{bmatrix} -d_{11} & 0 & 0 \\ 0 & -d_{12} & 0 \\ 0 & 0 & -d_{13} \end{bmatrix}, \qquad \Gamma_3 = \begin{bmatrix} d_{21} & 0 & 0 \\ 0 & d_{22} & 0 \\ 0 & 0 & d_{23} \end{bmatrix},\\
\Gamma_4 &= \begin{bmatrix} -10 - d_{31} & 10 & 0 \\ 28 & -1 - d_{32} & 0 \\ 0 & 0 & -\frac{8}{3} - d_{33} \end{bmatrix}.
\end{aligned} \tag{16}$$

We design the controllers u_1 and u_2 to be

$$\begin{aligned}
u_1 &= v_1 - g_2(x_2) + g_1(x_1),\\
u_2 &= v_2 + v_1 - g_3(x_3) + g_1(x_1),
\end{aligned} \tag{17}$$

where

$$v_1 = \begin{bmatrix} 0 & 0 & 0 & 0 & 0 & 0 \\ -38 & 0 & 0 & 0 & 0 & 0 \\ 0 & 0 & 0 & 0 & 0 & 0 \end{bmatrix} e,$$
$$v_2 = \begin{bmatrix} d_{11} - d_{21} & 0 & 0 & 0 & 0 & 0 \\ 38 & d_{12} - d_{22} & 0 & -38 & 0 & 0 \\ 0 & 0 & d_{13} - d_{23} & 0 & 0 & 0 \end{bmatrix} e. \tag{18}$$

The error systems (15) become

$$\dot{e} = \begin{bmatrix} \Gamma_1^* & \Gamma_2^* \\ \Gamma_3^* & \Gamma_4^* \end{bmatrix} e, \tag{19}$$

where

$$\Gamma_1^* = \begin{bmatrix} -10 - d_{11} - d_{21} & 10 & 0 \\ -10 & -1 - d_{12} - d_{22} & 0 \\ 0 & 0 & -\frac{8}{3} - d_{13} - d_{23} \end{bmatrix},$$
$$\Gamma_2^* = \begin{bmatrix} -d_{11} & 0 & 0 \\ 0 & -d_{12} & 0 \\ 0 & 0 & -d_{13} \end{bmatrix}, \quad \Gamma_3^* = \begin{bmatrix} d_{11} & 0 & 0 \\ 0 & d_{12} & 0 \\ 0 & 0 & d_{13} \end{bmatrix},$$
$$\Gamma_4^* = \begin{bmatrix} -10 - d_{31} & 10 & 0 \\ -10 & -1 - d_{32} & 0 \\ 0 & 0 & -\frac{8}{3} - d_{33} \end{bmatrix}. \tag{20}$$

If the conditions

$$-10 - d_{11} - d_{21} < 0, \quad -1 - d_{12} - d_{22} < 0,$$
$$-\frac{8}{3} - d_{13} - d_{23} < 0, \quad -10 - d_{31} < 0, \tag{21}$$
$$-1 - d_{32} < 0, \quad -\frac{8}{3} - d_{33} < 0$$

are satisfied, then Theorem 1 tells us that the error systems (19) are asymptotically stable at the origin under the controllers u_1 and u_2. It means that the synchronization of (13) is realized.

Fourth order Runge-Kutta integration method is used to numerical simulation with time step size 0.001. Let the initial conditions of the drive system and the response systems be $(x_{11}(0), x_{12}(0), x_{13}(0)) = (4, 5, -3)$, $(x_{21}(0), x_{22}(0), x_{23}(0)) = (5, 2, -5)$, and $(x_{31}(0), x_{32}(0), x_{33}(0)) = (11, 15, 10)$. respectively. And we choose that $d_{12} = d_{22} = d_{32} = d_{13} = d_{23} = d_{33} = 0$ and $d_{11} = d_{21} = d_{31} = 1$. The state trajectories of the error systems and chaotic systems are shown in Figures 1, 2, 3, and 4, respectively. It is easy to see that the state variables and the error variables all tend towards to less than 2 s under the controllers. Simulation results demonstrate that the convergence rates are much faster than the earlier research results proposed in the literature [19, 21]; then the effectiveness of the synchronization control schemes is confirmed.

Case 2. When the drive system and response systems are non-identical chaotic systems, the Chen system, Lü system,

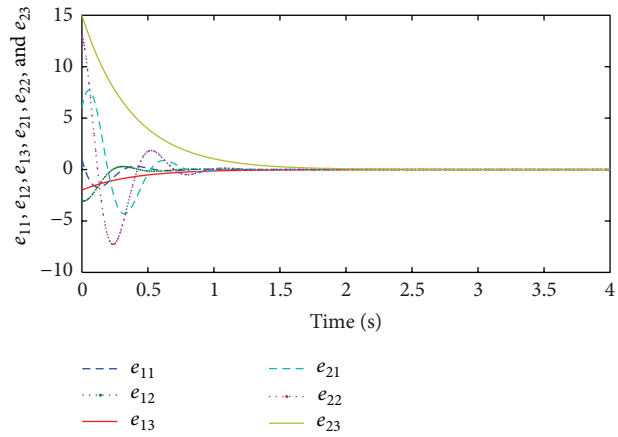

FIGURE 1: Dynamics of the variables e_{11}, e_{12}, e_{13}, e_{21}, and e_{22} and e_{23} of the error systems e_1 and e_2 with time t.

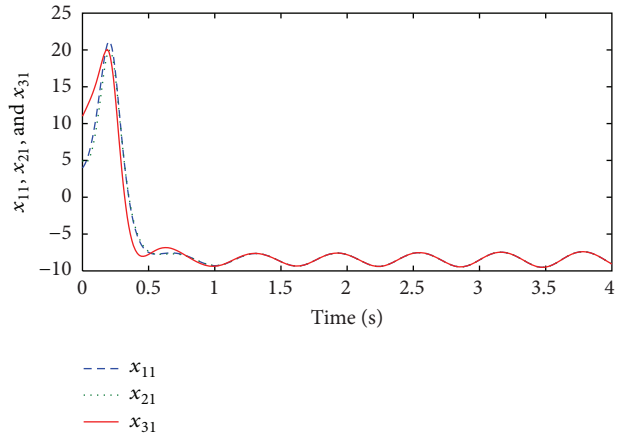

FIGURE 2: The state trajectories x_{11}, x_{21}, and x_{31} of the Lorenz systems with time t.

and Lorenz system are considered as drive system and response systems, respectively. They are described as follows:

$$\begin{aligned}
\dot{x}_{11} &= -35x_{11} + 35x_{12} + d_{11}(x_{31} - x_{11}), \\
\dot{x}_{12} &= -7x_{11} + 28x_{12} - x_{11}x_{13} + d_{12}(x_{32} - x_{12}), \\
\dot{x}_{13} &= -3x_{13} + x_{11}x_{12} + d_{13}(x_{33} - x_{13}), \\
\dot{x}_{21} &= -36x_{21} + 36x_{22} + d_{21}(x_{11} - x_{21}) + u_{11}, \\
\dot{x}_{22} &= 20x_{22} - x_{21}x_{23} + d_{22}(x_{12} - x_{22}) + u_{12}, \\
\dot{x}_{23} &= -3x_{23} + x_{21}x_{22} + d_{23}(x_{13} - x_{23}) + u_{13}, \\
\dot{x}_{31} &= -10x_{31} + 10x_{32} + d_{31}(x_{21} - x_{31}) + u_{21}, \\
\dot{x}_{32} &= 28x_{31} - x_{32} - x_{31}x_{33} + d_{32}(x_{22} - x_{32}) + u_{22}, \\
\dot{x}_{33} &= -\frac{8}{3}x_{33} + x_{31}x_{32} + d_{33}(x_{23} - x_{33}) + u_{23},
\end{aligned} \tag{22}$$

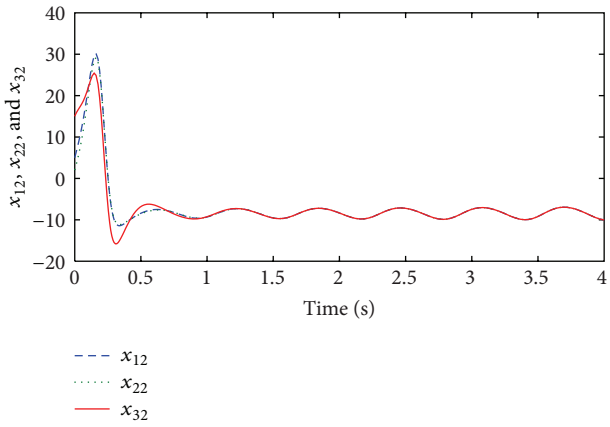

FIGURE 3: The state trajectories x_{12}, x_{22}, and x_{32} of the Lorenz systems with time t.

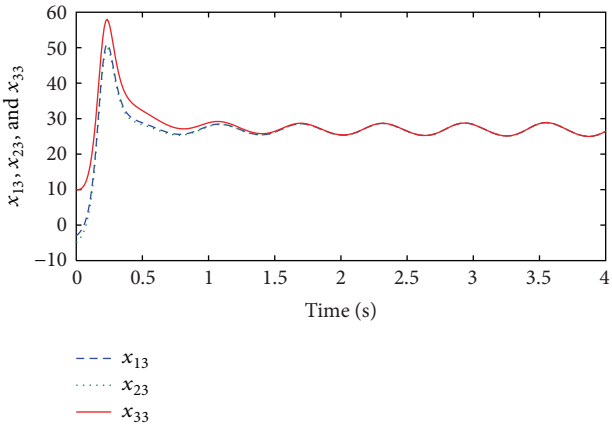

FIGURE 4: The state trajectories x_{13}, x_{23}, and x_{33} of the Lorenz systems with time t.

where

$$A_1 = \begin{bmatrix} -35 & 35 & 0 \\ -7 & 28 & 0 \\ 0 & 0 & -3 \end{bmatrix}, \quad A_2 = \begin{bmatrix} -36 & 36 & 0 \\ 0 & 20 & 0 \\ 0 & 0 & -3 \end{bmatrix},$$

$$A_3 = \begin{bmatrix} -10 & 10 & 0 \\ 28 & -1 & 0 \\ 0 & 0 & -\frac{8}{3} \end{bmatrix},$$

$$g_1(x_1) = \begin{bmatrix} 0 \\ -x_{11}x_{13} \\ x_{11}x_{12} \end{bmatrix}, \quad g_2(x_2) = \begin{bmatrix} 0 \\ -x_{21}x_{23} \\ x_{21}x_{22} \end{bmatrix},$$

$$g_3(x_3) = \begin{bmatrix} 0 \\ -x_{31}x_{33} \\ x_{31}x_{32} \end{bmatrix}, \tag{23}$$

and $D_1 = \mathrm{diag}(d_{11}, d_{12}, d_{13})$, $D_2 = \mathrm{diag}(d_{21}, d_{22}, d_{23})$, and $D_3 = \mathrm{diag}(d_{31}, d_{32}, d_{33})$ are the coupled matrices, and $u_1 = [u_{11}, u_{12}, u_{13}]^T$ and $u_2 = [u_{21}, u_{22}, u_{23}]^T$ are the control inputs.

Let the synchronization error state be $\dot{e}_{i-1} = \dot{x}_i - \dot{x}_{i-1}$, $(i = 2, 3)$. The error dynamical equations are

$$\dot{e} = \begin{bmatrix} \Delta_1 & \Delta_2 \\ \Delta_3 & \Delta_4 \end{bmatrix} e + \begin{bmatrix} -x_{11} - x_{12} + u_{11} \\ 7x_{11} - 8x_{12} - x_{21}x_{23} + x_{11}x_{13} + u_{12} \\ x_{21}x_{22} - x_{11}x_{12} + u_{13} \\ 26x_{21} + 26x_{22} + u_{21} - u_{11} \\ 28x_{21} - 21x_{22} - x_{31}x_{33} + x_{21}x_{23} + u_{22} - u_{12} \\ \frac{1}{3}x_{23} + x_{31}x_{32} - x_{21}x_{22} + u_{23} - u_{13} \end{bmatrix}, \tag{24}$$

where

$$\Delta_1 = \begin{bmatrix} -36 - d_{11} - d_{21} & 36 & 0 \\ 0 & 20 - d_{12} - d_{22} & 0 \\ 0 & 0 & -3 - d_{13} - d_{23} \end{bmatrix},$$

$$\Delta_2 = \begin{bmatrix} -d_{11} & 0 & 0 \\ 0 & -d_{12} & 0 \\ 0 & 0 & -d_{13} \end{bmatrix}, \quad \Delta_3 = \begin{bmatrix} d_{21} & 0 & 0 \\ 0 & d_{22} & 0 \\ 0 & 0 & d_{23} \end{bmatrix},$$

$$\Delta_4 = \begin{bmatrix} -10 - d_{31} & 10 & 0 \\ 28 & -1 - d_{32} & 0 \\ 0 & 0 & -\frac{8}{3} - d_{33} \end{bmatrix}. \tag{25}$$

The controllers u_1 and u_2 are designed as

$$u_1 = v_1 - (A_2 - A_1)x_1 - g_2(x_2) + g_1(x_1),$$
$$u_2 = v_2 + v_1 - (A_3 - A_1)x_1 - g_3(x_3) + g_1(x_1), \tag{26}$$

where

$$v_1 = \begin{bmatrix} 0 & 0 & 0 & 0 & 0 & 0 \\ -36 & 0 & 0 & 0 & 0 & 0 \\ 0 & 0 & 0 & 0 & 0 & 0 \end{bmatrix} e,$$
$$v_2 = \begin{bmatrix} d_{11} - d_{21} & 0 & 0 & 0 & 0 & 0 \\ 36 & d_{12} - d_{22} & 0 & -38 & 0 & 0 \\ 0 & 0 & d_{13} - d_{23} & 0 & 0 & 0 \end{bmatrix} e. \tag{27}$$

The error systems (24) become

$$\dot{e} = \begin{bmatrix} \Delta_1^* & \Delta_2^* \\ \Delta_3^* & \Delta_4^* \end{bmatrix} e, \tag{28}$$

where

$$\Delta_1^* = \begin{bmatrix} -36 - d_{11} - d_{21} & 36 & 0 \\ -36 & 20 - d_{12} - d_{22} & 0 \\ 0 & 0 & -3 - d_{13} - d_{23} \end{bmatrix},$$

$$\Delta_2^* = \begin{bmatrix} -d_{11} & 0 & 0 \\ 0 & -d_{12} & 0 \\ 0 & 0 & -d_{13} \end{bmatrix}, \quad \Delta_3^* = \begin{bmatrix} d_{11} & 0 & 0 \\ 0 & d_{12} & 0 \\ 0 & 0 & d_{13} \end{bmatrix},$$

$$\Delta_4^* = \begin{bmatrix} -10 - d_{31} & 10 & 0 \\ -10 & -1 - d_{32} & 0 \\ 0 & 0 & -\frac{8}{3} - d_{33} \end{bmatrix}. \tag{29}$$

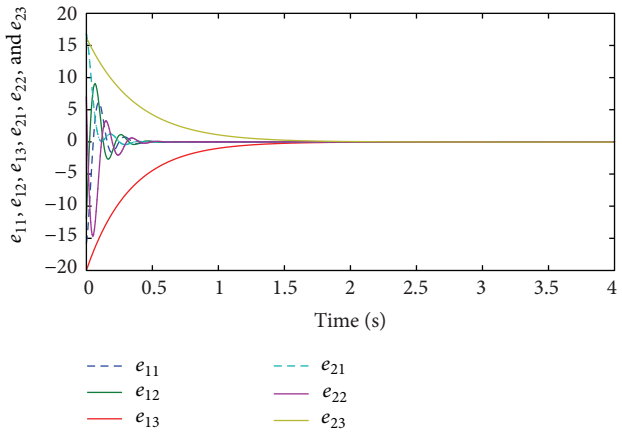

FIGURE 5: Dynamics of the variables e_{11}, e_{12}, and e_{13} of the error system e_1 with time t.

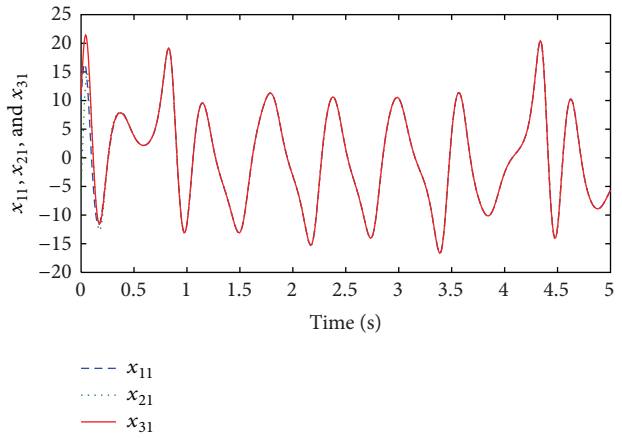

FIGURE 6: The state trajectories x_{11}, x_{21}, and x_{31} of the chaotic systems with time t.

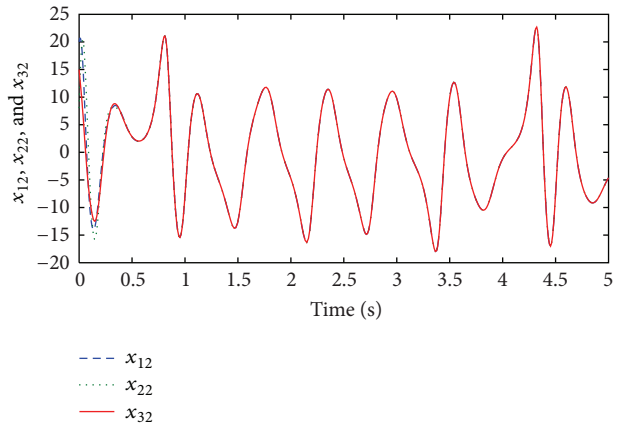

FIGURE 7: The state trajectories x_{12}, x_{22}, and x_{32} of the chaotic systems with time t.

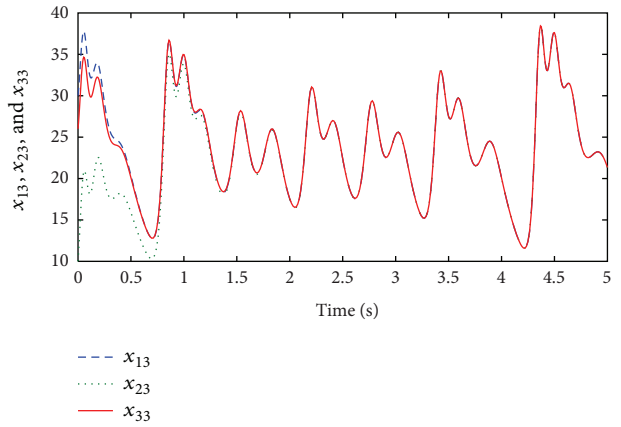

FIGURE 8: The state trajectories x_{13}, x_{23}, and x_{33} of the chaotic systems with time t.

From Theorem 1, we know that the conditions

$$\begin{aligned} &-36 - d_{11} - d_{21} < 0, \qquad 20 - d_{12} - d_{22} < 0, \\ &-3 - d_{13} - d_{23} < 0, \qquad -10 - d_{31} < 0, \\ &-1 - d_{32} < 0, \qquad -\frac{8}{3} - d_{33} < 0 \end{aligned} \tag{30}$$

ensure that the error systems (28) are asymptotically stable at the origin under the controllers u_1 and u_2. Thus, the synchronization between the response systems and the drive systems is realized.

Similar to Case 1, let the initial conditions of the drive system and the response systems be $(x_{11}(0), x_{12}(0), x_{13}(0)) = (10, 20, 30)$, $(x_{21}(0), x_{22}(0), x_{23}(0)) = (-5.8, 8, 10)$, and $(x_{31}(0), x_{32}(0), x_{33}(0)) = (11, 15, 26)$, respectively. And we choose that $d_{11} = d_{21} = d_{13} = d_{23} = d_{31} = d_{33} = 0$, $d_{12} = 10$, $d_{22} = 11$, and $d_{32} = 1$. The state trajectories of the error systems and chaotic systems are shown in Figures 5, 6, 7, and 8, respectively. It is easy to see that the state variables and the error variables all tend towards to less than 1.5 s under the controllers. Simulation results demonstrate that the convergence rates are much faster than the earlier research results proposed in the literature [19, 21]; then the effectiveness of the synchronization control schemes is confirmed.

4. Conclusions

This paper concerns the synchronization of N coupled chaotic systems with ring connection. A direct design control method is firstly used to design the controllers. The synchronization of N coupled chaotic systems is realized by coupling the state variables. This technology will undoubtedly improve performance of secret signaling and possess better application value in practice. Furthermore, our presented strategy can ensure strict synchronization between N coupled chaotic systems. This will lead to a rapid development in multilateral communications.

Acknowledgments

The author's work was supported in part by the Applied Mathematics Enhancement Program (AMEP) of Linyi University

and the National Natural Science Foundation of China, under Grants 61273012 and 61273218, by a project supported by the Scientific Research Fund of Zhejiang Provincial Education Department under Grant Y201223649, by a Project of Shandong Province Higher Educational Science and Technology Program under Grants J13LI11 and J12LI58.

References

[1] L. M. Pecora and T. L. Carroll, "Synchronization in chaotic systems," *Physical Review Letters*, vol. 64, no. 8, pp. 821–824, 1990.

[2] B. Nana, P. Woafo, and S. Domngang, "Chaotic synchronization with experimental application to secure communications," *Communications in Nonlinear Science and Numerical Simulation*, vol. 14, no. 5, pp. 2266–2276, 2009.

[3] C. Aguirre, D. Campos, P. Pascual, and E. Serrano, "Synchronization effects using a piecewise linear map-based spiking-bursting neuron model," *Neurocomputing*, vol. 69, no. 10–12, pp. 1116–1119, 2006.

[4] S. Tang and J. M. Liu, "Chaos synchronization in semiconductor lasers with optoelectronic feedback," *IEEE Journal of Quantum Electronics*, vol. 39, no. 6, pp. 708–715, 2003.

[5] J.-J. Yan, Y.-S. Yang, T.-Y. Chiang, and C.-Y. Chen, "Robust synchronization of unified chaotic systems via sliding mode control," *Chaos, Solitons and Fractals*, vol. 34, no. 3, pp. 947–954, 2007.

[6] S. Guan, C.-H. Lai, and G. W. Wei, "Phase synchronization between two essentially different chaotic systems," *Physical Review E*, vol. 72, no. 1, Article ID 016205, 8 pages, 2005.

[7] N. Cai, Y. W. Jing, and S. Y. Zhang, "Adaptive synchronization and anti-synchronization of two different chaotic systems," *Acta Physica Sinica*, vol. 58, no. 2, pp. 802–813, 2009.

[8] N. Cai, Y. Jing, and S. Zhang, "Generalized projective synchronization of different chaotic systems based on antisymmetric structure," *Chaos, Solitons and Fractals*, vol. 42, no. 2, pp. 1190–1196, 2009.

[9] J. Cao, D. W. C. Ho, and Y. Yang, "Projective synchronization of a class of delayed chaotic systems via impulsive control," *Physics Letters A*, vol. 373, no. 35, pp. 3128–3133, 2009.

[10] W. He and J. Cao, "Generalized synchronization of chaotic systems: an auxiliary system approach via matrix measure," *Chaos*, vol. 19, no. 1, Article ID 013118, 10 pages, 2009.

[11] Q. Gan, R. Xu, and P. Yang, "Synchronization of non-identical chaotic delayed fuzzy cellular neural networks based on sliding mode control," *Communications in Nonlinear Science and Numerical Simulation*, vol. 17, no. 1, pp. 433–443, 2012.

[12] J. Lu, J. Cao, and D. W. C. Ho, "Adaptive stabilization and synchronization for chaotic Lur'e systems with time-varying delay," *IEEE Transactions on Circuits and Systems I*, vol. 55, no. 5, pp. 1347–1356, 2008.

[13] W. Yu, G. Chen, J. Lü, and J. Kurths, "Synchronization via pinning control on general complex networks," *SIAM Journal on Control and Optimization*, vol. 51, no. 2, pp. 1395–1416, 2013.

[14] Q. Gan and Y. Liang, "Synchronization of chaotic neural networks with time delay in the leakage term and parametric uncertainties based on sampled-data control," *Journal of the Franklin Institute*, vol. 349, no. 6, pp. 1955–1971, 2012.

[15] Q.-L. Zhang, "Synchronization of multi-chaotic systems via ring impulsive control," *Journal of Control Theory and Applications*, vol. 27, no. 2, pp. 226–232, 2010.

[16] Y. Yu and S. Zhang, "Global synchronization of three coupled chaotic systems with ring connection," *Chaos, Solitons and Fractals*, vol. 24, no. 5, pp. 1233–1242, 2005.

[17] J.-A. Lu, X.-P. Han, Y.-T. Li, and M.-H. Yu, "Adaptive coupled synchronization among multi-Lorenz systems family," *Chaos, Solitons and Fractals*, vol. 31, no. 4, pp. 866–878, 2007.

[18] G. Grassi, "Propagation of projective synchronization in a series connection of chaotic systems," *Journal of the Franklin Institute*, vol. 347, no. 2, pp. 438–451, 2010.

[19] Y. Liu and L. Lü, "Synchronization of N different coupled chaotic systems with ring and chain connections," *Applied Mathematics and Mechanics*, vol. 29, no. 10, pp. 1299–1308, 2008.

[20] Y. Tang and J.-A. Fang, "Synchronization of N-coupled fractional-order chaotic systems with ring connection," *Communications in Nonlinear Science and Numerical Simulation*, vol. 15, no. 2, pp. 401–412, 2010.

[21] X. Chen and J. Qiu, "Synchronization of N different chaotic systems based on antisymmetric structure," *Mathematical Problems in Engineering*, vol. 2013, Article ID 742765, 6 pages, 2013.

[22] L.-X. Yang and J. Zhang, "Synchronization of three identical systems and its application for secure communication with noise perturbation," in *Proceedings of the International Conference on Information Engineering and Computer Science (ICIECS '09)*, pp. 1–4, Wuhan, China, December 2009.

Hindawi Publishing Corporation
Abstract and Applied Analysis
Volume 2013, Article ID 940809, 8 pages
http://dx.doi.org/10.1155/2013/940809

Research Article

Gossip Consensus Algorithm Based on Time-Varying Influence Factors and Weakly Connected Graph for Opinion Evolution in Social Networks

Lingyun Li,[1] Jie Zhou,[1] Demin Li,[2] Jinde Cao,[3,4] and Xiaolu Zhang[2]

[1] *School of Science, Donghua University, Shanghai 201620, China*
[2] *College of Information Science and Technology, Donghua University, Shanghai 201620, China*
[3] *Department of Mathematics, Southeast University, Nanjing 210096, China*
[4] *Department of Mathematics, King Abdulaziz University, Jeddah 21589, Saudi Arabia*

Correspondence should be addressed to Demin Li; deminli@dhu.edu.cn

Received 5 July 2013; Revised 25 August 2013; Accepted 27 August 2013

Academic Editor: Jianquan Lu

We provide a new gossip algorithm to investigate the problem of opinion consensus with the time-varying influence factors and weakly connected graph among multiple agents. What is more, we discuss not only the effect of the time-varying factors and the randomized topological structure but also the spread of misinformation and communication constrains described by probabilistic quantized communication in the social network. Under the underlying weakly connected graph, we first denote that all opinion states converge to a stochastic consensus almost surely; that is, our algorithm indeed achieves the consensus with probability one. Furthermore, our results show that the mean of all the opinion states converges to the average of the initial states when time-varying influence factors satisfy some conditions. Finally, we give a result about the square mean error between the dynamic opinion states and the benchmark without quantized communication.

1. Introduction

Individuals form beliefs on various economic, political, and social state based on information they receive from others, including friends, neighbors, and coworkers as well as local leaders and news sources. The society may face the tradeoff whether this process of information aggregation will lead to the formation of more accurate beliefs or to certain bias, which is led by the limit of communication and the change of mutual influence. Gossips, rumors, and other misinformation are an important form of social communications, and their spreading plays a significant role in human affairs. The spread of them can shape the public opinion in a country, greatly impact financial markets, and cause panic in a society during wars and epidemics outbreaks. The information content of rumors can range from simple gossip to advanced propaganda and marketing material. In practice, social groups are often swayed by misleading ads, media outlets, and political leaders, so they may hold on to incorrect and inaccurate beliefs. A central question we are interested in is to study the conditions under which exchange of information will lead to aggregation of dispersed information. We also pay attention to the gap between this consensus and the true value of the underlying state in society.

Social networks constitute a new method of studying social mechanism that has grown tremendously over the last decade. Decentralized is the inevitable trend of the development of network technology. In addition, the unprecedented number of interacting agents, the time-varying topology of agent interactions, and the unreliability of agents are key challenges for the analysis and design of this mechanism. Gossip algorithms, as an asynchronous time algorithm, have the special feature that each agent exchanges information and decisions with at most one neighboring agent in each time

slot. So, gossip algorithms have been proven to be an efficacious approach to achieve fault-tolerant information dissemination. Furthermore, these algorithms can be applied in such a decentralized, large scale, and dynamically distributed network very well. In social networks, gossip algorithms to solve consensus problems have attracted a lot of interest. Based on probabilistic quantized communication, whether a group of agents has to agree under the weakly connected graph and time-varying influence factors in the communication process, starting from different initial estimates is the problem we need to study in this paper.

Consensus problems have been discussed through the great number of different opinion formation models by a lot of people. To relax the requirement of the global clock synchronization, Boyd et al. [1] proposed a compelling gossip algorithms, which provides an asynchronous approach to treat average consensus and describe the randomized node interaction. Based on social network, Acemoglu et al. in [2] provided a gossip model to investigate the tension between information aggregation and the spread of misinformation, which individuals meet pairwise and exchange information, which is modeled as both individuals adopting the average of their beliefs. In [3], Shi and Johansson considered and solved a randomized optimal consensus problem for multiagent systems with stochastically time-varying topology.

Since communication constraints play a major role in consensus and related problems, Carli et al. in [4] considered the average consensus problem based on a deterministic or a randomized quantizer and studied the convergence based on pairwise gossip communications and updates. Yuan et al. [5] dealt with a more general probabilistic quantization case which is that the mixing parameter ranges from 0 to 1. In [6], Ceragioli and his collaborators considered continuous-time average consensus dynamics in which the agent's states are communicated through uniform quantizers. Recently, Wang et al. in [7] studied the problem of broadcast gossip average consensus with quantization constraints in the wireless sensor network. With the similar problem, Cai and Ishii [8] proposed the directed graphs with the least restrictive connectivity requirements.

We can know that the consensus problems in gossip algorithms [1–3] were important for large-scale information dissemination on the Internet, in the sensor network, and in peer-to-peer file sharing applications. Considering communication constraints and the spread of misinformation, more scholars [4–8] studied a class of gossip algorithms based on quantized communication, at the same time, they paid more attention to the time-invariant influence factors. According to the character of social network, we will not only consider communication constraints on strongly connected graph but also study with the broader topology and time-varying influence factors.

Our work has been influenced by reading the papers [8] which one based on strongly connected graph and [5] which also has the quantized communication. Compared to the former paper, our contribution is under the weaker assumption about the underlying topology, and thus broader discussion of opinion evolution will be given. Compared to the latter paper, we allow the information exchange between agents with time-varying influence factors, rather than the constant factors which one more precise and realistic in social network.

In this paper, we provide a new gossip consensus algorithm based on weakly connected graph to describe the randomized agent interactions and contain probabilistic quantized communication with time-varying influence factors. The paper is organized as follows: Section 2 introduces some descriptions of algorithm environment and our assumption, and gives a detailed description of the proposed algorithm. Section 3 provides the results that our algorithm indeed converges to a consensus almost surely, which is that all agents have the same opinion states, and this consensus value is a random variable. We also give a characterization of the expected value of this consensus with the influence factors satisfying some conditions. We also provide a result characterizing the convergence performance of the square mean error between the dynamic opinion and the average initial states. Section 4 gives some lemmas and the detailed proofs of the above results. We conclude the paper in Section 5.

2. Algorithm Description and Assumptions

In the following, we describe briefly the distributed average consensus problem along with the proposed consensus algorithm.

2.1. Description of the Environment. We consider a set $V = \{1, 2, \ldots, N\}$ of agents interacting and denote $\zeta = (V, E)$ as a directed and randomized graph, which we refer to as the social network. So, $(i, j) \in E$ and $(j, i) \in E$ are different. Each vertex of the graph is referred to as an agent, and each agent i begins with an initial belief $x_i(t)$ which evolves in discrete time t and represents its belief or opinion for every $i \in V$. The belief can be active when $x_i > 0$; otherwise, it can be negative and misleading when $x_i < 0$. Opinion belief represents the value of information. We devote $(1/N)\sum_{i=1}^{N} x_i(0)$ as the true value of the underlying aggregation state which represents the average of the dispersed initial states.

We use an asynchronous time algorithm introduced in [4] to describe interactions between agents. Particularly, we recognize that the information exchange results from bilateral communication under the circumstance of gossip, rumors, and misinformation. Moreover, each individual meets the other in her social neighborhoods according to a prespecified stochastic process and considers this stochastic process is representing an underlying social network such as friendships and information network. So, we assume that each agent communicates with the other agent at instances defined by a rate-one Poisson process independent of other agents.

In this algorithm, without loss of generality, at most, one node is meeting another at a given time [1]. Agent interactions are characterized by an $n \times n$ matrix $A = [a_{ij}]$ where $a_{ij} \geq 0$, and we can associate a unique diagraph $\zeta_A = (V, E_A)$ with A such that $(i, j) \in E_A$ if and only if $a_{ij} > 0$. We call $\zeta_A = (V, E_A)$ the induced graph A. We discretize time and suppose at time $k \geq 0$, agent i is chosen with probability $1/N$. In this case, agent i will meet agent $j \in V$ with probability a_{ij}. Following a meeting between i and j, there is a potential exchange

of information. Throughout, we assume that all events that happen in a meeting are independent of any other event that happened in the past. According to the above description, we can get the following definition.

Definition 1 (selection probabilities). Independent of time and agent state, at time $k \geq 0$,

(i) an agent $i \in V$ is selected with probability $1/N$,

(ii) for all i, the probabilities $a_{ii} = 0$,

(iii) agent i picks the edge (i, j) with probability a_{ij}, where $a_{ij} \geq 0$ for all i, j, $\sum_{j=1}^{N} a_{ij} = 1$.

From (iii), this implied that A is a row stochastic matrix.

In the social network, we want to reflect communication constraints by means of probabilistic quantization $\Phi(\cdot)$. For example, there exist the fact that words can't express meaning and everyone has different understanding so as to update partial information. In addition, people can understand themselves with the vague or fuzzy recognition sometimes. So we can use probabilistic quantization to show the actual opinion belief.

The probabilistic quantization has been introduced in [9]. The probabilistic quantization $\Phi : R \to R$ is defined as follows: suppose that $x \in R$ is bounded to a finite interval $[-I, I]$, and the interval is equally divided into $M-1$ subintervals with quantization points defined by the set $\theta = \{\theta_1, \theta_2, \ldots, \theta_M\}$, where $\theta_1 = -I$, $\theta_M = I$. Denote the interval as $\Delta = \theta_{i+1} - \theta_i$, for $i \in \{1, 2, \ldots, M-1\}$. Then, for $x \in [\theta_i, \theta_{i+1})$, $\Phi(x)$ is a random variable defined by

$$\Phi(x) = \begin{cases} \theta_i, & \text{with probability } \dfrac{(\theta_{i+1} - x)}{\Delta} \\ \theta_{i+1}, & \text{with probability } \dfrac{(x - \theta_i)}{\Delta}. \end{cases} \tag{1}$$

The following lemma gives two important properties of the probabilistic quantization.

Lemma 2 (see [10]). *For every $x \in [\theta_i, \theta_{i+1})$,*

$$E[\Phi(x)] = x, \qquad E\left[(x - \Phi(x))^2\right] \leq \frac{\Delta^2}{4}. \tag{2}$$

Note that $\Phi(x)$ is unbiased uniform quantization; that is, the quantized data $\Phi(x)$ is an unbiased representation of x.

2.2. Assumption. We consider a social network with the finite set $V = \{1, \ldots, N\}$ $(N \geq 3)$ of agents interacting. Each agent $i \in V$ starts with an initial belief which we denote by $x_i(0) \in [-I, I]$. Moreover, the underlying graph indicates potential interactions between agents.

Assumption 3 (connectivity see [11]). The underlying graph ζ_A is weakly connected.

Note that the graph ζ_A is the random graph. Here, we require that ζ_A keep the character of the weak connectivity.

Remark 4. Here, we can have a weaker assumption and a more extensive network. In the standing assumption of [8], the matrix A is supposed to have its largest eigenvalue equal to 1 and all other $N - 1$ eigenvalues strictly less than 1 in magnitude. This condition is equivalent with the underlying graph that is quasi-strongly connected. In order to guarantee convergence for the gossip algorithm discussed below, the assumption cannot be further weakened based on the following argument. If the weaker hold, they will be divide into two isolated groups at least in the network. As a result, agents in each group can only communicate with the others in the same group. So, the convergence for the whole network is impossible. If there is no-communication groups in fact, we also can apply our algorithm to each group. Moreover, most subsets of society are connected by means of several links, and the same seems to be true for indirect link via the Internet [2]. Therefore, Assumption 3 is a weaker assumption and weakly connected and random topology of social network reflects a wider social scope and relationship.

2.3. Description of the Consensus Algorithm. In society, we can usually listen to advice from other people, receive the influence of others, and eventually form their own views. Due to the change in the relationship over time and the limit in the communication, we will construct our average gossip algorithm based on quantized communication and time-varying impact factors. The gossip algorithms, as the name suggests, are built upon a gossip or rumor style unreliable, asynchronous information exchange protocol. At the same time, we use the symmetric gossip algorithm which is based on mutual trust between information exchangers. Let $x(t)$ denote the vector of all individual opinion value at the end of time instant t. Then, agent i and j can be connected with probability $A_{\langle i,j\rangle} = (1/N)(a_{ij} + a_{ji})$, and based bounded confidence and bilateral communication, the states of agent i and j evolve as follows:

$$\begin{aligned} x_i(t+1) &= (1 - S(t))\,\widehat{x}_i(t) + S(t)\,\widehat{x}_j(t), \\ x_j(t+1) &= S(t)\,\widehat{x}_j(t) + (1 - S(t))\,\widehat{x}_i(t), \\ x_k(t+1) &= \widehat{x}_k(t) \quad \text{for } k \neq i, j, \end{aligned} \tag{3}$$

where $\widehat{x}(t) = \Phi(x(t)) = [\Phi_1(x(t)), \Phi_2(x(t)), \ldots, \Phi_N(x(t))]$ and $S(t) \in (0, 1)$ is called the influence factor. The time-varying influence factor shows the size of the influence of each other, and each agent $i \in V$ starts with an initial belief $x_i(0) \in R$ and it is bounded to a finite interval $[-I, I]$. The agents' beliefs evolve according to the following stochastic update process. Furthermore, for the quantized version, the opinion states evolvement can be compactly written according to the following equation:

$$x(t+1) = A(t)\,\widehat{x}(t), \tag{4}$$

where the random matrix $A(t)$ satisfies

$$\text{Prob}\left(A(t) = I - S(t)\left(e_i - e_j\right)\left(e_i - e_j\right)^T\right) = A_{\langle i,j\rangle}, \tag{5}$$

and we define $A^{ij}(t) = I - S(t)(e_i - e_j)(e_i - e_j)^T$, where e_i, $i = 1, \ldots, N$ denotes the column vector in R^N having all entries equal to 0 except at a 1 in the ith position.

In the social network, we consider that probabilistic quantization $\Phi(\cdot)$ reflects communication constraints. For example, there exist the fact that words can not express meaning and everyone has different understanding so as to update partial information. In addition, people can understand themselves with the vague or fuzzy recognition in some times. But as time goes on and the increase of the number of the communication and information can get accurate expression with using $E[\Phi(x)] = x$. Furthermore, we are concerned that if each individual holds one opinion at the initial time, then can the dispersed group converge to a consensus? And if they can, what conditions must be needed? According to the above algorithm, we will talk about these problems as follows.

First, we know the convergence to a consensus means that a final unanimous consensus will be reached in some way. But what does the word "consensus" mean? From the view of the opinion algorithm, it means that an opinion vector in which all elements are the same. In other words, all individuals have the same opinion, which means a unanimous one. While final compromise means a compromise is reached for $t \to \infty$.

Then, in order to be convenient, we will follow the assumptions as above and give the results about the consensus.

3. Main Results

In this section, we provide our main convergence result based on the above algorithm. Particularly, we denote that despite the presence of quantized communication, with potentially very different initial opinions, the group will converge to a consensus almost surely, which all agents have the same opinion states. This consensus value is a random variable. We also provide the characterization of the expected value of this consensus under some conditions. In addition, we give a result about the square mean error between the dynamic opinion and the average initial states.

Here, we give a convergence theorem based on the topology of the underlying social network.

Theorem 5. *A global gossip consensus achieves the probabilistic consensus; that is,*

$$\Pr\left\{\lim_{t\to\infty} x(t) = c\widetilde{1}\right\} = 1, \tag{6}$$

where $\widetilde{1} \in R^N$ denotes the vector with all its entries equal to 1 and the random variable $c \in R$ satisfies

$$E[c] = \frac{1}{N}\widetilde{1}x(0), \tag{7}$$

when $S(t)$ satisfies $\sum_{t=0}^{\infty} S(t) = \infty$.

Remark 6. This result implies that the society will reach a dynamic consensus almost surely despite the presence of the quantized communication and the effect of influence factor under a weaker assumption that the underlying graph is weakly connected. Based on the network and the pattern of communication, all agents endowed with the different initial opinion will form the common opinion with probability 1, and the expected value of the common opinion will tend to be the true value of the underlying aggregation opinion when $S(t)$ satisfies some conditions. We also will discover that the above second conclusion still shows that even $S(t)$ is constant satisfying 0 to 1. In addition, either $S(t+1) > S(t)$ or $S(t+1) < S(t)$ for all t; that is, $S(t)$ is monotone, the conclusion is achieved only if $\sum_{t=0}^{\infty} S(t) = \infty$. Finally, in mathematics, the condition of divergent sequence is easier satisfied than that of convergent sequence. So, our condition can be satisfied in a rather wide range.

The following proposition provides the expectation of the error between the opinion states and the static average consensus.

Theorem 7. *The evolution of the square mean error from consensus of the algorithm satisfies*

$$E\left(\left\|x(t) - x_{\text{ave}}(t)\widetilde{1}\right\|^2\right) \le \left(1 - \frac{2}{N}S^*\lambda_2^*\right)^t \left\|x(0) - x_{\text{ave}}\widetilde{1}\right\|^2 + \frac{\Delta^2 N\left(N - 4S^* - 1\right)}{4S^*\lambda_2^*}, \tag{8}$$

where $S^* = \inf_{i\in N}\{S(i)(1 - S(t))\}$, $\lambda_2^* = \lambda_2^*(D - (A^T + A))$ for the given N, Δ.

Remark 8. We try to study the character of its square mean convergence and find that it does not meet this convergence. But from the above proposition, we can see the square mean error has an upper bound and estimate the convergence speed of the upper bound. The limit of the bound is $(\Delta^2 N(N - 4S^* - 1))/4S^*\lambda_2^*$ which depends on the quantized revolution, the second smallest eigenvalue of Laplacian matrix and the time-varying factors when $S^* \neq 0$.

4. Lemmas and Proofs

4.1. Average Matrix Properties

Lemma 9. *Define the expected value of $A(t)$ as*

$$\widetilde{A} = E[A(t)] = \frac{1}{N}\sum_{i,j} a_{ij}A^{ij}, \qquad \widehat{A} = E\left[A(t)^T A(t)\right], \tag{9}$$

then

$$\widetilde{A} = I - \frac{S(t)}{N}\left[D - \left(A + A^T\right)\right], \qquad \widehat{A} = I - \frac{2S(t)(1 - S(t))}{N}\left[D - \left(A + A^T\right)\right], \tag{10}$$

where $D = \text{diag}([D_1, D_2, \ldots, D_N])$ is the diagonal matrix with entries satisfying

$$D_i = \left(\sum_{j\neq i}\left(a_{ij} + a_{ji}\right)\right), \tag{11}$$

and for all $S(t) \in (0,1)$, $\widetilde{A}$, and $\widehat{A}$, respectively satisfies

$$\begin{aligned} \widetilde{A}\widetilde{1} &= \widetilde{1}, \qquad \widetilde{1}^T\widetilde{A} = \widetilde{1}^T, \\ \overline{A}\widetilde{1} &= \widetilde{1}, \qquad \widetilde{1}^T\overline{A} = \widetilde{1}^T, \qquad \rho\left(\widehat{A}\right) = 1, \end{aligned} \tag{12}$$

where $\widetilde{1} \in R^N$ denotes the vector with all its entries equal to 1.

Proof. From the fact that $\widetilde{A} = E[A(t)] = (1/N)\sum_{i,j} a_{ij}A^{ij}$, we can deduce that

$$\widetilde{A}_{ii} = 1 - \frac{S(t)\left[\sum_{j\neq i} a_{ij} + a_{ji}\right]}{N}, \qquad \widetilde{A}_{ij} = \frac{S(t)\left(a_{ij} + a_{ji}\right)}{N}, \tag{13}$$

then we can substitute these into the matrix $\widetilde{A}$, in the similar way, we can get $\widehat{A}$.

It is easy to see that the matrix $\widetilde{A}$ is the symmetric matrix and the sum of the row in $\widetilde{A}$ is 1. So, we have

$$\widetilde{A}\widetilde{1} = \widetilde{1}, \qquad \widetilde{1}^T\widetilde{A} = \widetilde{1}^T. \tag{14}$$

From the above equation, $\widehat{A}$ have the same character. So $\widetilde{1}$ is the eigenvector of the eigenvalue 1. Using the Gersgorin disc theorem [12], we have

$$0 \leq \lambda\left(D - \left(A^T + A\right)\right) \leq 2N, \tag{15}$$

where $\lambda(\cdot)$ denotes the eigenvalue of a symmetric matrix. Therefore,

$$\begin{aligned} 0 \leq 2S(t)(1 - S(t))\lambda\left(D - \left(A^T + A\right)\right) &\leq 4S(t) \\ \times (1 - S(t)) \leq 4\left(\frac{S(t) + 1 - S(t)}{2}\right)^2 &= 1. \end{aligned} \tag{16}$$

Then, the spectrum of $\widehat{A}$ is 1. □

Lemma 10 (see [13]). *Define $\{T_k\}$ is a sequence of real numbers with $T_k \in [0,1)$ for all $k \in [0,+\infty)$, then*

$$\sum_{k=0}^{\infty} T_k = \infty \quad \text{iff} \prod_{k=0}^{\infty}(1 - T_k) = 0. \tag{17}$$

4.2. The Proof of Theorem 5. Proof of Theorem 5: in the first part, we will prove the character of convergence. with loss of probability, we consider the integer quantization in the range $[1, m]$. Define a discrete Markov chain M with initial state $\widehat{x}(0)$, and the transition matrix is defined by the combination of the quantized gossip consensus algorithm $x(t+1) = A(t)\widehat{x}(t)$ and the probabilistic quantization operator $\Phi(\cdot)$.

Define $x_{\text{ave}}(t) = (1/N)\widetilde{1}^T x(t)$ and $x_{\text{ave}} = (1/N)\widetilde{1}^T x(0)$, when $t > 0$. Note that the gossip consensus algorithm satisfies

$$\left\|x(t+1) - x_{\text{ave}}(t+1)\,\widetilde{1}\right\| \leq \left\|x(t) - x_{\text{ave}}(t)\,\widetilde{1}\right\|, \tag{18}$$

the equality holds when the two agents chosen at time instant t have the same quantized state value. Thus, there is a nonzero probability that the strict inequality holds when the consensus is not achieved. Moreover, using the fact that $cA(t)\widetilde{1} = c\widetilde{1}$, we can derive

$$\widehat{x}(t+1) = \Phi[A(t)\widehat{x}(t)] = \Phi[\widehat{x}(t)] = \widehat{x}(t), \tag{19}$$

when $\widehat{x}(t) = c\widetilde{1}$. Then, following a similar line as in the proof of Theorem 1 in [13], we can prove that there exists a sequence of transitions with nonzero probability whose application yields absorption; that is, the probabilistic consensus is achieved.

In the second part, we will consider the character of mean about the state value.

We can use the Lebesgue dominated convergence theorem [14] to give

$$E\left(c\widetilde{1}\right) = E\left[\lim_{t\to\infty} x(t)\right] = \lim_{t\to\infty} E[x(t)]. \tag{20}$$

Then, we can derive the expression of $\lim_{t\to\infty} E[x(t)]$ and use the above equality to get the desired result. Now, define the quantization error as

$$u(t) = \widehat{x}(t) - x(t). \tag{21}$$

We can get

$$x(t+1) = A(t)x(t) + A(t)u(t). \tag{22}$$

Noting the property of the probabilistic quantization; that is, $E[u(t)] = 0$ and the fact that $A(t)$ and $u(t)$ are independent, so we can see that

$$\begin{aligned} E[x(t+1)] &= E[A(t)]E[x(t)] + E[A(t)]E[u(t)] \\ &= \widetilde{A}E[x(t)]. \end{aligned} \tag{23}$$

Therefore,

$$\begin{aligned} &\left\|E[x(t+1)] - x_{\text{ave}}\widetilde{1}\right\|^2 \\ &\quad = \left\{\widetilde{A}E[x(t)] - x_{\text{ave}}\widetilde{1}\right\}^T\left\{\widetilde{A}E[x(t)] - x_{\text{ave}}\widetilde{1}\right\} \\ &\quad = \left\{E[x(t)] - x_{\text{ave}}\widetilde{1}\right\}^T\left(\widetilde{A}^T\widetilde{A}\right)\left\{E[x(t)] - x_{\text{ave}}\widetilde{1}\right\} \\ &\quad = \left\{E[x(t)] - x_{\text{ave}}\widetilde{1}\right\}^T\left[I - \frac{S(t)}{N}\left(D - \left(A^T + A\right)\right)\right]^2 \\ &\qquad \times \left\{E[x(t)] - x_{\text{ave}}\widetilde{1}\right\}. \end{aligned} \tag{24}$$

Define $y(t) = E[x(t)] - x_{\text{ave}}\widetilde{1}$, we can see $y(0) \perp \widetilde{1}$, furthermore, on the basis of Lemma 9, we can see $y(t) \perp \widetilde{1}$, $\rho(\widetilde{A}) = 1$, and every possible sample of $\widetilde{A}$ is doubly stochastic, each sample of $\widetilde{A}^T\widetilde{A}$ is also doubly stochastic. This implied that $\widetilde{1}$ is the eigenvector corresponding to eigenvalue 1 of $\widetilde{A}^T\widetilde{A}$. Thus, we can conclude from the above equation that

$$\left\|E[x(t+1)] - x_{\text{ave}}\widetilde{1}\right\|^2 \leq \lambda_2\left(\widetilde{A}^T\widetilde{A}\right)\left\|E[x(t)] - x_{\text{ave}}\widetilde{1}\right\|^2, \tag{25}$$

where $\lambda_2(W)$ for a stochastic matrix W denotes the largest eigenvalue in magnitude excluding the eigenvalue at one.

Therefore,

$$\left\|y(t+1)\right\|^2 \le \left[1 - \frac{S(t)}{N}\lambda_2^*\left(D - \left(A^T + A\right)\right)\right]^2 \left\|y(t)\right\|^2. \tag{26}$$

Note that $D-(A^T+A)$ is actually the (weighted) Laplacian of the graph ζ_{A+A^T}. With Assumption 3, apparently $A + A^T$ is symmetric, and thus ζ_{A+A^T} one connected graphs [15], we have the multiple of λ_1^* is one and $\lambda_2^* > 0$, where λ_k^* is the kth smallest eigenvalue of $D-(A^T+A)$. On the other hand, since A is a stochastic matrix, it is straightforward to see that

$$\sum_{j=1, j\neq i} a_{ij} + a_{ji} < n \tag{27}$$

for all $i = 1, 2, \ldots, N$. According to Gersgorin's circle theorem, every eigenvalue of $D - (A^T + A)$ is $\lambda^* \in [0, 2N]$.

Then, we assume $\lambda_2^*[D - (A^T + A)] > N$, for the trace of $D - (A^T + A)$ is $2N$; then

$$\sum_{k=2}^{N} \lambda_2^*\left[D - \left(A^T + A\right)\right] > N \times (N-1) \tag{28}$$

since $N \ge 3$, $\sum_{k=2}^{N} \lambda_2^*[D - (A^T + A)] > \mathrm{Tr}[D - (A^T + A)]$.

It is impossible. So,

$$\lambda_2^*\left[D - \left(A^T + A\right)\right] \le N. \tag{29}$$

Now we conclude that for all t,

$$\begin{aligned}&\left[1 - \frac{S(t)}{N}\lambda_2^*\left(D - \left(A^T + A\right)\right)\right]^2 \\ &\qquad \le 1 - \frac{S(t)}{N}\lambda_2^*\left(D - \left(A^T + A\right)\right) < 1.\end{aligned} \tag{30}$$

Then,

$$\left\|y(t+1)\right\|^2 \le \prod_{t=0}^{\infty}\left[1 - \frac{S(t)}{N}\lambda_2^*\left(D - \left(A^T + A\right)\right)\right]\left\|y(0)\right\|^2. \tag{31}$$

Therefore, based on Lemma 10, we have

$$\lim_{t\to\infty}\left\|y(t)\right\| = 0. \tag{32}$$

So, we can get $E[c] = (1/N)\widetilde{1}x(0)$ when $S(t)$ satisfies $\sum_{t=0}^{\infty} S(t) = \infty$.

The proof is finished.

4.3. The Proof of Theorem 7. Proof of Theorem 7: defining

$$z(t+1) = x(t+1) - x_{\mathrm{ave}}(t+1)\,\widetilde{1} = (I - J)\,x(t+1), \tag{33}$$

where $J = (1/N)\widetilde{1}\widetilde{1}^T$; then, we can get

$$z(t+1) = (I - J)\,\widehat{x}(t) = A(t)\,z(t) + (I - J)\,A(t)\,u(t). \tag{34}$$

So,

$$\begin{aligned}&E\left[\left\|z(t+1)\right\|^2 \mid z(t)\right] \\ &\quad = z(t)^T E\left[A(t)^T A(t)\right] z(t) \\ &\qquad + E\left[z(t)^T A(t)^T (I - J)\,A(t)\,A(t)\,u(t)\right] \\ &\qquad + E\left[u(t)^T A(t)^T (I - J)\,A(t)\,A(t)\,z(t)\right] \\ &\qquad + E\left[u(t)^T A(t)^T (I - J)\,A(t)\,A(t)\,z(t)\right] \\ &\qquad + E\left[u(t)^T A(t)^T (I - J)^2 A(t)\,A(t)\,u(t)\right].\end{aligned} \tag{35}$$

Using the Proposition 3.4 in [4], it is easy to see that both the second and the third term of the right hand side of the above equation are zero. Thus, we can derive

$$\begin{aligned}&E\left[\left\|z(t+1)\right\|^2 \mid z(t)\right] \\ &\quad = z(t)^T E\left[A(t)^T A(t)\right] z(t) \\ &\qquad + E\left[u(t)^T\left(A(t)^T A(t) - J\right) u(t)\right] \\ &\quad = z(t)^T E\left[A(t)^T A(t)\right] z(t) + \sum_{i=1}^{N} \overline{A}_{ii} E\left[u_i^2(t)\right] \\ &\quad \le \lambda_2\left(\widehat{A}\right)\left\|z(t)\right\|^2 + \frac{\Delta^2}{4}\mathrm{trace}\left(\overline{A}\right) \\ &\quad = \lambda_2\left(\widehat{A}\right)\left\|z(t)\right\|^2 + \frac{\Delta^2}{4}\left[N - 4S(t)\left(1 - S(t)\right) - 1\right] \\ &\quad = \lambda_2\left(\widehat{A}\right)\left\|z(t)\right\|^2 + \frac{\Delta^2}{4}\left[N - 4S(t)\left(1 - S(t)\right) - 1\right] \\ &\quad = \lambda_2\left[I - \frac{2S(t)\left(1 - S(t)\right)}{N} \right. \\ &\qquad \left. \times\left(D - \left(A^T + A\right)\right)\right]\left\|z(t)\right\|^2 \\ &\qquad + \frac{\Delta^2}{4}\left[N - 4S(t)\left(1 - S(t)\right) - 1\right],\end{aligned} \tag{36}$$

where $\overline{A} = E[A(t)^T A(t) - J]$.

The second equality follows from the fact that $E[u_i(t)u_j(t)] = 0$ for $i \neq j$, and the inquiry follows from $E[u_i(t)^2] \le \Delta^2/4$. Furthermore, the last equality is obtained by using

$$\mathrm{trace}\left(\overline{A}\right) = \mathrm{trace}\left(\widehat{A} - J\right) = N - 4S(t)\left(1 - S(t)\right) - 1. \tag{37}$$

Then, repeatedly conditioning and using the iteration obtained above, we obtain, define $\lambda_2^* = \lambda_2^*(D-(A^T+A)) < N$

$$\begin{aligned}E\left[\left\|z(t+1)\right\|^2\right] &\le \prod_{i=k_0}^{t}\left(1 - \frac{2S(i)\left(1 - S(i)\right)}{N}\lambda_2^*\right)\left\|z(k_0)\right\|^2 \\ &\quad + \frac{\Delta^2}{4}\left[\sum_{i=k_0}^{t-1}\left(N - 4S(i)\left(1 - S(i)\right) - 1\right)\right]\end{aligned}$$

$$\times \prod_{j=i+1}^{t} \left(1 - \frac{4S(j)(1-S(j))}{N}\lambda_2^*\right) + \frac{\Delta^2}{4}\left[N - 4S(t)(1-S(t)) - 1\right], \tag{38}$$

when $t \geq 1$, $k_0 \leq t-1$, $k_0 \in N^+$ where

$$E\left[\|z(1)\|^2\right] \leq \left(1 - \frac{2S(0)(1-S(0))}{N}\lambda_2^*\right)\|z(0)\|^2 + \frac{\Delta^2}{4}\left[N - 4S(0)(1-S(0)) - 1\right], \tag{39}$$

when $t = 0$.

Define $S^* = \inf_{i\in N}\{S(i)(1-S(i))\}$.

Because of $S_i \in (0,1)$, $S^* \in [0,1)$; then

$$\begin{aligned} E\left(\|z(t+1)\|^2\right) &\leq \left[1 - \frac{2}{N}S^*\lambda_2^*\left(D - \left(A^T + A\right)\right)\right]\|z(0)\|^2 \\ &\quad + \frac{\Delta^2}{4}\left(N - 4S^* - 1\right) \\ &\quad \times \sum_{i=0}^{t}\left[1 - \frac{S^*}{N}\lambda_2^*\left(D - \left(A^T + A\right)\right)\right] \\ &\leq \left(1 - \frac{2}{N}S^*\lambda_2^*\right)^t\|z(0)\|^2 \\ &\quad + \frac{\Delta^2}{4}\left(N - 4S^* - 1\right)\sum_{i=0}^{t}\left(1 - \frac{S^*}{N}\lambda_2^*\right)^s. \end{aligned} \tag{40}$$

By Lemma 9, we can deduce that

$$E\left(\|z(t+1)\|^2\right) \leq \left(1 - \frac{2}{N}S^*\lambda_2^*\right)^t\|z(0)\|^2 + \frac{\Delta^2 N\left(N - 4S^* - 1\right)}{4S^*\lambda_2^*}. \tag{41}$$

This completes the proof.

5. Conclusions

In this paper, we have considered the consensus problem of gossip algorithm based on time-varying influence and weakly connected graph in the social network. Based on the gossip algorithm, we also pay attention to studying the effect of the probabilistic quantized communication.

We show that the group will achieve the probabilistic consensus value which is a random variable despite the presence of quantized communication, with potentially very different initial opinions. And we present the condition on the time-varying influence factors that guarantee the mean of consensus equals to the average initial states. We also provide a result about the square mean error which has an upper bound and the convergence speed of the upper bound can be estimated. The limit of the bound is dependent on the quantized revolution, the second smallest eigenvalue of Laplacian matrix, and the time-varying factors.

And some other interesting problems we will be concerned with in further research, such as the existence of agents who have different prejudices and whether the consensus can be reached with partial trust.

Acknowledgment

This research is supported by the National Science Foundation of China (NSFC) Grant no. 71171045 and funded by the Deanship of Scientific Research (DSR), King Abdulaziz University, under Grant no. (3-130/1434/HiCi). The authors acknowledge the technical and financial support of KAU.

References

[1] S. Boyd, A. Ghosh, B. Prabhakar, and D. Shah, "Randomized gossip algorithms," *IEEE Transactions on Information Theory*, vol. 52, no. 6, pp. 2508–2530, 2006.

[2] D. Acemoglu, A. Ozdaglar, and A. ParandehGheibi, "Spread of (mis)information in social networks," *Games and Economic Behavior*, vol. 70, no. 2, pp. 194–227, 2010.

[3] G. Shi and K. H. Johansson, "Randomized optimal consensus of multi-agent systems," *Automatica*, vol. 48, no. 12, pp. 3018–3030, 2012.

[4] R. Carli, F. Fagnani, P. Frasca, and S. Zampieri, "Gossip consensus algorithms via quantized communication," *Automatica*, vol. 46, no. 1, pp. 70–80, 2010.

[5] D. Yuan, S. Xu, H. Zhao, and Y. Chu, "Distributed average consensus via gossip algorithm with real-valued and quantized data for $0 < q < 1$," *Systems & Control Letters*, vol. 59, no. 9, pp. 536–542, 2010.

[6] F. Ceragioli, C. De Persis, and P. Frasca, "Discontinuities and hysteresis in quantized average consensus," *Automatica*, vol. 47, no. 9, pp. 1916–1928, 2011.

[7] N. Wang, D. Li, and Z. Yin, "Broadcast gossip algorithm with quantization," in *Proceedings of the 9th International Conference on Fuzzy Systems and Knowledge Discovery (FSKD '12)*, pp. 2143–2147, Sichuan, China, May 2012.

[8] K. Cai and H. Ishii, "Average consensus on general strongly connected digraphs," *Automatica*, vol. 48, no. 11, pp. 2750–2761, 2012.

[9] T. C. Aysal, M. J. Coates, and M. G. Rabbat, "Distributed average consensus with dithered quantization," *IEEE Transactions on Signal Processing*, vol. 56, no. 10, part 1, pp. 4905–4918, 2008.

[10] J.-J. Xiao and Z.-Q. Luo, "Decentralized estimation in an inhomogeneous sensing environment," *IEEE Transactions on Information Theory*, vol. 51, no. 10, pp. 3564–3575, 2005.

[11] G. Shi, M. Johansson, and K. H. Johansson, "Randomized gossip algorithm with unreliable communication," http://arxiv.org/abs/1203.6028.

[12] R. S. Varga, *Geršgorin and His Circles*, vol. 36 of *Springer Series in Computational Mathematics*, Springer, Berlin, Germany, 2004.

[13] G. Shi, M. Johansson, and K. H. Johansson, "How agreement and disagreement evolve over random dynamic networks," *IEEE Journal on Selected Areas in Communications*, vol. 31, no. 6, pp. 1061–1071, 2013.

[14] O. Kallenberg, *Foundations of Modern Probability*, Springer, New York, NY, USA, Second edition, 2002.

[15] C. Godsil and G. Royle, *Algebraic Graph Theory*, vol. 207 of *Graduate Texts in Mathematics*, Springer, New York, NY, USA, 2001.

Hindawi Publishing Corporation
Abstract and Applied Analysis
Volume 2013, Article ID 783279, 9 pages
http://dx.doi.org/10.1155/2013/783279

Research Article

Cucker-Smale Flocking with Bounded Cohesive and Repulsive Forces

Qiang Song,[1] Fang Liu,[2] Jinde Cao,[3,4] and Jianlong Qiu[5]

[1] *School of Electronics and Information, Hangzhou Dianzi University, Hangzhou 310018, China*
[2] *School of Information Engineering, Huanghuai University, Henan 463000, China*
[3] *Department of Mathematics, Southeast University, Nanjing 210096, China*
[4] *Department of Mathematics, King Abdulaziz University, Jeddah 21589, Saudi Arabia*
[5] *School of Science, Linyi University, Linyi, Shandong 276005, China*

Correspondence should be addressed to Jinde Cao; jdcao@seu.edu.cn

Received 6 July 2013; Accepted 27 August 2013

Academic Editor: A. M. Elaiw

This paper proposes two Cucker-Smale-type flocking models by introducing both cohesive and repulsive forces to second-order multiagent systems. Under some mild conditions on the initial state of the flocking system, it is shown that the velocity consensus of the agents can be reached independent of the parameter which describes the decay of communication rates. In particular, the collision between any two agents can always be avoided by designing an appropriate bounded repulsive function based on the initial energy of the flock. Numerical examples are given to demonstrate the effectiveness of the theoretical analysis.

1. Introduction

Over the past few decades, the flocking problem of multiagent systems has attracted increasing attention due to its wide applications in many fields such as unmanned air vehicles, mobile robots, and sensor networks. To simulate the collective behaviors of birds and fish, Reynolds [1] proposed three well-known flocking rules for multiagent systems, that is, center cohesion, collision avoidance, and velocity consensus. In [2], Vicsek et al. introduced a simple discrete time flocking model to study the emergence of autonomous agents moving in the plane with the same speed but with different headings. By using nonnegative matrix and algebraic graph theories, Jadbabaie et al. [3] provided the theoretical analysis for Vicsek's flocking model. Olfati-Saber [4] presented a systematic framework to design distributed flocking algorithms for multiagent systems. Tanner et al. [5] investigated the flocking behaviors of multiagent systems with fixed and switching network topologies. In [6], both theoretical and experimental results were given for a flock of mobile robots. In [7–10], some strategies were developed to ensure the connectivity of the time-varying communication topology.

In 2007, Cucker and Smale [11] proposed a flocking model to investigate the emergence behavior in multiagent systems. For a network of N autonomous agents, the continuous-time version of the Cucker-Smale flocking model is described as follows [11]:

$$\begin{aligned} \dot{x}_i(t) &= v_i(t), \quad i = 1, \ldots, N, \\ \dot{v}_i(t) &= \sum_{j=1, j\neq i}^{N} a_{ij}(x)\left(v_j - v_i\right), \end{aligned} \tag{1}$$

where $x_i(t)$ and $v_i(t) \in \mathbb{R}^n$ are the position and velocity states of the ith agent, respectively, $a_{ij}(x)$ is called the communication rate defined as

$$\begin{aligned} a_{ij}(x) &= \frac{H}{\left(1 + \left\|x_i - x_j\right\|^2\right)^{\beta}}, \quad i \neq j, \\ a_{ii}(x) &= 0, \end{aligned} \tag{2}$$

in which $\beta \geq 0$ determines the decay of $a_{ij}(x)$, $H > 0$, and $x = (x_1^T, \ldots, x_N^T)^T$.

In [11], Cucker and Smale studied the flocking behavior of model (1) and showed that the flock converges to a common velocity unconditionally when $\beta < 1/2$, while the stability of the flock depends on the initial positions and velocities when $\beta \geq 1/2$. The Cucker-Smale flocking model (1) has attracted much attention in recent years. Shen [12] investigated the flocking behavior of an extended Cucker-Smale model with hierarchical leadership. Ha and Liu [13] provided a simple proof for the Cucker-Smale model (1) and derived some conditions for reaching exponential flocking. Ha et al. [14] presented a Cucker-Smale-type model with nonlinear velocity couplings. Park et al. [15] proposed an augmented Cucker-Smale model by introducing interagent bonding forces. Perea et al. [16] successfully applied Cucker-Smale model (1) to the real-flight formation control in the Darwin space mission.

According to the flocking rules of Reynolds, one knows that the collision avoidance is not considered in the original Cucker-Smale model (1) and its variations [12–16]. To fix this drawback, Cucker and Dong [17] developed the following extended Cucker-Smale-type model with repelling forces:

$$\begin{aligned} \dot{x}_i(t) &= v_i(t), \quad i = 1, \ldots, N, \\ \dot{v}_i(t) &= \sum_{j=1, j\neq i}^{N} a_{ij}(x)\left(v_j - v_i\right) \\ &\quad + \left(\frac{1}{N}\sum_{i=1}^{N}\sum_{i>j}^{N}\left\|v_i - v_j\right\|^2\right)^{1/2} \\ &\quad \times \sum_{j=1, j\neq i}^{N} f\left(\left\|x_i - x_j\right\|^2\right)\left(x_i - x_j\right), \end{aligned} \tag{3}$$

where the differentiable function $f : (d_0, \infty) \to (0, \infty)$ satisfies $\int_{d_0}^{d_0+1} f(r)dr = \infty$ and $\int_{d_0+1}^{\infty} f(r)dr < \infty$ to ensure the collision avoidance among the agents, in which $d_0 > 0$ is a specified distance. Assuming that the initial positions of model (3) satisfy $\|x_i(0) - x_j(0)\| > d_0$ for all $i \neq j$, Cucker and Dong [17] showed that the flock asymptotically converges to a common velocity and the distance between any two agents is greater than d_0 when $\beta \leq 1/2$, while the convergence of the flock relies on the initial positions and velocities of the agents when $\beta > 1/2$. Note that when $\|x_i - x_j\| \to d_0^+$, one has $f(\|x_i - x_j\|^2) \to \infty$, which means that the repulsive force in model (3) is unbounded. However, in many practical cases, the actuator of an agent can only handle finite forces or torques due to its saturation. Therefore, it is imperative to design some bounded repulsive functions for Cucker-Smale-type flocking models.

Motivated by the above discussions, we propose two improved Cucker-Smale-type flocking models in this paper. The main contribution of this paper is three-fold. First, inspired by the flocking model developed by Park et al. [15] and the aggregation techniques proposed by Gazi and Passino [18, 19], this paper presents two control strategies for the Cucker-Smale model (1) to ensure the cohesiveness of the flocking system. Second, to overcome the actuator saturation of multiagent systems, this paper designs a class of bounded repulsive functions for Cucker-Smale model (1) such that the collision-free motion of the flock can always be guaranteed. Third, it is shown that the velocity convergence of two proposed flocking models in this paper can be achieved independent of the parameter β, which describes the decay of communication rate $a_{ij}(x)$. Due to these distinguishing features, the proposed flocking models in this paper significantly improve some previous work related to Cucker-Smale-type flocking.

The remainder of this paper is organized as follows. Section 2 formulates the asymptotical flocking problem and defines bounded repulsive functions. Section 3 proposes two improved Cucker-Smale models and investigates their flocking behaviors. Numerical examples are given in Section 4 to verify the theoretical analysis. Finally, some concluding remarks and future trends are stated in Section 5.

Notations. The standard notations are used throughout the paper. The superscript "T" represents the transpose of a vector or a matrix. $\mathbb{R}$ denotes the set of real numbers. For $x \in \mathbb{R}^n$, let $\|x\|$ be its Euclidean norm and let $\min_i\{x_i\}$ be its minimal element, and let $\langle\cdot,\cdot\rangle$ denote the inner product. Let $0_n = (0, \ldots, 0)^T \in \mathbb{R}^n$ be a vector with all zero entries. The symbol "∇" is the gradient operator.

2. Preliminaries

This section formulates the flocking problem of second-order multiagent systems, and defines a class of bounded repulsive functions to avoid interagent collisions.

2.1. Problem Formulation. Consider a second-order multiagent system consisting of N agents described by

$$\begin{aligned} \dot{x}_i(t) &= v_i, \quad i = 1, \ldots, N, \\ \dot{v}_i(t) &= u_i, \end{aligned} \tag{4}$$

where $x_i(t)$ and $v_i(t) \in \mathbb{R}^n$ are the position and velocity states of the ith agent, respectively, and $u_i \in \mathbb{R}^n$ is the control input for the ith agent.

Definition 1. According to the flocking rules proposed by Reynolds [1], multiagent system (4) is said to achieve asymptotical flocking if its solution satisfies the following conditions for all $1 \leq i, j \leq N, i \neq j$, and $t \geq 0$:

(i) flock cohesion: $\sup_{0\leq t<\infty}\|x_i(t) - x_j(t)\| < \infty$;

(ii) collision avoidance: $\|x_i(t) - x_j(t)\| > 0$;

(iii) velocity consensus: $\lim_{t\to\infty}\|v_i(t) - v_j(t)\| = 0$.

Remark 2. The first condition of the asymptotical flocking in Definition 1 indicates that each agent should stay close to the nearby flockmates to ensure the cohesiveness of the flock.

Remark 3. The collision in a multiagent system means that there exist at least two agents occupying the same space [4, 5, 7–9]. To ensure the collision-free motion of the flock,

the minimal interagent distance in multiagent system (4) should be always greater than zero.

2.2. Bounded Repulsive Functions. To avoid collisions in a multiagent system, one can design some artificial potential functions to create interagent repulsive forces [4–8, 17–19]. Up to date, most researchers utilize the negative gradients of unbounded potential functions to avoid collisions among agents [5, 7, 8, 17–19]. However, in many practical situations, the control input of a multiagent system should be bounded because no actuator could provide an infinite control force. In this paper, we will show that interagent collisions can be avoided by designing some appropriate bounded repulsive functions. Below we define a class of bounded repulsive functions.

Definition 4. For multiagent system (4), assume that the initial positions of the agents satisfy $\|x_i(0) - x_j(0)\| > 0$ for all $1 \le i, j \le N, i \ne j$. Let $\Psi : (0,\infty) \to (0,\infty)$ be a differentiable, nonnegative, and decreasing function with respective to the distance $\|x_i - x_j\|$ between agents i and j, such that

(i) $\nabla_{x_i}\Psi(\|x_i - x_j\|) = -g_r(\|x_i - x_j\|)(x_i - x_j)$. When $\|x_i - x_j\| \to 0^+$, $g_r(\|x_i - x_j\|) = P$; otherwise, $g_r(\|x_i - x_j\|) < P$,

(ii) $\lim_{\|x_i - x_j\| \to 0^+}\Psi(\|x_i - x_j\|) = Q$,

where $P, Q > 0$, and $g_r(\|x_i - x_j\|) > 0$ is a smooth and decreasing function in $(0,\infty)$. If $P < \infty$ and $Q < \infty$, the potential function Ψ is called a bounded repulsive function.

Remark 5. If $\lim_{\|x_i - x_j\| \to 0^+}\Psi(\|x_i - x_j\|) = \infty$, that is, $Q = \infty$, the repulsive function Ψ is unbounded.

Remark 6. A possible bounded repulsive function to satisfy Definition 4 can be chosen as follows:

$$\Psi\left(\left\|x_i - x_j\right\|\right) = Q\exp\left(-\mu\left\|x_i - x_j\right\|^2\right) \quad \text{for } \left\|x_i - x_j\right\| > 0, \tag{5}$$

where $0 < Q < \infty$ and $\mu > 0$.

Remark 7. Considering the symmetry of the potential function Ψ in Definition 4, that is, $\Psi(\|x_i - x_j\|) = \Psi(\|x_j - x_i\|)$, we have [5]

$$\begin{aligned} &\nabla_{x_i}\Psi\left(\left\|x_i - x_j\right\|\right) = -\nabla_{x_j}\Psi\left(\left\|x_i - x_j\right\|\right), \\ &\frac{d}{dt}\sum_{i=1}^{N}\sum_{j=1,j\ne i}^{N}\frac{1}{2}\Psi\left(\left\|x_i - x_j\right\|\right) \\ &\quad = \sum_{i=1}^{N} v_i^T \sum_{j=1,j\ne i}^{N}\nabla_{x_i}\Psi\left(\left\|x_i - x_j\right\|\right). \end{aligned} \tag{6}$$

3. Main Results

This section proposes two improved Cucker-Smale flocking models and investigates their flocking behaviors. In particular, some conditions are derived to ensure the collision-free motion of the flock.

3.1. Cucker-Smale Flocking with Bonding and Repulsive Forces. Recently, Park et al. [15] proposed an extended Cucker-Smale model as follows:

$$\begin{aligned} \dot{x}_i(t) &= v_i(t), \quad i = 1,\dots,N, \\ \dot{v}_i(t) &= \frac{\lambda}{N}\sum_{j=1,j\ne i}^{N}\psi\left(r_{ij}\right)\left(v_j - v_i\right) \\ &\quad + \frac{\sigma}{N}\sum_{j=1,j\ne i}^{N}\frac{K_1}{2r_{ij}^2} \\ &\quad \times \left\langle v_i - v_j, x_i - x_j\right\rangle\left(x_j - x_i\right) \\ &\quad + \frac{\sigma}{N}\sum_{j=1,j\ne i}^{N}\frac{K_2}{2r_{ij}}\left(r_{ij} - 2R\right)\left(x_j - x_i\right), \end{aligned} \tag{7}$$

where $\lambda, \sigma, K_1, K_2$, and R are positive parameters, $r_{ij} = \|x_i - x_j\|$, and the function $\psi(\cdot)$ is nonnegative.

In [15], it was shown that model (7) can exhibit cohesive flocking due to the bonding forces among the agents. However, the collision avoidance in model (7) was not addressed and thus should be resolved by adopting some new techniques. To improve model (7), we consider the following extended Cucker-Smale model with bonding and repulsive forces:

$$\begin{aligned} \dot{x}_i(t) &= v_i(t), \quad i = 1,\dots,N, \\ \dot{v}_i(t) &= \sum_{j=1,j\ne i}^{N}a_{ij}(x)\left(v_j - v_i\right) \\ &\quad + k_a\sum_{j=1,j\ne i}^{N}\frac{r_{ij} - \eta}{r_{ij}}\left(x_j - x_i\right) \\ &\quad - \sum_{j=1,j\ne i}^{N}\nabla_{x_i}\Psi\left(\left\|x_i - x_j\right\|\right), \end{aligned} \tag{8}$$

where $k_a > 0$, $\eta > 0$, $r_{ij} = \|x_i - x_j\|$, and $\Psi(\|x_i - x_j\|)$ is a bounded repulsive function described in Definition 4.

Remark 8. We will show that the terms $k_a\sum_{j=1,j\ne i}^{N}((r_{ij} - \eta)/r_{ij})(x_j - x_i)$ and $-\sum_{j=1,j\ne i}^{N}\nabla_{x_i}\Psi(\|x_i - x_j\|)$ in multiagent system (8) can yield bounded interagent bonding and repulsive forces, respectively.

The following result is very useful to derive the main results of this paper.

Lemma 9 (see [17]). *For $z_i \in \mathbb{R}$, $i = 1, \ldots, N$, let $\overline{z} = \sum_{i=1}^{N} z_i/N$ and $\widehat{z}_i = z_i - \overline{z}$. One has $\sum_{i=1}^{N-1}\sum_{j>i}^{N} \|\widehat{z}_j - \widehat{z}_i\|^2 = N\sum_{i=1}^{N}\|\widehat{z}_i\|^2$.*

Let x_c and v_c be the position and velocity of the mass center of system (8), respectively as follows:

$$x_c = \frac{\sum_{i=1}^{N} x_i}{N}, \qquad v_c = \frac{\sum_{i=1}^{N} v_i}{N}. \tag{9}$$

In view of $a_{ij}(x) = a_{ji}(x)$, $r_{ij} = r_{ji}$, and Remark 7, we can obtain $\dot{v}_c(t) = 0$. It follows that the velocity of the centroid of multiagent system (8) is a constant; that is, $v_c(t) = v_c(0)$ for all $t \geq 0$. Let $\widehat{x}_i = x_i - x_c$ and $\widehat{v}_i = v_i - v_c$. It is obvious to see that $\sum_{i=1}^{N}\widehat{x}_i = 0$ and $\sum_{i=1}^{N}\widehat{v}_i = 0$. Also, we have $\widehat{x}_i - \widehat{x}_j = x_i - x_j$ and $\widehat{v}_i - \widehat{v}_j = v_i - v_j$. Then, it follows that $\Psi(\|\widehat{x}_i - \widehat{x}_j\|) = \Psi(\|x_i - x_j\|)$ and $\nabla_{\widehat{x}_i}\Psi(\|\widehat{x}_i - \widehat{x}_j\|) = \nabla_{x_i}\Psi(\|x_i - x_j\|)$. Moreover, we have $r_{ij} = \|\widehat{x}_i - \widehat{x}_j\|$, whose time derivative is

$$\dot{r}_{ij}(t) = \frac{\left(\widehat{v}_i - \widehat{v}_j\right)^T\left(\widehat{x}_i - \widehat{x}_j\right)}{r_{ij}}. \tag{10}$$

Considering $\dot{x}_c = v_c$ and $\dot{v}_c = 0$, from (8) we have the following error system:

$$\begin{aligned}
\dot{\widehat{x}}_i(t) &= \widehat{v}_i(t), \quad i = 1, \ldots, N,\\
\dot{\widehat{v}}_i(t) &= \sum_{j=1, j\neq i}^{N} a_{ij}(\widehat{x})\left(\widehat{v}_j - \widehat{v}_i\right)\\
&\quad + k_a\sum_{j=1, j\neq i}^{N}\frac{r_{ij} - \eta}{r_{ij}}\left(\widehat{x}_j - \widehat{x}_i\right)\\
&\quad - \sum_{j=1, j\neq i}^{N}\nabla_{\widehat{x}_i}\Psi\left(\left\|\widehat{x}_i - \widehat{x}_j\right\|\right),
\end{aligned} \tag{11}$$

where $a_{ij}(\widehat{x}) = a_{ij}(x)$ and $\widehat{x} = \left(\widehat{x}_1^T(t), \ldots, \widehat{x}_N^T(t)\right)^T$.

To investigate the flocking behavior of multiagent system (8), we define the following energy function:

$$\begin{aligned}
W(t) &= \frac{1}{2}\sum_{i=1}^{N}\widehat{v}_i^T\widehat{v}_i + \frac{k_a}{4}\sum_{i=1}^{N}\sum_{j=1, j\neq i}^{N}\left(r_{ij} - \eta\right)^2\\
&\quad + \frac{1}{2}\sum_{i=1}^{N}\sum_{j=1, j\neq i}^{N}\Psi\left(\left\|\widehat{x}_i - \widehat{x}_j\right\|\right).
\end{aligned} \tag{12}$$

Theorem 10. *For a flock of N agents with dynamics* (8)*, assume that the initial energy defined by* (12) *is finite, the initial positions satisfy $\|x_i(0) - x_j(0)\| > 0$ for all $i \neq j$, and the repulsive function Ψ is chosen to be bounded according to Definition 4. Then, multiagent system* (8) *exhibits asymptotical flocking with the common velocity $v_c(0)$; that is, the velocity of the mass center, and the collision between any two agents can always be avoided if the repulsive function Ψ satisfies $W(0) < \Psi(0)$.*

Proof. Considering (10) and Remark 7, we compute the time derivative of $W(t)$ in (12) along the trajectory of (11) as follows:

$$\begin{aligned}
\dot{W}(t) &= \sum_{i=1}^{N}\widehat{v}_i^T\left[\sum_{j=1, j\neq i}^{N} a_{ij}(\widehat{x})\left(\widehat{v}_j - \widehat{v}_i\right)\right.\\
&\qquad + k_a\sum_{j=1, j\neq i}^{N}\frac{r_{ij} - \eta}{r_{ij}}\left(\widehat{x}_j - \widehat{x}_i\right)\\
&\qquad \left. - \sum_{j=1, j\neq i}^{N}\nabla_{\widehat{x}_i}\Psi\left(\left\|\widehat{x}_i - \widehat{x}_j\right\|\right)\right]\\
&\quad + \frac{k_a}{2}\sum_{i=1}^{N}\sum_{j=1, j\neq i}^{N}\frac{r_{ij} - \eta}{r_{ij}}\left(\widehat{v}_i - \widehat{v}_j\right)^T\left(\widehat{x}_i - \widehat{x}_j\right)\\
&\quad + \sum_{i=1}^{N}\widehat{v}_i^T\sum_{j=1, j\neq i}^{N}\nabla_{\widehat{x}_i}\Psi\left(\left\|\widehat{x}_i - \widehat{x}_j\right\|\right)\\
&= \sum_{i=1}^{N-1}\sum_{j>i}^{N}\left[a_{ij}(\widehat{x})\,\widehat{v}_i^T\left(\widehat{v}_j - \widehat{v}_i\right)\right.\\
&\qquad \left. + a_{ji}(\widehat{x})\,\widehat{v}_j^T\left(\widehat{v}_i - \widehat{v}_j\right)\right]\\
&\quad + k_a\sum_{i=1}^{N-1}\sum_{j>i}^{N}\left[\frac{r_{ij} - \eta}{r_{ij}}\widehat{v}_i^T\left(\widehat{x}_j - \widehat{x}_i\right)\right.\\
&\qquad \left. + \frac{r_{ji} - \eta}{r_{ji}}\widehat{v}_j^T\left(\widehat{x}_i - \widehat{x}_j\right)\right]\\
&\quad + \frac{k_a}{2}\sum_{i=1}^{N-1}\sum_{j>i}^{N}\left[\frac{r_{ij} - \eta}{r_{ij}}\left(\widehat{v}_i - \widehat{v}_j\right)^T\left(\widehat{x}_i - \widehat{x}_j\right)\right.\\
&\qquad \left. + \frac{r_{ji} - \eta}{r_{ji}}\left(\widehat{v}_j - \widehat{v}_i\right)^T\left(\widehat{x}_j - \widehat{x}_i\right)\right]\\
&= -\sum_{i=1}^{N-1}\sum_{j>i}^{N}a_{ij}(\widehat{x})\left(\widehat{v}_j - \widehat{v}_i\right)^T\left(\widehat{v}_j - \widehat{v}_i\right)\\
&\leq -\min_{j>i}a_{ij}(\widehat{x})\sum_{i=1}^{N-1}\sum_{j>i}^{N}\left(\widehat{v}_j - \widehat{v}_i\right)^T\left(\widehat{v}_j - \widehat{v}_i\right)\\
&= -N\min_{j>i}a_{ij}(\widehat{x})\sum_{i=1}^{N}\left\|\widehat{v}_i\right\|^2 \leq 0,
\end{aligned} \tag{13}$$

where we use $a_{ij}(\widehat{x}) = a_{ji}(\widehat{x})$ and $r_{ij} = r_{ji}$, and the fact that $\sum_{i=1}^{N-1}\sum_{j>i}^{N}\|\widehat{v}_j - \widehat{v}_i\|^2 = N\sum_{i=1}^{N}\|\widehat{v}_i\|^2$ (see Lemma 9) to obtain the third and the last equalities, respectively.

By (13), we have $\dot{W}(t) \leq 0$, which means that $W(t) \leq W(0) < \infty$ holds for all $t \geq 0$. Then, it follows from (12) that

$$\frac{k_a}{4}\sum_{i=1}^{N}\sum_{j=1, j\neq i}^{N}\left(r_{ij} - \eta\right)^2 \leq W(0). \tag{14}$$

Since $r_{ij} = r_{ji}$, from (14) we obtain $|r_{ij} - \eta| \leq \sqrt{2W(0)/k_a}$, which means that

$$\left\|x_i(t) - x_j(t)\right\| \leq \eta + \sqrt{\frac{2W(0)}{k_a}} < \infty, \quad i \neq j,\ t \geq 0. \tag{15}$$

Hence, the cohesion condition of Definition 1 is satisfied.

By (2) and (15), we have $a_{ij}(\widehat{x}) > 0$ for all $i \neq j$. In view of (13), we have $\dot{W}(t) \equiv 0$ if and only if $\widehat{v}_i(t) = 0_n, i = 1, \ldots, N$. Let $\widehat{v}(t) = (\widehat{v}_1^T(t), \ldots, \widehat{v}_N^T(t))^T$. Thus, the set $\mathscr{M} = \{\widehat{v}(t) \mid \widehat{v}(t) = 0_{Nn}\}$ is the largest invariant set contained in the set $\mathscr{D} = \{\widehat{v}(t) \mid \dot{W}(t) \equiv 0\}$ for error system (11). According to LaSalle's invariance principle [20], starting from any initial condition, every solution of system (11) approaches $\mathscr{M}$ as $t \to \infty$, that is, $\widehat{v}_i(t) \to 0_n, i = 1, \ldots, N$. So, the flock with dynamics (8) converges to a common velocity $v_c(0)$, that is, the velocity of the mass center.

Now we show that the collision between any two agents in multiagent system (8) can always be avoided if $W(0) < \Psi(0)$ is satisfied. Suppose that agents i and j collides at some time instant $t_1 > 0$. Then, we obtain $\Psi(\|\widehat{x}_i(t_1) - \widehat{x}_j(t_1)\|) = \Psi(\|x_i(t_1) - x_j(t_1)\|) = \Psi(0)$. From (12), we have $W(t_1) \geq \Psi(0)$. Considering the assumption of $\Psi(0) > W(0)$, we have $W(t_1) > W(0)$. However, $W(t_1) \leq W(0)$ always holds since $\dot{W}(t) \leq 0$. Hence, a contradiction occurs. Then, the distance between any two agents in multiagent system (8) should always be greater than zero, which ensures the collision-free motion of the flocking model (8).

Now, all three conditions of asymptotical flocking in Definition 1 hold. This completes the proof. □

Remark 11. From Theorem 10, we know that the velocity convergence of flocking model (8) is independent of the parameter β, which improves the original Cucker-Smale model and its existing variations.

Remark 12. The flocking model (8) theoretically ensures that any two agents will never collide during the time evolution of the system thus improving the augmented Cucker-Smale model (7).

Remark 13. From the proof of Theorem 10, we have $|r_{ij} - \eta| \leq \sqrt{2W(0)/k_a}$. Then, it follows that the term $k_a \sum_{j=1,j\neq i}^{N}((r_{ij} - \eta)/r_{ij})(x_j - x_i)\sqrt{2W(0)/k_a}$ in multiagent system (8) yields bounded bonding forces among agents satisfying $\|k_a \sum_{j=1,j\neq i}^{N}((r_{ij} - \eta)/r_{ij})(x_j - x_i)\| \leq (N-1)\sqrt{2k_aW(0)}$. If the repulsive function Ψ is bounded, the repulsive force in (8) is also bounded satisfying $\|\sum_{j=1,j\neq i}^{N}\nabla_{x_i}\Psi(\|x_i - x_j\|)\| \leq (N-1)\max_{i\neq j} g_r(\|x_i - x_j\|)\sup_{i\neq j}\|x_i - x_j\| \leq (N-1)P(\eta + \sqrt{2W(0)/k_a})$ by Definition 4 and (15).

Remark 14. From Theorem 10, we know that the bounded repulsive function Ψ for the flocking model (8) can be designed based on Definition 4 and the initial energy of the flock.

3.2. Cucker-Smale Flocking with Attractive and Repulsive Forces. For a network of agents, Gazi and Passino [18] proposed the following swarming model:

$$\begin{aligned}\dot{x}_i(t) = &-a\sum_{j=1,j\neq i}^{N}\left(x_i - x_j\right)\\ &+b\sum_{j=1,j\neq i}^{N}\left(x_i - x_j\right)\exp\left(-\frac{\left\|x_i - x_j\right\|^2}{c}\right),\end{aligned} \tag{16}$$

where a, b and c are positive parameters, the first and the second terms in the right-hand side describe the attraction and repulsion among the agents, respectively. Motivated by the aggregation technique in the swarming model (16), we introduce both attractive and repulsive forces to the original Cucker-Smale model (1) as follows:

$$\begin{aligned}\dot{x}_i(t) &= v_i(t), \quad i = 1, \ldots, N,\\ \dot{v}_i(t) &= \sum_{j=1,j\neq i}^{N} a_{ij}(x)\left(v_j - v_i\right)\\ &\quad + \frac{k_a}{N}\sum_{j=1,j\neq i}^{N}\left(x_j - x_i\right)\\ &\quad - \sum_{j=1,j\neq i}^{N}\nabla_{x_i}\Psi\left(\left\|x_i - x_j\right\|\right),\end{aligned} \tag{17}$$

where $k_a > 0$, and $\Psi(\|x_i - x_j\|)$ is a bounded repulsive function described in Definition 4.

Remark 15. Later, we will show that the terms $(k_a/N)\sum_{j=1,j\neq i}^{N}(x_j - x_i)$ and $-\sum_{j=1,j\neq i}^{N}\nabla_{x_i}\Psi(\|x_i - x_j\|)$ in (17) can yield bounded attractive and repulsive forces among the agents, respectively.

Let x_c and v_c be the position and the velocity of the mass center of multiagent system (17), respectively. It is easy to verify $\dot{v}_c = 0$, which means that the velocity of the centroid is constant. Let $\widehat{x}_i = x_i - x_c$ and let $\widehat{v}_i = v_i - v_c$. Note that $\sum_{j=1,j\neq i}^{N}(x_j - x_i) = N(x_c - x_i) = -N\widehat{x}_i$. From (17), we obtain the following error system:

$$\begin{aligned}\dot{\widehat{x}}_i(t) &= \widehat{v}_i(t), \quad i = 1, \ldots, N,\\ \dot{\widehat{v}}_i(t) &= \sum_{j=1,j\neq i}^{N} a_{ij}(\widehat{x})\left(\widehat{v}_j - \widehat{v}_i\right) - k_a\widehat{x}_i\\ &\quad - \sum_{j=1,j\neq i}^{N}\nabla_{\widehat{x}_i}\Psi\left(\left\|\widehat{x}_i - \widehat{x}_j\right\|\right).\end{aligned} \tag{18}$$

Construct the following energy function to study the flocking behavior of multiagent system (17):

$$W(t) = \frac{1}{2}\sum_{i=1}^{N}\widehat{v}_i^T\widehat{v}_i + \frac{k_a}{2}\sum_{i=1}^{N}\widehat{x}_i^T\widehat{x}_i + \frac{1}{2}\sum_{i=1}^{N}\sum_{j=1,j\neq i}^{N}\Psi\left(\left\|\widehat{x}_i - \widehat{x}_j\right\|\right). \tag{19}$$

Theorem 16. *For flocking system* (17)*, assume that the initial energy defined by* (19) *is finite, the initial positions satisfy* $\|x_i(0) - x_j(0)\| > 0$ *for all* $i \neq j$*, and the repulsive function* Ψ *is designed to be bounded based on Definition 4. Then, the flocking system* (17) *reaches velocity consensus on the common value* $v_c(0)$*, and the collision-free motion of the flock can be ensured if* $W(0) < \Psi(0)$ *holds.*

Proof. The proof can be carried out following the similar procedure for the proof of Theorem 10. The time derivative of $W(t)$ in (19) along the trajectory of (18) yields

$$\begin{aligned}
\dot{W}(t) &= \sum_{i=1}^{N}\widehat{v}_i^T\left[\sum_{j=1,j\neq i}^{N}a_{ij}(\widehat{x})\left(\widehat{v}_j - \widehat{v}_i\right) - k_a\widehat{x}_i - \sum_{j=1,j\neq i}^{N}\nabla_{\widehat{x}_i}\Psi\left(\left\|\widehat{x}_i - \widehat{x}_j\right\|\right)\right] \\
&\quad + k_a\sum_{i=1}^{N}\widehat{v}_i^T\widehat{x}_i + \sum_{i=1}^{N}\widehat{v}_i^T\sum_{j=1,j\neq i}^{N}\nabla_{\widehat{x}_i}\Psi\left(\left\|\widehat{x}_i - \widehat{x}_j\right\|\right) \\
&= \sum_{i=1}^{N-1}\sum_{j>i}^{N}\left[a_{ij}(\widehat{x})\widehat{v}_i^T\left(\widehat{v}_j - \widehat{v}_i\right) + a_{ji}(\widehat{x})\widehat{v}_j^T\left(\widehat{v}_i - \widehat{v}_j\right)\right] \\
&= -\sum_{i=1}^{N-1}\sum_{j>i}^{N}a_{ij}(\widehat{x})\left(\widehat{v}_j - \widehat{v}_i\right)^T\left(\widehat{v}_j - \widehat{v}_i\right) \\
&\leq -\min_{j>i}a_{ij}(\widehat{x})\sum_{i=1}^{N-1}\sum_{j>i}^{N}\left(\widehat{v}_j - \widehat{v}_i\right)^T\left(\widehat{v}_j - \widehat{v}_i\right) \\
&= -N\min_{j>i}a_{ij}(\widehat{x})\sum_{i=1}^{N}\left\|\widehat{v}_i\right\|^2.
\end{aligned} \tag{20}$$

By (20), we have $\dot{W}(t) \leq 0$. Thus, $W(t) \leq W(0) < \infty$ for all $t \geq 0$. From (19), we obtain

$$\frac{k_a}{2}\sum_{i=1}^{N}\widehat{x}_i(t)^T\widehat{x}_i(t) \leq W(0). \tag{21}$$

Then, it follows that $\|\widehat{x}_i\| = \|x_i - x_c\| \leq \sqrt{2W(0)/k_a}$, $i = 1,\ldots,N$, which indicates that the term $(k_a/N)\sum_{j=1,j\neq i}^{N}(x_j - x_i) = -k_a\widehat{x}_i$ in (17) creates attractive forces among agents such that the positions of all agents remain bounded in a ball centered at x_c with radius $R = \sqrt{2W(0)/k_a}$. Then, the distance between any two agents satisfies

$$\left\|x_i(t) - x_j(t)\right\| \leq 2R < \infty, \quad i \neq j,\ t \geq 0. \tag{22}$$

Since $\|x_i(t) - x_j(t)\| \leq 2R < \infty$, we have $a_{ij}(\widehat{x}) > 0$ for all $i \neq j$ by (2). Then, in view of (20), we have $\dot{W}(t) \equiv 0$ if and only if $\widehat{v}_i(t) = 0_n, i = 1,\ldots,N$. Following the similar lines in the proof of Theorem 10, we can show that the velocities of all agents in system (17) converge to the common velocity $v_c(0)$, and the distance between any two agents is always greater than zero if the bounded repulsive function Ψ satisfies $W(0) < \Psi(0)$. □

Remark 17. From the proof of Theorem 16, we have $\|\widehat{x}_i\| \leq \sqrt{2W(0)/k_a}$. Then, it follows that the term $(k_a/N)\sum_{j=1,i\neq j}^{N}(x_j - x_i) = -k_a\widehat{x}_i$ in (17) yields a bounded attractive force, that is, $k_a\|x_i\| \leq \sqrt{2k_aW(0)}$. If the repulsive function Ψ is bounded, the repulsive force in (17) is also bounded satisfying $\|\sum_{j=1,j\neq i}^{N}\nabla_{x_i}\Psi(\|x_i - x_j\|)\| \leq (N-1)\max_{i\neq j}g_r(\|x_i - x_j\|)\sup_{i\neq j}\|x_i - x_j\| \leq 2(N-1)P\sqrt{2W(0)/k_a}$ by Definition 4 and (22).

4. Numerical Results

This section provides two simulation examples to verify our theoretical results. The bounded repulsive function (5), that is, $\Psi(\|x_i - x_j\|) = Q\exp(-\mu\|x_i - x_j\|^2)$ for $\|x_i - x_j\| > 0$, is adopted to avoid interagent collisions. Define $d(t) = \min_{i\neq j}\|x_i(t) - x_j(t)\|$ to measure the proximity of the agents [17].

Example 18. Consider flocking model (8) with ten two-dimensional agents. Initially, the minimum distance between any two agents is 1.6584. The system parameters are chosen to be $H = 1$, $\beta = 0.5$, $k_a = 0.01$, and $\eta = 1.5$. The parameters of the repulsive function are taken as $Q = 140$ and $\mu = 3$. After some simple calculation using (12), we obtain $W(0) = 131.5835$ which is the initial energy of the flock. Considering $W(0) < \Psi(0) = Q = 140$, we know that the condition on the bounded repulsive function in Theorem 10 is satisfied. From Figure 1(a), we can see that the flock converges to a common velocity. The cohesiveness among agents is clearly shown in Figure 1(b), in which the symbols "+" and "o" denote the starting and ending points of the trajectory of an agent, respectively. In particular, from Figure 1(c), we note that collision avoidance in the flock is ensured because the minimal interagent distance is always greater than zero.

Example 19. Consider a multiagent system composed of ten two-dimensional agents described by dynamics (17) with $H = 1$, $\beta = 0.95$, and $k_a = 0.01$. The initial positions of the agents satisfy $\min_{i\neq j}\|x_i(0) - x_j(0)\| = 2.4876$. The parameters of the repulsive function are given by $Q = 40$ and $\mu = 1.8$. By (19), the initial energy of the flock is determined to be $W(0) = 34.0842$. Hence, the condition

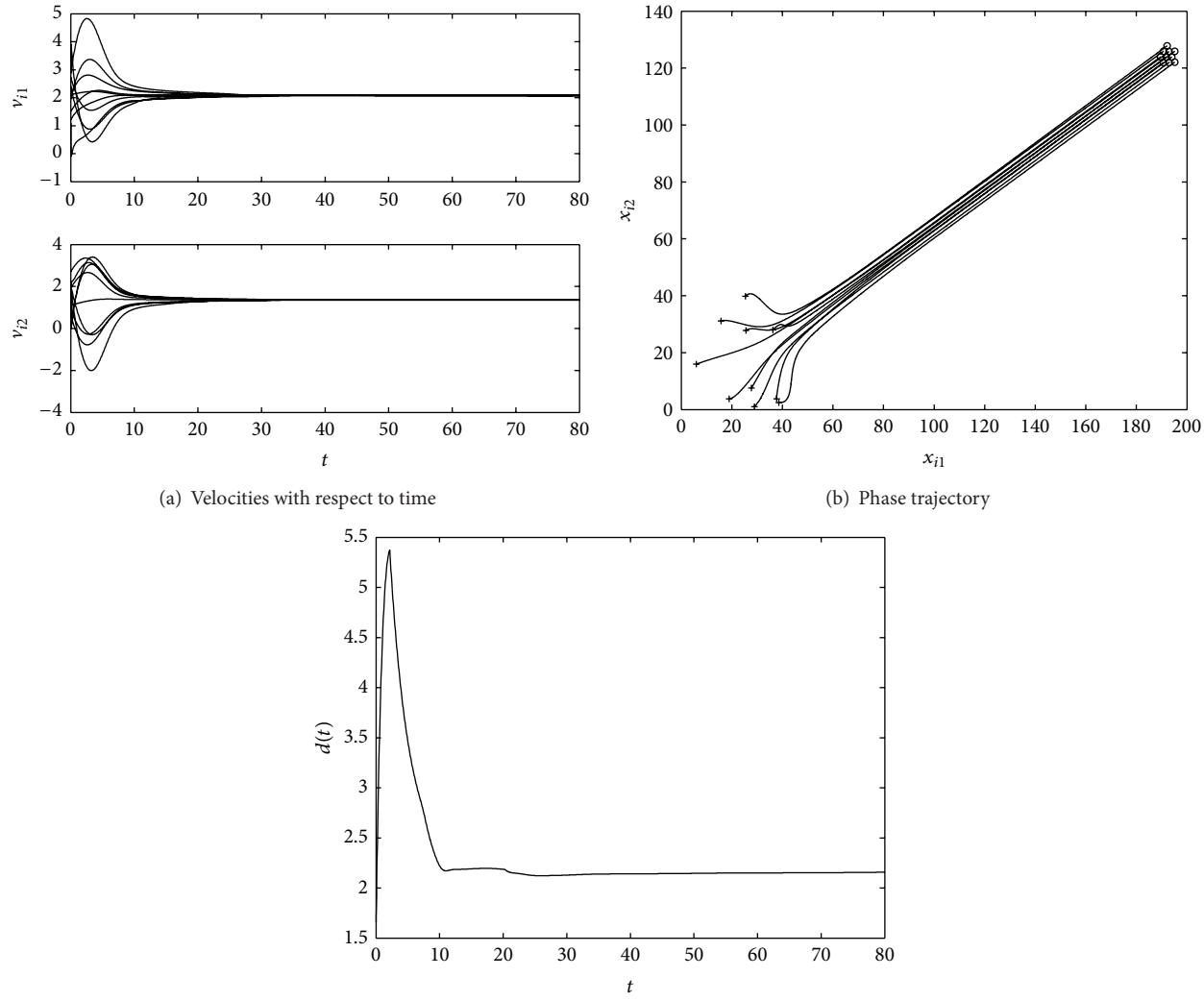

(a) Velocities with respect to time

(b) Phase trajectory

(c) Proximity $d(t)$ with respect to time

Figure 1: Flocking behavior of multiagent system (8) with ten two-dimensional agents.

for the bounded repulsive function in Theorem 16 holds in view of $W(0) < \Psi(0) = Q = 40$. Figure 2(a) shows that the flock achieves velocity consensus. The cohesive behavior of the flock is demonstrated by Figure 2(b). Figure 2(c) indicates that the interagent distance is always greater than zero which guarantees the collision-free motion of the agents.

5. Conclusions and Future Work

In this paper, we have proposed two Cucker-Smale-type flocking models with both cohesive and repulsive forces to improve the original Cucker-Smale model and its existing variations. It is shown that the velocity convergence of the flocking system is independent of the parameter β describing the decay of communication rates. We have also proved that the collision-free motion of the multiagent system can always be guaranteed by choosing an appropriate bounded repulsive function according to the initial energy of the flock. Up to date, the Cucker-Smale-type flocking models assume that each agent has the same sensing radius, which implies that the network topology is undirected. However, the sensing radii of the agents in a multiagent system may be different in many practical cases. In our future work, we will consider the Cucker-Smale flocking problem for multiagent systems with directed topologies.

Acknowledgments

This work was supported in part by the National Science Foundation of China under Grants 61273218, 61304172, 61272530, and 61273012, by the Natural Science Foundation of Henan Province of China under Grants 122102210027, 122300410220, and 2012XJGLX0521, by a project supported by the Scientific Research Fund of Zhejiang Provincial Education Department under Grant Y201223649 and by the Deanship of Scientific Research (DSR), King Abdulaziz University

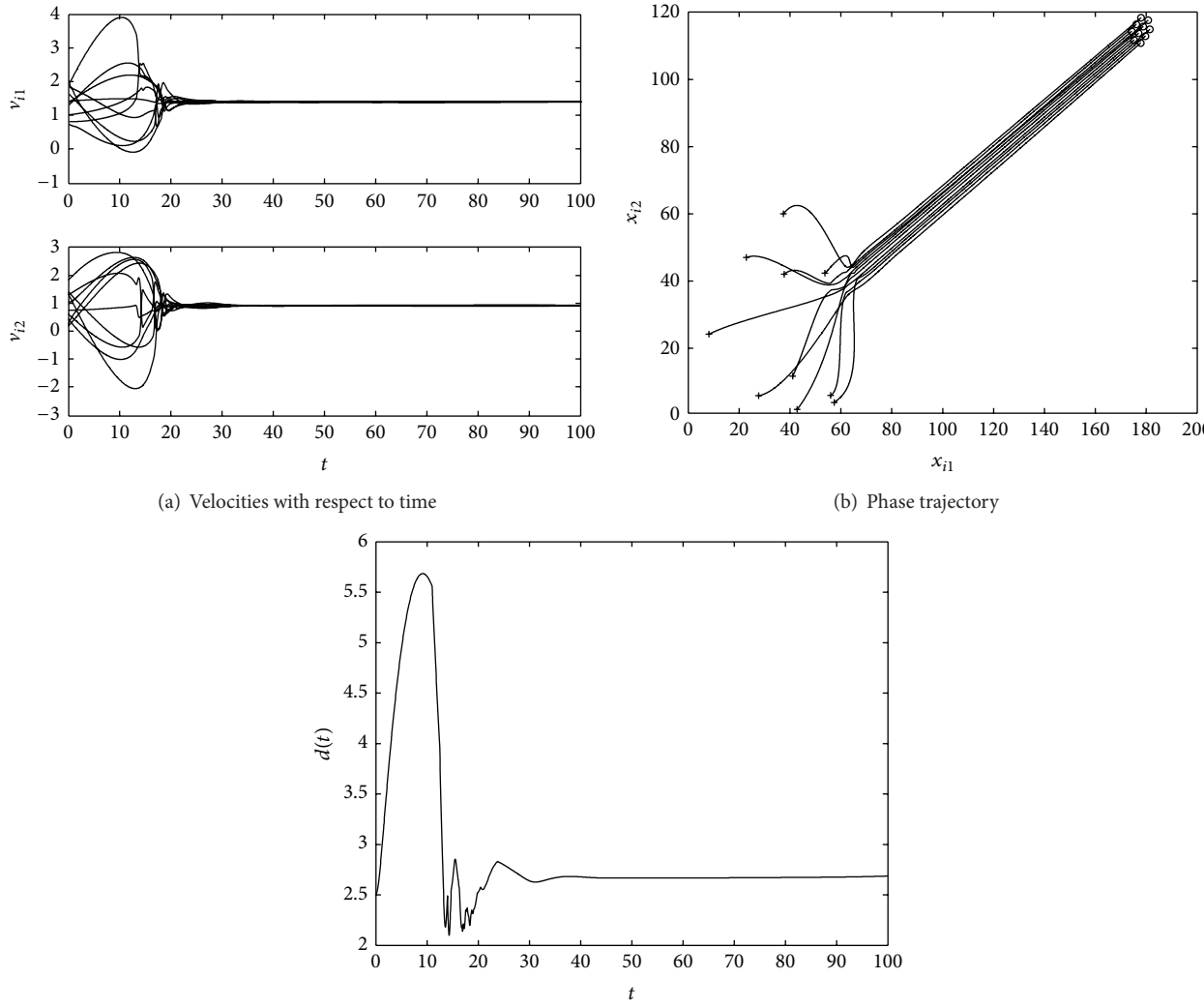

(a) Velocities with respect to time

(b) Phase trajectory

(c) Proximity $d(t)$ with respect to time

Figure 2: Flocking behavior of multiagent system (17) with ten two-dimensional agents.

(KAU), under Grant 3-130/1434/HiCi. The authors, therefore, acknowledge technical and financial support of KAU.

References

[1] C. W. Reynolds, "Flocks, herds, and schools: a distributed behavioral model," *Computer Graphics*, vol. 21, no. 4, pp. 25–34, 1987.

[2] T. Vicsek, A. Czirók, E. Ben-Jacob, I. Cohen, and O. Shochet, "Novel type of phase transition in a system of self-driven particles," *Physical Review Letters*, vol. 75, no. 6, pp. 1226–1229, 1995.

[3] A. Jadbabaie, J. Lin, and A. S. Morse, "Coordination of groups of mobile autonomous agents using nearest neighbor rules," *IEEE Transactions on Automatic Control*, vol. 48, no. 6, pp. 988–1001, 2003.

[4] R. Olfati-Saber, "Flocking for multi-agent dynamic systems: algorithms and theory," *IEEE Transactions on Automatic Control*, vol. 51, no. 3, pp. 401–420, 2006.

[5] H. G. Tanner, A. Jadbabaie, and G. J. Pappas, "Flocking in fixed and switching networks," *IEEE Transactions on Automatic Control*, vol. 52, no. 5, pp. 863–868, 2007.

[6] D. Gu and Z. Wang, "Leader-follower flocking: algorithms and experiments," *IEEE Transactions on Control Systems Technology*, vol. 17, no. 5, pp. 1211–1219, 2009.

[7] H. Su, X. Wang, and G. Chen, "A connectivity-preserving flocking algorithm for multi-agent systems based only on position measurements," *International Journal of Control*, vol. 82, no. 7, pp. 1334–1343, 2009.

[8] J. Zhou, X. Wu, W. Yu, M. Small, and J. Lu, "Flocking of multi-agent dynamical systems based on pseudo-leader mechanism," *Systems & Control Letters*, vol. 61, no. 1, pp. 195–202, 2012.

[9] G. Wen, Z. Duan, H. Su, G. Chen, and W. Yu, "A connectivity-preserving flocking algorithm for multi-agent dynamical systems with bounded potential function," *IET Control Theory & Applications*, vol. 6, no. 6, pp. 813–821, 2012.

[10] J. Zhu, J. Lü, and X. Yu, "Flocking of multi-agent non-holonomic systems with proximity graphs," *IEEE Transactions on Circuits and Systems I*, vol. 60, no. 1, pp. 199–210, 2013.

[11] F. Cucker and S. Smale, "Emergent behavior in flocks," *IEEE Transactions on Automatic Control*, vol. 52, no. 5, pp. 852–862, 2007.

[12] J. Shen, "Cucker-Smale flocking under hierarchical leadership," *SIAM Journal on Applied Mathematics*, vol. 68, no. 3, pp. 694–719, 2007.

[13] S. Y. Ha and J. G. Liu, "A simple proof of the Cucker-Smale flocking dynamics and mean-field limit," *Communications in Mathematical Sciences*, vol. 7, no. 2, pp. 297–325, 2009.

[14] S. Y. Ha, T. Ha, and J. H. Kim, "Emergent behavior of a Cucker-Smale type particle model with nonlinear velocity couplings," *IEEE Transactions on Automatic Control*, vol. 55, no. 7, pp. 1679–1683, 2010.

[15] J. Park, H. J. Kim, and S. Y. Ha, "Cucker-Smale flocking with inter-particle bonding forces," *IEEE Transactions on Automatic Control*, vol. 55, no. 11, pp. 2617–2623, 2010.

[16] L. Perea, G. Gómez, and P. Elosegui, "Extension of the Cucker-Smale control law to space flight formations," *Journal of Guidance, Control, and Dynamics*, vol. 32, no. 2, pp. 526–536, 2009.

[17] F. Cucker and J. G. Dong, "Avoiding collisions in flocks," *IEEE Transactions on Automatic Control*, vol. 55, no. 5, pp. 1238–1243, 2010.

[18] V. Gazi and K. M. Passino, "Stability analysis of swarms," *IEEE Transactions on Automatic Control*, vol. 48, no. 4, pp. 692–697, 2003.

[19] V. Gazi and K. M. Passino, "A class of attractions/repulsion functions for stable swarm aggregations," *International Journal of Control*, vol. 77, no. 18, pp. 1567–1579, 2004.

[20] H. K. Khalil, *Nonlinear Systems*, Prentice Hall, Englewood Cliffs, NJ, USA, 3rd edition, 2002.

Hindawi Publishing Corporation
Abstract and Applied Analysis
Volume 2013, Article ID 412189, 7 pages
http://dx.doi.org/10.1155/2013/412189

Research Article

Dynamic Average Consensus and Consensusability of General Linear Multiagent Systems with Random Packet Dropout

Wen-Min Zhou[1,2] and Jiang-Wen Xiao[1,2]

[1] *School of Automation, Huazhong University of Science and Technology, Wuhan 430074, China*
[2] *Key Laboratory of Image Processing and Intelligent Control of Education Ministry of China, Wuhan 430074, China*

Correspondence should be addressed to Jiang-Wen Xiao; jwxiao@mail.hust.edu.cn

Received 10 June 2013; Revised 19 August 2013; Accepted 27 August 2013

Academic Editor: Jianquan Lu

This paper is concerned with the consensus problem of general linear discrete-time multiagent systems (MASs) with random packet dropout that happens during information exchange between agents. The packet dropout phenomenon is characterized as being a Bernoulli random process. A distributed consensus protocol with weighted graph is proposed to address the packet dropout phenomenon. Through introducing a new disagreement vector, a new framework is established to solve the consensus problem. Based on the control theory, the perturbation argument, and the matrix theory, the necessary and sufficient condition for MASs to reach mean-square consensus is derived in terms of stability of an array of low-dimensional matrices. Moreover, mean-square consensusable conditions with regard to network topology and agent dynamic structure are also provided. Finally, the effectiveness of the theoretical results is demonstrated through an illustrative example.

1. Introduction

Multiagent systems (MASs) are kinds of networked systems in which each agent updates its states based on the information exchanges over communication networks. Due to their broad applications in many areas such as sensor networks [1], distributed computation [2], swarms and flocks [3], and formation control [4], the consensus problem of MASs has attracted increasing attention in recent years, and considerable interesting results have been obtained on this problem.

At the beginning, the consensus problem is investigated mainly for first-order and second-order MASs. Olfati-Saber and Murray [5] studied the consensus problem for a network of first-order integrators under various topology conditions, including directed or undirected, fixed or switching, and with or without communication time-delays; Hatano and Mesbahi [6] studied the asymptotic agreement of first-order continuous MASs over random information network based on stochastic stability analysis; Zhang and Tian [7] investigated the MASs consisting of discrete-time second-order agents under stochastic switching topology and proved that MASs can achieve mean-square consensus if and only if the union graphs in the topology set are connected. Sun et al. [8] investigated the finite-time consensus for first- and second-order leader-following Multiagent systems. In [9], Lin et al. further studied the consensus problems of a class of high-order Multiagent systems with dynamically changing topologies and time-delays and proved that the communication time-delays do not affect the stability of the Multiagent systems.

Recently, some researches on MASs with general linear dynamics have been conducted. Li et al. [10] proved that MASs with a communication topology having a spanning tree can reach consensus under an observe-type protocol if and only if each agent is stabilizable and detectable. Xu et al. [11] investigated the information structure for the consensusability of MASs under both fixed and switching topologies with dynamic output feedback control. In [12], Xu et al. further studied the leader-following consensus problem of discrete-time Multiagent systems with switching and

undirected topology by applying two kinds of distributed observer-based consensus protocols to each agent. Su and Huang [13] proved that if the system matrix is marginally stable and the dynamic graph is jointly connected, both the leaderless and the leader-following consensus problems for linear discrete-time Multiagent systems under switching network topology can be solved.

Note that most of the existing results on the consensus problem of MASs are derived from the assumption that the network communication environment is perfect. However, communication constraints which may deteriorate the performance of MASs are inevitable in practice. There are numerous studies focusing on the consensus problem for MASs with either communication time delay or presence of perturbation or both of them, such as [14–18], but as one of the main reasons for performance deterioration, packet dropout, which takes place frequently during the information exchange between agents, is not fully investigated. Therefore, it is of great significance to study the effect of packet dropout in MASs. Ren and Beard [19] studied the consensus problem for first-order continuous-time agents communicating via unreliable network through dynamically changing interaction topology method and proved that asymptotic consensus can be achieved if the union of the directed graph had a spanning tree frequently enough. Sun et al. [20] investigated the convergence and convergence speed for the second-order and the high-order discrete-time Multiagent systems with random networks and arbitrary weights. Zhang and Tian [21] investigated the mean-square consensus problem for continuous time second-order MASs disturbed by noise, variable delays, and occasional packet dropout and discussed the necessary and sufficient condition for mean-square robust consensusability. And in [22], Zhang and Tian further studied the consensus seeking problem for linear MASs, where each agent communicates via a weighted random lossy network and derived the maximum allowable loss probability.

Motivated by the above analysis, this paper is concerned with consensus problem of general linear discrete-time MASs with random packet dropout that happens during the information exchange between agents, which, to the best of our knowledge, has not been fully investigated until now. The contribution of this paper lies in the following: first, a distributed consensus protocol with weighted graph is proposed to address the packet dropout phenomenon; second, through introducing a new disagreement vector, the dynamic average consensus problem is studied based on the established new framework; third, the necessary and sufficient condition for MASs to reach mean-square consensus is derived in terms of stability of an array of low-dimensional matrices, which is easier to be used in reality; moreover, mean-square consensusable conditions with regard to network topology and agent dynamic structure are also provided.

The rest of this paper is organized as follows. In Section 2, modeling construction of Multiagent systems with packet dropout is proposed, and some useful lemmas are introduced. In Section 3, a new framework is derived to address the consensus problem of MASs. The consensusable conditions with regard to network topology and agent dynamic structure are presented in Section 4. In Section 5, an illustrative example is provided to demonstrate the effectiveness of our results. Concluding remarks are drawn in Section 6.

Notation. $\mathbb{R}^n$ and $\mathbb{R}^{m\times n}$ denote the n-dimensional Euclidean space and the set of $m \times n$ real matrix, respectively, and I_N represents an N-dimensional identity matrix. diag$\{\cdot\}$ refers to a diagonal matrix, or a block diagonal matrix. For matrices A and B, $A > B$ implies that A and B are symmetric matrices and that $A - B$ is positive definite. The superscript T and -1 mean transpose and inverse of a real matrix separately, and symbol $*$ in a symmetric matrix implies a block that can be induced by symmetry. $\lambda_{\min}(\cdot)$, $\lambda_{\max}(\cdot)$ and $\rho(\cdot)$, denote, respectively, the smallest eigenvalue, the largest eigenvalue and the spectral radius of a matrix. Prob$\{\cdot\}$ stands for the occurrence probability of a stochastic event and Prob$\{\cdot \mid \cdot\}$ the conditional probability. $E(\cdot)$ is the mathematical expectation operator. $\|\cdot\|$ and $\|\cdot\|_1$ stand the 2-norm and 1-norm respectively.

2. Problem Formulation and Preliminaries

Consider a system of N agents with identical general linear dynamics. The dynamic equation of agent i is described by

$$x_i(k+1) = Ax_i(k) + Bu_i(k), \quad i = 1, 2, \ldots, N, \tag{1}$$

where $x_i = [x_{i1}, x_{i2}, \ldots, x_{in}]^T \in R^n$ is the state variable, $u_i \in \mathbb{R}^m$ is the control input, and $A \in \mathbb{R}^{n\times n}$ and $B \in \mathbb{R}^{n\times m}$ are known constant matrices.

Suppose that there is a predesigned undirected fixed topology G which guarantees the effective communication between distinct nodes. This assumption is quite reasonable, since it is impossible to reach consensus under an unconnected topology. Denote N_i as the neighbor set of the node i and $A_G = [a_{ij}] \in R^{N\times N}$ as the weighted adjacency matrix of undirected graph G with $a_{ii} = 0$, and for any i belongs to set N_i, $a_{ij} = a_{ji} > 0$, otherwise, $a_{ij} = a_{ji} = 0$.

Under ideal communication environment, the commonly used linear distributed consensus protocol in MASs is as follows:

$$u_i(k) = K \sum_{j\in N_i} a_{ij}\left(x_j(k) - x_i(k)\right), \quad i = 1, 2, \ldots, N, \tag{2}$$

where $K \in \mathbb{R}^{m\times n}$ is the gain matrix.

As mentioned in Section 1, packet dropout is inevitable in practical environment. In this paper, Bernoulli distributed white sequence $\{\theta_{ij}(k)\}$ is introduced to model the unreliability of the link between agent i and agent j. At any given time instant k, for any $j \in N_i$, $\theta_{ij}(k)$ takes value in the set $\{0, 1\}$. Suppose that for any $i, j \in \{1, \ldots, N\}$, $\theta_{ij}(k)$ is mutually independent; that is, the packet dropout probability between each pair of agents is independent. When the packet is transmitted successfully between agent i and agent j, $\theta_{ij}(k) = 1$; when packet dropout takes place between agent i and agent j, $\theta_{ij}(k) = 0$, which can be described as

$$\theta_{ij}(k) = \begin{cases} 0, & \text{with probability } p_{ij}, \\ 1, & \text{with probability } 1 - p_{ij}, \end{cases} \tag{3}$$

where p_{ij} is the occurrence probability of packet dropout between i and j, and for any $j \notin N_i$, $\theta_{ij}(k) \equiv 0$, $p_{ij} \equiv 1$.

Besides, due to the occurrence of packet dropout, the topology of MAS (1) is no longer fixed. Denote $|N_i|$ as the number of agents in set N_i, S as the total number of the possible topologies. It is easy to see that $S = 2^{\sum_{i=1}^{N} |N_i|/2}$; then the topology of the MAS is changing among the set $\{G_1, \ldots, G_S\}$. Suppose that at certain time instant k, $\theta_{ij}(k) = \theta_{ij}^m$ and the network topology is G_m, then the occurrence probability of graph G_m, $m = 1, \ldots, S$, is

$$\pi_m = \prod_{i=1,\ i<j} \left(\theta_{ij}^m \left(1 - p_{ij}\right) + \left(1 - \theta_{ij}^m\right) p_{ij}\right). \tag{4}$$

Based upon the above analysis, the following distributed consensus protocol is employed in this paper:

$$u_i(k) = K \sum_{j \in N_i} \theta_{ij}(k)\, a_{ij} \left(x_j(k) - x_i(k)\right), \quad i = 1, \ldots, N, \tag{5}$$

where K is the state feedback gain matrix to be designed.

Substituting (5) into (1), the dynamic equation of agent i can be rewritten as

$$x_i(k+1) = Ax_i(k) + BK \sum_{j \in N_i} \theta_{ij}(k)\, a_{ij} \left(x_j(k) - x_i(k)\right). \tag{6}$$

Then, the states of MAS (1) evolve according to the following linear system:

$$x(k+1) = \left(I_N \otimes A - L_{\sigma(k)} \otimes (BK)\right) x(k), \tag{7}$$

where $x = [x_1^T, \ldots, x_N^T]^T$, $\sigma(\cdot) : Z^+ \to \{1, 2, \ldots, S\}$ is a stochastic process driven by an i.i.d. process and $L_{\sigma(k)} \in \{L_m\}$, where $L_m = [l_{ij}^m]_{N \times N}$, $m = 1, \ldots, S$, is the Laplacian matrix associated with G_m, with

$$l_{ij}^m = \begin{cases} \sum_{j=1}^{N} \theta_{ij}^m a_{ij}, & i = j, \\ -\theta_{ij}^m a_{ij}, & i \neq j. \end{cases} \tag{8}$$

Obviously, the Laplacian matrix L_m is a symmetric matrix with zero row sum that is, $\forall i \neq j$, $l_{ij} = l_{ji}$, and $\sum_{j=1}^{N} l_{ij}^m = 0$.

Before presenting our main results, the concepts of mean-square stability and mean-square consensus are introduced first, and along with them are some useful lemmas which play significant roles in the derivation of our results.

Definition 1 (see [23]). A closed-loop system is said to be mean-square stable, if for any $\varepsilon > 0$, there exists $\delta(\varepsilon) > 0$ such that for any $k > 0$, $E(\|x(k)\|^2) < \varepsilon$ holds when $E(\|x(0)\|^2) < \delta(\varepsilon)$. In addition, if $\lim_{k \to \infty} E(\|x(k)\|^2) = 0$ for any initial condition, then the closed-loop system is said to be globally mean-square asymptotically stable.

Definition 2. Multiagent system (1) with protocol (5) is said to reach consensus in mean-square sense, if for any initial distribution and initial states, $\lim_{k \to \infty} E(\|x_i(k) - x_j(k)\|^2) = 0$ holds for all $i, j \in \{1, \ldots, N\}$. Furthermore, if there exists a proper state feedback gain matrix K such that the Multiagent system can achieve mean-square consensus, then we say that system (1) is mean-square consensusable under protocol (5).

Lemma 3 (see [21]). *For any vector $z(k) \in \mathbb{R}^n$, denote $\overline{z}(k) := E(z(k) \otimes z(k))$, then there is*

$$E\left(\|z(k)\|^2\right) \leq \|\overline{z}(k)\|_1 \leq nE\left(\|z(k)\|^2\right). \tag{9}$$

Lemma 4 (see [6]). *For an undirected graph with n vertices, the Laplacian is a positive-semidefinite symmetric matrix, and the spectrum of a graph Laplacian is on the form*

$$0 = \lambda_1(L) \leq \lambda_2(L) \leq \cdots \leq \lambda_{n-1}(L) \leq \lambda_n(L), \tag{10}$$

with $\lambda_2(L) > 0$ if and only if the graph that corresponds to L is connected.

Lemma 5. *$\sum_{m=1}^{S} \pi_m L_m$ has only one zero eigenvalue, if and only if the union graph of the topology set $\{G_1, \ldots, G_S\}$ is connected.*

Proof. Since $\sum_{m=1}^{S} \pi_m L_m$ can be treated as a Laplacian matrix of a graph which has the same edges with the union graph of the topology set $\{G_1, \ldots, G_S\}$, then together with Lemma 4, it can be obtained that Lemma 5 holds. □

Lemma 6 (see [24]). *For any $A \in \mathbb{R}^{n \times n}$, there exist orthogonal matrix U and an upper triangular matrix V, such that*

$$U^T A U = V = \begin{bmatrix} \mu_1 & v_{12} & \cdots & v_{1n} \\ & \mu_2 & \cdots & v_{2n} \\ & & \ddots & \vdots \\ & & & \mu_n \end{bmatrix}, \tag{11}$$

where μ_i, $i = 1, \ldots, n$, are the eigenvalues of matrix A.

3. Necessary and Sufficient Conditions for Mean-Square Consensus

Introduce the following variable:

$$\delta_i(k) = x_i(k) - \frac{1}{N} \sum_{j=1}^{N} x_j(k). \tag{12}$$

Rewrite (12) in a compact form, which is

$$\delta(k) = \left(C \otimes I_n\right) x(k), \tag{13}$$

where $C = I_N - (1/N)\vec{1}\vec{1}^T$ and $\delta = [\delta_1^T, \ldots, \delta_N^T]^T \in R^{Nn}$ is the so-called disagreement vector.

It is easy to verify that δ evolves according to the following disagreement dynamics:

$$\delta(k+1) = \left(I_N \otimes A - L_{\sigma(k)} \otimes (BK)\right) \delta(k), \tag{14}$$

where $\delta(k)$ is defined in (7).

Since $E(\|\delta(k)\|^2) = E(x^T(k)(Q \otimes I_n)x(k))$, where $Q = C^TC = I_N - (1/N)\vec{1}\vec{1}^T$, it is easy to verify that

$$E\left(\|\delta(k)\|^2\right) = \frac{1}{2N}\sum_{i\neq j} E\left(\left\|x_j(k) - x_i(k)\right\|^2\right). \tag{15}$$

Equation (15) implies that the mean-square consensus problem can be solved if and only if $\lim_{k\to\infty} E(\|\delta(k)\|^2) = 0$. From Definitions 1 and 2, it is easy to see that the consensus problem of MAS (1) is converted to the mean square stability analysis of system (14).

Remark 7. If the system matrix A is Schur stable, which means all eigenvalues of A are located in the unit circle, MAS (1) would definitely reach consensus without the design of consensus protocol, since under this condition, for any $i \in \{1,\ldots,N\}$, x_i will converge to zero, and $\lim_{k\to\infty} E(\|x_i(k) - x_j(k)\|^2) = 0$ holds for sure. In view of this, we assume that not all eigenvalues of A are located in the unit circle.

Theorem 8. *For any initial distribution and initial states, Multiagent system* (1) *with the Bernoulli packet dropout between agents can achieve mean-square consensus under protocol* (1)*, if and only if*

$$\rho\left(A - \widehat{\lambda}_i BK\right) < 1, \tag{16}$$

where $\widehat{\lambda}_i$, $i = 2,\ldots,N$, *are the eigenvalues of matrix* $\sum_{m=1}^{S}\pi_m L_m$ *except one zero eigenvalue.*

Proof. Since for each $\sigma(k) = m$, $m = 1,\ldots,S$, $L_{\sigma(k)}$ is a symmetric matrix with zero row sum, and $w^T = (1/N)\vec{1}^T$ and $\vec{1}$ are, respectively, the left and right eigenvectors of $L_{\sigma(k)}$ associated with zero eigenvalue, we can construct an invertible matrix $T = \left[\vec{1}\ \ T_1\right]$ with $T^{-1} = \left[w\ \ T_2{}^T\right]^T$, such that

$$T^{-1}L_{\sigma(k)}T = \overline{L}_{\sigma(k)} = \begin{bmatrix} 0 & 0 \\ 0 & \widetilde{L}_{\sigma(k)} \end{bmatrix}, \tag{17}$$

where $T \in \mathbb{R}^{N\times N}$, $T_1 \in \mathbb{R}^{N\times(N-1)}$, $T_2 \in \mathbb{R}^{(N-1)\times N}$, and $\widetilde{L}_{\sigma(k)} = T_2 L_{\sigma(k)} T_1 \in R^{(N-1)\times(N-1)}$.

Introduce the following variable: $\varphi(k) = (T^{-1}\otimes I_n)\delta(k)$, where $\varphi = [\varphi_1^T,\ldots,\varphi_N^T]^T \in R^{Nn}$; then (14) can be denoted in terms of φ as

$$\varphi(k+1) = \left(I_N \otimes A - \overline{L}_{\sigma(k)} \otimes (BK)\right)\varphi(k). \tag{18}$$

Note that $\varphi_1 = (w^T \otimes I_n)\delta \equiv 0$, which implies that state φ_1 is always stable; thus, divide $\varphi(k)$ into two parts; that is, $\varphi(k) = [\varphi_1^T(k), \widehat{\varphi}^T(k)]^T$, with $\widehat{\varphi} = [\varphi_2^T,\ldots,\varphi_N^T]^T$, it can be derived from (17) and (18) that

$$\widehat{\varphi}(k+1) = \widetilde{A}_{\sigma(k)}\widehat{\varphi}(k), \tag{19}$$

where $\widetilde{A}_{\sigma(k)} = I_{N-1}\otimes A - \widetilde{L}_{\sigma(k)} \otimes (BK)$.

Similar to [21], let $\xi(k) = E(\widehat{\varphi}(k)\otimes\widehat{\varphi}(k))$; then $\xi(k)$ evolves according to

$$\xi(k+1) = \sum_{m=1}^{S}\pi_m\left(\widetilde{A}_m \otimes \widetilde{A}_m\right)\xi(k). \tag{20}$$

From Lemma 3, system (14) is mean-square stable if and only if system (20) is stable. Then, from the discrete-time system stability theory, it can be concluded that the necessary and sufficient condition for mean-square stability of (14) is $\rho(\sum_{m=1}^{S}\pi_m(\widetilde{A}_m \otimes \widetilde{A}_m)) < 1$.

Denote $\widetilde{A}_m = \Phi - \Psi_m K$ with $\Phi = I_{N-1}\otimes A$, $\Psi_m = \widetilde{L}_m \otimes B$, $K = I_{N-1}\otimes K$, and $K = \varepsilon K'$; then there is $\sum_{m=1}^{S}\pi_m(\widetilde{A}_m \otimes \widetilde{A}_m) = \Phi\otimes\Phi - \varepsilon(\sum_{m=1}^{S}\pi_m\Phi\otimes(\Psi_m K') + \sum_{m=1}^{S}\pi_m(\Psi_m K')\otimes\Phi) + \varepsilon^2\sum_{m=1}^{S}\pi_m(\Psi_m K')\otimes(\Psi_m K')$. The above equation can be treated as a perturbation of $\Phi\otimes\Phi$ by two terms depending on ε. For small enough ε, the above formula is equal to $\sum_{m=1}^{S}\pi_m(\widetilde{A}_m\otimes\widetilde{A}_m) = \Phi\otimes\Phi - \varepsilon(\sum_{m=1}^{S}\pi_m\Phi\otimes(\Psi_m K') + \sum_{m=1}^{S}\pi_m(\Psi_m K')\otimes\Phi)$. Meanwhile, $(\sum_{m=1}^{S}\pi_m\widetilde{A}_m)\otimes(\sum_{m=1}^{S}\pi_m\widetilde{A}_m) = \Phi\otimes\Phi - \varepsilon(\sum_{m=1}^{S}\pi_m\Phi\otimes(\Psi_m K') + \sum_{m=1}^{S}\pi_m(\Psi_m K')\otimes\Phi) + \varepsilon^2\sum_{m=1}^{S}(\pi_m\Psi_m K')\otimes(\pi_m\Psi_m K')$. Likewise, by applying perturbation argument, for a small enough ε, $\rho(\sum_{m=1}^{S}\pi_m(\widetilde{A}_m\otimes\widetilde{A}_m)) < 1$ is equivalent to

$$\rho\left(\left(\sum_{m=1}^{S}\pi_m\widetilde{A}_m\right)\otimes\left(\sum_{m=1}^{S}\pi_m\widetilde{A}_m\right)\right) < 1. \tag{21}$$

Next, it will be proved that (21) holds if and only if (16) is satisfied.

It can be seen from (18) that $\sum_{m=1}^{S}\pi_m\widetilde{L}_m$ has the same eigenvalue with $\sum_{m=1}^{S}\pi_m\overline{L}_m$ and $\sum_{m=1}^{S}\pi_m L_m$ except one zero eigenvalue. Besides, based on Lemma 6, there exists an orthogonal matrix $U \in R^{(N-1)\times(N-1)}$ such that

$$U^T\left(\sum_{m=1}^{S}\pi_m\widetilde{L}_m\right)U = \begin{bmatrix} \widehat{\lambda}_2 & * & \cdots & * \\ & \widehat{\lambda}_3 & \cdots & * \\ & & & \vdots \\ & & & \widehat{\lambda}_N \end{bmatrix}, \tag{22}$$

where $\widehat{\lambda}_i$, $i = 2,\ldots,N$, are the eigenvalues of matrix $\sum_{m=1}^{S}\pi_m L_m$ except one zero eigenvalue. It is easy to verify that $\sum_{m=1}^{S}\pi_m\widetilde{A}_m = I_{N-1}\otimes A - \sum_{m=1}^{S}\pi_m\widetilde{L}_m\otimes(BK)$ is similar to

$$\begin{bmatrix} A - \widehat{\lambda}_2 BK & * & \cdots & * \\ & A - \widehat{\lambda}_3 BK & \cdots & * \\ & & \ddots & \vdots \\ & & & A - \widehat{\lambda}_N BK \end{bmatrix}. \tag{23}$$

Based on the matrix theory, matrix $\sum_{m=1}^{S}\pi_m\widetilde{A}_m$ has the same eigenvalue with matrix (23), obviously $\rho(\sum_{m=1}^{S}\pi_m\widetilde{A}_m) < 1$, if and only if (16) is satisfied. Then, together with the properties of the Kronecker product, it is safe to say that (21) holds if and only if (16) is satisfied, which completes the proof. □

Remark 9. The contribution of Theorem 8 lies in the fact that it converts the consensus problem of MAS (1) into a set of matrices with the same dimensions as a single agent, which reduces the computational complexity greatly. Besides, while in most of the existing results each agent is guaranteed to achieve consensus with agent 1, see [7, 11, 21] for example, or to achieve average consensus, see [5], for example, in this paper a new disagreement vector is introduced to solve the consensus problem so that each agent will reach consensus on the average states of all agents, that is, dynamic average consensus.

4. Consensusability Analysis

Theorem 8 presents the numerical solution to consensus problem, which also implies the design method of consensus protocol. However, in practice, we are equally interested in that under what conditions MAS (1) has the ability to reach consensus and inequality (16) has a solution at the same time, that is, what are the consensusable conditions? In this section, we focus on addressing this problem.

Theorem 10. *Multiagent system* (1) *with the Bernoulli packet dropout between agents can achieve mean-square consensus under protocol* (5)*, if and only if the union graph of the topology set* $\{G_1, \ldots, G_S\}$ *is connected, and* (A, B) *is stabilizable.*

Proof. Necessity: define $E(L_{\sigma(k)}) = \sum_{m=1}^{S} \pi_m L_m$ as the expected Laplacian matrix and its corresponding graph as the expected graph. Since $E(L_{\sigma(k)})$ is a symmetric matrix, there exists an invertible matrix $\widehat{T} = \begin{bmatrix} \vec{1} & \widehat{F} \end{bmatrix}$ with $\widehat{T}^{-1} = \begin{bmatrix} w & \widehat{E}^T \end{bmatrix}^T$, such that

$$\widehat{T}^{-1} E\left(L_{\sigma(k)}\right) \widehat{T} = \Lambda = \begin{bmatrix} 0 & 0 \\ 0 & \widehat{\Delta} \end{bmatrix}, \tag{24}$$

where $\widehat{T} \in \mathbb{R}^{N\times N}$, $\widehat{F} \in \mathbb{R}^{N\times(N-1)}$, $\widehat{E} \in \mathbb{R}^{(N-1)\times N}$, w^T, which is defined in (18), is also the left eigenvalue of $E(L_{\sigma(k)})$ associated with zero eigenvalue, and $\widehat{\Delta} \in R^{(N-1)\times(N-1)}$ is a diagonal matrix with its diagonal elements being $\widehat{\lambda}_i$, $i = 2, \ldots, N$.

Denote $\phi(k) = E(\delta(k))$; then $\phi(k)$ evolves according to

$$\phi(k+1) = \left(I_N \otimes A - E\left(L_{\sigma(k)}\right) \otimes (BK)\right) \phi(k), \tag{25}$$

where $\phi = [\phi_1^T, \ldots, \phi_N^T]^T \in R^{Nn}$.

Similar to the proof in Theorem 8, introduce the following variable transformation: $\zeta(k) = (\widetilde{T}^{-1} \otimes I_n)\phi(k)$; then the dynamic equation of $\zeta(k)$ can be written as

$$\zeta(k+1) = \left(I_N \otimes A - \Lambda \otimes (BK)\right) \zeta(k), \tag{26}$$

where $\zeta = [\zeta_1^T, \ldots, \zeta_N^T]^T \in R^{Nn}$.

Notice that $\zeta_1(k) = (\widetilde{w}^T \otimes I_N)E(\delta(k)) \equiv 0$, divide $\zeta(k) = (\widetilde{w}^T \otimes I_N)E(\delta(k)) \equiv 0$ into two parts, that is, $\zeta(k) = [\zeta_1^T(k), \widetilde{\zeta}^T(k)]^T$, from (19) and (21), it can be derived that

$$\widetilde{\zeta}(k+1) = \begin{bmatrix} A - \widehat{\lambda}_2 BK & 0 & \cdots & 0 \\ & A - \widehat{\lambda}_3 BK & \cdots & 0 \\ & & \ddots & \vdots \\ & & & A - \widehat{\lambda}_N BK \end{bmatrix} \widetilde{\zeta}(k). \tag{27}$$

If the union graph of the topology set $\{G_1, \ldots, G_S\}$ is not connected, the expected graph is definitely not connected. It can be obtained from Lemma 3 that $0 = \widehat{\lambda}_2 \le \widehat{\lambda}_3 \le \cdots \le \widehat{\lambda}_N$. Due to the fact that not all eigenvalues of A are located in the unit circle, there exists an initial state such that $\lim_{k\to\infty}\zeta(k) \neq 0$ and $\lim_{k\to\infty}E(\delta(k)) \neq 0$ thus; system (14) is not mean-square stable since $E(\|\delta(k)\|^2) \ge \|E(\delta(k))\|^2$, and consequently, Multiagent system (1) cannot achieve mean-square consensus.

Besides, if (A, B) is unstabilizable, it is impossible to guarantee that $\rho(A - \widehat{\lambda}_i BK) < 1$, $i = 2, \ldots, N$, even if the topology condition is satisfied, and system (27) is still not guaranteed to be stable.

Sufficiency: It can be derived from Lemma 5 that when the union of the graphs in the topology set is connected, all eigenvalues of $\sum_{m=1}^{S} \pi_m \widetilde{L}_m$ are positive; that is, $\widehat{\lambda}_i > 0$, $i = 2, \ldots, N$. Therefore, when the union graph of the topology set $\{G_1, \ldots, G_S\}$ is connected and (A, B) is stablizable, there exists a proper gain matrix K such that $\rho(A - \widehat{\lambda}_i BK) < 1$, $i = 2, \ldots, N$. The proof is completed. □

Remark 11. In [21], for two-order continuous-time MASs with $A = \left[\begin{smallmatrix} 0 & 1 \\ 0 & 0 \end{smallmatrix}\right]$, $B = \left[\begin{smallmatrix} 0 \\ 1 \end{smallmatrix}\right]$, which implies that (A, B) is stablizable, Zhang and Tian prove that the MAS can reach mean-square consensus if and only if the union graph is connected, while in this paper, it is verified theoretically that the stabilizability of (A, B) is essential for achieving consensus.

5. Numerical Simulation

Consider an MAS consisted of four agents, with its prior fixed weighted communication topology being $N_1 = \{2\}$, $N_2 = \{1, 3\}$, $N_3 = \{2, 4\}$, $N_4 = \{3\}$, $a_{12} = 2$, $a_{23} = 2$, $a_{34} = 3$; then there are eight graphs in the topology set $\{G_1, \ldots, G_8\}$. Assume that the packet dropout probability between each pair of agents is 0.1.

Each agent is described by a three-order difference equation, with

$$A = \begin{bmatrix} 0.6 & 0 & 0.2 \\ 0.3 & 0.3 & 0.4 \\ 0 & 0 & 1.2 \end{bmatrix}, \qquad B = \begin{bmatrix} 0 \\ 0 \\ 1 \end{bmatrix}. \tag{28}$$

Obviously, each agent is unstable since the eigenvalues of A are 0.6, 0.3, and 1.2, and (A, B) is stablizable. By applying Theorem 8, it can be obtained that

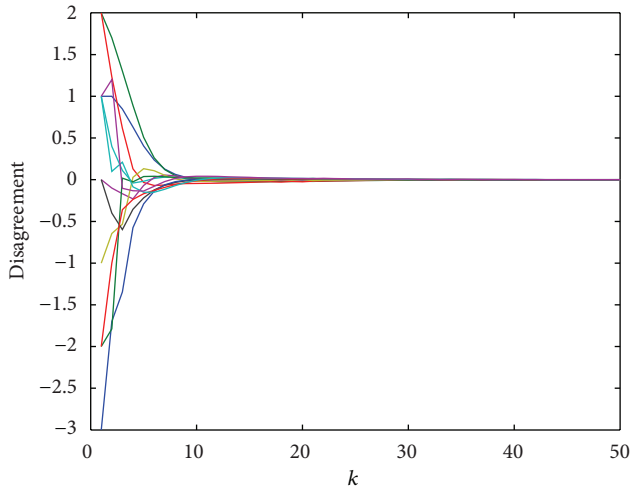

FIGURE 1: The disagreement values between agents under consensus protocol (5).

$K = [0.1111 \ -0.0000 \ 0.1944]$, such that $\rho(A - \widehat{\lambda}_i BK) = 0.8910 < 1$. Suppose the initial conditions are $x_{10} = [2 \ 3 \ 2]^T$, $x_{20} = [2 \ 1 \ -1]^T$, $x_{30} = [1 \ -2 \ -3]^T$, and $x_{40} = [-1 \ 2 \ -2]^T$; the simulation results are shown in Figure 1.

6. Conclusion

We have studied the consensus problem of general linear discrete-time Multiagent systems (MASs) with random packet dropout that happens during information exchange between agents. The packet dropout phenomenon is characterized as being a Bernoulli random process. A distributed consensus protocol with weighted graph is proposed to address the packet dropout phenomenon. By constructing a new disagreement vector, a new framework is established to solve the consensus problem. Then, through introducing a common linear transformation for the switching system, together with the control theory, the perturbation argument, and the matrix theory, the necessary and sufficient condition for MASs to reach mean-square consensus is derived in terms of stability of an array of low-dimensional matrices. Moreover, mean-square consensusable conditions with regard to network topology and agent dynamic structure are also provided.

It is worth pointing out that this paper is only a first step; the consensus problem of linear discrete time MASs, which may be affected by many other factors including time-delay, and noise, is not fully investigated, and this is of our research interest in the future.

Acknowledgments

This work is supported by the National Natural Science Foundation of China under Grants 61074124 and 61374171, the Project-Sponsored by SRF for ROCS, SEM, the Fundamental Research Funds for the Central Universities, HUST, under Grant 2012TS020, and the Graduate Fund of Innovation and Entrepreneurship, Hust, under Grant HF-11-18-2013.

References

[1] S. Kar and J. M. F. Moura, "Distributed consensus algorithms in sensor networks: quantized data and random link failures," *IEEE Transactions on Signal Processing*, vol. 58, no. 3, pp. 1383–1400, 2010.

[2] N. A. Lynch, *Distributed Algorithms*, Morgan Kaufmann, San Francisco, Calif, USA, 1997.

[3] H. G. Tanner, A. Jadbabaie, and G. J. Pappas, "Flocking in fixed and switching networks," *IEEE Transactions on Automatic Control*, vol. 52, no. 5, pp. 863–868, 2007.

[4] R. S. Dong and Z. Y. Geng, "Consensus based formation control laws for systems on Lie groups," *Systems & Control Letters*, vol. 62, no. 2, pp. 104–111, 2013.

[5] R. Olfati-Saber and R. M. Murray, "Consensus problems in networks of agents with switching topology and time-delays," *IEEE Transactions on Automatic Control*, vol. 49, no. 9, pp. 1520–1533, 2004.

[6] Y. Hatano and M. Mesbahi, "Agreement over random networks," *IEEE Transactions on Automatic Control*, vol. 50, no. 11, pp. 1867–1872, 2005.

[7] Y. Zhang and Y.-P. Tian, "Consentability and protocol design of multi-agent systems with stochastic switching topology," *Automatica*, vol. 45, no. 5, pp. 1195–1201, 2009.

[8] F. Sun, J. Chen, Z.-H. Guan, L. Ding, and T. Li, "Leader-following finite-time consensus for multi-agent systems with jointly-reachable leader," *Nonlinear Analysis: Real World Applications*, vol. 13, no. 5, pp. 2271–2284, 2012.

[9] P. Lin, Z. Li, Y. Jia, and M. Sun, "High-order multi-agent consensus with dynamically changing topologies and time-delays," *IET Control Theory & Applications*, vol. 5, no. 8, pp. 976–981, 2011.

[10] Z. K. Li, Z. S. Duan, G. R. Chen, and L. Hang, "Consensus of multi-agent systems and synchronization of complex networks: a unified viewpoint," *IEEE Transactions on Circuits and Systems*, vol. 57, no. 1, pp. 213–224, 2010.

[11] J. Xu, L. H. Xie, T. Li, and K. Y. Lum, "Consensus of multi-agent systems with general linear dynamics via dynamic output feedback control," *IET Control Theory Applications*, vol. 7, no. 1, pp. 108–115, 2013.

[12] X. L. Xu, S. Y. Cheng, W. Huang, and L. X. Gao, "Leader-following consensus of discrete-time multi-agent systems with observer-based protocols," *Neurocomputing*, vol. 118, pp. 334–341, 2013.

[13] Y. F. Su and J. Huang, "Two consensus problems for discrete-time multi-agent systems with switching network topology," *Automatica*, vol. 48, no. 9, pp. 1988–1997, 2012.

[14] P. Lin and Y. Jia, "Multi-agent consensus with diverse time-delays and jointly-connected topologies," *Automatica*, vol. 47, no. 4, pp. 848–856, 2011.

[15] Z. H. Wu and H. J. Fang, "Improvement for consensus performance of multi-agent systems based on delayed-state-derivative feedback," *Journal of Systems Engineering and Electronics*, vol. 23, no. 1, pp. 137–144, 2012.

[16] Z. H. Wu, L. Peng, L. B. Xie, and J. W. Wen, "Stochastic bounded consensus tracking of leader-follower multi-agent systems with measurement noises based on sampled-data with

small sampling delay," *Physica A*, vol. 392, no. 4, pp. 918–928, 2013.

[17] W. Zhu, "Consensus of multiagent systems with switching jointly reachable interconnection and time delays," *IEEE Transactions on Systems, Man, and Cybernetics A*, vol. 42, no. 2, pp. 348–358, 2012.

[18] Y. G. Sun and L. Wang, "H_∞ consensus of second-order multiagent systems with asymmetric delays," *Systems & Control Letters*, vol. 61, no. 8, pp. 857–862, 2012.

[19] W. Ren and R. W. Beard, "Consensus seeking in multiagent systems under dynamically changing interaction topologies," *IEEE Transactions on Automatic Control*, vol. 50, no. 5, pp. 655–661, 2005.

[20] F. L. Sun, Z.-H. Guan, X.-S. Zhan, and F.-S. Yuan, "Consensus of second-order and high-order discrete-time multi-agent systems with random networks," *Nonlinear Analysis: Real World Applications*, vol. 13, no. 5, pp. 1979–1990, 2012.

[21] Y. Zhang and Y.-P. Tian, "Consensus of data-sampled multiagent systems with random communication delay and packet loss," *IEEE Transactions on Automatic Control*, vol. 55, no. 4, pp. 939–943, 2010.

[22] Y. Zhang and Y.-P. Tian, "Maximum allowable loss probability for consensus of multi-agent systems over random weighted lossy networks," *IEEE Transactions on Automatic Control*, vol. 57, no. 8, pp. 2127–2132, 2012.

[23] C. Z. Zhang, G. Feng, H. J. Gao, and Y. Zhao, "State feedback controller design of networked control systems with multiple packet dropouts," in *Proceedings of the 29th Chinese Control Conference (CCC '10)*, pp. 5839–5844, July 2010.

[24] F. Z. Zhang, *Matrix Theory*, Springer, New York, NY, USA, 1999.

Hindawi Publishing Corporation
Abstract and Applied Analysis
Volume 2013, Article ID 612342, 8 pages
http://dx.doi.org/10.1155/2013/612342

Research Article

Third-Order Leader-Following Consensus in a Nonlinear Multiagent Network via Impulsive Control

Xiaomei Li,[1] Zhongjun Ma,[1] Chunhai Li,[1] and Jinde Cao[2]

[1] *School of Mathematics and Computing Science, Guilin University of Electronic Technology, Guilin 541004, China*
[2] *Department of Mathematics, Southeast University, Nanjing 210096, China*

Correspondence should be addressed to Zhongjun Ma; mzj1234402@163.com

Received 15 June 2013; Accepted 24 August 2013

Academic Editor: Qiankun Song

Many facts indicate that the impulsive control method is a finer method, which is simple, efficient, and low in cost, for achieving consensus. In this paper, based on graph theory, Lyapunov stability theory, and matrix theory, a novel impulsive control protocol is given to realize the consensus of the multiagent network. Numerical simulations are performed to verify the theoretical results.

1. Introduction

In the past few years, consensus of multiagent networks has been intensively studied in many fields, such as biological, social, mathematical, and physical sciences ones [1–5]. Generally speaking, consensus refers to designing a system algorithm or protocol such that all agents asymptotically reach an agreement on their states. In particular, leader-following consensus means that there exists a virtual leader which specifies an objective for all agents to follow. Recently, some first-order and second-order leader-following consensus problems were discussed by lots of researchers [6–10], and then some novel system algorithms were given via some different control methods, such as pinning control, delay coupling control, adaptive control, and impulsive control [9–14]. In addition, Qin et al. considered consensus in the second-order multiagent system with communication delay in [15, 16]. Particularly, some multiagent networks cannot be controlled continuously. At this time, the impulsive control becomes a more desirable alternative. The impulsive control is low in cost and then has been widely applied in many fields, such as information science, system control, life science, communication security, and space techniques [17–19]. In the above senses, the impulsive control is very effective for achieving consensus of a multiagent network.

In some real networks, the connections between part nodes are sometimes a failure, and then the network topology may dynamically change over time. Therefore, it is indispensable to consider the case that the network topology is switching. As much as we know, most of the relevant studies focus on second-order consensus for multiagent networks [11, 12]. When the agent states are influenced by speeds, positions, and accelerations, it is necessary and significative to research the third-order consensus problem of a multiagent network with switching topology. At present, just few works considered the third-order consensus problem. In [20], adaptive third-order leader-following consensus of a nonlinear multiagent network with perturbations was addressed, without using the impulsive control method. In [11], impulsive consensus problem of second-order multiagent network with switching topologies was investigated, without considering its own dynamics. In this paper, we consider the third-order consensus problem in a multiagent network with the aforementioned four characters, that is, leader-following, own dynamics, switching topology, and impulsive control. By using the graph theory, Lyapunov stability theory, and matrix theory, some sufficient conditions are obtained to realize the third-order leader-following consensus.

The rest of this paper is designed as follows. Some necessary preliminaries are stated in Section 2. The consensus of a multiagent network is discussed in Section 3. Numerical examples are given to verify the theoretical results in Section 4. Finally, in Section 5, conclusions are presented.

2. Preliminaries

2.1. Multiagent Network. Information exchange among agents can be modeled by an interaction graph. Let $G = \{V, E, A\}$ be a weighted diagraph with a node set $V = \{1, \ldots, N\}$, an edge set $E \subseteq V \times V$, and a weight adjacency matrix $A = (a_{ij})_{N\times N}$. A directed edge denoted by (i, j) means that j has access to node i; that is, node j can receive information from node i. The elements of matrix A are defined such that $a_{ij} > 0$ for $(j, i) \in E$, while $a_{ij} = 0$ for $(j, i) \notin E$. Let $a_{ii} = 0$ for $i \in V$. The set $\aleph_i = \{j \in V \mid (j, i) \in E\}$ is used as the neighbor set of node i. When the communication topology is switching, the neighbor set is time-varying, and then $\aleph_i(t) = \{j \in V : a_{ij}(t) > 0\}$. Let

$$a_{ij}(t) = \begin{cases} 1, & j \in \aleph_i(t), \\ 0, & \text{otherwise.} \end{cases} \tag{1}$$

The out-degree of node i is defined by $\deg(i) = \sum_{j=1}^{N} a_{ij} = \sum_{j\in\aleph_i} a_{ij} = d_i$. If the degree matrix of digraph G is $D = \text{diag}(d_1, \ldots, d_N)$, then the Laplacian matrix of digraph G is $L = D - A$.

A directed path from node i to node j in the directed graph G is a sequence of edges $(i, j_1), (j_1, j_2), \ldots, (j_l, j)$ with distinct nodes j_k, $k = 1, \ldots, l$. A digraph G has a directed spanning tree if there exists at least one node called root which has a directed path to all the other nodes.

For a leader-follower multiagent network, suppose that the leader (labeled by 0) is denoted by node 0, and the followers are denoted by the nodes $1, 2, \ldots, N$. The graph $\overline{G}$ is consisting of the leader and the followers with communication topology. The connection weight between the ith follower and the leader is represented by $b_i, i \in V$. If the ith follower is connected to the leader, then $b_i > 0$; otherwise, $b_i = 0$. Let $B = \text{diag}\{b_1, b_2, \ldots, b_N\}$.

Following, we address the multiagent network with switching topology. The set $\Omega = \{\overline{G}_1, \overline{G}_2, \ldots, \overline{G}_m\}$ is used as a set of the graphs with all possible topology, which includes all possible graphs (involving N agents and a leader). We define a switching signal $\tau : [0, +\infty) \to \mathrm{P} = \{1, 2, \ldots, m\}$, which determines the topology structure that corresponds to the network. When the topology is switching, the Laplacian matrix L and the matrix B are also switching, which are denoted by $L_{\tau(t)}$ and $B_{\tau(t)}$.

The following assumptions are needed to derive our main results.

Assumption 1 (see [21]). Assume that there exists a constant $\gamma > 0$, such that the vector-valued function f satisfies the condition

$$\begin{aligned} &(u - w)^T \left(f(t, x, v, u) - f(t, y, z, w)\right) \\ &\quad \le \gamma \Big((x - y)^T (x - y) + (v - z)^T (v - z) \\ &\qquad + (u - w)^T (u - w) \Big) \end{aligned} \tag{2}$$

for any $x, y, z, u, v, w \in R^n$.

2.2. Impulsive Control System. Impulsive control systems can be classified into three types based on the characteristics of plants and control laws [22].

A type-I impulsive control system [22] is given by

$$\begin{aligned} \dot{X} &= \mathbf{F}(t, X), \quad t \neq \tau_k(X), \\ \Delta X &= \mathbf{U}(k, Y), \quad t = \tau_k(X), \\ Y &= \mathbf{G}(t, X), \end{aligned} \tag{3}$$

where X and Y are the state variable and the output, respectively. $\mathbf{U}(k, Y)$ is the impulsive control law. In this kind of system, the control input is implemented by the "sudden jumps" of some state variables.

Definition 2 (see [22]). For $t \neq \tau_k(X)$, we define the time derivative of the function $V(t, X)$ with respect to system (3) as

$$\dot{V}(t, X) \triangleq \frac{\partial V(t, X)}{\partial t} + \frac{\partial V(t, X)}{\partial X} \mathbf{F}(t, X). \tag{4}$$

Type-II and type-III impulsive control systems and more theoretical results are present in [22].

In this paper, a type-I impulsive control system is considered.

3. Main Results

Consider that a nonlinear multiagent network consists of N agents with third-order dynamics:

$$\begin{aligned} \dot{x}_i(t) &= v_i(t), \qquad \dot{v}_i(t) = u_i(t), \\ \dot{u}_i(t) &= f\left(t, x_i(t), v_i(t), u_i(t)\right), \\ &\qquad i = 1, 2, \ldots, N, \end{aligned} \tag{5}$$

where $x_i = (x_{i1}, \ldots, x_{in}^T) \in R^n$, $v_i = (v_{i1}, \ldots, v_{in})^T \in R^n$, and $u_i = (u_{i1}, \ldots, u_{in})^T \in R^n$ are the position, velocity, and acceleration states of the ith agent, respectively, and $f = (f_1, \ldots, f_n)^T \in R^n$ is a nonlinear vector-valued continuous function used to describe the self-dynamics of the ith agent.

The virtual leader of the multiagent network (5) is an isolated agent described by

$$\begin{aligned} \dot{x}_0(t) &= v_0(t), \qquad \dot{v}_0(t) = u_0(t), \\ \dot{u}_0(t) &= f\left(t, x_0(t), v_0(t), u_0(t)\right), \end{aligned} \tag{6}$$

where $x_0 \in R^n$, $v_0 \in R^n$, and $u_0 \in R^n$ are the position, velocity, and acceleration of the virtual leader, respectively.

For $t \in (t_{k-1}, t_k)$, the state variables $x_i(t)$, $v_i(t)$, $u(t)$ of the system (5) do dynamically change with ordinary differential equations. And at the moment t_k, if the $x_i(t)$, $v_i(t)$, $u(t)$ supervise the impulsive control, then it can result in the jump. Based on the above senses and the impulsive controller of [11]

and applying impulsive control to (5), we have the following consensus scheme for the multiagent system:

$$\begin{aligned}
\dot{x}_i(t) &= v_i(t), \quad (t \neq t_k),\\
\dot{v}_i(t) &= u_i(t), \quad (t \neq t_k),\\
\dot{u}_i(t) &= f(t, x_i(t), v_i(t), u_i(t)), \quad (t \neq t_k),\\
\Delta x_i(t_k) &\triangleq x_i(t_k^+) - x_i(t_k^-)\\
&= C_k\Bigg(\sum_{j\in\mathcal{N}_i(t_k)} a_{ij}(t_k)\left(x_i(t_k) - x_j(t_k)\right)\\
&\qquad + b_i(t_k)\left(x_i(t_k) - x_0(t_k)\right)\Bigg),\\
\Delta v_i(t_k) &\triangleq v_i(t_k^+) - v_i(t_k^-)\\
&= C_k\Bigg(\sum_{j\in\mathcal{N}_i(t_k)} a_{ij}(t_k)\left(v_i(t_k) - v_j(t_k)\right)\\
&\qquad + b_i(t_k)\left(v_i(t_k) - v_0(t_k)\right)\Bigg),\\
\Delta u_i(t_k) &\triangleq u_i(t_k^+) - u_i(t_k^-)\\
&= C_k\Bigg(\sum_{j\in\mathcal{N}_i(t_k)} a_{ij}(t_k)\left(u_i(t_k) - u_j(t_k)\right)\\
&\qquad + b_i(t_k)\left(u_i(t_k) - u_0(t_k)\right)\Bigg),\\
x_i(t_0^+) &= x_i(t_0), \quad (t_0 \geq 0), \qquad x_i(t_k^-) = x_i(t_k),\\
v_i(t_0^+) &= v_i(t_0), \quad (t_0 \geq 0), \qquad v_i(t_k^-) = v_i(t_k),\\
u_i(t_0^+) &= u_i(t_0), \quad (t_0 \geq 0), \qquad u_i(t_k^-) = u_i(t_k),
\end{aligned} \tag{7}$$

where $\Delta x_i(t_k)$, $\Delta v_i(t_k)$, $\Delta u_i(t_k)$ are the jump of the position, velocity, and acceleration of the ith follower agent at the moment t_k, respectively, $x_i(t_k^+) = \lim_{h\to 0^+} x_i(t_k + h)$, $x_i(t_k^-) = \lim_{h\to 0^-} x_i(t_k + h)$, $v_i(t_k^+) = \lim_{h\to 0^+} v_i(t_k + h)$, $v_i(t_k^-) = \lim_{h\to 0^-} v_i(t_k + h)$, $u_i(t_k^+) = \lim_{h\to 0^+} u_i(t_k + h)$, $u_i(t_k^-) = \lim_{h\to 0^-} u_i(t_k + h)$, $C_k \in R^{n\times n}$ is the impulsive controller gain at the moment t_k, the moments of impulsive satisfy $0 \leq t_0 < t_1 < t_2 < \cdots < t_k < t_{k+1} < \cdots$, and $\lim_{k\to+\infty} t_k = +\infty$, $\Delta t_k = t_k - t_{k-1} \leq \rho < +\infty$ is the impulsive interval, where $k = 1, 2, \ldots$.

Let $x_i(t) - x_0(t) = \hat{x}_i(t)$, $v_i(t) - x_0(t) = \hat{v}_i(t)$, $u_i(t) - u_0(t) = \hat{u}_i(t)$, $\hat{x}(t) = (\hat{x}_1^T(t), \hat{x}_2^T(t), \ldots, \hat{x}_N^T(t))^T$, $\hat{v}(t) = (\hat{v}_1^T(t), \hat{v}_2^T(t), \ldots, \hat{v}_N^T(t))^T$, $\hat{u}(t) = (\hat{u}_1^T(t), \hat{u}_2^T(t), \ldots, \hat{u}_N^T(t))^T$, $e(t) = (\hat{x}^T(t), \hat{v}^T(t), \hat{u}^T(t))^T$; then the error system with (6) and (7) can be written as

$$\begin{aligned}
\dot{e}(t) &= He(t) + W, \quad (t \neq t_k),\\
\Delta e(t_k) &= \overline{C}_k e(t_k),\\
e(t_0^+) &= e(t_0),
\end{aligned} \tag{8}$$

where

$$\begin{aligned}
H &= \begin{pmatrix} O_{nN\times nN} & I_{nN\times nN} & O_{nN\times nN}\\ O_{nN\times nN} & O_{nN\times nN} & I_{nN\times nN}\\ O_{nN\times nN} & O_{nN\times nN} & O_{nN\times nN}\end{pmatrix},\\
W &= \begin{pmatrix} O_{nN\times 1}\\ O_{nN\times 1}\\ F(t, x(t), v(t), u(t)) - 1_N\\ \otimes f(t, x_0(t), v_0(t), u_0(t))\end{pmatrix},\\
&F(t, x(t), v(t), u(t))\\
&= \left(f^T(t, x_1(t), v_1(t), u_1(t)), \ldots,\right.\\
&\qquad \left. f^T(t, x_N(t), v_N(t), u_N(t))\right)^T,\\
&1_N = (1, \ldots, 1)^T \in R^N,\\
\overline{C}_k &= \operatorname{diag}\left((L_{\tau(k)} + B_{\tau(k)}) \otimes C_k, (L_{\tau(k)} + B_{\tau(k)}) \otimes C_k,\right.\\
&\qquad \left.(L_{\tau(k)} + B_{\tau(k)}) \otimes C_k\right),
\end{aligned} \tag{9}$$

$L_{\tau(k)}$ and $B_{\tau(k)}$ are associated with the switching interconnection graph at time t_k, $\tau(k) \in \mathrm{P}$.

Definition 3. Denote $e_{xi}(t) = \|x_i(t) - x_0(t)\|$, $e_{vi}(t) = \|v_i(t) - v_0(t)\|$ and $e_{ui}(t) = \|u_i(t) - u_0(t)\|$. The multiagent network (7) with the virtual leader (6) is said to achieve third-order leader-following consensus if the solution of (8) satisfies $\lim_{t\to+\infty} e_{xi}(t) = 0$, $\lim_{t\to+\infty} e_{vi}(t) = 0$, and $\lim_{t\to+\infty} e_{ui}(t) = 0$, $i = 1, 2, \ldots, N$ for any initial condition.

Basing on graph theory, Lyapunov function method, matrix theory, and the proof of Theorem 1 in [11], we have the following theorem.

Theorem 4. *Under Assumption 1, if there exists* $0 < \varphi < 1$ *such that*

$$\delta_k e^{\mu(\Delta t_k)} < \varphi, \tag{10}$$

where δ_k *and* μ *are the maximum eigenvalues of matrices*

$$\left(I_{3nN\times 3nN} + \overline{C}_k\right)^T \left(I_{3nN\times 3nN} + \overline{C}_k\right), \tag{11}$$

$$\begin{pmatrix} 2\gamma I_{nN\times nN} & I_{nN\times nN} & O_{nN\times nN}\\ I_{nN\times nN} & 2\gamma I_{nN\times nN} & I_{nN\times nN}\\ O_{nN\times nN} & I_{nN\times nN} & 2\gamma I_{nN\times nN}\end{pmatrix}, \tag{12}$$

respectively, then the third-order leader-following consensus in the multiagent network (7) *is achieved.*

Proof. Consider the following Lyapunov function:

$$V(e(t)) = e^T(t)\,e(t). \tag{13}$$

For any $t \in (t_{k-1}, t_k]$, the time derivative of $V(e(t))$ along the trajectory of (8) is

$$\begin{aligned}
\mathbf{D}V(e(t)) &= (\dot{e}(t))^T e(t) + e^T(t)\,\dot{e}(t)\\
&= e^T(t)\left(H + H^T\right)e(t) + 2W^T e(t)\\
&= e^T(t)\left(H + H^T\right)e(t)\\
&\quad + 2\widehat{u}^T(t)\left(F(t, x(t), v(t), u(t)) - 1_N \otimes f(t, x_0(t), v_0(t), u_0(t))\right)\\
&= e^T(t)\left(H + H^T\right)e(t)\\
&\quad + 2\sum_{i=1}^{N}\widehat{u}_i^T(t)\left(f(t, x_i(t), v_i(t), u_i(t)) - f(t, x_0(t), v_0(t), u_0(t))\right)\\
&\le e^T(t)\left(H + H^T\right)e(t)\\
&\quad + 2\gamma\sum_{i=1}^{N}\left(\widehat{x}_i^T(t)\,\widehat{x}_i(t) + \widehat{v}_i^T(t)\,\widehat{v}_i(t) + \widehat{u}_i^T(t)\,\widehat{u}_i(t)\right)\\
&= e^T(t)\left(H + H^T\right)e(t)\\
&\quad + e^T(t)\begin{pmatrix} 2\gamma I_{nN\times nN} & 0_{nN\times nN} & 0_{nN\times nN}\\ 0_{nN\times nN} & 2\gamma I_{nN\times nN} & 0_{nN\times nN}\\ 0_{nN\times nN} & 0_{nN\times nN} & 2\gamma I_{nN\times nN}\end{pmatrix}e(t)\\
&= e^T(t)\begin{pmatrix} 2\gamma I_{nN\times nN} & I_{nN\times nN} & 0_{nN\times nN}\\ I_{nN\times nN} & 2\gamma I_{nN\times nN} & I_{nN\times nN}\\ 0_{nN\times nN} & I_{nN\times nN} & 2\gamma I_{nN\times nN}\end{pmatrix}e(t)\\
&\le \mu V(e(t)).
\end{aligned} \tag{14}$$

Moreover, for any $t \in (t_{k-1}, t_k]$,

$$0 \le V(e(t)) \le V\left(t_{k-1}^+\right)e^{\mu(t-t_{k-1})}. \tag{15}$$

For $t = t_k^+$, similar to the proof of Theorem 1 in [11], we have

$$\begin{aligned}
V\left(e\left(t_k^+\right)\right) &= e^T\left(t_k^+\right)e\left(t_k^+\right)\\
&= \left(e(t_k) + \Delta e(t_k)\right)^T\left(e(t_k) + \Delta e(t_k)\right)\\
&= e^T(t_k)\left(I_{3nN\times 3nN} + \overline{C}_k\right)^T\left(I_{3nN\times 3nN} + \overline{C}_k\right)e(t_k);
\end{aligned} \tag{16}$$

that is,

$$V\left(e\left(t_k^+\right)\right) \le \delta_k V\left(e(t_k)\right). \tag{17}$$

Consequently, according to (10) and (15), we obtain

$$V\left(e\left(t_k^+\right)\right) \le \delta_k V\left(t_{k-1}^+\right)e^{\mu(t_k - t_{k-1})} \le \varphi V\left(t_{k-1}^+\right). \tag{18}$$

By recurrence, we have

$$V\left(e\left(t_k^+\right)\right) \le \varphi^k V(t_0). \tag{19}$$

Then,

$$\lim_{k\to+\infty} V\left(e\left(t_k^+\right)\right) = 0. \tag{20}$$

Using $\Delta t_k = t_k - t_{k-1} \le \rho < +\infty$ and (15),

$$\lim_{t\to+\infty} V(e(t)) = 0; \tag{21}$$

that is,

$$\lim_{t\to+\infty} e(t) = 0. \tag{22}$$

Therefore, third-order leader-following consensus in the multiagent network (5) is achieved under the impulsive controllers (7). □

Remark 5. According to the proof of Theorem 4, it is not necessary that all the graphs $G_1, G_2, \ldots, G_m$ have directed spanning tree.

On the basis of Gersgorin disk theorem [23], we get $\mu \le 2(\gamma+1)$. For $(I_{3nN\times 3nN} + \overline{C}_k)^T(I_{3nN\times 3nN} + \overline{C}_k) = I_{3\times 3}\otimes[(I_{nN\times nN} + (L_{\tau(k)} + B_{\tau(k)})\otimes C_k)^T(I_{nN\times nN} + (L_{\tau(k)} + B_{\tau(k)})\otimes C_k)]$, accordingly, δ_k is equal to the maximum eigenvalue of $(I_{nN\times nN} + (L_{\tau(k)} + B_{\tau(k)})\otimes C_k)^T(I_{nN\times nN} + (L_{\tau(k)} + B_{\tau(k)})\otimes C_k)$. Therefore, we have the following Corollary 6 (recalling $\Delta t_k = t_k - t_{k-1} \le \rho$ and $\mathrm{P} = \{1, 2, \ldots, m\}$).

Corollary 6. *Under Assumption 1, if there exists* $0 < \varphi < 1$ *such that*

$$\delta e^{2(\gamma+1)\rho} < \varphi, \tag{23}$$

where $\delta = \sup\{\delta_k\}$, δ_k *is the maximum eigenvalue of the matrix* $(I_{nN\times nN} + (L_{\tau(k)} + B_{\tau(k)}) \otimes C_k)^T(I_{nN\times nN} + (L_{\tau(k)} + B_{\tau(k)}) \otimes C_k)$*; then, the third-order leader-following consensus in the multiagent network* (7) *is achieved.*

4. Numerical Simulations

In this section, we give some numerical examples to verify the theory results given in the previous section.

Consider the following nonlinear function f for multiagent network:

$$f(x_i(t), v_i(t), a_i(t)) = \begin{pmatrix} 2a_{i2} + \left(|a_{i1} + 1| - |a_{i1} - 1|\right)\\ a_{i1} - a_{i2} + a_{i3}\\ -2\cos x_{i1} + 2\cos v_{i1} - a_{i2} - a_{i3}\end{pmatrix}. \tag{24}$$

It is easy to verify that the nonlinear function f in (24) satisfies Assumption 1. (Let $\gamma = 5$).

Following, we consider that the topology of the multiagent network is switching ($\mathrm{P} = \{1, 2\}$).

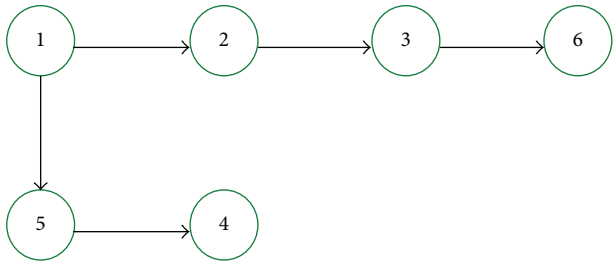

Figure 1: Spanning tree of graph G_1.

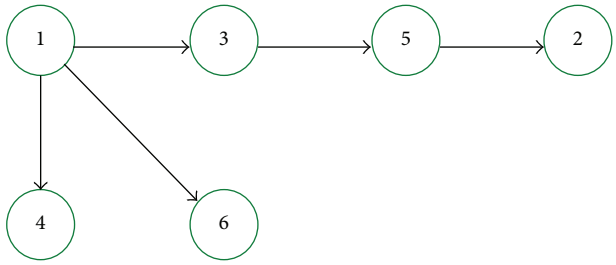

Figure 2: Spanning tree of graph G_2.

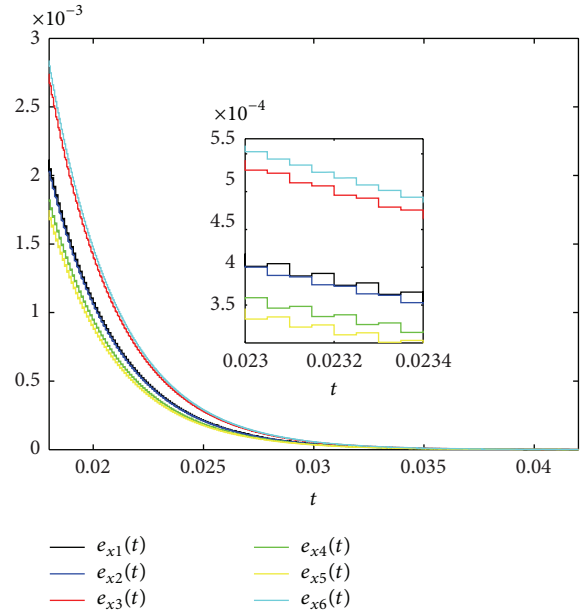

Figure 3: Position errors $e_{xi}(t)$ of system (7) with a directed spanning tree.

Example 7. Assume that the graphs G_1, G_2 have directed spanning trees. The directed spanning trees of G_1, G_2 are described in Figures 1 and 2. The corresponding matrices of the graphs G_1, $\overline{G}_1$, G_2, $\overline{G}_2$ are A_1, B_1, A_2, B_2, respectively, where

$$A_1 = \begin{pmatrix} 0 & 0 & 1 & 1 & 0 & 0 \\ 1 & 0 & 1 & 0 & 0 & 0 \\ 0 & 1 & 0 & 0 & 0 & 1 \\ 1 & 0 & 0 & 0 & 1 & 0 \\ 1 & 0 & 0 & 0 & 0 & 0 \\ 0 & 0 & 1 & 0 & 1 & 0 \end{pmatrix},$$

$$A_2 = \begin{pmatrix} 0 & 0 & 0 & 1 & 0 & 1 \\ 1 & 0 & 0 & 0 & 1 & 0 \\ 1 & 1 & 0 & 0 & 0 & 0 \\ 1 & 0 & 0 & 0 & 1 & 0 \\ 0 & 1 & 1 & 0 & 0 & 0 \\ 1 & 0 & 1 & 0 & 0 & 0 \end{pmatrix},$$

$$B_1 = \operatorname{diag}(0,1,0,1,0,0), \qquad B_2 = \operatorname{diag}(1,0,0,0,1,0). \tag{25}$$

In time intervals $[t_{4k-1}, t_{4k})$, the corresponding matrices are $A_2, B_2, k = 1, 2, \ldots$. In other time intervals, the corresponding matrices are A_1, B_1. We choose the impulsive gains C_{k1}, C_{k2} with topology $\overline{G}_1$ and $\overline{G}_2$, respectively, as follows:

$$C_{k1} = \begin{pmatrix} -0.04 & 0 & 0 \\ 0 & -0.04 & 0 \\ 0 & 0 & -0.04 \end{pmatrix},$$

$$C_{k2} = \begin{pmatrix} -0.05 & 0 & 0 \\ 0 & -0.05 & 0 \\ 0 & 0 & -0.05 \end{pmatrix}. \tag{26}$$

Let the equidistant impulsive interval $\Delta t_k = t_k - t_{k-1} = 0.00005$. Then, $\rho = 0.00005$. There exists $\varphi = 0.9995$, which satisfies the inequality (23) of Corollary 6. From Figures 3, 4, and 5, we can see that the position errors $e_{xi}(t)$, the velocity errors $e_{vi}(t)$, and the acceleration errors $e_{ai}(t)$ converge to zero quickly.

Example 8. Assume that the graphs G_1, G_2 do not contain directed spanning trees. Let the corresponding matrices of the graphs G_3, $\overline{G}_3$, G_4, $\overline{G}_4$ be A_3, B_3, A_4, B_4, respectively, where

$$A_3 = \begin{pmatrix} 0 & 1 & 0 & 0 & 0 & 0 \\ 0 & 0 & 0 & 0 & 0 & 0 \\ 0 & 0 & 0 & 0 & 0 & 0 \\ 1 & 0 & 1 & 0 & 0 & 0 \\ 0 & 1 & 1 & 0 & 0 & 0 \\ 0 & 0 & 0 & 1 & 1 & 0 \end{pmatrix},$$

$$A_4 = \begin{pmatrix} 0 & 0 & 1 & 0 & 0 & 0 \\ 1 & 0 & 0 & 1 & 0 & 0 \\ 0 & 1 & 0 & 1 & 0 & 0 \\ 0 & 0 & 0 & 0 & 0 & 0 \\ 0 & 0 & 0 & 0 & 0 & 0 \\ 1 & 0 & 0 & 0 & 1 & 0 \end{pmatrix},$$

$$B_3 = \operatorname{diag}(0,1,1,0,0,0), \qquad B_4 = \operatorname{diag}(0,0,0,1,1,0). \tag{27}$$

Similar to Example 7, in time intervals $[t_{4k-1}, t_{4k})$, the corresponding matrices are $A_4, B_4, k = 1, 2, \ldots$, while in other time intervals, the corresponding matrices are A_3, B_3.

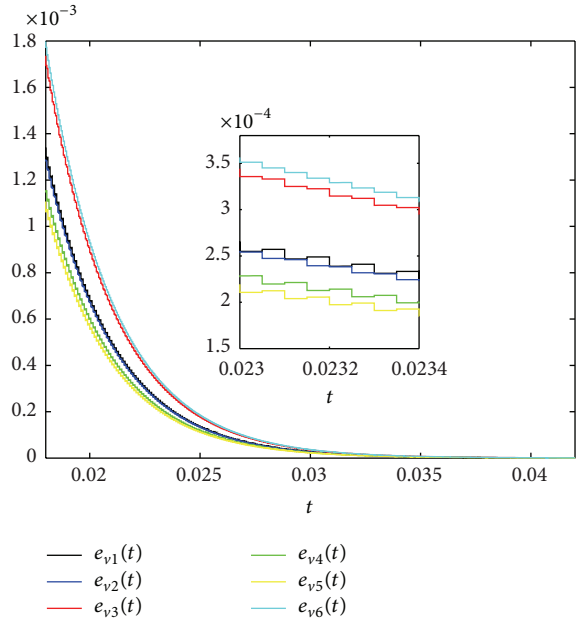

Figure 4: Velocity errors $e_{vi}(t)$ of system (7) with a directed spanning tree.

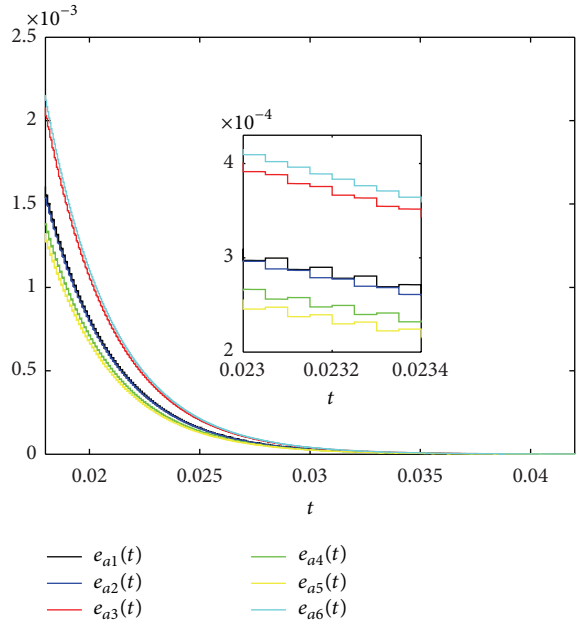

Figure 5: Acceleration errors $e_{ai}(t)$ of system (7) with a directed spanning tree.

We choose the impulsive gain C_{k3}, C_{k4} with topology $\overline{G}_3$ and $\overline{G}_4$, respectively, as follows:

$$C_{k3} = \begin{pmatrix} -0.07 & 0 & 0 \\ 0 & -0.07 & 0 \\ 0 & 0 & -0.07 \end{pmatrix},$$
$$C_{k4} = \begin{pmatrix} -0.08 & 0 & 0 \\ 0 & -0.08 & 0 \\ 0 & 0 & -0.08 \end{pmatrix}. \quad (28)$$

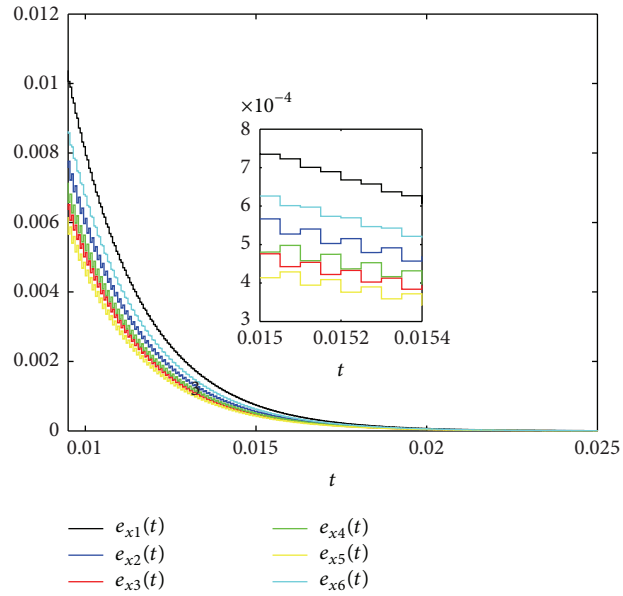

Figure 6: Position errors $e_{xi}(t)$ of system (7) without a directed spanning tree.

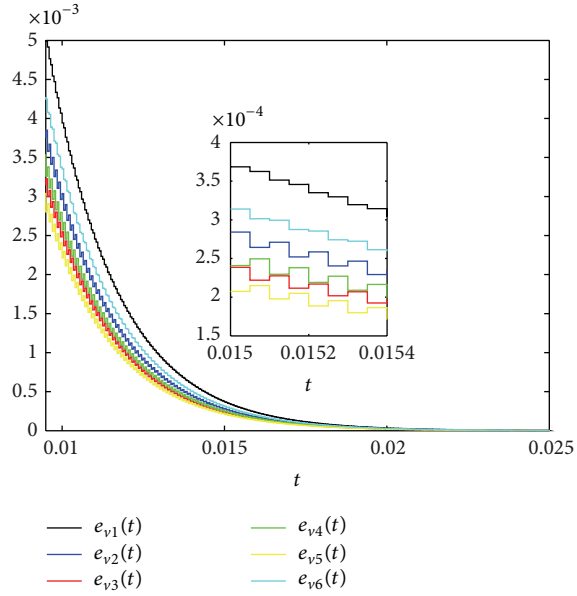

Figure 7: Velocity errors $e_{vi}(t)$ of system (7) without a directed spanning tree.

Let the equidistant impulsive interval $\Delta t_k = t_k - t_{k-1} = 0.00005$. Then, $\rho = 0.00005$. By some calculations, we can know that there exists $\varphi = 0.9995$, which satisfies the inequality (23) of Corollary 6. From Figures 6, 7, and 8, we can see that the position errors $e_{xi}(t)$, the velocity errors $e_{vi}(t)$, and the acceleration errors $e_{ai}(t)$ converge to zero quickly. It shows that the condition on a directed spanning tree is not necessary to realize consensus of the multiagent network (7) under the impulsive control. In addition, the researchers considered the second-order multiagent system

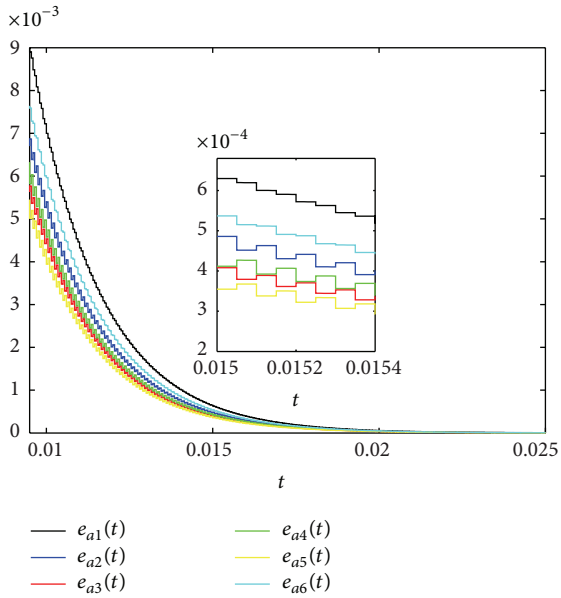

FIGURE 8: Acceleration errors $e_{ai}(t)$ of system (7) without a directed spanning tree.

with communication delay in [21, 22]. In our future work, we will study the third-order consensus problem for the multiagent systems with communication delay.

5. Conclusion

By using graph theory, Lyapunov stability theory, and matrix theory, third-order leader-following consensus problem of a nonlinear multiagent network is studied in this paper. By designing proper impulsive controllers, a new criterion on realizing consensus in the multiagent network with switching topology is achieved. Finally, numerical simulations are provided to illustrate the theoretical results. In our future work, we will study the third-order consensus problem for the multiagent systems with communication delay.

Acknowledgments

This work was supported by the National Natural Science Foundation of China (nos. 60964006, 61004101, and 11162004) and the Science Foundation of Guangxi Province, China (no. 2013GXNSFAA019006).

References

[1] T. Vicsek, A. Czirok, E. B. Jacob, I. Cohen, and O. Schocher, "Novel type of phase transition in a system of self-driven particles," *Physical Review Letters*, vol. 75, pp. 1226–1229, 1995.

[2] A. Jadbabaie, J. Lin, and A. S. Morse, "Coordination of groups of mobile autonomous agents using nearest neighbor rules," *IEEE Transactions on Automatic Control*, vol. 48, no. 6, pp. 988–1001, 2003.

[3] J. Q. Lu, D. Ho, and J. Kurths, "Consensus over directed static networks with arbitrary finite communication delays," *Physical Review E*, vol. 80, no. 6, Article ID 066121, 7 pages, 2009.

[4] J. H. Qin, W. X. Zheng, and H. J. Gao, "Consensus of multiple second-order vehicles with a time-varying reference signal under directed topology," *Automatica*, vol. 47, no. 9, pp. 1983–1991, 2011.

[5] R. Olfati-Saber and R. M. Murray, "Consensus problems in networks of agents with switching topology and time-delays," *IEEE Transactions on Automatic Control*, vol. 49, no. 9, pp. 1520–1533, 2004.

[6] K. Peng and Y. P. Yang, "Leader-following consensus problem with a varying-velocity leader and time-varying delays," *Physica A*, vol. 388, pp. 193–208, 2009.

[7] C. Q. Ma, T. Li, and J. F. Zhang, "Consensus control for leader-following multi-agent systems with measurement noises," *Journal of Systems Science & Complexity*, vol. 23, no. 1, pp. 35–49, 2010.

[8] W. W. Yu, G. R. Chen, and M. Cao, "Distributed leader-follower flocking control for multi-agent dynamical systems with time-varying velocities," *Systems & Control Letters*, vol. 59, no. 9, pp. 543–552, 2010.

[9] Q. Song, J. D. Cao, and W. W. Yu, "Second-order leader-following consensus of nonlinear multi-agent systems via pinning control," *Systems & Control Letters*, vol. 59, no. 9, pp. 553–562, 2010.

[10] J. P. Hu and Y. G. Hong, "Leader-following coordination of multi-agent systems with coupling time delays," *Physica A*, vol. 374, no. 2, pp. 853–863, 2007.

[11] Q. Zhang, S. H. Chen, and C. C. Yu, "Impulsive consensus problem of second-order multi-agent systems with switching topologies," *Communications in Nonlinear Science and Numerical Simulation*, vol. 17, no. 1, pp. 9–16, 2012.

[12] H. B. Jiang, Q. S. Bi, and S. Zheng, "Impulsive consensus in directed networks of identical nonlinear oscillators with switching topologies," *Communications in Nonlinear Science and Numerical Simulation*, vol. 17, no. 1, pp. 378–387, 2012.

[13] H. B. Jiang, J. J. Yu, and C. G. Zhou, "Consensus of multi-agent linear dynamic systems via impulsive control protocols," *International Journal of Systems Science*, vol. 42, no. 6, pp. 967–976, 2011.

[14] X. Han and J.-A. Lu, "Impulsive control induced effects on dynamics of single and coupled ODE systems," *Nonlinear Dynamics*, vol. 59, no. 1-2, pp. 101–111, 2010.

[15] J. H. Qin and H. J. Gao, "A sufficient condition for convergence of sampled-data consensus for double-integrator dynamics with nonuniform and time-varying communication delays," *IEEE Transactions on Automatic Control*, vol. 57, no. 9, pp. 2417–2422, 2012.

[16] J. Qin, H. Gao, and W. X. Zheng, "Second-order consensus for multi-agent systems with switching topology and communication delay," *Systems & Control Letters*, vol. 60, no. 6, pp. 390–397, 2011.

[17] Z. C. Yang and D. Y. Xu, "Stability analysis and design of impulsive control systems with time delay," *IEEE Transactions on Automatic Control*, vol. 52, no. 8, pp. 1448–1454, 2007.

[18] H. B. Jiang, J. J. Yu, and C. G. Zhou, "Robust fuzzy control of nonlinear fuzzy impulsive systems with time-varying delay," *IET Control Theory & Applications*, vol. 2, no. 8, pp. 654–661, 2008.

[19] Y. G. Sun, L. Wang, and G. M. Xie, "Average consensus in networks of dynamic agents with switching topologies and multiple time-varying delays," *Systems & Control Letters*, vol. 57, no. 2, pp. 175–183, 2008.

[20] M. Sun, Y. Chen, L. Cao, and X. F. Wang, "Adaptive third-order leader following consensus of nonlinear multi-agent systems with perturbations," *Chinese Physics Letters*, vol. 29, no. 2, Article ID 020503, 2012.

[21] C. Hu, J. Yu, H. J. Jiang, and Z. D. Teng, "Synchronization of complex community networks with nonidentical nodes and adaptive coupling strength," *Physics Letters A*, vol. 375, no. 5, pp. 873–879, 2011.

[22] T. Yang, *Impulsive Control Theory*, Springer, New York, NY, USA, 2001.

[23] R. Bhatia, *Matrix Analysis*, Springer, New York, NY, USA, 1997.

Hindawi Publishing Corporation
Abstract and Applied Analysis
Volume 2013, Article ID 638496, 10 pages
http://dx.doi.org/10.1155/2013/638496

Research Article

Asymptotic Stability and Exponential Stability of Impulsive Delayed Hopfield Neural Networks

Jing Chen,[1] Xiaodi Li,[2,3] and Dequan Wang[4]

[1] *Department of Mathematics, Shandong University, Jinan 250100, China*
[2] *School of Mathematical Sciences, Shandong Normal University, Jinan 250014, China*
[3] *Research Center on Logistics Optimization and Prediction of Engineering Technology, Jinan, Shandong 250014, China*
[4] *School of Computer Science, Fudan University, Shanghai 200433, China*

Correspondence should be addressed to Xiaodi Li; sodymath@163.com

Received 27 June 2013; Accepted 11 August 2013

Academic Editor: Jinde Cao

A criterion for the uniform asymptotic stability of the equilibrium point of impulsive delayed Hopfield neural networks is presented by using Lyapunov functions and linear matrix inequality approach. The criterion is a less restrictive version of a recent result. By means of constructing the extended impulsive Halanay inequality, we also analyze the exponential stability of impulsive delayed Hopfield neural networks. Some new sufficient conditions ensuring exponential stability of the equilibrium point of impulsive delayed Hopfield neural networks are obtained. An example showing the effectiveness of the present criterion is given.

1. Introduction

In the last several years, Hopfield neural networks (HNN) have received especially considerable attention due to their extensive applications in solving optimization problem, traveling salesman problem, and many other subjects in recent years [1–9]. In hardware implementation of neural networks, time delays are inevitably present due to the finite switching speeds of the amplifiers. Hence, it is vital to investigate the stability of delayed HNN. Recently, various results for the stability of delayed HNN are obtained via different approaches. In [3], Rakkiyappan and Balasubramaniam studied the exponential stability for fuzzy impulsive neural networks by utilizing the Lyapunov-Krasovskii functional and the linear matrix inequality approach. In [8], Li studied the global robust stability for stochastic interval neural networks with continuously distributed delays of neutral type based on the similar methods. In [9], Xia et al. derived some sufficient conditions for the synchronization problem of coupled identical Yang-Yang type fuzzy cellular neural networks with time-varying delays based on using the invariance principle of functional differential equations.

On the other hand, impulsive differential equations have attracted a great deal of attention due to its potential applications in biological systems, chemical reactions, and various results are obtained; for instance, see [10–14]. Impulses can make unstable systems stable, and stable systems can become unstable after impulse effects. Hence, the stability properties of impulsive HNN with time delays have become an important topic of theoretical studies and have been investigated by many researchers; see [5, 6, 15–22]. In [5], Zhang and Sun obtained a result for the uniform stability of the equilibrium point of the impulsive HNN systems with time delays by using Lyapunov functions and analysis technique. In [6], global exponential stability of impulsive delay HNN is investigated by applying the piecewise continuous vector Lyapunov function.

The purpose of this paper is to present some sufficient conditions for uniform asymptotic stability and global exponential stability of impulsive HNN with time delays by means of constructing the extended impulsive Halanay inequality which is different from that given in [23], Lyapunov functional methods, and linear matrix inequality approach.

The results here are also discussed from the point of view of thier comparison with the earlier results. Our results improve and generalize the earlier results. At last, we discuss an example to illustrate the advantage of the results we obtained.

2. Systems Description and Preliminaries

Let $\mathbb{R}$ denote the set of real numbers, let $\mathbb{R}_+$ denote the set of nonnegative real numbers, and let $\mathbb{R}^n$ denote the n-dimensional real space equipped with the Euclidean norm $\|\cdot\|$.

Consider the following impulsive and delayed HNN model:

$$\begin{aligned} x_i'(t) &= -c_i x_i(t) + \sum_{j=1}^{n} a_{ij} f_j\left(x_j(t)\right) \\ &\quad + \sum_{j=1}^{n} b_{ij} g_j\left(x_j\left(t-\tau_j(t)\right)\right) + I_i, \quad t \neq t_k,\ t \geq t_0, \\ \Delta x_i|_{t=t_k} &= x_i\left(t_k\right) - x_i\left(t_k^-\right), \quad i \in \Lambda,\ k = 1,2,\ldots, \end{aligned} \tag{1}$$

where $\Lambda = \{1,2,\ldots,n\}$. $n \geq 2$ corresponds to the number of units in a neural network; the impulse times t_k satisfy $0 \leq t_0 < t_1 < \cdots < t_k < \cdots, \lim_{k\to+\infty} t_k = +\infty$; x_i corresponds to the membrane potential of the unit i at time t; c_i is positive constant; f_j, g_j denote, respectively, the measures of response or activation to its incoming potentials of the unit j at time t and $t - \tau_j(t)$; constant a_{ij} denotes the synaptic connection weight of the unit j on the unit i at time t; constant b_{ij} denotes the synaptic connection weight of the unit j on the unit i at time $t - \tau_j(t)$; I_i is the input of the unit i; $\tau_j(t)$ is the transmission delay of the jth neuron such that $0 < \tau_j(t) \leq \tau, t \geq t_0$, and $j \in \Lambda$.

Assume that system (1) is supplemented with initial conditions of the form

$$x(s) = \phi(s), \quad s \in \left[t_0 - \tau, t_0\right], \tag{2}$$

where $x(s) = (x_1(s), x_2(s), \ldots, x_n(s))^T$, $\phi(s) = (\phi_1(s), \phi_2(s), \ldots, \phi_n(s))^T \in PC([t_0-\tau, t_0], \mathbb{R}^n)$, and $PC(I, \mathbb{R}^n) = \{\psi : I \to \mathbb{R}^n$, which is continuous everywhere except at finite number of points t_k, at which $\psi(t_k^+)$ and $\psi(t_k^-)$ exist and $\psi(t_k^+) = \psi(t_k)\}$. For any given $t \geq t_0$, $\psi \in PC([t-\tau, t], \mathbb{R}^n)$, the norm of ψ is defined by $\|\psi\|_\tau = \sup_{t-\tau\leq\theta\leq t}|\psi(\theta)|$. For any $\sigma \geq 0$, let $PC_\delta(\sigma) = \{\psi \in PC([\sigma-\tau, \sigma], \mathbb{R}^n) : \|\psi\| < \delta\}$.

In this paper, we assume that some conditions are satisfied, so that the equilibrium point of (1) without impulse does exist denoted by $x^* = (x_1^*, x_2^*, \ldots, x_n^*)^T$; see [2, 5]. Impulsive operator is viewed as perturbation of the equilibrium point of system (1) without impulsive effects. We assume that $\Delta x_i|_{t=t_k} = x_i(t_k) - x_i(t_k^-) = d_k^{(i)}(x_i(t_k^-) - x^*)$, $d_k^{(i)} \in \mathbb{R}$, and $i \in \Lambda, k = 1,2,\ldots$.

Since x^* is an equilibrium point of (1), one can derive from (1) that the transformation $y_i = x_i - x_i^*, i \in \Lambda$, transforms system (1) into the following system:

$$\begin{aligned} y_i'(t) &= -c_i y_i(t) + \sum_{j=1}^{n} a_{ij}\Omega_j\left(y_j(t)\right) \\ &\quad + \sum_{j=1}^{n} b_{ij}\Gamma_j\left(y_j\left(t-\tau_j(t)\right)\right), \quad t \neq t_k,\ t \geq t_0, \\ y_i\left(t_k\right) &= \left(1 + d_k^{(i)}\right) y_i\left(t_k^-\right), \quad i \in \Lambda,\ k = 1,2,\ldots, \end{aligned} \tag{3}$$

where $\Omega_j(y_j(t)) = f_j(x_j^* + y_j(t)) - f_j(x_j^*)$, $\Gamma_j(y_j(t)) = g_j(x_j^* + y_j(t-\tau_j(t))) - g_j(x_j^*)$.

Clearly, x^* is uniformly asymptotically stable for system (1) if and only if the trivial solution of system (3) is uniformly asymptotically stable. Hence, we only need to prove the stability of the trivial solution of system (3).

Remark 1. If $x_i(t_k) = d_k^{(i)} x_i(t_k^-)$, then we cannot get $y_i(t_k) = d_k^{(i)} y_i(t_k^-)$ through the transformation $y_i = x_i - x_i^*$. So some of the results [5] are incorrect.

The following notations will be used throughout the paper. The notation A^T and A^{-1} means the transpose of and the inverse of a square matrix A. Let $y(t) = (y_1(t), y_2(t), \ldots, y_n(t))^T, y_\tau = (y_1(t-\tau_1(t)), y_2(t-\tau_2(t)), \ldots, y_n(t-\tau_n(t)))^T; C = \mathrm{diag}[-c_1, -c_2, \ldots, -c_n]^T$, $A = (a_{ij})_{n\times n}$, $B = (b_{ij})_{n\times n}$, $D_k = \mathrm{diag}[1 + d_k^{(1)}, 1 + d_k^{(2)}, \ldots, 1 + d_k^{(n)}]^T$; $\Omega(y) = [\Omega_1(y_1), \Omega_2(y_2), \ldots, \Omega_n(y_n)]^T$, $\Gamma(y_\tau) = [\Gamma_1(y_1(t-\tau_1(t))), \Gamma_2(y_2(t-\tau_2(t))), \ldots, \Gamma_n(y_n(t-\tau_n(t)))]^T$. Then system (3) with initial condition becomes

$$\begin{aligned} y'(t) &= Cy(t) + A\Omega\left(y(t)\right) + B\Gamma\left(y_\tau\right), \quad t \neq t_k,\ t \geq t_0, \\ y\left(t_k\right) &= D_k y\left(t_k^-\right), \quad k = 1,2,\ldots, \\ y\left(t_0+\theta\right) &= \varphi(\theta), \quad \theta \in [-\tau, 0], \end{aligned} \tag{4}$$

where $\varphi(\theta) = x(t_0+\theta) - x^*$.

We introduce some definitions as follows.

Definition 2 (see [10]). The function $V(t,s) : [0,\infty) \times \mathbb{R}^n \to \mathbb{R}_+$ belongs to class v_0 if

- (A_1) V is continuous on each of the sets $[t_{k-1}, t_k) \times \mathbb{R}^n$ and $\lim_{(t,z)\to(t_k^-,s)} V(t,z) = V(t_k^-, s)$ exists;
- (A_2) $V(t,s)$ is locally Lipschitzian in s and $V(t,0) \equiv 0$.

Definition 3 (see [10]). Let $V \in v_0$, for any $(t,s) \in [t_{k-1}, t_k) \times \mathbb{R}^n$; the upper right-hand Dini derivative of $V(t,s)$ along the solution of (4) is defined by

$$\begin{aligned} &D^+V\left(t, \psi(0)\right) \\ &= \frac{\limsup_{h\to 0^+}\left\{V\left(t+h, y\left(t,\psi\right)(t+h)\right) - V\left(t,\psi(0)\right)\right\}}{h}. \end{aligned} \tag{5}$$

Definition 4 (see [11]). Assume that $y(t) = y(\sigma,\varphi)(t)$ is the solution of (4) through (σ,φ). Then the zero solution of (4) is said to be

(1) uniformly stable, if for any $\sigma \geq t_0$ and $\varepsilon > 0$, there exists a $\delta = \delta(\varepsilon) > 0$ such that $\varphi \in PC_\delta(\sigma)$ implies that $\|y(\sigma,\varphi)(t)\| < \varepsilon, t \geq \sigma$;

(2) uniformly asymptotically stable, if it is uniformly stable, and there exists a $\delta > 0$ such that for any $\varepsilon > 0$, $\sigma \geq t_0$, there is a $T = T(\varepsilon) > 0$ such that $\varphi \in PC_\delta(\sigma)$ implies that $\|y(\sigma,\varphi)(t)\| < \varepsilon, t \geq \sigma + T$;

(3) globally exponentially stable, if for any $\varphi \in PC([-\tau, 0], \mathbb{R}^n)$, there exist constants $M, \mu > 0$ such that

$$\|y(t)\| < M\|\varphi\|_\tau e^{-\mu(t-\sigma)}, \quad t \geq \sigma. \tag{6}$$

In this paper, we always assume that the following assumption holds:

(H_0) there exist constants $M, N > 0$ such that

$$\Omega^T(y)\Omega(y) \leq My^T y, \qquad \Gamma^T(y_\tau)\Gamma(y_\tau) \leq Ny_\tau^T y_\tau. \tag{7}$$

In addition, we have the following basic lemmas.

Lemma 5 (see [24]). *For any vectors $a, b \in \mathbb{R}^n$, the inequality*

$$\pm 2a^T b \leq a^T X a + b^T X^{-1} b \tag{8}$$

holds, in which X is any $n \times n$ matrix with $X > 0$.

Lemma 6 (see [25]). *Assume that there exist constants $P, Q > 0$ and $m(t) \in PC([t_0 - \tau, \infty), \mathbb{R}_+)$ such that*

(i) *for $t = t_k$, $m(t_k) \leq \gamma_k m(t_k^-)$, $\gamma_k > 0$ are constants and satisfy $\max_{k\in\mathbb{Z}_+}\{1/\gamma_k, 1\} < P/Q$;*

(ii) *for $t \geq t_0$, $t \neq t_k$,*

$$D^+ m(t) \leq -Pm(t) + Q\widetilde{m}(t), \tag{9}$$

where $\widetilde{m}(t) = \sup_{t-\tau\leq s\leq t} m(s)$.

Then for $t \geq t_0$,

$$m(t) \leq \widetilde{m}(t_0)\left(\prod_{t_0<t_k\leq t}\gamma_k\right)e^{-\lambda(t-t_0)}, \tag{10}$$

where λ satisfies the following inequality:

$$0 < \lambda \leq P - Q\max_{k\in\mathbb{Z}_+}\left\{\frac{1}{\gamma_k}, 1\right\}\cdot e^{\lambda\tau}. \tag{11}$$

3. Main Results

In this section, we will establish some theorems which provide sufficient conditions for uniformly asymptotically stable and global exponential stability of system (1).

Theorem 7. *The equilibrium point the system* (1) *is uniformly asymptotically stable, if there exists $n \times n$ symmetric, and positive definite matrix P satisfies the following conditions:*

(H_1) $\overline{\eta} \doteq \prod_{k=1}^{\infty}\max\{\eta_k, 1\} < \infty$, *where η_k is the largest eigenvalue of $P^{-1}D_k P D_k$;*

(H_2) $\lambda_3 < (-M-N)/\lambda_1$, *where λ_1 is the smallest eigenvalue of P and λ_3 is the largest eigenvalue of $P^{-1}(CP + PC + PAA^TP + PBB^TP)$.*

Proof. First, we will prove that the zero solution of system (4) is uniformly stable. For any $\varepsilon > 0$, we may choose a $\delta > 0$ such that $\delta \leq \sqrt{(\lambda_1/\overline{\eta}\lambda_2)}\varepsilon$, where λ_2 is the largest eigenvalue of P. For any $\sigma \geq t_0, \varphi \in PC_\delta(\sigma)$, let $y(t) = y(\sigma,\varphi)(t)$ be a solution of (4) through $(\sigma,\varphi), \sigma \geq t_0$ (for convenience, that we assume $\sigma = t_0$); then we can prove that $\|y(t)\| < \varepsilon, t \geq t_0$.

Consider the following Lyapunov function: $V(t, y(t)) = y^T(t)Py(t)$; then we have

$$\lambda_1\|y(t)\|^2 \leq V(t, y(t)) \leq \lambda_2\|y(t)\|^2. \tag{12}$$

By virtue of Lemma 5, we obtain for $t \in [t_k, t_{k+1}), k = 1, 2, \ldots,$

$$\begin{aligned}
&D^+V(t,y(t))\big|_{(4)}\\
&= \left(y^T(t)\right)'Py(t) + y^T(t)Py'(t)\\
&= \left(Cy(t) + A\Omega(y(t)) + B\Gamma(y_\tau)\right)^T Py(t)\\
&\quad + y^T(t)P\left(Cy(t) + A\Omega(y(t)) + B\Gamma(y_\tau)\right)\\
&= y^T(t)CPy(t) + \Omega^T(y(t))A^TPy(t)\\
&\quad + \Gamma^T(y_\tau)B^TPy(t) + y^T(t)PCy(t)\\
&\quad + y^T(t)PA\Omega(y(t)) + y^T(t)PB\Gamma(y_\tau)\\
&= y^T(t)(CP + PC)y(t)\\
&\quad + 2\Omega^T(y(t))A^TPy(t) + 2\Gamma^T(y_\tau)B^TPy(t)\\
&\leq y^T(t)(CP + PC)y(t)\\
&\quad + \Omega^T(y(t))\Omega(y(t)) + y^T(t)PAA^TPy(t)\\
&\quad + \Gamma^T(y_\tau)\Gamma(y_\tau) + y^T(t)PBB^TPy(t)\\
&\leq y^T(t)\left(CP + PC + PAA^TP + PBB^TP\right)y(t)\\
&\quad + \Omega^T(y(t))\Omega(y(t)) + \Gamma^T(y_\tau)\Gamma(y_\tau)\\
&\leq \lambda_3 y^T(t)Py(t) + My^T(t)y(t) + Ny_\tau^T y_\tau\\
&\leq \lambda_3 y^T(t)Py(t) + M\lambda_1^{-1}y^T(t)Py(t)\\
&\quad + N\lambda_1^{-1}y_\tau^T Py_\tau\\
&\leq \left[\lambda_3 + M\lambda_1^{-1}\right]y^T(t)Py(t) + N\lambda_1^{-1}y_\tau^T Py_\tau.
\end{aligned} \tag{13}$$

First, it is obvious that for $t_0 - \tau \leq t \leq t_0$,

$$\lambda_1\|y(t)\|^2 \leq V(t, y(t)) \leq \lambda_2\delta^2 \leq \overline{\eta}^{-1}\lambda_1\varepsilon^2. \tag{14}$$

Then we can prove that for $t \in [t_0, t_1)$,

$$V(t, y(t)) \leq \overline{\eta}^{-1}\lambda_1\varepsilon^2. \tag{15}$$

Suppose that this is not true; then there exists $\widehat{t} \in [t_0, t_1)$ such that $V(\widehat{t}, y(\widehat{t})) > \overline{\eta}^{-1}\lambda_1\varepsilon^2$.

Set

$$\check{t} = \sup\left\{t \mid s \in [t_0, t), V(s, y(s)) \le \overline{\eta}^{-1}\lambda_1\varepsilon^2\right\}. \tag{16}$$

It is obvious that $\check{t} < \widehat{t}$. Then it follows that

(I_a) $V(t, y(t)) \le \overline{\eta}^{-1}\lambda_1\varepsilon^2$, $t \in [t_0, \check{t})$;

(II_a) $V(\check{t}, y(\check{t})) = \overline{\eta}^{-1}\lambda_1\varepsilon^2$;

(III_a) for any $\delta > 0$, there exists $t_\delta \in (\check{t}, \check{t} + \delta)$ such that $V(t_\delta, y(t_\delta)) > \overline{\eta}^{-1}\lambda_1\varepsilon^2$.

So

$$V\left(\check{t}, y\left(\check{t}\right)\right) = \overline{\eta}^{-1}\lambda_1\varepsilon^2 \ge V\left(t, y_\tau\right), \quad \check{t} - \tau \le t \le \check{t}. \tag{17}$$

In view of condition (H_2), from (13), we obtain

$$\begin{aligned} D^+V\left(\check{t}, y\left(\check{t}\right)\right) &\le \left[\lambda_3 + M\lambda_1^{-1}\right] y^T\left(\check{t}\right) Py\left(\check{t}\right) + N\lambda_1^{-1} y_\tau^T P y_\tau \\ &\le \left[\lambda_3 + M\lambda_1^{-1} + N\lambda_1^{-1}\right] V\left(\check{t}, y\left(\check{t}\right)\right) \\ &< 0, \end{aligned} \tag{18}$$

which is a contradiction with (III_a). Hence, (15) holds. Considering

$$\begin{aligned} V\left(t_1, y\left(t_1\right)\right) &= y^T\left(t_1\right) Py\left(t_1\right) \\ &= y^T\left(t_1^-\right) D_1 P D_1 y\left(t_1^-\right) \\ &\le \eta_1 y^T\left(t_1^-\right) Py\left(t_1^-\right) \\ &= \eta_1 V\left(t_1^-, y\left(t_1^-\right)\right) \\ &\le \eta_1\overline{\eta}^{-1}\lambda_1\varepsilon^2 \\ &\le \max\left\{\eta_1, 1\right\}\overline{\eta}^{-1}\lambda_1\varepsilon^2, \end{aligned} \tag{19}$$

we will prove that for $t \in [t_1, t_2)$,

$$V\left(t, y\left(t\right)\right) \le \max\left\{\eta_1, 1\right\}\overline{\eta}^{-1}\lambda_1\varepsilon^2. \tag{20}$$

Suppose that this is false; then we can define

$$\vec{t} = \sup\left\{t \mid s \in [t_1, t), V\left(s, y\left(s\right)\right) \le \max\left\{\eta_1, 1\right\}\overline{\eta}^{-1}\lambda_1\varepsilon^2\right\}. \tag{21}$$

Similarly, we can obtain

(I_b) $V(t, y(t)) \le \max\{\eta_1, 1\}\overline{\eta}^{-1}\lambda_1\varepsilon^2, t \in [t_1, \vec{t})$;

(II_b) $V(\vec{t}, y(\vec{t})) = \max\{\eta_1, 1\}\overline{\eta}^{-1}\lambda_1\varepsilon^2$;

(III_b) for any $\delta > 0$, there exists $t_\delta \in (\vec{t}, \vec{t} + \delta)$ such that $V(t_\delta, y(t_\delta)) > \max\{\eta_1, 1\}\overline{\eta}^{-1}\lambda_1\varepsilon^2$.

So

$$\begin{aligned} V\left(\vec{t}, y\left(\vec{t}\right)\right) = \max\left\{\eta_1, 1\right\}\overline{\eta}^{-1}\lambda_1\varepsilon^2 \ge V\left(t, y_\tau\right), \\ \vec{t} - \tau \le t \le \vec{t}. \end{aligned} \tag{22}$$

In fact, if $\vec{t} - \tau \ge t_1$, then it is obvious that inequality (22) holds. If $\vec{t} - \tau < t_1$, then $V(t, y_\tau) \le \overline{\eta}^{-1}\lambda_1\varepsilon^2 \le \max\{\eta_1, 1\}\overline{\eta}^{-1}\lambda_1\varepsilon^2 = V(\vec{t}, y(\vec{t}))$. So, inequality (22) still holds.

Considering condition (H_2), from (13), we obtain

$$\begin{aligned} D^+V\left(\vec{t}, y\left(\vec{t}\right)\right) &\le \left[\lambda_3 + M\lambda_1^{-1}\right] y^T\left(\vec{t}\right) Py\left(\vec{t}\right) + N\lambda_1^{-1} y_\tau^T P y_\tau \\ &\le \left[\lambda_3 + M\lambda_1^{-1} + N\lambda_1^{-1}\right] V\left(\vec{t}, y\left(\vec{t}\right)\right) \\ &< 0, \end{aligned} \tag{23}$$

which contradicts (III_b). Hence, (20) holds.

By induction hypothesis, we may prove, in general, that for $t \in [t_m, t_{m+1})$,

$$V\left(t, y\left(t\right)\right) \le \prod_{k=1}^{m} \max\left\{\eta_k, 1\right\}\overline{\eta}^{-1}\lambda_1\varepsilon^2; \tag{24}$$

that is,

$$V\left(t, y\left(t\right)\right) \le \prod_{t_0 < t_k \le t} \max\left\{\eta_k, 1\right\}\overline{\eta}^{-1}\lambda_1\varepsilon^2. \tag{25}$$

Finally, we arrive at

$$\lambda_1\left\|y(t)\right\|^2 \le V\left(t, y\left(t\right)\right) \le \lambda_1\varepsilon^2, \quad t \ge t_0. \tag{26}$$

Therefore, we obtain $\|y(t)\| < \varepsilon, t \ge t_0$. In view of the choice of δ, the zero solution of (4) is uniformly stable; that is, the equilibrium point of (1) is uniformly stable.

Next we show the uniformly asymptotical stability. For any given $G > 0$, we find a corresponding $\delta > 0$ such that for any $\varphi \in PC_\delta(\sigma)$ implies that $\|y(t)\| = \|y(t_0, \varphi)(t)\| \le G$, $t \ge \sigma = t_0$; that is, $V(t, y(t)) \le \lambda_2 G^2$.

For any small $\varepsilon \in (0, G)$, we choose $\vec{N} = \vec{N}(\varepsilon) \in \mathbb{Z}_+$ such that

$$\sqrt{\frac{\vec{N}\lambda_1}{2\lambda_2}}\varepsilon < G \le \sqrt{\frac{\left(\vec{N} + 1\right)\lambda_1}{2\lambda_2}}\varepsilon, \tag{27}$$

$$\vec{N} > \frac{-N}{\lambda_3\lambda_1 + M + N}. \tag{28}$$

In fact, it is feasible to choose small enough $\varepsilon \in (0, G)$ such that $\vec{N}$ in (27) is large enough to satisfy (28).

Since $\overline{\eta} \doteq \prod_{k=1}^{\infty}\max\{\eta_k, 1\} < \infty$ implies that $\sum_{k=1}^{\infty}(\max\{\eta_k, 1\} - 1) < \infty$, there exists sufficient large $N^\star \in \mathbb{Z}_+$ such that

$$\begin{aligned} \sum_{i=N^\star}^{\infty}\left(\max\left\{\eta_i, 1\right\} - 1\right) &\le \frac{\lambda_1\varepsilon^2}{6\lambda_2 G^2}, \\ \max\left\{\eta_k, 1\right\} &< \frac{1}{6\vec{N}} + 1, \quad k \ge N^\star. \end{aligned} \tag{29}$$

Let

$$w_1 = \frac{\left[1 + \sum_{k=1}^{\infty}\left(\max\left\{\eta_k, 1\right\} - 1\right)\right]\lambda_2 G^2}{\left|\left[\lambda_1\lambda_3 + M + N\right]\vec{N} + N\right|} \cdot \frac{2}{\varepsilon^2} + 1. \tag{30}$$

Next we show that there exists $T_1 \in [N^\star, N^\star + w_1]$ such that

$$V(T_1, y(T_1)) < \frac{\lambda_1 \varepsilon^2}{2} \vec{N}. \tag{31}$$

Or else, for all $t \in [N^\star, N^\star + w_1]$,

$$V(t, y(t)) \geq \frac{\lambda_1 \varepsilon^2}{2} \vec{N}. \tag{32}$$

Thus, we get

$$V(t, y(t)) + \frac{\lambda_1 \varepsilon^2}{2} \geq \frac{\lambda_1 \varepsilon^2}{2} \left(\vec{N} + 1\right) \geq \lambda_2 G^2 > V(\xi, y_\tau), \quad t - \tau \leq \xi \leq t. \tag{33}$$

From (13), we have

$$\begin{aligned} D^+ V(t, y(t))\big|_{(4)} &\leq \left[\lambda_3 + M\lambda_1^{-1}\right] y^T(t) P y(t) \\ &\quad + N\lambda_1^{-1} y_\tau^T P y_\tau \\ &\leq \left[\lambda_3 + M\lambda_1^{-1}\right] V(t, y(t)) \\ &\quad + N\lambda_1^{-1} \left(V(t, y(t)) + \frac{\lambda_1 \varepsilon^2}{2}\right) \\ &\leq \left[\lambda_3 + M\lambda_1^{-1} + N\lambda_1^{-1}\right] V(t, y(t)) + \frac{\varepsilon^2}{2} N \\ &\leq \left[\lambda_3 + M\lambda_1^{-1} + N\lambda_1^{-1}\right] \frac{\lambda_1 \varepsilon^2}{2} \vec{N} + \frac{\varepsilon^2}{2} N \\ &\leq \left\{\left[\lambda_3 \lambda_1 + M + N\right] \vec{N} + N\right\} \frac{\varepsilon^2}{2}. \end{aligned} \tag{34}$$

Integrating the above inequality from $N^\star$ to $N^\star + w_1$, we have

$$\begin{aligned} &V(N^\star + w_1, y(N^\star + w_1)) \\ &\quad \leq V(N^\star, y(N^\star)) + \left\{\left[\lambda_3 \lambda_1 + M + N\right] \vec{N} + N\right\} \frac{\varepsilon^2}{2} w_1 \\ &\qquad + \sum_{N^\star < t_k < N^\star + w_1} \left[V(t_k) - V(t_k^-)\right] \\ &\quad \leq V(N^\star, y(N^\star)) + \left\{\left[\lambda_3 \lambda_1 + M + N\right] \vec{N} + N\right\} \frac{\varepsilon^2}{2} w_1 \\ &\qquad + \sum_{N^\star < t_k < N^\star + w_1} \left[\max\{\eta_k, 1\} - 1\right] V(t_k^-) \\ &\quad \leq \lambda_2 G^2 + \left\{\left[\lambda_3 \lambda_1 + M + N\right] \vec{N} + N\right\} \frac{\varepsilon^2}{2} w_1 \\ &\qquad + \sum_{N^\star < t_k < N^\star + w_1} \left[\max\{\eta_k, 1\} - 1\right] \lambda_2 G^2 \\ &\quad \leq \left\{\left[\lambda_3 \lambda_1 + M + N\right] \vec{N} + N\right\} \frac{\varepsilon^2}{2} w_1 \\ &\qquad + \left\{1 + \sum_{N^\star < t_k < N^\star + w_1} \left[\max\{\eta_k, 1\} - 1\right]\right\} \lambda_2 G^2 \\ &\quad < 0, \end{aligned} \tag{35}$$

which is a contradiction. So (31) holds. We may choose $T_1 = N^\star + w_1$.

We next claim that for all $t > T_1$,

$$V(t, y(t)) < \left(\frac{\vec{N}}{2} + \frac{1}{4}\right) \lambda_1 \varepsilon^2. \tag{36}$$

Suppose that this is not true; then there exists a $\tau_2 > T_1$ such that

$$V(\tau_2, y(\tau_2)) \geq \left(\frac{\vec{N}}{2} + \frac{1}{4}\right) \lambda_1 \varepsilon^2, \tag{37}$$

and for $T_1 < t < \tau_2$,

$$V(t, y(t)) < \left(\frac{\vec{N}}{2} + \frac{1}{4}\right) \lambda_1 \varepsilon^2. \tag{38}$$

Suppose that $T_1 \in [t_m, t_{m+1})$, $m \in \mathbb{Z}_+$. We claim that $\tau_2 \geq t_{m+1}$. Otherwise, $\tau_2 \in [T_1, t_{m+1})$. Since (31) holds, it is clear that there exists a $\tau_1 \in [T_1, \tau_2)$ such that

$$\begin{aligned} V(\tau_1, y(\tau_1)) &= \frac{\vec{N}}{2} \lambda_1 \varepsilon^2, \\ V(\tau_1, y(\tau_1)) &\leq V(t, x(t)) \leq V(\tau_2, x(\tau_2)), \quad \tau_1 \leq t \leq \tau_2. \end{aligned} \tag{39}$$

Furthermore, we note that

$$V(t, y(t)) + \frac{\lambda_1 \varepsilon^2}{2} \geq \frac{\lambda_1 \varepsilon^2}{2} \left(\vec{N} + 1\right) \geq \lambda_2 G^2 > V(\xi, y_\tau), \quad t - \tau \leq \xi \leq t. \tag{40}$$

From (13), we have

$$D^+ V(t, y(t)) \leq \left\{\left[\lambda_3 \lambda_1 + M + N\right] \vec{N} + N\right\} \frac{\varepsilon^2}{2} < 0, \quad \tau_1 \leq t \leq \tau_2, \tag{41}$$

which implies that

$$V(\tau_2, y(\tau_2)) \leq V(\tau_1, y(\tau_1)). \tag{42}$$

This is a contradiction.

Hence, we obtain $\tau_2 \geq t_{m+1}$; without loss of generality, we may suppose that $\tau_2 \in [t_{m+q}, t_{m+q+1})$, $q \geq 1$. Next we first claim that there exists $\tau_1 > 0$ satisfying $\tau_2 > \tau_1 > T_1$ such that

$$V(\tau_1, y(\tau_1)) \geq \frac{\vec{N}}{2} \lambda_1 \varepsilon^2. \tag{43}$$

Suppose that this is false; then for all $t \in (T_1, \tau_2)$,

$$V(t, y(t)) < \frac{\vec{N}}{2}\lambda_1\varepsilon^2, \tag{44}$$

which implies that $\tau_2 = t_{m+q}$ in view of (37). Consequently, we have

$$\begin{aligned} V\left(t_{m+q}, y\left(t_{m+q}\right)\right) &\geq \left(\frac{\vec{N}}{2} + \frac{1}{4}\right)\lambda_1\varepsilon^2, \\ V\left(t_{m+q}^-, y\left(t_{m+q}^-\right)\right) &< \frac{\vec{N}}{2}\lambda_1\varepsilon^2, \end{aligned} \tag{45}$$

which implies that

$$\begin{aligned} &\left(\max\left\{\eta_{m+q}, 1\right\} - 1\right)\lambda_2 G^2 \\ &\quad \geq \left(\max\left\{\eta_{m+q}, 1\right\} - 1\right) V\left(t_{m+q}^-, y\left(t_{m+q}^-\right)\right) > \frac{1}{4}\lambda_1\varepsilon^2. \end{aligned} \tag{46}$$

Hence, we get $\max\{\eta_{m+q}, 1\} > 1 + (\lambda_1\varepsilon^2/4\lambda_2 G^2)$, which contradicts (29). So (43) holds.

Therefore, there are two situations $\tau_2 > t_{m+q}$ and $\tau_2 = t_{m+q}$. Next we discuss them, respectively.

(b_1) If $\tau_2 > t_{m+q}$, let

$$\begin{aligned} \widetilde{\tau_1} = \inf_{\tau_1 \leq t < \tau_2} \Bigg\{ & t \mid s \in [t, \tau_2], \frac{\vec{N}}{2}\lambda_1\varepsilon^2 \leq V(s, y(s)) \\ & < V(\tau_2, y(\tau_2)) \Bigg\}. \end{aligned} \tag{47}$$

We first show that $\widetilde{\tau_1} < t_{m+q}$. Suppose on the contrary that $\widetilde{\tau_1} \in [t_{m+q}, \tau_2)$; then

$$\begin{aligned} V(t, y(t)) + \frac{\lambda_1\varepsilon^2}{2} &\geq \frac{\lambda_1\varepsilon^2}{2}\left(\vec{N} + 1\right) \\ &\geq \lambda_2 G^2 > V(\xi, y_\tau), \\ t - \tau \leq \xi \leq t, &\quad t \in \left[\widetilde{\tau_1}, \tau_2\right]. \end{aligned} \tag{48}$$

From (13), we have

$$\begin{aligned} D^+V(t, y(t)) &\leq \left\{\left[\lambda_3\lambda_1 + M + N\right]\vec{N} + N\right\}\frac{\varepsilon^2}{2} < 0, \\ &\widetilde{\tau_1} \leq t \leq \tau_2, \end{aligned} \tag{49}$$

which implies that

$$V(\tau_2, y(\tau_2)) \leq V(\widetilde{\tau_1}, y(\widetilde{\tau_1})); \tag{50}$$

which is a contradiction with the definition of $\widetilde{\tau_1}$. Thus we obtain that $\widetilde{\tau_1} < t_{m+q}$. Suppose that $\widetilde{\tau_1} \in [t_{m+k}, t_{m+k+1}), 1 \leq k < q$.

We also have two cases.

(b_{1a}) If $\widetilde{\tau_1}$ is not impulsive point, that is to say $\widetilde{\tau_1} > t_{m+k}$, then considering the definition of $\widetilde{\tau_1}$, we have

$$V(\widetilde{\tau_1}, y(\widetilde{\tau_1})) = \frac{\vec{N}}{2}\lambda_1\varepsilon^2. \tag{51}$$

By the same argument as the above mentioned, we obtain that (48) still holds.

Hence, from (13), we get

$$\begin{aligned} \left(\frac{\vec{N}}{2} + \frac{1}{4}\right)\lambda_1\varepsilon^2 &\leq V(\tau_2, y(\tau_2)) \\ &\leq V(\widetilde{\tau_1}, y(\widetilde{\tau_1})) + \sum_{i=m+k+1}^{m+q}\left[V(t_i) - V(t_i^-)\right] \\ &\leq \frac{\vec{N}}{2}\lambda_1\varepsilon^2 + \sum_{i=m+k+1}^{m+q}\left(\max\{\eta_i, 1\} - 1\right)V(t_i^-) \\ &\leq \frac{\vec{N}}{2}\lambda_1\varepsilon^2 + \sum_{i=m+k+1}^{m+q}\left(\max\{\eta_i, 1\} - 1\right)\lambda_2 G^2, \end{aligned} \tag{52}$$

which implies that

$$\frac{1}{4}\lambda_1\varepsilon^2 \leq \sum_{i=m+k+1}^{m+q}\left(\max\{\eta_i, 1\} - 1\right)\lambda_2 G^2, \tag{53}$$

which is a contradiction with (29). So $\widetilde{\tau_1}$ is some impulsive point.

(b_{1b}) If $\widetilde{\tau_1}$ is some impulsive point, that is to see $\widetilde{\tau_1} = t_{m+k}$, then from the definition of $\widetilde{\tau_1}$, it is clear that

$$V(\widetilde{\tau_1}^-, y(\widetilde{\tau_1}^-)) = V(t_{m+k}^-, y(t_{m+k}^-)) < \frac{\vec{N}}{2}\lambda_1\varepsilon^2, \tag{54}$$

which implies that

$$\begin{aligned} V(\widetilde{\tau_1}, y(\widetilde{\tau_1})) &= V(t_{m+k}, y(t_{m+k})) \\ &\leq \eta_{m+k}V(t_{m+k}^-, y(t_{m+k}^-)) \\ &< \eta_{m+k}\frac{\vec{N}}{2}\lambda_1\varepsilon^2 \\ &\leq \max\{\eta_{m+k}, 1\}\frac{\vec{N}}{2}\lambda_1\varepsilon^2. \end{aligned} \tag{55}$$

On the other hand, note that inequality (48) still holds; from (13) and (29), we have

$$\begin{aligned}\left(\frac{\vec{N}}{2}+\frac{1}{4}\right)\lambda_1\varepsilon^2 &\le V\left(\tau_2, y\left(\tau_2\right)\right)\\ &\le V\left(\widetilde{\tau_1}, y\left(\widetilde{\tau_1}\right)\right)\\ &\quad+\sum_{i=m+k+1}^{m+q}\left[V\left(t_i\right)-V\left(t_i^-\right)\right]\\ &< \max\left\{\eta_{m+k},1\right\}\frac{\vec{N}}{2}\lambda_1\varepsilon^2\\ &\quad+\sum_{i=m+k+1}^{m+q}\left(\max\left\{\eta_i,1\right\}-1\right)V\left(t_i^-\right),\end{aligned}\tag{56}$$

which implies that

$$\begin{aligned}\frac{1}{4}\lambda_1\varepsilon^2 &\le \left(\max\left\{\eta_{m+k},1\right\}-1\right)\frac{\vec{N}}{2}\lambda_1\varepsilon^2\\ &\quad+\sum_{i=m+k+1}^{m+q}\left(\max\left\{\eta_i,1\right\}-1\right)\lambda_2G^2\\ &\le \frac{1}{6\vec{N}}\frac{\vec{N}}{2}\lambda_1\varepsilon^2\\ &\quad+\sum_{i=m+k+1}^{m+q}\left(\max\left\{\eta_i,1\right\}-1\right)\lambda_2G^2.\end{aligned}\tag{57}$$

That means

$$\frac{1}{6}\lambda_1\varepsilon^2 < \sum_{i=m+k+1}^{m+q}\left(\max\left\{\eta_i,1\right\}-1\right)\lambda_2G^2,\tag{58}$$

which contradicts (29).

Hence, the first situation $\tau_2 > t_{m+q}$ is impossible.

(b_2) If $\tau_2 = t_{m+q}$, then by the same arguments as in the proof in (b_1) and (43), we have

$$V\left(\tau_2^-, y\left(\tau_2^-\right)\right) > \frac{\vec{N}}{2}\lambda_1\varepsilon^2.\tag{59}$$

Then let

$$\begin{aligned}\widetilde{\tau_1} = \inf_{\tau_1\le t<\tau_2}\Bigg\{t \mid s\in\left[t,\tau_2\right],\ &\frac{\vec{N}}{2}\lambda_1\varepsilon^2\\ &\le V\left(s,y\left(s\right)\right) < V\left(\tau_2,y\left(\tau_2\right)\right)\Bigg\}.\end{aligned}\tag{60}$$

The rest of the arguments are omitted. Finally we can find our desirable contradiction. Hence, (36) holds.

With above mentioned, the same arguments as before, if we replace T_1 with N^*, then there exists a $T_2 = T_1 + w_1 = N^* + 2w_1$ such that for $t > T_2$,

$$V\left(t, y\left(t\right)\right) < \frac{\vec{N}}{2}\lambda_1\varepsilon^2.\tag{61}$$

Let T_2 replace T_1; then there exists a $T_3 = N^* + 3w_1$ such that for $t > T_3$,

$$V\left(t, y\left(t\right)\right) < \left(\frac{\vec{N}}{2}-\frac{1}{4}\right)\lambda_1\varepsilon^2.\tag{62}$$

By induction hypothesis, we may prove, in general, that there exists a $T_{2\vec{N}} = N^* + 2\vec{N}w_1$ such that $t > T_{2\overleftarrow{N}}$,

$$V\left(t, y\left(t\right)\right) < \left(\frac{\vec{N}}{2}-\frac{\vec{N}-2}{2}\right)\lambda_1\varepsilon^2 = \lambda_1\varepsilon^2.\tag{63}$$

Therefore, we obtain that $\|y(t)\| < \varepsilon, t > N^* + 2Nw_1$. In view of the choice of N^*, $\vec{N}$, and w_1, the zero solution of (4) is uniformly asymptotically stable; that is, the equilibrium point of (1) is uniformly asymptotically stable. The proof of Theorem 7 is therefore complete. □

Let $|1 + d_k^{(i)}| \ne |1 + d_k^{(j)}|, c_i \ne c_j, i \ne j, i, j \in \Lambda, k = 1, 2, \ldots,$ in Theorem 7; then we can have the following result.

Corollary 8. *The equilibrium point of system* (1) *is uniformly asymptotically stable, if there exists n×n symmetric and positive definite matrix P satisfying*

(I_1) $\overline{\eta} \doteq \prod_{k=1}^{\infty}\max\{\max_{i\in\Lambda}(1+d_k^{(i)})^2, 1\} < \infty$;

(I_2) $\lambda_3 < (-M-N)/\lambda_1$, *where* λ_1 *is the smallest eigenvalue of* P *and* λ_3 *is the largest eigenvalue of* $2C + AA^TP + BB^TP$.

Remark 9. For using the less conservative conditions in Theorem 7, our results obviously improve some results established in the earlier references. In [5], condition $y(t_k) = Dy(t_k^-)$ holds for all $k \in \mathbb{Z}_+$; here note in our Theorem 7 that we only require that the solutions satisfy the hypothesis (H_1) at impulsive points. In addition, our conditions are without requirement of the range of the largest eigenvalues of $P^{-1}D^TPD$ on $(0, 1)$, which are milder than the restrictions in [5].

By utilizing Lemma 6, we will give some sufficient conditions for globally exponential stability of the equilibrium point of system (1).

Theorem 10. *Assume that there exists* $n \times n$ *symmetric and positive definite matrix* P *such that* $\lambda_1 > 0$ *is the smallest eigenvalue of* P, λ_3 *is the largest eigenvalue of* $P^{-1}(CP + PC + PAA^TP + PBB^TP)$, η_k *is the largest eigenvalue of* $P^{-1}D_kPD_k$, *and* λ_1, λ_3 *and* η_k *satisfy the following conditions:*

(H_3) *one has*

$$\lambda_3 + \frac{M}{\lambda_1} + \frac{N}{\lambda_1}\cdot\max_{k\in\mathbb{Z}_+}\left\{\frac{1}{\eta_k}, 1\right\} < 0,\tag{64}$$

(H_4) *there exist constants* $\mathbb{U}(>0), \delta(\ge 0)$ *such that* $\delta < \mu$ *and the following inequality*

$$\sum_{k=1}^{m}\ln\eta_k - \delta\left(t_m - t_0\right) < \mathbb{U} \quad \forall m\in\mathbb{Z}_+ \text{ holds},\tag{65}$$

where μ satisfies the following inequality:

$$0 < \mu \le -\lambda_3 - \frac{M}{\lambda_1} - \frac{N}{\lambda_1}\max_{k\in\mathbb{Z}_+}\left\{\frac{1}{\eta_k}, 1\right\} \cdot e^{\mu\tau}. \tag{66}$$

Then the equilibrium point of the system (1) *is globally exponentially stable, and the exponential convergence rate is equal to $(\mu - \delta)/2$.*

Proof. Let $y(t) = y(\sigma, \varphi)(t)$ be a solution of (4) through (σ, φ), $\sigma \ge t_0$ (for convenience, we assume that $\sigma = t_0$). We next will prove that the zero solution of (4) is globally exponentially stable. Construct the Lyapunov functional as in Theorem 7; that is, $V(t, y(t)) = y^T(t)Py(t)$; then we obtain the following:

(1) $\lambda_1\|y(t)\|^2 \le V(t, y(t)) \le \lambda_2\|y(t)\|^2$, where λ_2 is the largest eigenvalue of P;

(2) for $t \in [t_k, t_{k+1})$, $k = 1, 2, \ldots$,

$$\begin{aligned} D^+V(t, y(t))\big|_{(4)} &\le \left[\lambda_3 + M\lambda_1^{-1}\right] y^T(t) Py(t) \\ &\quad + N\lambda_1^{-1} y_\tau^T P y_\tau; \end{aligned} \tag{67}$$

(3) $V(t_k, y(t_k)) \le \eta_k V(t_k^-, y(t_k^-))$.

From (2), we have for $t \in [t_k, t_{k+1})$, $k = 1, 2, \ldots$,

$$D^+V(t, y(t))\big|_{(4)} \le -PV(t, y(t)) + Q\widetilde{V}(t, y(t)), \tag{68}$$

where $\widetilde{V}(t) = \sup_{t-\tau\le s\le t}V(s)$, $P = -\lambda_3 - M\lambda_1^{-1}$, and $Q = N\lambda_1^{-1}$.

For any $t \ge t_0$, suppose that $t \in [t_m, t_{m+1})$, $m \ge 0$. By Lemma 6 and condition (H_4), we obtain

$$\begin{aligned} V(t) &\le \widetilde{V}(t_0)\left(\prod_{k=1}^{m}\eta_k\right)e^{-\mu(t-t_0)} \\ &\le \widetilde{V}(t_0)\, e^{\mathbb{U}} \cdot e^{\delta(t_m - t_0)} \cdot e^{-\mu(t-t_0)} \\ &\le \widetilde{V}(t_0)\, e^{\mathbb{U}} \cdot e^{\delta(t-t_0)} \cdot e^{-\mu(t-t_0)} \\ &\le \lambda_2 e^{\mathbb{U}}\|\varphi\|_\tau^2 e^{-(\mu-\delta)(t-t_0)}, \end{aligned} \tag{69}$$

where μ satisfies inequality (66).

Hence, we obtain for any $t \ge t_0$,

$$\|y(t)\| \le e^{(1/2)\mathbb{U}}\sqrt{\frac{\lambda_2}{\lambda_1}}\|\varphi\|_\tau e^{-((\mu-\delta)/2)(t-t_0)}, \quad t \ge t_0, \tag{70}$$

where μ satisfies inequality (66).

Therefore, the zero solution of system (4) is globally exponentially stable; that is, the equilibrium point of system (1) is globally exponentially stable. The proof of Theorem 10 is complete. □

Remark 11. In Theorem 10, if $\sup_{n\in\mathbb{Z}_+}(\prod_{k=1}^{n}\eta_k) < \infty$, then we can choose $\delta = 0$ in condition (H_3).

Let $\eta_k \in (0, 1], k = 1, 2, \ldots$ in Theorem 7; then we can have the following result.

Corollary 12. *Assume that there exists $n \times n$ symmetric and positive definite matrix P such that λ_1 is the smallest eigenvalue of P, λ_3 is the largest eigenvalue of $P^{-1}(CP + PC + PAA^TP + PBB^TP)$, η_k is the largest eigenvalue of $P^{-1}D_kPD_k$, and condition*

$$\lambda_1\lambda_3 + M + N < 0 \quad \textit{holds}. \tag{71}$$

Then the equilibrium point of the system (1) *is globally exponentially stable, and the exponential convergence rate is equal to $\mu/2$, where μ satisfies the following inequality:*

$$0 < \mu \le -\lambda_3 - \frac{M}{\lambda_1} - \frac{N}{\lambda_1}\max_{k\in\mathbb{Z}_+}\eta_k \cdot e^{\mu\tau}. \tag{72}$$

4. Example

In this section, we present a numerical example to illustrate our results.

Example 1. We consider Example 1 in [2] as follows:

$$\begin{aligned} u_1'(t) &= -2.5u_1(t) - 0.5f(u_1(t)) \\ &\quad + 0.1f(u_2(t)) - 0.1f(u_1(t-\tau)) \\ &\quad + 0.2f(u_2(t-\tau)) - 1, \\ u_2'(t) &= -2u_1(t) + 0.2f(u_1(t)) \\ &\quad - 0.1f(u_2(t)) + 0.2f(u_1(t-\tau)) \\ &\quad + 0.1f(u_2(t-\tau)) + 4, \end{aligned} \tag{73}$$

with impulses

$$\begin{aligned} d_k^{(1)} &= \sqrt{1 + \frac{1}{2k^2}} - 1, \\ d_k^{(2)} &= \sqrt{1 + \frac{1}{k^2}} - 1, \quad t_k = k,\ k \in \mathbb{Z}_+. \end{aligned} \tag{74}$$

The delayed feedback matrixes A, B, and C are

$$\begin{aligned} C &= \begin{pmatrix} -2.5 & 0 \\ 0 & -2 \end{pmatrix}, \qquad A = \begin{pmatrix} -0.5 & 0.1 \\ 0.2 & -0.1 \end{pmatrix}, \\ B &= \begin{pmatrix} -0.1 & 0.2 \\ 0.2 & 0.1 \end{pmatrix}. \end{aligned} \tag{75}$$

Since the activation function in [2] is described by $f = f_i = 0.5(|x + 1| - |x - 1|), i = 1, 2$, then we have $M = N = 1$. We may choose $P = E$ (unit matrix); then $\lambda_1 = \lambda_2 = 1$. Note that

$$\begin{aligned} P^{-1}D_kPD_k = D_k^2 &= \begin{pmatrix} 1 + \dfrac{1}{2k^2} & 0 \\ 0 & 1 + \dfrac{1}{k^2} \end{pmatrix}, \\ P^{-1}\left(CP + PC + PAA^TP + PBB^TP\right) & \\ = 2C + AA^T + BB^T & \\ = \begin{pmatrix} -4.69 & -0.11 \\ -0.11 & -3.9 \end{pmatrix} = \Delta. & \end{aligned} \tag{76}$$

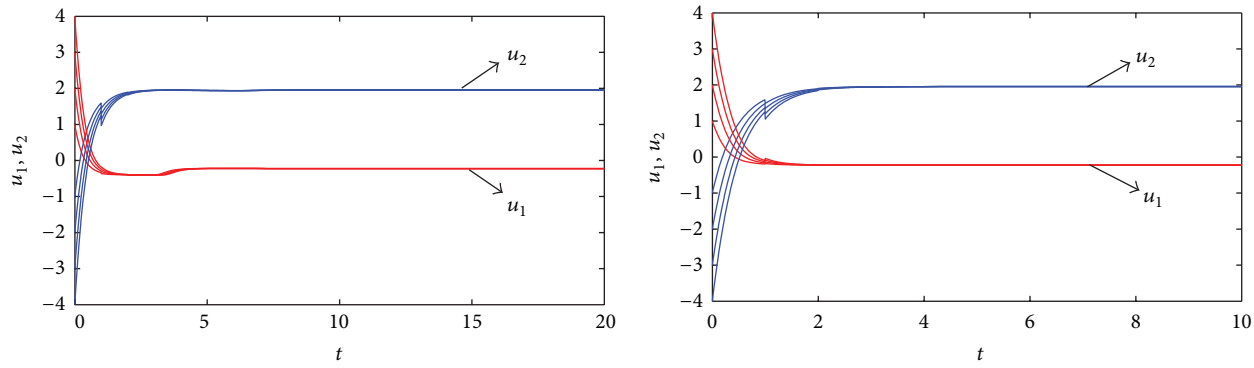

FIGURE 1: (a) State trajectories of system (73) with impulses (74) and $\tau = 3$. (b) State trajectories of system (73) with impulses (79) and $\tau = 0.17$.

then we get $\eta_k = 1 + 1/k^2$, $\overline{\eta} = \prod_{k=1}^{\infty}(1 + 1/k^2) < \infty$. Matrix Δ's characteristic equation is

$$\lambda^2 + 8.59\lambda + 18.2789 = 0. \tag{77}$$

By a straightforward calculation, we obtain that the largest characteristic root $\lambda_3 \approx -3.885 < -2$. By Theorem 7, the equilibrium point of system (73) is uniformly asymptotically stable with impulses (74) for any $\tau > 0$, which is shown in Figure 1(a).

However, the criteria in [5] are invalid here. In fact, condition $y(t_k) = Dy(t_k^-)$ is not satisfied here. Moreover, because of the impulsive effect, the criteria in [2] are also invalid here. Therefore, our results are less conservative than those given result in [2, 5].

Furthermore, let $\tau = 0.17$. Note that $\prod_{k=1}^{\infty}(1 + 1/k^2) < \infty, \lambda_3 = -3.885 < -2$; then one can choose $\delta = 0$ in Theorem 10. So all conditions of Theorem 10 are satisfied. Therefore, the equilibrium point of system (73) is globally exponentially stable, and the exponential convergence rate is equal to μ, where $\mu > 0$ satisfies

$$\mu + e^{0.17\mu} - 2.885 < 0. \tag{78}$$

If $d_k^{(1)}, d_k^{(2)}$ in above example are given as follows:

$$d_k^{(1)} = \begin{cases} \sqrt{2.2} - 1, & k = 2n - 1, \\ \sqrt{0.23} - 1, & k = 2n,\ n \in \mathbb{Z}_+, \end{cases}$$
$$d_k^{(2)} \begin{cases} \sqrt{1.7} - 1, & k = 2n - 1, \\ \sqrt{0.4} - 1, & k = 2n,\ n \in \mathbb{Z}_+, \end{cases} \tag{79}$$

then we finally get $\lambda_3 = -3.885 < -3.500, \delta = 0$. So all conditions of Theorem 10 are still satisfied. Therefore, the equilibrium point of system (73) is globally exponentially stable with impulses (79), and the exponential convergence rate is equal to μ, where $\mu > 0$ satisfies

$$\mu + 2.5e^{0.17\mu} - 2.885 < 0. \tag{80}$$

The simulation is shown in Figure 1(b). However, it is easy to check that the impulsive delayed Halanay inequality in [23, 26] is not feasible here. Thus our results can be applied to the case not covered in [23, 26].

5. Conclusion

The uniform asymptotic stability and global exponential stability of impulsive HNN with time delays are considered in this paper. Some new stability conditions are obtained by means of constructing the extended impulsive Halanay inequality, Lyapunov functional methods, and linear matrix inequality approach. Moreover, our results can be applied to the case not covered in some other existing criteria. Hence, the results extend and improve the earlier publications. An example is given to illustrate the feasibility of the results and the effects of impulses.

Acknowledgments

This work was jointly supported by the Project of Shandong Province Higher Educational Science and Technology Program (J12LI04), Research Fund for Excellent Young and Middle-Aged Scientists of Shandong Province (BS2012DX039), and National Natural Science Foundation of China (11226136, 11301308).

References

[1] Q. Zhang, X. Wei, and J. Xu, "Delay-dependent global stability condition for delayed Hopfield neural networks," *Nonlinear Analysis: Real World Applications*, vol. 8, no. 3, pp. 997–1002, 2007.

[2] Q. Zhang, X. Wei, and J. Xu, "Delay-dependent global stability results for delayed Hopfield neural networks," *Chaos, Solitons & Fractals*, vol. 34, no. 2, pp. 662–668, 2007.

[3] R. Rakkiyappan and P. Balasubramaniam, "On exponential stability results for fuzzy impulsive neural networks," *Fuzzy Sets and Systems*, vol. 161, no. 13, pp. 1823–1835, 2010.

[4] X. Liao and D. Xiao, "Globally exponential stability of Hopfield neural networks with time varying delays," *Acta Electronica Sinica*, vol. 28, no. 4, pp. 87–90, 2000.

[5] Y. Zhang and J. Sun, "Stability of impulsive neural networks with time delays," *Physics Letters A*, vol. 348, no. 1-2, pp. 44–50, 2005.

[6] Z. C. Yang and D. Y. Xu, "Global exponential stability of Hopfield neural networks with variable delays and impulsive

effects," *Applied Mathematics and Mechanics*, vol. 27, pp. 1517–1522, 2006.

[7] X. Li and X. Fu, "Global asymptotic stability of stochastic Cohen-Grossberg-type BAM neural networks with mixed delays: an LMI approach," *Journal of Computational and Applied Mathematics*, vol. 235, no. 12, pp. 3385–3394, 2011.

[8] X. Li, "Global robust stability for stochastic interval neural networks with continuously distributed delays of neutral type," *Applied Mathematics and Computation*, vol. 215, no. 12, pp. 4370–4384, 2010.

[9] Y. Xia, Z. Yang, and M. Han, "Synchronization schemes for coupled identical Yang-Yang type fuzzy cellular neural networks," *Communications in Nonlinear Science and Numerical Simulation*, vol. 14, no. 9-10, pp. 3645–3659, 2009.

[10] D. D. Baĭnov and P. S. Simeonov, *Systems with Impulsive Effect Stability Theory and Applications*, Ellis Horwood, New York, NY, USA, 1989.

[11] X. Fu, B. Yan, and Y. Liu, *Introduction of Impulsive Differential Systems*, Science Press, Beijing, China, 2005.

[12] Y. Xia, "Impulsive effect on the delayed cohen-grossberg-type BAM neural networks," *Neurocomputing*, vol. 73, no. 13–15, pp. 2754–2764, 2010.

[13] Y. Xia and P. J. Y. Wong, "Global exponential stability of a class of retarded impulsive differential equations with applications," *Chaos, Solitons & Fractals*, vol. 39, no. 1, pp. 440–453, 2009.

[14] A. O. Ignatyev, "On the stability of invariant sets of systems with impulse effect," *Nonlinear Analysis: Theory, Methods & Applications A*, vol. 69, no. 1, pp. 53–72, 2008.

[15] Z. Guan and G. Chen, "On delayed impulsive Hopfield neural networks," *Neural Networks*, vol. 12, no. 2, pp. 273–280, 1999.

[16] Z. Guan, J. Lam, and G. Chen, "On impulsive autoassociative neural networks," *Neural Networks*, vol. 13, no. 1, pp. 63–69, 2000.

[17] R. Rakkiyappan, P. Balasubramaniam, and J. Cao, "Global exponential stability results for neutral-type impulsive neural networks," *Nonlinear Analysis: Real World Applications*, vol. 11, no. 1, pp. 122–130, 2010.

[18] X. Li and R. Rakkiyappan, "Impulse controller design for exponential synchronization of chaotic neural networks with mixed delays," *Communications in Nonlinear Science and Numerical Simulation*, vol. 18, no. 6, pp. 1515–1523, 2013.

[19] X. Liu, K. L. Teo, and B. Xu, "Exponential stability of impulsive high-order Hopfield-type neural networks with time-varying delays," *IEEE Transactions on Neural Networks*, vol. 16, no. 6, pp. 1329–1339, 2005.

[20] S. Mohamad, K. Gopalsamy, and H. Akça, "Exponential stability of artificial neural networks with distributed delays and large impulses," *Nonlinear Analysis: Real World Applications*, vol. 9, no. 3, pp. 872–888, 2008.

[21] H. Gu, "Mean square exponential stability in high-order stochastic impulsive BAM neural networks with time-varying delays," *Neurocomputing*, vol. 74, no. 5, pp. 720–729, 2011.

[22] Y. Zhang, "Robust exponential stability of uncertain impulsive neural networks with time-varying delays and delayed impulses," *Neurocomputing*, vol. 74, no. 17, pp. 3268–3276, 2011.

[23] Z. Yang and D. Xu, "Stability analysis of delay neural networks with impulsive effects," *IEEE Transactions on Circuits and Systems I*, vol. 52, pp. 517–521, 2005.

[24] X. Liao, G. Chen, and E. N. Sanchez, "LMI-based approach for asymptotically stability analysis of delayed neural networks," *IEEE Transactions on Circuits and Systems I*, vol. 49, no. 7, pp. 1033–1039, 2002.

[25] X. Fu and X. Li, "Global exponential stability and global attractivity of impulsive Hopfield neural networks with time delays," *Journal of Computational and Applied Mathematics*, vol. 231, no. 1, pp. 187–199, 2009.

[26] J. Zhou, L. Xiang, and Z. Liu, "Synchronization in complex delayed dynamical networks with impulsive effects," *Physica A*, vol. 384, no. 2, pp. 684–692, 2007.

Hindawi Publishing Corporation
Abstract and Applied Analysis
Volume 2013, Article ID 308675, 10 pages
http://dx.doi.org/10.1155/2013/308675

Research Article

Crime Busting Model Based on Dynamic Ranking Algorithms

Yang Cao,[1] Xiaotian Xu,[2,3] and Zhijing Ye[1]

[1] *College of Telecommunications and Information Engineering, Nanjing University of Posts and Telecommunications, Nanjing 210023, China*
[2] *College of Overseas Education, Nanjing University of Posts and Telecommunications, Nanjing 210023, China*
[3] *School of Engineering and Computing Sciences, New York Institute of Technology, Old Westbury, NY 11568-8000, USA*

Correspondence should be addressed to Yang Cao; caoyeacy@njuptsast.org

Received 28 May 2013; Accepted 11 June 2013

Academic Editor: Xinsong Yang

This paper proposed a crime busting model with two dynamic ranking algorithms to detect the likelihood of a suspect and the possibility of a leader in a complex social network. Signally, in order to obtain the priority list of suspects, an advanced network mining approach with a dynamic cumulative nominating algorithm is adopted to rapidly reduce computational expensiveness than most other topology-based approaches. Our method can also greatly increase the accuracy of solution with the enhancement of semantic learning filtering at the same time. Moreover, another dynamic algorithm of node contraction is also presented to help identify the leader among conspirators. Test results are given to verify the theoretical results, which show the great performance for either small or large datasets.

1. Introduction

Nowadays, many crimes are committed by collaboration of conspirators. Therefore, with the interconnections of conspirators, a complicated conspirator network can be spawned. However, many conspirators still sustain their social ties with the outside, and thus conspirator network often hides in a greater social network.

To identify the hidden conspirators' network from a complex social network, it calls for us to discover the hidden conspirators' network and analyze its unique features to detect the leader. Those features of networks can be captured from various information, such as topological properties of the network, semantic network analysis of their messages interactions, and other prior knowledge, which contains known conspirators, known nonconspirators, and background of the entire social network.

To study this network, manual approach is the most comprehensive method. However, it would become extremely ineffective and inefficient with large database. From many pervious work [1–4], to deal with the problem of large database, people have used the graphic-based centrality measures of network to study the characteristics of conspirators. Criminals with high betweenness centrality are usually brokers, while those with high degree centrality appreciate better profit by running higher risks [1]. Morselli also proposed that leaders of a criminal organization tend to balance profit and risk by making a careful trade-off between out-degree and betweenness centrality [2].

However, those static centrality approaches, which only utilize graphical properties, tend to overlook many other imperative analytical information such as the network topology, the sematic meaning of people's interactions. Therefore, the idea of complex network analysis, including subnetwork detection and block-modeling, has been introduced to detect the inner patterns of interactions between social actors [3]. Despite they shed light on the internal structures of networks, these approaches are still burdened with intimidating complexity with large databases.

Inspired by the discussions above, the suspicious ranking system must be modified carefully to combine these pieces of information with network topology and centrality. Meanwhile, topics with higher frequency and more contacts to known conspirators may increase the crime probability. To provide a better solution to this problem, an advanced dynamic network mining approach with semantic network

analysis will be introduced in this paper. Notably, based on modifying the definition of centrality, dynamic cumulative nominating algorithm to measure each people's suspicion will be adopted to serve our model better, which will reduce computational expensiveness than most other topology-based approaches. In the meantime, with the enhancement of semantic learning, the accuracy of solution will be also increased. Furthermore, with deeper analysis of the structure of the possible conspirator network, node contraction algorithm will be presented to help identify the leader among conspirators. As a final point, the traditional centrality approach is also performed to verify the inner agreement and connection with our approach. Through that way, a priority list based on the possibility of the suspect and suspect's leader rank will be dynamically adjusted with new clues added. Eventually, the model will be promoted into a more common place which can be applied in other networks.

The algorithms will be tested with the data from ICM 2012 problem [5] which shows the great performance for either small or large datasets.

2. Overall Assumptions and Preliminaries

2.1. Overall Assumptions

(i) A conspirator knows all other members in the conspiracy.

(ii) A nonconspirator does not know who conspirators are and hence treats conspirators and nonconspirators equally.

(iii) A conspirator is reluctant to mention to an outsider topics related to crime.

(iv) Conspirators tend not to talk frequently with each other about irrelevant topics.

(v) The leader of the conspiracy is the most inseparable of the whole conspirators' network.

(vi) The information of known conspirators and nonconspirators is valid.

(vii) The information offered in materials is complete and reliable. All the messages and the topics represent their thoughts, ignoring that someone lies during the eavesdropping.

2.2. Models Preliminaries

2.2.1. Degree. Degree is defined as the number of edges linked to a node in graph. It can be written as $\deg(v)$. In directed graph, the number of incident edges is input degree $\deg_{\text{in}}(v)$. The number of emergent edges is output degree $\deg_{\text{out}}(v)$.

2.2.2. Centrality. Centrality of nodes indicates the relative importance of nodes within a graph. It can be utilized to determine the center of the suspicious network. Here are three popular types of centrality.

(i) Degree Centrality. Degree centrality refers to the centrality of a node with respect to other adjacent nodes. In suspicious network, it reflects activeness of a member. More links to a member means more possible the member be the leader. For a given graph $G := (V, E)$ with V set of nodes and E set of edges, the normalized degree centrality of node i is

$$C_D(i) = \frac{\sum_{j=1}^{N} K\left(e_{ij}\right)}{N-1}, \quad i \neq j, \tag{1}$$

where $K(e_{ij})$ = the number of conversations between v_i and v_j. e_{ij} = binary variable represents whether there is a link between two nodes. If there is one or more conversation from v_i to v_j, $e_{ij} = 1$, otherwise the value is 0; $N = \text{count}(v_j)$.

(ii) Betweenness Centrality. Betweenness centrality measures how much a node acts as a medium along the shortest path between two other nodes. It helps analyzing who has bigger possibility to be an intermediary to exchange information between two other members. Member with high betweenness centrality also plays an important role in suspicious networks. The normalized betweenness centrality is

$$C_B(i) = \frac{\sum_{j=1}^{N} \sum_{k<j}^{N} \omega_{j,k}(i)}{N-1}, \quad i \neq j, \tag{2}$$

where $\omega_{j,k}$ shows whether the shortest path between two nodes passing node i.

2.2.3. Symbol Chart. For some symbol and their meaning, see Table 1.

Table 1: Symbol.

Symbols	Meaning
$\deg(v)$	Degree of a node
$C_D(i)$	Degree centrality
$C_B(i)$	Betweenness centrality
$\omega_{j,k}$	The shortest path between two nodes passing node i
l	Number of topics in one conversation
$K(e_{ij})$	The number of conversations with same person
$\widetilde{q_i^{n+1}}$	The nomination score of the node v_i after $(n+1)$ iteration
q_i^n	The normalized nomination score of the node v_i after n iteration
a_{ij}	The element in the adjacent matrix of the effect network
w_t	Empirical weight of topic's effect, in our case $w_t = 15$
$T(v_{ij})$	Unified topic's suspicion degree, from v_j to v_i

3. Analysis of Suspicious Topics

3.1. Statistical Analysis. Topics among known conspirators are important information which can be utilized to analyse conspirator's characteristics on choosing topics. According to the statistical characteristics, some unknown conspirators can be unearthed and some people's suspicion can be eliminated.

Table 2: Topics among known conspirators.

	Jean	Alex	Elsie	Paul	Ulf	Yao	Harvey
Jean		**11***			8		14
Alex			1	**13***	**11***	3, **7***	
Elsie		**11***			**13***		
Paul	**11***		**7***		**7***		4
Ulf		**7***, **11***, **13***				**13***	
Yao	**13***	**7***, **11***, **13***	**7***, 9		**13***		2, **7***
Harvey						**13***	

Suspicious topics are in bold with *.

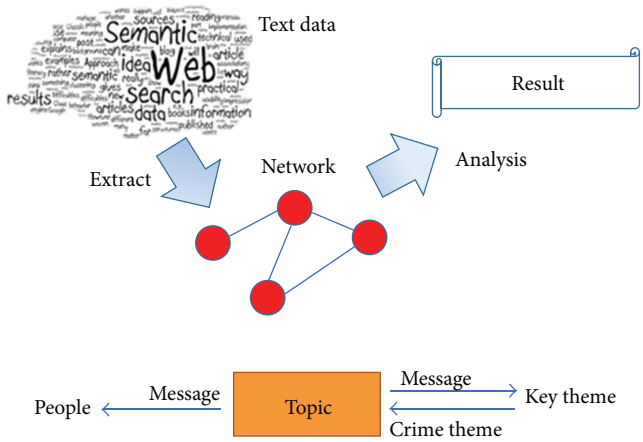

Figure 1: Semantic network analysis procedure.

After analyzing the test data from ICM 2012, Table 2 displays the topics relation matrix among known conspirators, and then Table 3 illustrates the comparison of suspicious topic among different kinds of groups. As we know, conspirators usually talk about known suspicious topics (topics 7, 11, 13) and rarely mention irrelevant topics to other conspirators. Therefore, a suspect person is more likely to be a conspirator if conspirators often talk about suspicious topics with him. Conversely, a person who often receives irrelevant information is probably innocent.

To sum up, the conclusion is as follows.

(i) Topic 13 has more conspiracy possibility than topics 11, 7.

(ii) Topic 11 has more suspects involved. It is an active topic among the suspects and conspirators.

(iii) Topic 7 has larger frequency among suspects.

3.2. Semantic Network Analysis

3.2.1. Background. Semantic network is a network which represents semantic relations between concepts. This is often used as a form of knowledge representation. It is a directed or undirected graph consisting of vertices, which represents concepts and edges. Semantic network analysis, a machine learning technique to analyse large amount of messages in the foundation of semantic network, is commonly used in search engines. It can predict user's identity and inclination according to the frequently used searching words of the user. So, semantic analysis can be used to separate given topics into more detailed parts [6].

The term text analysis describes a set of linguistic, statistical, and machine learning techniques that model and structure the information content of textual sources for business intelligence, exploratory data analysis, research, or investigation. It attaches importance only to the text itself [7, 8]. Semantic network analysis represents human's knowledge and text analysis puts an emphasis on textual data processing. The procedure of semantic network analysis is demonstrated in Figure 1.

3.2.2. Basic Assumptions

(i) The meaning of a word could be represented by the set of its verbal associations [9].

(ii) Social network analysis is based on an assumption of the importance of relationships among interacting units [10].

3.2.3. Step Procedures and Results

Step 1. Series of suspicious words and themes related to crime will be extracted from the known suspicious messages in Topic.xls.

After machine learning of topic semantic diffusion [11], four suspicious factors are chosen by the system as follows:

(1) *Economic information*

(2) *Spanish words*

(3) *Codes*

(4) *Known conspirators' names.*

Step 2. It is easy for us to analyze the connection between the original topics and suspicious topics. Then we sort out topics that are related to these pieces of criminal information exacted. So, more topics are related to crime. We called the topics that were not suspicious topics and did not contain the key theme or word as normal topic.

Step 3. Since the number of conspiratorial topics has increased, in order to distinguish the degree of suspicion, we assign different topics to different weights again, depending on how much they are related to crime. In the process of calculating the topic weight, 4 variables i_1, i_2, i_3, i_4 are promoted to represent these 4 factors. The value of the four variables is either 1 or 0. Then, the suspicion degree of topics based on four factors can be presented as

$$\deg_s = k_1 i_1 + k_2 i_2 + k_3 i_3 + k_4 i_4, \quad (3)$$

where k_1, k_2, k_3, k_4 are coefficients of each factor and $k_1 + k_2 + k_3 + k_4 = 1$.

In order to simplify analysis, we assign same importance to the four factors, which means $k_1 = k_2 = k_3 = k_4 = 0.25$.

Table 3: Suspicious topics frequency comparison.

	Innocent-innocent	Innocent-conspirators	Innocent-suspect	Suspect-conspirators	Conspirators-conspirators
Topic 7*	0%	0%	8.03%	12.28%	**25%**
Topic 11*	0%	0%	4.16%	8.77%	**21.43%**
Topic 13*	0%	9.09%	0%	5.26%	**28.57%**
Sum	0%	9.09%	12.5%	26.3%	**75%**

Table 4: The suspicion degree of topics.

Topic	Suspicious keywords	$\deg_s$
1	Stock price (1)	0.25
2	Spanish (2)	0.25
3		0
4	Paige (4)	0.25
5	Security (3), Chris (4)	0.5
6	Paige (4)	0.25
7*	Spanish (2), codes (3), (4)	0.75
8		0
9	Jean (4)	0.25
10		0
11*	Accounting (1), flaws (3), (4)	0.75
12	Spanish (2)	0.25
13*	Key in the conspiracy plan	1
14	High price (1)	0.25
15	Computer security (3), Paige (4)	0.5

Table 5: 5 types of topics.

	Type 1	Type 2	Type 3	Type 4	Type 5
Topics	13*	7*, 11*	5, 15	1, 2, 4, 6, 9, 12, 14	3, 8, 10
$\deg_s$	1	0.75	0.5	0.25	0

According to former equation, the suspicion degrees of all 15 topics are shown in Table 4.

Based on the suspicion degree of each topic, 15 topics can be divided into 5 types as shown in Table 5.

Similar to pervious statistical analysis, Tables 4 and 5 suggest that suspicious topics 7, 11, 13 are highly relevant to crime for their bigger weight. Topics 5, 15 show some clues about crime and other topics indicate little connections with crime.

Step 4. In order to simplify the situation of multitopic and multiconversation with the same person, a unified topic suspicion degree of topic is defined in terms of each topic's suspicion degree. For conversation with multitopics, the suspicion degree of each topic is sum up to as the numerator of the unified topic suspicion degree. For the situation of multiconversation with same person for more than one time, an average value will be calculated. Therefore, the unified topic suspicion degree can be represented as

$$T\left(v_{ij}\right) = \frac{\sum_{k=1}^{K(v_{ij})} \sum_{l} \deg_s}{K\left(e_{ij}\right)}; \quad v_{ij} \neq 0 \text{ or } K\left(v_{ij}\right) \geq 1, \tag{4}$$

where l = number of topics in one conversation and $K(e_{ij})$ = the number of conversations between v_i and v_j.

This suspicion degree is a significant indicator to determine a person's identity.

4. Cumulative Nominating Algorithm

4.1. Algorithm Descriptions. The likelihood of conspirators' nodes in the social network can be regarded as the reputation in the small network of conspirators. Thus, the priority list can be obtained from the algorithm of cumulative nominating. The nomination scores indicate the importance of a particular node in the small network of conspirator, which reflect the suspicious degree of a suspect. This algorithm can be specifically described as 4 simple principles [12].

(1) The new nomination of a node not only includes its pervious nomination scores but also contains the effect of the pervious nomination scores of nodes which it is connected to. To sum up, the nomination score includes 2 parts: pervious scores and effect of others [13, 14].

(2) The effect of others includes other's scores, topic, and the manage identity.

(3) The initial nomination scores are the conditions of the problem, which is conspirators = 1, suspect = 0.5, and innocent people = 0. Normalization is done after each term of nomination in order to adapt to different size networks.

(4) After enough time of nomination cycle, when the nomination scores of suspect are enough for discrimination but not higher than the score of known conspirator, we believe that the irritation can be stopped and the higher cumulative nomination scores, the higher suspicious degree.

The entire cumulative process can be express as

$$\widetilde{q_i^{n+1}} = q_i^n + \sum_j a_{ij} q_j^n, \tag{5}$$

where $\widetilde{q_i^{n+1}}$ = the nomination score of the node v_i after $(n+1)$ iteration, q_i^n = the normalized nomination score of the node v_i after n iteration, and a_{ij} = the element in the adjacent matrix of the effect network.

Considering the effect of topic and the manage identity, a_{ij} can be defined as

$$a_{ij} = \frac{w_t \cdot T\left(e_{ji}\right) - w_m \cdot e_{ji} \cdot M\left(v_i\right)}{\deg_{\text{out}}\left(v_j\right) + 1}, \tag{6}$$

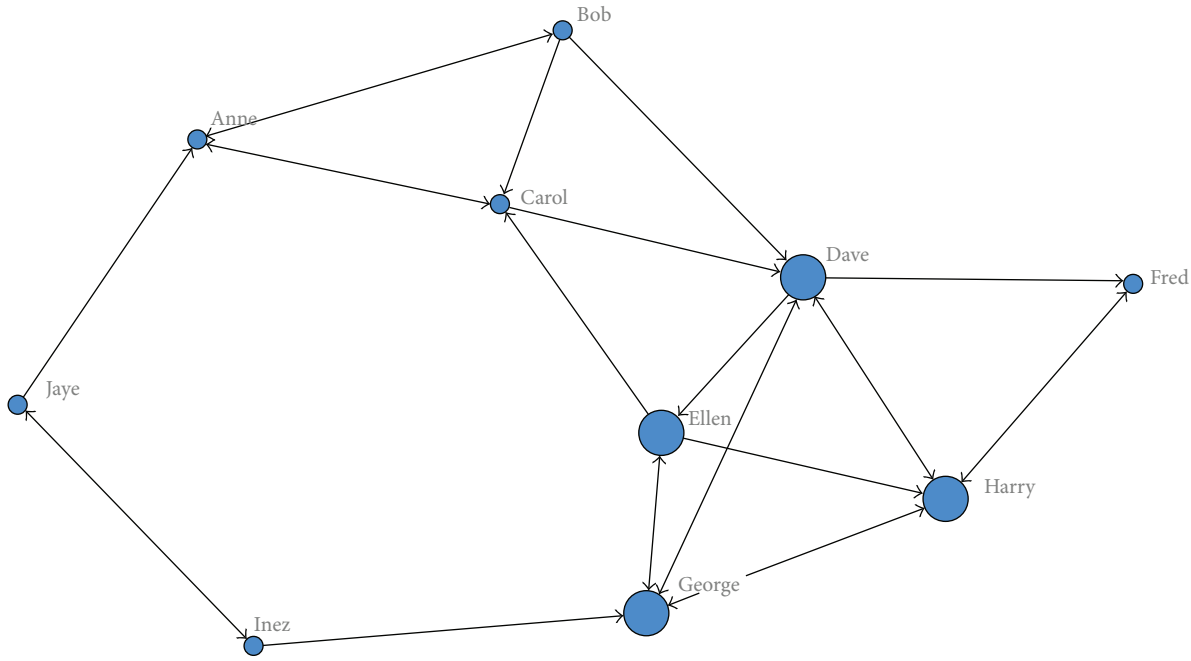

Figure 2: Topological clustering results of EZ case.

where w_t = empirical weight of topic's effect, in our case $w_t = 15$, $T(e_{ji})$ = unified topic's suspicion degree, from v_j to v_i, and w_m = empirical weight of manage identity's effect, in our case $w_m = 1$; $M(v_j)$ = binary keying variable, if v_j is a senior manager, $M(v_j) = 1$, otherwise the value is 0. (The senior manager is able to talk more sensitive topics, while others who talk those topics seem suspicious.)

In order to adapt the model to network with different size, normalization is required to be done after each term of iteration. Because of this, the normalized nomination function can be expressed as

$$q_i^{n+1} = \begin{cases} 1 & \widetilde{q_i^{n+1}} \geq 1 \\ N \cdot \widetilde{q_i^{n+1}} & 0 < \widetilde{q_i^{n+1}} < 1 \\ 0 & \widetilde{q_i^{n+1}} \leq 0 \end{cases} \tag{7}$$

whereby $\sum_i q_i^n = \sum_i q_i^0$, $q_i^n \in [0, 1]$;

$$\text{Normalization parameter } N = \frac{\sum_i q_i^0 - \text{count}\left(q_i^{n+1} = 1\right)}{\sum_{q_i^{n+1} \neq 1} \widetilde{q_i^{n+1}}}. \tag{8}$$

Known conspirators $q_i^0 = 1$, suspect $q_i^0 = 0.5$, and known innocent people $q_i^0 = 0$.

During the iteration, if $\text{count}(q_i^{n+1} = 1) > \text{count}(q_i^0 = 1)$, the iteration can stop and the final priority list is obtained based on the nomination score q_i^n.

4.2. Case Validation. Here, we use two given cases from ICM 2012 to verify our algorithm.

4.2.1. EZ Case. EZ case can be utilized to verify our model because of its similar suspicious network, small data quantity, and known result. Given data of EZ case will be substituted into the cumulative nominating algorithm in our model. The supervisor has offered some information:

(1) Dave, George are known conspirators and Anne, Jaye are known nonconspirators;

(2) 28 messages with 5 topics among 10 people;

(3) Ellen, Carol were found based on supervisor's analysis, but Carol was misjudged;

(4) Bob admitted his involvement in conspiracy;

(5) supervisor was pretty sure that Inez was involved.

After degree clustering, the topological results of EZ case are shown in Figure 2. In addition, based on semantic analysis, topics 1, 3, 5 are considered as suspicious topics and, respectively, weighted as 1, 1, and 1. Other topics are weighted as 0.

Test result is shown in Figure 3.

The test result shows that Dave, George, Inez, Jaye, and Ellen are the top five of all 10 people. This result is partly same to supervisor's result.

Moreover, Inez is identified by our model and Carol is also misjudged. The test result also corresponds with known result.

Bob shows low possibility in our result because he has few conversations with other people especially known conspirators and he often talks about nonsuspicious topics.

Therefore, our analysis model displays higher accuracy than supervisor's model.

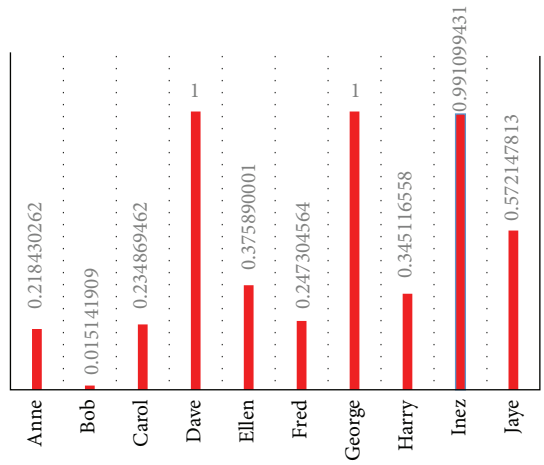

Figure 3: Priority list of EZ case.

4.2.2. Complex Case. The following are information that ICM 2012 has previously provided to us [5]:

(i) all 83 office workers' names;

(ii) 15 short descriptions of the topics;

(iii) 364 links of the nodes that transmit messages and the topic code numbers;

(iv) 7 known conspirators: Jean, Alex, Elsie, Paul, Ulf, Yao, and Harvey;

(v) 8 known nonconspirators: Darlene, Tran, Jia, Ellin, Gard, Chris, Paige, and Este;

(vi) senior managers of the company: Jerome, Delores, and Gretchen.

Two new clues are added as follows:

(i) topic 1 is also connected to the conspiracy;

(ii) Chris is one of the conspirators.

(1) Without New Clues. For complex case, ICM has offered us some information as shown below:

(i) 364 links of the nodes that transmit messages and the topic code numbers;

(ii) 7 known conspirators: Jean, Alex, Elsie, Paul, Ulf, Yao, and Harvey;

(iii) 8 known nonconspirators: Darlene, Tran, Jia, Ellin, Gard, Chris, Paige, and Este;

(iv) senior managers of the company: Jerome, Delores, and Gretchen.

After degree clustering, the topological results of complex case are shown in Figure 4. According to the given data in "Messages.xls", "Names.xls", and Topics.xls, a priority list based on cumulative nominating algorithm that shows the likelihood of one's being conspirator is obtained in Figure 5.

(2) With New Clues. New clues: topic 1 is also connected to the conspiracy and Chris is one of the conspirators.

After changing Chris's $q^0 = 1$, and changing Topic 1's $\deg_s = 1$, the result is obtained as Figure 6.

Even though the new clues cannot coincide with the original one, the former actually fluctuates slightly surrounding the latter. That is to say, they are quite similar to some extent. As to the big difference of the last node (Chris), it is a result when Chris becomes a known conspirator. Therefore, the model still works well and the list remains stable even if some conditions have changed.

After the iterative computation, the known conspirators' scores remain equal to one, while some known innocent persons' scores change rapidly, which is reasonable because in later clues some known innocent persons may also change into the conspirators, like Chris.

However, this algorithm cannot distinguish the possible leader from the known conspirators and high suspicious suspects because the nomination scores of known conspirators are all the same equal to one.

5. Node Contraction Algorithm

5.1. Algorithm Description. The model based on cumulative nomination algorithm cannot clearly differentiate nodes with high score. Hence, a new analyzing method should be introduced to compare the difference among nodes within conspiracy. The leader can be finally identified by this method.

Node contraction method [15–17] combines the node to be measured with its adjacent nodes into a new node and compares the importance of each contracted node based on its network agglomeration degree. This method suggests that the most important node is the one whose contraction leads to the largest increase of the networks agglomeration. Both degree and position are considered in node contraction.

Assume v_i is a node within graph $G = (V, E)$, the adjacent nodes of v_i with total number of k_i will combine with v_i, and then a new node v_i' substitutes the original $k_i + 1$ nodes.

As shown in Figure 7, if a node's agglomeration degree is $\Phi(G)$, the contracted agglomeration degree can be represented as $\Phi(G * v_i)$. If v_i is really important, the contracted network can be well agglomerated [18, 19].

The agglomeration degree of network depends on two factors, the connection ability among each node and the amount of nodes within the network N. The connection ability can be measured by an average distance L which refers to the mathematical average of distance between two nodes (node pair). The agglomeration degree of network is defined as

$$\Phi(G) = \frac{1}{N \times L} = \frac{N-1}{\sum_{i \neq j} d_{ij}}, \tag{9}$$

where $N \geq 2$, d_{ij} = distance between v_i and v_j, $0 < \Phi \leq 1$.

Then, the importance of node v_i is expressed as

$$\mathrm{IMC}(v_i) = \left[1 - \frac{\Phi(G)}{\Phi(G \cdot v_i)}\right] \cdot q_i, \tag{10}$$

where $G \cdot v_i$ = graph after contraction of v_i.

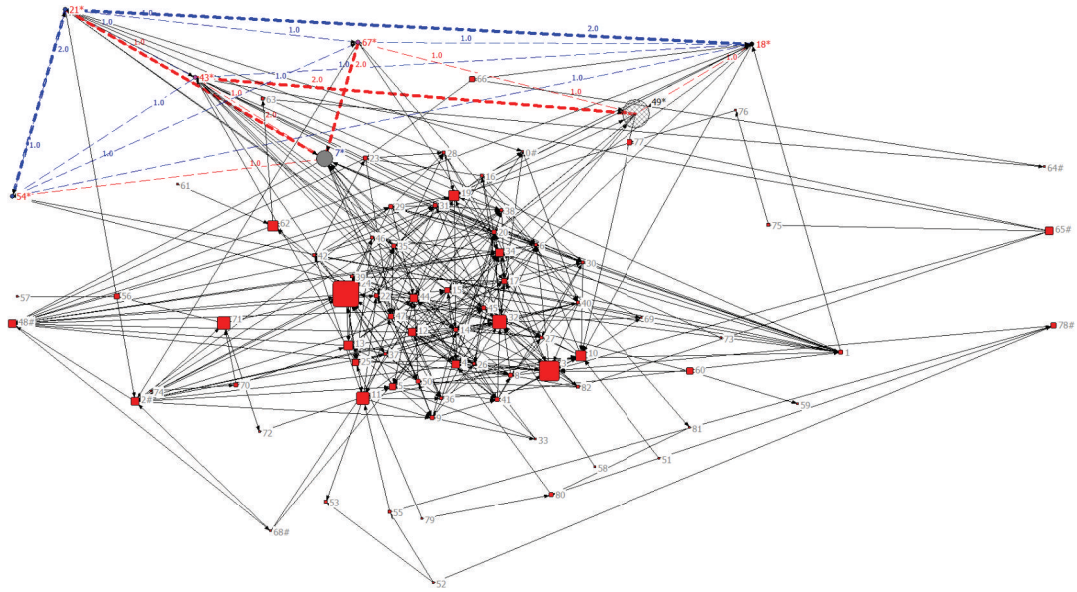

Figure 4: Topological clustering results of complex case.

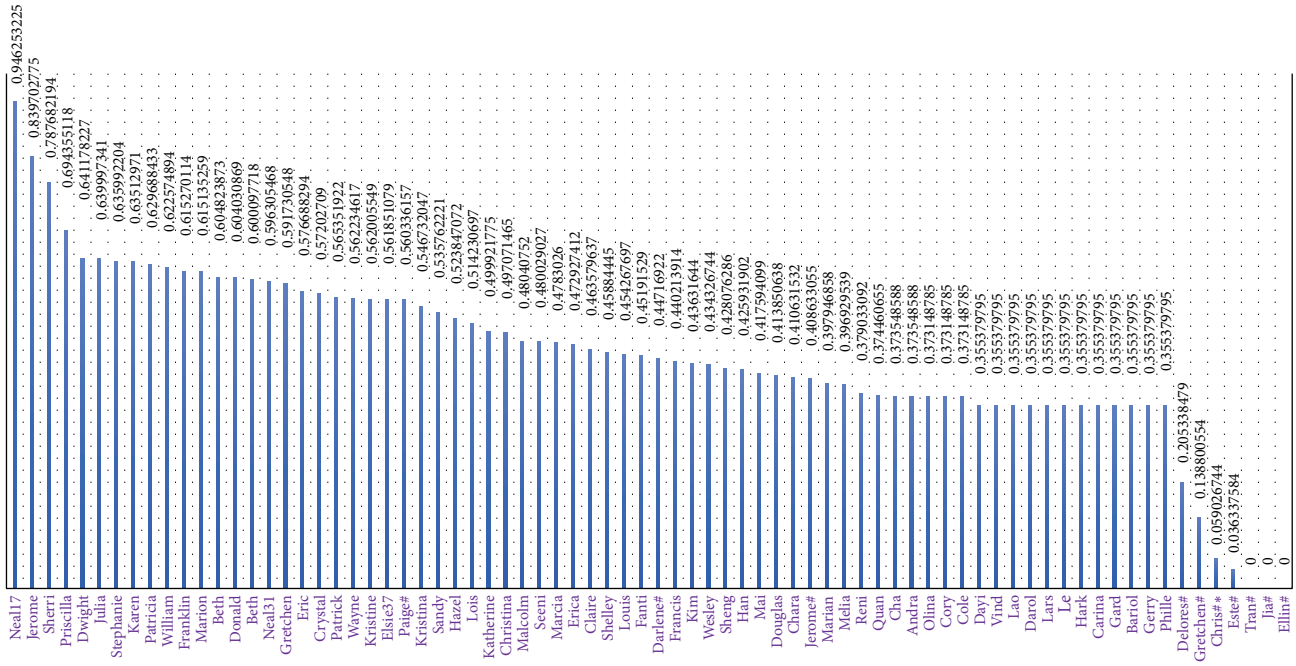

Figure 5: Suspect nomination priority list without new clues.

The node v_i plays more important role if it has more links k_i, because more other node pairs' shortest paths pass through it and the average distance after contraction will be highly reduced. In a conspiracy, the leader often connects with more people than other conspirators and messages between two subordinates often pass through the leader. This two properties can indicate a person's importance.

Basic steps of node contraction are shown below.

Step 1. Calculate the distance between a node pair (v_i, v_j), which is d_{ij}.

Step 2. Calculate the initial agglomeration degree $\Phi(G)$ of the network.

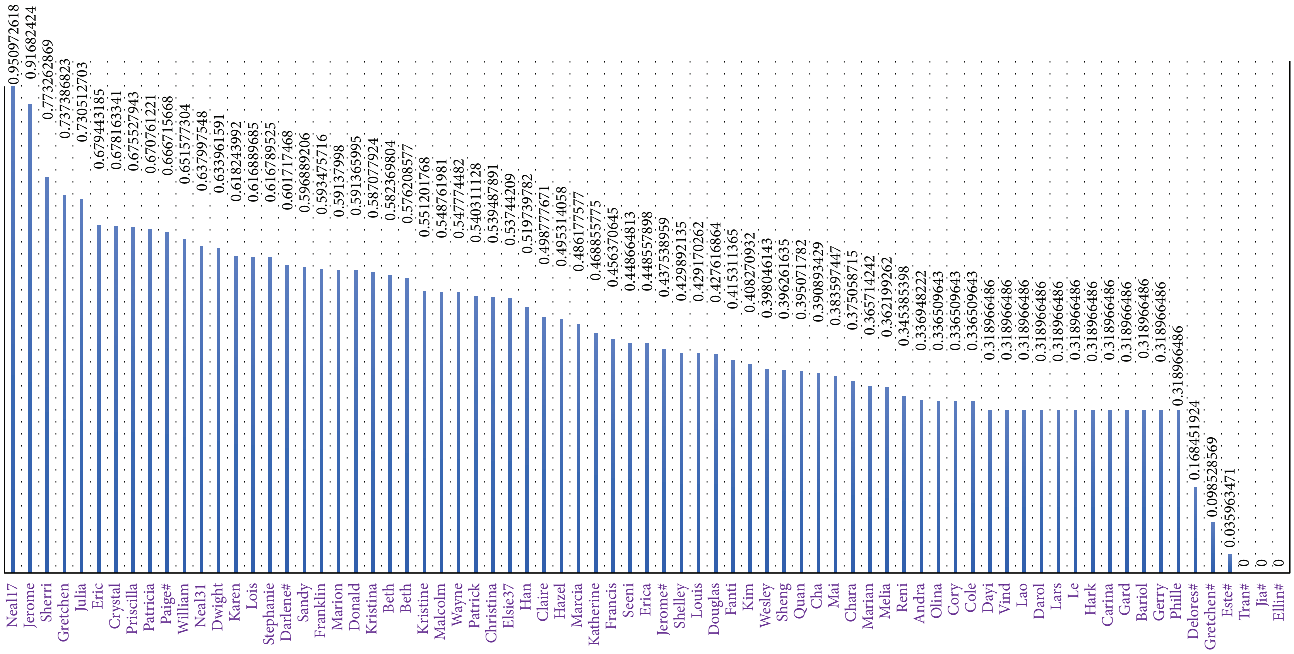

FIGURE 6: Suspect nomination priority list with new clues.

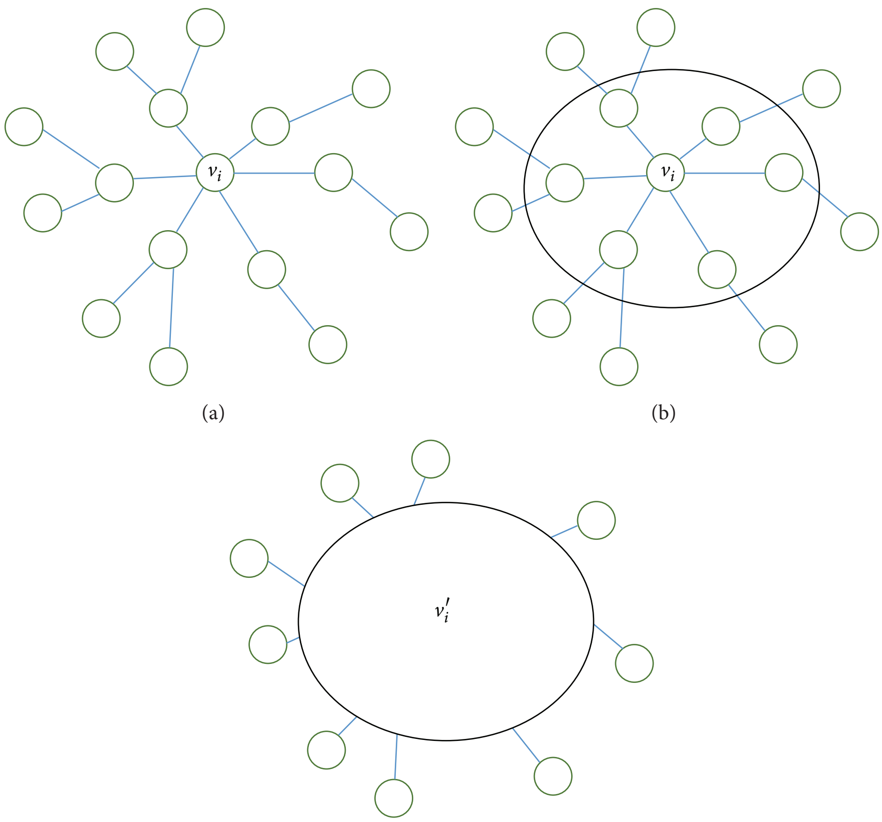

(a) (b) (c)

FIGURE 7: Illustration of node contraction.

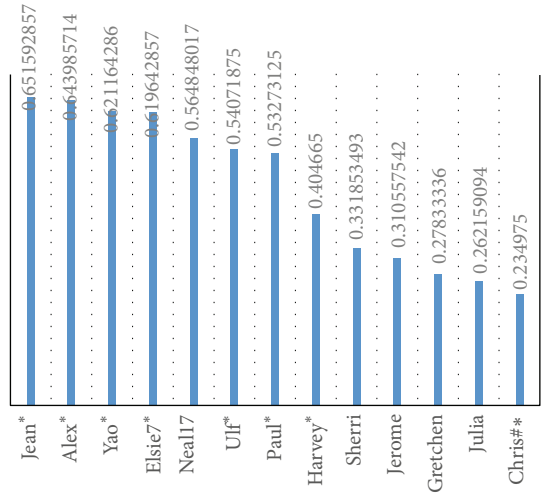

Figure 8: Leader Rankbased on IMC.

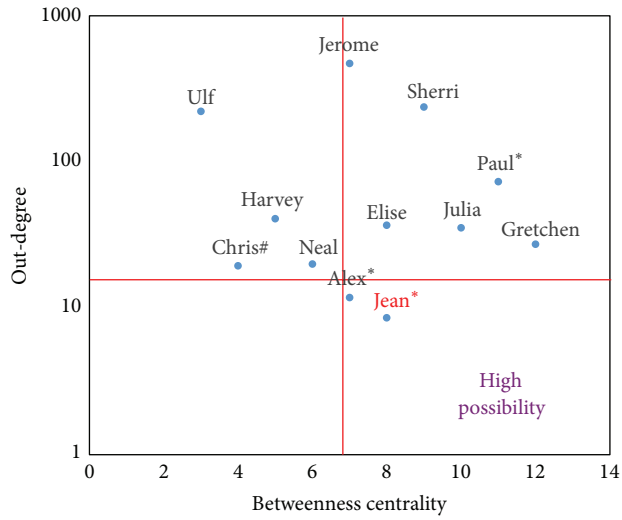

Figure 9: Joint distribution of betweenness centrality and out-degree. (Yao's out-degree is 0, which means he could not be the leader empirically.)

Step 3. Calculate the importance of v_i.

(a) Calculate d'_{lj} of all node pairs (v_l, v_j) after contraction.

(b) Calculate $\Phi(G * v_i)$.

(c) Calculate $\mathrm{ICM}(v_i)$.

5.2. Leader Rank Result. Suspicion score q_i of each node can be obtained from results of former model. Nodes with suspicion score bigger than 70% can be taken into node contraction method. Because the final purpose is identifying the leader, we only consider people with high suspicion score and compare the importance of these people. The person with biggest importance value is judged as leader of the conspiracy. The result is shown in Figure 8.

From Figure 8, Jean ranks first among all 13 people. So, Jean can be considered to be the leader of the conspiracy network.

5.3. Centrality Theory Support. Centrality-based analysis of criminal networks finds that a leader of a criminal organization tends to carefully balance out-degree and betweenness-centrality. It has been proposed that the leader usually maintains a high betweenness centrality but a relatively low out-degree, for enhancing efficiency while ensuring safety [2].

In Figure 9, Jean has high relatively betweenness centrality with relatively low out-degree, which is in accord with his identity of a leader. Thus, our conclusion that Jean is the leader is thus empirically supported by centrality theory.

6. Model Promotion

Networks have a typical pattern that they all consist of nodes and links. In most cases, nodes and links contain many related information. So, such kind of network can be analyzed by mathematical method. For our model takes full account of interactions among nodes and weights of different related information, it can also be utilized in other similar cases, such as: social network and biological network.

A common approach of network analysis is presented below.

(1) Observe the characteristics of the network and transform the complex relations among each individual into an abstract mathematical network with each individual as nodes and relations as links or edges.

(2) If detailed information of the network is unknown, figure out the basic parameters of each node within the network, degree and centrality. These parameters can roughly reflect the importance of each person.

(3) For some certain cases, semantic network analysis should be applied to weigh the suspicion degree to increase accuracy. What is more, the effect of interconnection among individuals should be considered. Combining suspicion degree with interaction, a cumulative score of each node can be calculated. After iteration, one can identify, prioritize, and categorize similar nodes in a network database.

(4) Use node contraction method to measure the importance of each individual within a small ensemble. The core of the network is the one with biggest importance.

In a contagion network, the source of disease can be found. Infected individuals and uninfected ones can be segregated by making use of our model. This model is beneficial for the institution of disease control and prevention to prevent contagion spreading.

7. Conclusions and Further Discussion

In this paper, we have proposed a crime busting model with two dynamic ranking algorithms—cumulative nominating

algorithm and node contraction algorithm in order to detect the likelihood of a suspect and their leader in a complex social network. The contributions and further discussion of our results are list as follows.

7.1. Contributions

(i) *Comprehensive*: we take both the message and node position into consideration for identifying, prioritizing, and categorizing. So, the solution of our model pursues high credibility, while reducing the misjudgment rate.

(ii) *Reasonable*: the result of our model matches perfectly with the experience, which proves the rationality and correctness of our model.

(iii) *Extendable*: the result of simulation shows that our model can be applied in other fields, not just crime busting.

(iv) *Flexible*: we cannot judge a person to be conspiratorial or innocent only based on the message traffic. Since everything may be an accident, our model has its false positive rate which allows the unexpected things to happen.

7.2. Further Discussion. In fact, our research on crime network is just remaining in the beginning, and many problems are waiting to be done. First, the criminal psychology is not taken into consideration while some simple examples show that some people may lie during the taping. Second, since there is no clear criteria for the classification, those conspirators who are slightly behind may be changed while the conspirators ranking in the front remain unchanged.

In near future, many areas should be studied further, for instance, how to apply semantic network analysis more efficiently to discover the potential linkage between the messages and scientifically classify them into different groups, how to dynamically and automatically select reasonable criteria for the classification, and so forth.

Appendix

Data Declarations for ICM 2012 Problem

(i) "Elsie" is given as one of the known conspirators. It is an important data in this problem. However, there are two "Elsie" with node number "7" and "37". According to some statistics about the message with suspicious topics, it suggests that Elsie with number 7 is more likely to be the known conspirator than the other Elsie. Therefore, we consider Elsie with node number 7 as known conspirator.

(ii) There are two "Gretchen" with node number "4" and "32." After analyzing some basic statistics, "Gretchen 32" is found to have more message exchanges than "Gretchen 4." For common sense, managers have more communication than others. So, Gretchen with node number 32 should be regarded as one of the senior managers in this problem.

(iii) "Topic 18" appears in line 215 of "Messages.xls," but "Topic.xls" only contains 15 topics. So, we ignore this data to correct the error.

(iv) "Dolores" is misspelled as "Delores" in "name.xls." This small error should be fixed.

References

[1] V. E. Krebs, "Mapping networks of terrorist cells," *Connections*, vol. 24, pp. 43–52, 2002.

[2] C. Morselli, "Assessing vulnerable and strategic positions in a criminal network," *Journal of Contemporary Criminal Justice*, vol. 26, no. 4, pp. 382–392, 2010.

[3] J. Xu and H. Chen, "Untangling criminal networks: a case study," in *Intelligence and Security Informatics*, vol. 2665, pp. 232–248, 2003.

[4] C. Arney and K. Coronges, "Judges' commentary: modeling for crime busting," *UMAP Journal*, vol. 33, no. 3, p. 293, 2012.

[5] COMAP, "2012 ICM problem," 2012, http://www.comap.com/undergraduate/contests/mcm/contests/2012/problems/.

[6] J. F. Sowa, "Semantic networks," in *Encyclopedia of Cognitive Science*, 2006.

[7] R. Feldman and J. Sanger, *The Text Mining Handbook: Advanced Approaches in Analyzing Unstructured Data*, Cambridge University Press, 2006.

[8] R. Bilisoly, *Practical Text Mining with Perl*, vol. 2, John Wiley & Sons, Hoboken, NJ, USA, 2008.

[9] M. Sharples, D. Hogg, C. Hutchinson, S. Torrance, and D. Young, *Computers and Thought: A Practical Introduction to Artificial Intelligence*, MIT Press, 1989.

[10] U. Gretzel, "Social network analysis: introduction and resources," 2001, http://lrs.ed.uiuc.edu/tse-portal/analysis/social-network-analysis/.

[11] Y. Freund, R. Iyer, R. E. Schapire, and Y. Singer, "An efficient boosting algorithm for combining preferences," *Journal of Machine Learning Research*, vol. 4, no. 6, pp. 933–969, 2003.

[12] A. Meaden and D. Hacker, *Problematic and Risk Behaviours in Psychosis: A Shared Formulation Approach*, Routledge, 2010.

[13] J. A. Zhang and X. E. Guo, "Trust model based on dynamic recommendation in P2P network," *Computer Engineering*, vol. 36, no. 1, pp. 174–180, 2010.

[14] F. Autrel, N. Cuppens-Boulahia, and F. Cuppens, "Reaction policy model based on dynamic organizations and threat context," in *Data and Applications Security XXIII*, vol. 5645 of *Lecture Notes in Computer Science*, pp. 49–64, Springer, 2009.

[15] Y. J. Tan, J. Wu, and H. Z. Deng, "Evaluation method for node importance based on node contraction in complex networks," *System Engineering Theory and Practice*, vol. 26, no. 11, pp. 79–83, 2006.

[16] M. Perkowitz and O. Etzioni, "Adaptive web sites: conceptual cluster mining," in *Proceedings of the 16th International Joint Conference on Artificial Intelligence*, pp. 264–269, July 1999.

[17] R. Cooley, B. Mobasher, and J. Srivastava, "Web mining: information and pattern discovery on the World Wide Web," in *Proceedings of the IEEE 9th IEEE International Conference on Tools with Artificial Intelligence*, pp. 558–567, November 1997.

[18] J. M. Kleinberg, "Authoritative sources in a hyperlinked environment," *Journal of the ACM*, vol. 46, no. 5, pp. 604–632, 1999.

[19] G. W. Flake, S. Lawrence, and C. L. Giles, "Efficient identification of web communities," in *Proceedings of the 6th ACM SIGKDD International Conference on Knowledge Discovery and Data Mining*, pp. 150–160, August 2000.